361 p.

NASA Contractor Report 172439

Vortex Flap Technology: A Stability and Control Assessment

K. M. Carey And G. E. Erickson

Northrop Corporation, Aircraft Division
Hawthorne, CA 90250

Contract NAS1-17533
November 1984

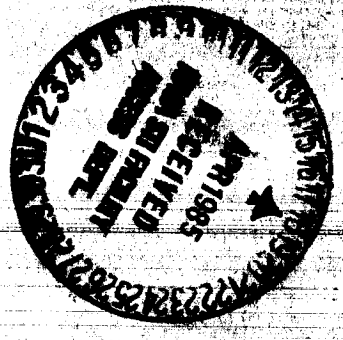

National Aeronautics and
Space Administration

Langley Research Center
Hampton, Virginia 23665

NASA Contractor Report 172439

Vortex Flap Technology: A Stability and Control Assessment

K. M. Carey And G. E. Erickson

Northrop Corporation, Aircraft Division
Hawthorne, CA 90250

Contract NAS1-17533
November 1984

NASA
National Aeronautics and
Space Administration

Langley Research Center
Hampton Virginia 23665

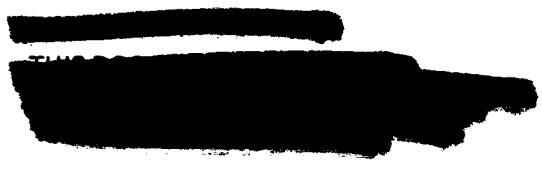

FOREWORD

This document is the final report of the "Vortex Flap Technology: A Stability and Control Assessment" program, which was conducted under Contract NAS1-17533, as part of the on-going NASA Vortex Flap Technology Program. The NASA Technical Monitor for this contract was Mr. Long P. Yip of NASA Langley Research Center, Flight Dynamics Branch.

Acknowledgement is given to Mr. Heinz A. Gerhardt, Manager of Aerodynamics Research at Northrop, and to the following individuals at Northrop who contributed to the program: Tom Widynski, plotting routines and data handling; Bob Lucas, Lee Keraly, and Ralph Jaffke, instrumentation; and Dale Hollingsworth, model fabrication.

TABLE OF CONTENTS

TABLE OF CONTENTS (Cont'd)

LIST OF SYMBOLS

The longitudinal aerodynamic coefficients are referred to the wind-axes system while the lateral-directional aerodynamic coefficients are referred to the body-axes system. The moment reference center was located at .40 $\bar{c}$ for all configurations.

ENGLISH SYMBOLS

a. c.	aerodynamic center
AR	aspect ratio
b	span
c	local chord
$\bar{c}$	mean aerodynamic chord
C_D	drag coefficient
C_L	lift coefficient
$C_{L_{max}}$	maximum lift coefficient
C_ℓ	body-axis rolling moment coefficient
C_{ℓ_β}	body-axis rolling moment derivative due to sideslip angle
$C_{\ell_{\delta_f}}$	body-axis rolling moment derivative due to trailing-edge flap deflection angle
$C_{\ell_{\delta_n}}$	body-axis rolling moment derivative due to leading-edge flap deflection angle
$C_{\ell_{\delta_v}}$	body-axis rolling moment derivative due to tail deflection angle

LIST OF SYMBOLS (Cont'd)

C_m	pitching moment coefficient
$C_{m_{/\beta/}}$	pitching moment due to sideslip angle
$C_{m_{C_N}}$	pitching moment due to normal force coefficient
$C_{m_{\delta_f}}$	pitching moment due to trailing-edge flap deflection angle
C_n	body-axis yawing moment coefficient
C_{n_β}	body-axis yawing moment derivative due to sideslip angle
$C_{n_{\beta_{dyn}}}$	dynamic directional stability parameter, a value for I_z/I_x of 8 was used
$C_{n_{\delta_f}}$	body-axis yawing moment derivative due to trailing-edge flap deflection angle
$C_{n_{\delta_n}}$	body-axis yawing moment derivative due to leading-edge flap deflection angle
$C_{n_{\delta_v}}$	body-axis yawing moment derivative due to tail deflection angle
C_s	potential flow leading-edge suction coefficient
C_Y	sideforce coefficient
C_{Y_β}	sideforce derivative due to sideslip angle
c.g.	center of gravity
CPU	upper surface static pressure coefficient

LIST OF SYMBOLS (Cont'd)

d	maximum body width
h	canard height above wing plane
I_z/I_x	moment-of-inertia ratio
ℓ	distance between canard apex and wing apex
LEX	leading-edge extension
S_{ref}	reference area
S	local wing semispan
S (flap hingeline)	local semispan distance relative to flap hinge-line
VLM	Vortex Lattice Method
x	chordwise distance measured along wing (tail) centerline
x/c	non-dimensional chordwise distance
y	spanwise distance measured from wing centerline
y/s	non-dimensional span distance
z	vertical distance measured normal to model centerline
z/d	non-dimensional vertical distance

GREEK SYMBOLS

α	angle of attack, deg.
β	angle of sideslip, deg.
δ_f	trailing-edge flap deflection angle, deg.; positive trailing-edge down
δ_n	leading-edge flap deflection angle, deg.; positive leading-edge down
δ_v	vertical tail deflection angle, deg.; positive trailing-edge right
λ	taper ratio
Λ_{LE}	leading-edge sweep angle, deg.
Λ_{TE}	trailing-edge sweep angle, deg.

LIST OF TABLES

LIST OF FIGURES

LIST OF FIGURES (Cont'd)

LIST OF FIGURES (Cont'd)

LIST OF FIGURES (Cont'd)

LIST OF FIGURES (Cont'd)

LIST OF FIGURES (Cont'd)

LIST OF FIGURES (Cont'd)

LIST OF FIGURES (Cont'd)

LIST OF FIGURES (Cont'd)

LIST OF FIGURES (Cont'd)

LIST OF FIGURES (Cont'd)

LIST OF FIGURES (Cont'd)

LIST OF FIGURES (Cont'd)

LIST OF FIGURES (Cont'd)

LIST OF FIGURES (Cont'd)

LIST OF FIGURES (Cont'd)

LIST OF FIGURES (Cont'd)

LIST OF FIGURES (Cont'd)

LIST OF FIGURES (Cont'd)

LIST OF FIGURES (Cont'd)

SUMMARY

This report presents results of a comprehensive low-speed wind tunnel investigation and data analysis of leading-edge vortex flap effects on representative aircraft configurations. The wind tunnel data were analyzed to determine the effects of analytically- and empirically-designed vortex flaps on the static longitudinal and lateral-directional aerodynamic, stability, and control characteristics of wings having leading-edge sweep angles of 45 to 76.5 degrees. Sensitivity of the characteristics to several configuration modifications were also assessed, including flap planform and apex geometry effects, leading- and trailing-edge flap deflection effects, fuselage upwash and forebody effects, and centerline tail and outboard fin effects. The data, composed of force, moment and surface static pressure measurements and flow visualization, were obtained in the Northrop 21- by 30-inch low-speed wind tunnel.

Leading-edge vortex flaps were analytically designed using the NASA Langley extended version of the Vortex Lattice Method with Suction Analogy. The design procedure produces a flap shape which corresponds to the flow situation of vortex separation everywhere along the leading-edge with primary reattachment at the deflected flap hingeline. Although test results indicate that this is not necessarily the flow situation which yields maximum improvements in performance, the design procedure is a useful tool for the preliminary sizing of leading-edge flaps.

Leading-edge vortex flap deflection of 30 degrees normal to the flap hingeline results in the greatest performance improvements on moderately-swept wings; vortex flap effectiveness decreases with increasing leading-edge sweep. Wing upper surface static pressure distributions and flow visualization revealed that the ability of the VLM-designed vortex flaps to maintain a concentrated vortex along the deflected control surface is quite limited. The vortex migrates off the deflected flap at angles of attack

below the typical maneuver range. Leading-edge controller tabs, although an effective means of enhancing the vortex strength at a given angle of attack, exacerbate this situation.

Comparisons of flap planforms revealed that the longitudinal characteristics favor the tapered, empirically-designed flap, while the lateral-directional characteristics favor the inverse-tapered VLM-designed vortex flap, although some of the effects are configuration-dependent. The aerodynamic and stability characteristics of vortex-flapped configurations are quite sensitive to slight modifications of the flap apex. Small changes in apex geometry significantly affect the vortex flow-field and burst characteristics. The configurations also display sensitivity to trailing-edge sweep angle and wing vertical position. Closely-coupled canards, nose strakes, and outboard fins have very favorable effects on the lateral stability characteristics and the dynamic directional stability parameter of selected vortex-flapped configurations, to the extent they were examined in this investigation. Trailing-edge flap deflection increases vortex flap effectiveness. Significant maneuvering performance gains can be achieved by suitable combination of vortex flap and trailing-edge flap deflection angles.

INTRODUCTION

Advanced fighter aircraft with a requirement for supersonic capability must also achieve high levels of transonic sustained and instantaneous maneuverability. Under transonic maneuver conditions however, it is difficult to maintain attached flow on thin, sharp-edged wings of moderate-to-high sweep. Such wings are characterized by organized flow separation in the form of concentrated vortices. These powerful rotational flows induce the required high lift but also promote high levels of drag due to the loss of leading-edge suction, as shown in Figure 1.

The vortex flap concept evolved from early investigations by Boeing and NASA researchers (References 1-8) as a simple separated flow design alternative to the severe wing warping characteristic of attached flow designs. The vortex flap concept, illustrated in Figure 2, takes advantage of leading-edge flow separation by developing a concentrated vortex on a forward-facing surface. The vortex-induced suction pressures act on the deflected flap to produce both aerodynamic lift and thrust components, thereby reducing drag. Ideally, the leading-edge vortex is maintained on the flap along its entire spanwise length with primary reattachment at or near the flap hingeline and attached flow over the wing upper surface, as shown in Figure 3. The flaps tend to be of inverse taper planform to accommodate the growth of the vortex along the span.

The majority of investigations performed to date have emphasized the maneuver performance enhancement of vortex-flapped wings with leading-edge sweep of 60 degrees and greater. Interestingly, recent and on-going studies have shown that vortex flaps are most effective when applied to wings of moderate sweep (45 to 55 degrees). Little attention has been given to the impact of vortex flaps on the stability and control characteristics of wings with moderate-to-high sweep. In addition, a systematic study of vortex flap planform effects has not been performed in previous investigations.

Accordingly, this program was initiated to expand the low-speed experimental data base on vortex-flapped wings of cropped delta and cranked planform with leading-edge sweep angles ranging from 45 to 76.5 degrees. Emphasis was placed on the static longitudinal and lateral-directional stability and control characteristics. A comprehensive test program was performed involving a unique combination of force and moment measurements, wing surface pressure measurements, and flow visualization. Numerous configuration effects were examined which provided a better understanding of the vortex flap flow phenomena and forebody-wing, canard-wing, and wing-tail vortex interactions. Comparisons were made of vortex flaps with inverse taper and "conventional" taper planform and with leading-edge controller tabs (tabbed flaps) to assess the "optimum" vortex flap shape.

PROGRAM SUMMARY

The primary objective of the program was to conduct a detailed low speed wind tunnel investigation addressing the longitudinal and lateral-directional stability and control characteristics of vortex-flapped wings with moderate-to-high sweep. The three-task program consisted of vortex flap-wing design and fabrication, wind tunnel testing, and data analysis as described in the following paragraphs.

Task I - Design and Fabrication of Leading-Edge Vortex Flaps

The first task involved the design and fabrication of leading-edge vortex flaps in conjunction with wing planforms suitable for advanced tactical aircraft configurations. The extended version of the NASA-Langley Vortex Lattice Method with Suction Analogy (VLM-SA) of References 9 and 10 was used to design full- and part-span vortex flaps for cropped delta and cranked wings with leading-edge sweep angles ranging from 45 degrees to 76.5 degrees as shown in Figure 4. The design conditions corresponded to a Mach number of 0, vortex flap deflection normal to the hingeline of 30 degrees, and a nominal lift coefficient of 0.5.

The design condition of a 30-degree deflection angle was based on results from a previous low-speed diagnostic wind tunnel test which indicated that a 30-degree vortex flap deflection angle was the most effective. Smaller deflection angles did not provide a strong concentrated leading-edge vortex which could be maintained on the flap at low-to-moderate angles of attack and larger deflection angles tended to promote hingeline separation. Flap deflection angle was not scheduled with angle of attack. Strict adherence to the design conditions (see Reference 10) resulted in the curved vortex flap planforms depicted in Figure 4.

Three of the eighteen designs incorporated trailing-edge sweep variations of 15- and 30-degrees forward and 15 degrees aft on the 65-degree cropped delta wing with full-span flap. Tabbed vortex flaps were developed for the 60- and 65-degree cropped delta and the 70/50-degree cranked wings, as shown in Figure 5. Tabbed flaps are described in detail in Reference 1. The tabbed flap total chord was equal to the VLM-designed vortex flap chord and the ratio of tab length to total chord length was 1 to 3. Vortex flaps of conventional taper were designed for comparison to the inverse-tapered vortex flaps and are illustrated in Figure 6. Geometric details of all wings are provided in Table 1. Wing reference area includes flap area. Task I activity concluded with the fabrication of the wing flap geometries for testing in conjunction with an existing versatile fighter fuselage.

Task II - Low-Speed Wind Tunnel Test

The second task involved wind tunnel testing in the Northrop 21- by 30-inch low-speed diagnostic facility. Six-component force and moment data were obtained up to high angles of attack at zero and non-zero sideslip angles. The wind tunnel test program was organized into five series as outlined in Figure 7. Parametric tests were conducted to assess the effects on longitudinal and lateral-directional stability and control characteristics of: 1) vortex flap-wing geometry; 2) vortex flap deflection; 3) vortex

flap apex modification; 4) inverted leading-edge flap deflection; 5) trailing-edge flap deflection; 6) centerline and outboard vertical tail; 7) wing height variation; 8) nose strakes; and 9) close-coupled canards. Differential inverted leading-edge and trailing-edge flap deflections for roll control were tested along with deflections of all-moveable centerline and outboard vertical tails for yaw control. Wing upper surface flow visualization was performed on selected configurations using a fluorescent oil flow technique to determine primary reattachment and secondary separation lines. A laser light sheet technique was used on a more limited basis for off-body vortex flow visualization.

Task III - Wind Tunnel Data Analysis

The third task involved a detailed analysis of the wind tunnel force and moment data, wing surface pressure distributions, and flow visualization results. The static longitudinal and lateral-directional aerodynamic, stability and control characteristics were determined for all configurations. An assessment was also made of the ability of the Vortex Lattice Method design procedure to develop effective leading-edge vortex flaps. Task III activity culminated in the development of a useful data base which was documented in a final report.

EXPERIMENTAL APPROACH

Model and Apparatus

The designed vortex flap-wing geometries were fabricated from 0.05-inch thick metal using equipment available at the diagnostic test facility. Thirty-eight pairs of wings were built for force testing, including twenty-four pairs of wings with vortex flaps deflected 30 degrees and 14 pairs of wings with undeflected flaps. The sharp leading-edged wings were beveled

on the lower surface and variations of leading- and trailing-edge flap deflection angles were obtained using hand-brake equipment to bend the flaps about a specified hingeline. The wings were painted black to provide suitable contrast for the fluorescent surface flow visualization.

The surface patterns are helpful in understanding the flow-field associated with the leading-edge vortex. Interpretations of the patterns can be made based on the following explanation and the illustrations in Figure 8. The side and plan views show: 1) the primary separation, fixed at the sharp leading-edge, which produces the vortex sheet; 2) the primary attachment which divides the fluid that is drawn into the core and flows outboard toward the leading-edge from that which passes it by and continues over the surface; 3) the fluid near the surface which can't negotiate the adverse pressure gradient it meets under the vortex core and separates as a secondary vortex sheet (rotating in the opposite sense to the primary); and 4) the secondary attachment line which divides the flow from the fluid drawn into the secondary vortex. The position of the secondary separation line is not fixed and depends on the condition of the boundary layer and on the Reynolds number.

Four pairs of wings were instrumented for pressure testing. The 65-degree cropped delta and the 70/50-degree cranked wings with VLM-designed flaps and tabbed flaps were instrumented with three spanwise rows of 0.01-inch diameter upper surface static pressure taps as shown in Figure 9.

All-moveable flat-plate centerline vertical tail and outboard-vertical tail surfaces, illustrated in Figure 10, were fabricated from the same sheet metal stock. The total tail volume of the twin outboard tails was equal to that of the centerline tail. Three pairs of outboard tails were made with incidence angles of -10, 0, and +10 degrees. The centerline tail and outboard fins were subsequently instrumented with surface static pressure orifices distributed in two spanwise rows as shown in Figure 11. Testing was performed in conjunction with the 70/50-degree cranked wing.

The test-bed for the vortex flap-wing geometries was an existing generic fighter fuselage. The model, shown in Figure 12, is constructed of composite materials and features removeable forebody, canopy, vertical tail, and high-, mid-, and low-wing positions.

Force and moment data were obtained using an internal, six-component strain-gage balance. Wing surface static pressures were measured with Scanivalve instrumentation using two modules of a five-pack. Pressure tubing was mounted on the wing lower surface and routed inboard to the model centerline.

Test Conditions and Procedures

Diagnostic Facility - The Northrop low-speed wind tunnel, shown in Figure 13, is a self-contained facility, including equipment and material for basic model fabrication, apparatus for photography and color video recording, a data acquisition system, flow visualization capabilities, and supporting personnel. The open-return, fan-driven tunnel has a 21- by 30-inch test section which is a 0.25-scale model of the Northrop 7- by 10-foot low-speed wind tunnel. The model is sting-mounted via a vertically-traversing strut providing a 40-degree angle-of-attack range and a range of sideslip angle from -10 to +10 degrees. Tunnel speed is variable up to 145 ft/sec, corresponding to a Reynolds number of 900,000 per foot.

The diagnostic facility is a useful and highly-efficient tool providing valid and repeatable quantitative information regarding aerodynamic trends. It is an effective means of evaluating new concepts and preliminary designs. Diagnostic model fabrication and testing are governed by simplicity and low cost. This experimental approach provides a foundation for more detailed testing of higher-quality models in larger-scale wind tunnels. Six-component forces and moments obtained in the 21- by 30-inch wind tunnel on generic and specific fighter configurations compare reasonably well with data obtained on similar models tested in the Northrop 7- by 10-foot facility, up to angles of attack approaching 30 degrees.

Test Procedure

The wind tunnel investigation was performed at a freestream dynamic pressure of 20 psf corresponding to a Reynolds number of 0.78 (10^6) per foot. Six-component force and moment data were obtained at angles of attack from 0 to 30 degrees (to 40 degrees on selected configurations) in 2-degree increments at zero and five degrees of sideslip. Sideslip "sweeps" from -10 to +10 degrees in 5-degree increments were performed at selected angles of attack. This capability was developed specifically for use in the NASA contract testing. All data were corrected for sting deflection, blockage, and wall effects. Upper surface static pressure measurements were taken at seleted angles of attack and at sideslip angles from -10 to +10 degrees. The pressure distributions were obtained independently of force and moment measurements.

Surface oil flow visualization was performed at selected angles of attack and at 0 and ± 5 degrees of sideslip on selected configurations. The surface flow visualization was performed using a mixture of fluorescent powder, oil, and kerosene, which was "painted" on the model prior to each run. The flow pattern was established within several seconds. Upon evaporation of the kerosene, a "permanent" record of the surface pattern was established to provide information on attached and vortex-domonated flows. The oil flow patterns were exposed to ultraviolet light and photographs were taken with a 35-mm SLR camera with 2X converter using ASA 400 Tri-X pan film.

Off-body flow visualization was performed on a limited basis using a laser light sheet technique which was recently developed for use in the Northrop diagnostic facility to examine the cross-sectional structure of vortical flows. A 35mW helium-neon laser was used to illuminate smoke particles formed by the reaction of ammonia and sulfur dioxide gases and introduced into the freestream ahead of the model by a hand-held smoke wand. The traversal of the laser system, mounted on a platform above the test

section, in the freestream direction made possible the visualization of the streamwise development of the vortex flow. Video equipment was used to record the flow development from a side view.

The wind tunnel data acquisition system is portable and self-contained. The data system uses a Cromemco Z-2, S-100 based computer system. Front-end signal conditioning is provided for all standard-type measuring devices such as strain gages, pressure transducers, and thermocouples. The front-end hardware is computer-controlled to permit real time as well as post-test data reduction. Both raw and reduced data are stored on floppy discs. The computer software was already available for this test and other software is available for special applications. The computer supports a FORTRAN IV Compiler for program development.

When the wind tunnel test was completed, the reduced data were transferred from floppy discs to a 9-track magnetic tape. The 9-track tape was then loaded into the IBM Main Computing System. The data were manipulated on the IMB system and plotted on a Tektronix 4014-1 terminal with hard copy unit using existing stability and control derivative routines and plotting packages modified for use in the NASA contract.

The lateral-directional stability derivatives were obtained by subtracting the two spline-fitted rolling moment curves (at zero and five degrees of sideslip) at interpolated points, dividing by the constant sideslip angle, and spline-fitting the resulting curve. Similarly, the longitudinal stability derivatives were obtained by determining C_{m_α} and C_{N_α} from their respective spline-fitted curves, dividing C_{m_α} by C_{N_α} at interpolated values, and spline-fitting the resulting curve.

DISCUSSION OF RESULTS

The results of the wind tunnel test, including force and moment data, pressure measurements, and flow visualization, will be presented and discussed in sections organized as follows:

1) Effects of Deflected Vortex Flaps

2) Comparisons of Flap Effects
   a) Comparison of Full- and Part-Span Vortex Flaps
   b) Comparison of Tabbed and Plain Vortex Flaps
   c) Comparison of Conventional and Vortex Flaps

3) Configuration Effects
   a) Trailing-Edge Sweep Variation Effects
   b) Wind Vertical Position Effects
   c) Nose Strake Effects
   d) Canard Effects
   e) Flap Apex Modification Effects

4) Flap Deflection Angle Effects
   a) Leading-Edge Flap Effects
   b) Trailing-Edge Flap Effects
   c) Differential Flap Deflections for Roll Control

5) Vertical Tail Effects
   a) Outboard Fin Effects
   b) Tail Deflection Effects

Effects of Deflected Vortex Flaps

The effects of a 30-degree deflection of the VLM-designed vortex flaps on the static longitudinal aerodynamic characteristics of the eleven basic wings examined are shown in Figures 14 through 24. In general, the designed full-span vortex flap results in a reduction in the lift coefficient at a given angle of attack, an increase in maximum lift, a decrease in drag-due-to-lift, and a nose-down increment in the pitching moment with little effect on the longitudinal stability level. Vortex flap deflection reduces vortex strength which in turn reduces the lift coefficient at a constant angle of attack. The increased $C_{L_{max}}$ trend is due to improved flow separation and vortex stability characteristics. The drag improvements are quite significant on the wings of moderate sweep; however, as the leading-edge sweep increases, vortex flap effectiveness decreases. For example, at a typical maneuver C_L of 0.5, the C_D due to vortex flap deflection on the 45-degree delta wing is 45% whereas the C_D for the same conditions on the 70-degree delta wing is 16%.

The designed part-span vortex flap results in a decrease in lift coefficient below $C_{L_{max}}$ and slight nose down pitching moment increments at low-to-moderate angles of attack. The effect of part-span vortex flap deflection on induced-drag is minimal, due to the development of a multiple vortex system and adverse interaction between the respective vortex flows which were observed in surface flow patterns and will be discussed in a later section.

A plausible explanation for the reduced vortex flap effectiveness on the higher swept wings is as follows. The VLM design method yielded large flaps on the more highly-swept wings. Deflection of these large leading-edge control surfaces requires a much higher angle of attack to achieve a given lift. In addition, as wing sweep is increased the vortex is displaced away from the wing surface and quickly migrates off the deflected flap surface as angle of attack is increased. On the moderately-swept wings, the leading-edge vortex is better maintained on the flap surface to higher angles of attack than on the more highly-swept wings. This effect is

apparent from wing upper surface flow patterns. Figures 25-27 are photographs of the flow patterns on the 50-, 60-, and 70-degree cropped delta wings, respectively, taken at an angle of attack of 24° and zero sideslip. It is evident that the vortex-induced primary reattachment lines move inboard as the leading-edge sweep is increased at a constant angle of attack.

In addition, even under conditions where the vortex acts principally on the deflected flap, the aerodynamic thrust component due to vortex-induced suction pressures is smaller on wings of greater sweep. This is due to the more aft inclinations of the suction force which acts normal to the flap surface. Also, for the design flap condition of $\delta_n = 30°$, the flap deflection angle measured streamwise decreases with increasing wing sweep.

The static longitudinal stability derivative, $\partial C_m/\partial C_N$, is plotted against angle of attack for the designed vortex flapped configurations in Figures 28-38. Designed Vortex flaps delay to higher angles of attack the stable break in the longitudinal stability curve. However, designed flaps generally do not affect the character of the stability curve.

Coupling between the longitudinal and lateral-directional axes is represented by the parameter $C_{m_{|\beta|}}$, which is indicative of the tendency to pitch due to sideslip. It is desireable to have as small a positive value of this parameter as possible or a negative value to avoid increasing the angle of attack by pitching up in sideslip. A negative slope of the $C_{m_{|\beta|}}$ curve in the stall or post-stall region is desireable to promote stall recovery.

The variation of the pitch-sideslip coupling parameter with angle of attack is shown in Figures 39-49. Vortex flap deflection reduces the nose-up pitching moment due to sideslip and reduces the slope of the curve at angles of attack greater than 10°. These effects are less pronounced on the configurations with deflected part-span vortex flaps due to vortex development from the undeflected portion of the wing leading-edge.

The effects of vortex flaps on the static lateral-directional stability derivatives, $\partial C_\ell/\partial\beta$, $\partial C_N/\partial\beta$, and $\partial C_Y/\partial\beta$, are shown in Figures 50-60. With undeflected flaps the wings exhibit large variations in rolling moment at high angles of attack and consequent fluctuations in lateral stability, produced by asymmetric vortex breakdown in sideslip. The unstable break in the lateral stability curve occurs at higher angles of attack with increasing wing sweep. At higher attitudes, the stable variation of C_{ℓ_β} with α can be attributed to more symmetric wing flow separation characteristics. In this region, the wings of moderate sweep exhibit massive, unsteady flow separation and, therefore, fluctuations in the rolling moment. This unsteady flow situation was especially noticeable during wing upper surface flow visualization. The kerosene was very slow in evaporating, indicative of low-energy flow. The surface flow patterns were ill-defined and exhibited abrupt fluctuations at fixed angle of attack. In contrast, the surface patterns on the more highly-swept wings were characterized by a strong rotational flow, although vortex bursting occurred well upstream of the wing trailing-edge.

At low angles of attack, designed vortex flaps reduce lateral stability due to vortex separation on the flap underside and provides stable increments to the lateral stability at moderate angles of attack as a result of reduced tip separation. At high angles of attack the designed vortex flaps delay the onset of vortex breakdown and reduce burst asymmetries. These effects serve to delay the unstable break in and diminish the large oscillations of the C_{ℓ_β} curve.

These trends were not exhibited by the more highly-swept 70-degree cropped delta and 76.5/66.5-degree cranked wings. Vortex flap deflection has a destabilizing effect throughout the angle of attack range. The vortex flaps on these configurations represent a large percentage of the total wing area. Deflection of these large surfaces suppresses vortex development at low angles and significantly reduces vortex strength at higher angles of attack, which reduces the magnitude of C_{ℓ_β}.

At low angles of attack, leading-edge vortex flap deflection contributes small stable increments to the directional stability due to vortex suction pressures acting on the back-side of the flap. At moderate angles of attack the deflected flap is destabilizing directionally on the more highly-swept configurations. This may be the result of reduced vortex-tail interaction since the wing vortical flow is of reduced strength and is displaced outboard with flap deflection. Vertical tail-off tests would be required to confirm this hypothesis. At high angles of attack, the unfavorable sidewash which results from vortex bursting over the wing adversely affects the directional stability although the fluctuations in the unstable yawing moments are reduced by the deflection of the vortex flaps.

Vortex flap deflection induces small variations in the sideforce due to sideslip at the low-to-moderate angles of attack for all but the most moderately swept. At the high angles of attack the sharp changes in the slope of the sideforce curves are reduced by vortex flap deflection on the moderately swept wings. On the most highly-swept wings, vortex flap deflection induces a positive increment in C_{Y_β} at all angles of attack, consistent with reduced load on the vertical tail.

Figures 61-63 present the variations of lift and rolling moment with sideslip at several angles of attack on the 50-degree and 65-degree cropped delta and 70/50-degree cranked wings. The 50-degree cropped delta wing exhibits a nominal variation of lift with sideslip up to 24 degrees as shown in Figure 61. The rolling moment variation with sideslip is stable at all angles of attack, although the magnitude of the rolling moment coefficient decreases with increased angle of attack. The moderately swept wing does not generate a strong vortex system and is therefore not sensitive to vortex burst asymmetries and the consequent aerodynamic nonlinearities at high angles of attack.

Figures 62 and 63 show similar variations of lift and rolling moment with sideslip on the 65-degree cropped delta and 70/50-degree cranked wings. At the higher attitudes, the stable rolling moment coefficients are greater in magnitude in comparison to the 50-degree swept wing due to the increased vortex-induced effects. Sideslip "sweeps" were not performed at sufficiently high α's to incur pronounced nonlinearities associated with asymmetric core breakdown.

Dynamic Directional Stability Parameter, $C_{n_{\beta_{dyn}}}$: 50-Degree and 65-Degree Cropped and 70/50-Degree Cranked Wings

The parameter $C_{n_{\beta_{dyn}}}$ (see Reference 11) is a measure of the directional stability about the flight path under dynamic conditions. It is computed from:

$$C_{n_{\beta_{dyn}}} = C_{n_\beta} \cos \alpha - \frac{I_z}{I_x} C_{\ell_\beta} \sin \alpha .$$

Generally used to predict yaw departure, negative values of $C_{n_{\beta_{dyn}}}$ indicate the possibility of directional divergence. A moment-of-inertia ratio (I_z/I_x) of 8 was used as a representative value for an advanced tactical fighter configuration in calculating the dynamic directional stability parameter.

Figures 64-66 present the effect of a 30-degree deflection of the vortex flaps on $C_{n_{\beta_{dyn}}}$ for the 50-degree and 65-degree cropped delta and 70/50-degree cranked wings. The 50-degree cropped delta wing maintains positive values of $C_{n_{\beta_{dyn}}}$ up to the maximum angle of attack tested. Vortex flap deflection increases the positive values of the dynamic directional stability parameter in the angle of attack range of 7 to 22 degree but reduces $C_{n_{\beta_{dyn}}}$ significantly at higher angles of attack. Vortex flap deflection has no effect on the angle of attack at which the minimum value of $C_{n_{\beta_{dyn}}}$ occurs.

Figure 65 shows positive values of $C_{n_{\beta_{dyn}}}$ for the 65-degree cropped delta wing up to an angle of attack of 27 degrees with vortex flaps undeflected and to 29 degrees with flaps deflected. Vortex flap deflection results in positive increments to $C_{n_{\beta_{dyn}}}$ at angles of attack greater than 20 degrees. However, the large negative values of the parameter at angles of attack greater than approximately 29 degrees indicate the configuration is susceptible to yaw departure.

The configuration with the 70/50-degree cranked wing exhibits large, negative $C_{n_{\beta_{dyn}}}$ values above 29 degrees angle of attack, as shown in Figure 66. This effect is mitigated somewhat by vortex flap deflection. Similar to the results obtained on the 65-degree cropped delta wing, the static lateral stability derivative (Figure 58a) is the primary driver of the $C_{n_{\beta_{dyn}}}$ parameter.

Upper Surface Static Pressure Distributions: 65 Degree Cropped Delta Wing

Figures 67 and 68 present the effect of sideslip angle on the 65-degree cropped delta wing upper surface static pressure distributions at α= 16 degrees and α= 24 degrees. Vortex flap deflection angle is fixed at 30 degrees. Upper surface static pressure coefficient, CPU, is plotted against span distance, Y (PORT), normalized by the vortex flap hingeline span distance, S (FLAP HINGELINE). Pressures outboard of a non-dimensional span location of 1.0 are on the deflected vortex flap; pressures inboard of this position are on the main wing.

Results at α=16 degrees generally reveal a reduction in the peak vortex-induced suction pressures on the windward and leeward wings as sideslip angle is increased. The location of the peak pressures on the windward wing is sensitive to sideslip angle, displaying an inboard shift due to sideslip. However, the peak pressure magnitudes on the windward and leeward wings are comparable at a given measurement station.

Flow-field asymmetries due to sideslip are more pronounced at α=24 degrees. A consistent reduction in the peak suction pressures occurs on the windward wing. In fact, the absence of a pronounced peak in the pressure distributions at the aft measurement station is indicative of vortex breakdown. In contrast, the peak vortex-induced suction pressures on the leeward wing increase at the forward measurement station and are insensitive to sideslip at the mid- and aft stations. In addition, there is a marked outboard shift in the location of the peak pressures. These flow-field characteristics correlate well with the reduced lateral stability and with the variation of lift and rolling moment with sideslip shown previously in Figures 54 and 62, respectively, at similar angles of attack.

Upper Surface Static Pressure Distributions: 70/50-Degree Cranked Wing

Figures 69 and 70 illustrate the effect of sideslip on the cranked wing surface pressures at α=16 degrees and α=24 degrees, respectively. Upper surface static pressure distributions on the windward and leeward wings are presented at two measurement stations ahead of the leading-edge break (x/c=.422 and x/c=.678) and one station aft of the break (x/c=.848). Vortex flap deflection is fixed at 30 degrees.

Sideslip has only a small effect on the wing surface pressures at α=16 degrees. On the windward wing, the magnitude of the peak suction pressures induced by the vortical flow shed from the more highly-swept inboard leading edge is not sensitive to sideslip angle. However, the locations of the peak pressures ahead of and behind the planform break are more outboard and inboard, respectively, at sideslip. The reduced suction peak on the deflected flap of the outboard wing panel is the result of an effective increase in the streamwise deflection and associated reduction in vortex strength. On the leeward wing, the peak suction pressures are generally lower in magnitude as the sideslip angle is increased. This is indicative of a displacement of the leading-edge vortex away from the wing surface.

Similar effects of sideslip on the wing surface pressures are observed at α=24 degrees. The test results indicate that the maximum suction pressures are maintained on the deflected flap at the forward measurement station on the windward and leeward wings. Migration of the vortex off the flap is evident at the mid station on both wings. In addition, a small, concentrated vortex is maintained on the outboard vortex flap segments. The pressure distributions provide no indication of vortex breakdown effects. In fact, the surface pressure data trends correlate well with the high level of lateral stability exhibited by the cranked wing at α=24 degrees.

Comparison of Flap Effects

Comparison of Full- and Part-Span Vortex Flaps

Full- and part-span vortex flaps were designed for the 65- and 70-degree cropped delta and the 70/50-degree cranked wings, as shown in Figures 71-73. Comparisons of the static longitudinal aerodynamic and stability characteristics of the three wing planforms with full- and outboard part-span flaps deflected 30 degrees are shown in Figures 74-79.

The deflected full-span flap results in higher maximum lift, lower induced drag, and less nose-up pitching moments than the part-span flap on the 65-degree cropped delta wing. These trends also apply to the 70-degree cropped delta wing, although it was not tested up to $C_{L_{max}}$.

In contrast, the 70/50-degree cranked wing with part-span flap exhibits higher lift throughout the range of angles tested and lower drag-due-to-lift at high lift coefficients, relative to the full-span flap. These results are consistent with wing surface pressure measurements which revealed the development of a strong vortex from the inboard, undeflected portion of the wing leading-edge. This vortex induced an effect analogous to a wing leading-edge extension (LEX). Similar to the cropped delta wing results, the part-span flap promotes nose-up pitching moments in comparison to the configuration with full-span flap.

The effects of flap deflection on the coupling parameter, $C_{m_{/\beta/}}$, plotted against angle of attack, are show in Figures 80-82. The full-span vortex flaps result in less nose-up pitching moment due to sideslip for all configurations.

Comparisons of the effects of 30° full- and part-span vortex flap deflections on the lateral-directional stability characteristics of the three configurations are shown in Figures 83-85. The results are somewhat configuration dependent. Compared to the part-span flap, the full-span flap on the 65-degree cropped delta wing results in significantly higher lateral stability above 10 degrees angle of attack and delays to higher angles the unstable break in the stability curve. In contrast, on the 70-degree cropped delta and the 70/50-degree cranked wings the full-span flaps exhibits reduced lateral stability relative to the part-span flap throughout most of the angle-of-attack range. However, the full-span flap on the 70-degree cropped delta wing eliminates the large oscillations in lateral stability exhibited by the wing with part-span flap.

The comparisons show no significant differences between the effects of the full- and part-span flaps on the directional stability characteristics nor on the sideforce due to sideslip. In general, the wings with part-span flaps are slightly more stable in yaw at low angles of attack, whereas the full-span flap tends to delay the onset of directional instability to slightly higher angles of attack.

Figures 86, 87 and 88 are photographs of upper surface flow patterns on the 65-degree and 70-degree cropped delta and 70/50-degree cranked wings with full- and part-span flaps, respectively. All patterns correspond to a flap deflection of 30 degrees at an angle of attack of 12 degrees and zero sideslip. The photos show that a dual-vortex system is generated by the part-span flap configuration: one vortex develops from the undeflected inboard portion and another emanates from the deflected flap.

The local increase in vortex strength along the undeflected leading-edge accounts for the increased non-linear lift in the moderate angle of attack range and the nose-up pitching moment increments associated with the part-span flaps. The single concentrated vortex emanating from the deflected full-span flap induces a greater thrust component since the vortex acts on a larger forward facing surface area, which accounts for the lower induced-drag associated with the full-span flap.

Due to the shorter generating length of both the flap vortex and the inboard vortex, the part-span flap configuration develops more pronounced vortex bursting at the moderate-to-high angles of attack. This is also an explanation for the reduced maximum lift typically exhibited by the part-span flap configurations. In addition, the wings with part-span flaps are more prone to vortex-burst asymmetries in sideslip at moderate angles of attack.

It should be noted that the lateral stability characteristics of the wings with part-span flaps are sensitive to small changes in the flap apex geometry. Consequently, the trends established in Figures 74-85 are not necessarily universal. This topic will be addressed in more detail in a later section.

Comparison of Tabbed and Plain Vortex Flaps

Comparisons of the longitudinal aerodynamic and stability characteristics of the 60- and 65-degree cropped delta and the 70/50-degree cranked wings with tabbed and plain vortex flaps deflected 30 degrees, illustrated in Figures 89-91, are shown in Figures 92-97. In general, the wings with tabbed vortex flaps exhibit higher lift and lower drag at high lift. These results are indicative of the increased vortex strength arising from the controller tabs. The tabs had no effect on the longitudinal stability characteristics of the cropped delta wings and only slightly increased the pitch instability of the cranked wing at high lift.

The comparisons in Figures 98-100 indicate that pitching moment due to sideslip is insensitive to this variation in flap geometry.

Figures 101-103 present comparisons of the lateral-directional stability characteristics. The plain vortex flap on the 60-degree cropped delta wing results in significantly higher levels of lateral stability in

comparison to the wing with the tabbed vortex flap throughout most of the angle of attack range. This trend also applies to the 65-degree cropped delta and 70/50-degree cranked wings, although the effect is considerably less. Significantly, the configurations with deflected tabbed vortex flaps maintain lateral stability at high angles of attack while the plain vortex flapped-configurations become unstable. Although data were not obtained on the tabbed flaps for comparison to the plain flaps at the highest angles it appears that this trend would be maintained.

There is little difference in the respective directional stability characteristics although the tabbed flap is somewhat less unstable than the plain vortex flap at high angles of attack.

The laser light sheet technique was applied to the 65-degree cropped delta wing with both flap configurations to analyze the respective flow field structures. Results from the flow visualization studies indicate that the tabbed vortex flap configuration was more effective in trapping the vortex along the wing leading-edge than was the plain vortex flap at low angles of attack. However, the vortex was maintained on the plain vortex flap to higher angles of attack, particularly in the .4 to .6 C_L range, than on the tabbed vortex flap.

Upper Surface Static Pressure Distributions With Tabbed Vortex Flaps: 65-Degree Cropped Delta and 70/50-Degree Cranked Wings

Figures 104 and 105 show the effect of sideslip angle on the 65-degree cropped delta and 70/50-degree cranked wing pressure distributions with tabbed vortex flaps deflected 30 degrees. The cropped delta wing results obtained at α=12 degrees reveal nominal effects due to sideslip on the magnitude and location of the peak suction pressures on the windward and leeward wings. The vortex is effectively "captured" at this angle of attack by the unique tabbed flap geometry. Similar results are obtained on the cranked wing, although the maximum vortex-induced suction levels generally decrease with sideslip.

Comparison of Upper Surface Static Pressure Distributions with VLM-Designed and Tabbed Vortex Flaps: 65-Degree Croped Delta and 70/50-Degree Cranked Wings

Figures 106 and 107 compare the pressure distributions on the 65-degree cropped delta wing with VLM-designed and tabbed vortex flaps at α=8 degrees and α=12 degrees, respectively. A similar comparison at α=12 degrees is presented in Figure 108 corresponding to the 70/50-degree cranked wing.

The results obtained on the cropped delta wing reveal consistently higher suction levels at the forward and middle pressure measurement stations with the tabbed vortex flap. The data trends show the effectiveness of the controller tabs to manipulate the leading-edge vortex strength at a given angle of attack.

The test data comparisons on the cranked wing reveal more pronounced variations in the pressure distributions. The stronger vortex on the wing with tabbed flap is evidenced by the significant increase in the suction levels on the deflected flap at all measurement stations. In addition, the larger (and stronger) vortex on the outboard tabbed flap segment induces primary flow reattachment near the hingeline, thereby alleviating flow separation in this region.

The pressure data trends correlate well with increased lift obtained in force measurements and more concentrated vortex observed in laser lightsheet flow visualization of the tabbed-flap configurations.

Vortex Flap Planform Effects

Vortex flaps of conventional taper were empirically designed for the 60-, 65-, and 70-degree cropped delta and the 70/50-degree cranked wings for comparison to VLM-designed vortex flaps of equal exposed area. The eight

configurations are shown in Figures 109-112. The term "conventional" is somewhat misleading since it implies attached flow as opposed to vortex flow. It is apparent from surface flow visualization that flaps of conventional taper on thin wings of moderate-to-high sweep are also vortex-flow dominated at moderate-to-high angles of attack. However, because of the difference in flap chord variation, the flow situations are quite different. The VLM-design procedure provides a flap shape, typically of inverse taper, corresponding to the flow condition of vortex separation everywhere along the leading-edge with primary reattachment at the hingeline of the deflected flap. The tapered planform, on the other hand, tends to have regions of vortex-dominated flow with reattachment non-coincident with the hingeline. Flaps of sufficient taper will also feature mixed regions of attached flow inboard and vortex flow outboard.

Comparisons of the effects of VLM-designed and tapered flaps deflected 30 degrees on the longitudinal aerodynamic and stability characteristics of the four wing planforms are shown in Figures 113-120. The VLM-designed vortex flaps yield consistently lower lift at a given angle of attack and higher drag in comparison to the tapered flaps. The wings with VLM-designed vortex flaps also exhibit consistently greater pitch instability and more nose-up pitching moment due to sideslip.

Figures 121-124 present comparisons of the lateral-directional stability characteristics. The VLM-designed flaps deflected to 30 degrees generally result in a higher level of lateral stability than the conventionally-tapered flaps. This effect is due to the larger flap chord outboard which delays tip stall to higher angles of attack. This trend does not apply to the 70-degree cropped delta wing, however. Wing surface pressure measurements obtained on the wing with VLM-designed vortex flap indicate that the pronounced inverse taper flap planform significantly reduces vortex strength near the tip. The results from the 70-degree swept wing suggest that lateral stability favors a stronger vortex outboard, as is the case with the tapered flap.

For all the configurations examined, the tapered flaps result in lower directional stability at low-to-moderate angles of attack and greater instability at high angles of attack.

Configuration Effects

Trailing-Edge Sweep Effects

Vortex flaps were designed for the 65-degree swept wing with trailing-edge sweep angles of 0°, ±15°, and -30°, as shown in Figure 125. Neither the 15-degree forward sweep nor the 15-degree aft sweep had a significant effect on the size of the vortex flap required to meet the VLM-design criteria. However, 30-degree forward sweep required an 8-10% increase in the flap local chord length. All flaps were designed for a 30-degree deflection angle.

The static longitudinal aerodynamic and stability characteristics for the range of trailing-edge sweep are shown in Figures 126-127. Aspect ratio appears to be the dominant effect on lift, with the cropped arrow wing developing higher lift throughout the angle of attack range tested. The markedly improved drag polar associated with the cropped arrow (Λ_{TE} = +15°) wing is the result of higher aspect ratio and the larger ratio of vortex flap-to-wing area. The cropped arrow wing exhibits reduced pitch instability. This can also be attributed to the effectively larger vortex flap and to a slight forward shift in the .40$\bar{c}$ location.

Consistent with these trends, the cropped arrow planform with vortex flap deflected 30 degrees develops less nose-up pitching moment due to sideslip. This result is shown in Figure 127.

The effects of trailing-edge sweep variation on the lateral-directional stability characteristics are shown in Figure 128. The cropped diamond planforms exhibit reduced lateral stability at low-to-moderate angles of attack relative to the baseline cropped delta configuration. In contrast, the cropped arrow configuration generally improves lateral stability in the same angle of attack range. The latter, however, shows considerably reduced levels of lateral stability at higher angles of attack due to the more severe vortex breakdown asymmetry that is characteristic of arrow wings.

The higher stability levels associated with the cropped arrow wing are probably due to an increase in tail volume, which results from the forward shift of the reference c.g. and reduced wing area, rather than an aerodynamic effect. Similarly, the reduced directional stability of the diamond wing is probably due to a reduction of tail volume because of the aft shift of the reference c.g. and an increase in wing area.

Wing Vertical Position Effects

The 65-degree cropped delta wing with full-span vortex flaps deflected 30 degrees was tested at three non-dimensional wing vertical positions, $z/d = -0.20, 0.0, +0.20$, with z measured normal to the model centerline and non-dimensionalized by the maximum body width, d.

The longitudinal aerodynamic and stability characteristics with the high-, mid-, and low-wing positions are shown in Figures 129-130. Relative to the mid-wing position, the high- and low-wing positions result in increased lift, less induced-drag at mid-to-high lift, and slight nose-up pitching moment increments with no change in longitudinal stability.

Wing upper surface flow visualization, however, revealed no discernible changes in the flow patterns due to wing height variation. Specifically, the vortex-induced primary reattachment and secondary separation lines appeared insensitive to wing position on the body.

Figure 131 illustrates the effect of wing vertical position on the lateral-directional stability characteristics. Compared to the baseline mid-wing position, the low-wing and high-wing configurations exhibit lower and higher levels of lateral stability, respectively. These effects on the lateral stability are due to the different flow fields the configurations experience due to the crossflow around the fuselage. In sideslip, the low wing configuration experiences downwash on the windward wing and upwash on the leeward wing, while the high-wing configuration experiences upwash on the windward wing and downwash on the leeward wing. These situations contribute positive and negative rolling moment increments to the baseline conditions, respectively, consistent with the classical fuselage crossflow effect on lateral stability. The unstable break in the lateral stability curve occurs at virtually the same angle of attack for all three configurations.

At low-to-moderate angles of attack there is no significant difference in the directional stability of the low-, mid-, and high-wing configurations. At moderate-to-high angles of attack, the high-wing results in lower yaw instability while the low-wing position results in increased instability. The variations in directional stability due to wing position can once again be attributed to fuselage crossflow effects rather than any changes in the vortex flap aerodynamics.

Effect of Wing Vertical Position on Upper Surface Static Pressure Distributions: 65-Degree Cropped Delta Wing

For completeness, pressure distributions are presented in Figure 132 corresponding to mid- and low-wing positions at α=16 degrees with vortex flap deflected to 30 degrees. The magnitude and location of the peak vortex-induced suction pressures are relatively insensitive to wing vertical location on the fuselage. These results are consistent with upper surface flow visualization which revealed no measurable changes in the vortex migratory behavior due to wing height variation.

Nose Strake Effects

The nose strakes shown in Figure 133 were empirically designed and mounted at the nose maximum half-breadth. The strakes were fabricated from .05-inch thick sheet metal and were joined by a thin strip of metal. The strip joining the strakes was fitted into a slot in the nose of the model such that the strakes were flush with the surface with no protuberances. The nose strakes were tested in conjunction with the 65-degree cropped delta and 70/50-degree cranked wings. Vortex flap effects were examined on the cranked wing with deflection angles of 0 and 30 degrees; the cropped delta wing was tested with a 30 degree flap deflection. Trailing-edge flaps were undeflected.

The effect of vortex flap deflection on the longitudinal aerodynamic and stability characteristics of the cranked wing with nose strakes is presented in Figures 134 and 135. Based on a comparison with vortex flap effects on the same configuration without strakes, shown previously in Figures 22, 36, and 47, it is evident that the strakes do not alter the vortex flap effects on the lift and drag characteristics. However, they do cause more nose-down pitching moment increments and a more significant reduction of the pitch-sideslip coupling parameter due to flap deflection.

Figure 136 shows the effect of vortex flap deflection on the lateral-directional stability characteristics of the configuration with nose strakes for comparison to the effects on the configuration without strakes, given in Figure 58. Both configurations yield similar trends in the lateral stability although the strakes-off configuration results in more improvement in C_{ℓ_β} at moderate-to-high angles of attack due to vortex flap deflection. Although the strakes-on configuration generates higher levels of directional stability than does the strakes-off configuration, vortex flap deflection has a more detrimental effect on the former.

Figures 137-140 illustrate the effects of the strakes on the static longitudinal aerodynamic and stability characteristics of the 65-degree cropped delta and 70/50-degree cranked wings, both with vortex flaps deflected to 30 degrees. The strake-induced lift produces nose-up pitching moment increments, increased pitch instability, and more nose-up pitching moment due to sideslip. However, the strakes have minimal effect on total lift and drag.

Figures 141 and 142 show the effects of the nose strakes on the lateral-directional stability characteristics. The strakes result in increased lateral stability at moderate-to-high angles of attack. In addition, the strakes enable directional stability to be maintained to higher angles of attack and considerably reduce the directional instability at high angles of attack.

The effect on $C_{n_{\beta_{dyn}}}$ of nose strakes in conjunction with the 70/50-degree cranked wing with vortex flaps deflected to 30 degrees is illustrated in Figure 143. Consistent with the improved lateral-directional stability shown previously in Figure 142a, the strakes result in positive values of the dynamic directional stability parameter up to approximately 34 degrees.

To isolate the effect of the nose strake flow field, a component build-up was conducted in conjunction with the 70/50-degree cranked wing. Figures 144 and 145 provide some insight into the contributions to lateral-directional stability of the various airframe components. The test data suggest that a favorable interaction of the strake vortex system with the windward wing flow field is the primary source of the increased dihedral effect. At high angles of attack, a slight increase in windward wing vortex stability can promote a large increase in lateral stability. This effect has been observed in several investigations of advanced fighter aircraft configurations. The main contribution to increased directional stability is the direct suction effect induced by the windward strake vortex. Secondary effects due to strake vortex system interaction with the centerline tail may also contribute to the enhanced stability. Increased lateral and directional stability due to nose strakes located at the maximum half-breadth has been demonstrated in wind tunnel and flight tests of the Northrop YF-17 (Reference 12).

Canard Effects

A pair of canards were empirically designed on the basis of results obtained in References 13 and 14, and were tested in conjunction with the 65-degree delta wing with full-span vortex flaps deflected 30 degrees. Canard area was not included in the reference area. The objective of this portion of the wind tunnel investigation was not to optimize canard-wing interactions but, rather, to obtain representative results of canard effects on a vortex-flapped wing.

The canards, illustrated in Figure 146, were tested at a non-dimensional height, h/b, of 0.085 above the wing plane, where h and b are the canard height and wing span, respectively. Two longitudinal positions, ℓ, non-dimensionalized by the wing mean aerodynamic chord, $\bar{c}$, were investigated and corresponded to $\ell/\bar{c}$=.40 and $\ell/\bar{c}$=.27. Here, ℓ was defined as the distance between the canard apex and the wing apex. The canard incidence angle was 0 degrees.

The effects of the canards on the static longitudinal aerodynamic and stability characteristics are presented in Figures 147-148. The canards promote a more pronounced nonlinearity of the lift curve at high angles of attack due to canard-wing vortex interaction, induced-drag reductions at high lift, large nose-up pitching moment increments, and increased pitch instability. Longitudinal trim conditions will require canard deflections which may affect these results which are based on zero canard deflection.

Figure 149 presents canard effects on the lateral-directional stability characteristics. Canard downwash improves the windward wing flow separation characteristics and, consequently, results in large increases in lateral stability at moderate-to-high angles of attack. The data suggest that the canards delay the onset of asymmetric vortex breakdown on the wing and consequently delay the corresponding unstable break in the lateral stability curve. Concurrent with these favorable effects are unstable increments in directional stability at low-to-moderate angles of attack. The canard alone

would be stabilizing directionally based on the sideforce due to sideslip data which indicates that the canards induce positive sideforce increments.

Figure 150 shows the effect of canards on the variations of lift and rolling moment with sideslip on the 65-degree cropped delta wing. The canards have negligible effect on the lift loss at sideslip. However, the data indicate that the canards result in a more stable variation of rolling moment with sideslip at α=24 degrees.

Figure 151 shows the effect of the effect of canards on the dynamic directional stability parameter for the 65-degree cropped delta wing. Above 20 degrees angle of attack the canards result in large positive increments to $C_{n_{\beta_{dyn}}}$. This effect is due largely to the improved lateral stability characteristics arising from a favorable canard-wing flow field interaction.

Figure 152 presents the effect of the canard on the wing upper surface static pressure distributions at an angle of attack of 24 degrees. Only the right wing was instrumented with pressure orifices. Consequently, test data were obtained at positive and negative sideslip angles to access canard effects on windward and leeward wing surface pressures, respectively.

The addition of the canards results in an outboard shift of the peak vortex-induced suction pressures at all measurement stations, indicating an improvement in the migratory behavior of the wing leading-edge vortex. For example, with canards on, the vortex remains on the flap up to approximately the mid-measurement station (x/c=.576). With canards off, the vortex has migrated off the flap upstream of the first station (x/c=.405). The latter position is inboard of the canard tip and, consequently, exhibits lower peak suction pressures due to canard downwash effects. The mid- and aft-pressure measurement stations are outboard of the canard tip and generally develop slightly higher suction levels as a result of the canard-induced upwash field.

The canard has a pronounced effect on the wing upper surface pressure distributions in sideslip. Results are presented in Figure 153 corresponding to α=24 degrees and β=10 degrees. The pressure distributions on the windward wing (Figures 153a -153c)exhibit a significant increase in the magnitude of the peak suction pressures and an outboard shift in the position of the suction peaks at all measurement stations. These results are indicative of enhanced wing leading-edge vortex stability and downward displacement of the vortex core due to the canard-induced downwash field. In contrast, the canard generally decreases the vortex-induced effects on the leeward wing (Figures 153d - 153f), presumably because of premature "lifting away" of the vortex from the wing surface and possible core breakdown due to canard upwash. The pressure distributions correlate well with the large increase in lateral stability shown previously in Figure 146.

Canard deflection necessary for longitudinal trim would certainly affect the interaction of the canard flow-field with the wing and tail surfaces and therefore will affect the surface static pressure distributions as well as the lateral-directional stability trends. The results presented here should be interpreted accordingly since zero canard incidence is unlikely, particularly at high angles of attack.

Vortex Flap Apex Modification Effects

Modifications were made to the apex of the part-span vortex flaps on the 65-degree cropped delta and the 70/50-degree cranked wings. A streamwise cut was made in the flap and the curved apex region inboard of the cut was removed, as shown in Figure 154. Test results were obtained with vortex flaps deflected to 30 degrees. The data are not corrected for the slight change in wing area.

The effects of these modifications on the static longitudinal aerodynamic characteristics are shown in Figures 155 and 156. In general, the wings with unmodified flaps exhibit higher lift, less drag at high lift, and more nose-up pitching moments. The unmodified vortex flap on the 65-degree cropped delta wing results in higher maximum lift. This trend appears to

be applicable to the 70/50-degree cranked wing, although the latter was not tested up to $C_{L_{max}}$. Surface flow patterns indicate that the modified apex is conducive to unorganized flow separation just downstream of the wing-flap junction and to the development of a counter-rotating vortex along the streamwise edge. In contrast, the unmodified apex promotes the smooth development of a leading-edge vortex from the deflected flap surface. These effects, in combination with the reduced flap area and earlier vortex bursting, account for the higher drag and lower lift associated with the modified vortex flap at high α's.

Figures 157 and 158 illustrate the effects of the flap modifications on the longitudinal stability characteristics. The flap apex modification has a minimal effect on the longitudinal stability level of the cropped delta wing. However, the modified flap increases pitch stability on the cranked wing. The cropped delta wing exhibits less nose-up pitching moment due to sideslip with the modified flap; nose down pitching moments due to sideslip are developed on the cranked wing.

Figures 159 and 160 present the lateral stability characteristics of the 65-degree cropped delta and 70/50-degree cranked wings with the original and the modified part-span vortex flaps deflected to 30 degrees. The modified flap on the cropped delta wing exhibits significantly higher levels of lateral stability at moderate and high angles of attack and a delayed onset of the unstable break in the C_{ℓ_β} curve. In contrast, the modified flap on the cranked wing results in lower, although still favorable, lateral stability. However, the modified flap maintains lateral stability up to the highest angles of attack tested while the original flap becomes unstable.

Surface flow patterns on the 65-degree cropped delta wing indicate that the streamwise edge of the modified part-span flap appears to reduce the interaction of the flap vortex with the vortical flow that is generated by the undeflected portion of the wing leading-edge. Wing upper surface static pressure distributions obtained in another investigation on the 65-degree cropped delta wing with unmodfied flap indicate that at moderate-to-high

angles of attack the vortices merge. This single, concentrated vortex system is prone to large asymmetries in the core breakdown positions. The modified flap, however, enables a distinct two-vortex system to be maintained to higher angles of attack. Although the vortices break down sooner due to their relatively short generating lengths, the vortex flow-field exhibits reduced breakdown asymmetries in sideslip. This effect is analogous to wind tunnel and water tunnel results obtained on an advanced LEX-wing fighter configuration in Reference 15. In the latter study it was found that truncating the LEX apex region decreased $C_{L_{max}}$ but enhanced high-lateral stability as a result of reduced vortex burst asymmetries.

An understanding of the conflicting results obtained on the cranked wing is again aided by wing surface pressure measurements obtained in another study are shown in Figures 161 and 162. In contrast to the part-span flap on the 65-degree cropped delta wing, the part-span flap on the cranked wing is not an efficient vortex generator. Although the sweep angle discontinuity is not large, pressure measurements indicate that the variation of flap chord across the span is sufficient to promote a two-vortex system on the deflected flap. However, only the vortex shed from the inner flap segment is of any consequence. The flap apex modification serves to reduce the generating length of this vortical flow. The beneficial effect on roll stability of a strong vortex outboard is thereby reduced.

The original and modified flaps result in similar directional stability trends for both wing planforms, as shown in Figures 163 and 164.

Two apex modifications were made to the full-span vortex flap of the 60-degree cropped delta wing as shown in Figure 165. In one case, the inboard 25 percent of the exposed vortex flap span was removed and the remaining portion was deflected to 30 degrees. In the other case a streamwise cut was made in the flap at a distance of 25 percent of the exposed half-span. The inboard segment was undeflected while the outboard segment was deflected to 30 degrees.

Figures 166 and 167 illustrate the effects of the former modification on the static longitudinal aerodynamic and stability characteristics. The results do not reflect the changes in reference area which resulted from the modification. The flap alteration promoted a significant reduction in maximum lift, increased drag-due-to-lift; a small, stable shift in longitudinal stability level; and reduced nose-up pitching moment due to sideslip at moderate and high angles of attack. These results can be attributed to earlier breakdown of the wing leading-edge vortex system.

Figure 168 shows the effects of removing the inboard flap area on the lateral-directional stability characteristics. The modified flap promotes lower levels of lateral stability at low and moderate angles of attack which is due to the weakened primary vortex system. At high angles of attack, lateral stability is improved, although the variation of C_{ℓ_β} with α is oscillatory. Consistent with the part-span flap flow-field discussed in a previous section, a two-vortex system is developed. Since wing flow separation is more pronounced at high angles of attack on the wing with the part-span flap, there is less potential for significant vortex breakdown asymmetries in sideslip. Consequently, the lateral stability characteristics are improved at high attitudes in comparison to results obtained with the unmodified, full-span flap. Directional stability is also improved above 25° angle of attack with the part-span flap.

The second flap modification was tested in an attempt to minimize the lift loss at high α's while retaining the increased roll stability associated with the part-span flap. Relative to the wing with unmodified flap, this configuration exhibits slightly reduced maximum lift, greater induced-drag, increased nose-up pitching moments with little change in longitudinal stability, and more nose-up pitching moment due to sideslip, as depicted in Figures 169 and 170. Figure 171 shows the lateral-directional stability characteristics. Evidently, this flap modification does not significantly alter the vortex flow field since the lateral stability characteristics are similar for both flap configurations. At high angles of attack, the vortices that are shed from the two flap segments merge into a single,

concentrated vortex system. Inherent in the latter is pronounced vortex breakdown asymmetry in sideslip. The modified flap does, however, result in less directional stability at low-to-moderate angles of attack and reduced instability at high angles.

A systematic study of the effects of vortex flap apex geometry on the longitudinal and lateral-directional aerodynamic and stability characteristics of fighter wings was performed in a parallel investigation under Air Force sponsorship. Vortex flaps featuring curved leading-edges with zero- and finite-chord near the apex were tested along with vortex-flapped configurations with straight leading-edges. In all cases, the experimental data indicate that a curved apex with finite chord alleviates flow separation from the deflected flap hingeline. However, as shown in Figure 172, a straight leading-edge yields higher maximum lift, less drag at high lift, and reduced pitch instability. Figure 173 shows that both the straight and curved leading-edge geometries provide lateral stability throughout the angle of attack range.

Flap Deflection Effects

A detailed study was conducted to assess the effects of leading- and trailing-edge flap deflection angles on the 50-, 60-, and 65-degree cropped delta wings and of trailing-edge flap deflection angles on the 70/50-degree cranked wing. The wing-flap geometries are shown in Figure 174. Full-span leading-edge vortex flap deflection angles of -30, 0, 30, 45, and 60 degrees were tested along with part-span trailing-edge flap deflection angles of 0, 15, and 30 degrees. Differential deflections of trailing-edge flaps and inverted leading-edge flaps for roll control were examined on the 60-degree cropped delta wing. It should be kept in mind that the vortex flaps were designed for a deflection angle of 30°.

Leading Edge Flap Deflection Effects

The effect of leading-edge vortex flap deflection angles on the static longitudinal aerodynamic and stability characteristics are shown in Figures 175-180. Increased flap deflection generally results in increased lift loss at low-to-moderate angles of attack, higher maximum lift, improved drag polar, and reduced pitch instability. Nose-down pitching moment increments increase from $\delta_n = 30°$ to $\delta_n = 45°$, but decrease from $\delta_n = 45°$ to $\delta_n = 60°$. As flap deflection angle is increased from 0°, reductions in drag-due-to-lift are delayed to higher lift coefficients. In addition, nose-up pitching moment due to sideslip is considerably reduced as flap deflection angle is increased. The data show that the effects are greatest on the 50-degree cropped delta wing.

Upper surface flow patterns show that the leading-edge flap deflection delays the migration of the vortex off the flap to higher angles of attack. However, when the vortex flap deflection is greater than 45 degrees, flow separation and vortex formation from the hingeline occur. This flow situation accounts for the small changes in the pitching moment characteristics between flap deflection angles of 45 and 60 degrees.

The effects of leading-edge vortex flap deflection angle on the lateral-directional stability characteristics are shown in Figures 181 - 183. The 50-degree cropped delta wing exhibits significant reduction in lateral-directional stability at high angles of attack due to increased leading-edge flap deflection angle. The lateral-directional stability of the 60- and 65-degree cropped delta wing were not significantly affected by increased leading-edge flap deflection angle. Increased flap deflection angle results in larger unstable increments in lateral stability at low-to-moderate angles of attack and delays the unstable C_{ℓ_β} break to higher angles of attack. However, leading-edge flap deflections of 45 and 60 degrees cause large fluctuations in lateral stability at moderate-to-high angles of attack due to the unsteady flow separation from the flap hingeline.

The flap deflection angles does not significantly affect the directional stability derivative at low angles of attack. However, increased flap deflection generally reduces the onset angle of attack for yaw instability with subsequent greater instability at high angles of attack.

Inverted Leading-Edge Vortex Flap Effects

The effects of a 30-degree upward deflection on the vortex flaps on the longitudinal aerodynamic and stability characteristics of the 60- and 65-degree cropped delta wing are shown in Figures 184-187. The inverted flaps promote large lift increments at typical approach angles of attack, primarily due to increased vortex strength. Inverted deflection decreases lift at higher angles of attack due to earlier vortex bursting, increases drag as a result of an aft rotation of the vortex lift vector, and causes nose-up pitching moment increments as a result of the inverse camber. The inverted flaps have a minimal effect on the longitudinal stability level. However, the inverted flap configurations exhibit greater nose-up pitching moment due to sideslip.

Figures 188-189 show the effects of inverted vortex flaps on the lateral-directional stability characteristics. Except at very low angles of attack, the wings with upward deflected flaps develop much lower levels of lateral stability. In addition, the inverted flaps promote an earlier unstable break in the lateral stability curve. These effects are due to the more pronounced vortex breakdown asymmetries in sideslip. The inverted flap on the windward wing has an increased effective streamwise deflection which results in increased vortex strength but, concurrently, earlier onset of vortex breakdown.

Trailing-Edge Flap Deflection Effects

Figures 190-221 illustrate the effects of trailing-edge flap deflection on the static longitudinal aerodynamic and stability characteristics of the 50-, 60-, and 65-degree cropped delta and 70/50-degree cranked wings.

For a given leading-edge flap deflection angle, deflecting the trailing-edge flap increases lift, reduces drag at moderate-to-high lift, and induces large nose-down pitching moment increments. In general, a pronounced unstable break in the pitching moment curve occurs at high lift with trailing-edge flap deflected, due to earlier vortex breakdown. However, pitching moment due to sideslip is greatly reduced.

Significant performance gains can be achieved by suitable combination of vortex flap and trailing-edge flap deflections. Downward deflection of the trailing-edge flap increases the upwash at the leading-edge at a constant angle of attack, thereby increasing the suction pressures on the deflected vortex flap. Thus, the deflected trailing-edge flap has a very favorable influence on the vortex flap effectiveness.

Figures 222-225 present the effect of vortex flap deflection on the longitudinal control derivative, $C_{m_{\delta_f}}$. Vortex flap deflection generally reduces trailing-edge flap longitudinal control effectiveness at low-to-moderate angles of attack. The inconsistent results associated with a 60-degree vortex flap deflection are presumably due to the strong vortex shed from the flap hingeline. At high angles of attack, pitch control is increased on the cropped delta wings as a result of vortex flap deflection. This effect decreases, however, with increasing wing sweep. In all cases, as trailing-edge flap deflection is increased, flap longitudinal control effectiveness diminishes. This is the result of trailing-edge flap flow separation and earlier tip stall.

The effects of trailing-edge flap deflection angle on the lateral-directional stability characteristics are shown in Figures 226-241. At low angles of attack, trailing-edge flap deflection results in stable increments in lateral stability which increase with increased deflection angle. This effect is due to increased circulation about the windward wing

and increased separation on the outward portion of the leeward wing. At higher angles of attack, trailing-edge flap deflection generally results in large destabilizing effects on C_{ℓ_β} and C_{n_β} due to increased vortex breakdown asymmetry in sideslip. The results obtained on the 50-degree cropped delta wing at angles of attack greater than 20 degrees should be interpreted with the understanding that the unsteady flow separation from this wing at high angles of attack promotes large fluctuations in the lateral-directional stability derivatives. This effect decreases rapidly with increased wing sweep, since a well-organized vortex flow can be maintained to higher angles of attack on the more slender planforms.

Vortex flap deflection enhances, and extends to higher angles of attack, the dihedral effect due to trailing-edge flap deflection. In addition, the deflected vortex flap reduces the destabilizing effects on C_{ℓ_β} at high angles of attack arising from trailing-edge control surface deflection by limiting vortex breakdown asymmetry due to sideslip.

The lateral stability characteristics with vortex flaps deflected to 60 degrees warrant discussion. The highly-oscillatory variation of C_{ℓ_β} with α is the result of the strong vortices that are shed from the leading-edge flap hingeline region. Since there is no "aerodynamically-sharp" edge from which these vortices form, the vortex behavior is very sensitive to model oscillation, tunnel turbulence, etc. Consequently, the hingeline vortex development and breakdown phenomena are unsteady.

A major shortcoming of inverted leading-edge flaps is illustrated in Figure 234 corresponding to the 60-degree cropped delta wing. At typical approach angles of attack, the inverted leading-edge flap in combination with trailing-edge flap deflection promotes very large destabilizing effects on lateral stability. This effect can be attributed to more severe vortex burst asymmetry.

When the leading-edge flaps are undeflected, trailing-edge flap deflection typically has a favorable effect on the directional stability at low-to-moderate angles of attack and delays the angle of attack at which C_{n_β} becomes negative. Vortex flap deflection serves to diminish these effects.

Differential Flap Deflection Effects

The part-span trailing-edge flaps on the 60-degree cropped delta wing were deflected differentially such that the right flap was down 30 degrees while the left flap remained undeflected. The leading-edge vortex flaps were symmetrically deflected to 30 degrees. Figures 242 and 243 show the resulting rolling and yawing moment variations with angle of attack. Results obtained at zero sideslip indicate that a differentially deflected trailing-edge flap is a powerful roll control device at all angles of attack. Concurrent with the negative rolling moments are large proverse yawing moment increments. Although one would expect positive yaw increments due to the increased induced drag on the right wing, this is not the case due to apparent wing leading-edge vortex-induced sidewash effect on the centerline tail. Because of the proximity of the wing trailing-edge to the centerline vertical tail, the sidewash induces a positive sideforce, which must be in the vicinity of the tail in order to promote a positive C_y, as shown in Figure 244. Vertical tail-off tests would be required to confirm this hypothesis.

Figure 245 illustrates the roll control effectiveness of the differentially-deflected flaps. The configuration yields roll control effectivesess throughout the angle of attack range. The large yawing moments due to trailing-edge control surface input are depicted in Figure 246.

Full-span leading-edge vortex flaps were deflected upward differentially on the 60-degree cropped delta wing. The right flap was deflected up to 30 degrees and the left flap was undeflected. Trailing-edge flap deflection angle was 0 degrees. The resulting rolling and yawing moment

variations with angle of attack are presented in Figures 247 and 248, respectively. This configuration provides rolling moment increments at low angles of attack. At higher angles of attack, rolling moment increments in opposition to control surface input occur due to the earlier onset of vortex burst asymmetries. This flow-field effect also results in destabilizing yawing moment increments.

The lateral-directional control derivatives are shown in Figures 249 and 250. The results show that differentially-inverted leading-edge flaps provide roll control at angles of attack less than 10 degrees. However, they exhibit undesireable reversal and roll control effectiveness.

Vertical Tail Effects

The effects of outboard fins, fin deflection, and centerline tail deflection were examined in conjunction with the 70/50-degree cranked wing with leading-edge vortex flaps deflected to 0 and 30 degrees. The outboard fins had the same tail volume as the centerline tail and were located at a non-dimensional span distance, y/s, of approximately 0.68. The principal objective of this portion of the wind tunnel investigation was to obtain representative results showing the effects of outboard tail surfaces on the leading-edge vortex behavior and longitudinal and lateral-directional stability and characteristics. No attempt was made to optimize the fin location.

Outboard Fin Effects

The effects of vortex flap deflection on the longitudinal aerodynamic and stability characteristics of the 70/50-degree cranked wing with outboard fins are shown in Figures 251 and 252 for comparison to the vortex flap effects on the identical wing planform with centerline tail shown previously

in Figures 22, 36, and 47. Consistent with previously discussed results, vortex flap deflection reduces lift at a given angle of attack, reduces drag at constant lift, has little effect on the pitching moment, and reduces the pitching moment due to sideslip. However, compared to the flap deflection effects on the configuration with a centerline tail, the configuration with outboard fins yields reduced lift loss and better drag polar improvements. Significantly, the outboard fin configuration continues to yield drag reductions throughout the lift coefficient range, while the centerline tail configuration shows an increase in drag for lift coefficients above .9. Pitching moment and longitudinal stability are similar for the two configurations although the outboard fin configuration does not show as much improvement in the pitch-sideslip coupling as does the centerline tail configuration.

The effect of vortex flap deflection on the lateral-directional stability characteristics of the 70/50-degree cranked wing with outboard fins are illustrated in Figure 253. The effects on the stability trends are similar to those on the 70/50-degree cranked wing with centerline tail shown in Figure 58.

A comparison of the outboard fin and centerline tail effects with vortex flaps deflected to 30 degrees on the static longitudinal aerodynamic and stability characteristics are shown in Figures 254 and 255. Relative to the centerline tail, the outboard fins result in significantly lower lift at angles of attack above 14 degrees, reduced maximum lift, higher drag-due-to-lift at moderate and high lift, and more nose-up pitching moments. The reduced lift and increased drag are due to earlier vortex breakdown and a lower effective aspect ratio associated with the addition of the outboard fins. In addition, the latter promote increased pitch instability and nose-up pitching moments due to sideslip.

These results can be better understood by examining the wing upper surface static pressure distributions. The location of the pressure ports

on the 70/50-degree cranked wing are illustrated in Figure 256. Figure 257 presents the effect of outboard fins on the wing upper surface static pressure coefficient. Results are shown at angles of attack of 16 and 24 degrees at two chordwise locations, x/c = .678 and x/c = .848. Sideslip angle is zero degrees. This discontinuity in the pressure distribution at the aft measurement station is due to the presence of the tail surface. At the forward measurement station, the pressure distributions with outboard fin off reveal a suction peak associated with the primary leading-edge vortex. The vortex has migrated off the inboard vortex flap segment and induces the inboard negative pressure peak at the aft measurement station. The more pronounced suction levels near the leading-edge are due to a small, concentrated vortex on the deflected outboard flap surface. At the aft station, addition of the vertical fin promotes a large reduction in the suction pressures and an inboard displacement of the peak pressure associated with the inboard vortex. These effects indicate vortex breakdown and a more inboard trajectory of the vortical flow. The concurrent reduction in leading-edge upwash along the outboard wing panel results in lower suction pressures and an outboard shift in the peak pressure locations on the outer flap segment. An upstream effect due to the fins is evident in the pressure distributions at the forward station. Although the effects are considerably less pronounced, the presence of the fins reduces the vortex-induced suction pressures. The surface pressure measurements are, therefore, consistent with the reduced lift, increased drag, and nose-up pitching moment increments associated with the fins.

A comparison of the effects of outboard fins and centerline tail on the lateral-directional stability characteristics are shown in Figure 258. The fins reduce the dihedral effect at low angles of attack and significantly increase lateral stability at moderate and high angles. The reduced lateral stability at low angles of attack may be due simply to the lower position of the fin center pressure, and hence smaller moment arm, compared to that of the centerline tail. At higher attitudes where the leading-edge vortices are a dominant feature of the flow-field, the fins reduce and even eliminate

vortex breakdown asymmetry due to sideslip and promote corresponding large increases in lateral stability. In comparison to the configuration with centerline tail the outboard fins reduce the directional stability and promote an earlier onset of yaw instability.

The increased lateral stability due to addition of the outboard fins is consistent with wing upper surface static pressure distributions. Figure 259 presents windward and leeward wing surface pressures at two measurement stations, x/c = .678 and .848, corresponding to angles of attack of 16 and 24 degrees and sideslip angles of 5 and 10 degrees. The results at the aft measurement station reveal large reductions in the vortex-induced suction pressures on the windward and leeward wings due to the presence of the fins. The effects, however, are generally more pronounced on the leeward wing, particularly at large sideslip angle where inboard vortex impingement with the tail surface occurs. Under these conditions, the upstream influence of the fin on the wing surface pressures becomes more severe. In contrast, the windward leading-edge vortex is displaced away from the vertical fin as sideslip angle is increased, thereby mitigating the tail influence on vortex stability. These factors result in enhanced roll stability at high angles of attack.

Figure 260 compares the variations of rolling moment and lift coefficient with sideslip on the 70/50-degree cranked wing with outboard fins and centerline tail. Consistent with the variations with sideslip of the peak suction pressure magnitude and location, the configuration with outboard fins exhibits large variations in rolling moment with sideslip relative to the centerline tail at the higher angle of attack.

Figure 261 compares the dynamic directional stability parameter of the outboard fin and centerline tail configurations. Relative to the configuration with centerline tail, the outboard fins promote positive increments to $C_{n_{\beta_{dyn}}}$ at moderate-to-high angles of attack. This can be attributed principally to the reduced vortex breakdown asymmetry and, hence, improved C_{ℓ_β} characteristics shown previously in Figure 258.

An examination of the surface flow patterns established on the cranked wing and outboard fin combination yields further insight into the flow-field. Figure 262 illustrates the surface flow patterns on the 70/50-degree cranked wing with vortex flaps deflected to 30 degrees, and on the windward and leeward sides of both vertical fins at 16 degrees angle of attack and 5 degrees of sideslip. For reference, the flow patterns on the wing without fin are also shown. The fins provide a fence-like effect, limiting the vortex-induced spanwise flow. In addition, comparison of the secondary separation line locations on the wings with and without fins indicates that the presence of the fins causes an inboard displacement of the leading-edge vortices, particularly on the leeward wing. On the downwind, or suction, side of the leeward fin the flow is separated from the wing-tail junction to the tail mid-span and attached near the tip. On the inboard side of the leeward and windward fins the surface flow patterns reveal the scrubbing action due to the wing vortex interacting with the lower portion of the fin in addition to a tail-generated vortex near the tip. On the outboard, or pressure, side of the windward tail the flow is generally streamwise, indicative of attached flow.

Additional evidence that, relative to the centerline tail, the outboard fins are immersed in an unfavorable flow-field is provided by tail surface static pressure measurements. Figures 263 and 264 show the effect of sideslip angle on the pressure distributions on the outboard fin and centerline tail suction and pressure sides at α= 16 and 24 degrees. The net lifting pressures, C_{p_L}, on the outboard fins indicate the latter are relatively ineffective lift-generating surfaces. In contrast, the centerline tail is exposed to less adverse vortex-induced sidewash and maintains lift effectiveness to high angles of attack.

Tail Deflection Effects

The effects of a +10 degree centerline tail deflection on the longitudinal and lateral-directional stability characteristics of the 70/50-degree cranked wing with vortex flaps deflected to 30 degrees are illustrated in Figure 265 and 266. The tail deflection has no effect on the longitudinal stability but results in greater nose-up pitching moments due to sideslip at moderate-to-high angles of attack. The configuration with the deflected tail displays less lateral stability at low-to-moderate angles of attack although a pronounced unstable break in the C_{ℓ_β} curve is delayed to higher angles of attack. There is no change in directional stability due to tail deflection.

The effects of symmetric deflection of the outboard fins to +10 and -10 degrees on the longitudinal and lateral-directional stability characteristics are depicted in Figures 267 and 268. The tail deflections have no significant effect on the longitudinal stability or on the longitudinal and lateral-directional coupling parameter. Both deflection angles have a destabilizing effect on C_{ℓ_β} up to about 24 degrees angle of attack. Directional stability is also reduced due to fin deflection at low-to-moderate angles of attack, although the configurations with deflected fins exhibit slightly less directional instability at high α's.

Figure 269 presents the control effectiveness of the outboard fins with symmetric deflections of -10 degrees at zero sideslip. The roll control effectiveness, $C_{\ell_{\delta_v}}$, is favorable throughout the angle of attack range. The yaw control effectiveness, $C_{n_{\delta_v}}$, diminishes and becomes unfavorable at high angles of attack.

A comparison of the control effectiveness of the centerline tail and outboard fins deflected 10 degrees is shown in Figure 270. Consistent with the higher levels of lateral stability associated with the outboard fins,

this configuration exhibits greater roll control effectiveness, relative to the centerline tail configuration. And, despite the lower levels of directional stability, the deflected outboard fins are also a more effective yaw control device than is the deflected centerline tail.

CONCLUDING REMARKS

A detailed low-speed wind tunnel investigation was conducted to determine the effects of analytically- and empirically-designed leading-edge vortex flaps on the static longitudinal and lateral-directional aerodynamic, stability, and control characteristics of fighter wings having sweep angles of 45 degrees to 76.5 degrees. A determination was made of the sensitivity of the configuration forces and moments, wing surface pressures, and flowfield to symmetric and differential vortex flap and trailing-edge flap deflection angles; vortex flap planform, apex geometry, and controller tabs; trailing-edge sweep angle; wing position on the fuselage; nose strakes; closely-coupled canards; and centerline and outboard tail deflection angles. The wind tunnel tests were performed in the Northrop 21-by 30-inch facility using an existing generic fighter fuselage model at angles of attack up to 40 degrees, sideslip angles to $\pm$ 10 degrees, and free-stream dynamic pressure of approximately 20 psf (130/ft/sec).

The Vortex Lattice Method-Suction Analogy design procedure yields full-span vortex flaps of approximately constant chord planform on the wings of moderate sweep angle (45 degrees to 55 degrees) and of inverse taper planform on the more highly-swept wings. The curved leading edge in the apex and tip regions is an outcome of the vortex flap design procedure and has little basis in the real flow. The vortex flap size increases with increased wing sweep, and varies from approximately 10-15 percent of the wing area on the moderately-swept planforms to nearly 30 percent on the most slender wings. The design procedure is a useful tool for the preliminary sizing of leading-edge vortex flaps. However, the design criteria of vortex flow along the entire spanwise length of the deflected flap with flow reattachment at the hingeline can only be met for the given set of design conditions by the wings of lower leading-edge sweep. As sweep increases, the vortex flow cannot be maintained on the flap and migrates onto the upper surface beginning at the tip and moving inboard with increasing sweep.

In general, the VLM-designed full-span vortex flap results in a reduction in the lift coefficient at angles of attack below the planar wing stall, increased maximum lift, decreased drag-due-to-lift, nose-down pitching moment increments, reduced pitch instability, and less nose-up pitching moment due-to-sideslip. These effects are typically more pronounced as vortex flap deflection angle is increased. Performance improvements due to a 30-degree vortex flap deflection normal to the hingeline are greatest on the wings of moderate sweep angle. On the more highly-swept wings, the large vortex flap size promotes a greater reduction in potential flow lift which limits the maneuver performance enhancement. A vortex flap on a wing of given sweep angle exhibits only limited ability to maintain a concentrated vortical flow along the entire length of the deflected surface. At typical transonic sustained maneuver lift coefficients, the migration of the vortex off the flap is delayed by increased flap deflection angle. However, the favorable suction effect on the forward-facing surface is offset to an extent by flow separation from the deflected flap hingeline. Experimental observations indicate that the leading-edge flaps deflected to angles up to 60 degrees (measured normal to the hingeline) are dominated by vortex separation at moderate-to-high lift coefficients. The presence of a concentrated vortical flow on the deflected flap is easily discernible in upper surface flow patterns and static pressure distributions. However, the vortex structure in the cross-plane is not well-defined by an existing laser lightsheet technique except at high angles of attack where the vortex is large and of increased strength.

Vortex flap deflection typically reduces lateral stability at low angles of attack due to flow separation on the flap underside. At moderate and high angles of attack, the deflected flap reduces tip separation, delays the onset of vortex breakdown asymmetry, and reduces the burst asymmetry once it occurs. These effects serve to increase the dihedral effect at those angles of attack. Exceptions to this trend are the 70-degree cropped delta and 76.5/66.5-degree cranked wings which experience adverse effects on roll stability at all angles of attack. This anomaly in the lateral stability behavior is an apparent result of the suppression of the

leading-edge vortices at low-to-moderate angles of attack and a significant decrease in vortex strength at high attitudes due to deflection of the large control surfaces. The lateral stability characteristics of a wing of given sweep angle, within the range of wing planforms examined in the present study, are generally unsteady when the vortex flaps are deflected to large angles. This effect is due to the development of a strong, but unsteady, vortex from the flap hingeline.

The effect of vortex flap deflection on the directional stability is not large. The yaw instability exhibited by the planar wing at high angles of attack is adversely affected by vortex flap deflection. In general, the deflected vortex flaps promote positive increments to the dynamic directional stability parameter, $C_{n_{\beta_{dyn}}}$, due to the increased dihedral effect.

The effects on the longitudinal characteristics of VLM-designed partial-span vortex flaps that extend from 25 percent of the exposed wing span to the wing tip are similar, but less pronounced. In comparison to results obtained with the full-span flaps, the partial-span geometries yield consistently lower maximum lift, higher induced drag, and more nose-up pitching moments in conjunction with the 65- and 70-degree cropped delta wings. The test data show that the part-span flap results in a two-vortex system of reduced stability at high angles of attack.

Comparisons of the lateral-directional stability characteristics of the cropped delta and cranked wings with full- and part-span flaps reveal a configuration dependence. The 65-degree cropped delta wing with full-span flap exhibits significantly higher lateral stability. In contrast, the 70-degree cropped delta and 70/50-degree cranked wings develop higher roll stability in combination with the deflected partial-span flaps.

The aerodynamic and stability characteristics are very sensitive to small changes in the flap apex geometry. Streamwise cuts to the apex regions of the part-span flaps on the 65-degree cropped delta and 70/50-degree cranked wings promote earlier bursting of the vortex system with resultant lift loss, drag increase, and increased pitch instability. The effects on lateral stability are configuration-dependent. The cropped delta wing develops significantly higher levels of lateral stability while the cranked wing exhibits consistently lower but stable dihedral effect throughout the angle of attack range tested.

Inverted leading-edge flap deflection results in large increases in lift, higher drag, nose-up pitching moment increments, and more nose-up pitching moment due-to-sideslip at typical approach angles of attack. The increased vortex breakdown asymmetry due to upward deflection of the vortex flap results in large, unstable increments to roll stability.

Roll control due to differential deflection of an inverted leading-edge flap is limited to low angles of attack due to vortex breakdown effects.

Leading-edge controller tabs are an effective means of manipulating the vortex strength at a given angle of attack. Relative to the plain vortex flaps, the tabbed flaps result in higher lift and less drag at high lift. The increased vortex size arising from the tab deflection, however, causes an earlier migration of the vortical flow off the deflected flap. A comparison of the lateral-directional stability characteristics of the wings with plain and tabbed vortex flaps indicate that the former exhibit more lateral stability at the low angle of attack range. At high attitudes, however, the configurations with tabbed flaps maintain lateral stability while those with plain flaps become unstable.

Empirically-designed vortex flaps of tapered planform yield increased lift, lower drag at moderate-to-high lift, and less pitch instability in comparison to the analytically-designed flaps of inverse taper planform. The inverse-tapered flap generally results in slightly higher levels of lateral stability due to its larger tip chord. The experimental results indicate that the flow situation corresponding to vortex separation everywhere along the leading edge with primary reattachment at the hingeline is not necessarily "optimal."

Downward deflection of a part-span trailing-edge flap increases the vortex flap effectiveness due to increased upwash and the resulting higher suction pressures on the forward-facing surface. However, trailing-edge flap longitudinal control effectiveness decreases with increasing trailing-edge flap deflection angle due to flow separation on the trailing-edge flap. In general, trailing-edge flap deflection increases the lateral stability at low angles of attack, decreases the dihedral effect at higher angles, and promotes stable increments to the directional stability. In addition, vortex flap deflection enhances the trailing-edge flap pitch control effectiveness at high angles of attack.

The aerodynamic and stability characteristics of a vortex-flapped wing are sensitive to trailing-edge sweep angle. The results of the 65-degree cropped delta wing with vortex flap deflected to 30 degrees indicate that the cropped arrow wing (Λ_{TE} = +15°) develops higher lift, lower drag, and reduced pitch instability compared to the cropped delta (Λ_{TE} = 0°) and cropped diamond (Λ_{TE} = -15°, -30°) planforms. These results are due to the higher aspect ratio and larger ratio of vortex flap-to-wing area of the former wing. The cropped arrow planform exhibits better lateral stability characteristics at low and moderate angles of attack while the cropped diamond planforms maintain higher levels of lateral stability at higher attitudes.

The results of testing the 65-degree cropped delta wing at three vertical positions show that the high- and low-wing positions result in increased lift, reduced drag at mid-to-high lift, and slight nose-up pitching moment increments with no change in longitudinal stability, relative to the baseline mid-wing position. Consistent with the classical fuselage crossflow effect on lateral stability, the low- and high-wing configurations exhibit lower and higher levels of lateral stability, respectively, than the mid-wing position. At moderate-to-high angles of attack, the high-wing configuration exhibits less directional stability while the low-wing configuration exhibits increased instability. Wing upper surface flow visualization revealed no discernible changes in the flow patterns due to wing height variations. In addition, upper surface static pressure distributions demonstrate that he magnitude and location fo the peak vortex-induced suction pressures are relatively insensitive to wing vertical location on the fuselage.

Strakes mounted at the nose maximum half-breadth have minimal effect on the total lift and drag characteristics of the 65-degree cropped delta and 70/50-degree cranked wings but induce nose-up pitching moment increments, increased pitch instability, and nose-up pitching moments due to sideslip. The strakes result in increased lateral stability at moderate and high angles of attack, delay the onset of directional instability, and greatly reduce the directional instability at high angles of attack. The increased dihedral effect is due primarily to a favorable forebody-wing flow-field interaction. The improvements in directional stability are attributed to a direct strake vortex-induced suction effect on the forebody. The strakes also result in large, positive increments to $C_{n_{\beta_{dyn}}}$. Nose strake effects on vortex flap effectiveness are limited to pitching moment and directional stability characteristics: the strakes result in more nose-down pitching moment increments and reduced $C_{m_{|\beta|}}$ with flap deflection, and increase directional stability.

Closely-coupled canards, at zero incidence angle, in conjunction with the 65-degree cropped delta wing result in a more pronounced vortex-induced nonlinearity of the lift curve at high angles of attack, lower drag at high lift, increased pitch instability, and more nose-up pitching moment due to sideslip. The lateral instability is improved at moderate-to-high angles of attack due to a favorable canard-wing flow-field interation. The canards also result in large positive increments to the dynamic directional stability parameter. Test data indicate that the canards improve the effectiveness of the leading-edge vortex flaps, although canard deflection required for longitudinal trim would have a significant effect on the data presented.

A comparison of the effects of vortex flap deflection on the 70/50-degree cranked wing with centerline tail and outboard vertical fins indicates that the latter configuration enhances vortex flap effectiveness, yielding reduced lift loss and more significant drag polar impovements. However, the outboard fins on the 70/50-degree cranked wing with vortex flaps deflected to 30 degrees promote earlier vortex breakdown with resultant lift loss at moderate-to-high angles of attack, increased drag, and pitch in stability, relative to the configuration with the centerline tail. The fins increase the lateral stability at moderate and high altitudes due to reduced vortex breakdown asymmetry. In comparison to the configuration with centerline vertical tail, the fins reduce the directional stability but promote positive increments to $C_{n_{\beta_{dyn}}}$ due to the increased dihedral effect. In addition, the deflected fins display greater roll and yaw control effectiveness than the deflected centerline tail.

RECOMMENDATIONS

Although the relative merits of various flap planforms have been identified, the "optimum" shape for particular wing planforms has yet to be determined. Wind tunnel testing at both subsonic and transonic speeds is recommended to identify the optimal leading-edge flap planform and size suitable for advanced tactical aircraft configurations. Further investigation is also recommended to design vortex flaps specifically for wings of cropped delta and cropped diamond planforms with leading-edge sweep angles of 40 to 60 degrees, since the results indicate that vortex flaps are most effective on such configurations. In conjunction with these wings, an evaluation of the effects of trailing-edge flap size and span is recommended.

A low-speed wind tunnel investigation is recommended of segmented leading-edge flaps to enhance the high angle of attack lateral stability of fighter wings without compromising the sustained turn capability.

Flap optimization on a moderately-swept wing with leading-edge extension (LEX) warrants study. In addition, an evaluation of a deflectable LEX to alleviate pitch instability at high angles of attack should be made.

The influence of close-coupled canards on the leading-edge flap design merits further testing and evaluation. A more thorough investigation of the optimum canard planform and position relative to the wing should be conducted, and the investigation should account for the canard deflection required for pitch trim.

It is recommended that further testing be performed addressing outboard fin effects. Various spanwise and chordwise locations as well as asymmetric deflection angles (i.e. "toe-in" and "toe-out" configurations) should be examined to investigate the sensitivity of the vortex flow-field about a cranked wing with deflected leading-edge flaps to outboard fin position and orientation. A more complete measure of surface static pressure distributions should be made to gain a better understanding of the complex flow-field. Various wing planforms should be tested in conjunction with the fins to assess wing-fin interactions.

REFERENCES

1. Tinoco, E. N. and Yoshihara, H., "Subcritical Drag Minimization for Highly-Swept Wings with Leading-Edge Vortices," AGARD-CP-247, October, 1978.

2. Rao, D. M., "Leading-Edge 'Vortex Flaps' for Enhanced Subsonic Aerodynamics of Slender Wings," ICAS Paper No. 80-13.5, 1980.

3. Johnson, T. D., Jr. and Rao, D. M., "Experimental Study of Delta Wing Leading-Edge Devices for Drag Reduction at High Lift," NASA CR 165846, February, 1982.

4. Schoonover, W. E., Jr. and Ohlson, W. E., "Wind-Tunnel Investigation of Vortex Flaps on a Highly-Swept Interceptor Configuration," ICAS Paper No. 82-6.7.3, August 1982.

5. Hom, H. W., Hahne, D. E., and Morris, O. A., "Low-Speed Investigation of the Maneuver Capability of Supersonic Fighter Wings," AIAA Paper No. 83-0416, January, 1983.

6. Frink, N. T., "Analytical Study of Vortex Flaps on Highly-Swept Delta Wings," ICAS Paper No. 82-6.7.2, August, 1982.

7. Luckring, J. M., Schoonover, W. E., Jr., and Frink, N. T., "Recent Advances in Applying Free Vortex Sheet Theory for the Estimation of Vortex Flow Aerodynamics," AIAA Paper No. 82-0095, January 1982.

8. Marchman, J. F., Plentovich, E. B. and Manor, D., "Performance Improvement of Delta Wings at Subsonic Speeds Due to Vortex Flaps," AIAA Paper No. 80-1802, March, 1980.

9. Lamar, J. E., and Herbert, H. E., "Production Version of the Extended NASA-Langley Vortex Lattice FORTRAN Computer Program." Volume I - User's Guide, NASA TM-83303, April, 1982.

10. Frink, N. T., "Concept for Designing Vortex Flap Geometries," NASA TP-2233, December, 1983.

11. Moul, M. T., and Paulson, J. W., "Dynamic Lateral Behavior of High-Performance Aircraft," NACA RM L58E16, 1958.

12. Skow, A. M., Titiriga, A., Jr., and Moore, W. A., "Forebody/Wing Vortex Interactions and Their Influence on Departure and Spin Resistance," AGARD-CP-247, October, 1978.

13. Gloss, Blair B., "Effect of Wing Planform and Canard Location and Geometry on the Longitudinal Aerodynamic Characteristics of a Close-Coupled Canard Model at Subsonic Speeds," NASA TN-7910, 1975.

14. Er-El, J. and Seginer, A., "The Leading-Edge Vortex Trajectory of Close-Coupled Canard Configurations and Their Breakdown Characteristics," AIAA Paper No. 83-1817, 1983.

15. Erickson, G. E., "Water Tunnel Flow Visualization and Wind Tunnel Data Analysis of the F/A-18" NASA CR-165859, May, 1982.

TABLE 1. WING GEOMETRY DETAILS

Λ_{LE}, deg	S_{ref}, in^2	$\bar{c}$, in	b/2, in	FLAP PLANFORM	DESIGNATION	AR	λ
45	43.86	4.82	5.1	Vortex, full-span	W_o	2.37	.277
50	47.8	5.34	5.08	Vortex, full-span	W_1	2.16	.206
55	48.8	5.90	4.67	Vortex, full-span	W_2	1.79	.203
60	51.1	6.24	4.98	Vortex, full-span	W_3	1.66	.081
65	59.1	7.49	4.60	Vortex, full-span	W_4	1.43	.169
65	56.7	7.08	4.60	Vortex, part-span	W_5	1.49	.181
70	53.9	7.99	3.96	Vortex, full-span	W_6	1.16	.201
70	52.4	7.50	3.96	Vortex, part-span	W_7	1.20	.205
70/50	51.0	7.39	4.59	Vortex, full-span	W_8	1.65	.101
70/50	57.8	7.73	4.59	Vortex, part-span	W_9	1.69	.147
76.5/66.5	55.8	8.97	3.94	Vortex, full-span	W_{10}	1.11	.028
50	47.8	5.34	5.08	Conventional	W_{12}	2.16	.206
55	48.8	5.90	4.67	Conventional	W_{13}	1.79	.203
60	51.1	6.24	4.98	Conventional	W_{14}	1.66	.081
65	59.1	7.49	4.60	Conventional	W_{15}	1.43	.169
70	53.9	7.99	3.96	Conventional	W_{16}	1.16	.201
70/50	51.0	7.39	4.59	Conventional	W_{17}	1.65	.101
65[1]	53.40	6.69	4.60	Vortex, full-span	W_{18}	1.58	.191
65[2]	64.46	8.26	4.60	Vortex, full-span	W_{19}	1.31	.153
65[3]	70.65	9.15	4.60	Vortex, full-span	W_{20}	1.19	.138
60	51.1	6.24	4.98	Tabbed vortex	W_{21}	1.66	.081
65	59.1	7.49	4.60	Tabbed vortex	W_{22}	1.43	.169
70/50	51.0	7.39	4.59	Tabbed vortex	W_{24}	1.65	.101
65[4]	59.1	7.99	4.60	Tabbed vortex	W_{25}	1.43	.169
65[4]	59.1	7.99	4.60	Tabbed vortex	W_{26}	1.43	.169
70/50[4]	51.0	7.39	4.59	Vortex, full-span	W_{27}	1.65	.101
70/50[4]	51.0	7.39	4.59	Tabbed vortex	W_{28}	1.65	.101

1. +15° trailing-edge sweep
2. -15° trailing-edge sweep
3. -30° trailing-edge sweep
4. Pressure-instrumented wings

Note: Wing reference area includes flap area.

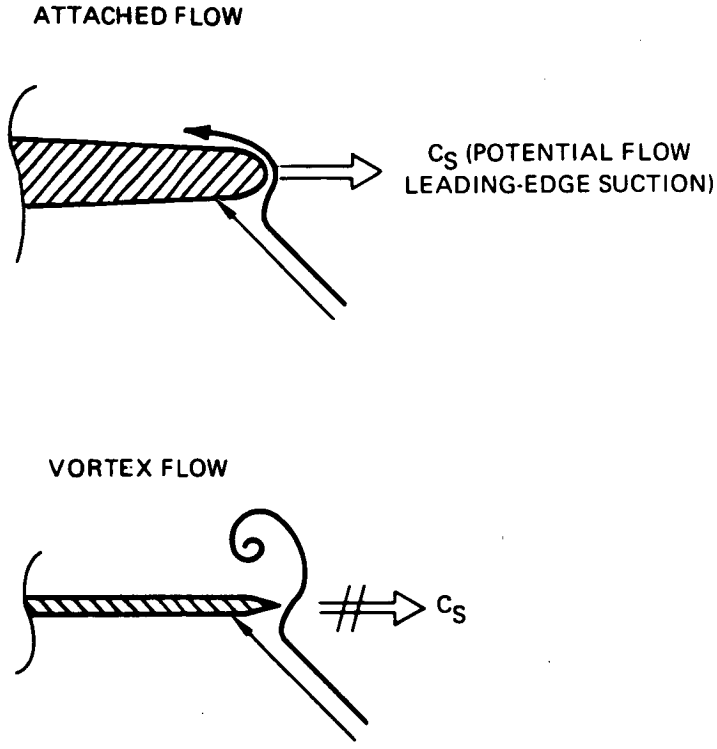

Figure 1. Loss of Leading-Edge Suction Due to Flow Separation at the Sharp Edge.

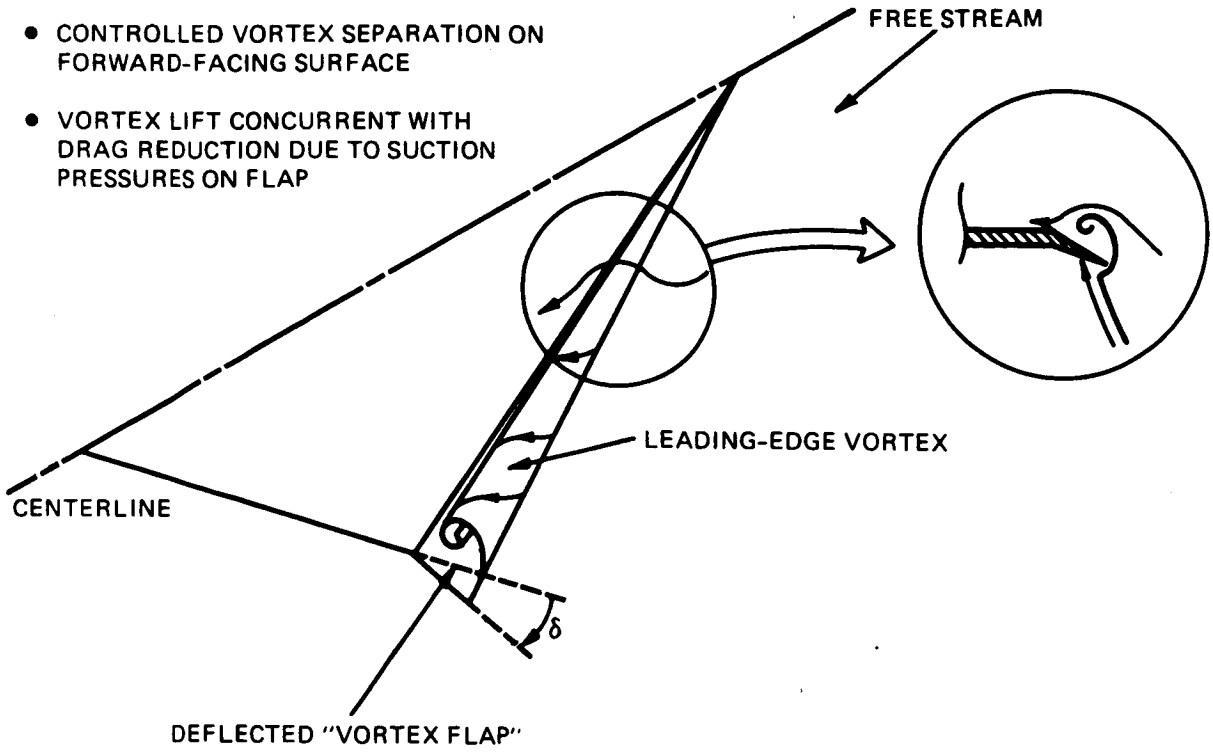

Figure 2. Leading-Edge Vortex Flap Concept.

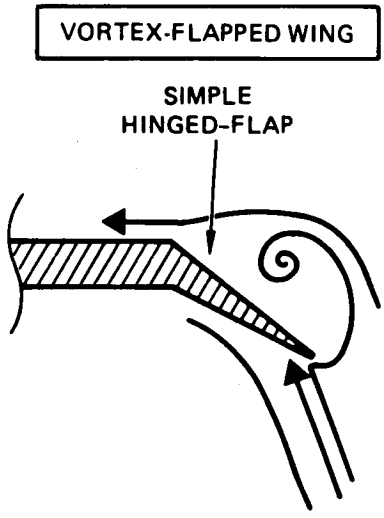

Figure 3. "Ideal" Vortex Flow Situation.

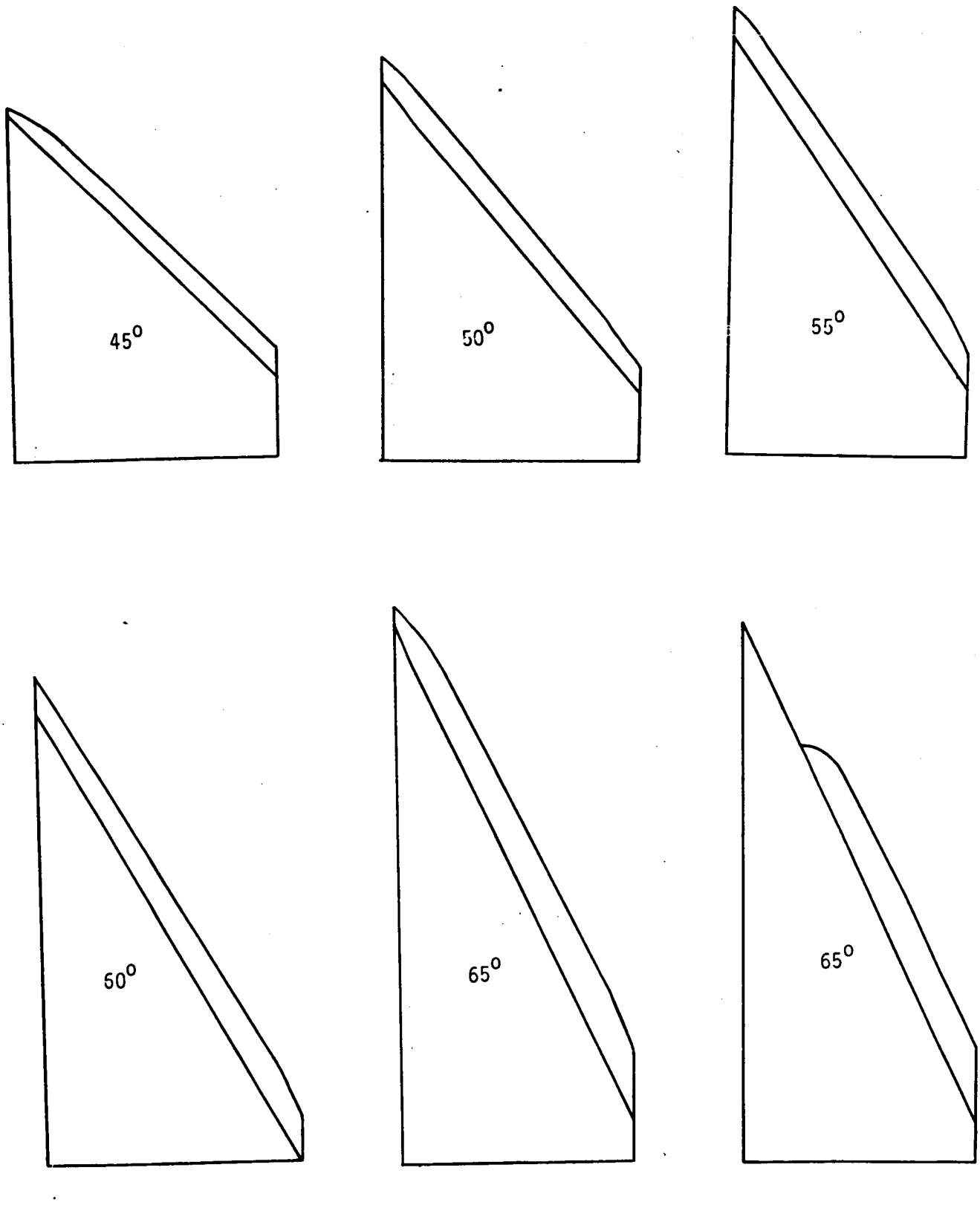

Figure 4. VLM-Designed Vortex Flap-Wing Geometries (Exposed Wings Shown).

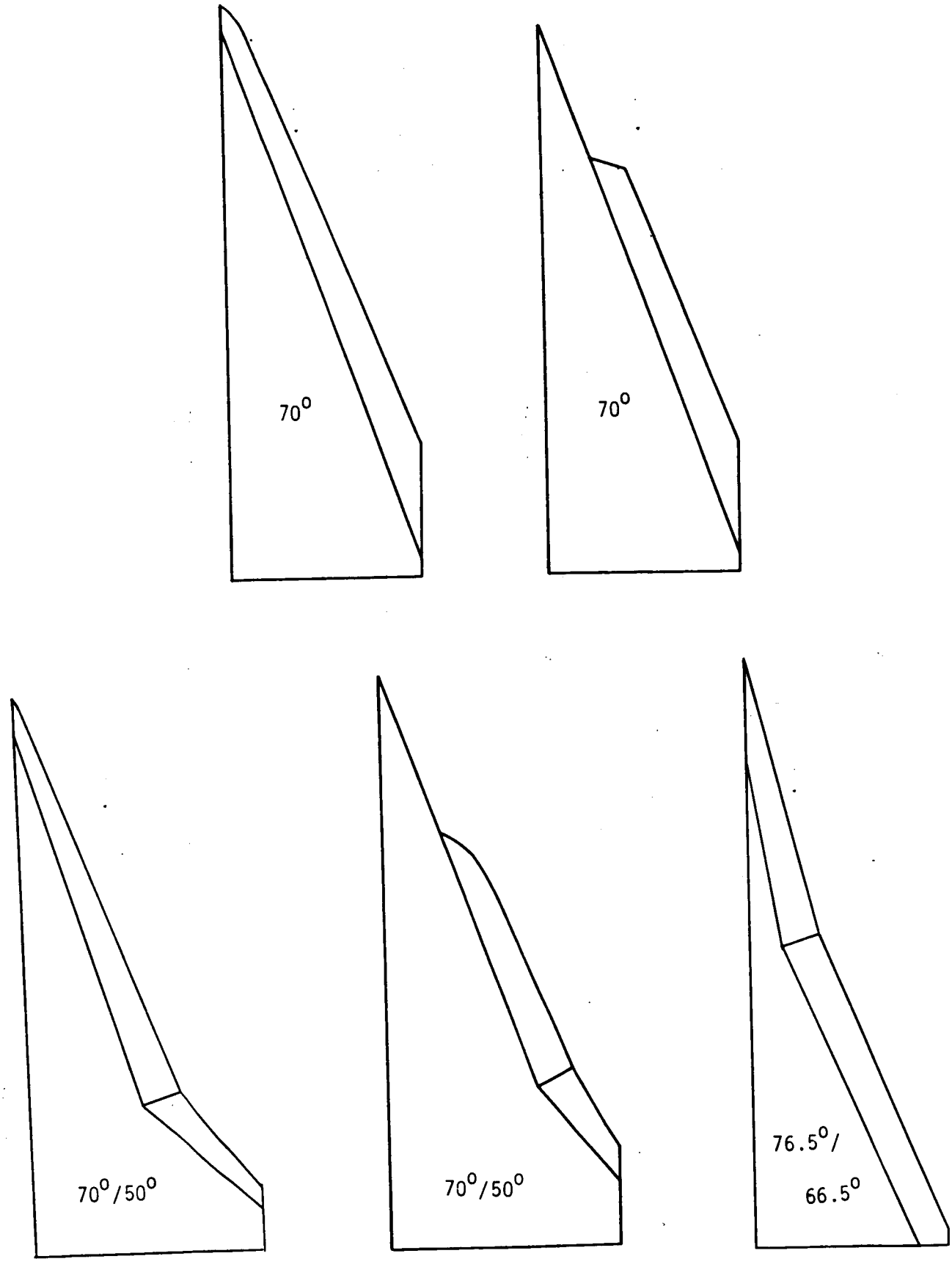

Figure 4. Continued.

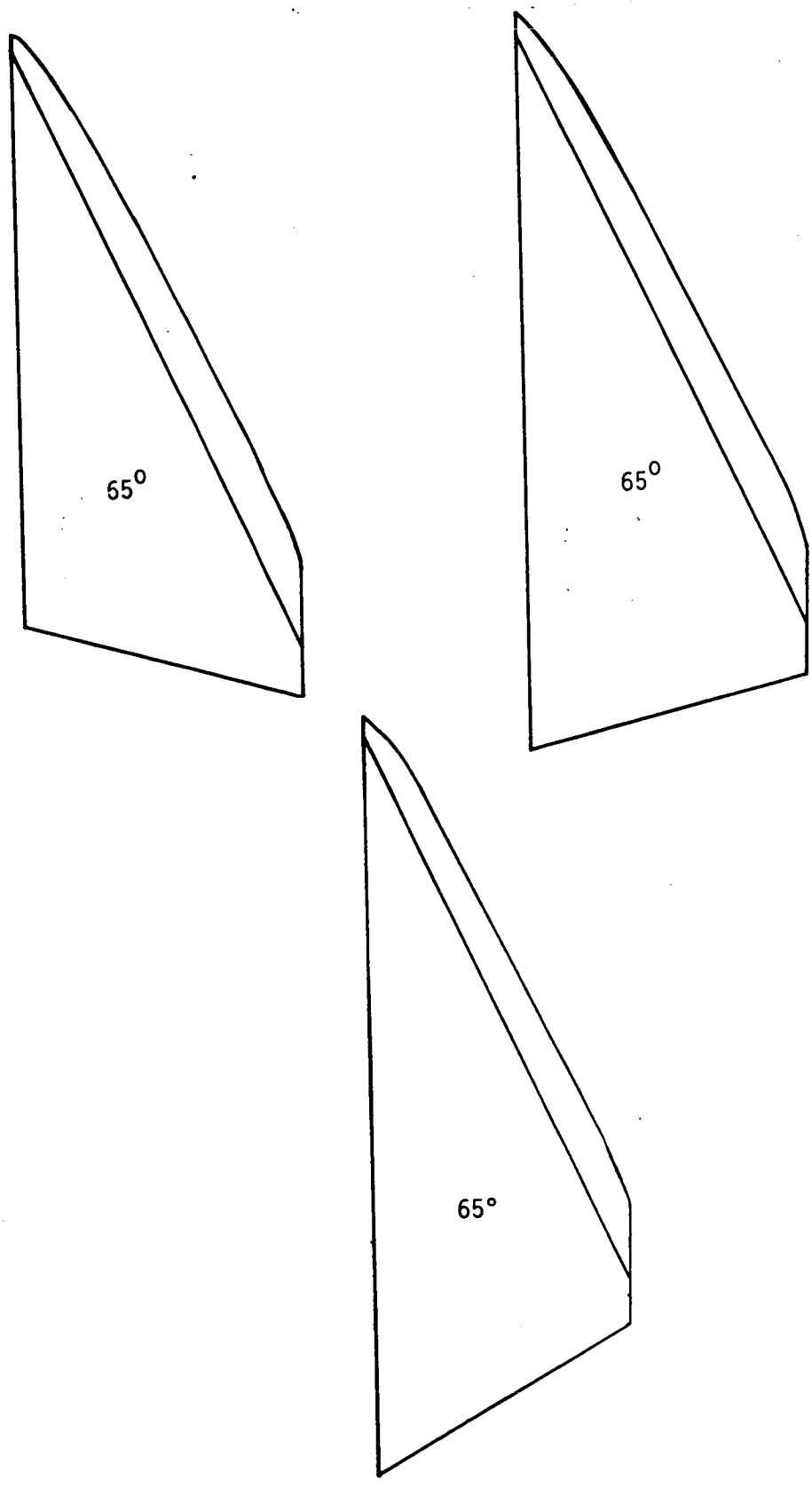

Figure 4. Concluded.

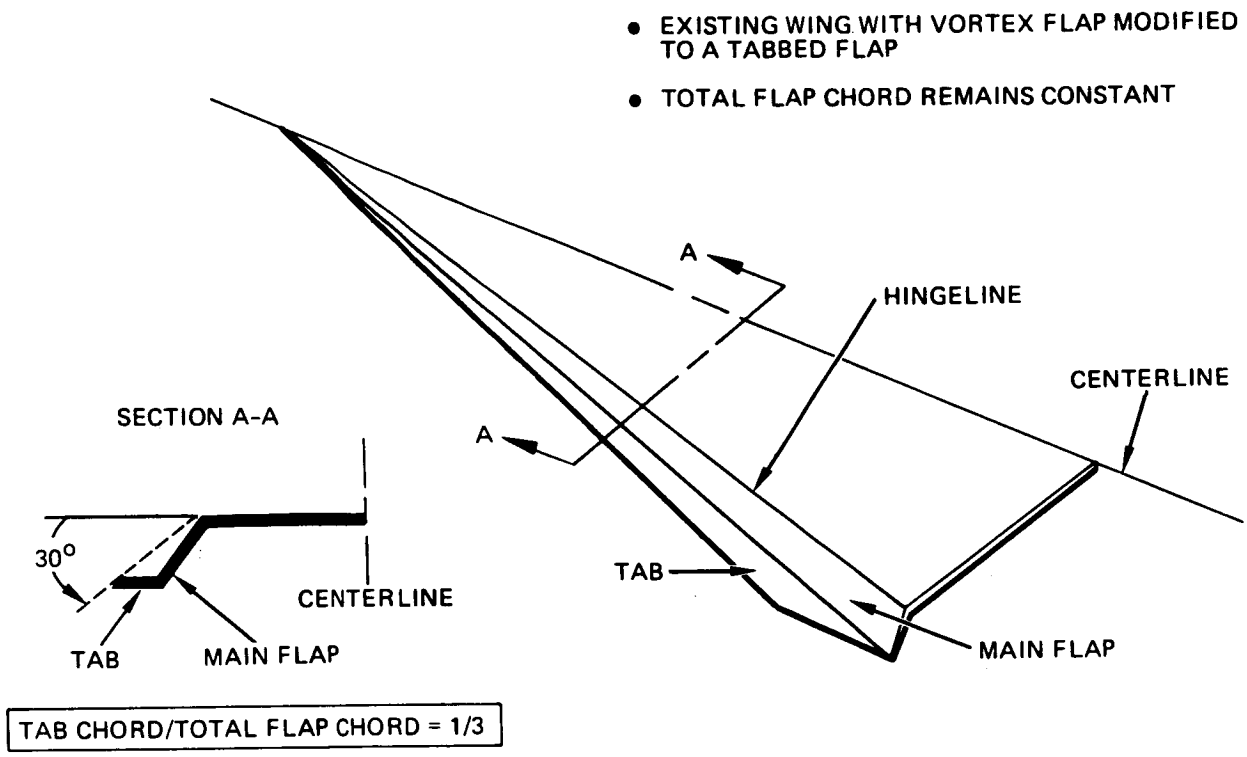

a) Definition of Tabbed Flap

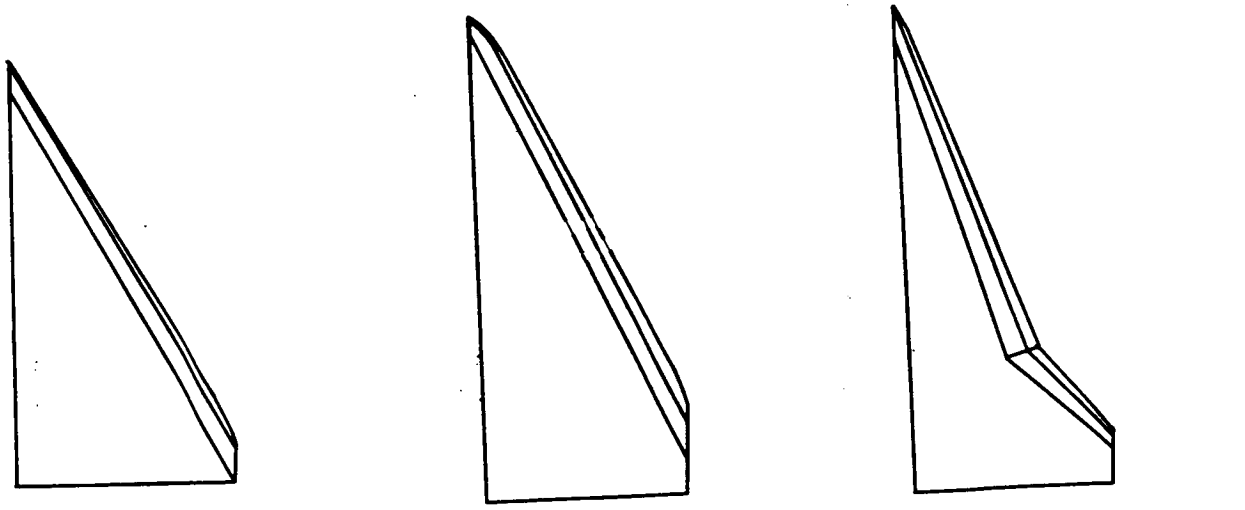

60-Degree Cropped Delta Wing

65-Degree Cropped Delta Wing

70/50-Degree Cranked Wing

b) Tabbed Flaps

Figure 5. Empirically-Designed "Tabbed" Vortex Flap-Wing Geometries (Exposed Wing Shown)

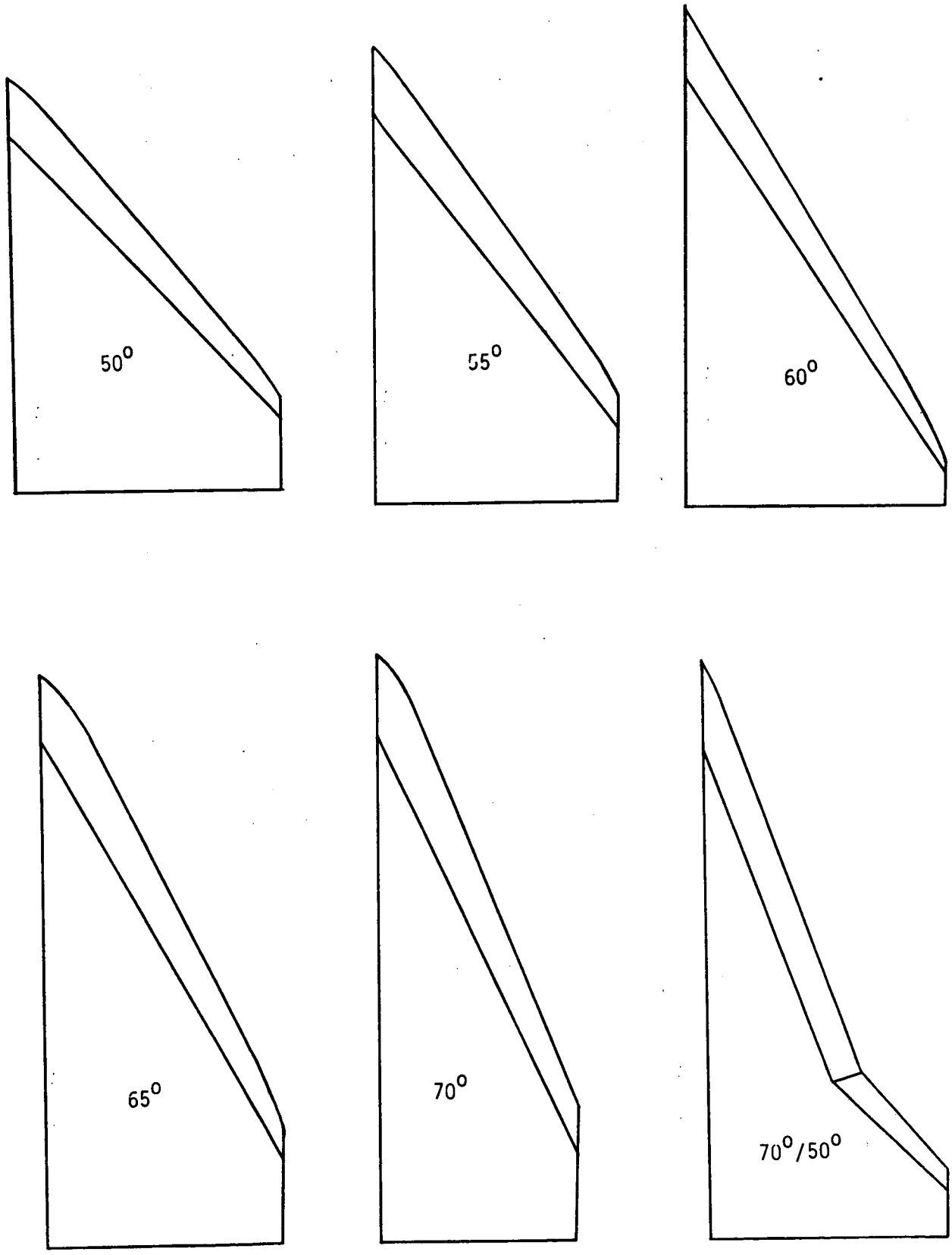

Figure 6. Empirically-Designed Vortex Flaps of Conventional Taper (Exposed Wing Shown)

SERIES A - Screening of 18 designed vortex flap/wing geometries and 6 empirically-developed conventional-flapped wings

- cropped delta and cranked wings with sweep angles from 45^{o} to 76.5^{o}
- trailing-edge sweep variations
- two vortex flap deflection angles (0^{o}, 30^{o})
- "tabbed" vortex flaps
- sideslip "sweeps" on all configurations (-10^{o}, -5^{o}, 0^{o}, $+5^{o}$, $+10^{o}$)
- surface and off-body flow visualization

SERIES B - More detailed testing of 4 selected vortex flap/wing geometries and 1 tabbed flap

- five vortex flap deflection angels (0^{o}, 30^{o}, 45^{o}, 60^{o}, -30^{o})
- three trailing-edge flap deflection angles (0^{o}, 15^{o}, 30^{o})
- differential trailing-edge and inverted leading-edge flap deflections for roll control
- pressure-instrument 2 "plain" and 2 "tabbed" vortex flap/wing geometries
- sideslip "sweeps" on selected configurations (-10^{o} - + 10^{o})
- surface and off-body flow visualization

SERIES C - Testing of 2 vortex flap/wing geometries for fuselage upwash and nose strake effects

- two vortex flap deflection angles (0^{o}, 30^{o})
- two trailing-edge flap deflection angles (0^{o}, 30^{o})
- nose strakes at max. half-breadth
- three wing positions (z/d=-0.2, 0, +0.2)
- sideslip sweeps on all configurations
- surface and off-body flow visualization

SERIES D - Vortex Flap Apex Modifications

- streamwise cuts of 2 part-span vortex flaps
- differential deflection of segmented vortex flap
- removal of inboard 25% of exposed full-span flap
- surface flow visualization

SERIES E - Testing of single vortex flap/cranked wing geometry for vertical tail effects

- two vortex flap deflection angles (0^{o}, 30^{o})
- two trailing-edge flap deflection angle (0^{o}, 30^{o})
- two vertical tail configurations (single centerline and twin outboard tails)
- three tail deflections (0^{o}, $\pm 10^{o}$)
- sideslip sweeps on selected configurations
- pressure-instrument tail and wings
- surface and off-body flow visualization

Figure 7. Five-Series Test Outline

C-2

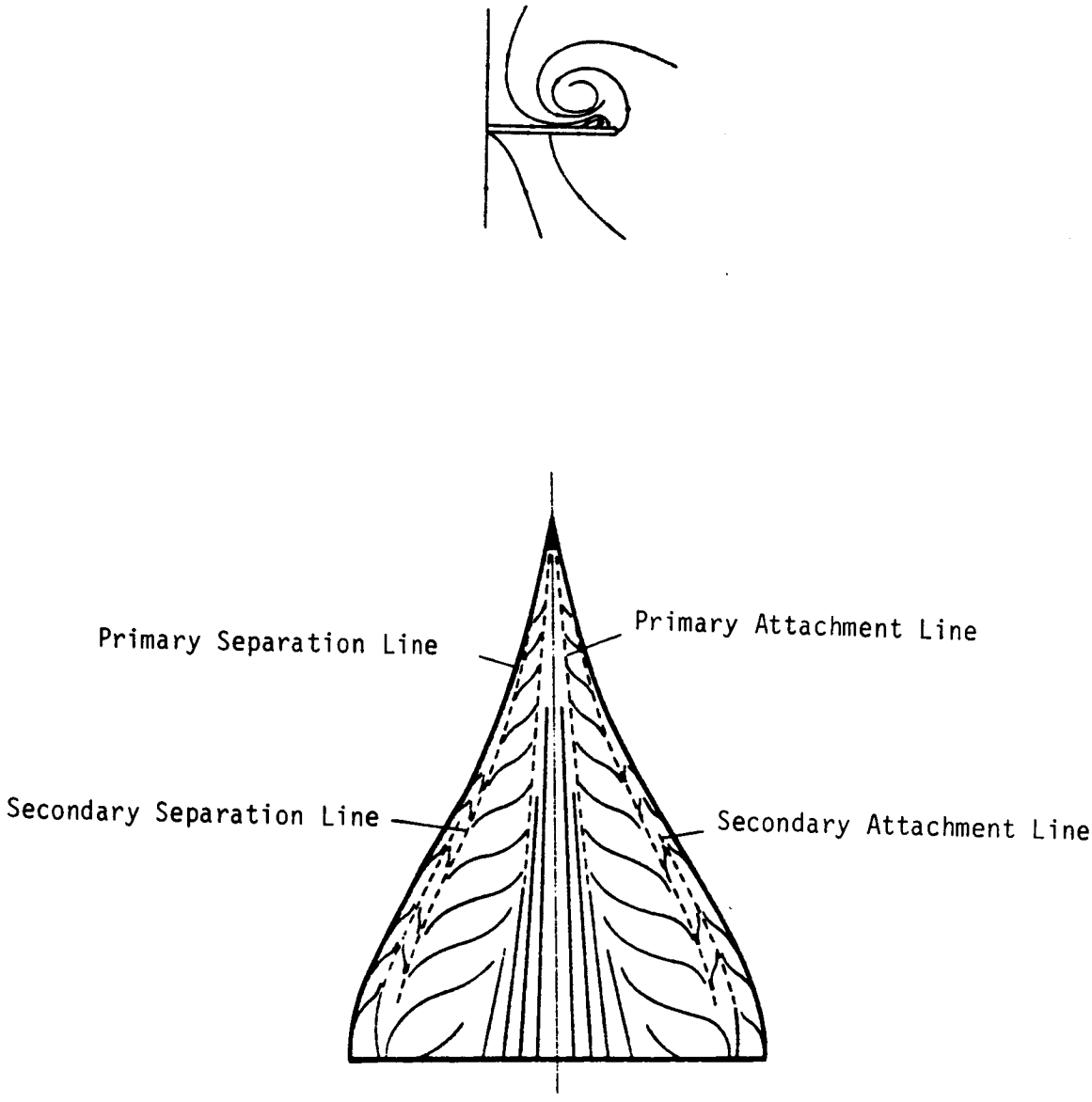

Figure 8. Example of Surface Flow Pattern

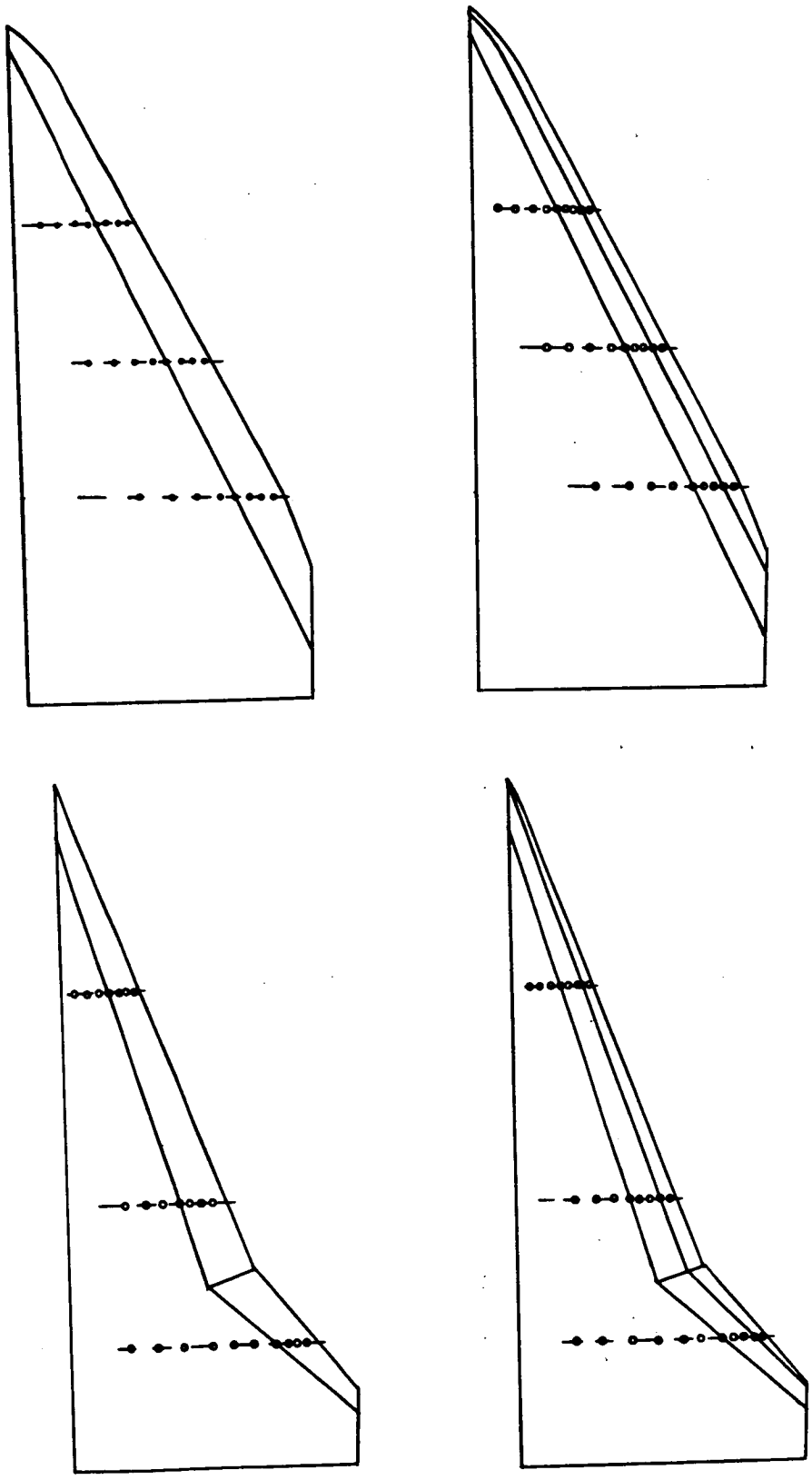

Figure 9. Pressure-Instrumented Wings
(Exposed Wing Shown)

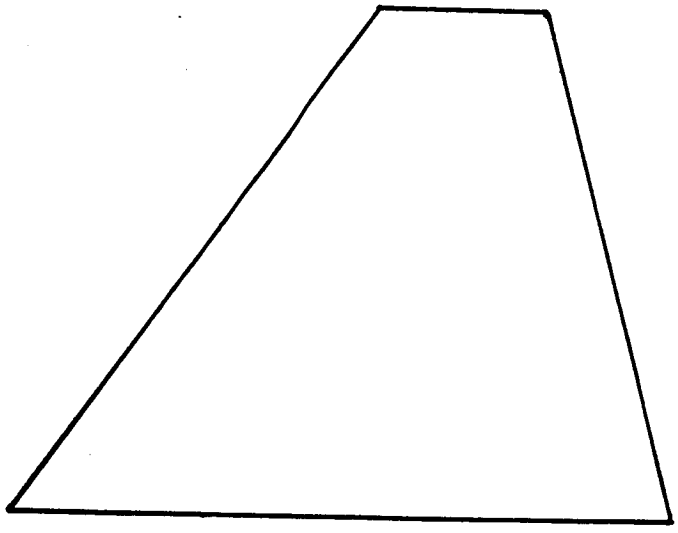

a) Centerline Vertical Tail (Exposed Tail Shown)

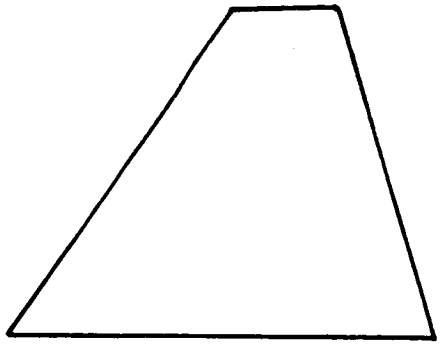

b) Outboard Vertical Tail (Exposed Tail Shown)

Figure 10. Vertical Tails

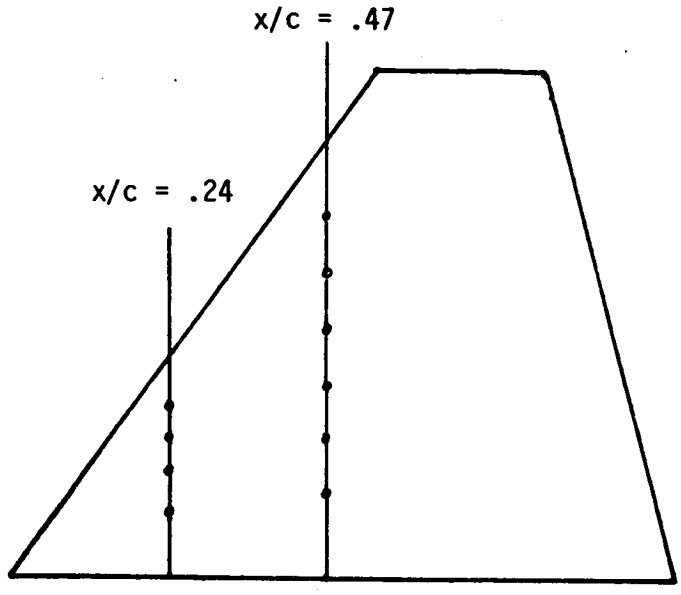

a) Centerline Vertical Tail (Exposed Tail Shown)

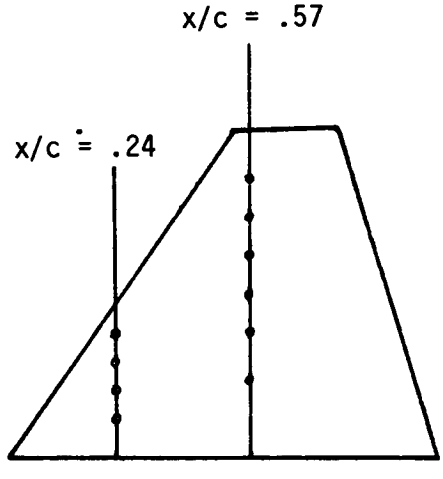

b) Outboard Vertical Tail (Exposed Tail Shown)

Figure 11. Pressure-Instrumented Tails.

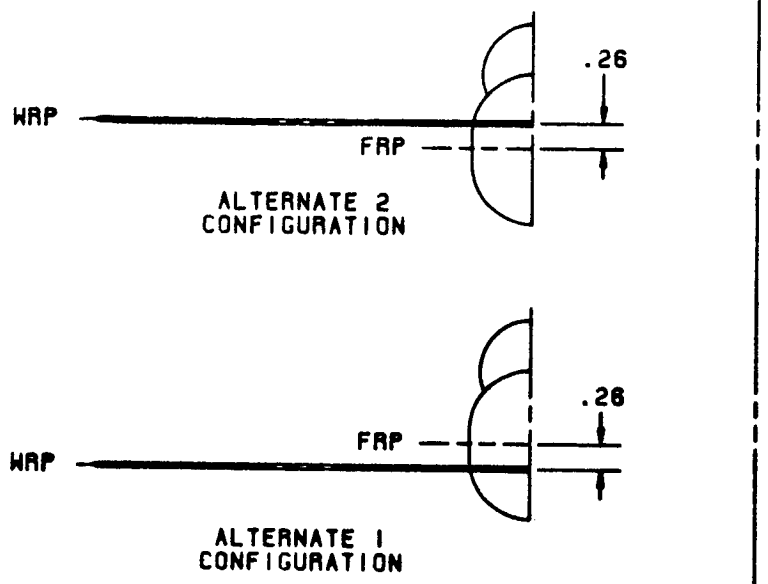

ALTERNATE WING LOCATIONS

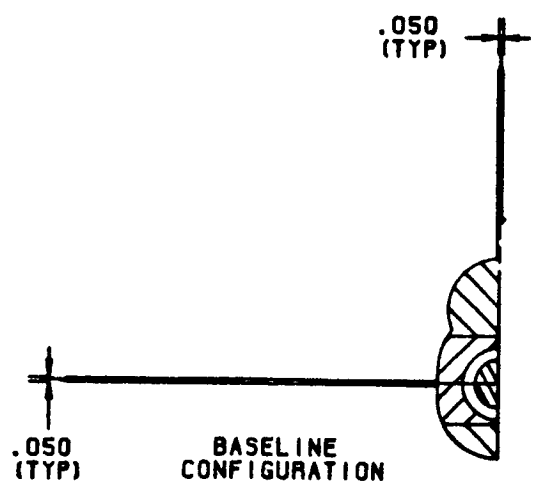

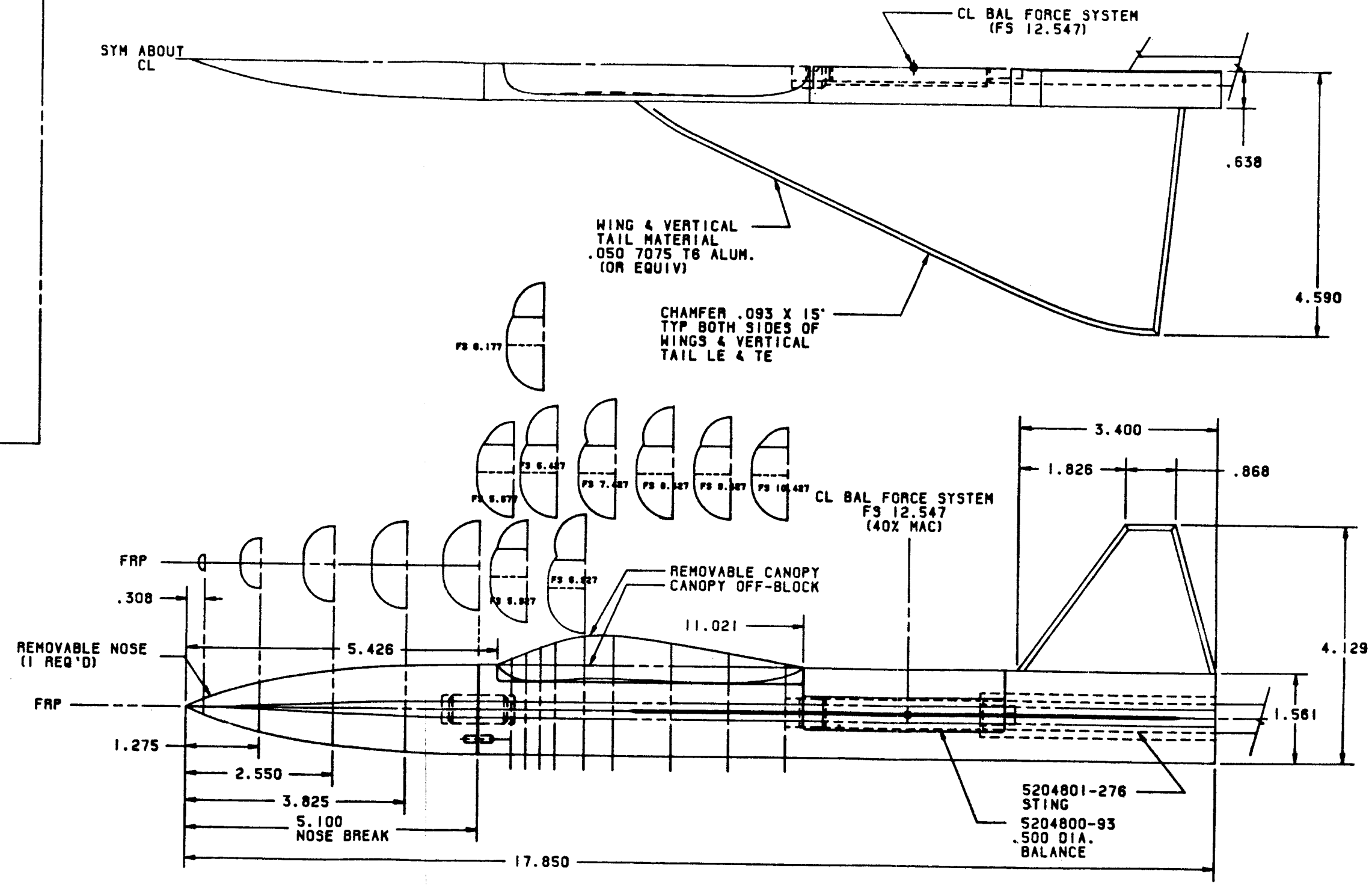

Figure 12. Generic Fighter Model

FOLDOUT FRAME

FOLDOUT FRAME

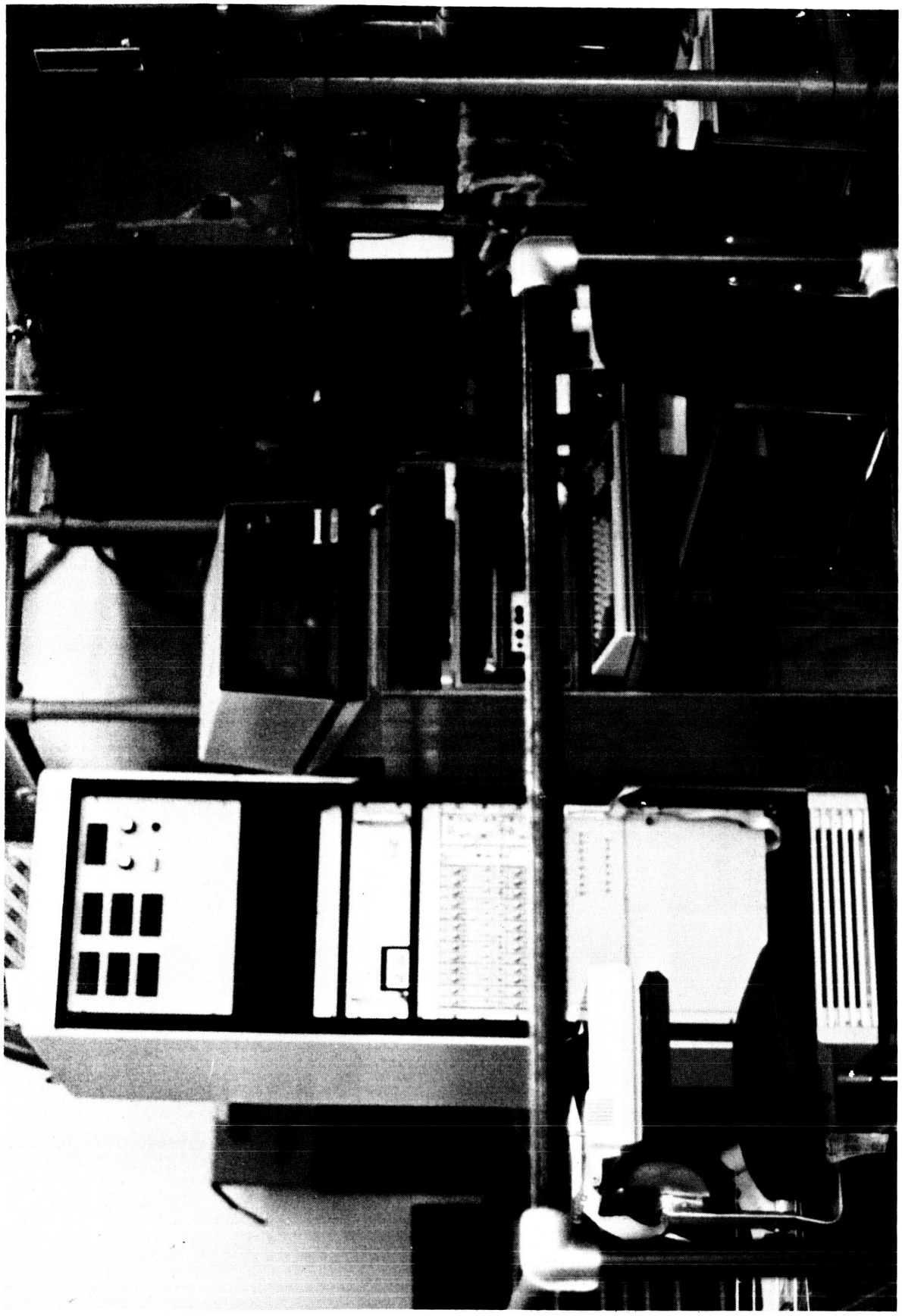

Figure 13. Photograph of Diagnostic Wind Tunnel Facility.

THIS PAGE INTENTIONALLY LEFT BLANK

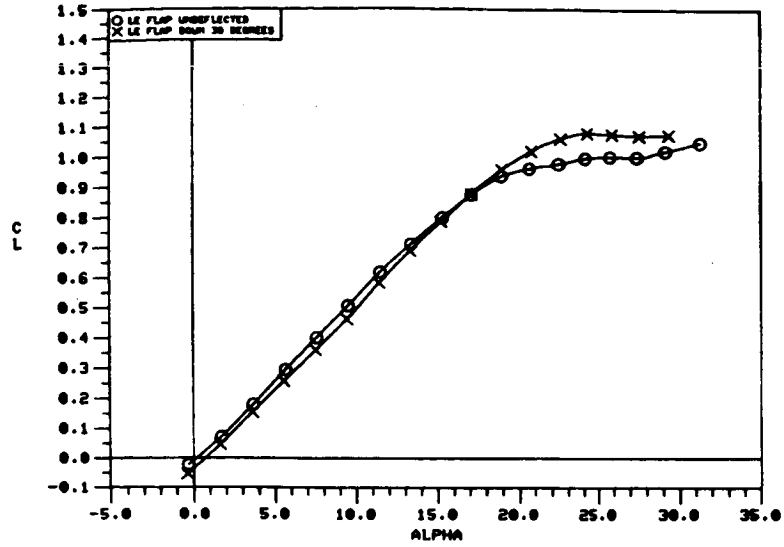

O LE FLAP UNDEFLECTED
X LE FLAP DOWN 30 DEGREES

a) C_L vs. α

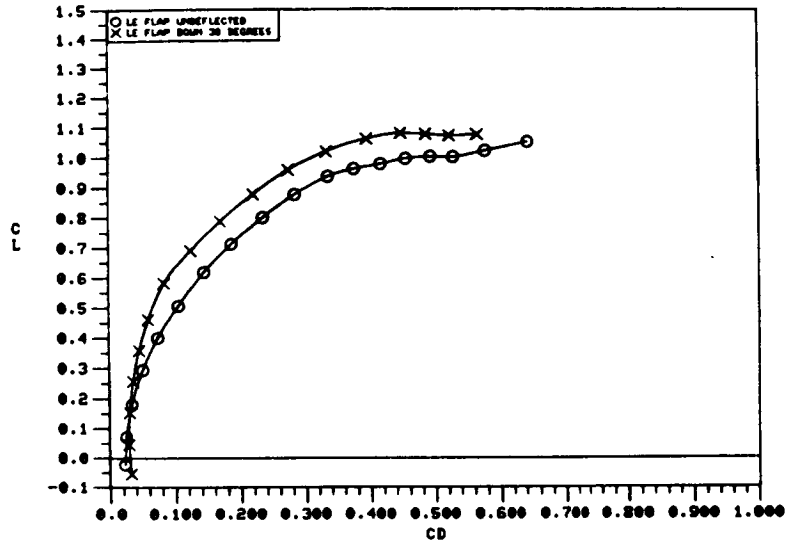

b) C_L vs. C_D

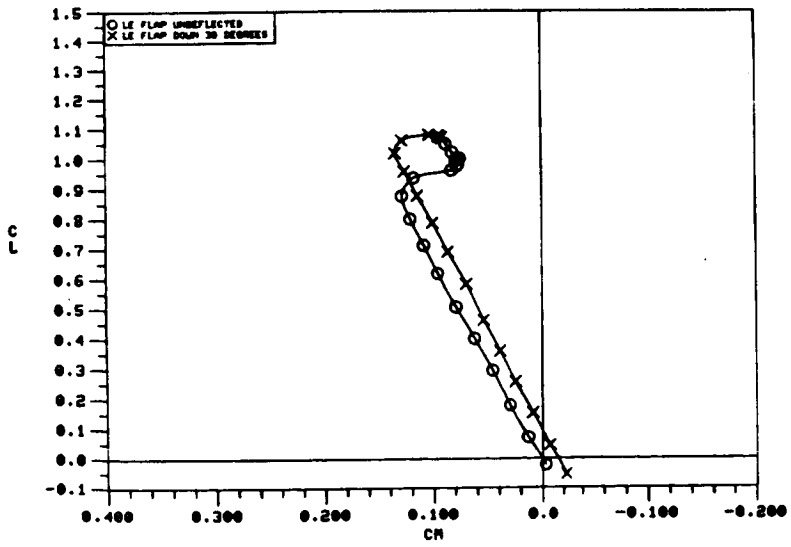

c) C_L vs. C_m

Figure 14. Effect of Deflected Vortex Flap on the Static Longitudinal Aerodynamic Characteristics of the 45-Degree Cropped Delta Wing.

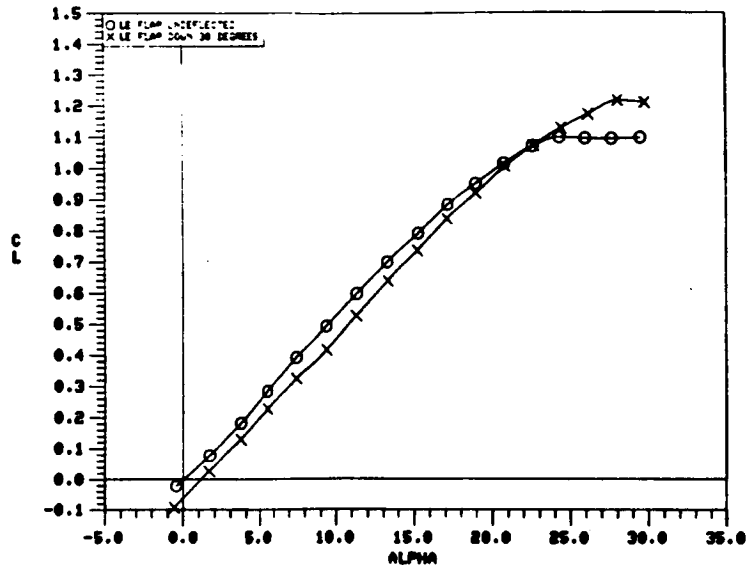

a) C_L vs. α

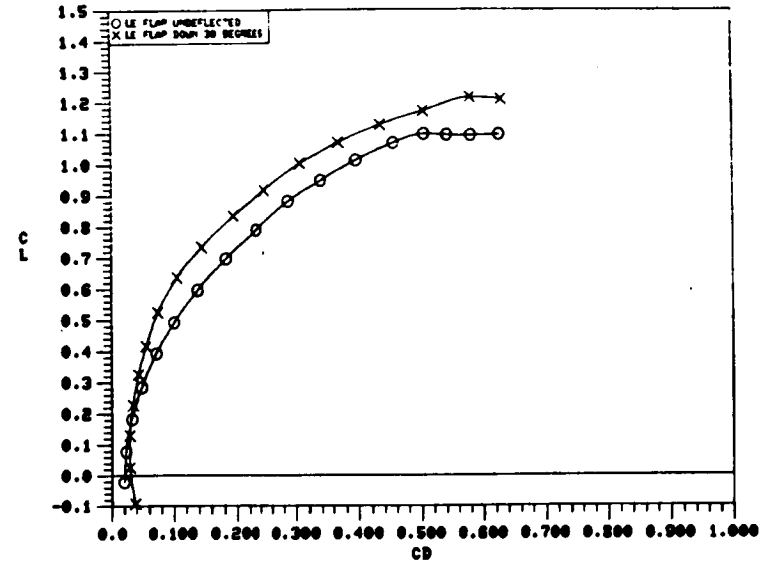

b) C_L vs. C_D

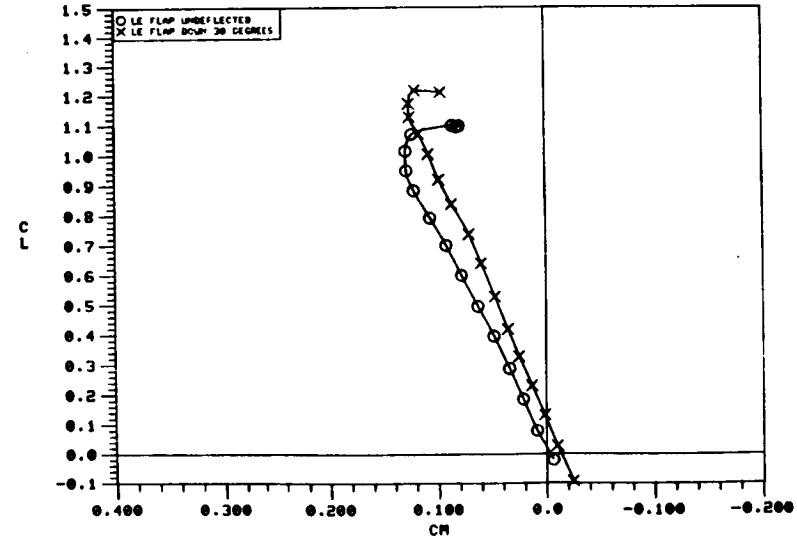

c) C_L vs. C_m

Figure 15. Effect of Deflected Vortex Flap on the Static Longitudinal Aerodynamic Characteristics of the 50-Degree Cropped Delta Wing.

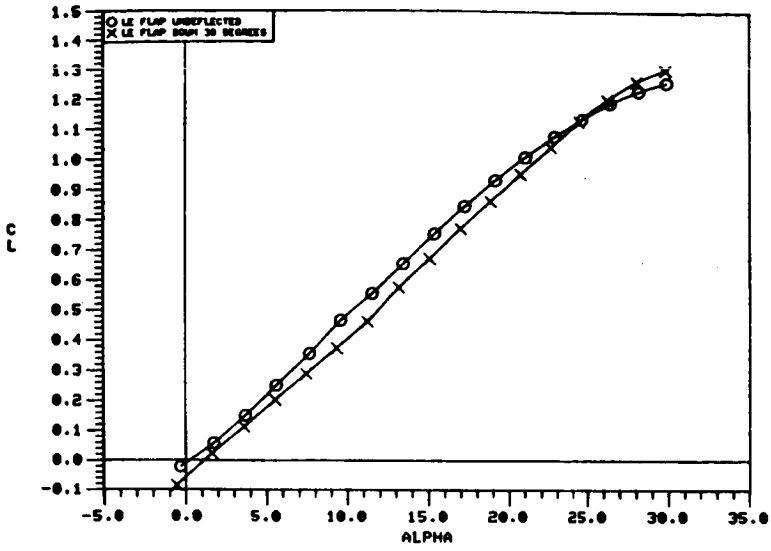

0 LE FLAP UNDEFLECTED
X LE FLAP DOWN 30 DEGREES

a) C_L vs. α

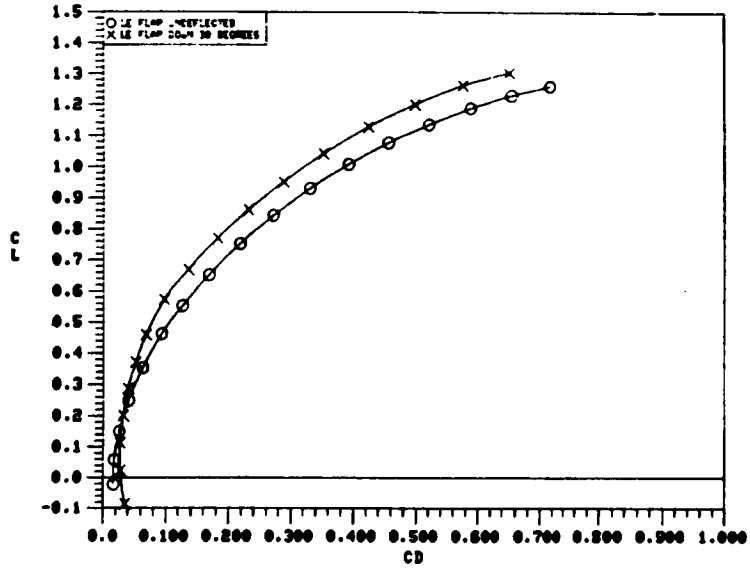

b) C_L vs. C_D

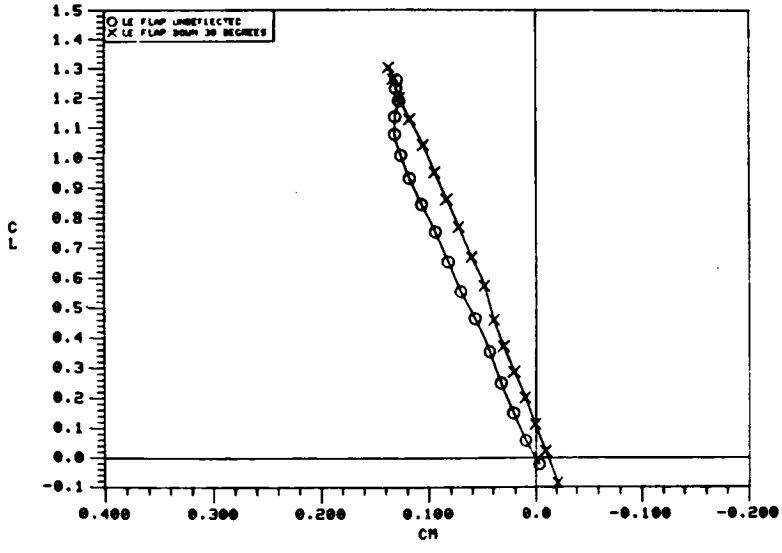

c) C_L vs. C_m

Figure 16. Effect of Deflected Vortex Flap on the Static Longitudinal Aerodynamic Characteristics of the 55-Degree Cropped Delta Wing.

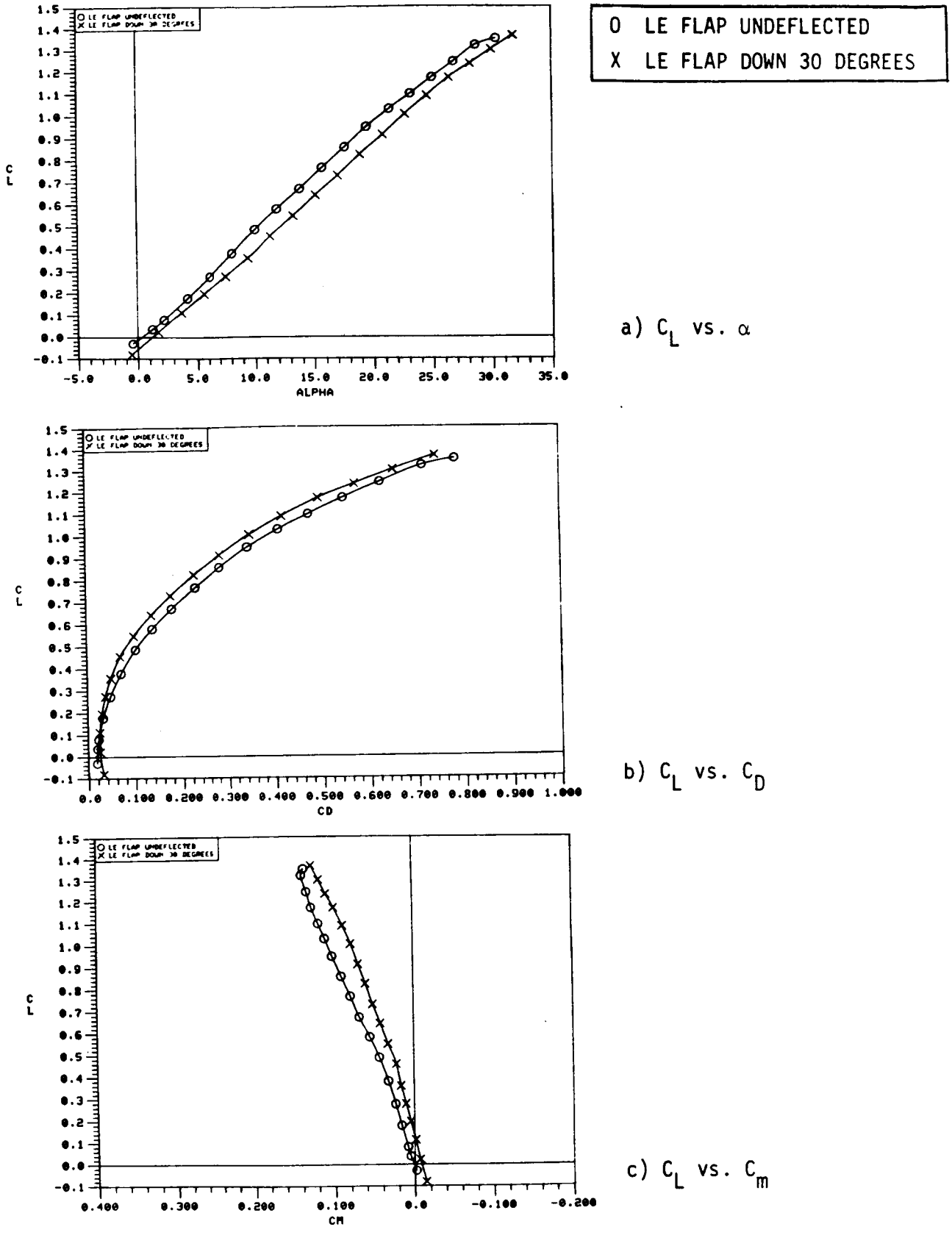

a) C_L vs. α

b) C_L vs. C_D

c) C_L vs. C_m

Figure 17. Effect of Deflected Vortex Flap on the Static Longitudinal Aerodynamic Characteristics of the 60-Degree Cropped Delta Wing.

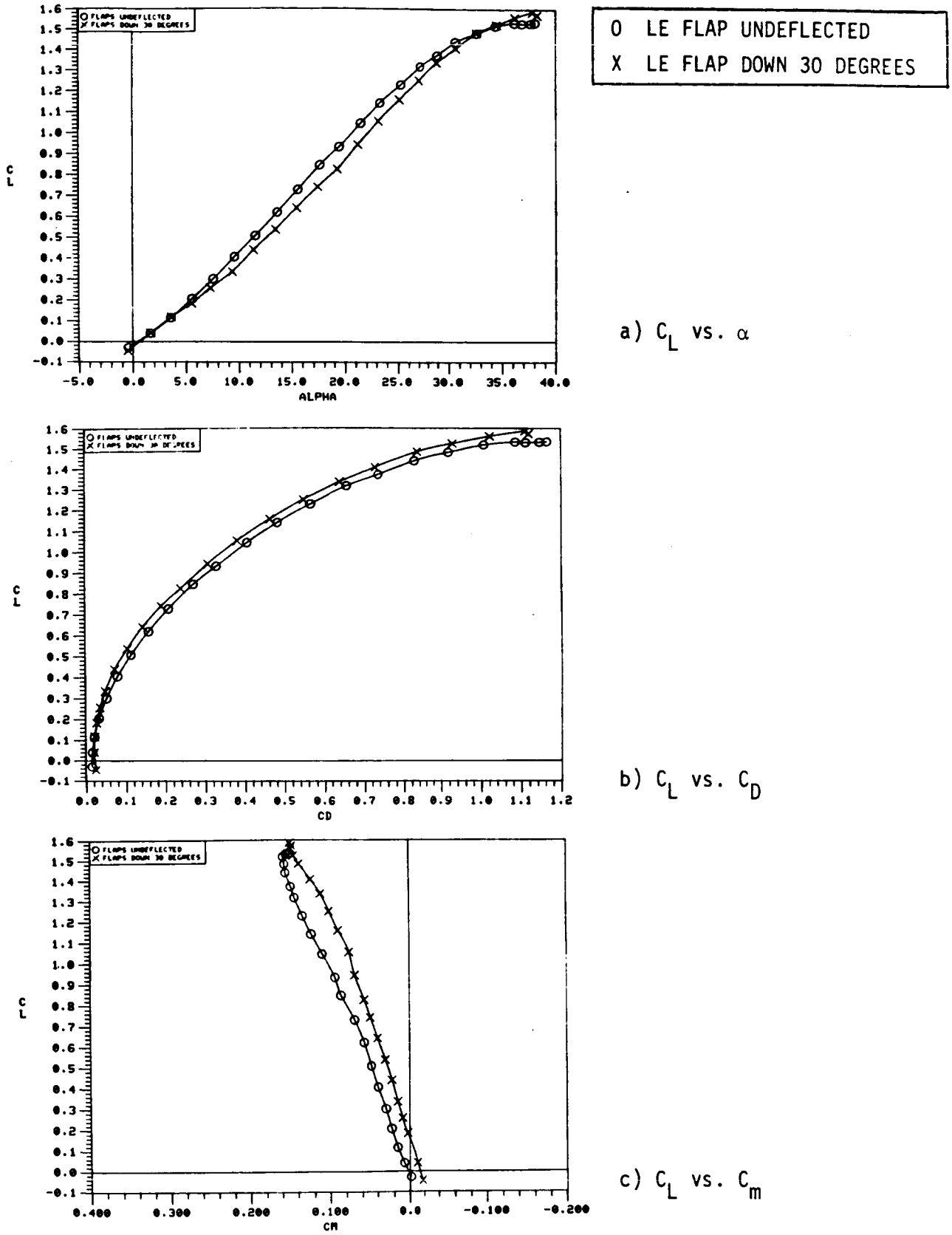

a) C_L vs. α

b) C_L vs. C_D

c) C_L vs. C_m

Figure 18. Effect of Deflected Vortex Flap on the Static Longitudinal Aerodynamic Characteristics of the 65-Degree Cropped Delta Wing.

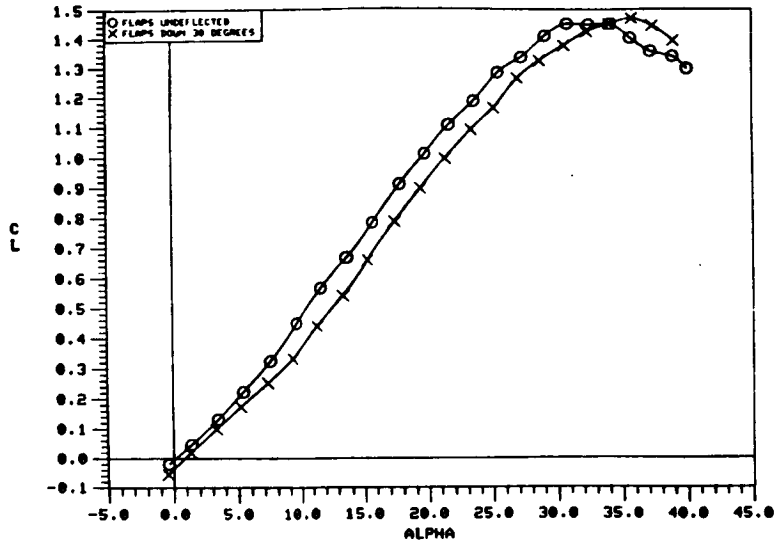

a) C_L vs. α

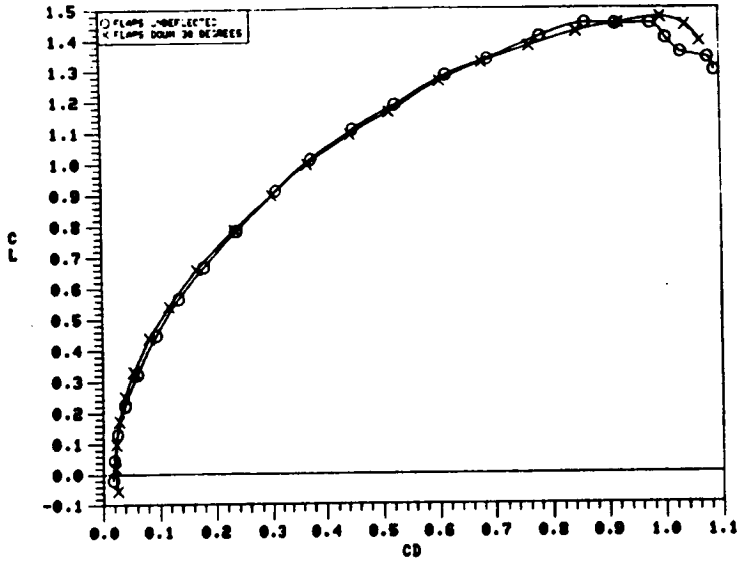

b) C_L vs. C_D

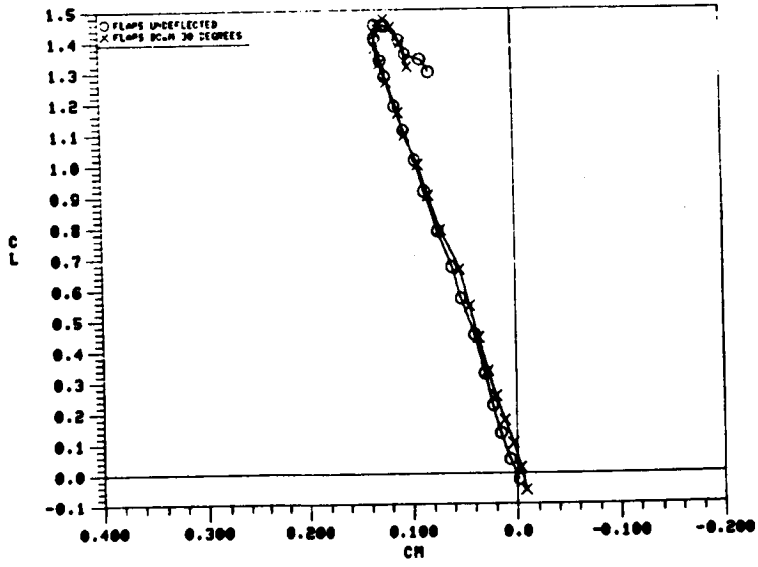

c) C_L vs. C_m

Figure 19. Effect of Deflected Vortex Flap on the Static Longitudinal Aerodynamic Characteristics of the 65-Degree Cropped Delta Wing With Part-Span Flap.

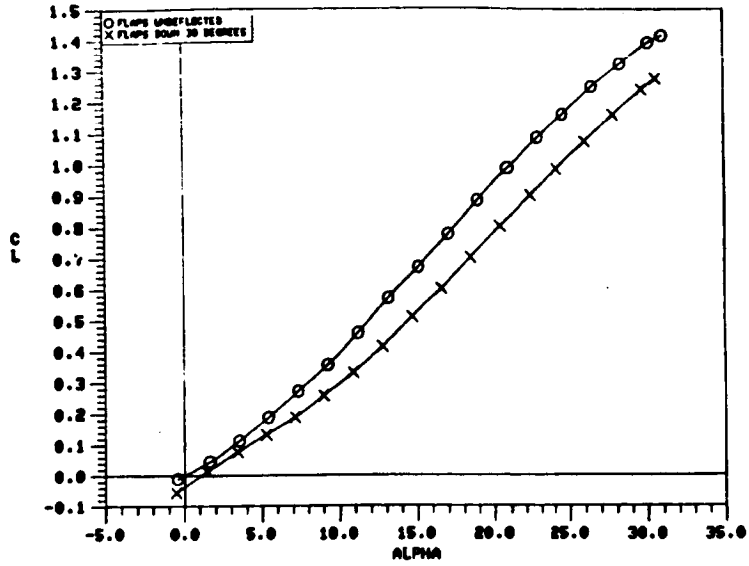

a) C_L vs. α

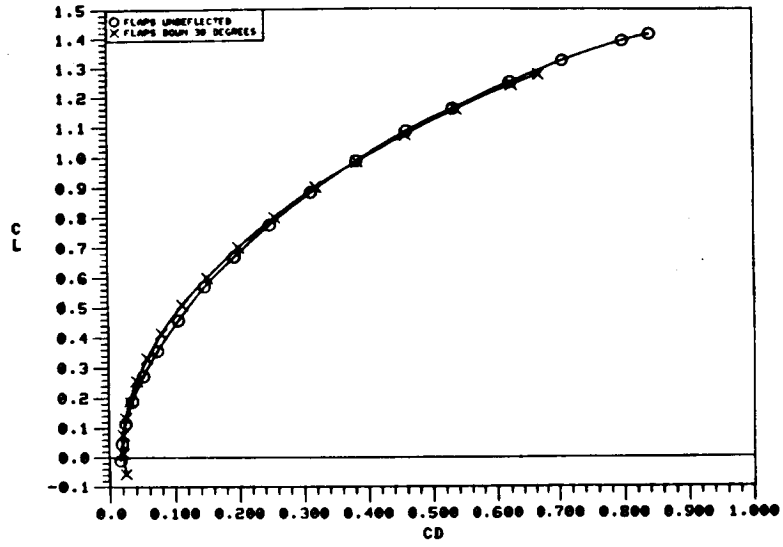

b) C_L vs. C_D

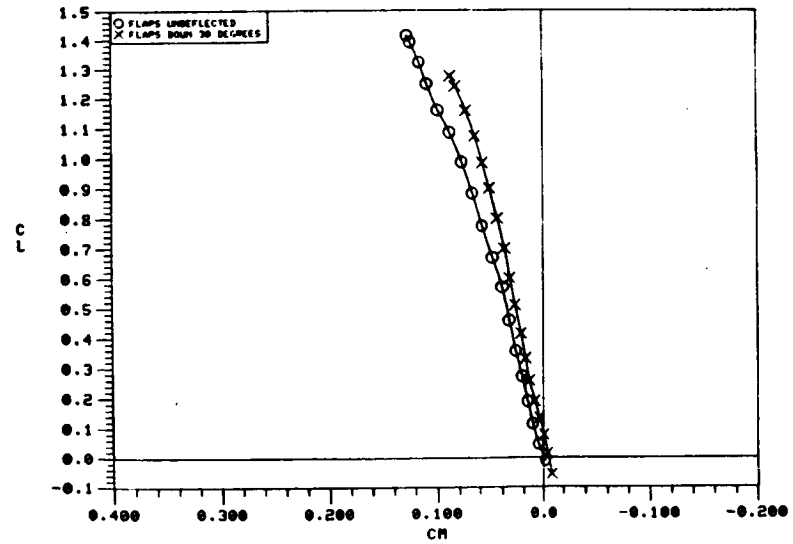

c) C_L vs. C_m

Figure 20. Effect of Deflected Vortex Flap on the Static Longitudinal Aerodynamic Characteristics of the 70-Degree Cropped Delta Wing.

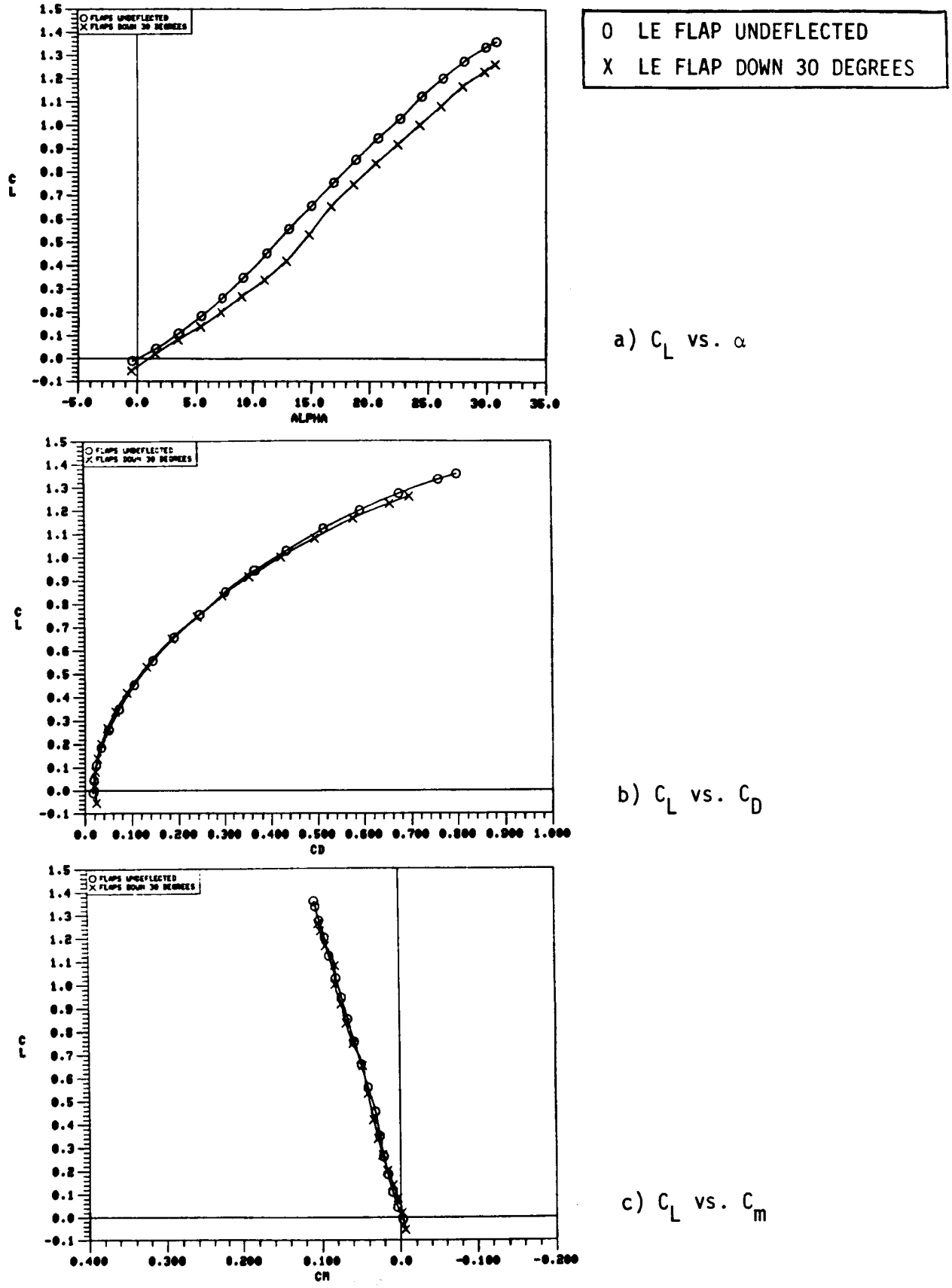

Figure 21. Effect of Deflected Vortex Flap on the Static Longitudinal Aerodynamic Characteristics of the 70-Degree Cropped Delta Wing With Part-Span Flap.

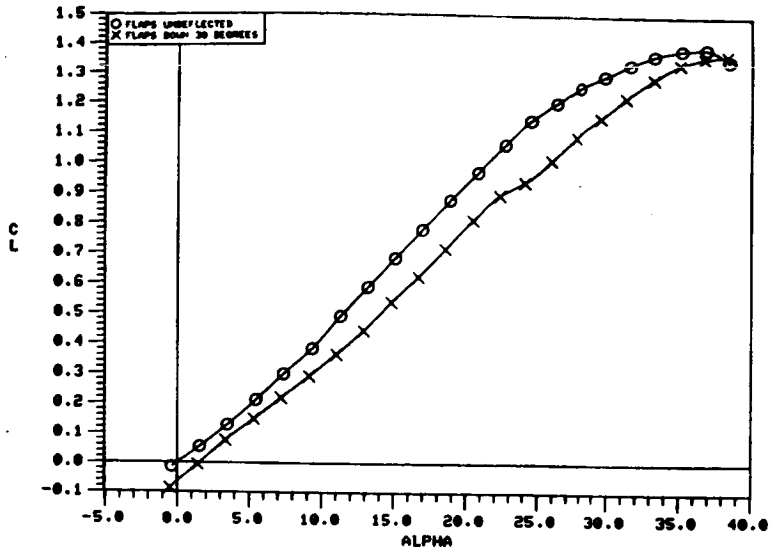

O	LE FLAP UNDEFLECTED
X	LE FLAP DOWN 30 DEGREES

a) C_L vs. α

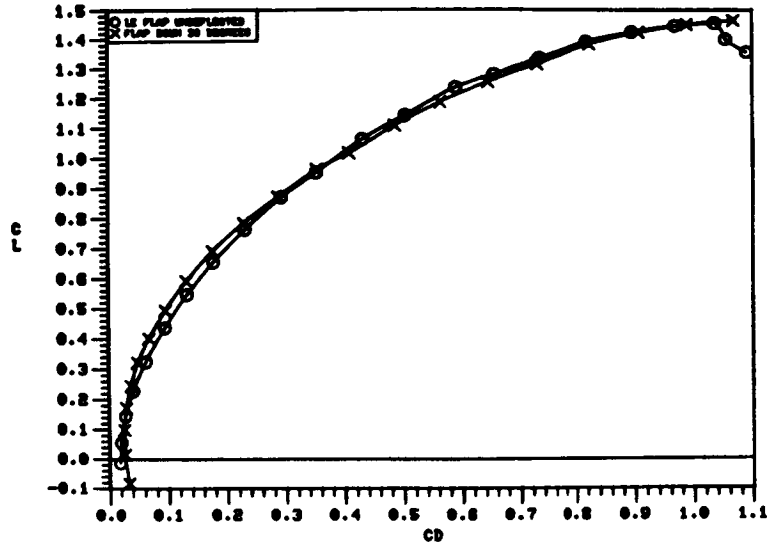

b) C_L vs. C_D

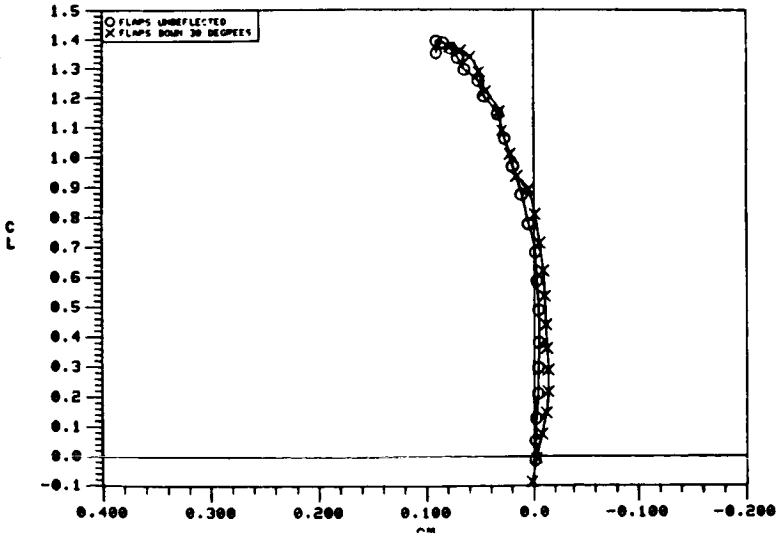

c) C_L vs. C_m

Figure 22. Effect of Deflected Vortex Flap on the Static Longitudinal Aerodynamic Characteristics of the 70/50-Degree Cranked Wing.

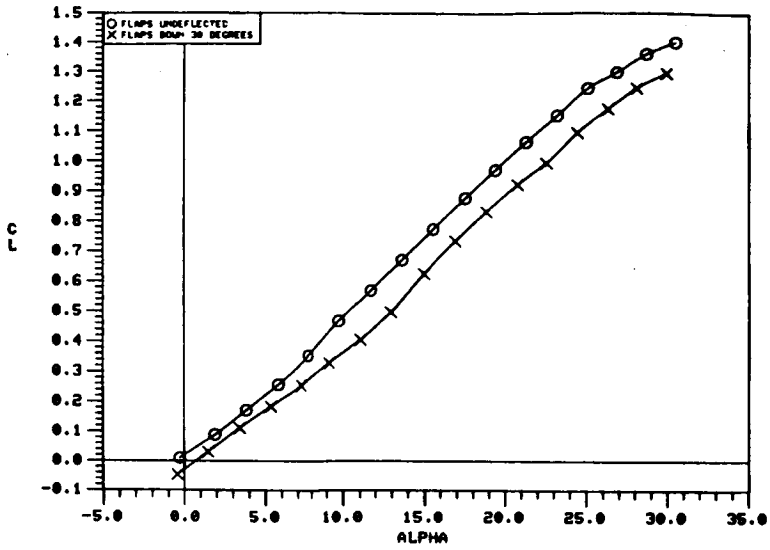

O LE FLAP UNDEFLECTED
X LE FLAP DOWN 30 DEGREES

a) C_L vs. α

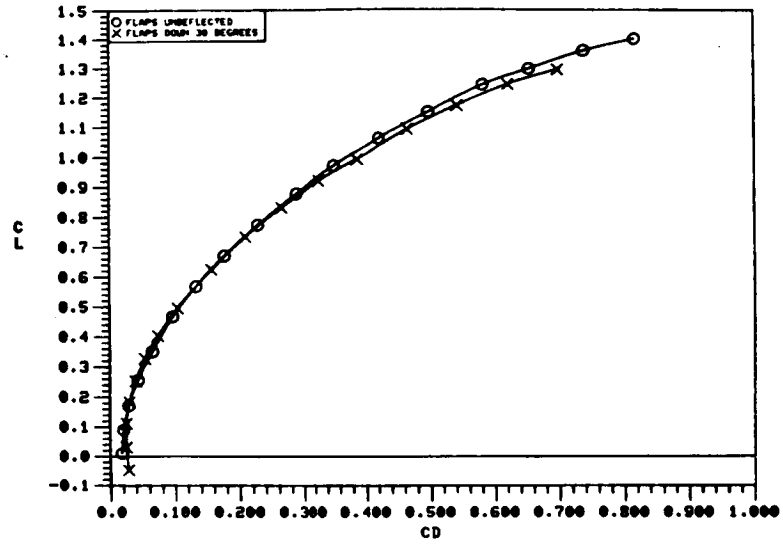

b) C_L vs. C_D

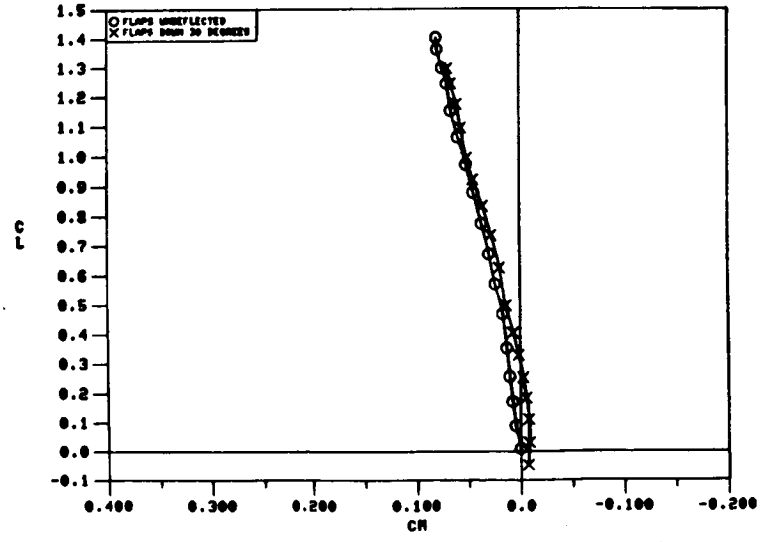

c) C_L vs. C_m

Figure 23. Effect of Deflected Vortex Flap on the Static Longitudinal Aerodynamic Characteristics of the 70/50-Degree Cranked Wing With Part-Span Flap.

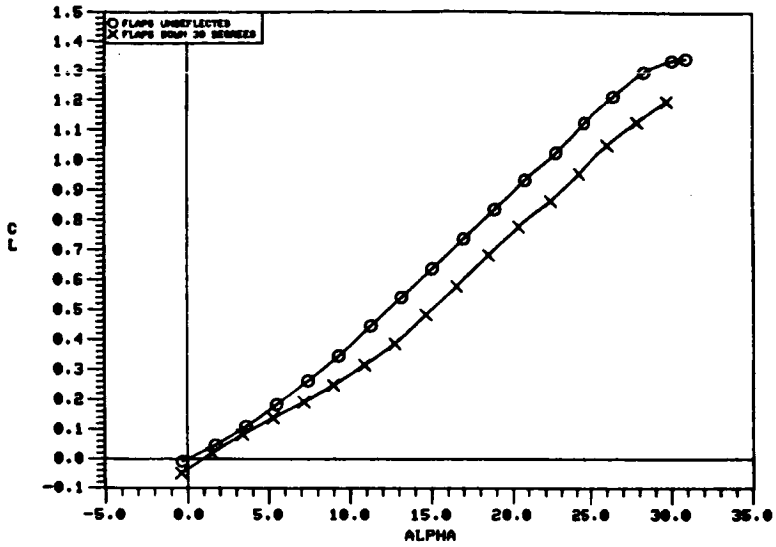

O LE FLAP UNDEFLECTED
X LE FLAP DOWN 30 DEGREES

a) C_L vs. α

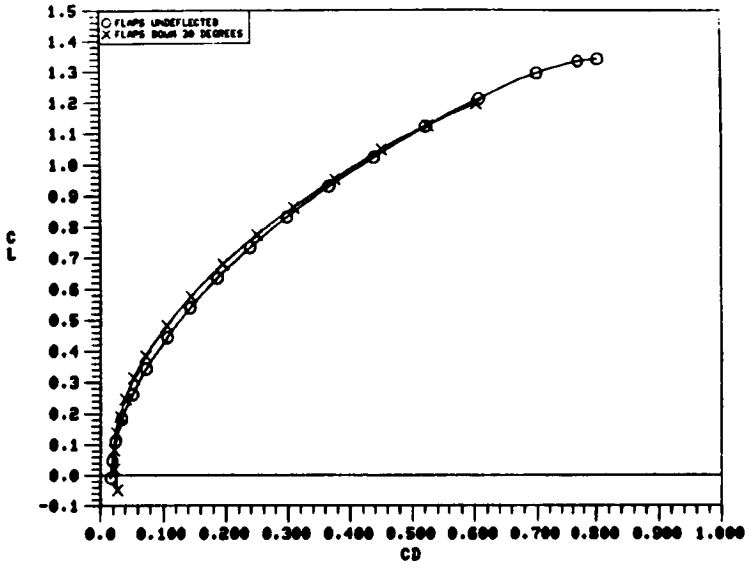

b) C_L vs. C_D

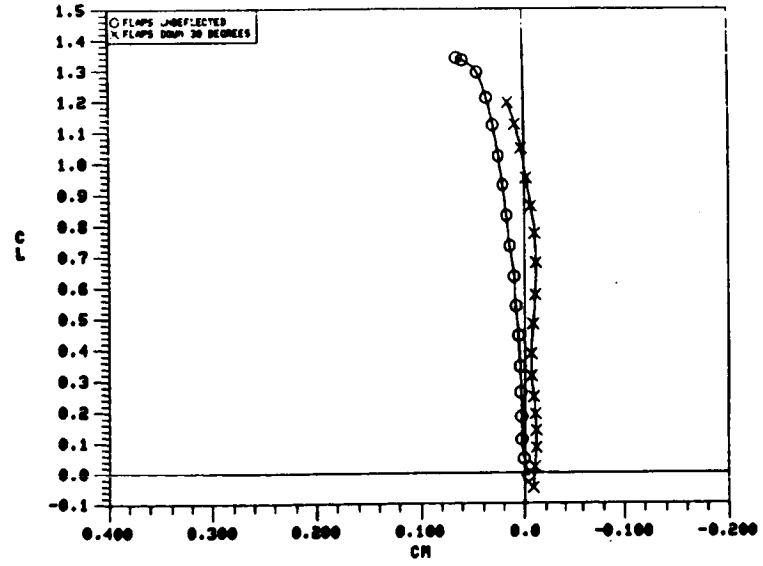

c) C_L vs. C_m

Figure 24. Effect of Deflected Vortex Flap on the Static Longitudinal Aerodynamic Characteristics of the 76.5/66.5-Degree Cranked Wing.

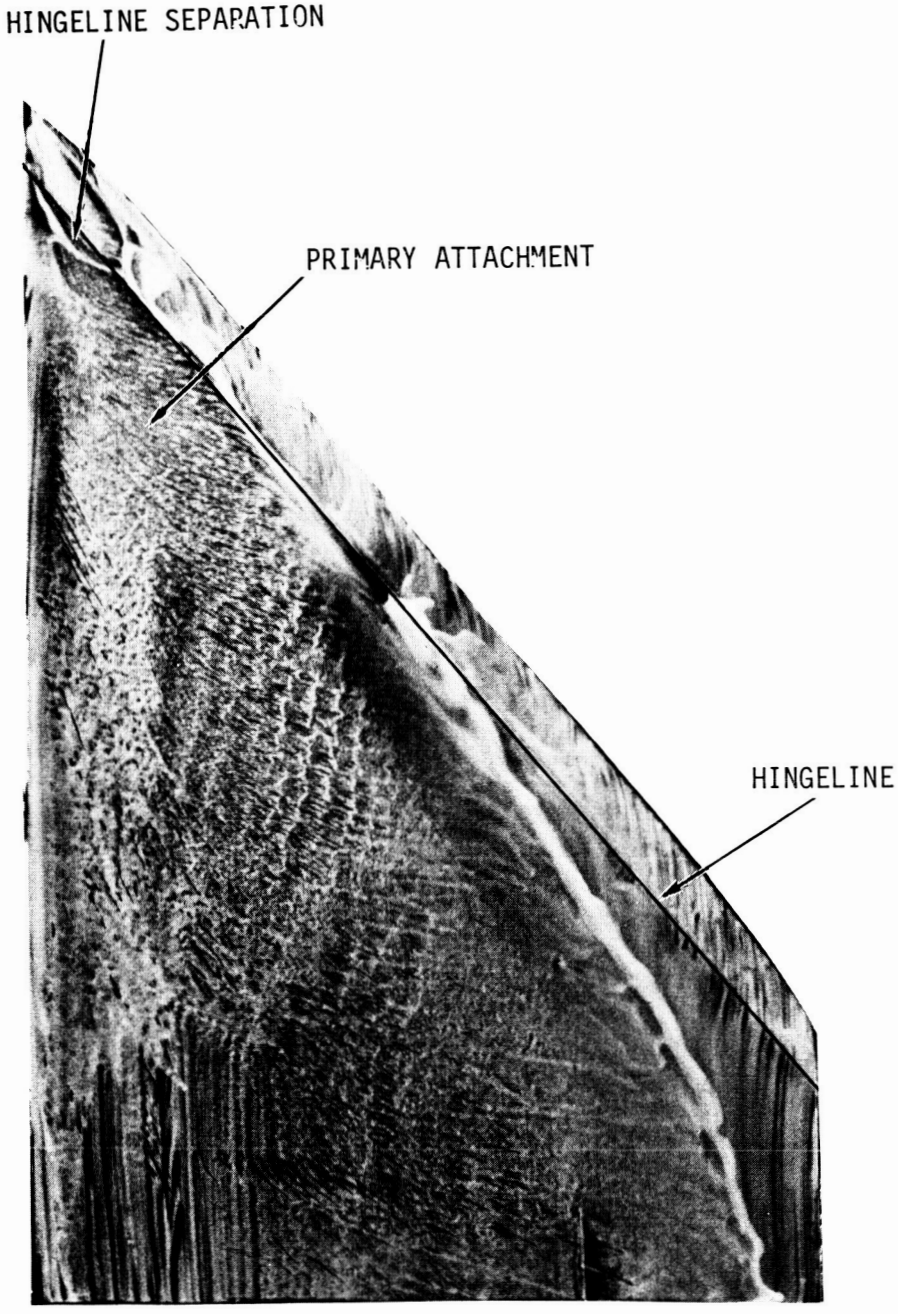

Figure 25. Upper Surface Flow Patterns of the 50-degree Cropped Delta Wing, δ_n = 30°, α= 24°, β= 0°.

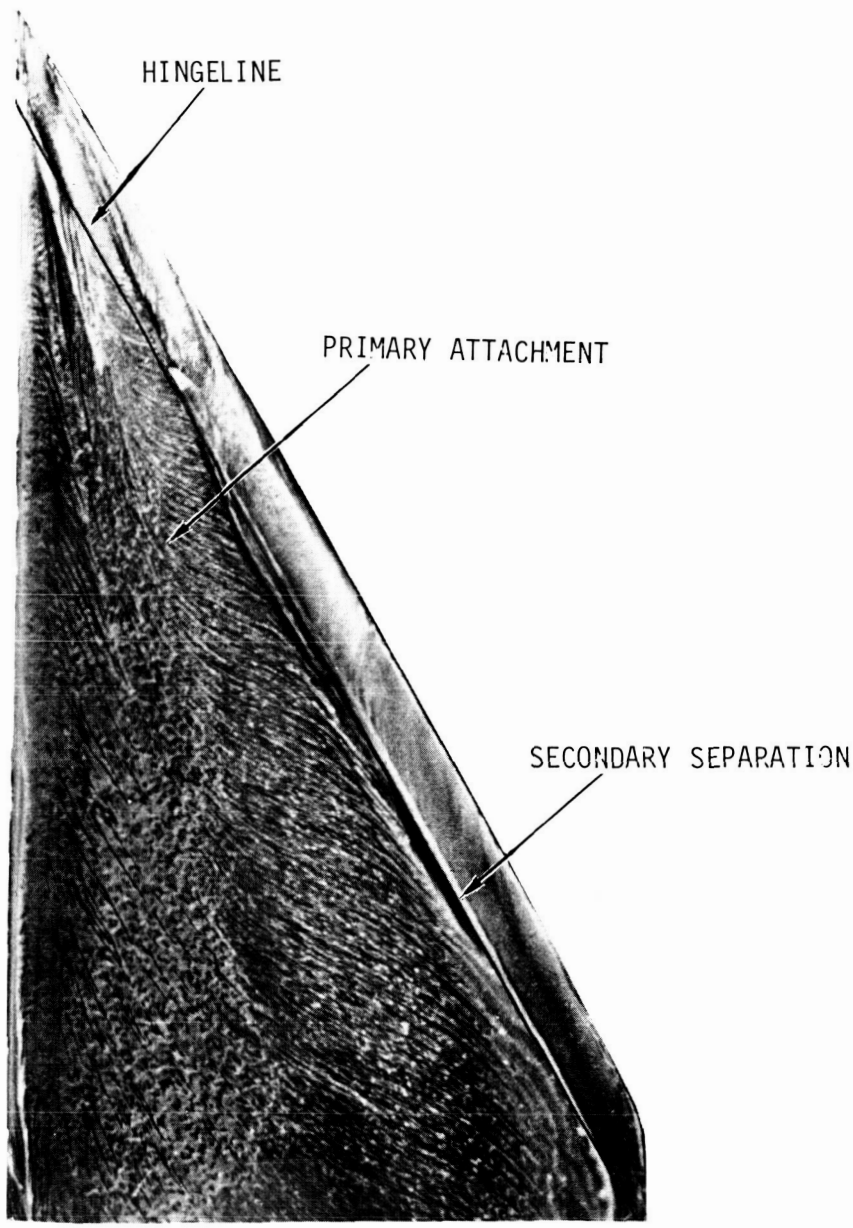

Figure 26. Upper Surface Flow Patterns of the 60-degree Cropped Delta Wing, $\delta_n = 30°$, $\alpha = 24°$, $\beta = 0°$.

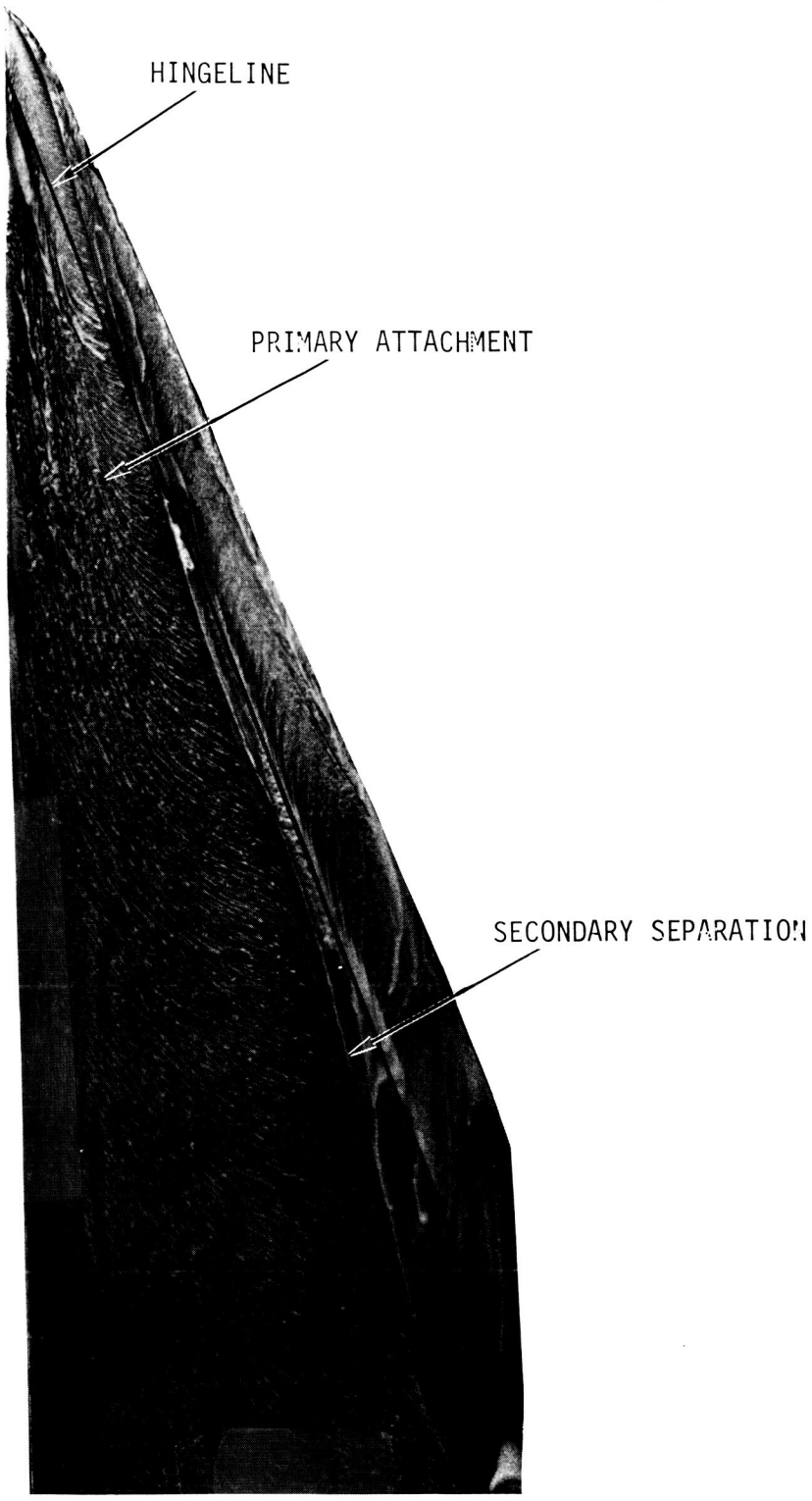

Figure 27. Upper Surface Flow Patterns of the 70-degree Cropped Delta Wing, $\delta_n = 30°$, $\alpha = 24°$, $\beta = 0°$.

O	LE FLAP UNDEFLECTED
X	LE FLAP DOWN 30 DEGREES

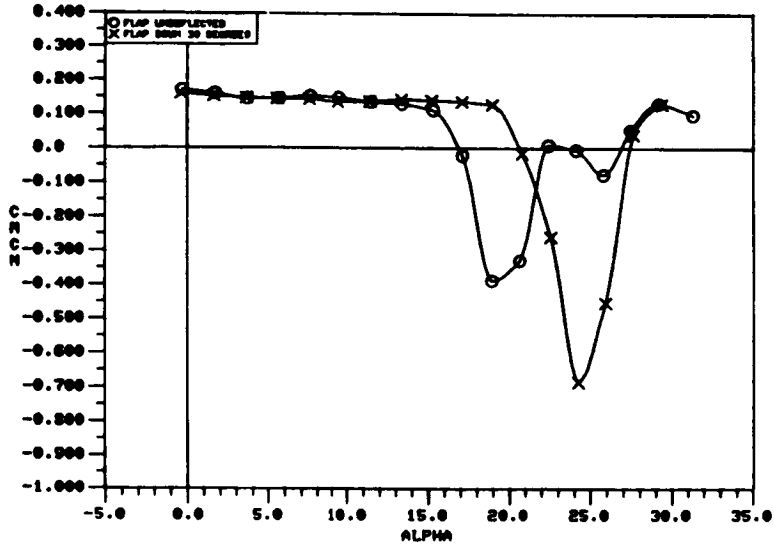

$C_{m_{C_N}}$ vs. α

Figure 28. Effect of Deflected Vortex Flap on the Static Longitudinal Stability Characteristics of the 45-Degree Cropped Delta Wing.

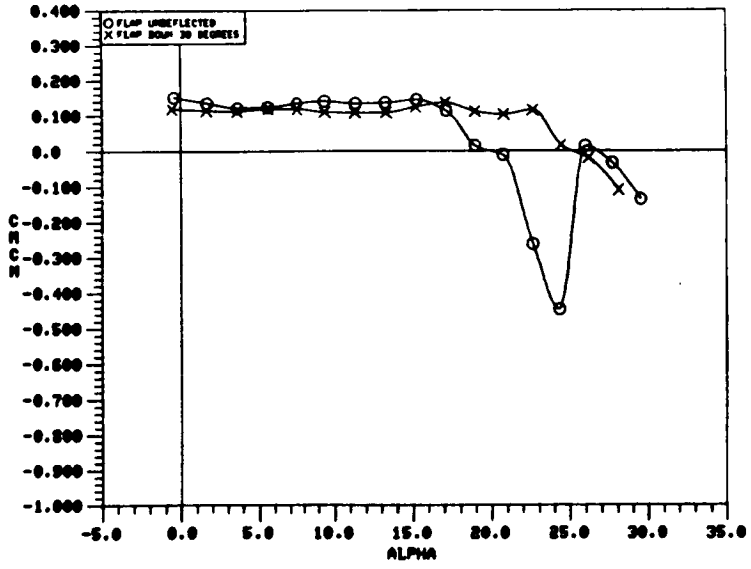

$C_{m_{C_N}}$ vs. α

Figure 29. Effect of Deflected Vortex Flap on the Static Longitudinal Stability Characteristics of the 50-Degree Cropped Delta Wing.

O	LE FLAP UNDEFLECTED
X	LE FLAP DOWN 30 DEGREES

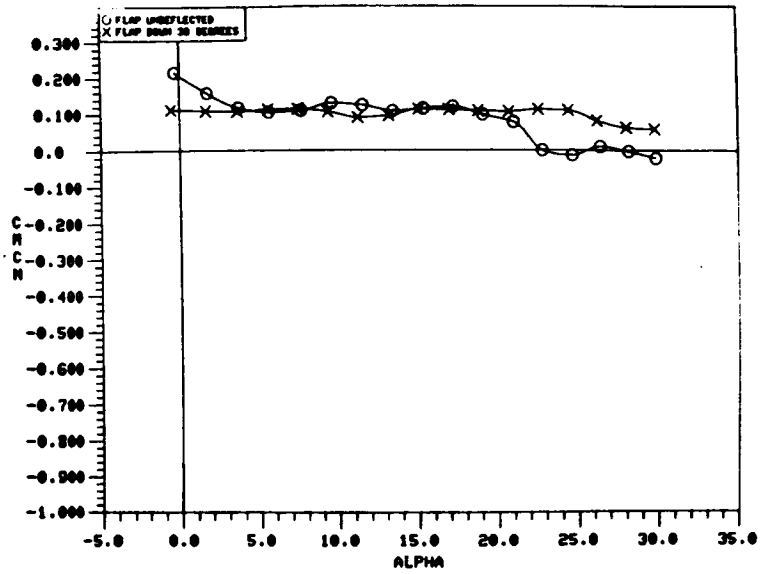

$C_{m_{C_N}}$ vs. α

Figure 30. Effect of Deflected Vortex Flap on the Static Longitudinal Stability Characteristics of the 55-Degree Cropped Delta Wing.

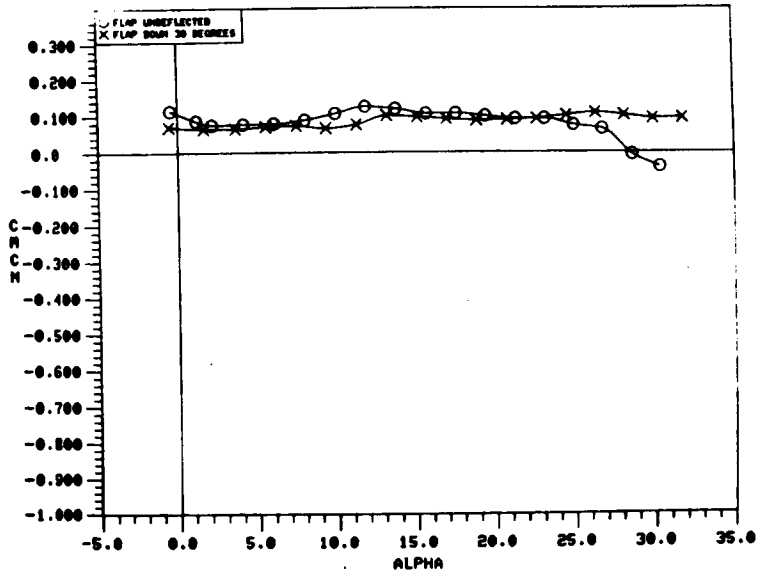

$C_{m_{C_N}}$ vs. α

Figure 31. Effect of Deflected Vortex Flap on the Static Longitudinal Stability Characteristics of the 60-Degree Cropped Delta Wing.

O LE FLAP UNDEFLECTED
X LE FLAP DOWN 30 DEGREES

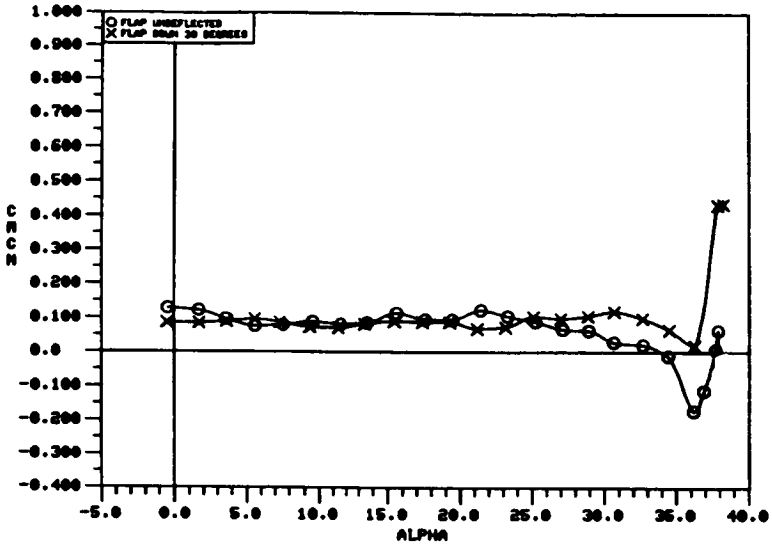

$C_{m_{C_N}}$ vs. α

Figure 32. Effect of Vortex Flap Deflection on the Static Longitudinal Stability Characteristics of the 65-Degree Cropped Delta Wing.

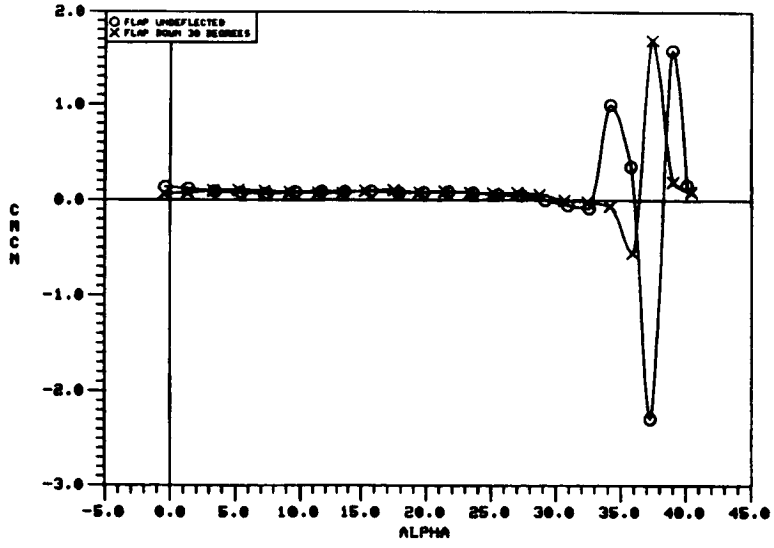

$C_{m_{C_N}}$ vs. α

Figure 33. Effect of Deflected Vortex Flap on the Static Longitudinal Stability Characteristics of the 65-Degree Cropped Delta Wing with Part-Span Flap.

O	LE FLAP UNDEFLECTED
X	LE FLAP DOWN 30 DEGREES

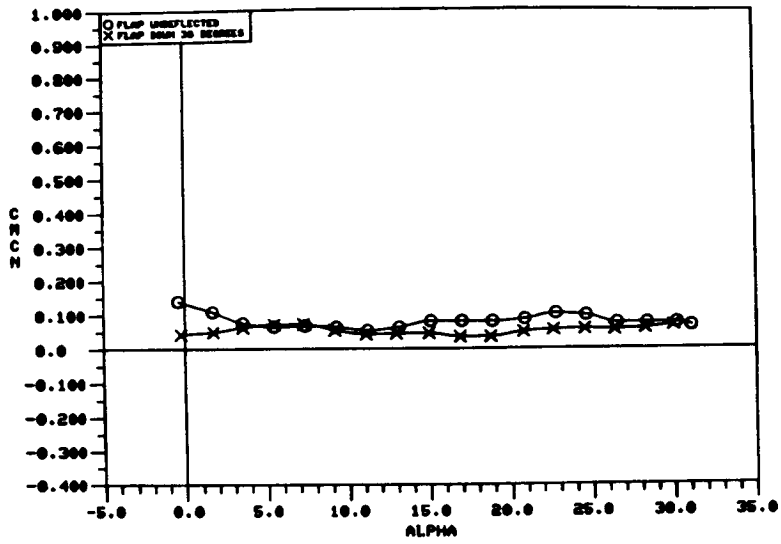

$C_{m_{C_N}}$ vs. α

Figure 34. Effect of Deflected Vortex Flap on the Static Longitudinal Stability Characteristics of the 70-Degree Cropped Delta Wing.

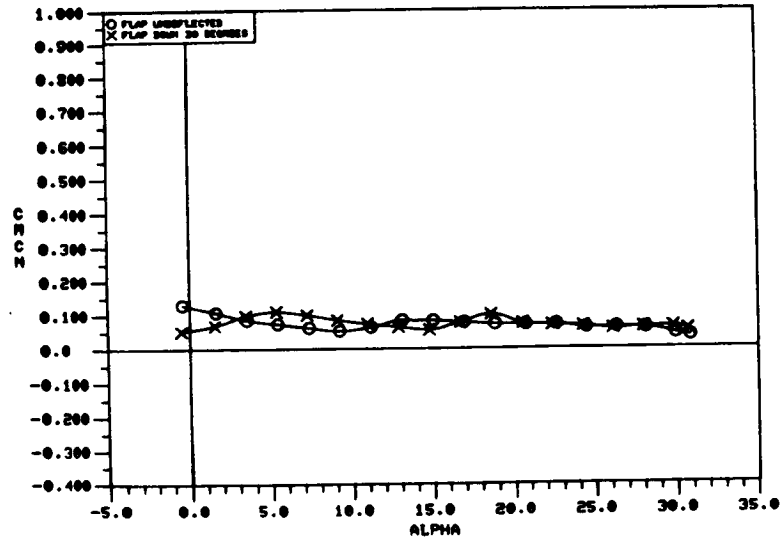

$C_{m_{C_N}}$ vs. α

Figure 35. Effect of Deflected Vortex Flap on the Static Longitudinal Stability Characteristics of the 70-Degree Cropped Delta Wing with Part-Span Flap.

O	LE FLAP UNDEFLECTED
X	LE FLAP DOWN 30 DEGREES

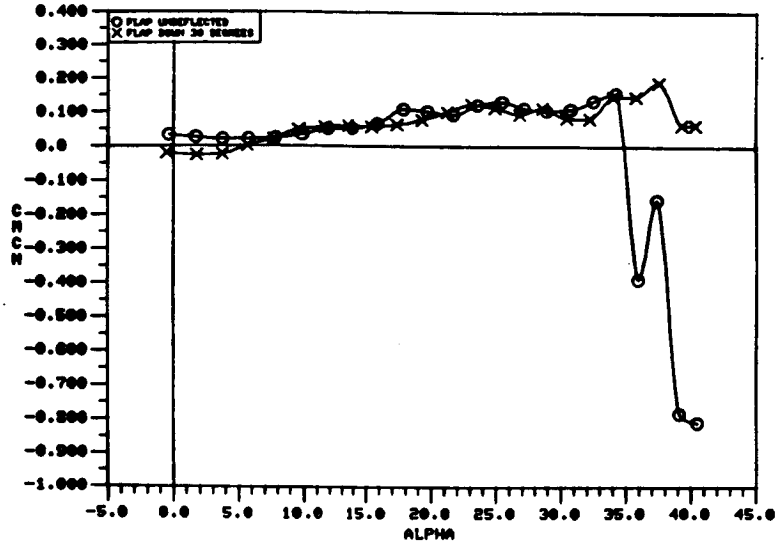

$C_{m_{C_N}}$ vs. α

Figure 36. Effect of Deflected Vortex Flap on the Static Longitudinal Stability Characteristics of the 70/50-Degree Cranked Wing.

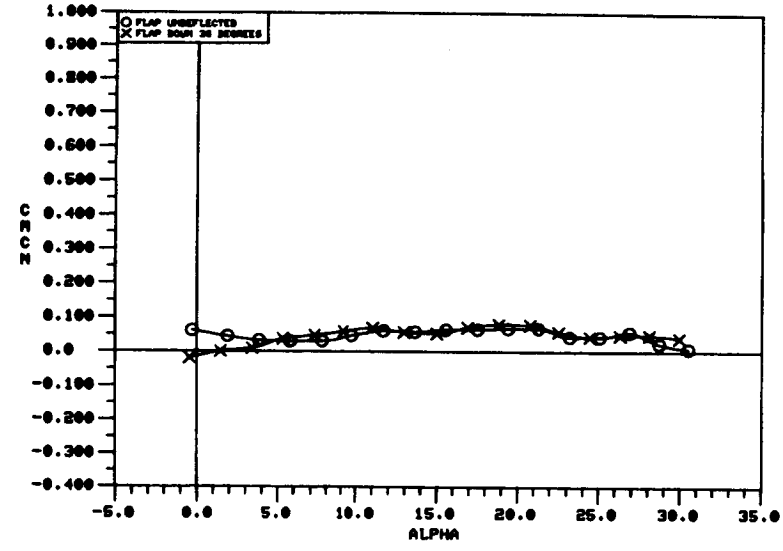

$C_{m_{C_N}}$ vs. α

Figure 37. Effect of Deflected Vortex Flap on the Static Longitudinal Stability Characteristics of the 70/50-Degree Cranked Wing with Part-Span Flap.

O	LE FLAP UNDEFLECTED
X	LE FLAP DOWN 30 DEGREES

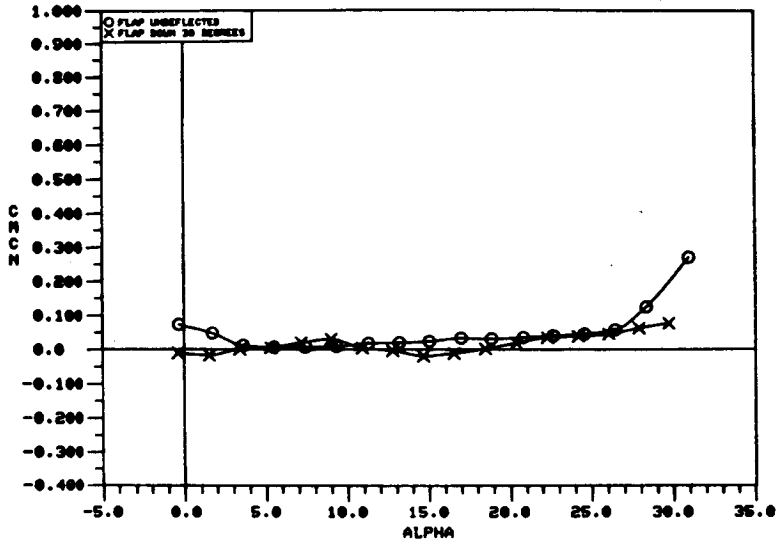

$C_{m_{C_N}}$ vs. α

Figure 38. Effect of Deflected Vortex Flap on the Static Longitudinal Stability Characteristics of the 76.5/66.5-Degree Cranked Wing.

O	LE FLAP UNDEFLECTED
X	LE FLAP DOWN 30 DEGREES

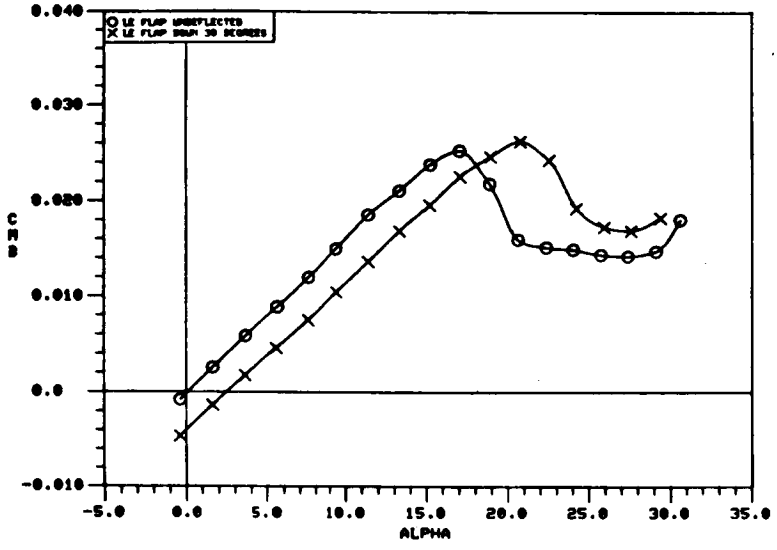

C_{m_β} vs. α

Figure 39. Effect of Deflected Vortex Flap on the Pitch-Sideslip Coupling Parameter of the 45-Degree Cropped Delta Wing.

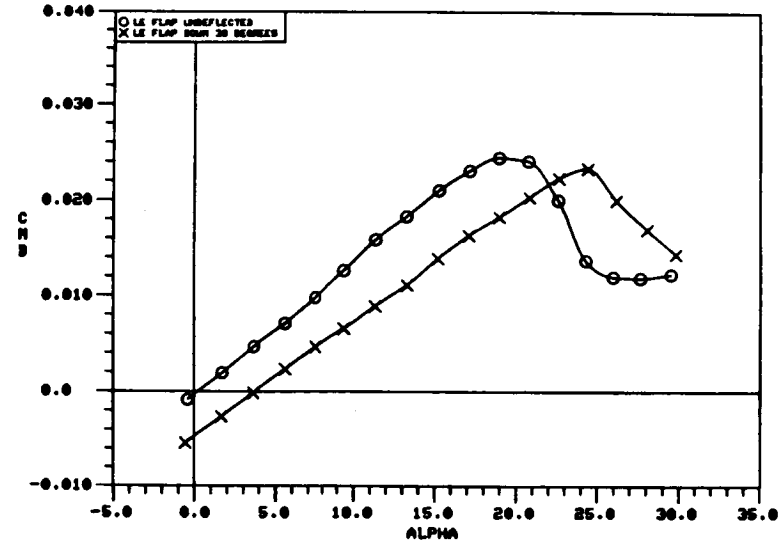

C_{m_β} vs. α

Figure 40. Effect of Deflected Vortex Flap on the Pitch-Sideslip Coupling Parameter of the 50-Degree Cropped Delta Wing

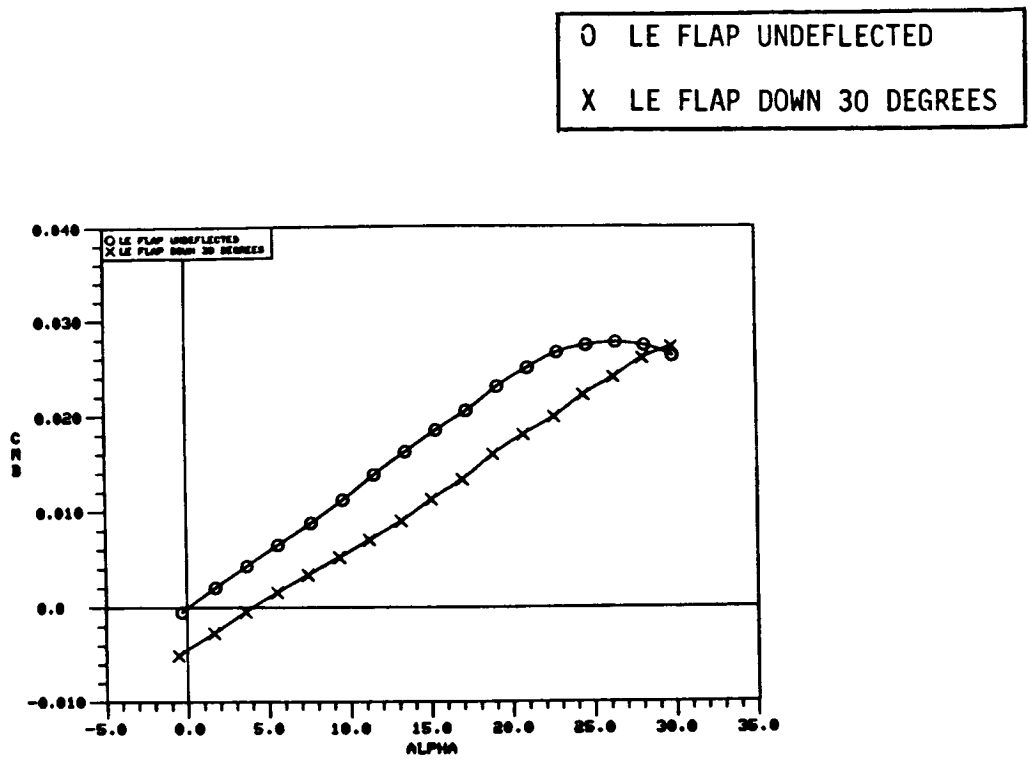

C_{m_β} vs. α

Figure 41. Effect of Deflected Vortex Flap on the Pitch-Sideslip Coupling Parameter of the 55-Degree Cropped Delta Wing.

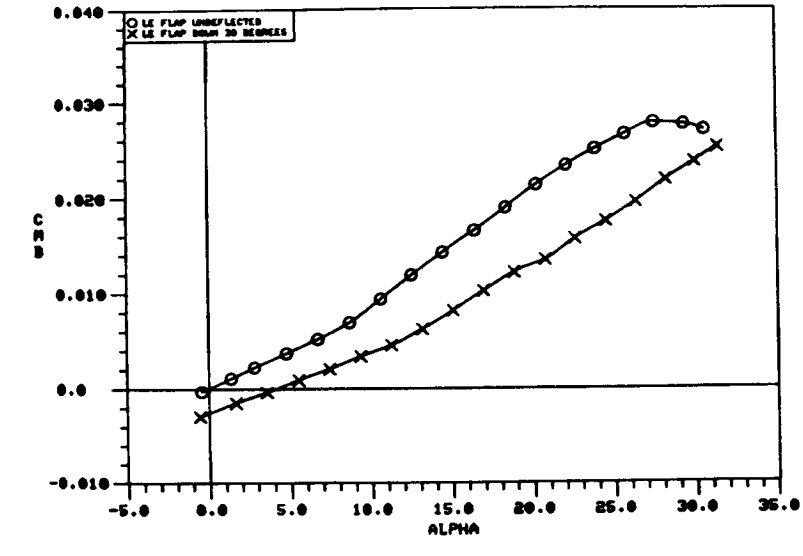

C_{m_β} vs. α

Figure 42. Effect of Deflected Vortex Flap on the Pitch-Sideslip Coupling Parameter of the 60-Degree Cropped Delta Wing

O	LE FLAP UNDEFLECTED
X	LE FLAP DOWN 30 DEGREES

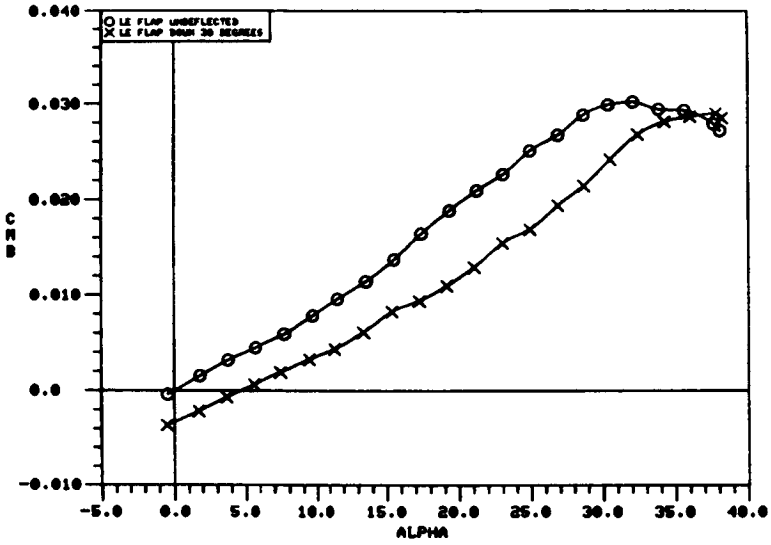

C_{m_β} vs. α

Figure 43. Effect of Deflected Vortex Flap on the Pitch-Sideslip Coupling Parameter of the 65-Degree Cropped Delta Wing.

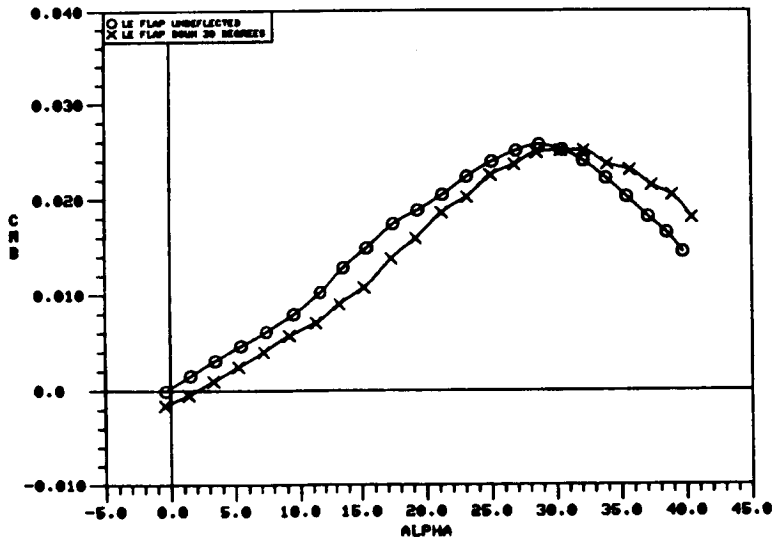

C_{m_β} vs. α

Figure 44. Effect of Deflected Vortex Flap on the Pitch-Sideslip Coupling Parameter of the 65-Degree Cropped Delta Wing with Part-Span Flap.

O	LE FLAP UNDEFLECTED
X	LE FLAP DOWN 30 DEGREES

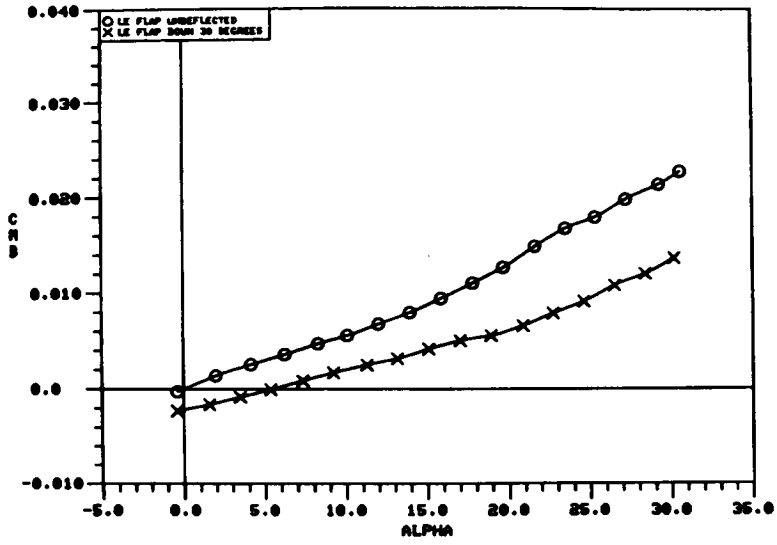

C_{m_β} vs. α

Figure 45. Effect of Deflected Vortex Flap on the Pitch-Sideslip Coupling Parameter of the 70-Degree Cropped Delta Wing.

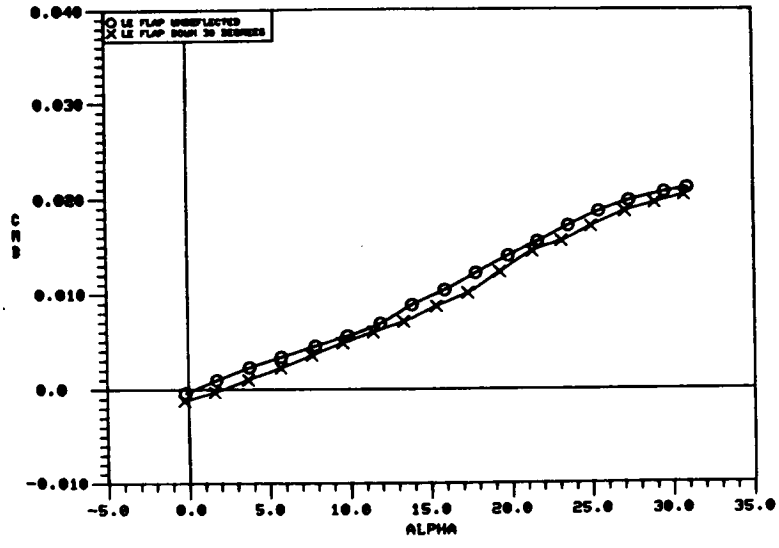

C_{m_β} vs. α

Figure 46. Effect of Deflected Vortex Flap on the Pitch-Sideslip Coupling Parameter of the 70-Degree Cropped Delta Wing with Part-Span Flap.

O LE FLAP UNDEFLECTED
X LE FLAP DOWN 30 DEGREES

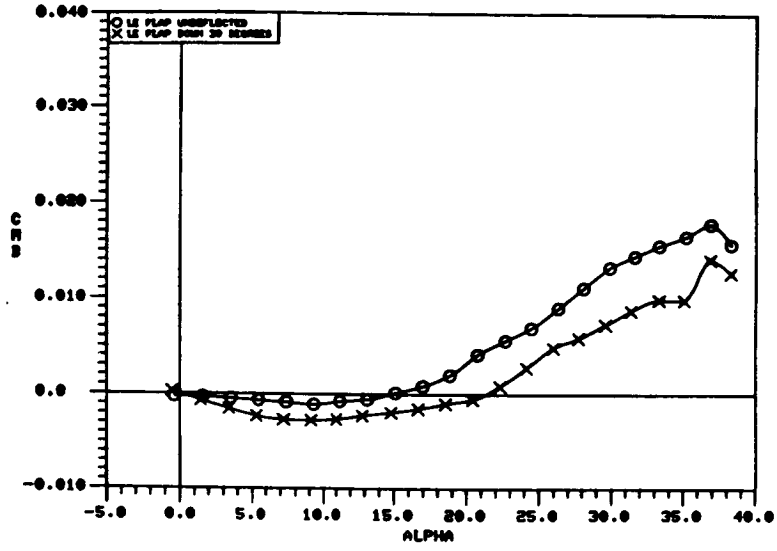

C_{m_β} vs. α

Figure 47. Effect of Deflected Vortex Flap on the Pitch-Sideslip Coupling Parameter of the 70/50-Degree Cranked Wing.

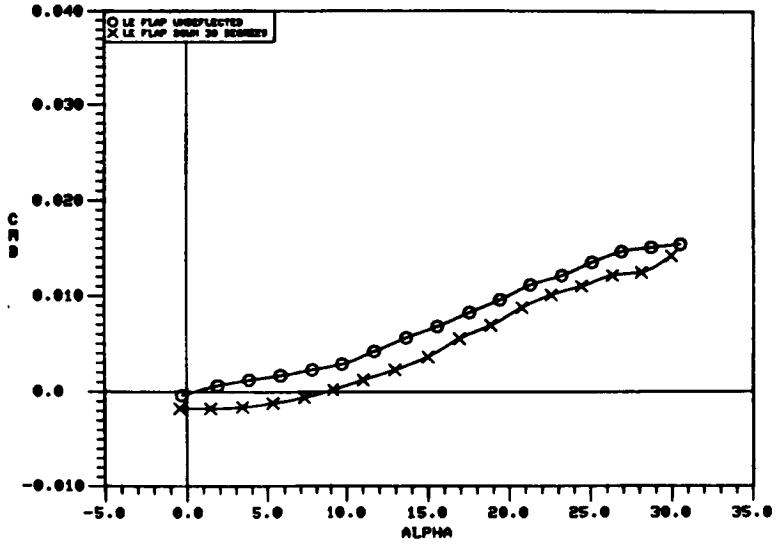

C_{m_β} vs. α

Figure 48. Effect of Deflected Vortex Flap on the Pitch-Sideslip Coupling Parameter of the 70/50-Degree Cranked Wing with Part-Span Flap.

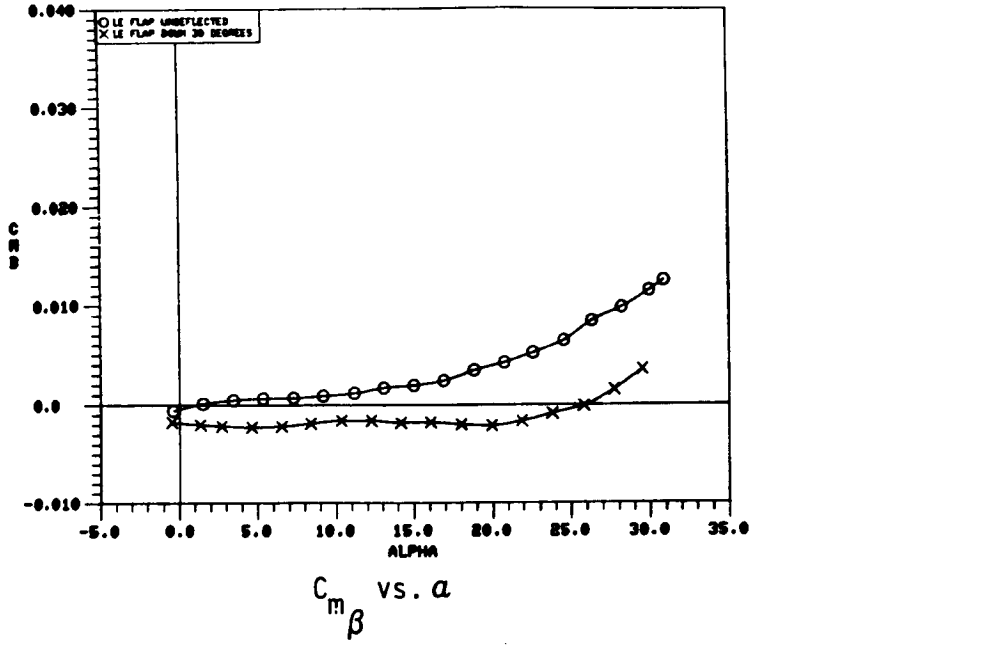

Figure 49. Effect of Deflected Vortex Flap on the Pitch-Sideslip Coupling Parameter of the 76.5/66.5-Degree Cranked Wing.

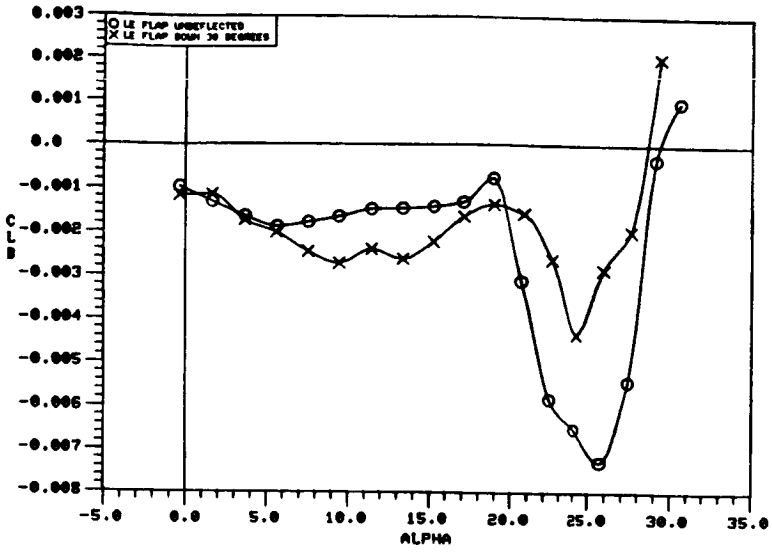

O LE FLAP UNDEFLECTED
X LE FLAP DOWN 30 DEGREES

a) C_{ℓ_β} vs. α

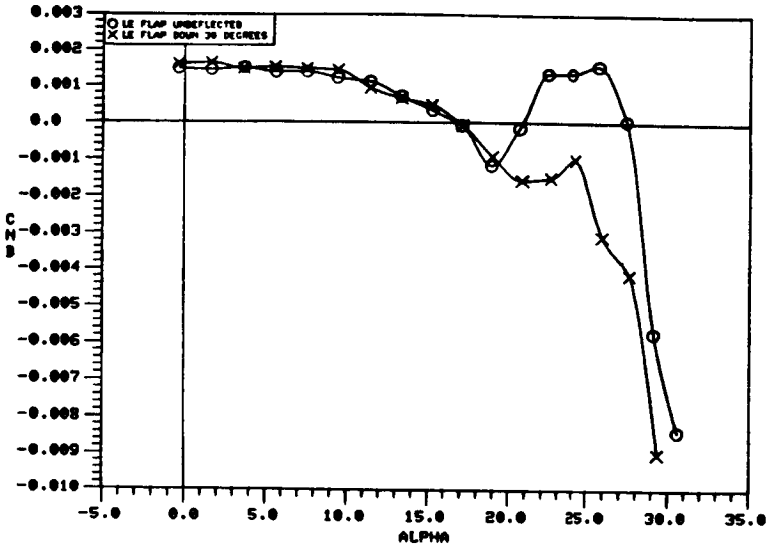

b) C_{n_β} vs. α

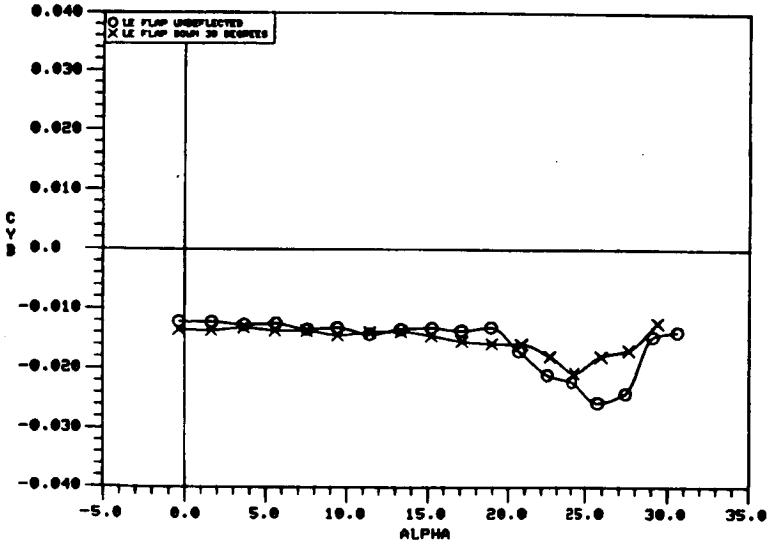

c) C_{Y_β} vs. α

Figure 50. Effect of Deflected Vortex Flap on the Static Lateral-Directional Stability Characteristics of the 45-Degree Cropped Delta Wing.

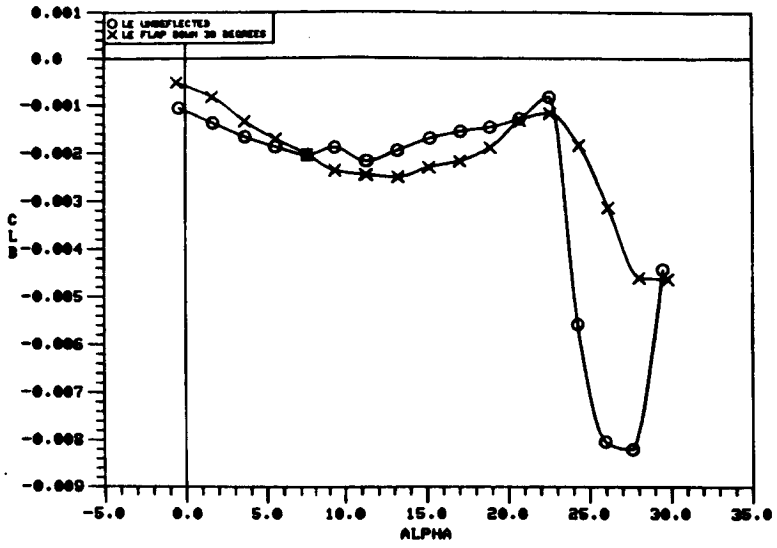

O LE FLAP UNDEFLECTED
X LE FLAP DOWN 30 DEGREES

a) C_{ℓ_β} vs. α

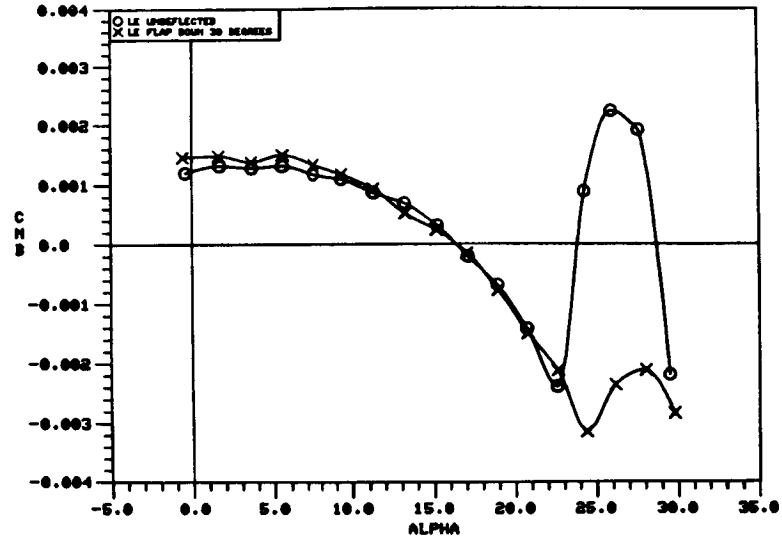

b) C_{n_β} vs. α

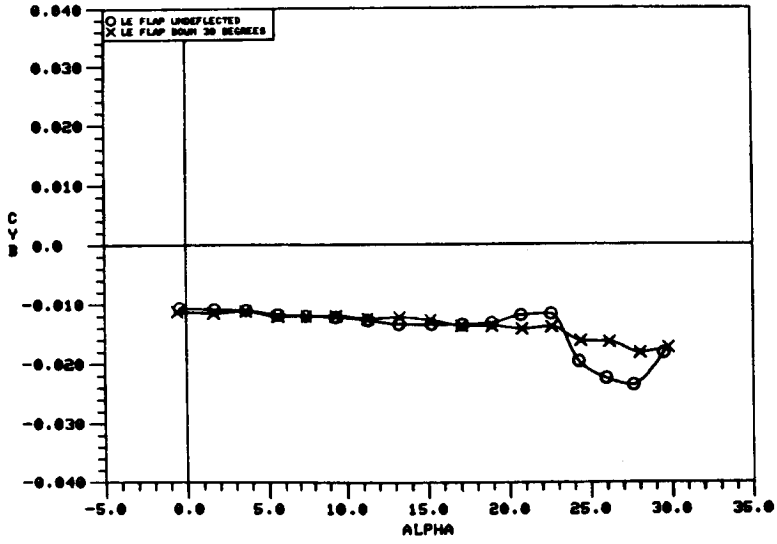

c) C_{Y_β} vs. α

Figure 51. Effect of Deflected Vortex Flap on the Static Lateral-Directional Stability Characteristics of the 50-Degree Cropped Delta Wing.

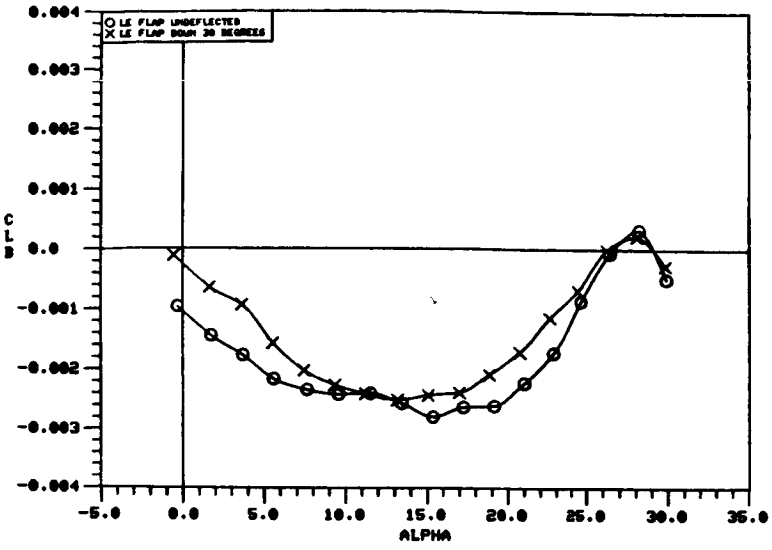

a) C_{ℓ_β} vs. α

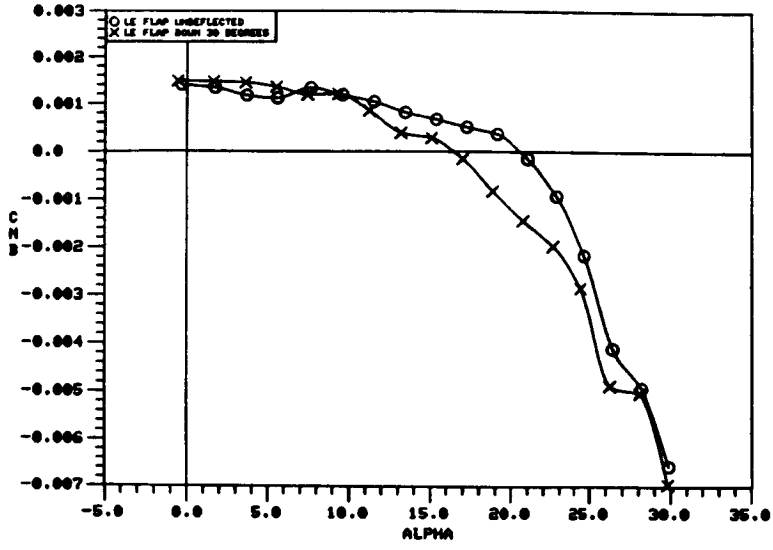

b) C_{n_β} vs. α

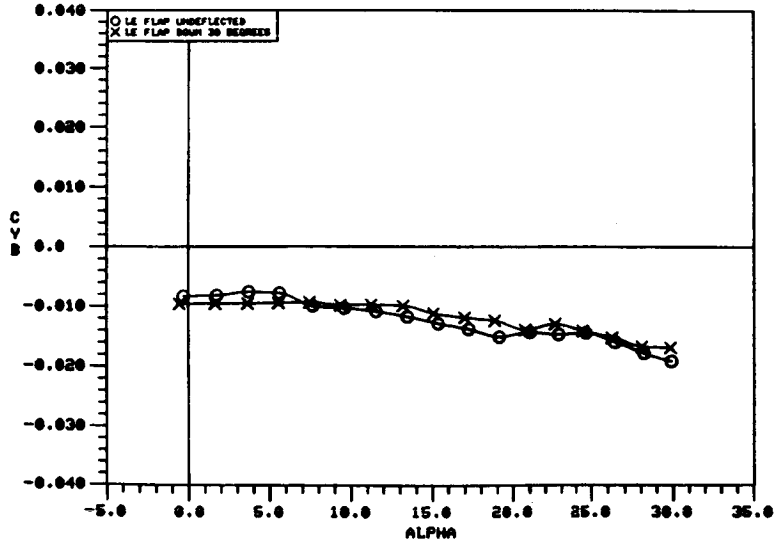

c) C_{Y_β} vs. α

Figure 52. Effect of Deflected Vortex Flap on the Static Lateral-Directional Stability Characteristics of the 55-Degree Cropped Delta Wing.

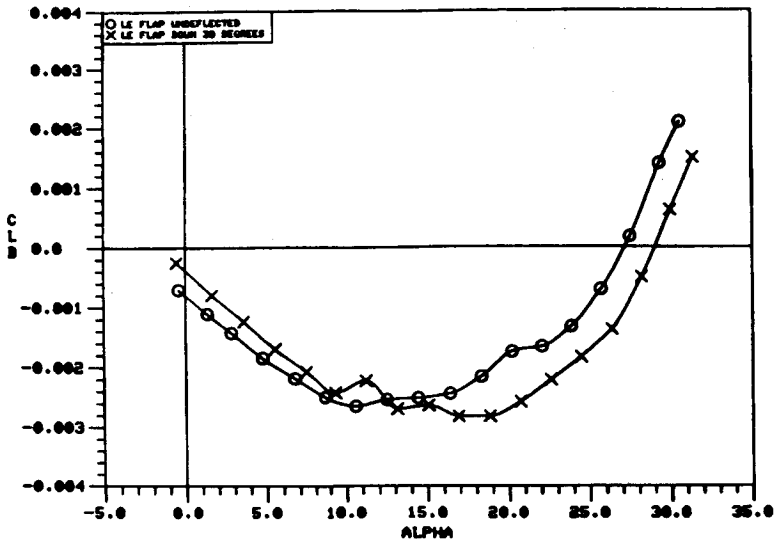

a) C_{ℓ_β} vs. α

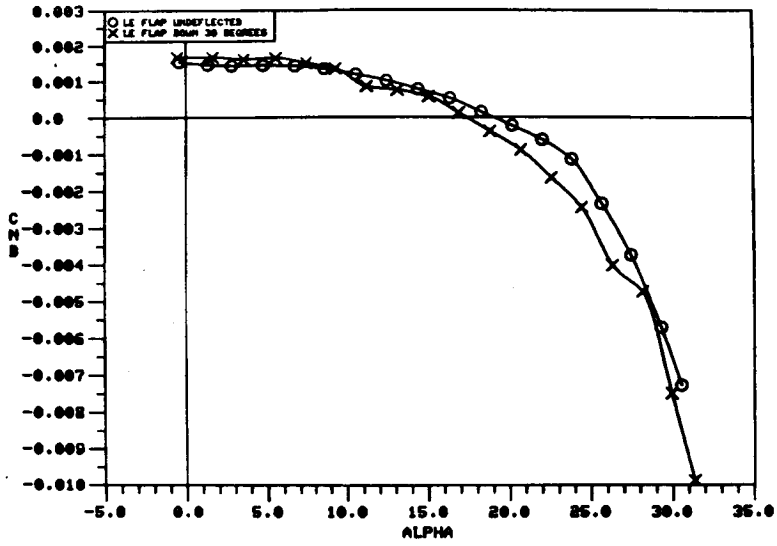

b) C_{n_β} vs. α

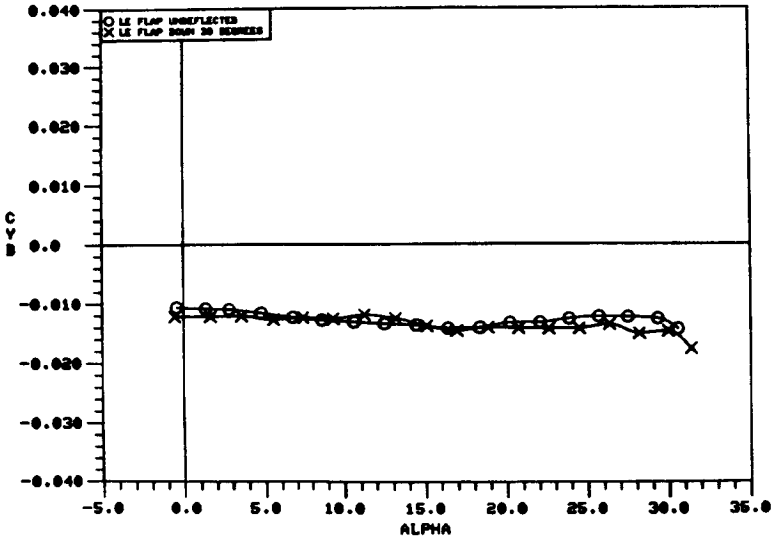

c) C_{Y_β} vs. α

Figure 53. Effect of Deflected Vortex Flap on the Static Lateral-Directional Stability Characteristics of the 60-Degree Cropped Delta Wing.

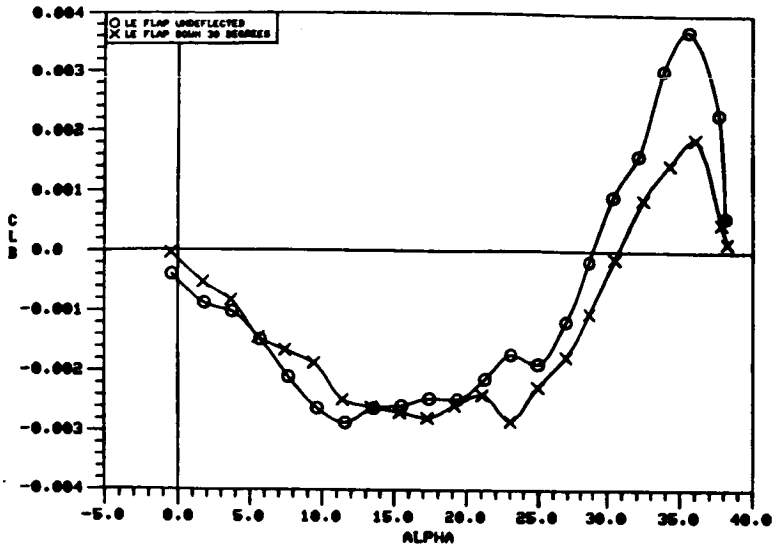

O LE FLAP UNDEFLECTED
X LE FLAP DOWN 30 DEGREES

a) C_{ℓ_β} vs. α

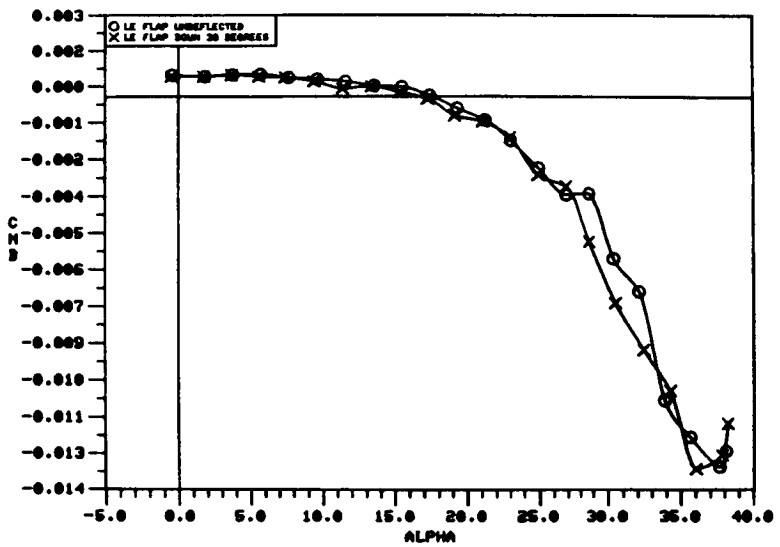

b) C_{n_β} vs. α

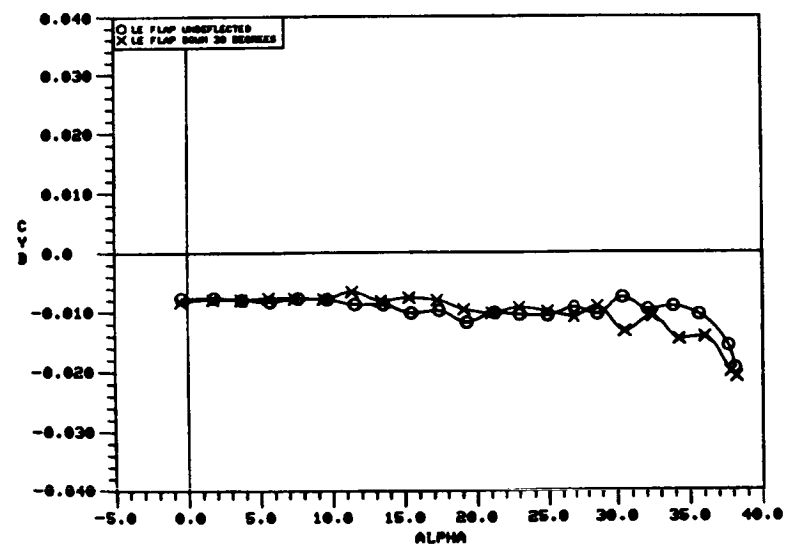

c) C_{Y_β} vs. α

Figure 54. Effect of Deflected Vortex Flap on the Static Lateral-Directional Stability Characteristics of the 65-Degree Cropped Delta Wing.

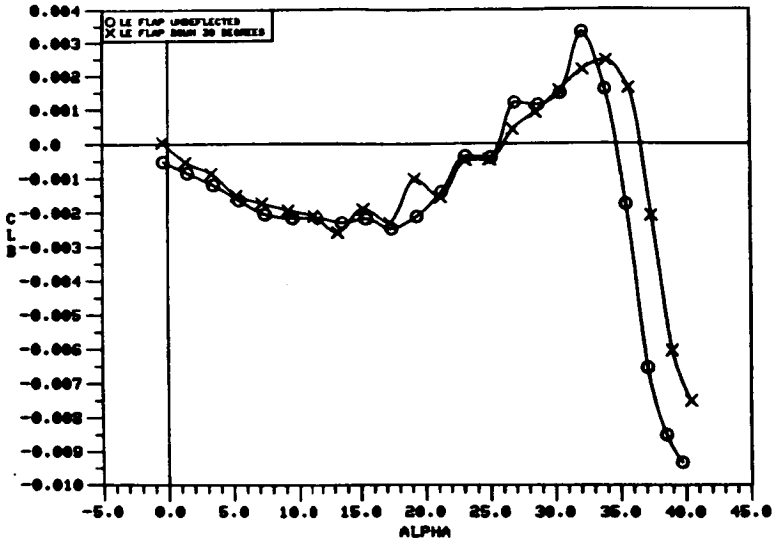

O LE FLAP UNDEFLECTED
X LE FLAP DOWN 30 DEGREES

a) C_{ℓ_β} vs. α

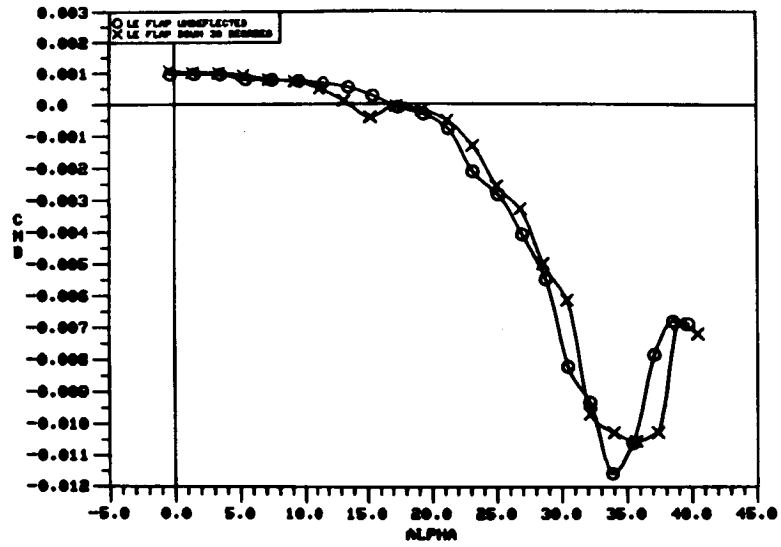

b) C_{n_β} vs. α

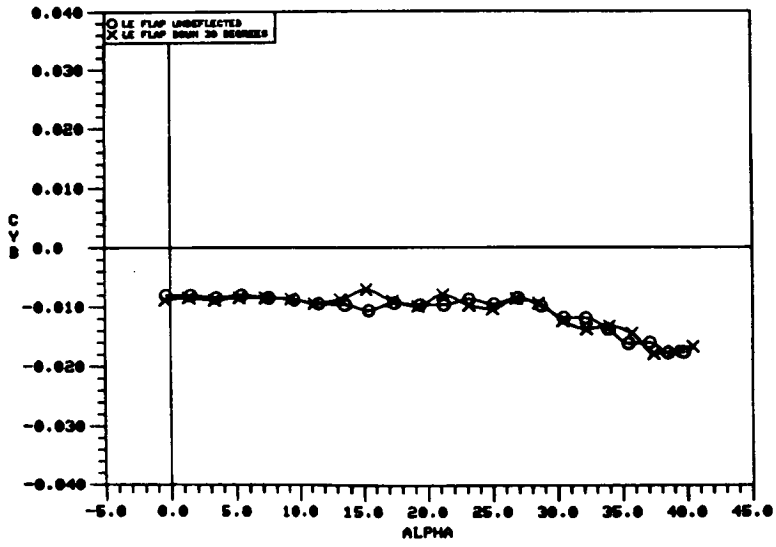

c) C_{Y_β} vs. α

Figure 55. Effect of Deflected Vortex Flap on the Static Lateral-Directional Stability Characteristics of the 65-Degree Cropped Delta Wing with Part-Span Flap.

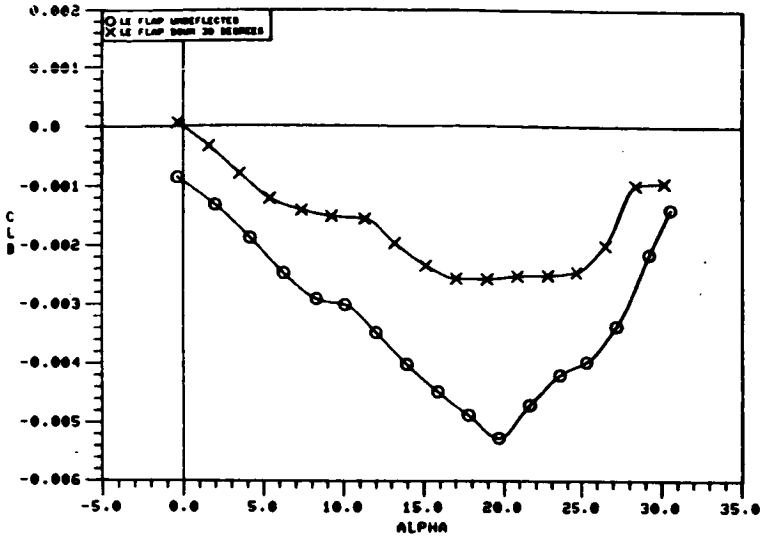

a) C_{ℓ_β} vs. α

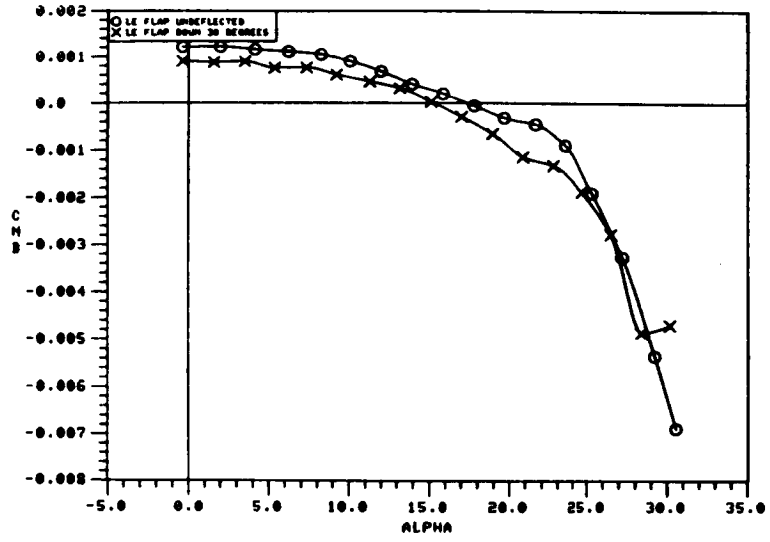

b) C_{n_β} vs. α

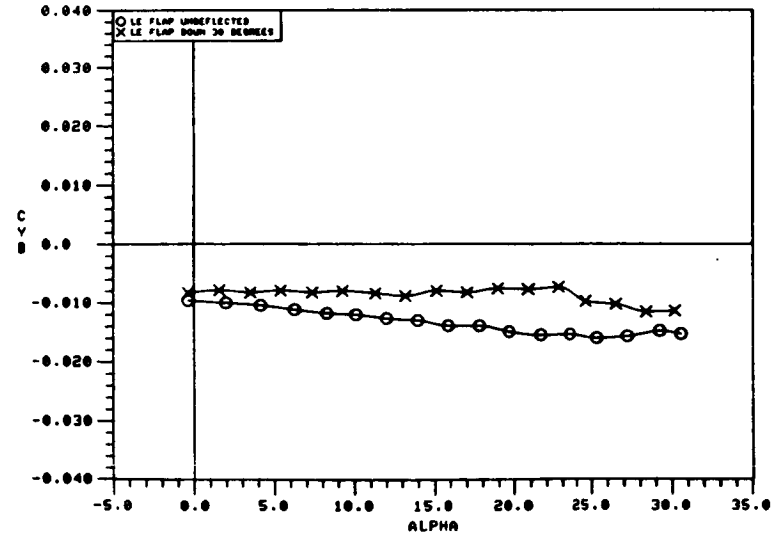

c) C_{Y_β} vs. α

Figure 56. Effect of Deflected Vortex Flap on the Static Lateral-Directional Stability Characteristics of the 70-Degree Cropped Delta Wing

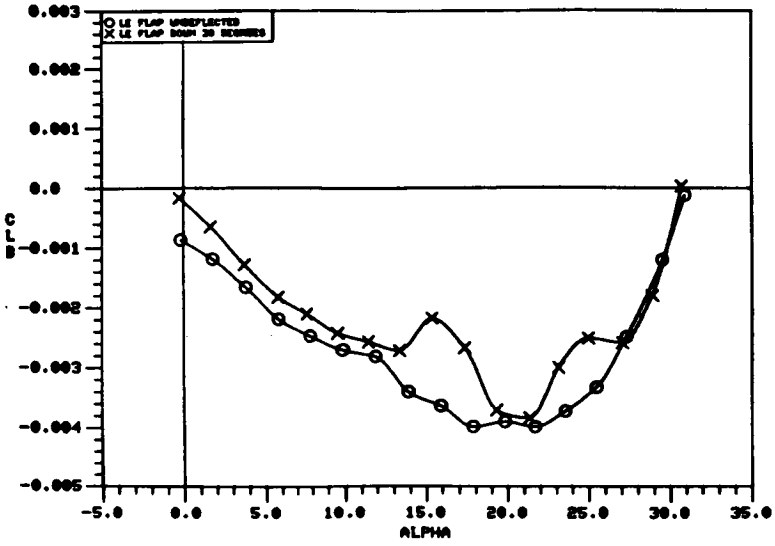

a) C_{ℓ_β} vs. α

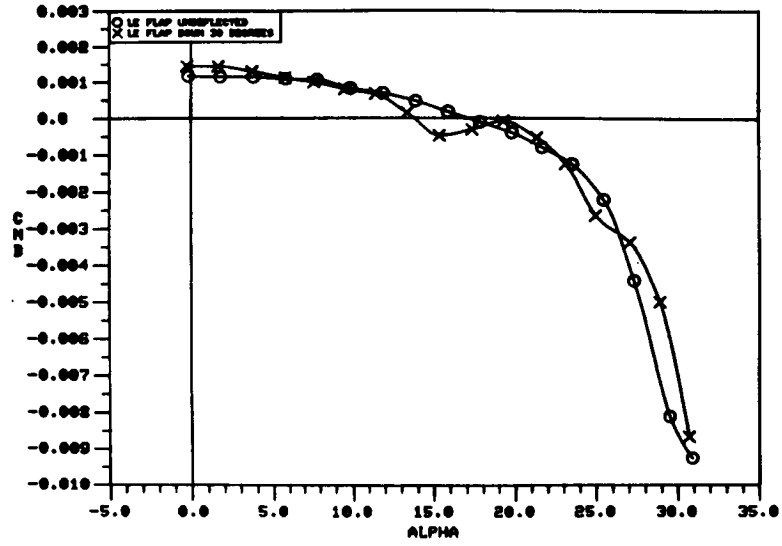

b) C_{n_β} vs. α

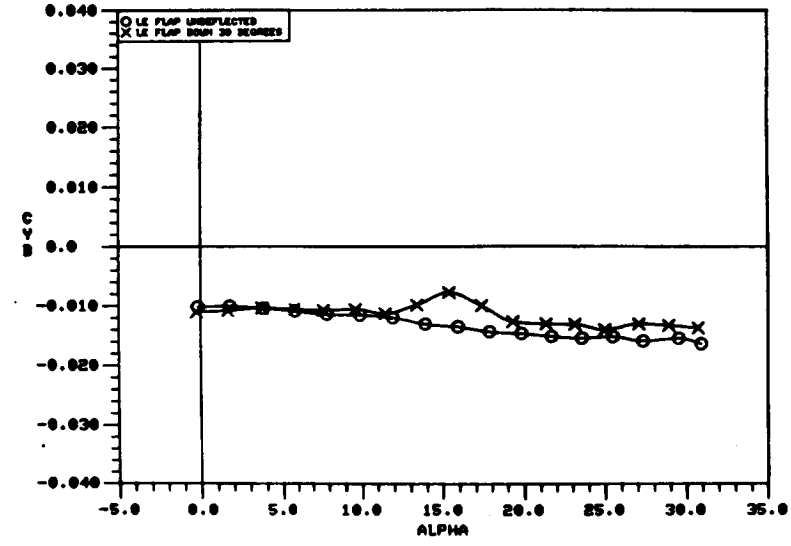

c) C_{Y_β} vs. α

Figure 57. Effect of Deflected Vortex Flap on the Static Lateral-Directional Stability Characteristics of the 70-Degree Cropped Delta Wing with Part-Span Flap.

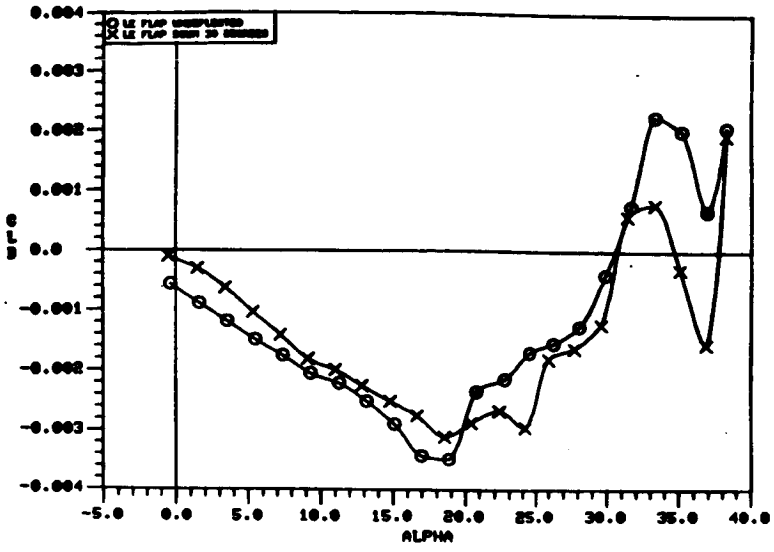

a) C_{ℓ_β} vs. α

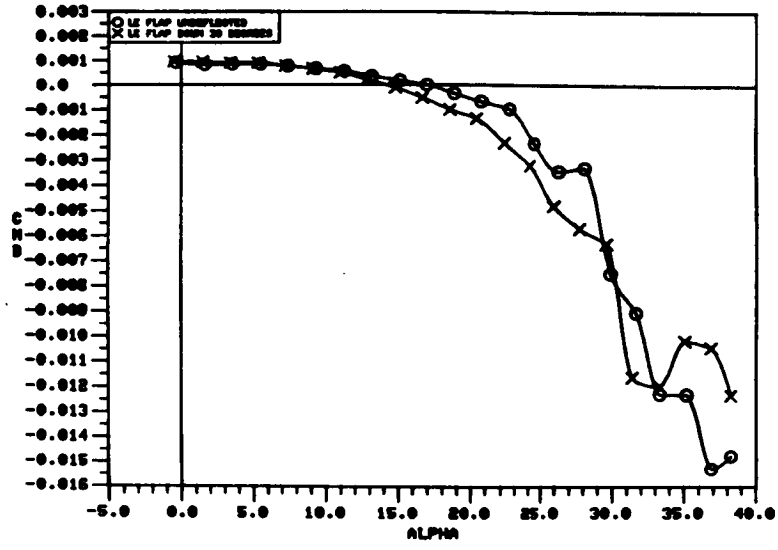

b) C_{n_β} vs. α

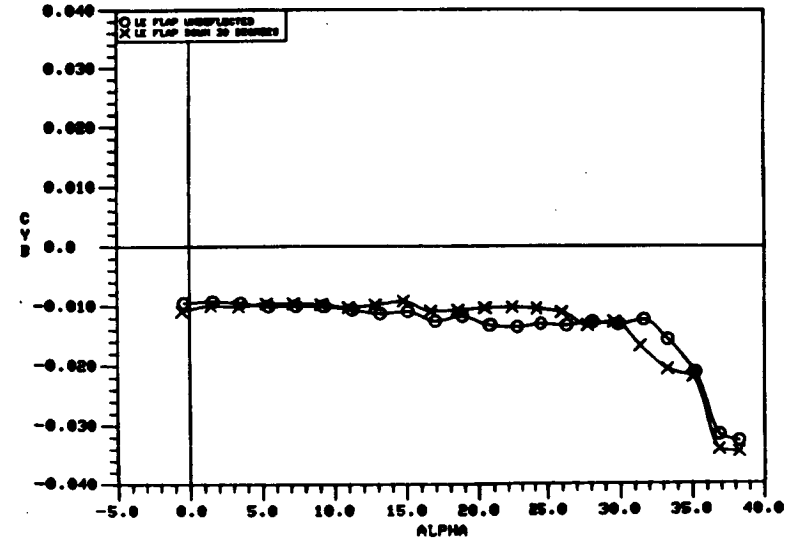

c) C_{Y_β} vs. α

Figure 58. Effect of Deflected Vortex Flap on the Static Lateral-Directional Stability Characteristics of the 70/50-Degree Cranked Wing

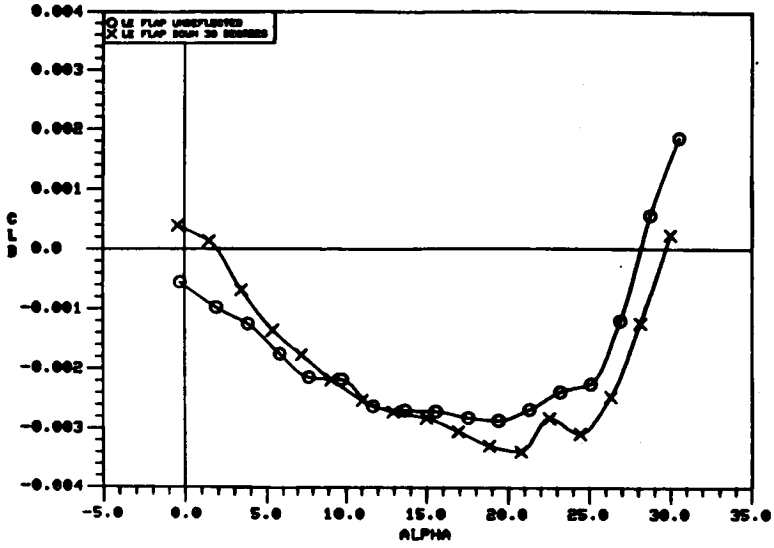

a) C_{ℓ_β} vs. α

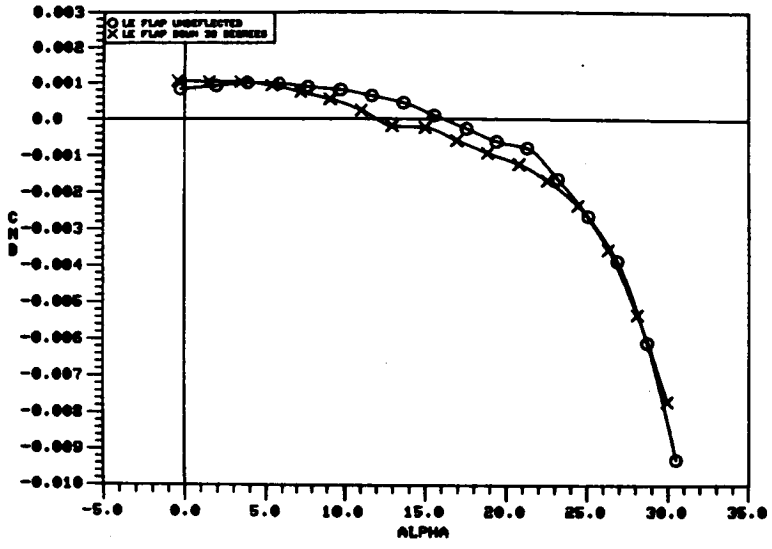

b) C_{n_β} vs. α

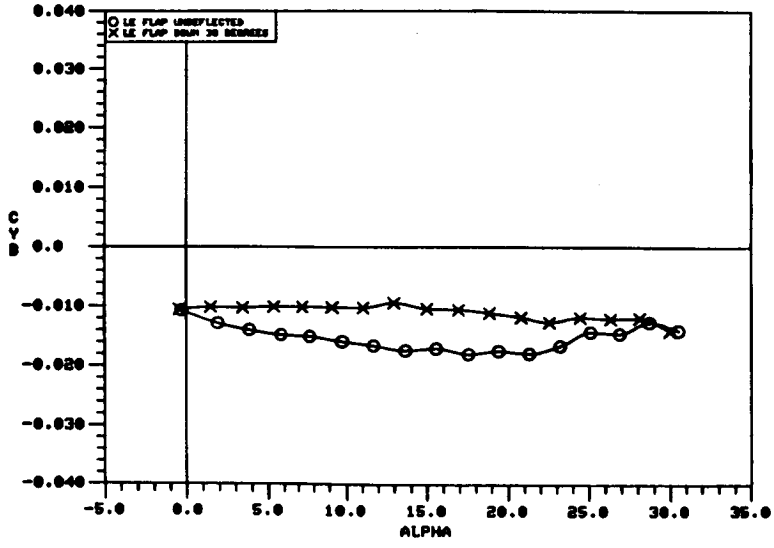

c) C_{Y_β} vs. α

Figure 59. Effect of Deflected Vortex Flap on the Static Lateral-Directional Stability Characteristics of the 70/50-Degree Cranked Wing with Part-Span Flap.

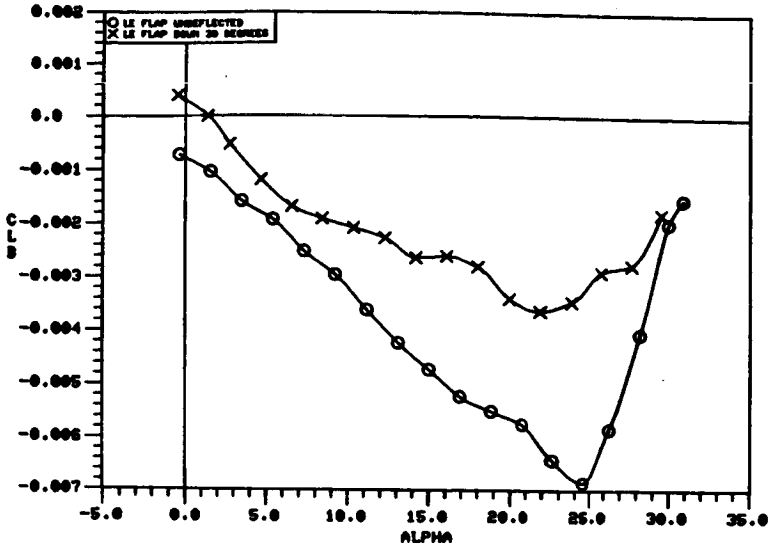

a) C_{ℓ_β} vs. α

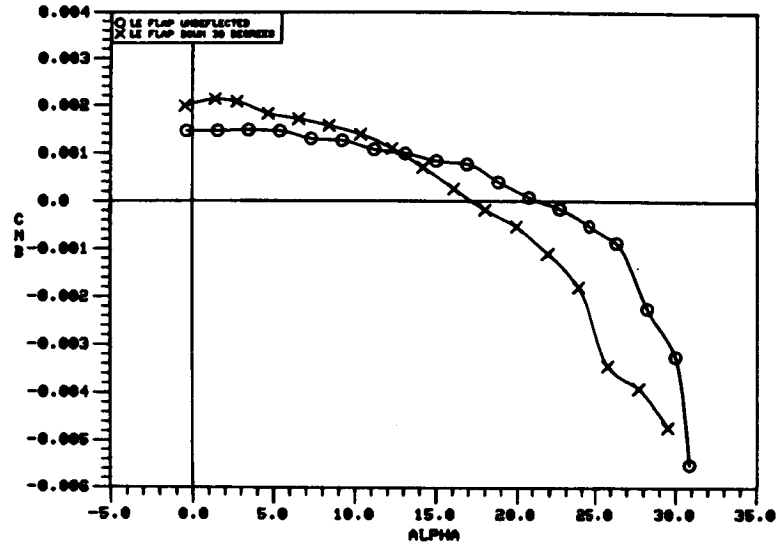

b) C_{n_β} vs. α

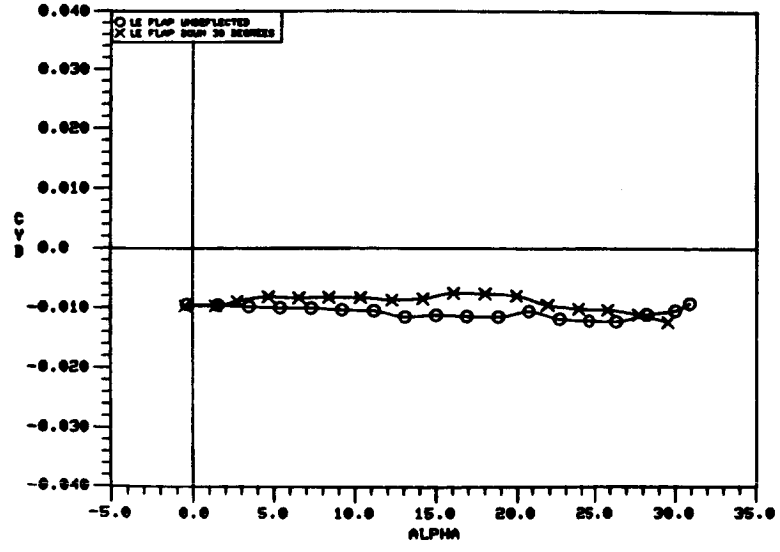

c) C_{Y_β} vs. α

Figure 60. Effect of Deflected Vortex Flap on the Static Lateral-Directional Stability Characteristics of the 76.5/66.5-Degree Cranked Wing

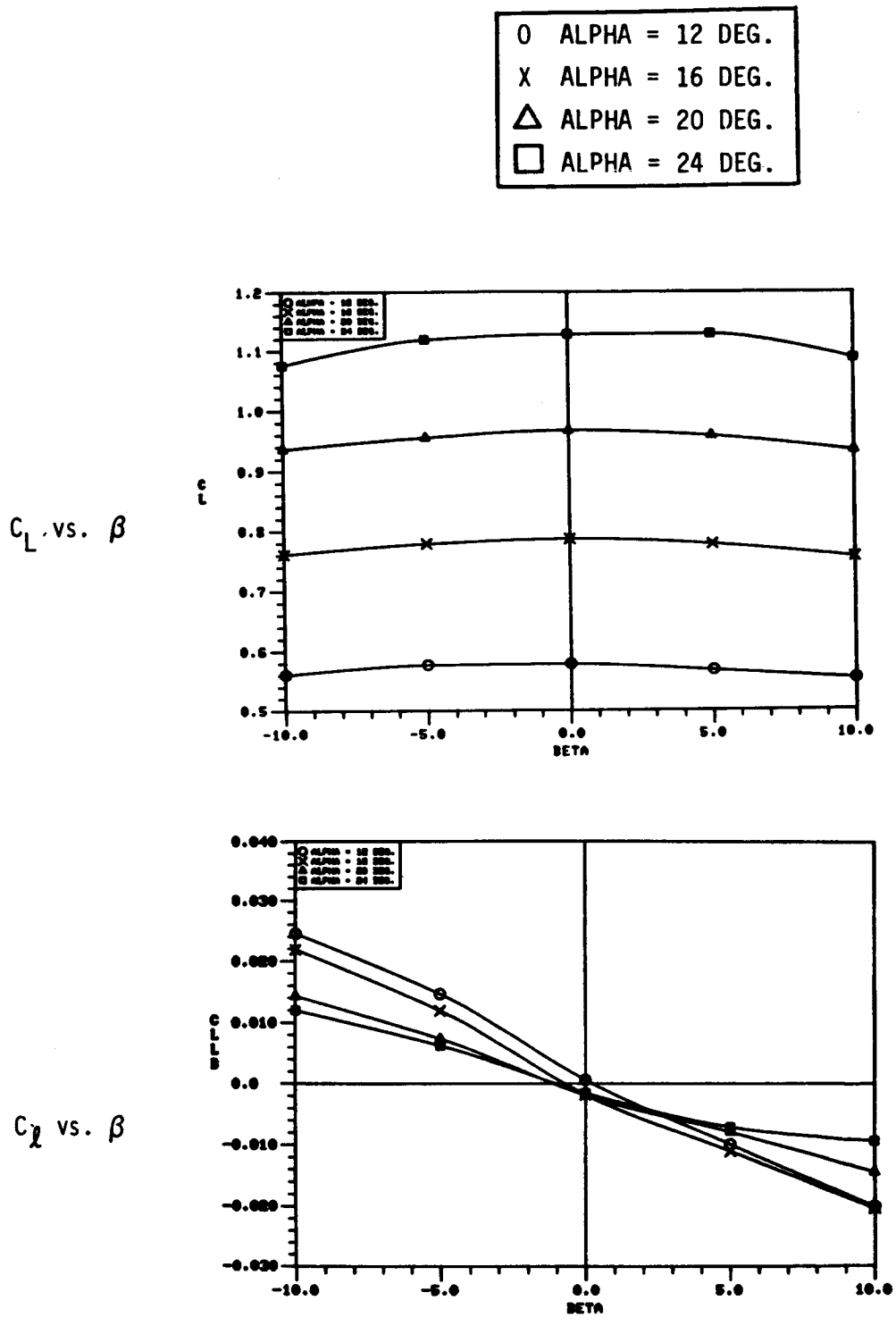

Figure 61. Effect of Deflected Vortex Flap on the 50-Degree Cropped Delta Wing Lift and Rolling Moment Variation with Sideslip.

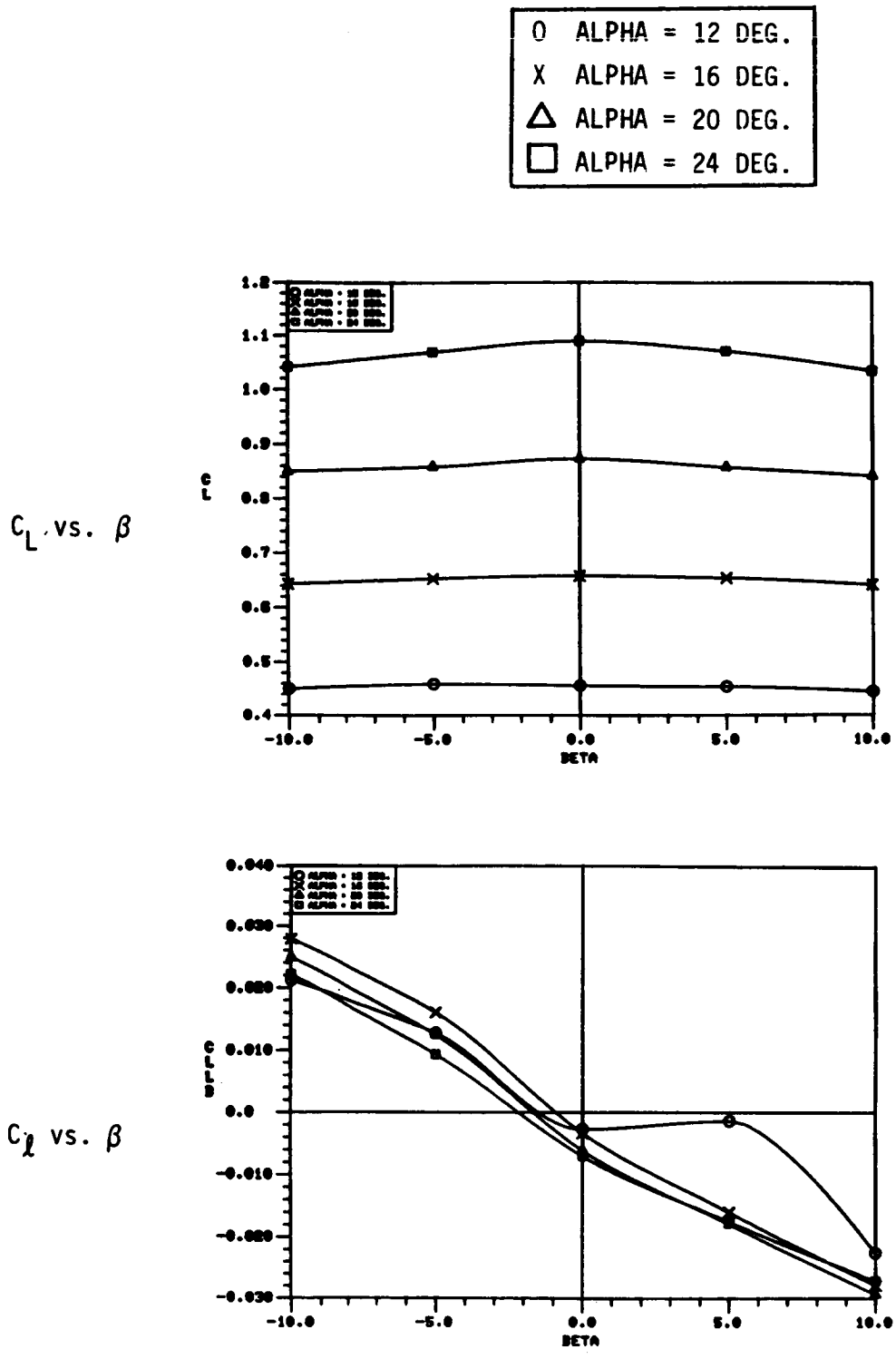

Figure 62. Effect of Angle of Attack on the 65-Degree Cropped Delta Wing Lift and Rolling Moment Variation with Sideslip.

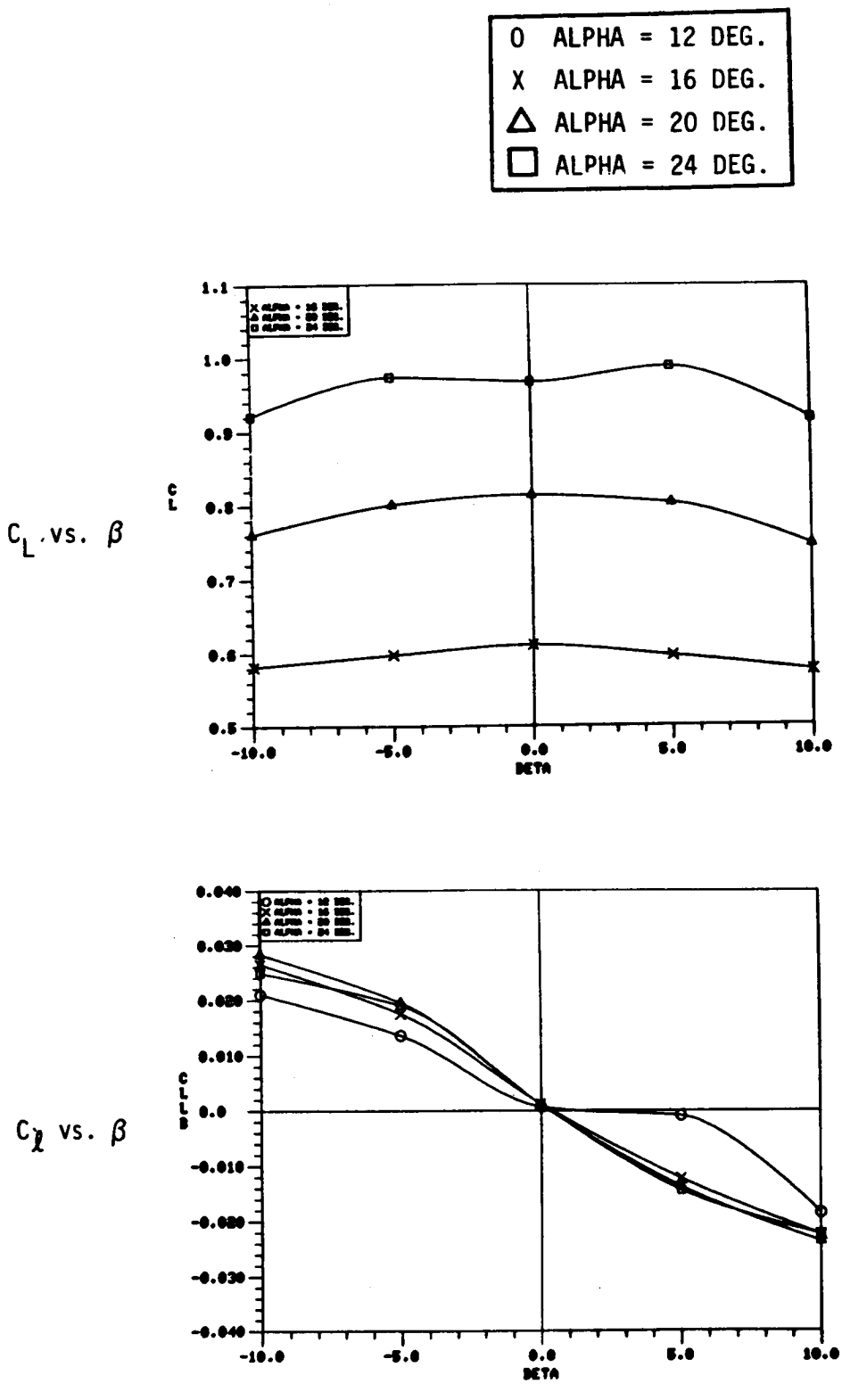

Figure 63. Effect of Angle of Attack on the 70/50-Degree Cranked Wing Lift and Rolling Moment Variation with Sideslip.

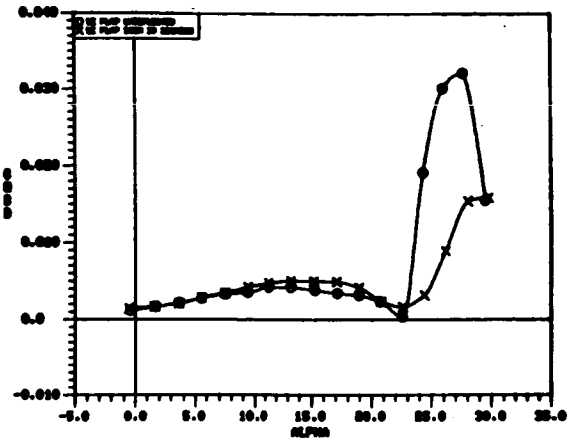

O LE FLAP UNDEFLECTED
X LE FLAP DOWN 30 DEGREES

$C_{n_{\beta_{dyn}}}$ vs α

Figure 64. Effect of Deflected Vortex Flap on the 50-Degree Cropped Delta Wing Dynamic Directional Stability Parameter.

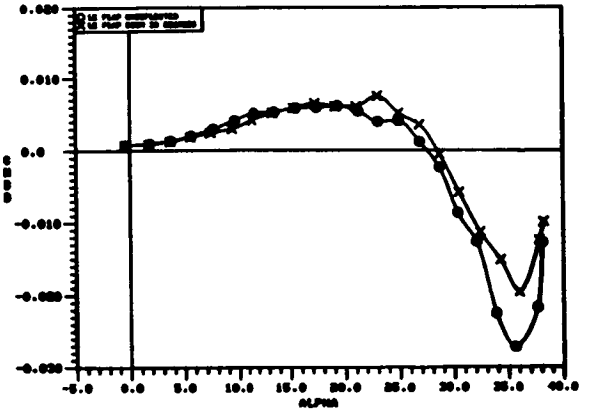

$C_{n_{\beta_{dyn}}}$ vs α

Figure 65. Effect of Deflected Vortex Flap on the 65-Degree Cropped Delta Wing Dynamic Directional Stability Paremeter.

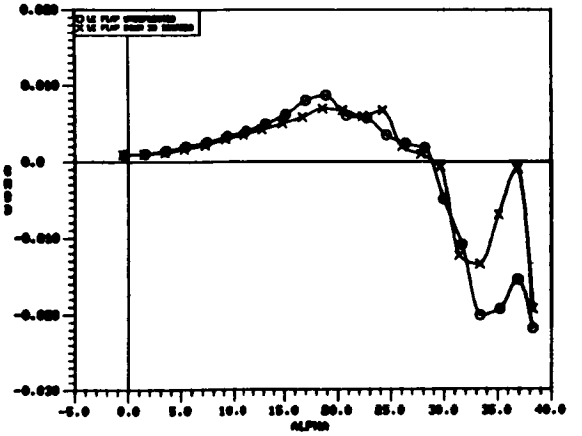

$C_{n_{\beta_{dyn}}}$ vs α

Figure 66. Effect of Deflected Vortex Flap on the 70/50-Degree Cranked Wing Dynamic Directional Stability Parameter.

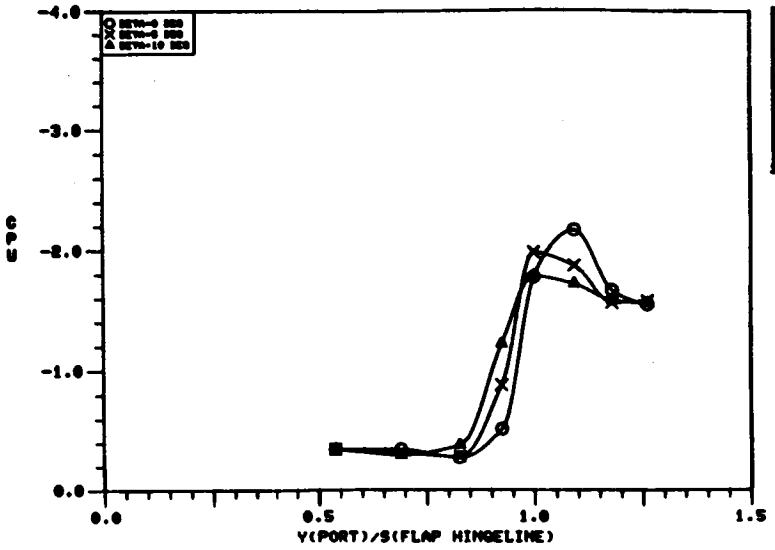

O BETA = 0 DEG.
X BETA = 5 DEG.
△ BETA = 10 DEG.

a) Windward Wing,
α = 16 , x/c = .405

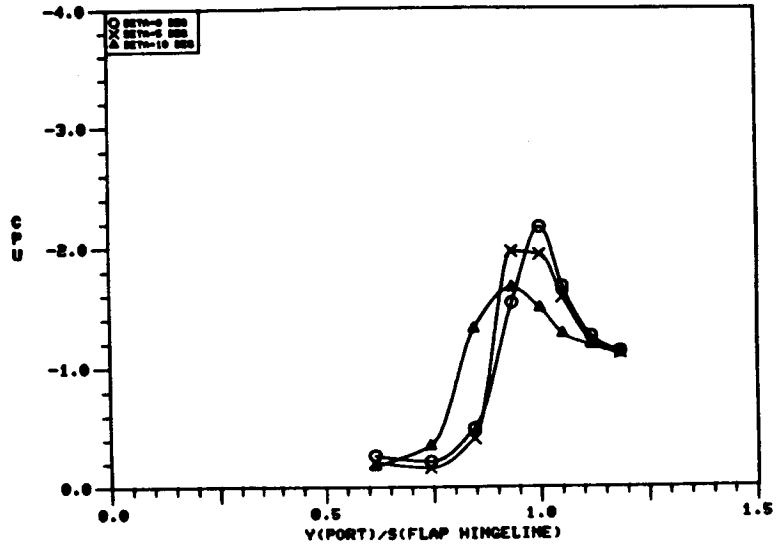

b) Windward Wing,
α = 16 , x/c = .576

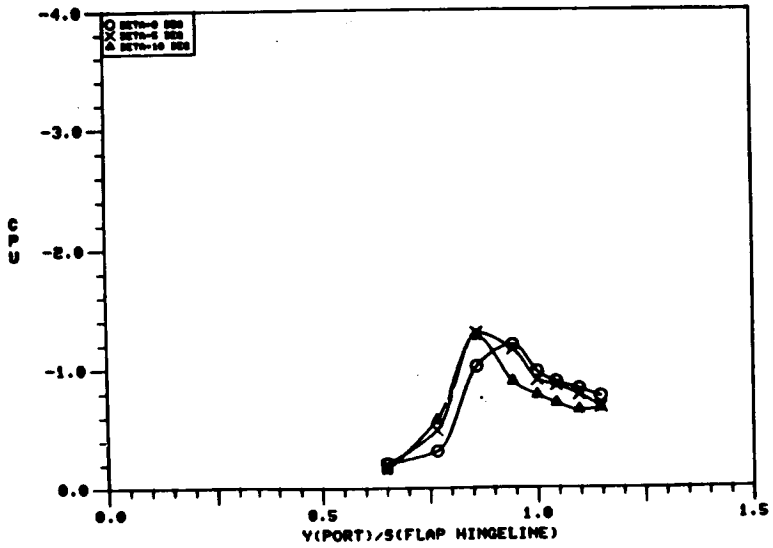

c) Windward Wing,
α = 16 , x/c = .748

Figure 67. Effect of Sideslip Angle on the 65-Degree Cropped Delta Wing Upper Surface Static Pressure Distributions at α = 16°, Vortex Flap Deflected to 30°.

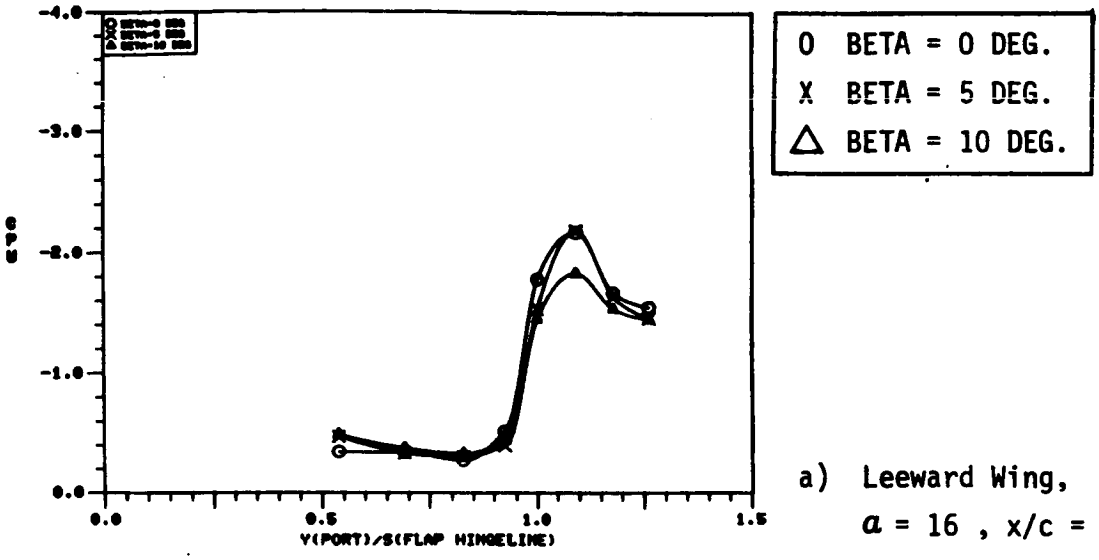

a) Leeward Wing, α = 16 , x/c = .405

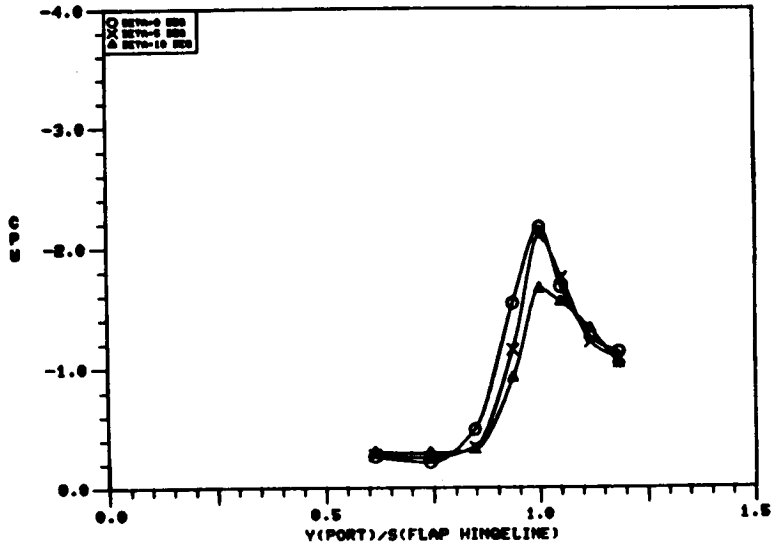

b) Leeward Wing, α = 16 , x/c = .576

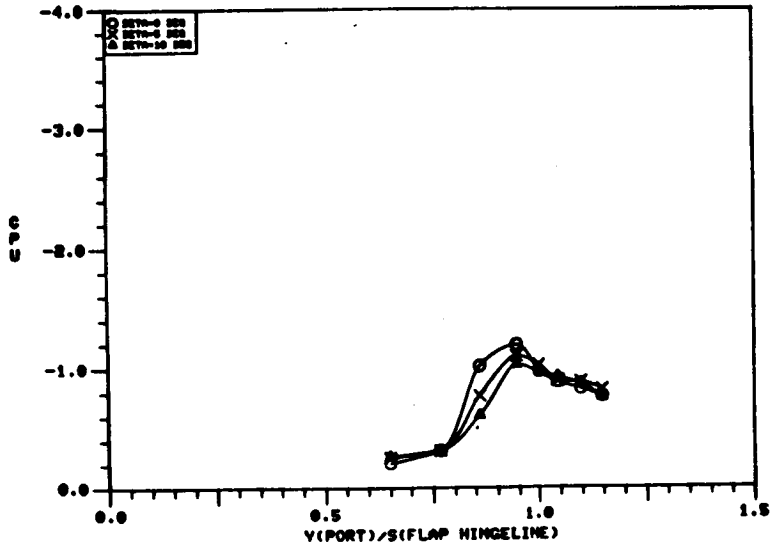

c) Leeward Wing, α = 16 , x/c = .748

Figure 67. Concluded

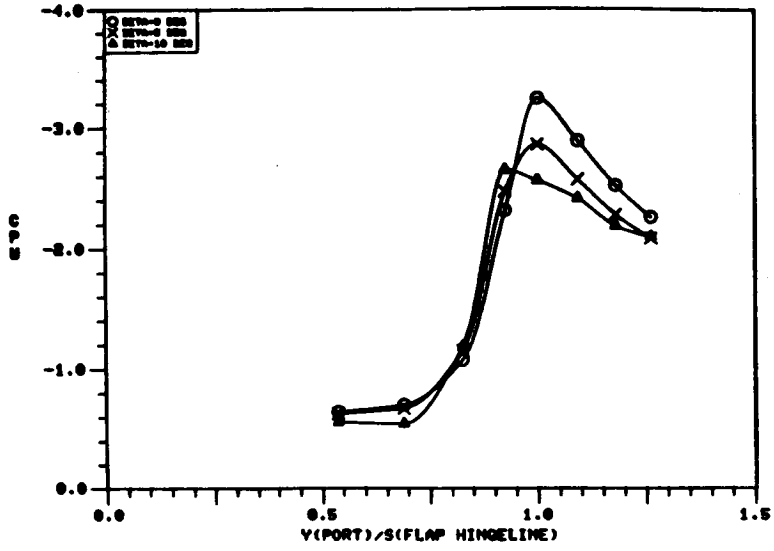

O	BETA = 0 DEG.
X	BETA = 5 DEG.
Δ	BETA = 10 DEG.

a) Windward Wing, α = 24, x/c = .405

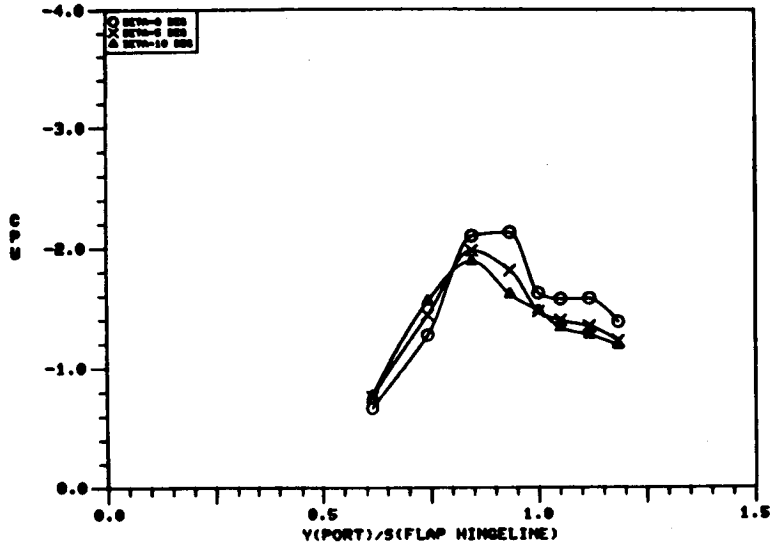

b) Windward Wing, α = 24, x/c = .576

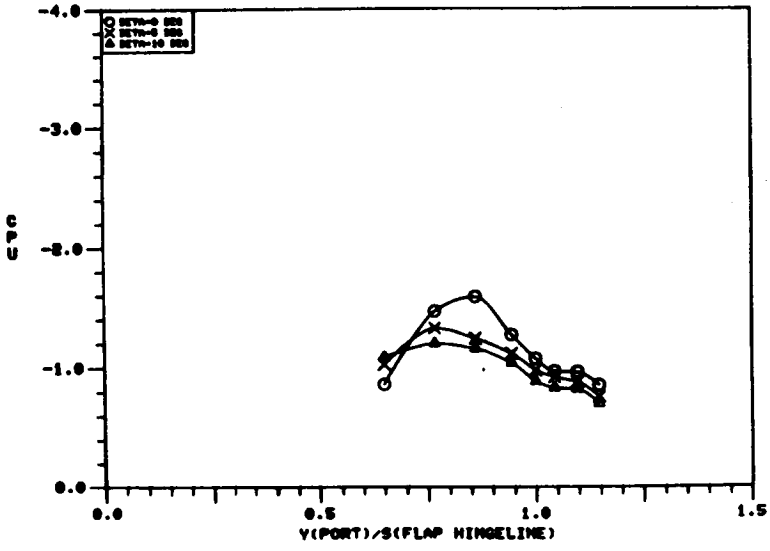

c) Windward Wing, α = 24, x/c = .748

Figure 68. Effect of Sidelsip Angle on the 65-Degree Cropped Delta Wing Upper Surface Static Pressure Distributions at α = 24°, Vortex Flap Deflected to 30°.

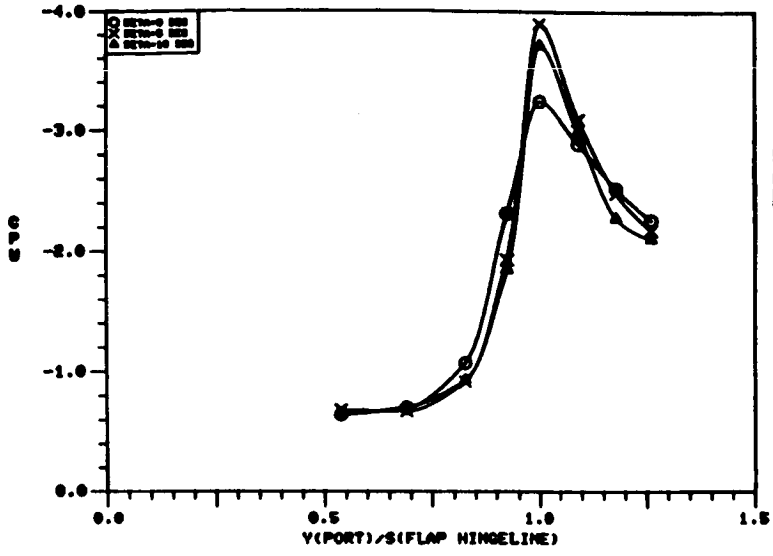

O BETA = 0 DEG.

X BETA = 5 DEG.

Δ BETA = 10 DEG.

a) Leeward Wing, α = 24, x/c = .405

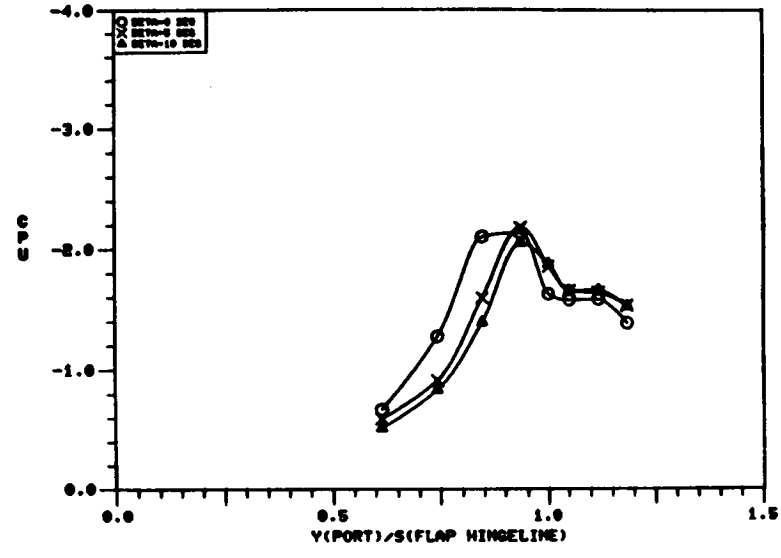

b) Leeward Wing, α = 24, x/c = .576

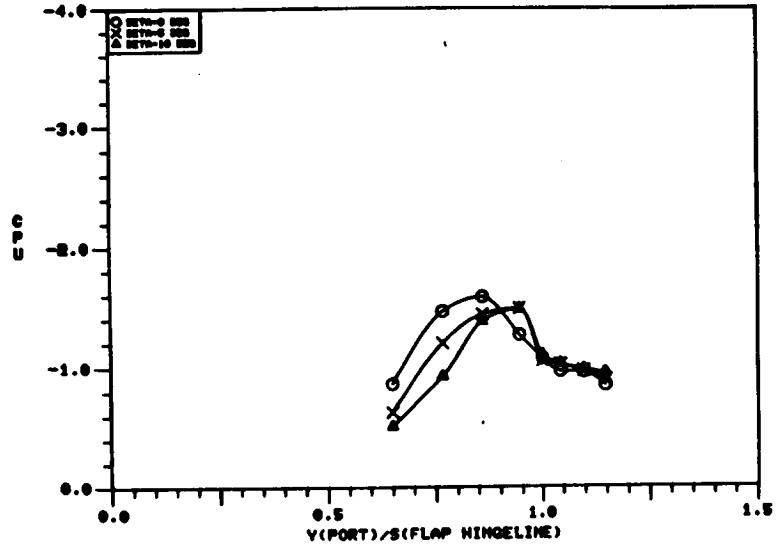

c) Leeward Wing, α = 24, x/c = .748

Figure 68. Concluded.

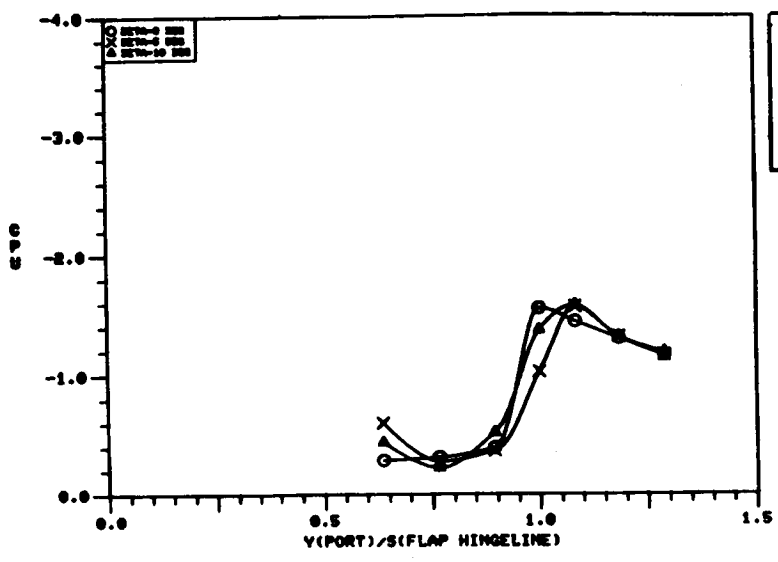

O BETA = 0 DEG.
X BETA = 5 DEG.
△ BETA = 10 DEG.

a) Windward Wing, α = 16 , x/c = .422

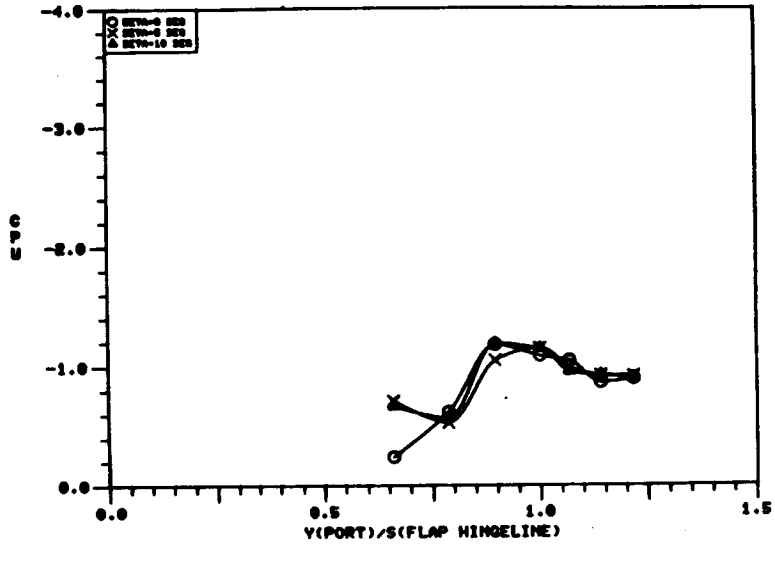

b) Windward Wing, α = 16 , x/c = .678

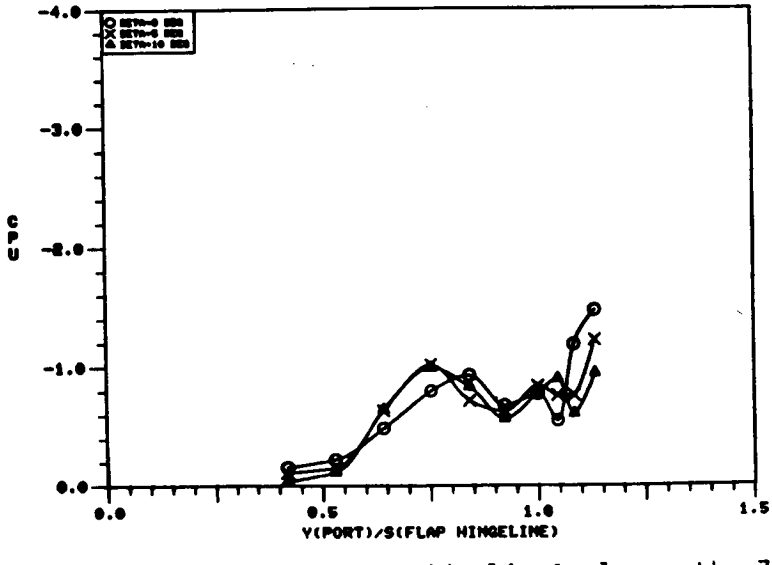

c) Windward Wing, α = 16 , x/c = .848

Figure 69. Effect of Sideslip Angle on the 70/50-Degree Cranked Wing Upper Surface Static Pressure Distributions at α= 16°, Vortex Flap Deflected to 30°.

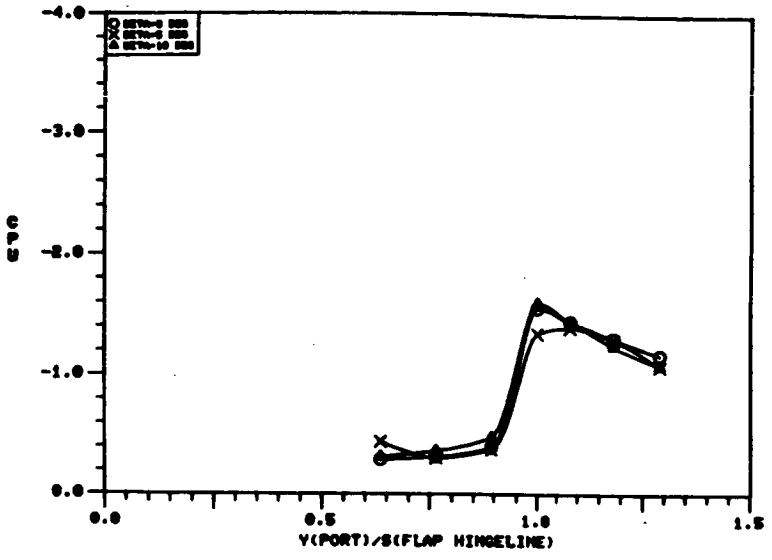

O BETA = 0 DEG.
X BETA = 5 DEG.
△ BETA = 10 DEG.

a) Leeward Wing,
α = 16 , x/c = .422

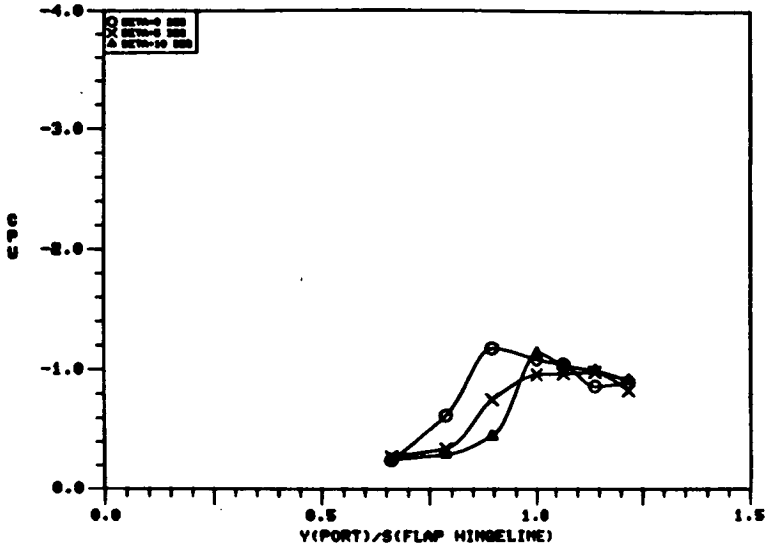

b) Leeward Wing,
α = 16 , x/c = .678

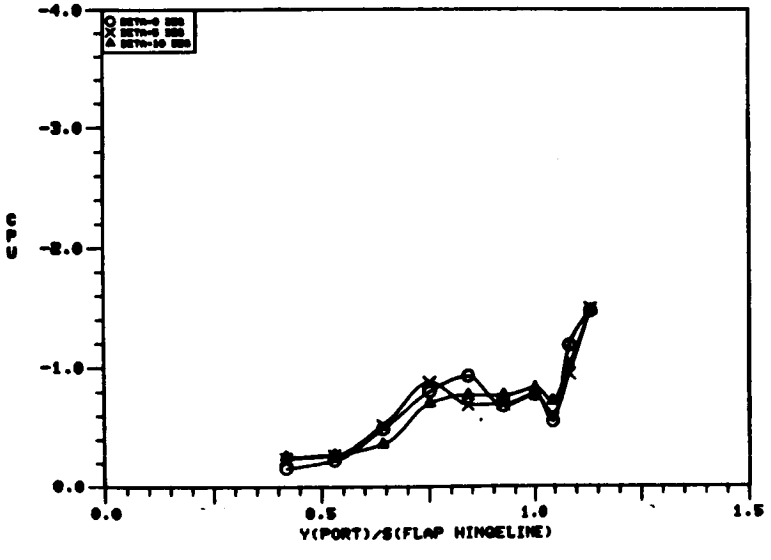

c) Leeward Wing,
α = 16 , x/c = .848

Figure 69. Concluded.

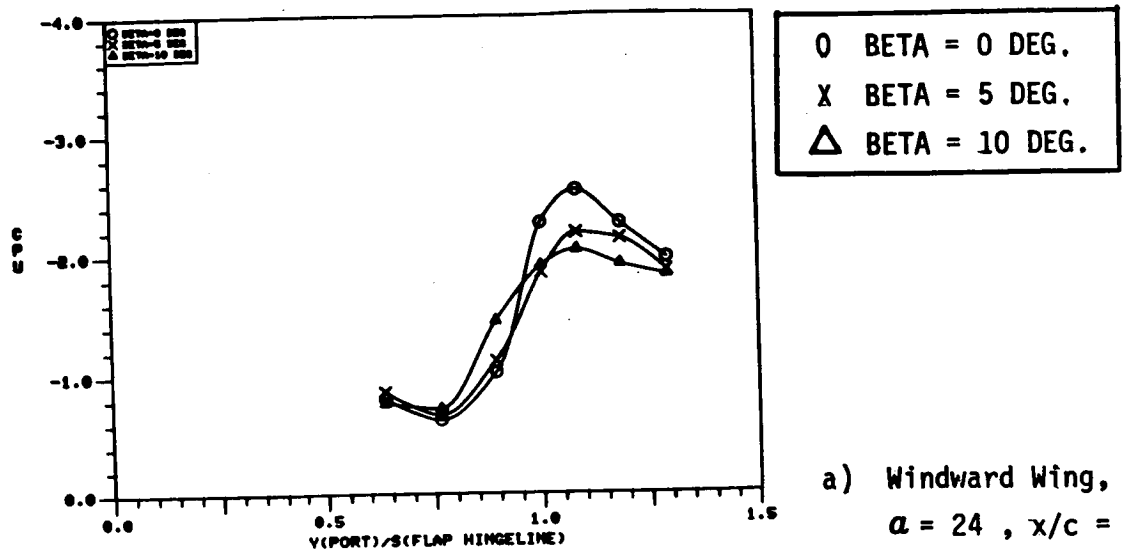

a) Windward Wing,
α = 24 , x/c = .422

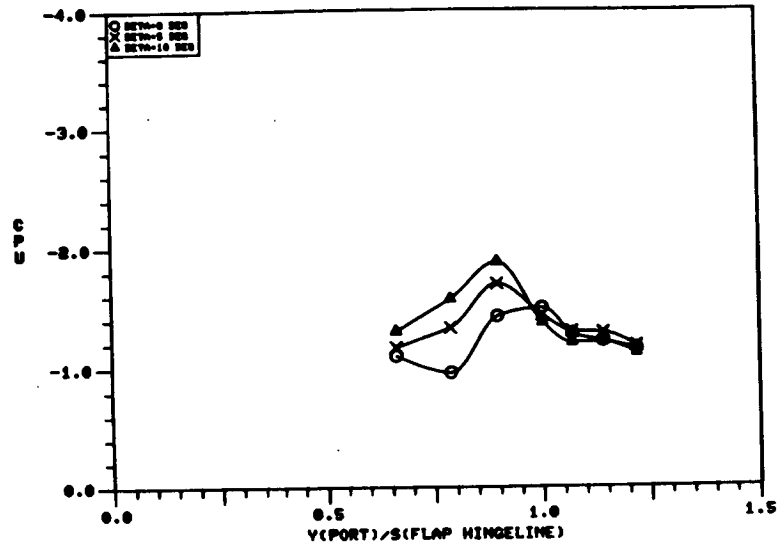

b) Windward Wing,
α = 24 , x/c = .678

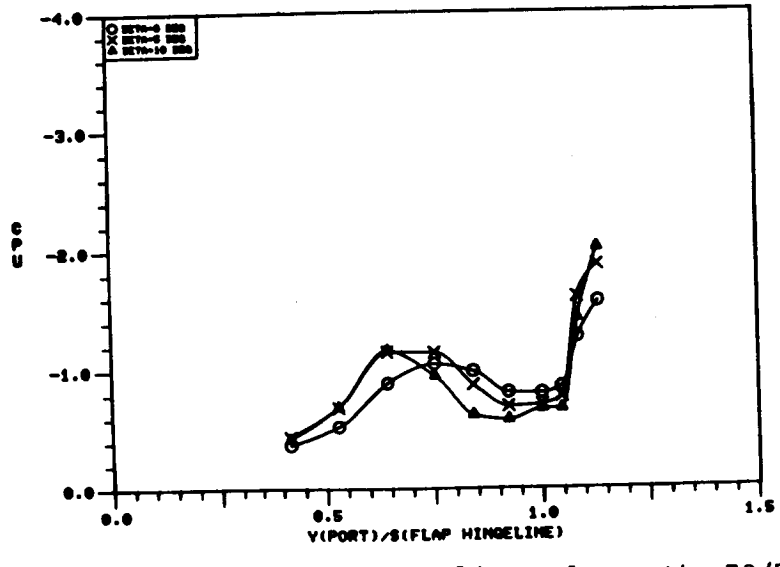

c) Windward Wing,
α = 24 , x/c = .848

Figure 70. Effect of Sideslip Angle on the 70/50-Degree Cranked Wing Upper Surface Static Pressure Distriutions at α= 24°, Vortex Flap Deflected to 30°.

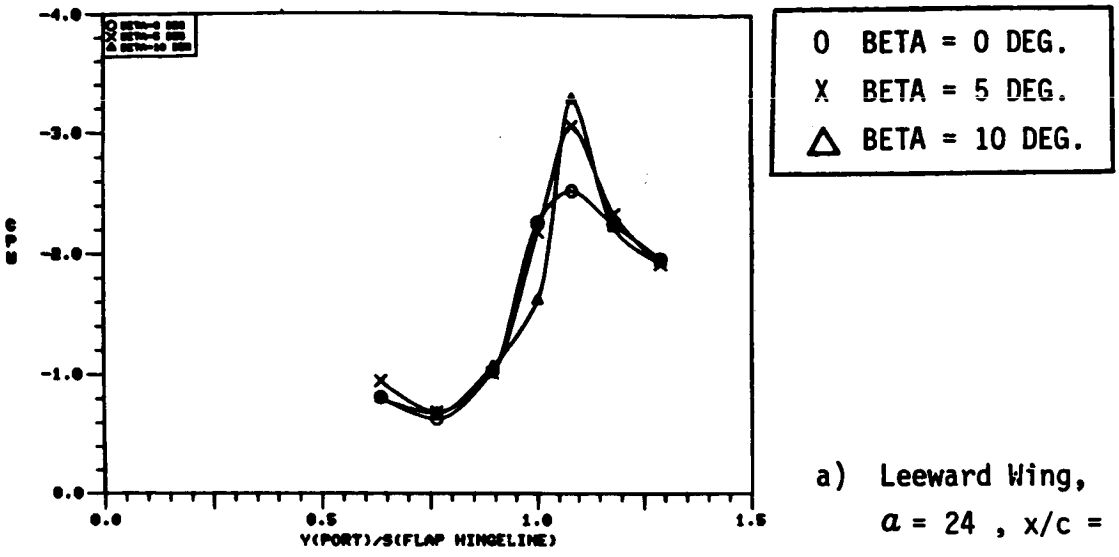

a) Leeward Wing,
α = 24 , x/c = .422

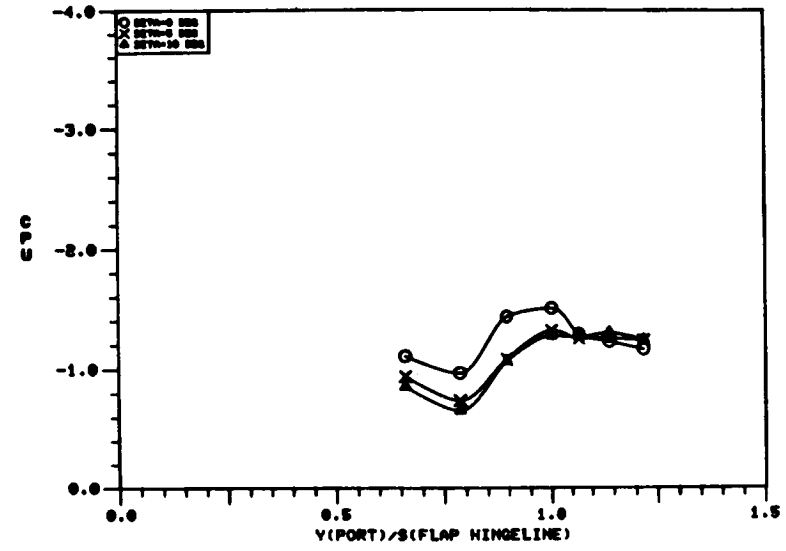

b) Leeward Wing,
α = 24 , x/c = .678

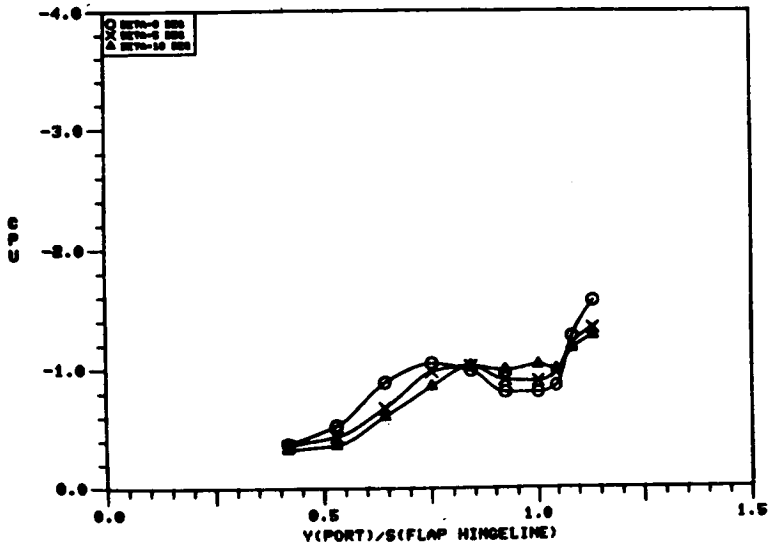

c) Leeward Wing,
α = 24 , x/c = .848

Figure 70. Concluded.

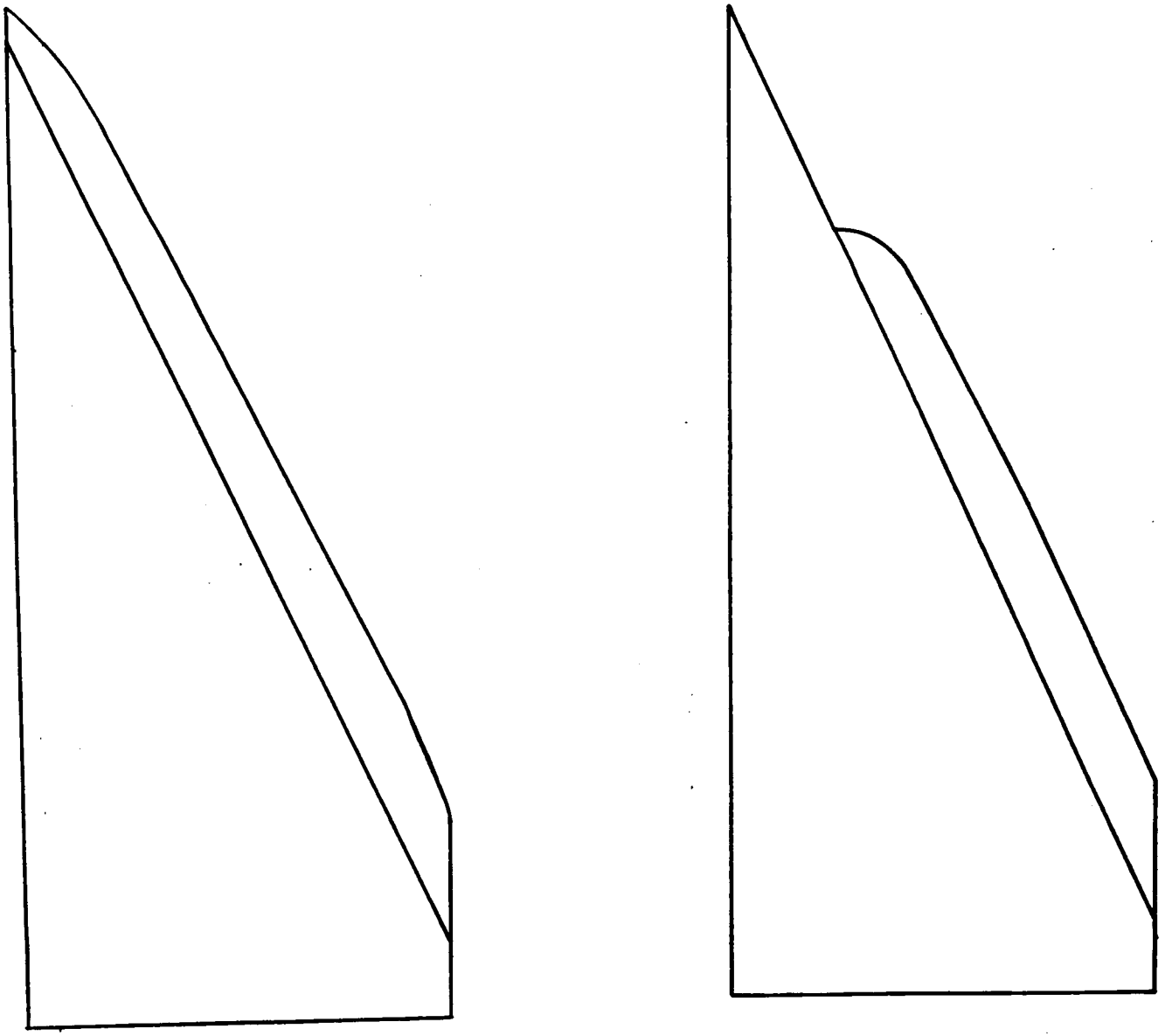

a) Full-Span Vortex Flap

b) Part-Span Vortex Flap

Figure 71. 65-Degree Cropped Delta Wing

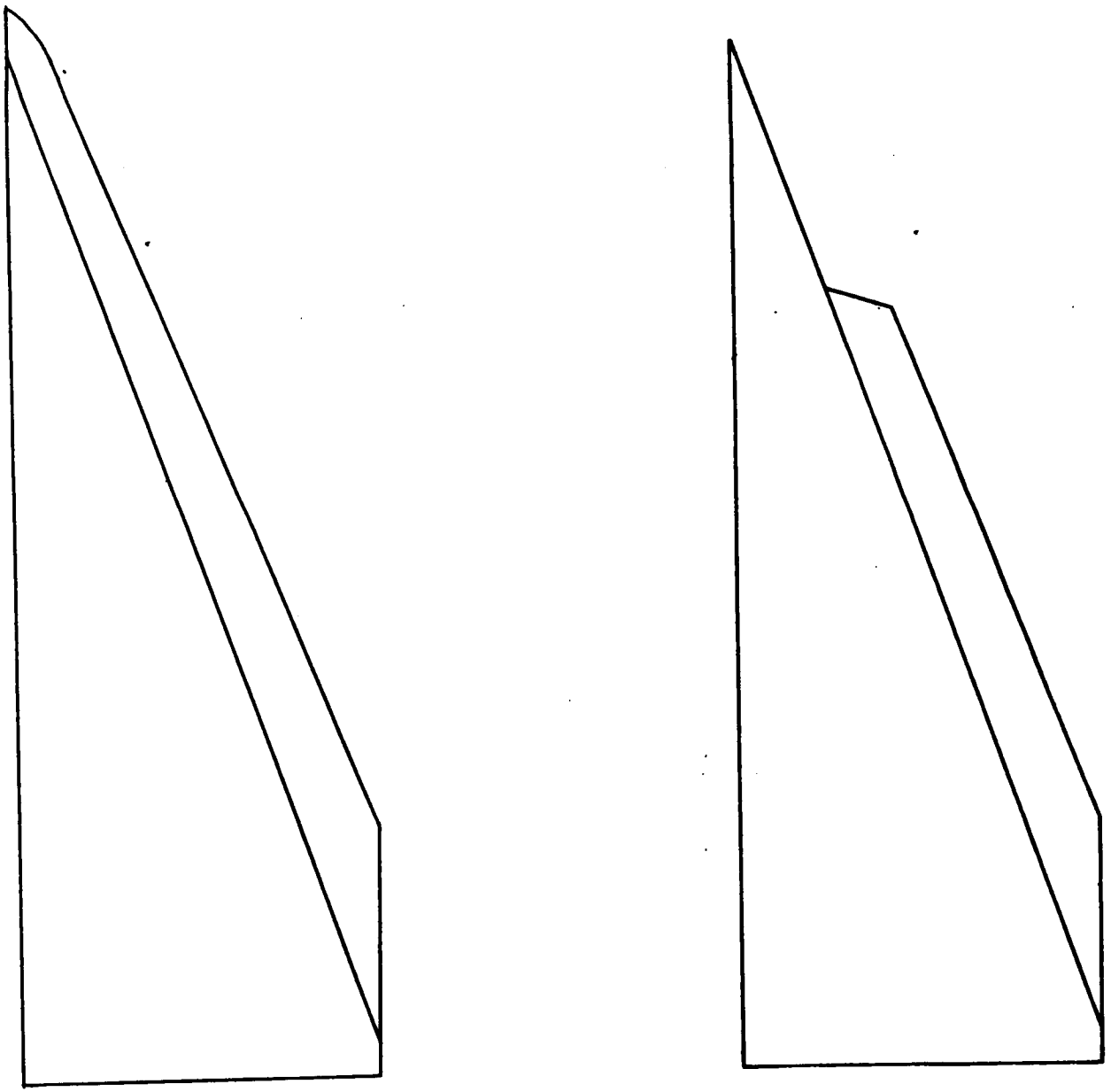

a) Full-Span Vortex Flap

b) Part-Span Vortex Flap

Figure 72. 70-Degree Cropped Delta Wing

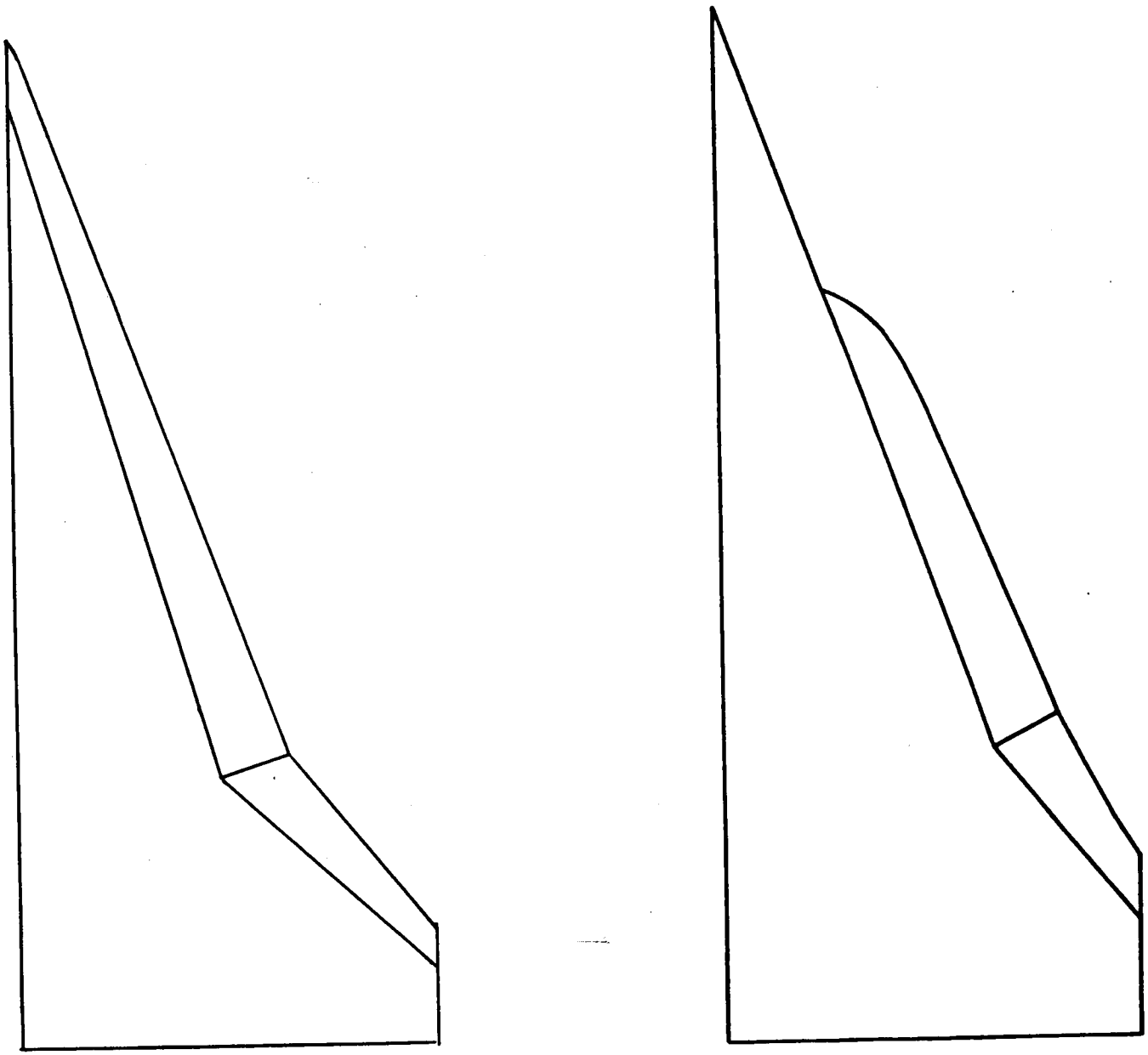

a) Full-Span Vortex Flap

b) Part-Span Vortex Flap

Figure 73. 70/50-Degree Cranked Wing

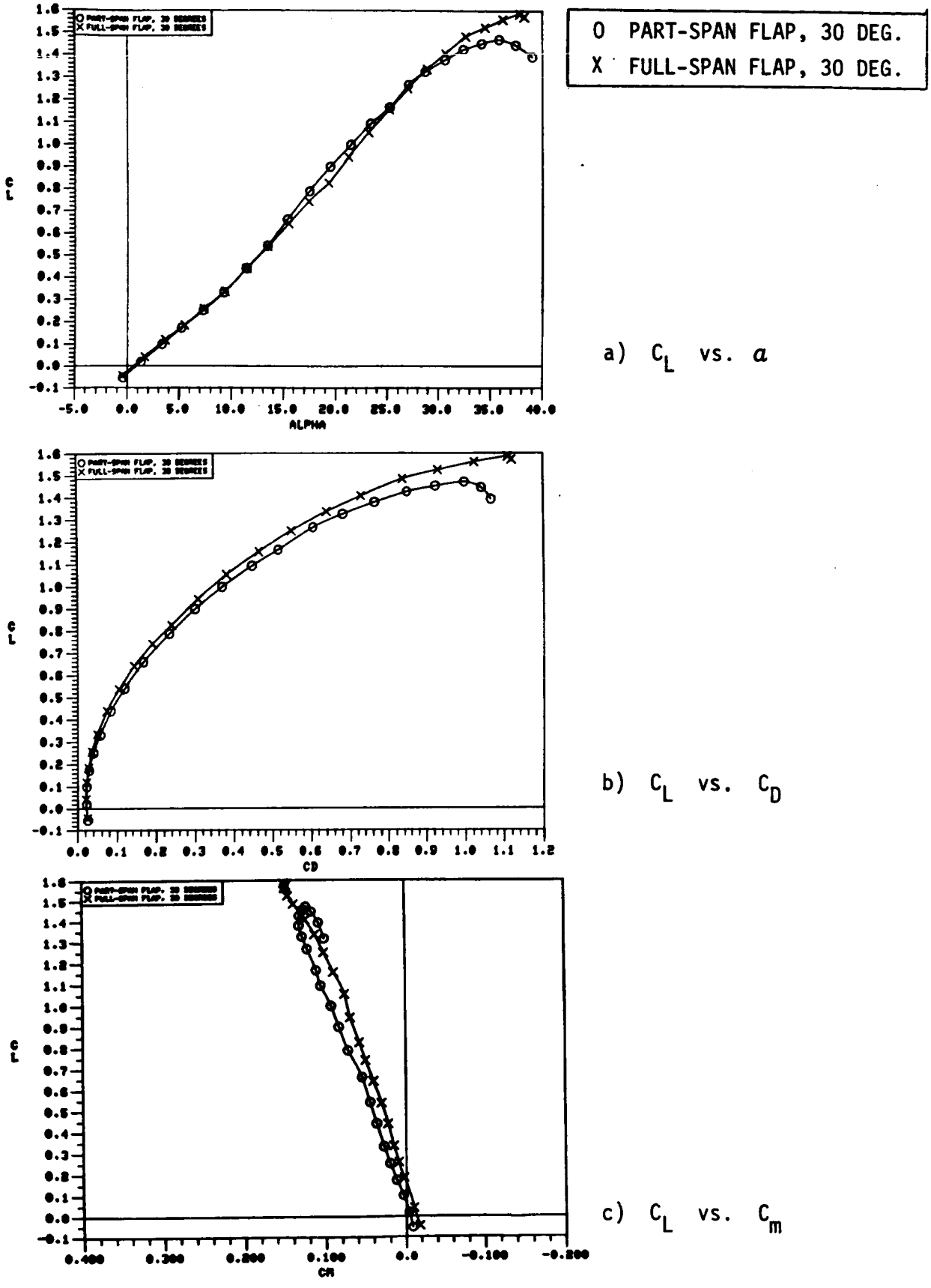

a) C_L vs. α

b) C_L vs. C_D

c) C_L vs. C_m

Figure 74. Comparison of the Static Longitudinal Aerodynamic Characteristics of the 65-degree Cropped Delta Wing with Full- and Part-Span Flaps.

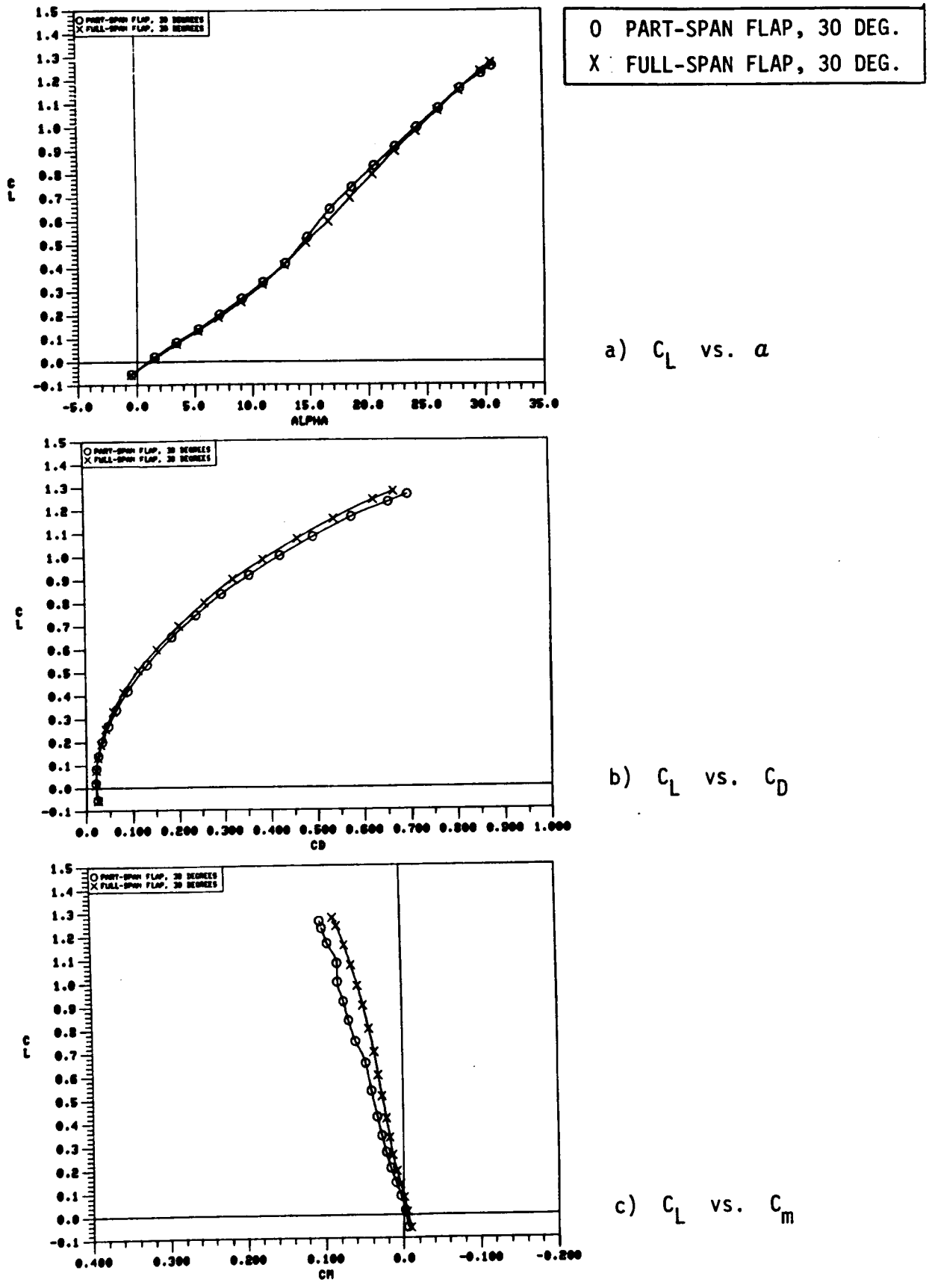

Figure 75. Comparison of the Static Longitudinal Aerodynamic Characteristics of the 70-Degree Cropped Delta Wing with Full- and Part-Span Flaps.

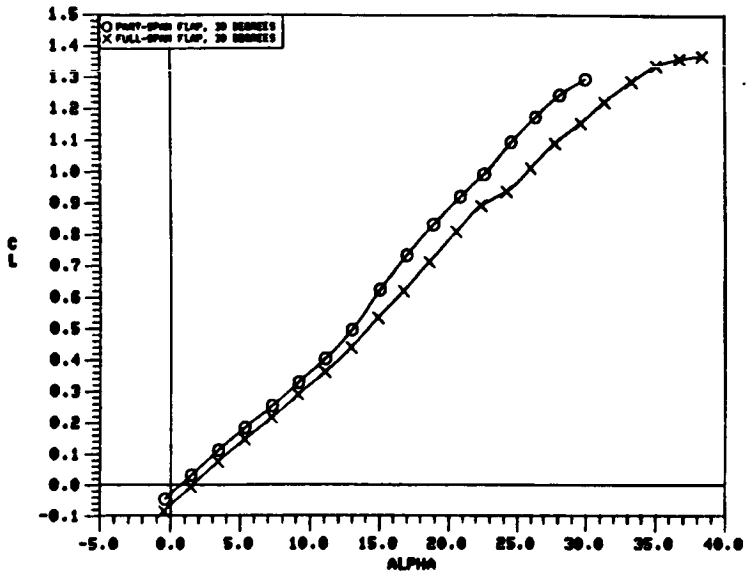

a) C_L vs. α

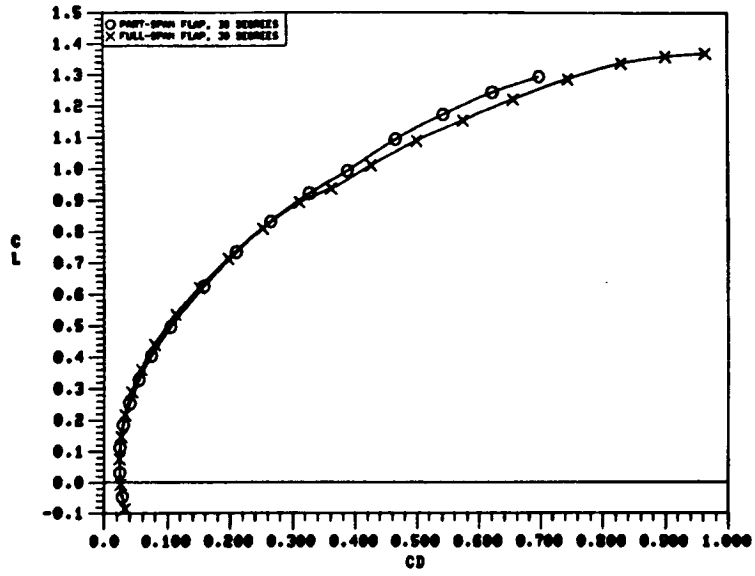

b) C_L vs. C_D

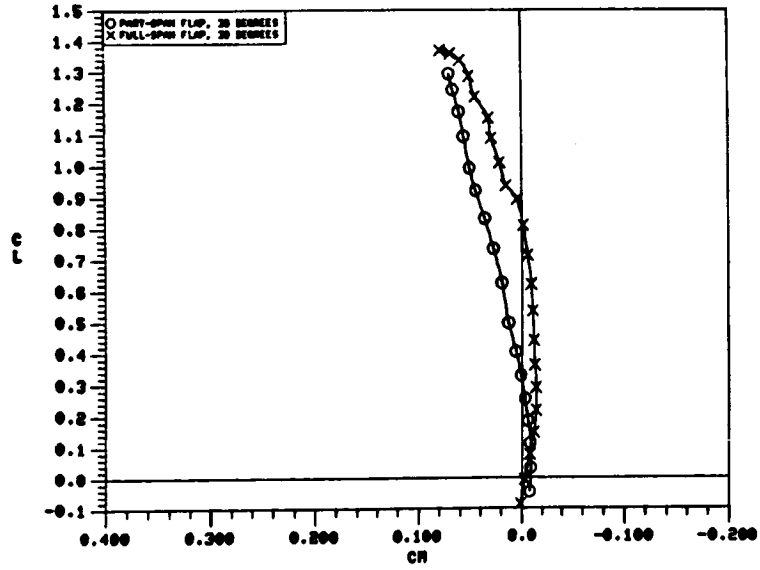

c) C_L vs. C_m

Figure 76. Comparison of the Static Longitudinal Aerodynamic Characteristics of the 70/50-Degree Cranked Wing with Full- and Part-Span Flaps.

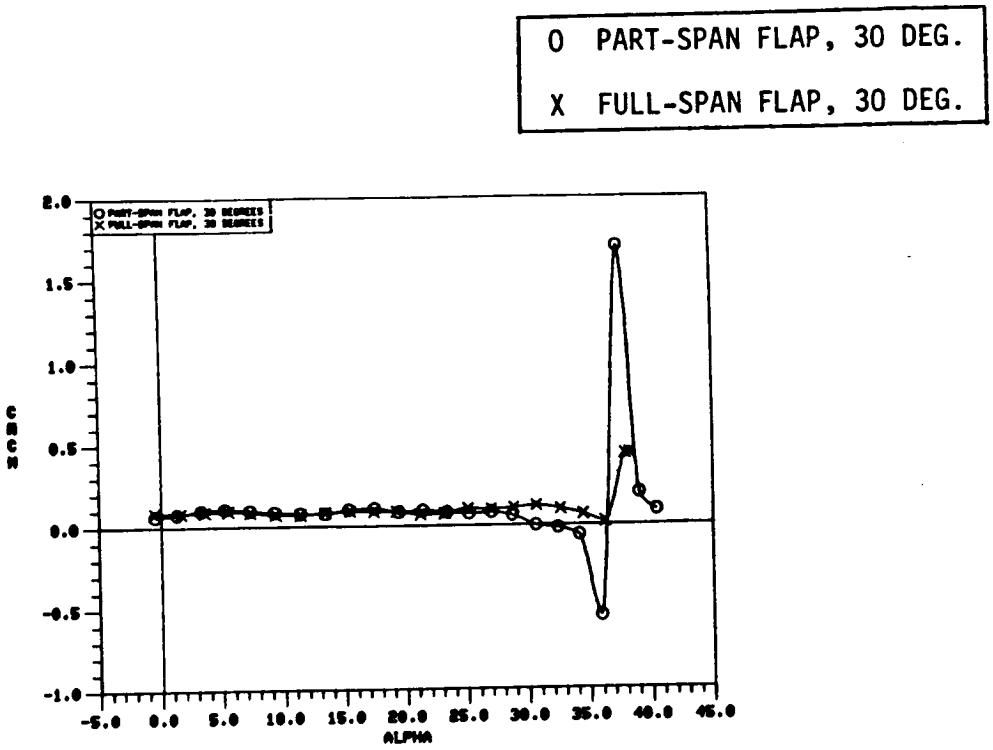

$C_{m_{C_N}}$ vs. α

Figure 77. Comparison of the Static Longitudinal Stability Characteristics of the 65-Degree Cropped Delta Wing with Full- and Part-Span Flaps.

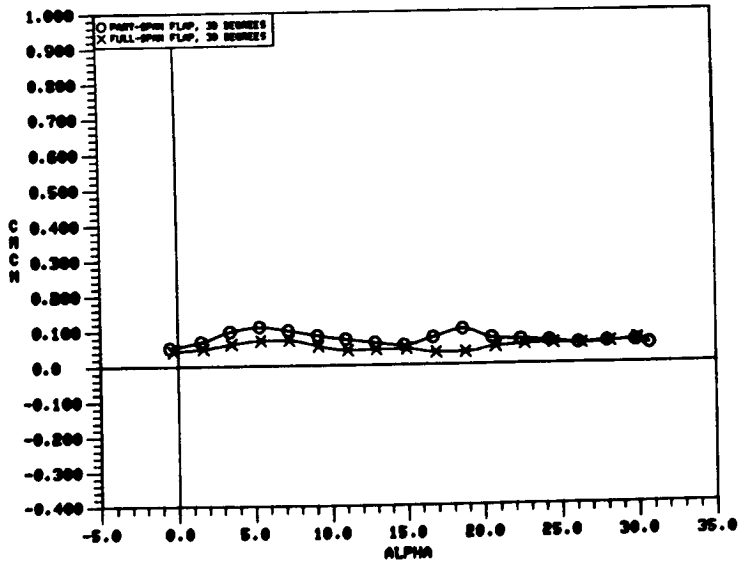

$C_{m_{C_N}}$ vs. α

Figure 78. Comparison of the Static Longitudinal Aerodynamic Characteristics of the 70-Degree Cropped Delta Wing with Full- and Part-Span Flaps.

O	PART-SPAN FLAP, 30 DEG.
X	FULL-SPAN FLAP, 30 DEG.

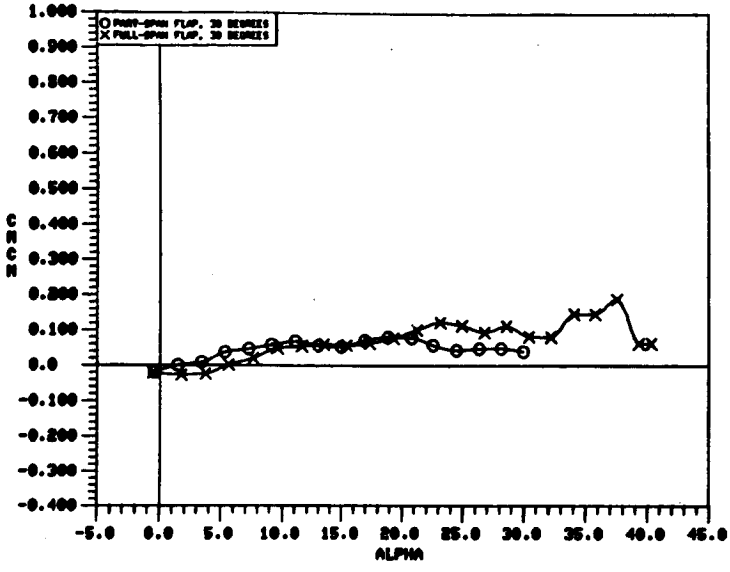

$C_{m_{C_N}}$ vs. α

Figure 79. Comparison of the Static Longitudinal Stability Characteristics of the 70/50-Degree Cranked Wing with Full- and Part-Span Flaps.

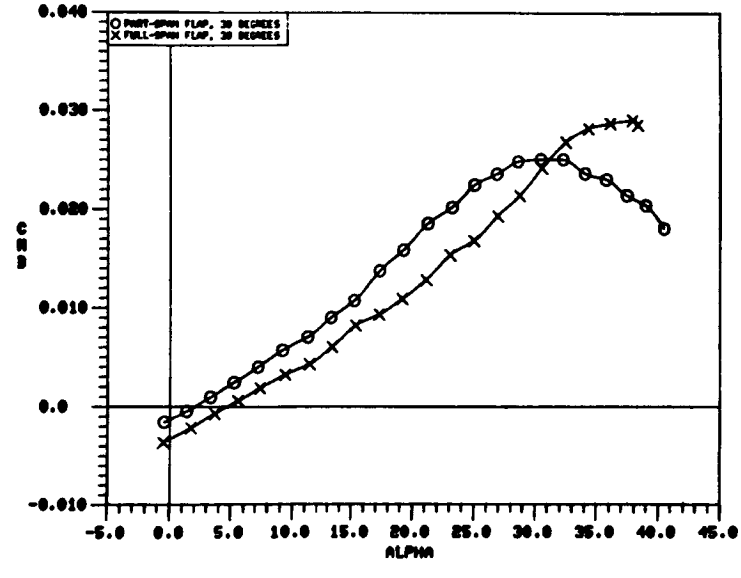

C_{m_β} vs. α

Figure 80. Comparison of the Pitch-Sideslip Coupling Parameter of the 65-Degree Cropped Delta Wing with Full- and Part-Span Flaps.

O	PART-SPAN FLAP, 30 DEG.
X	FULL-SPAN FLAP, 30 DEG.

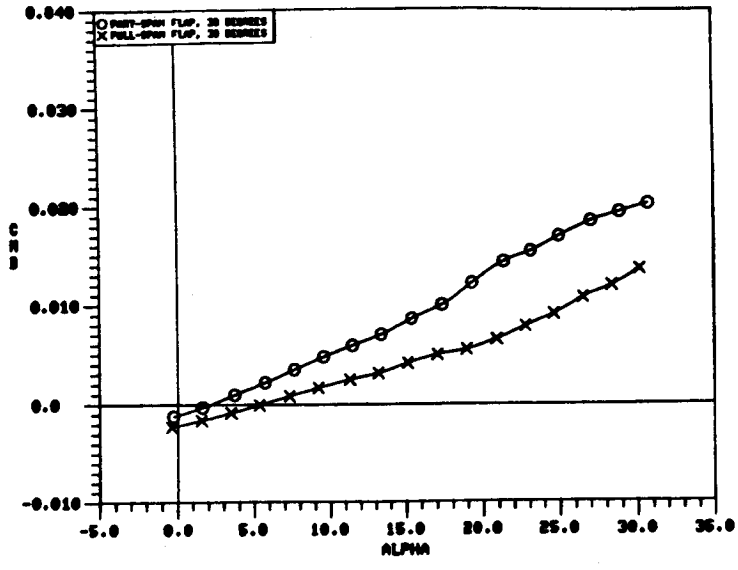

C_{m_β} vs. α

Figure 81. Comparison of the Pitch-Sideslip Coupling Parameter of the 70-Degree Cropped Delta Wing with Full- and Part-Span Flaps.

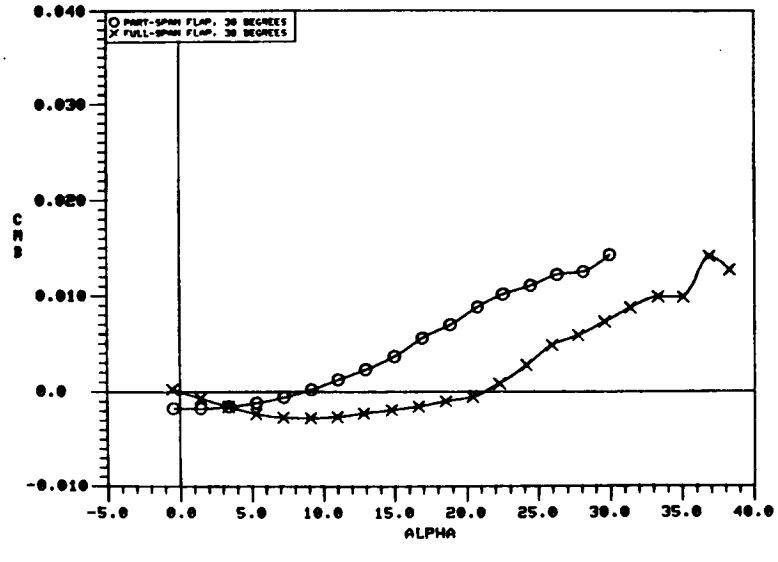

C_{m_β} vs. α

Figure 82. Comparison of the Pitch-Sideslip Coupling Parameter of the 70/50-Degree Cranked Wing with Full- and Part-Span Flaps.

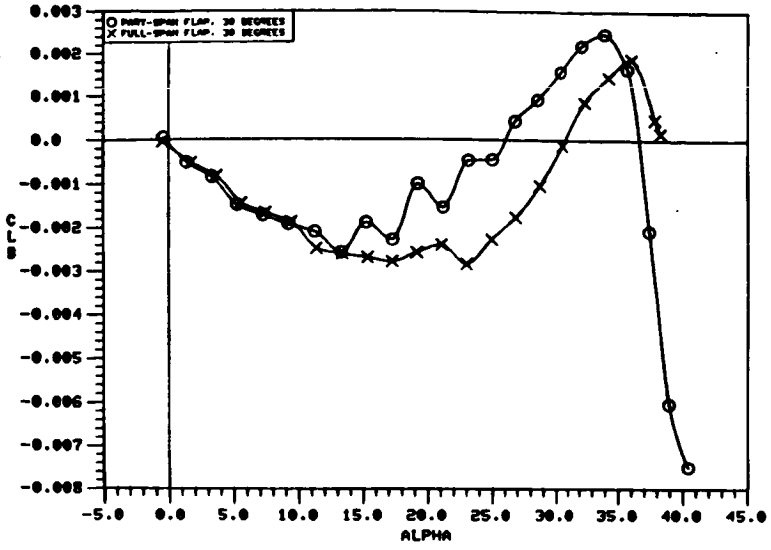

a) C_{ℓ_β} vs. α

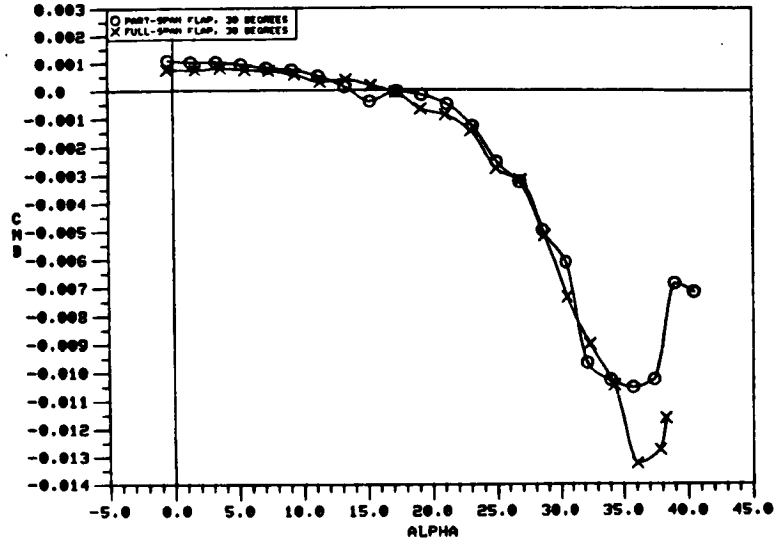

b) C_{n_β} vs. α

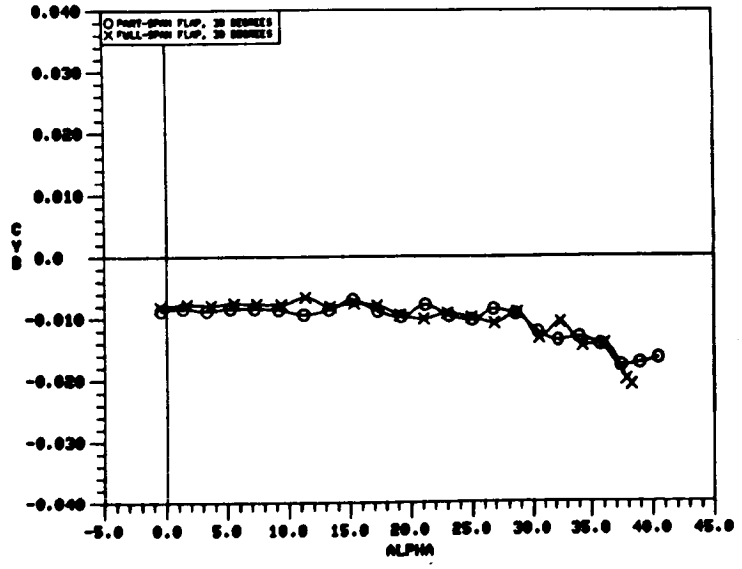

c) C_{Y_β} vs. α

Figure 83. Comparison of the Static Lateral-Directional Stability Characteristics of the 65-Degree Cropped Delta Wing with Full- and Part-Span Flaps.

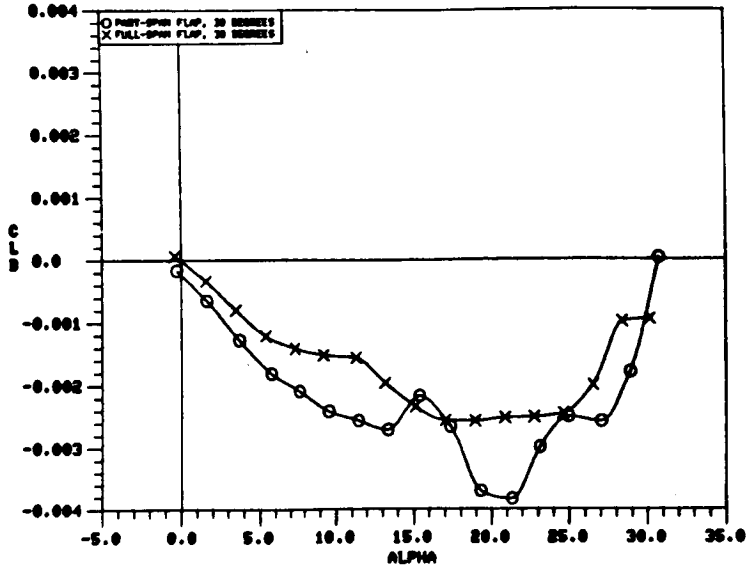

a) C_{ℓ_β} vs. α

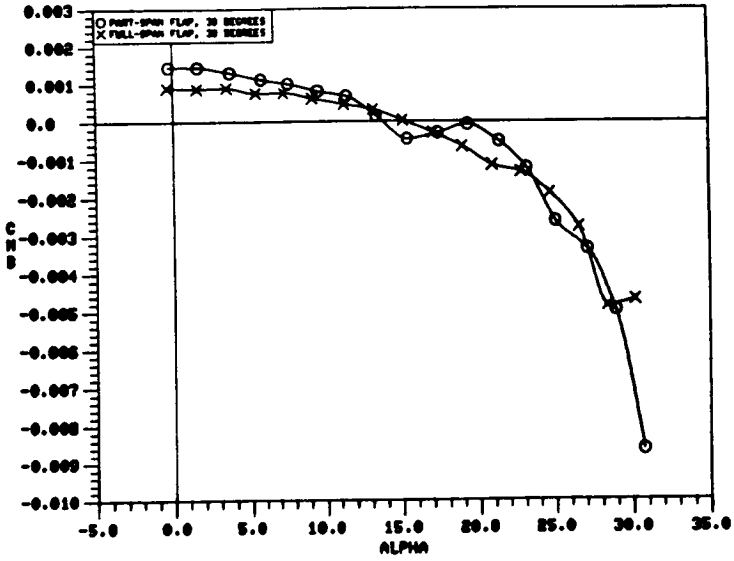

b) C_{n_β} vs. α

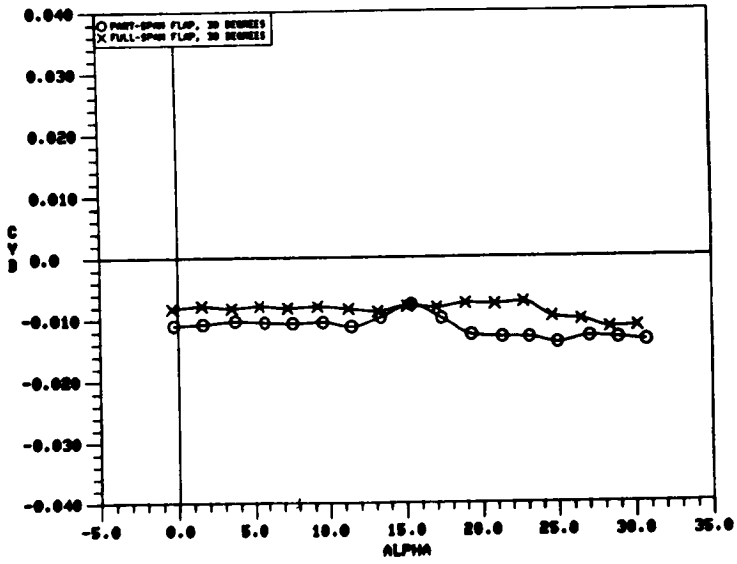

c) C_{Y_β} vs. α

Figure 84. Comparison of the Static Lateral-Directional Stability Characteristics of the 70-Degree Cropped Delta Wing with Full- and Part-Span Flaps.

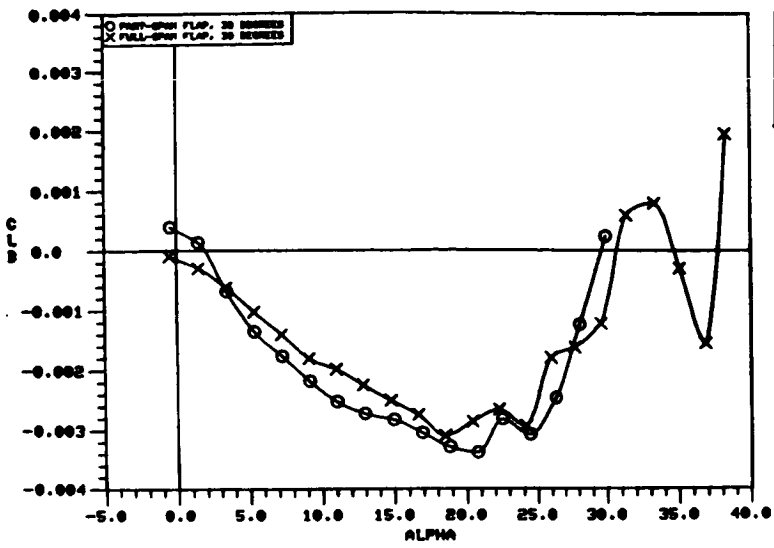

a) C_{ℓ_β} vs. α

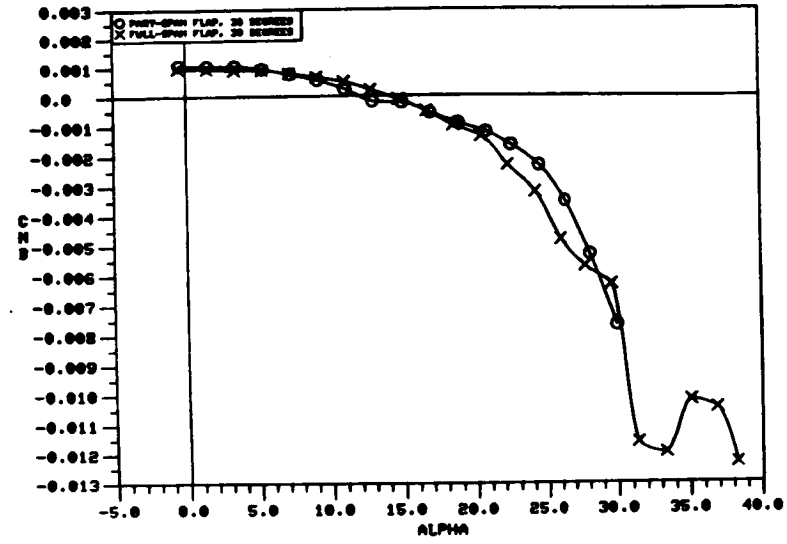

b) C_{n_β} vs. α

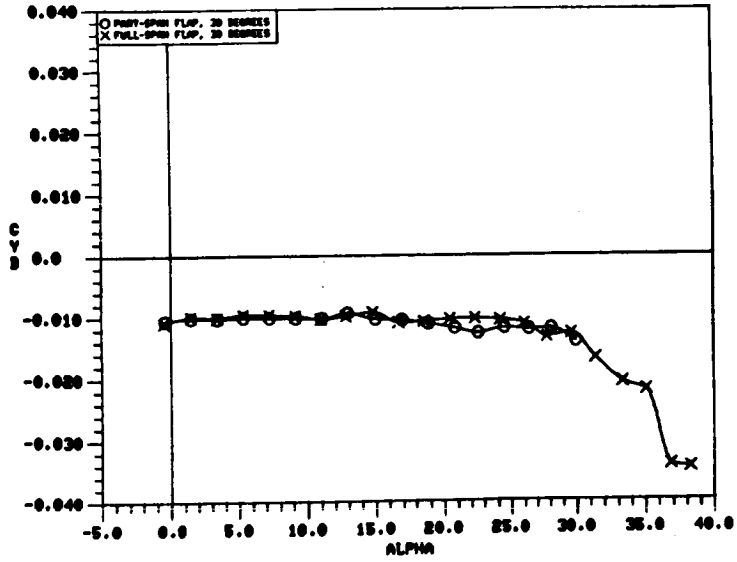

c) C_{Y_β} vs. α

Figure 85. Comparison of the Static Lateral-Directional Stability Characteristics of the 70/50-Degree Cranked Wing with Full- and Part-Span Flaps.

ORIGINAL PAGE IS
OF POOR QUALITY

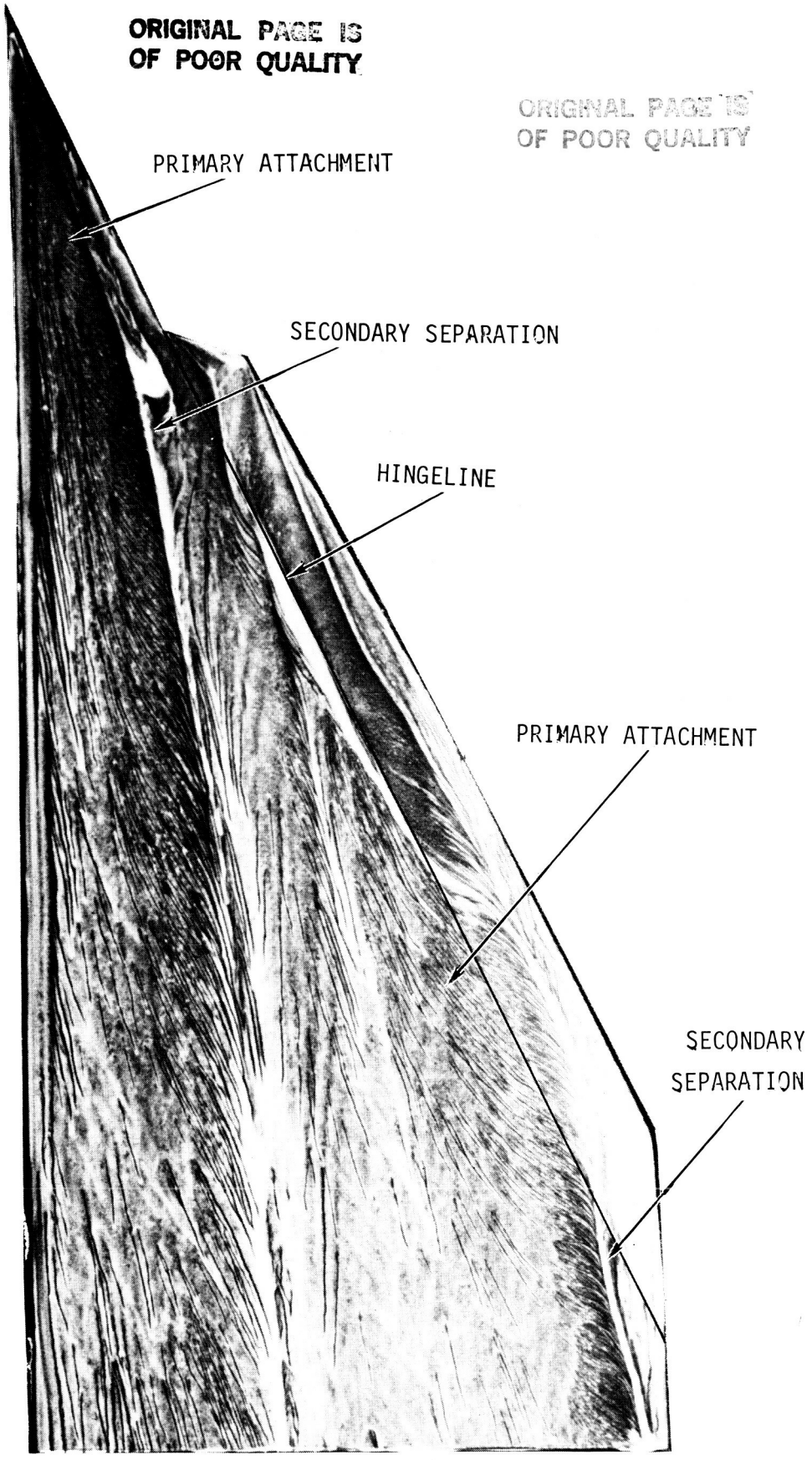

Figure 86. Upper Surface Flow Patterns of the 65-Degree Cropped Delta Wing, $\delta_n = 30°$, $\alpha = 12°$, $\beta = 0°$.

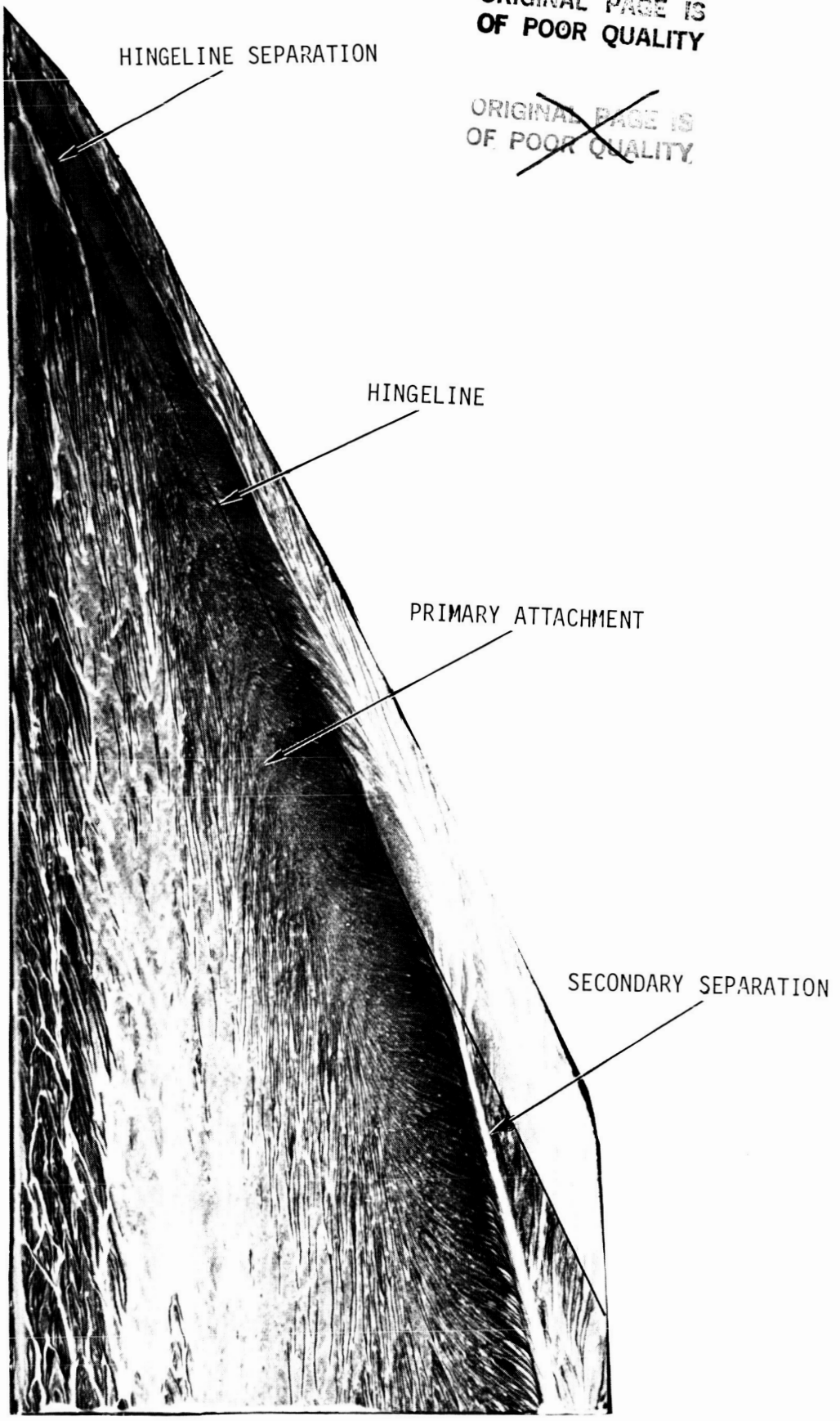

Figure 86. Concluded.

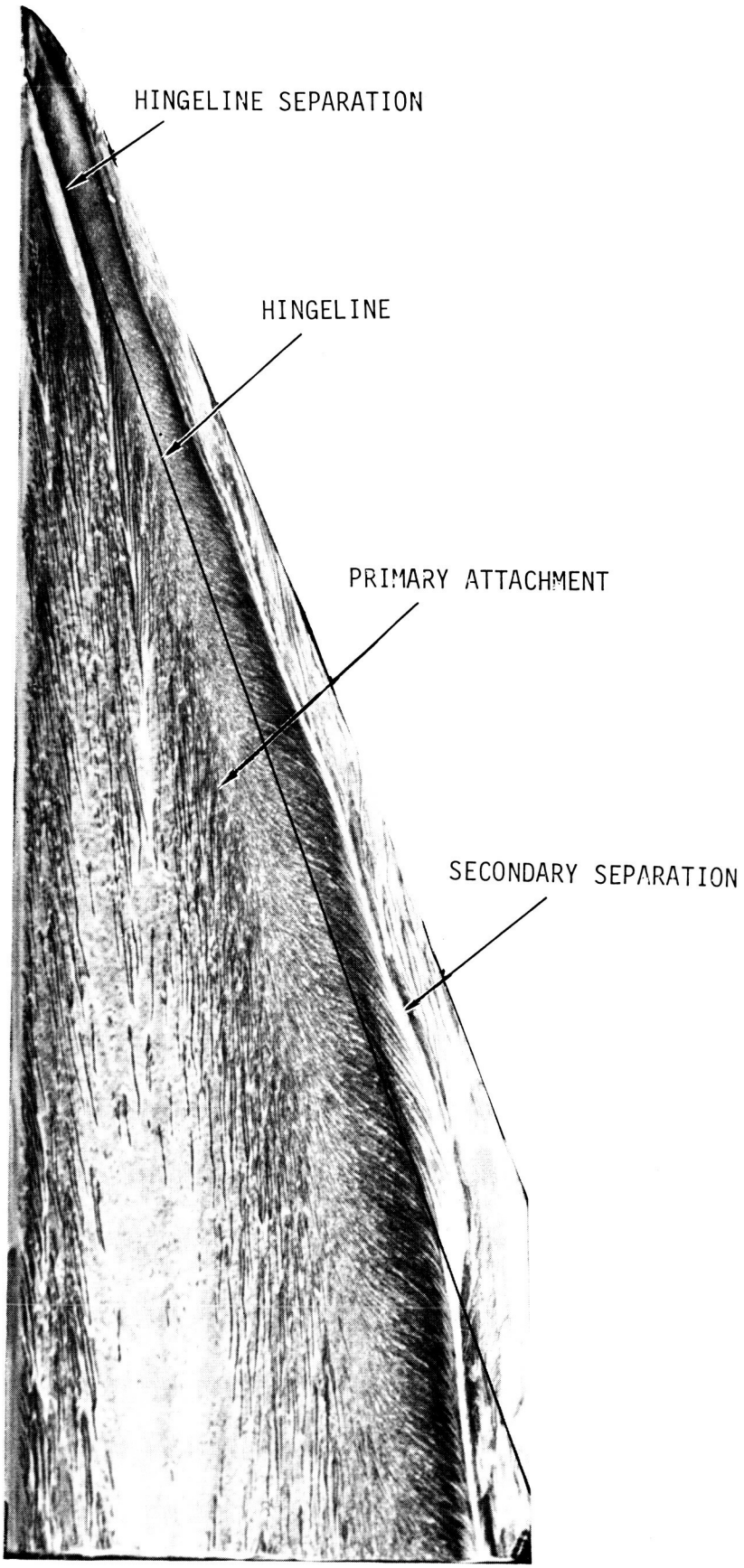

Figure 87. Upper Surface Flow Patterns of the 70-Degree Cropped Delta Wing, $\delta_n = 30°$, $\alpha = 12°$, $\beta = 0°$.

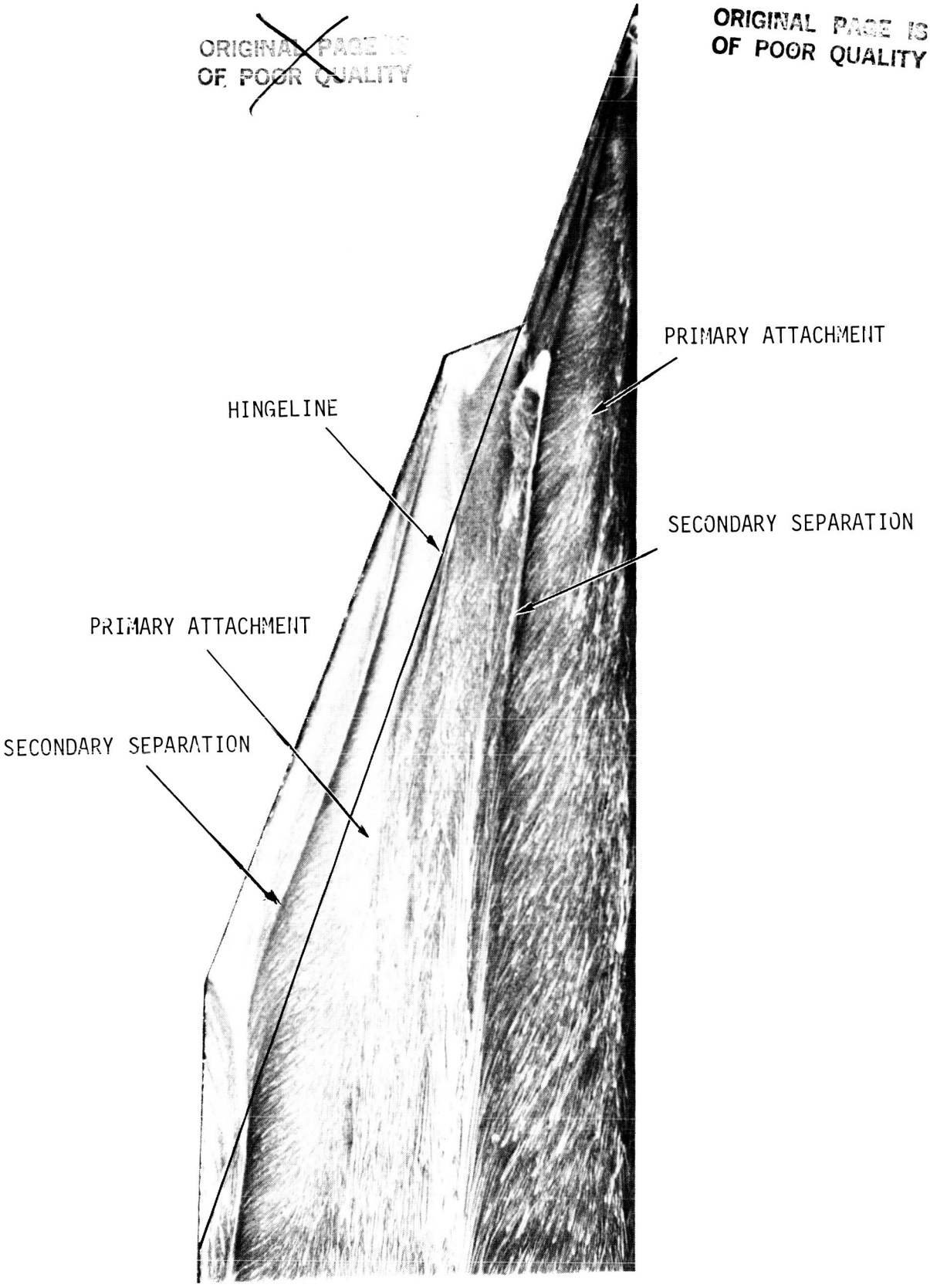

Figure 87. Concluded.

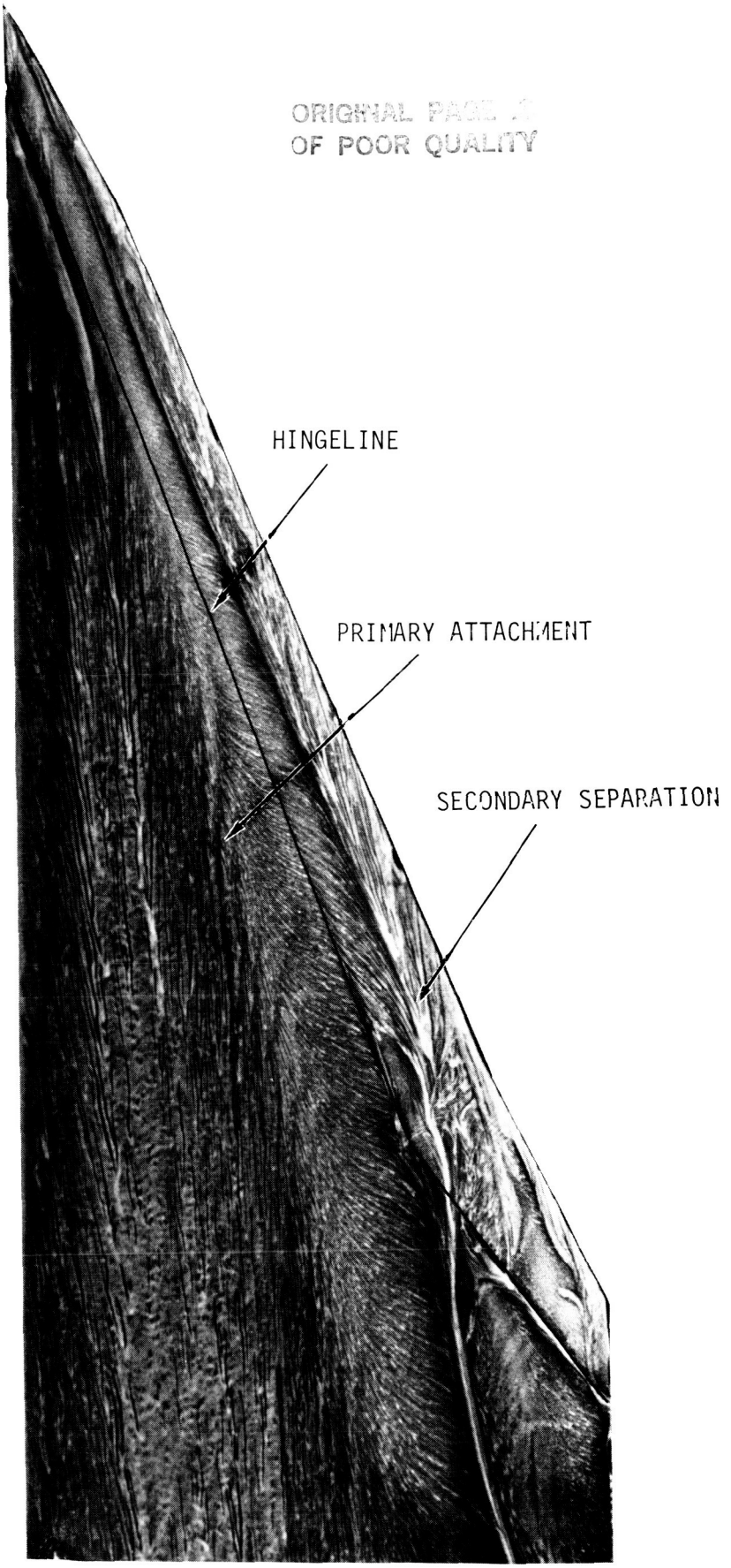

Figure 88. Upper Surface Flow Patterns of the 70/50-Degree Cropped Cranked Wing, δ_n = 30°, α = 12°, β = 0°.

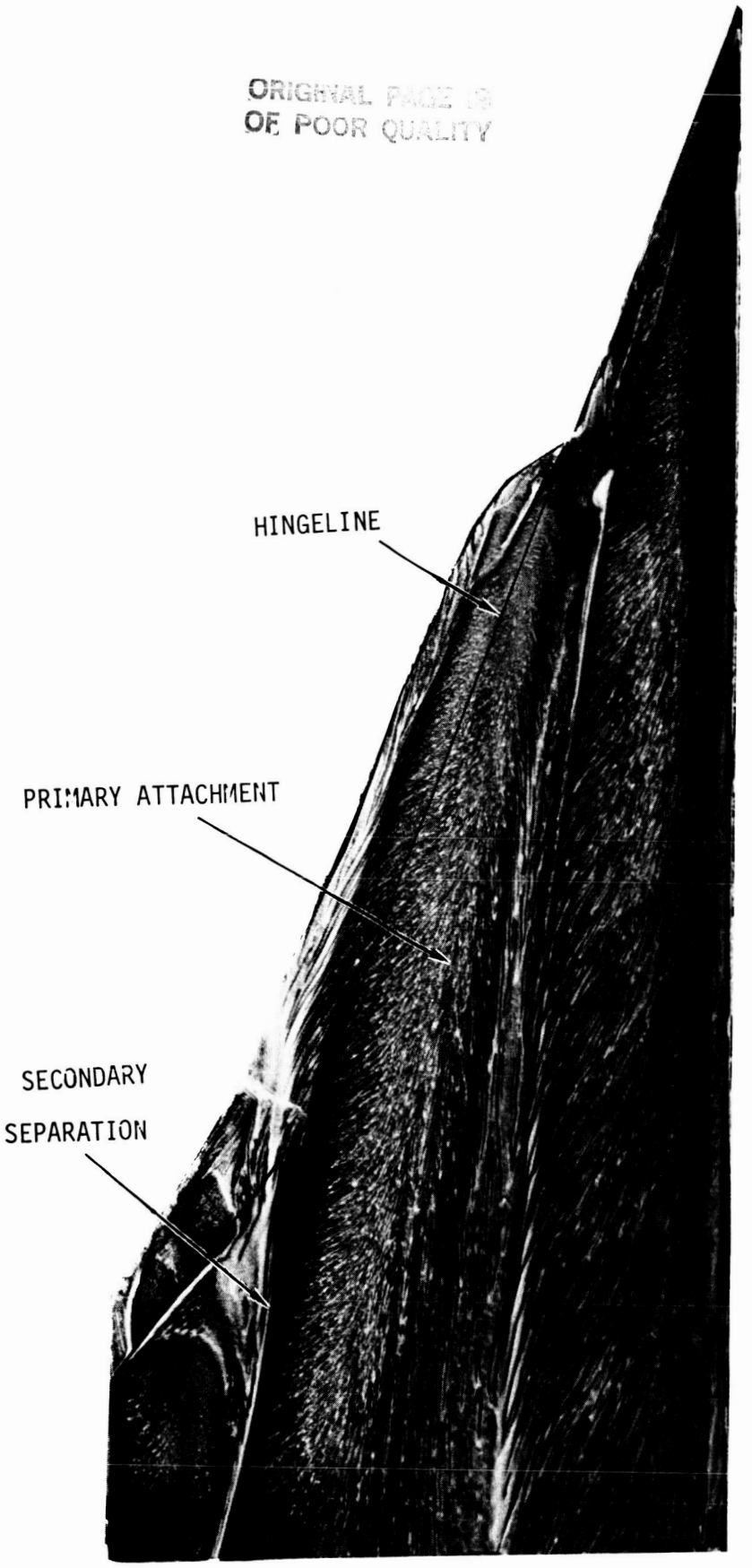

Figure 88. Concluded.

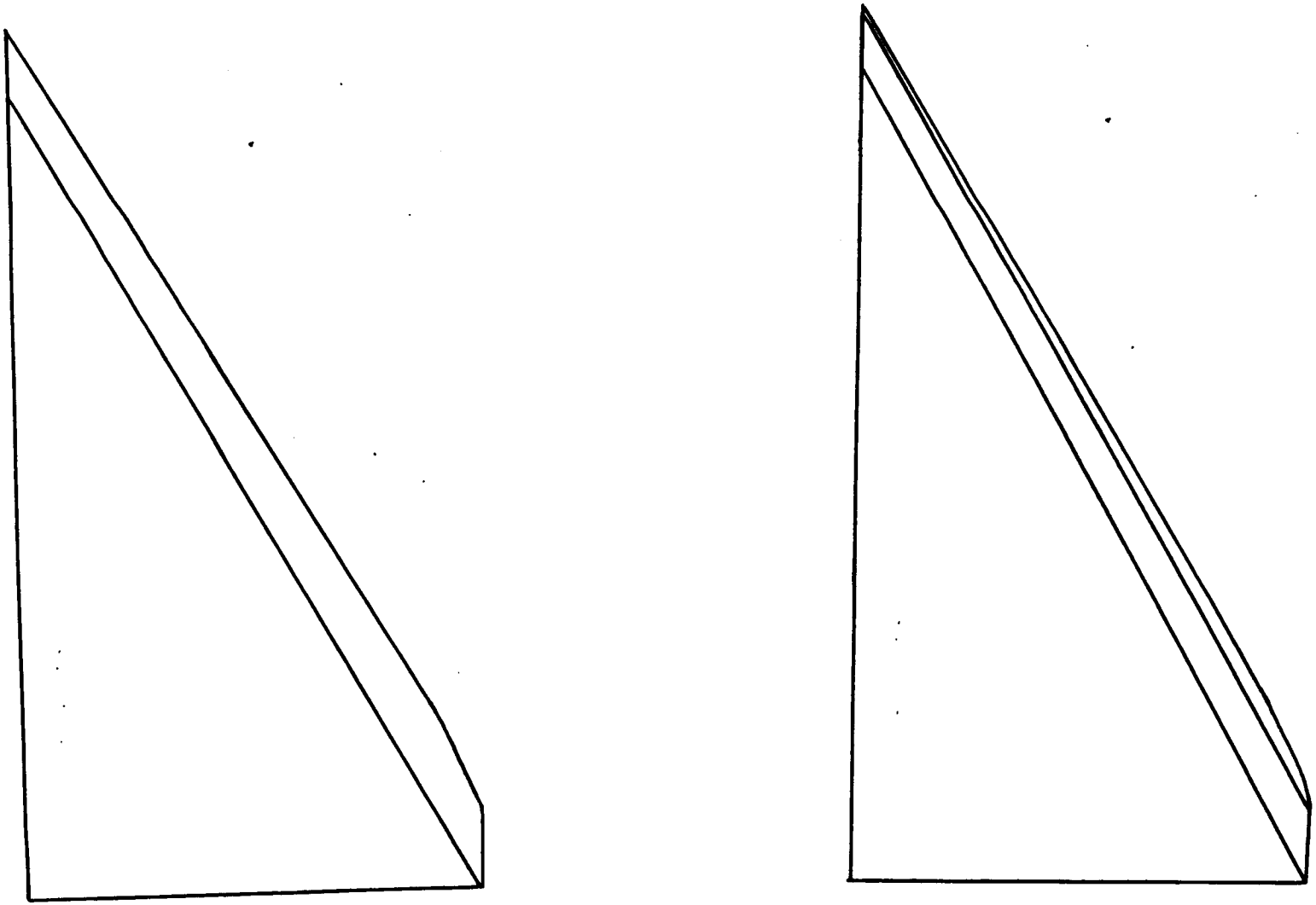

a) Plain Vortex Flap

b) Tabbed Vortex Flap

Figure 89. 60-Degree Cropped Delta Wing

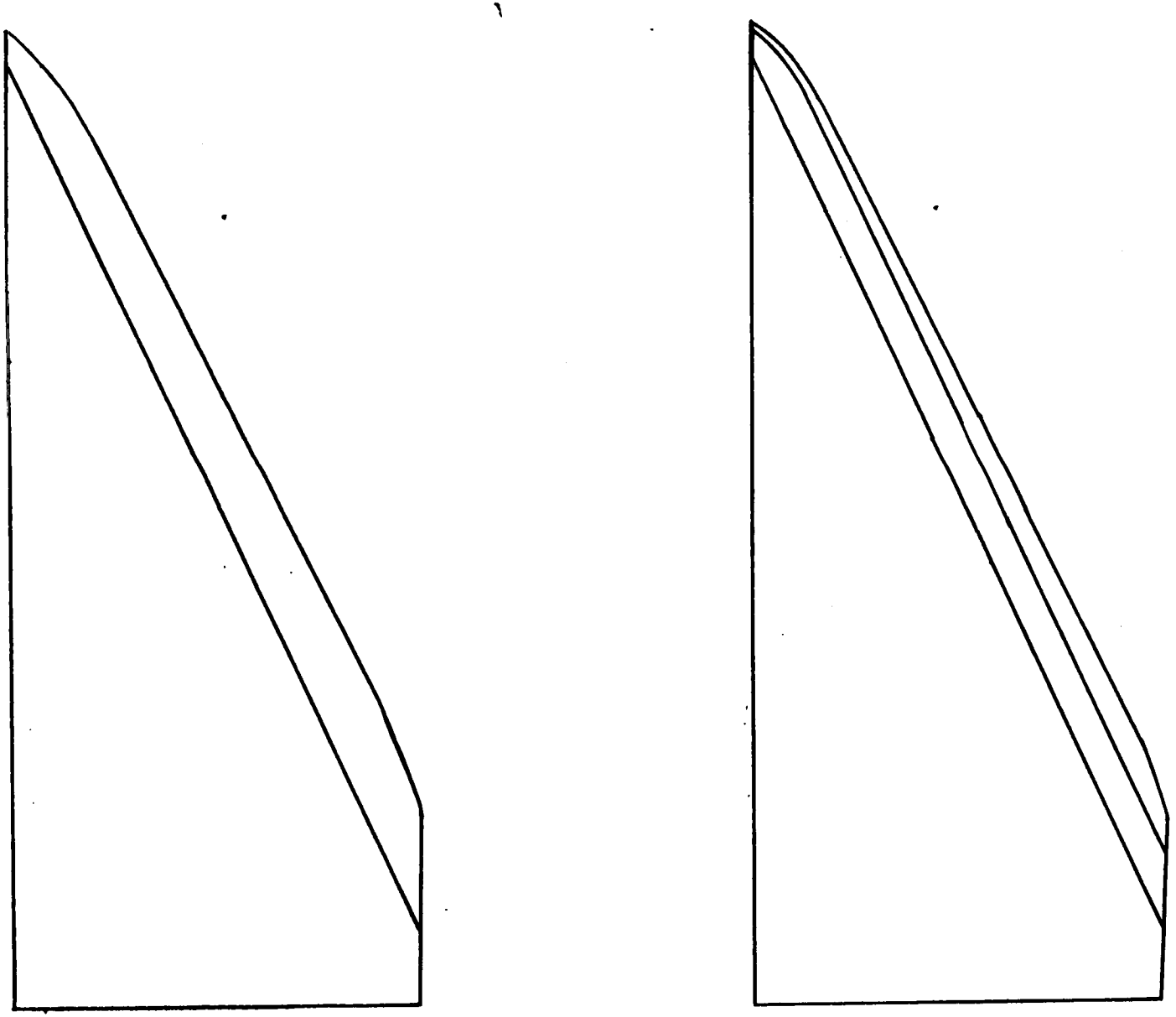

a) Plain Vortex Flap

b) Tabbed Vortex Flap

Figure 90. 65-Degree Cropped Delta Wing

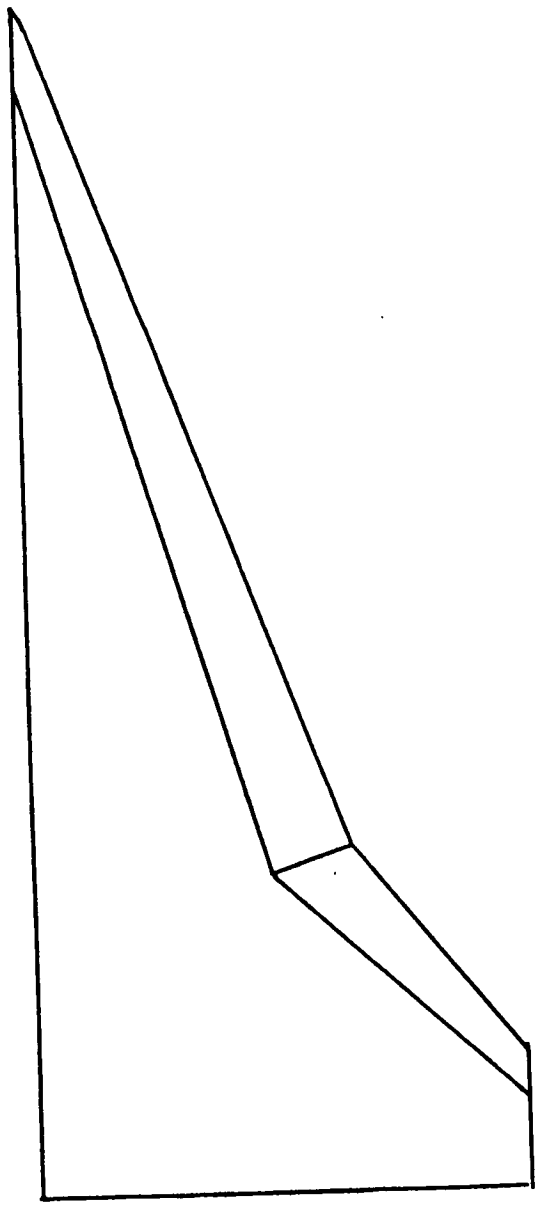

a) Plain Vortex Flap

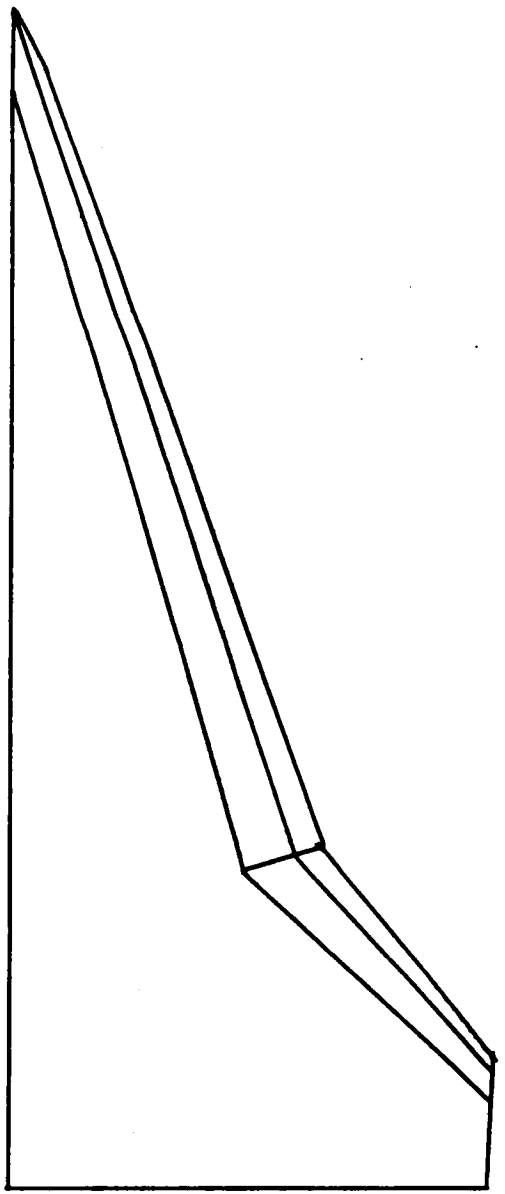

b) Tabbed Vortex Flap

Figure 91. 70/50-Degree Cranked Wing

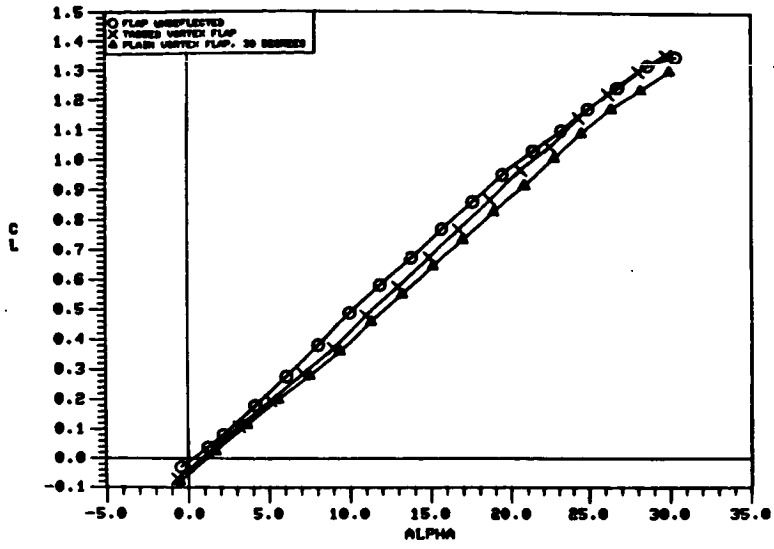

O FLAP UNDEFLECTED

X TABBED VORTEX FLAP, 30 DEG.

△ PLAIN VORTEX FLAP, 30 DEG.

a) C_L vs. α

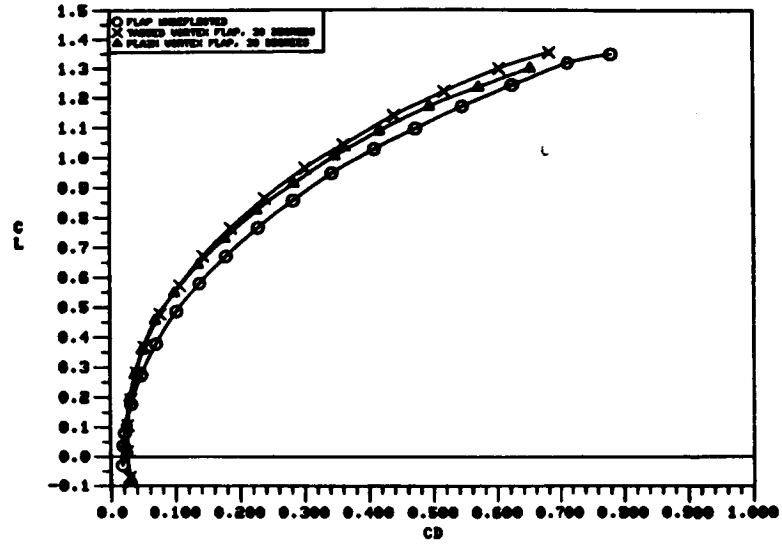

b) C_L vs. C_D

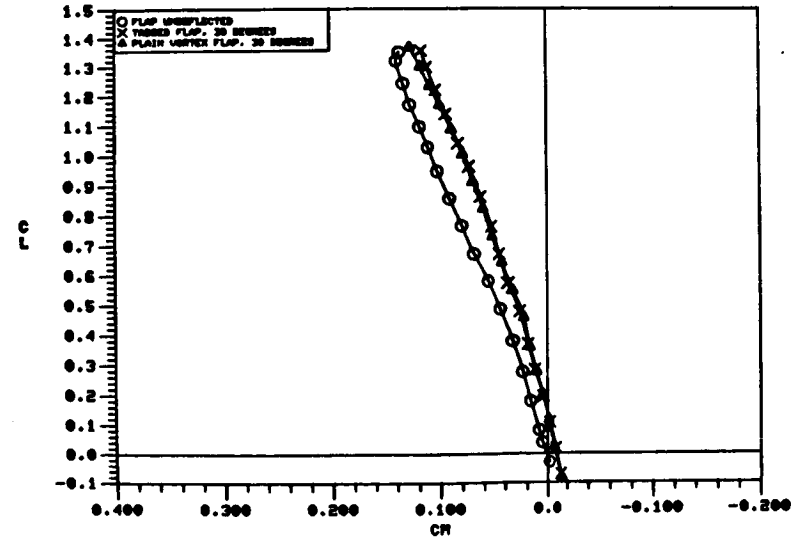

c) C_L vs. C_m

Figure 92. Comparison of the Static Longitudinal Aerodynamic Characteristics of the 60-Degree Cropped Delta Wing with Tabbed and Plain Vortex Flaps

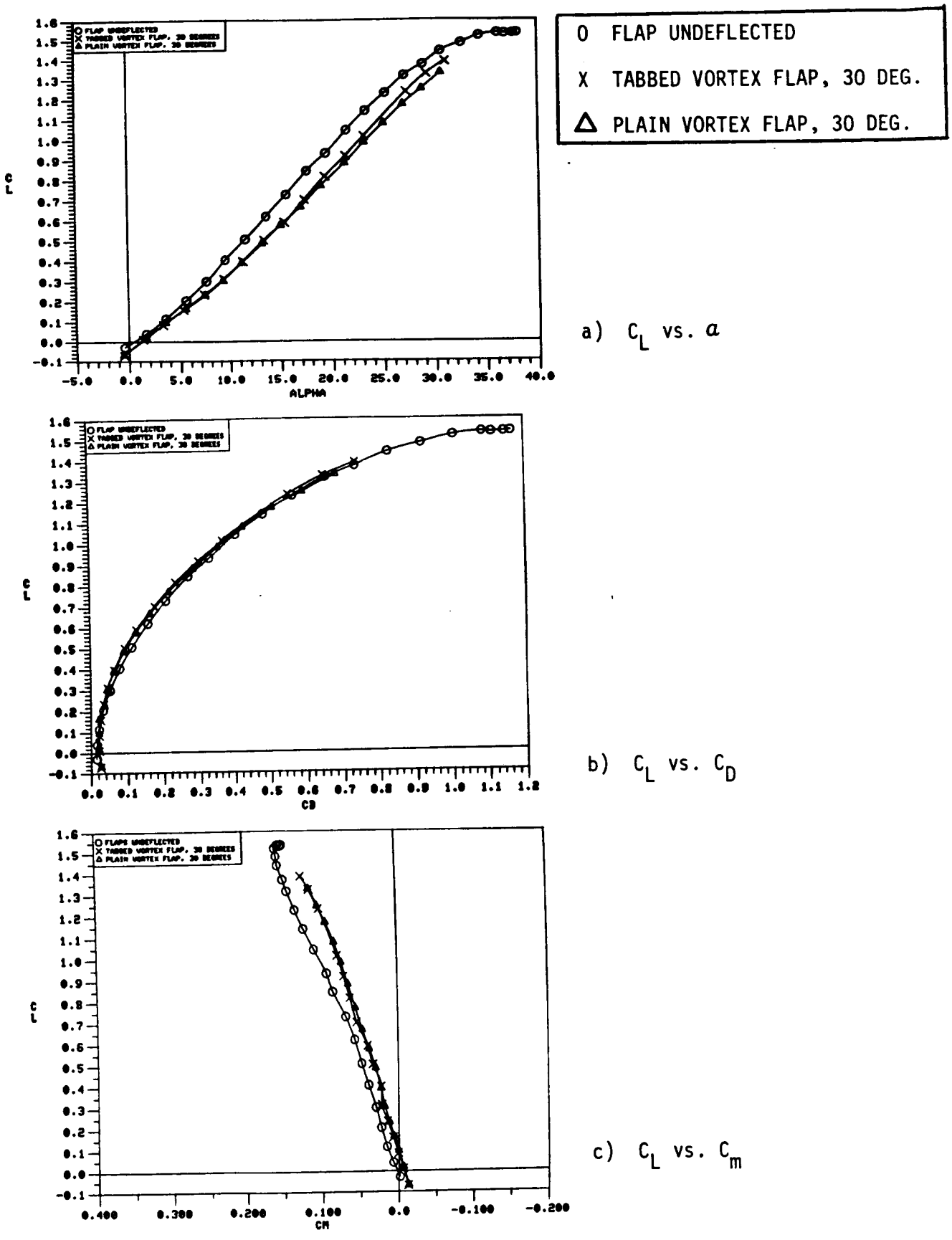

a) C_L vs. α

b) C_L vs. C_D

c) C_L vs. C_m

Figure 93. Comparison of the Static Longitudinal Aerodynamic Characteristics of the 65-Degree Cropped Delta Wing with Tabbed and Plain Vortex Flaps

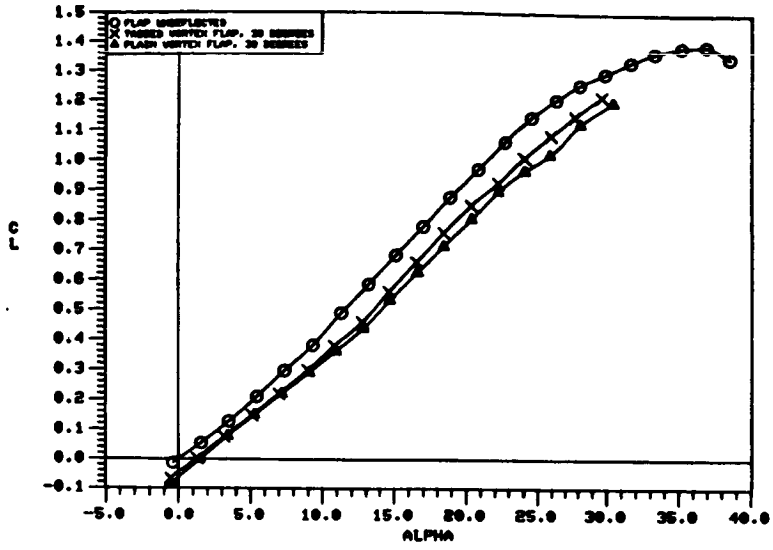

a) C_L vs. α

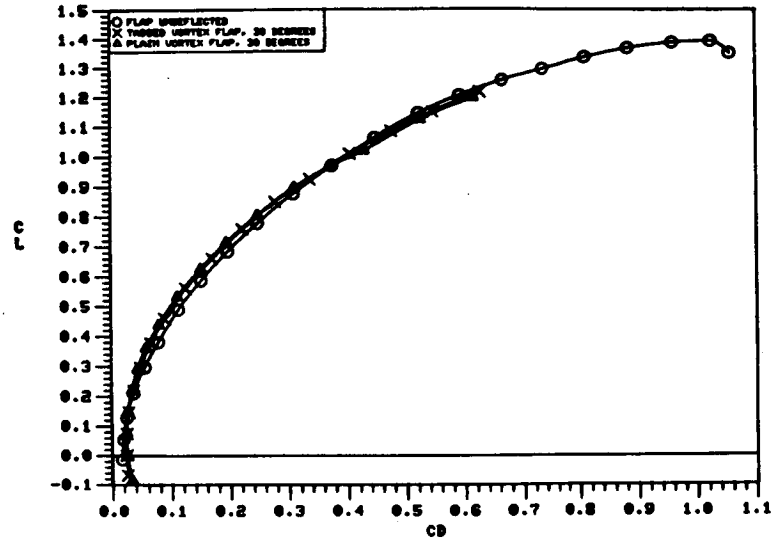

b) C_L vs. C_D

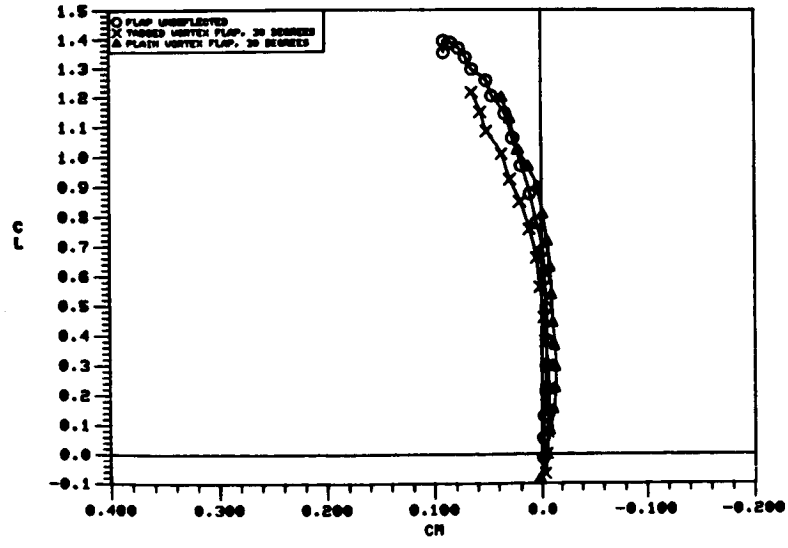

c) C_L vs. C_m

Figure 94. Comparison of the Static Longitudinal Aerodynamic Characteristics of the 70/50-Degree Cranked Wing with Tabbed and Plain Vortex Flaps

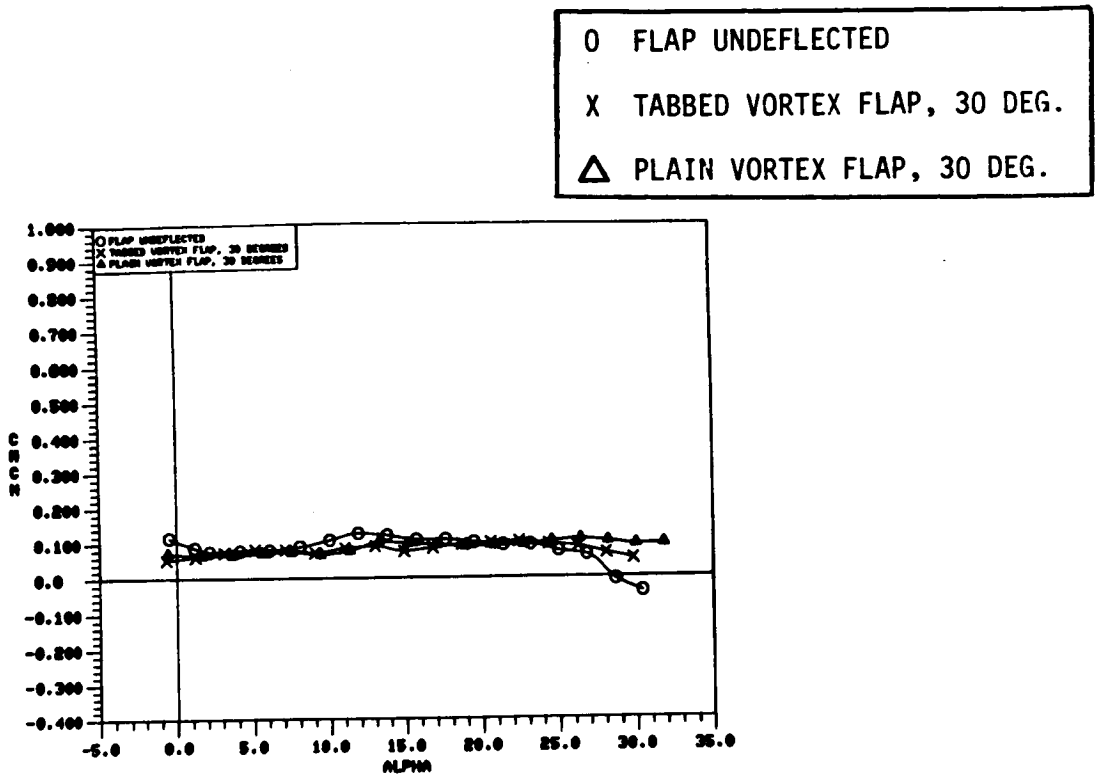

$C_{m_{C_N}}$ vs. α

Figure 95. Comparison of the Static Longitudinal Stability Characteristics of the 60-Degree Cropped Delta Wing with Tabbed and Plain Vortex Flaps.

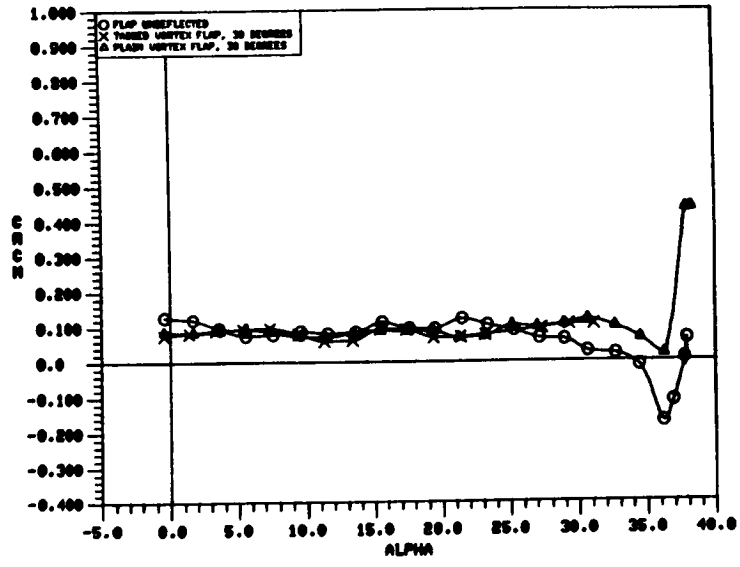

$C_{m_{C_N}}$ vs. α

Figure 96. Comparison of the Static Longitudinal Stability Characteristics of the 65-Degree Cropped Delta Wing with Tabbed and Plain Vortex Flaps

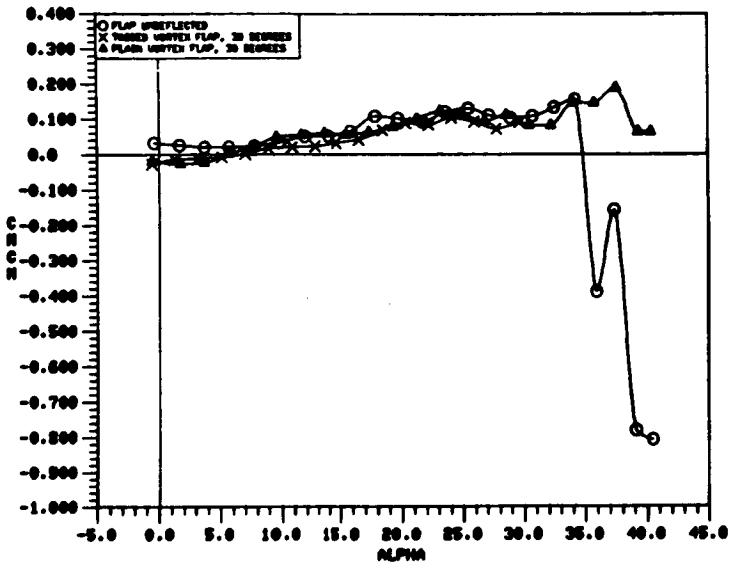

$C_{m_{C_N}}$ vs. α

Figure 97. Comparison of the Static Longitudinal Stability Characteristics of the 70/50-Degree Cranked Wing with Tabbed and Plain Vortex Flaps.

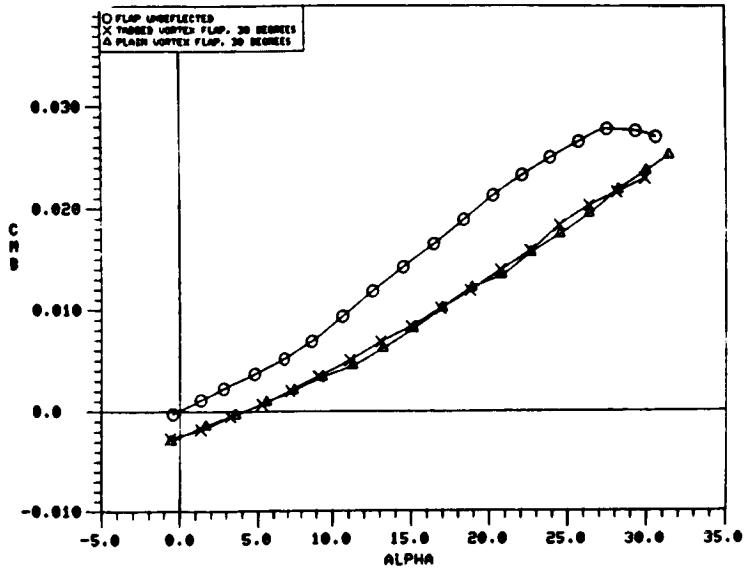

C_{m_β} vs. α

Figure 98. Comparison of the Pitch-Sideslip Coupling Parameter of the 60-Degree Cropped Delta Wing with Tabbed and Plain Vortex Flaps

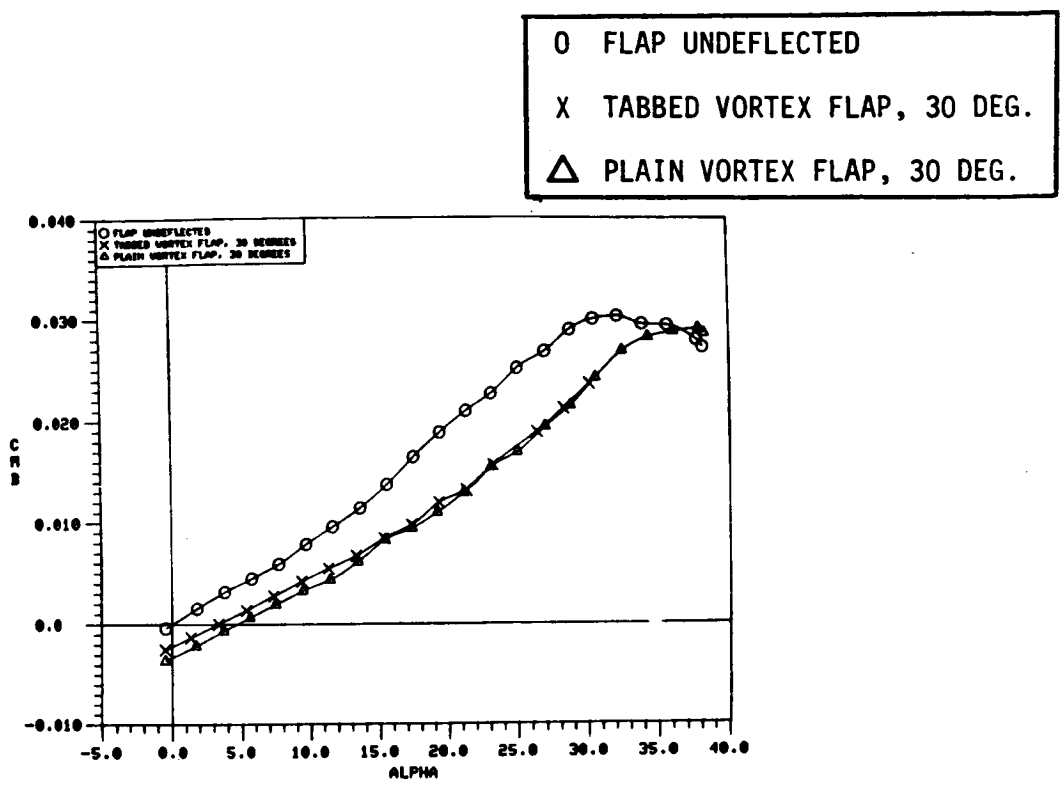

C_{m_β} vs. α

Figure 99. Comparison of the Pitch-Sideslip Coupling Parameter of the 65-Degree Cropped Delta Wing with Tabbed and Plain Vortex Flaps.

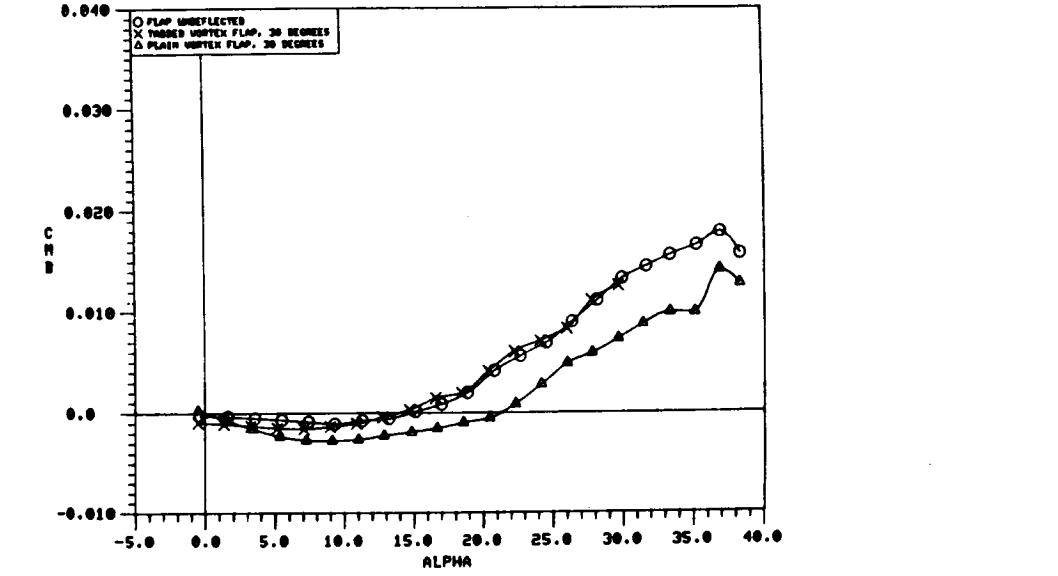

C_{m_β} vs. α

Figure 100. Comparison of the Pitch-Sideslip Coupling Parameter of the 70/50-Degree Cranked Wing with Tabbed and Plain Vortex Flaps

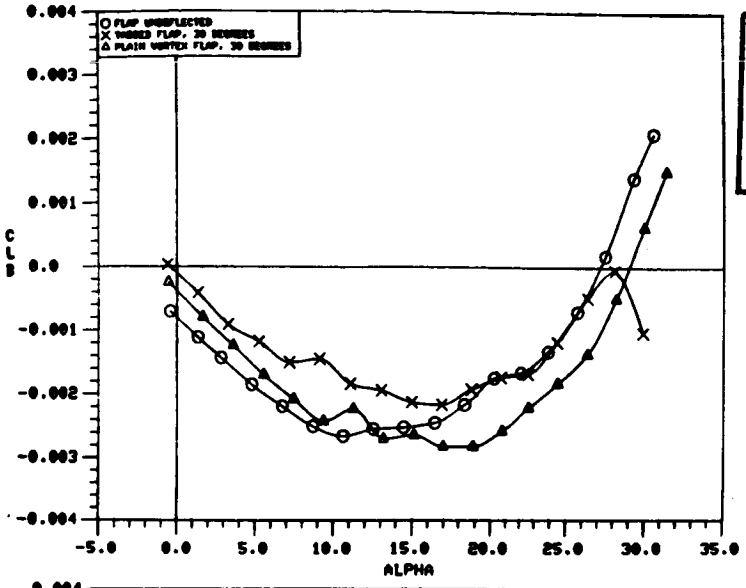

a) C_{ℓ_β} vs. α

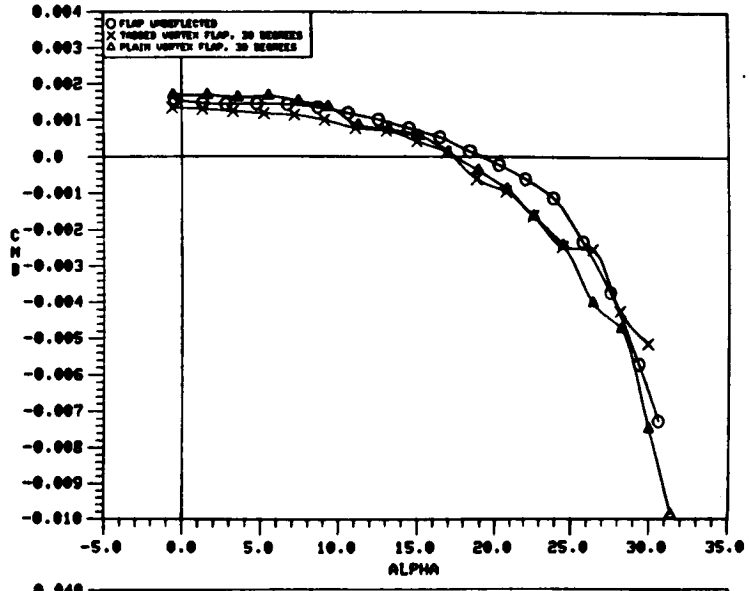

b) C_{n_β} vs. α

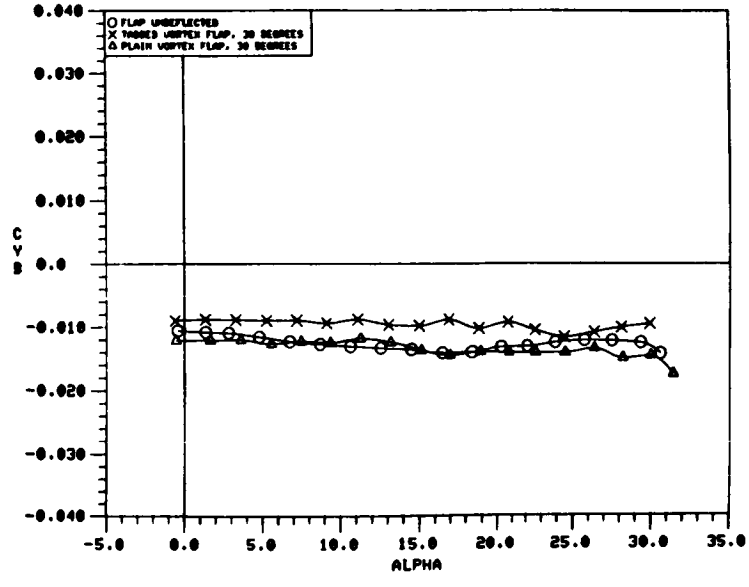

c) C_{Y_β} vs. α

Figure 101. Comparison of the Static Lateral-Directional Stability Characteristics of the 60-Degree Cropped Delta Wing with Tabbed and Plain Vortex Flaps.

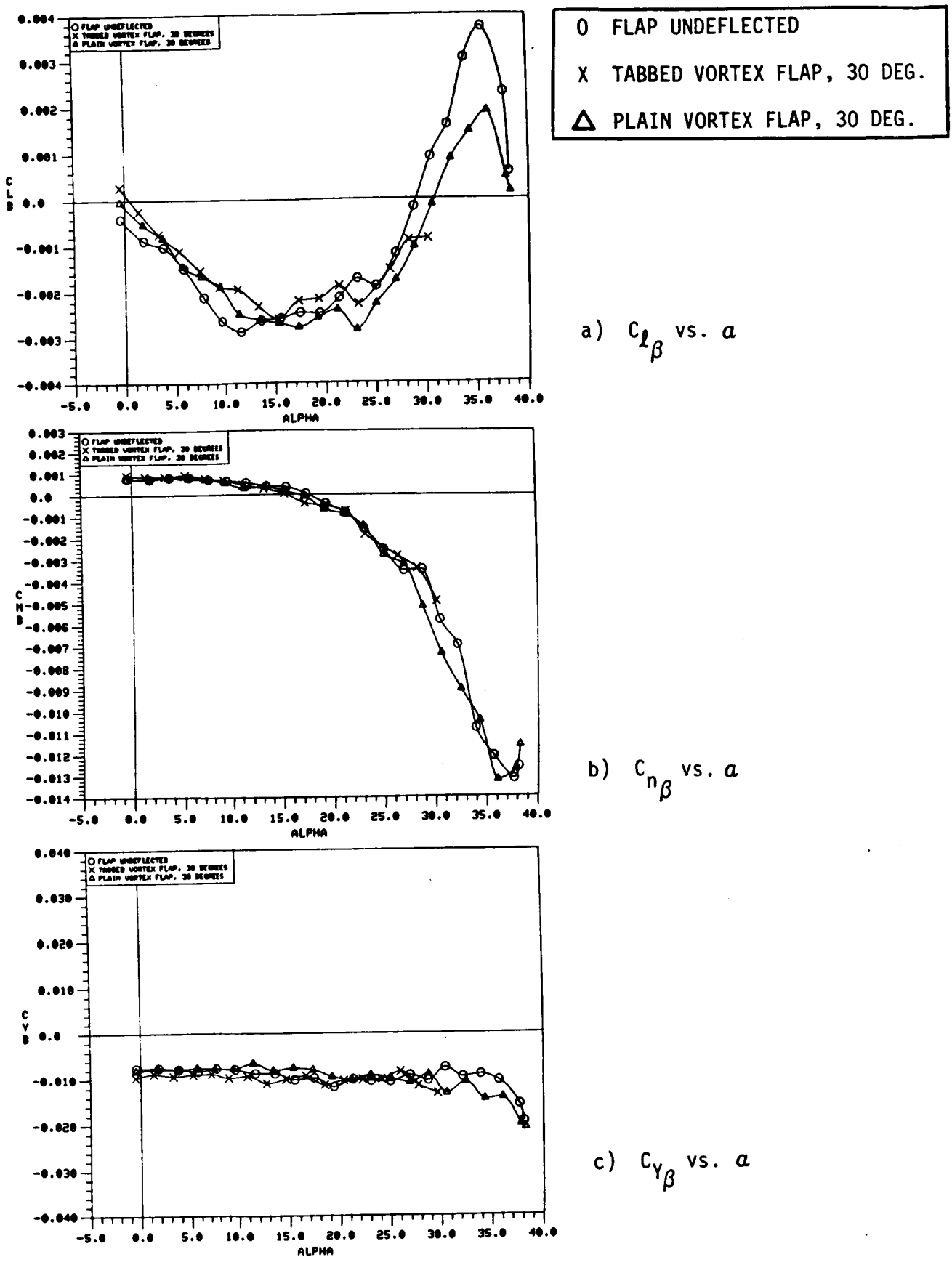

Figure 102. Comparison of the Static Lateral-Directional Stability Characteristics of the 65-Degree Cropped Delta Wing with Tabbed and Plain Vortex Flaps.

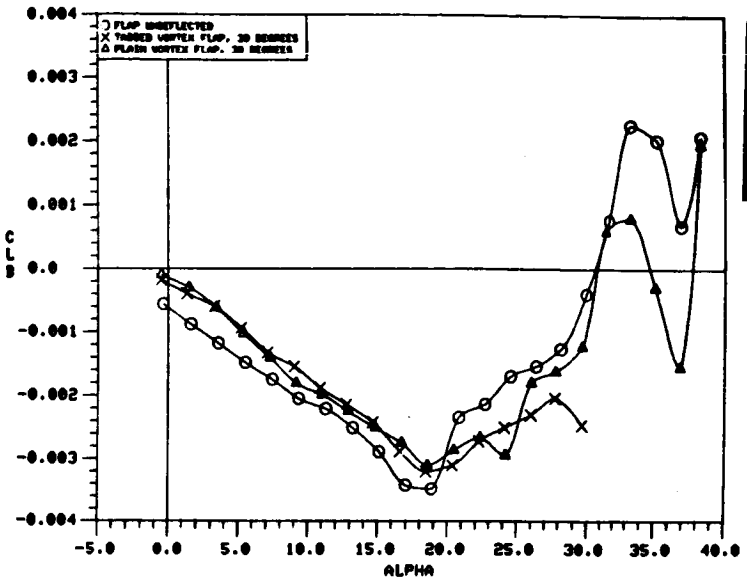

a) C_{ℓ_β} vs. α

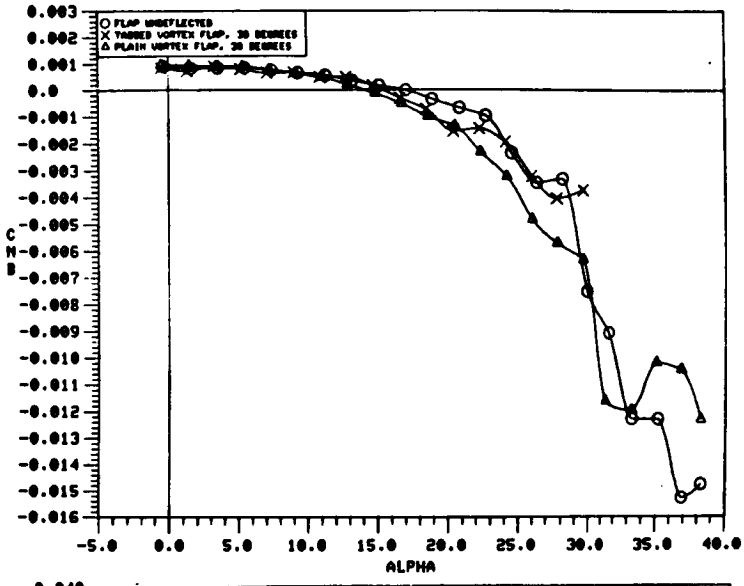

b) C_{n_β} vs. α

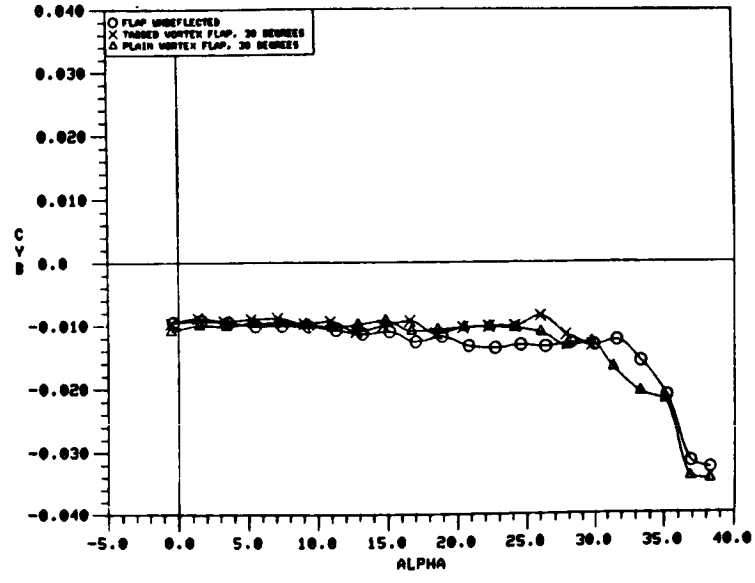

c) C_{Y_β} vs. α

Figure 103. Comparison of the Static Lateral-Directional Stability Characteristics of the 70/50-Degree Cranked Wing with Tabbed and Plain Vortex Flaps.

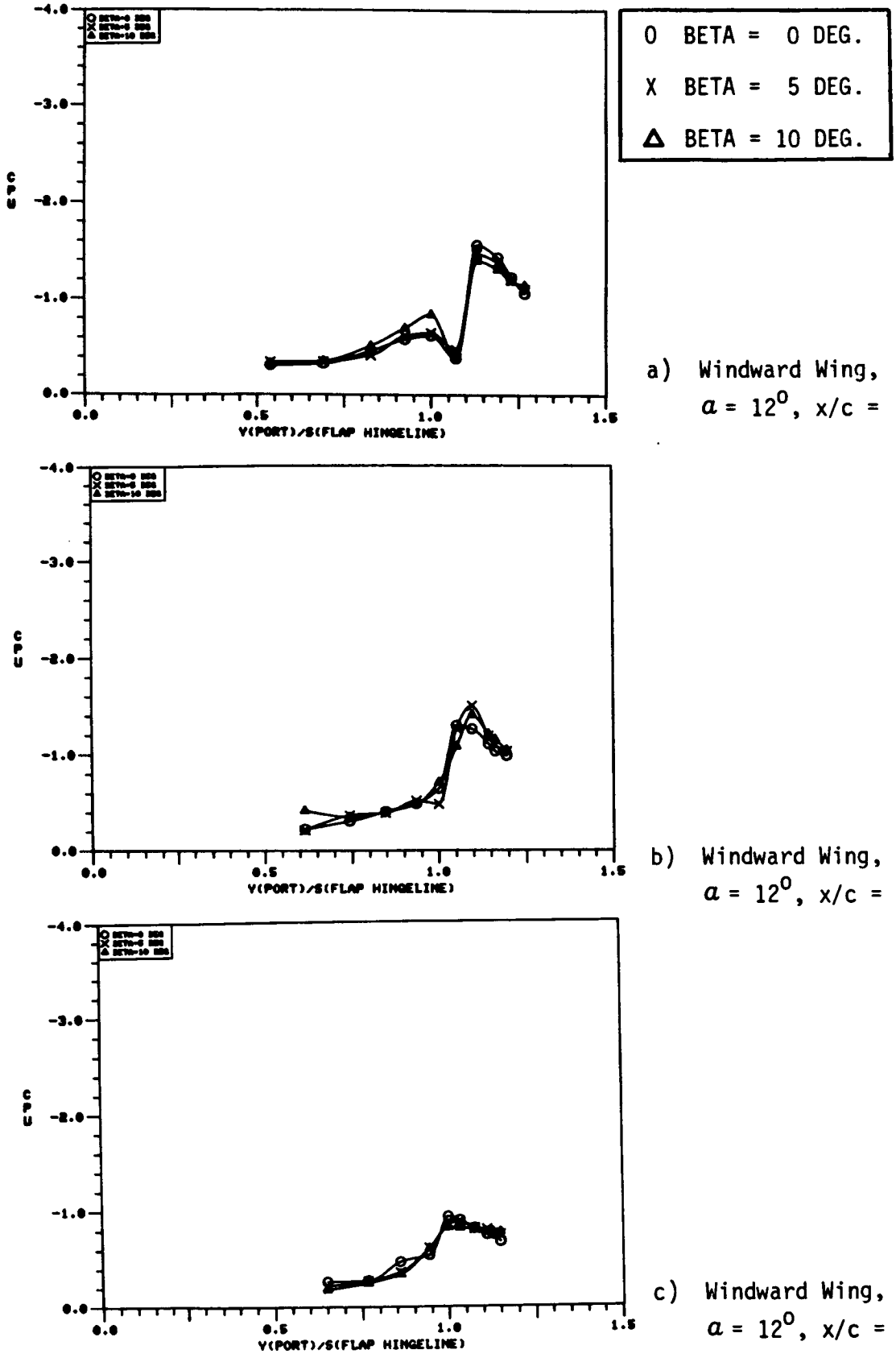

Figure 104. Effect of Sideslip Angle on the 65-Degree Cropped Delta Wing Upper Surface Pressure Distributions with Tabbed Vortex Flap.

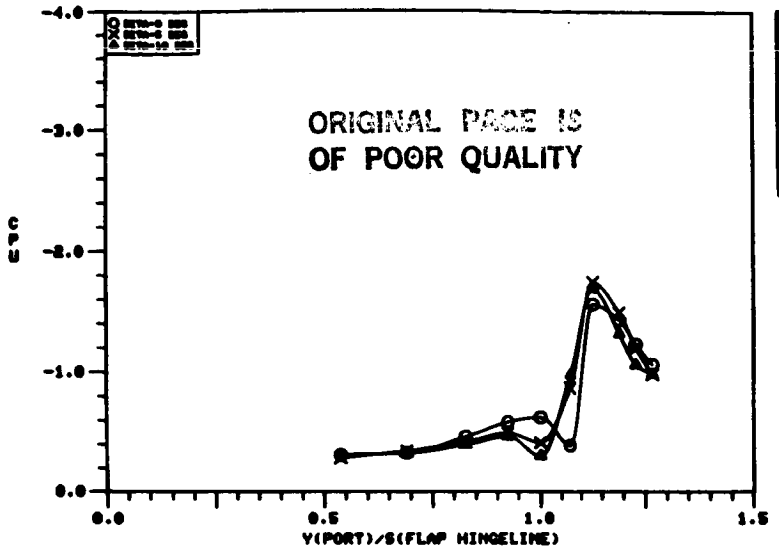

O	BETA =	0 DEG.
X	BETA =	5 DEG.
Δ	BETA =	10 DEG.

a) Leeward Wing, $\alpha = 12^{0}$, x/c = .405

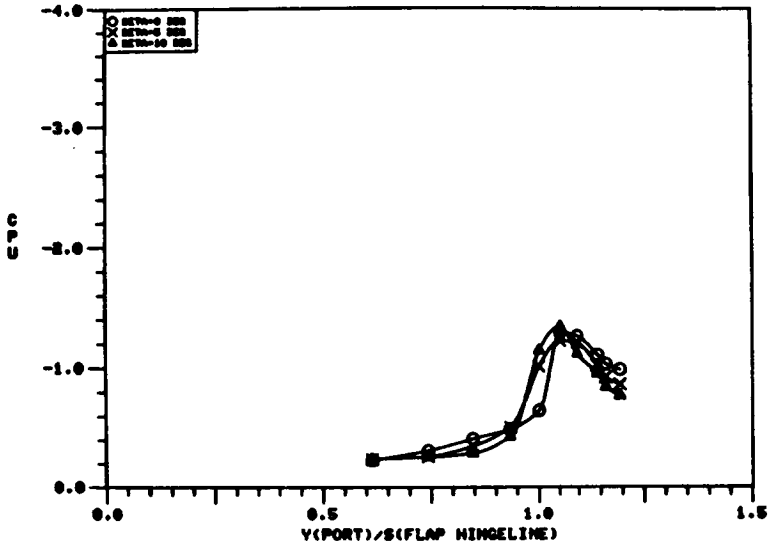

b) Leeward Wing, $\alpha = 12^{0}$, x/c = .576

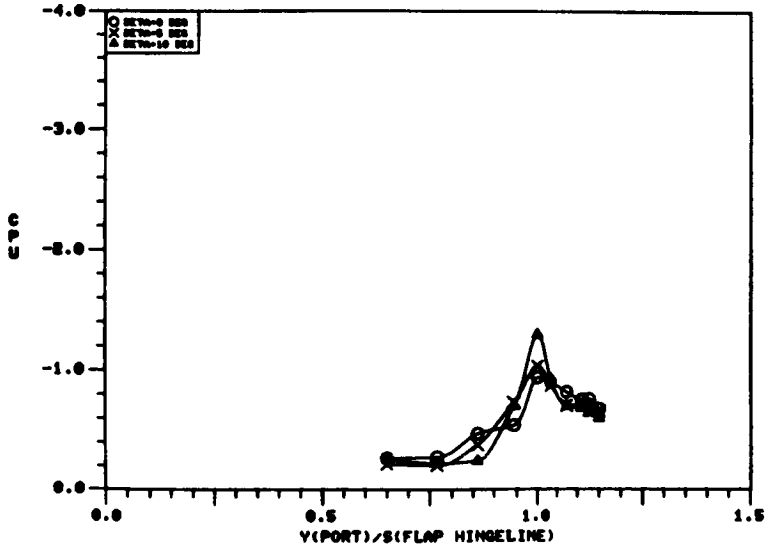

c) Leeward Wing, $\alpha = 12^{0}$, x/c = .748

Figure 104. Concluded.

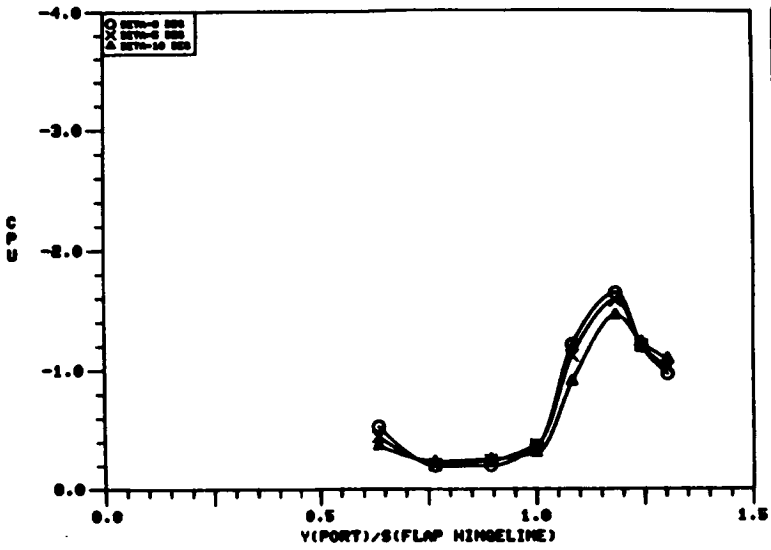

0 BETA = 0 DEG.

X BETA = 5 DEG.

Δ BETA = 10 DEG.

a) Windward Wing, $\alpha = 12^{o}$, x/c = .422

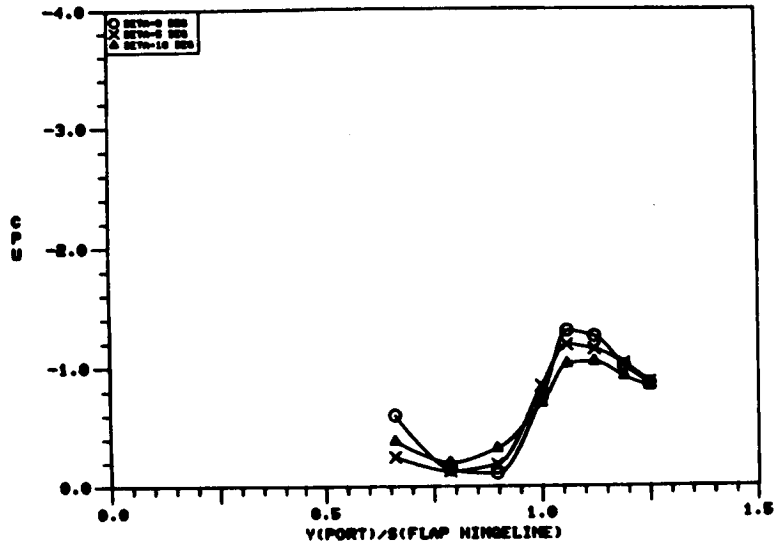

b) Windward Wing, $\alpha = 12^{o}$, x/c = .678

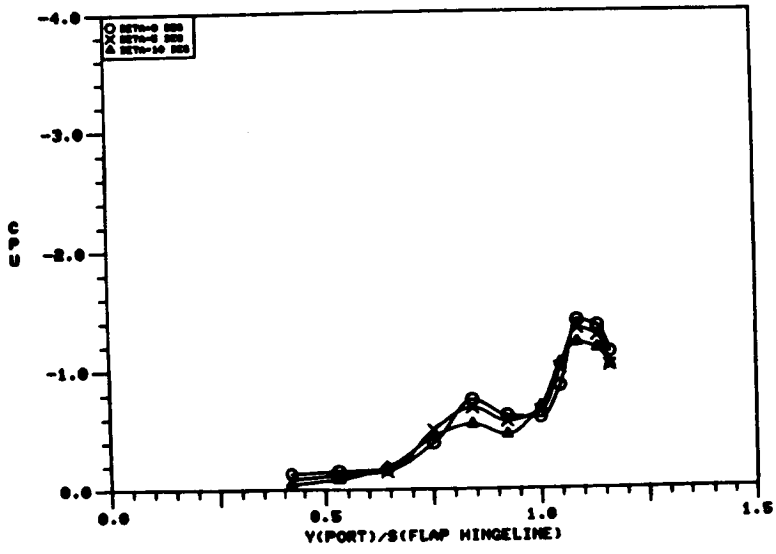

c) Windward Wing, $\alpha = 12^{o}$, x/c = .848

Figure 105. Effect of Sideslip Angle on the 70/50-Degree Cranked Wing Upper Surface Pressure Distributions with Tabbed Vortex Flaps.

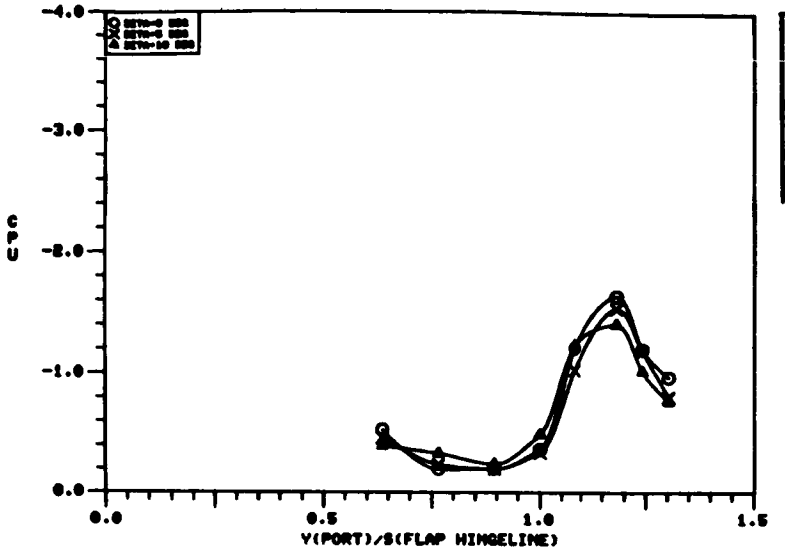

O	BETA = 0 DEG.
X	BETA = 5 DEG.
Δ	BETA = 10 DEG.

a) Leeward Wing, $\alpha = 12^{0}$, x/c = .422

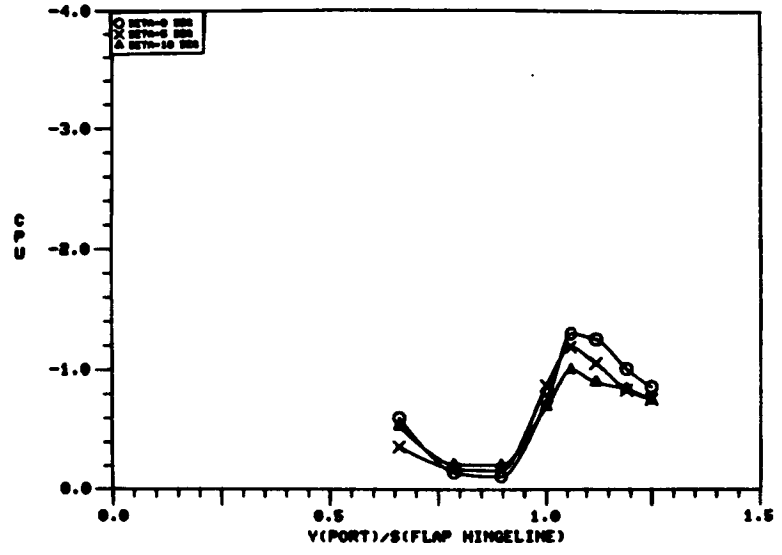

b) Leeward Wing, $\alpha = 12^{0}$, x/c = .678

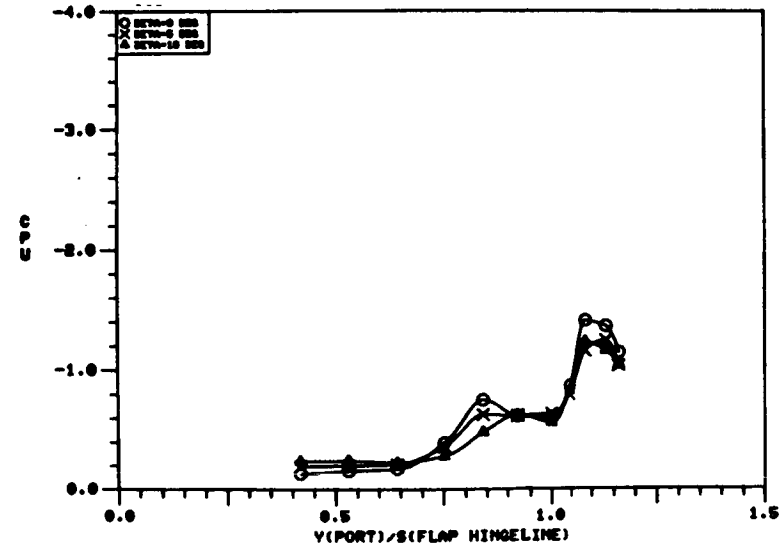

c) Leeward Wing, $\alpha = 12^{0}$, x/c = .848

Figure 105. Concluded.

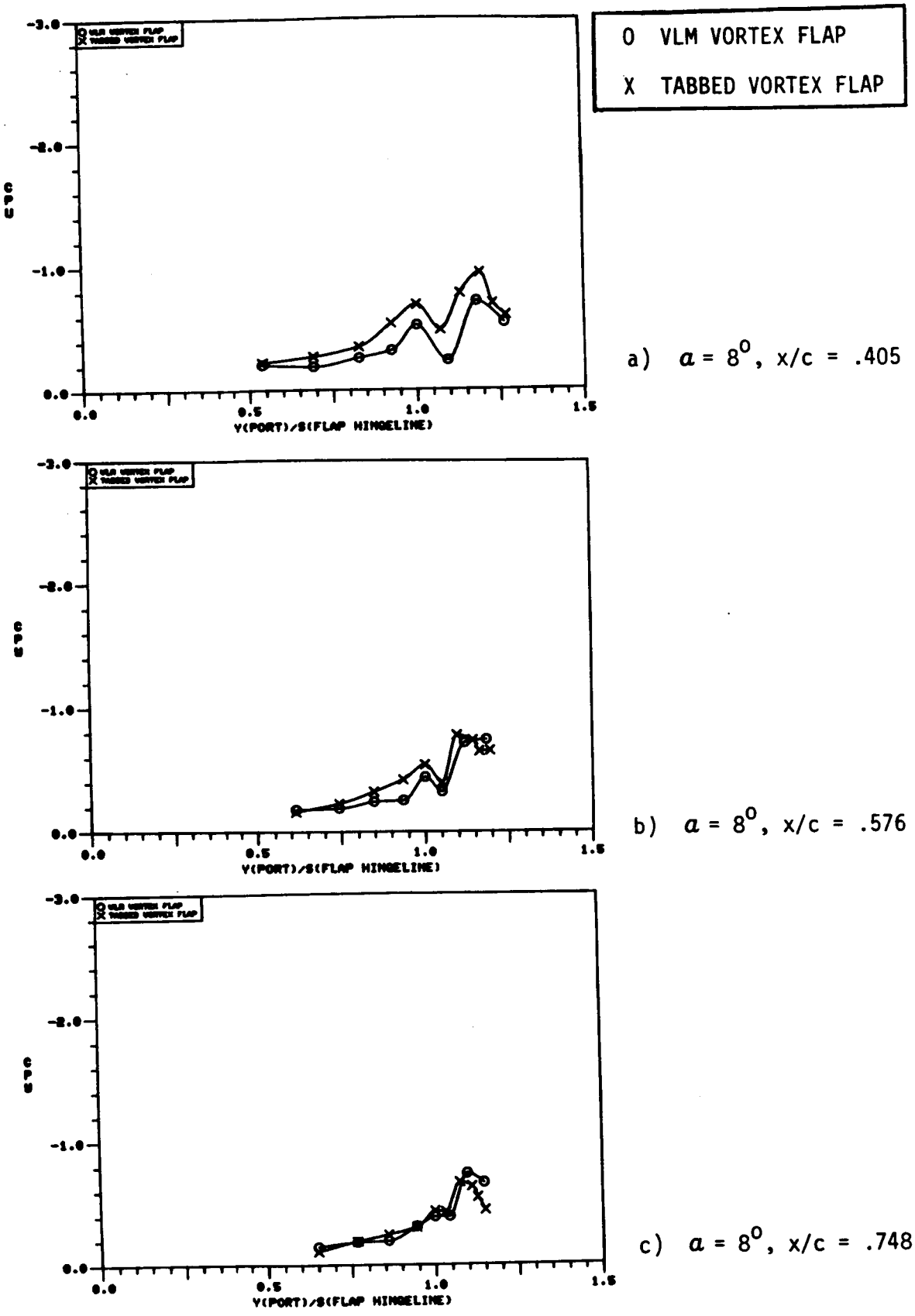

a) $\alpha = 8^{o}$, x/c = .405

b) $\alpha = 8^{o}$, x/c = .576

c) $\alpha = 8^{o}$, x/c = .748

Figure 106. Comparison of the 65-Degree Cropped Delta Wing Upper Surface Pressure Distribution with Tabbed and Plain Vortex Flaps.

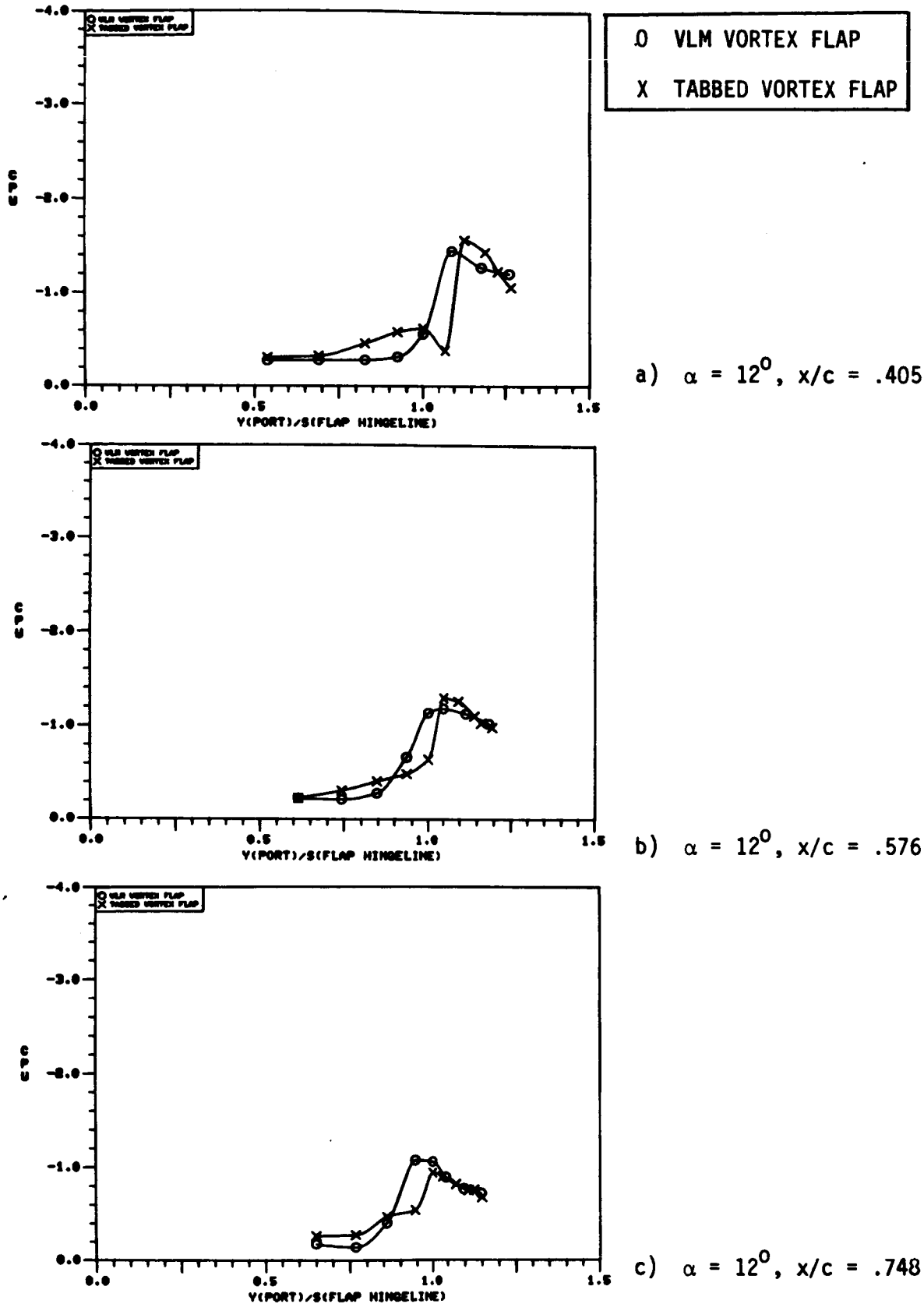

a) $\alpha = 12^{o}$, x/c = .405

b) $\alpha = 12^{o}$, x/c = .576

c) $\alpha = 12^{o}$, x/c = .748

Figure 107. Comparison of the 65-Degree Cropped Delta Wing Upper Surface Pressure Distribution with Tabbed and Plain Vortex Flaps.

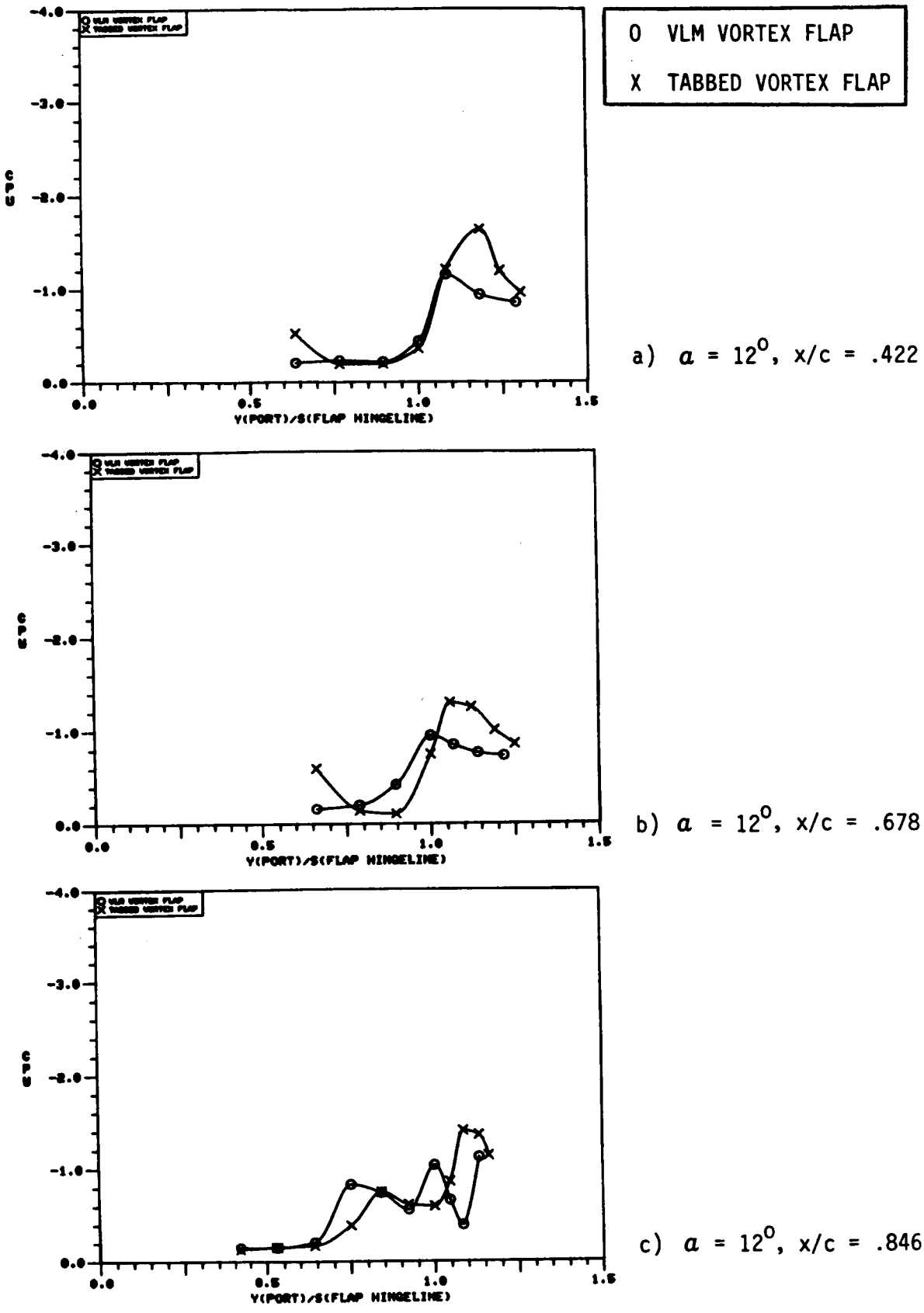

Figure 108. Comparison of the 70/50-Degree Cranked Wing Upper Surface Pressure Distribution with Tabbed and Plain Vortex Flaps.

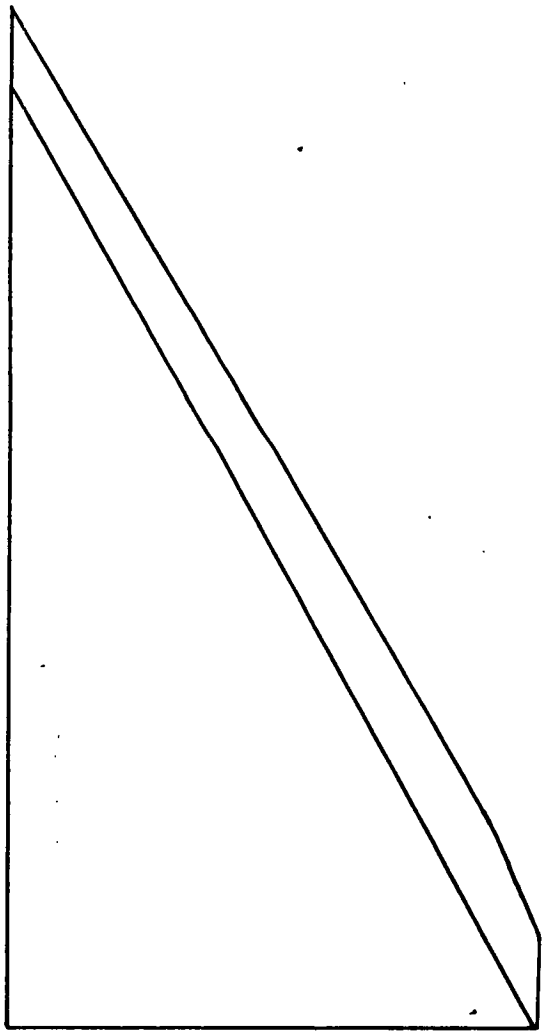

a) VLM-Designed Vortex Flap

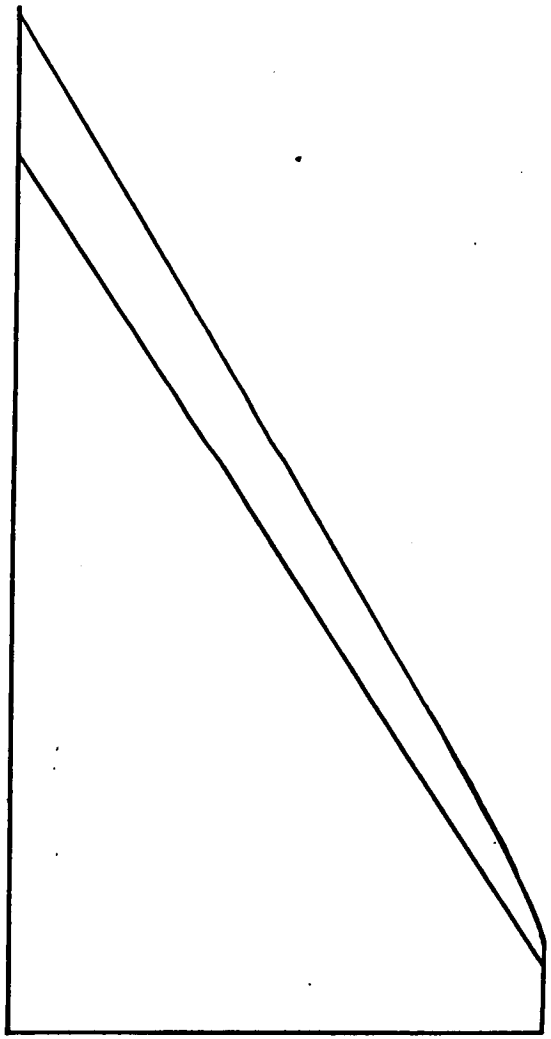

b) Tapered Vortex Flap

Figure 109. 60-Degree Cropped Delta Wing

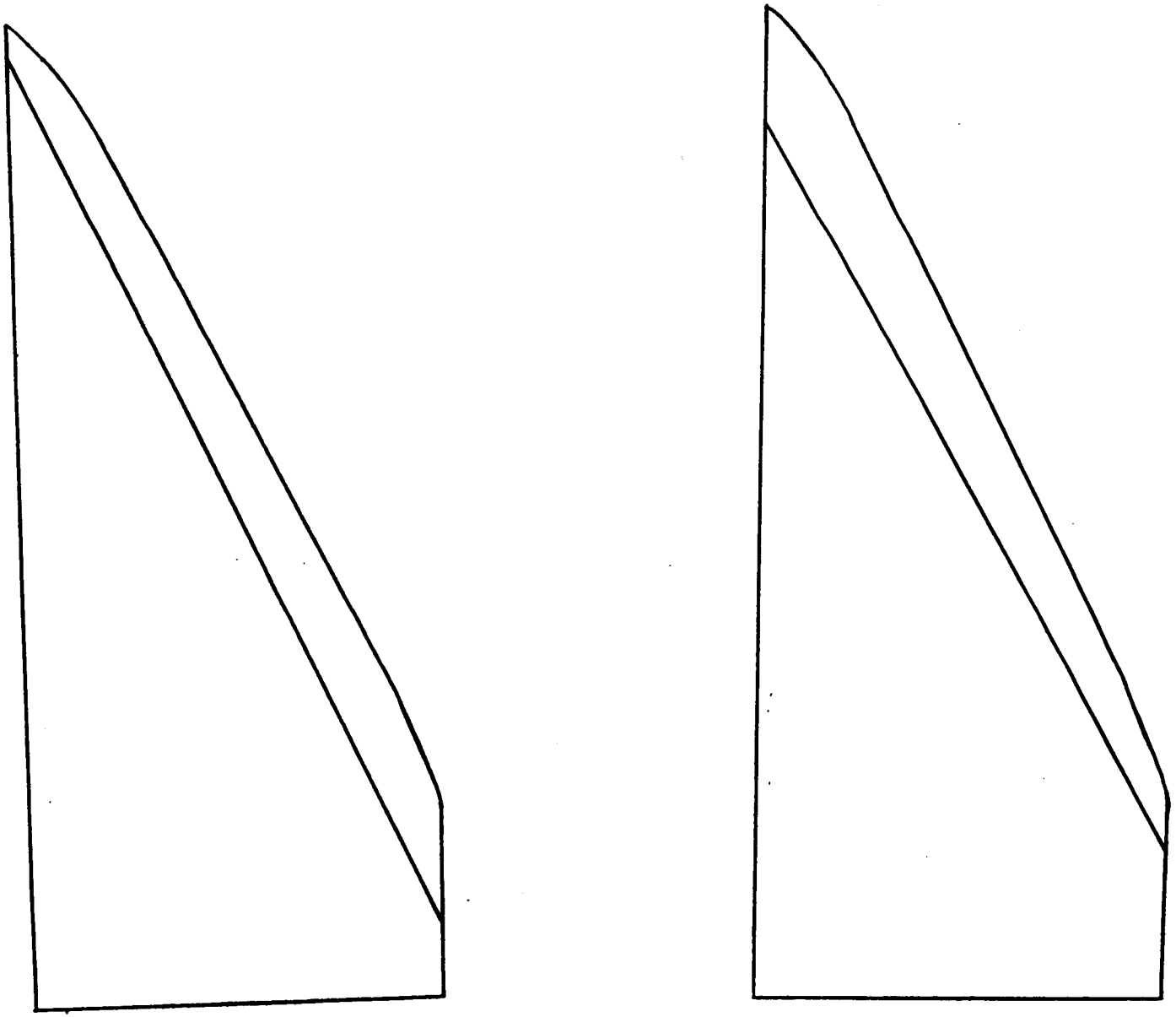

a) VLM-Designed Vortex Flap

b) Tapered Vortex Flap

Figure 110. 65-Degree Cropped Delta Wing

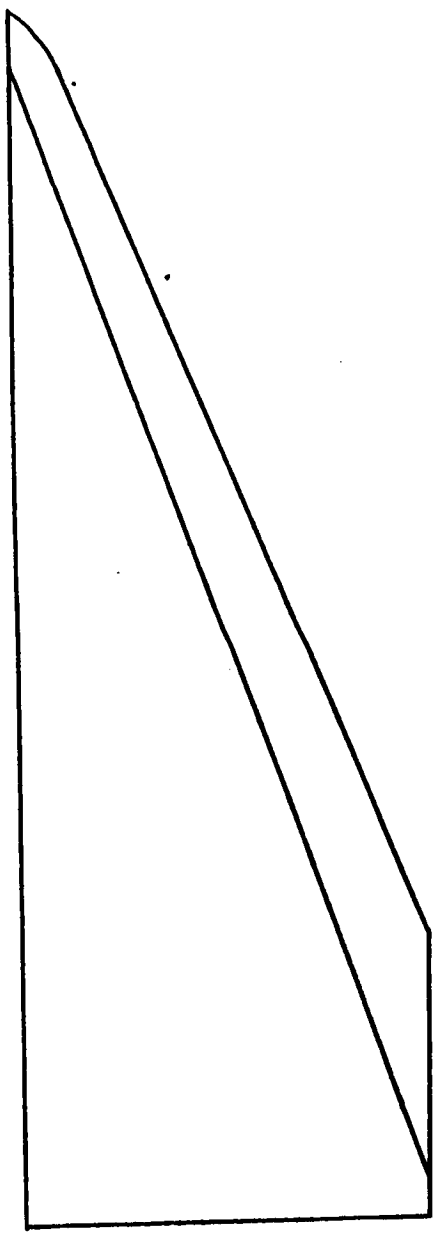

a) VLM-Designed Vortex Flap

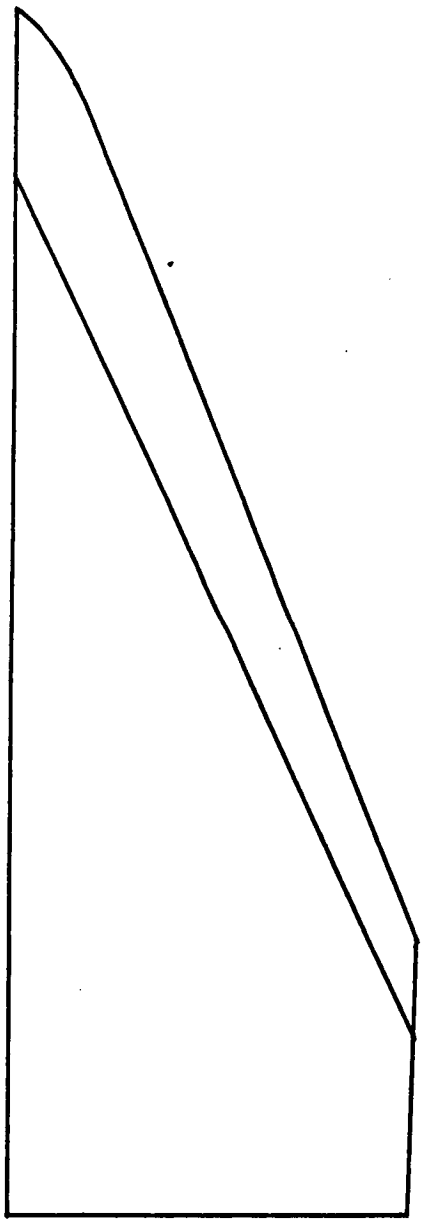

b) Tapered Vortex Flap

Figure 111. 70-Degree Cropped Delta Wing

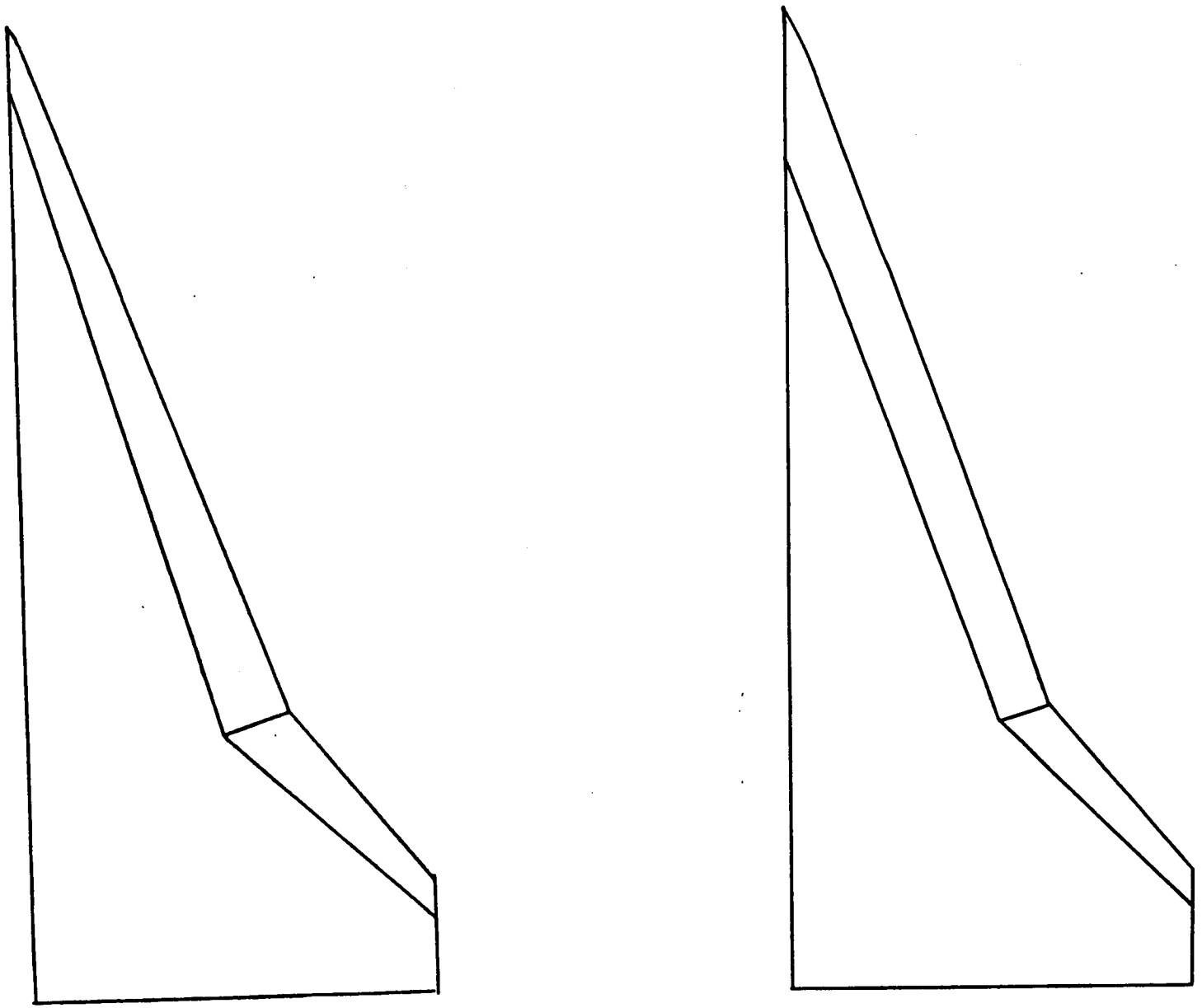

a) VLM-Designed Vortex Flap

b) Tapered Vortex Flap

Figure 112. 70/50-Degree Cranked Wing

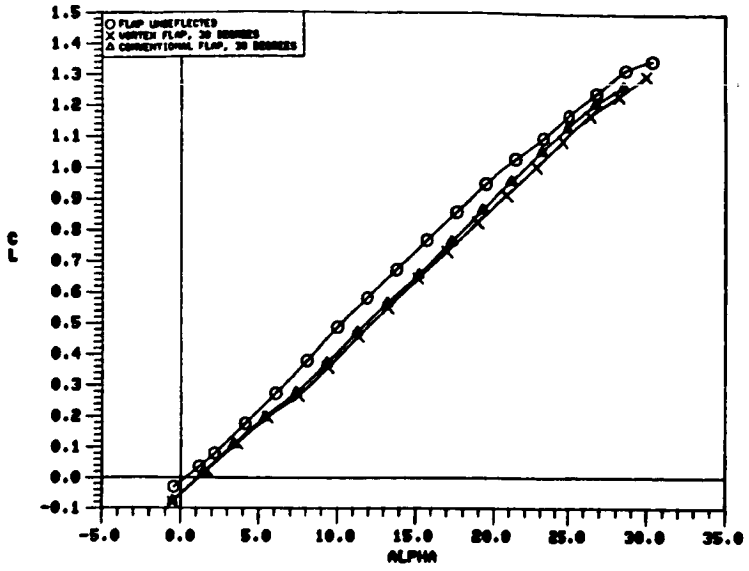

a) C_L vs. α

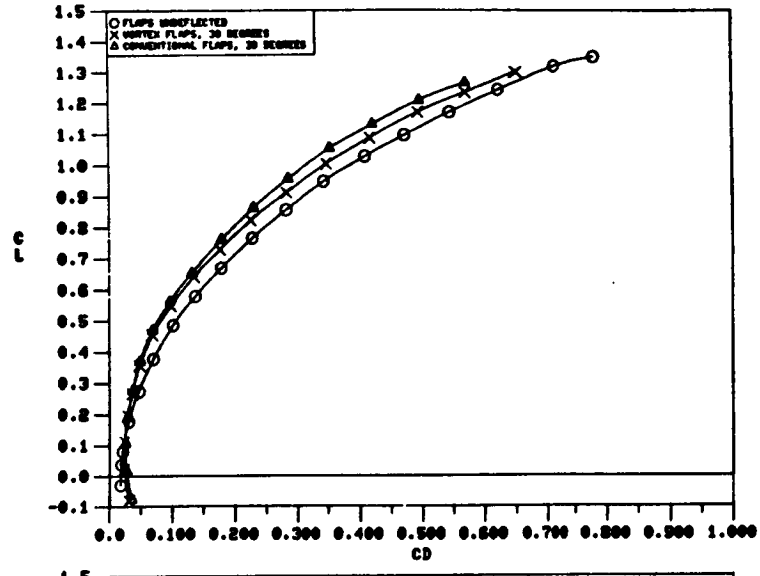

b) C_L vs. C_D

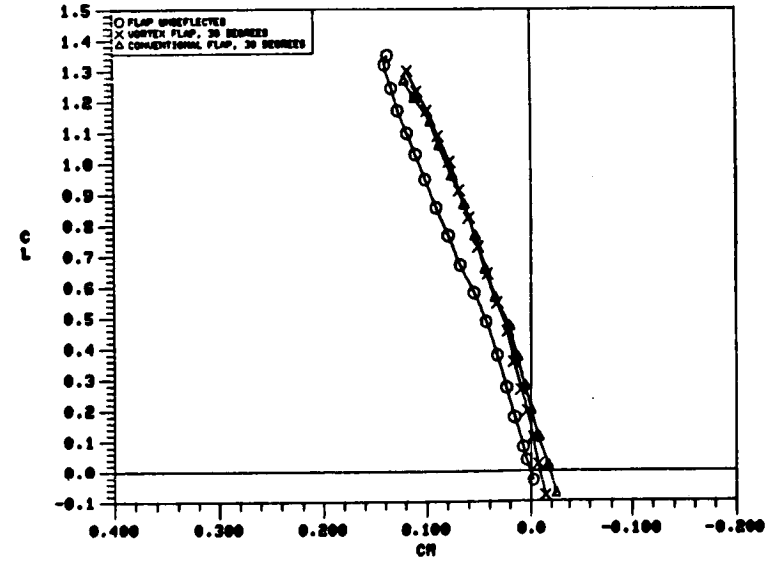

c) C_L vs. C_m

Figure 113. Comparison of the Static Longitudinal Aerodynamics Characteristics of the 60-Degree Cropped Delta Wing with VLM-Designed and Tapered Flaps.

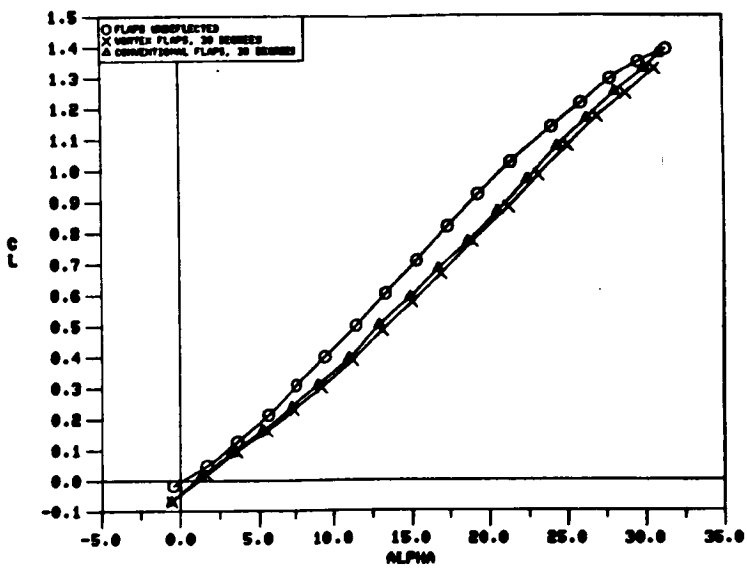

0 FLAP UNDEFLECTED

X VLM - DESIGNED FLAP, 30 DEG.

Δ TAPERED FLAP, 30 DEG.

a) C_L vs. α

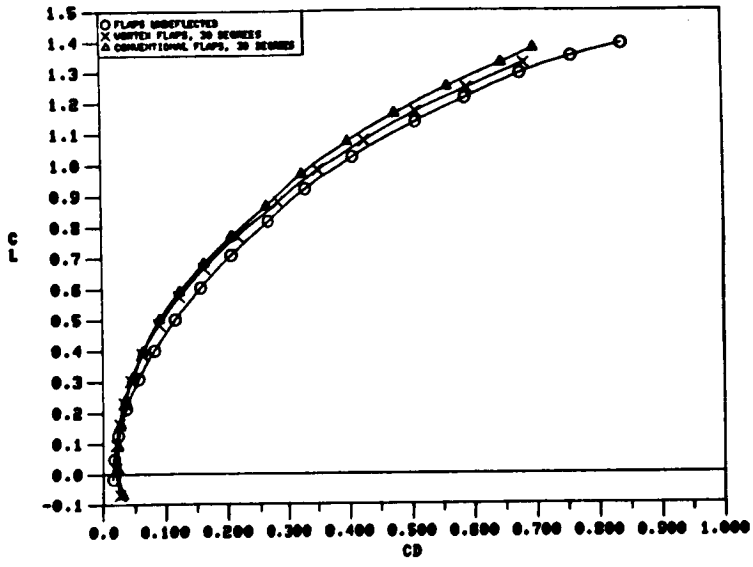

b) C_L vs. C_D

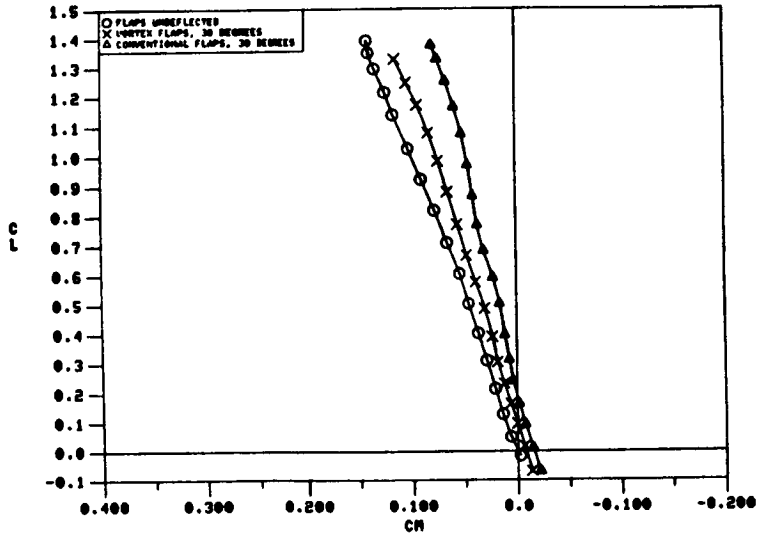

c) C_L vs. C_m

Figure 114. Comparison of the Static Longitudinal Aerodynamics Characteristics of the 65-Degree Cropped Delta Wing with VLM-Designed and Tapered Flaps.

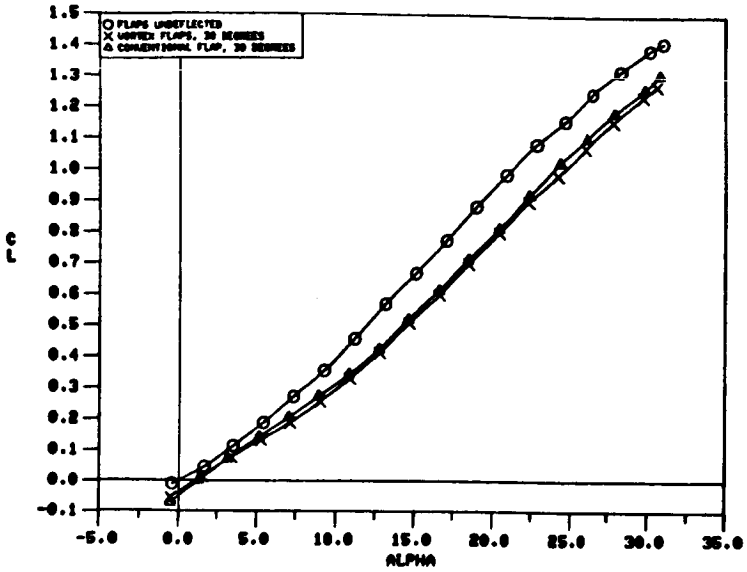

a) C_L vs. α

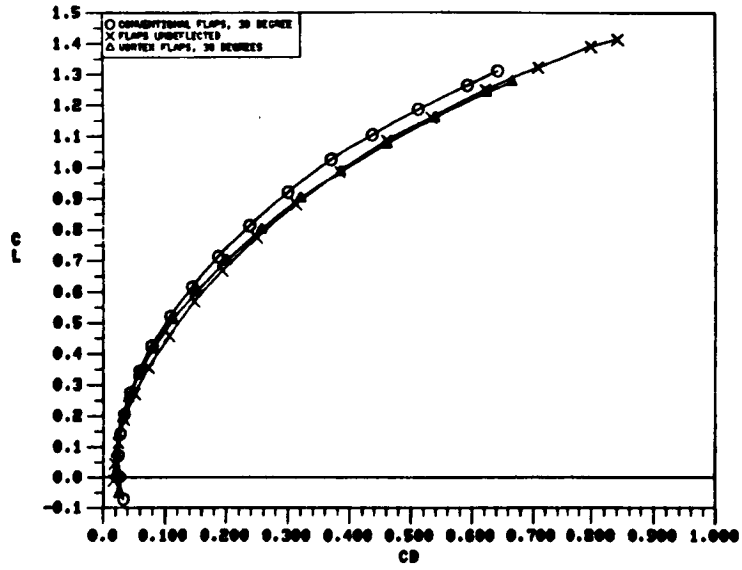

b) C_L vs. C_D

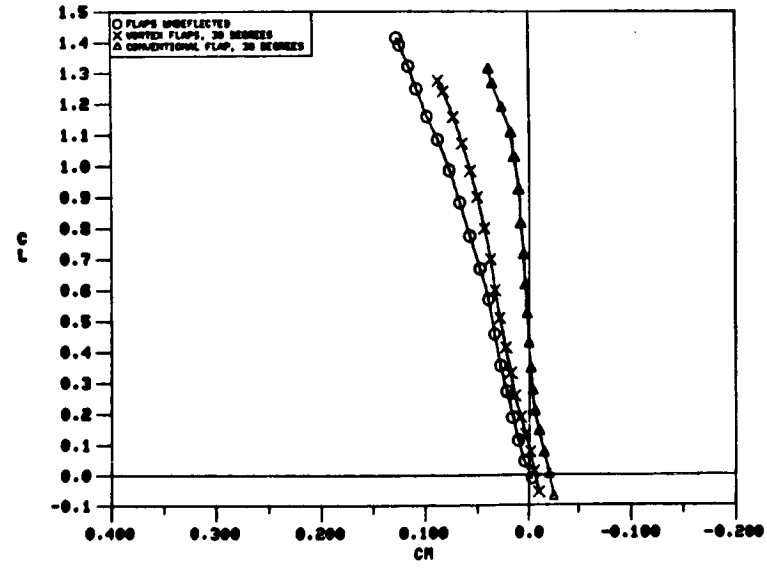

c) C_L vs. C_m

Figure 115. Comparison of the Static Longitudinal Aerodynamics Characteristics of the 70-Degree Cropped Delta Wing with VLM-Designed and Tapered Flaps.

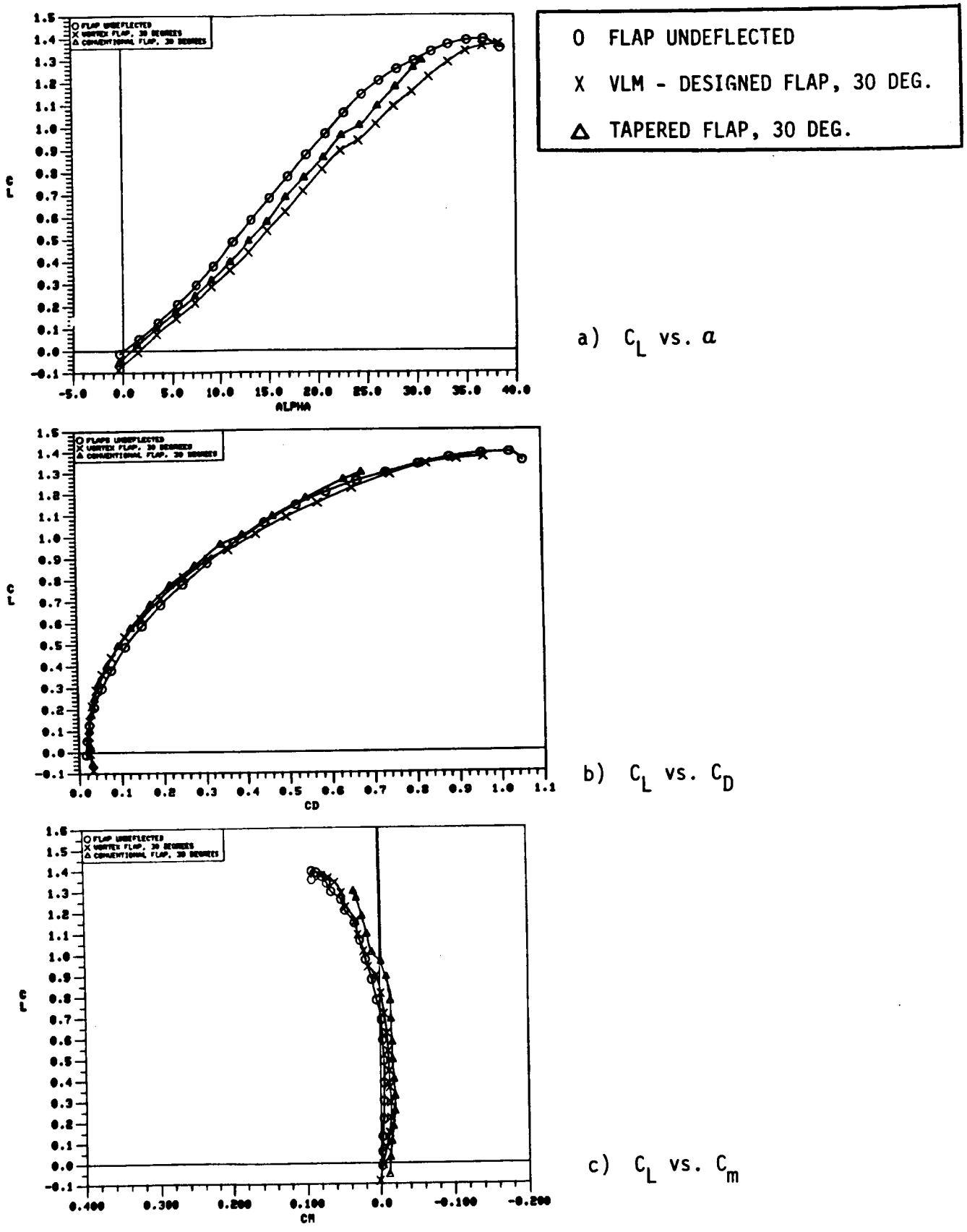

a) C_L vs. α

b) C_L vs. C_D

c) C_L vs. C_m

Figure 116. Comparison of the Static Longitudinal Aerodynamics Characteristics of the 70/50-Degree Cranked Wing with VLM-Designed and Tapered Flaps.

O	FLAP UNDEFLECTED
X	VLM-DESIGNED FLAP, 30 DEG.
Δ	TAPERED FLAP, 30 DEG.

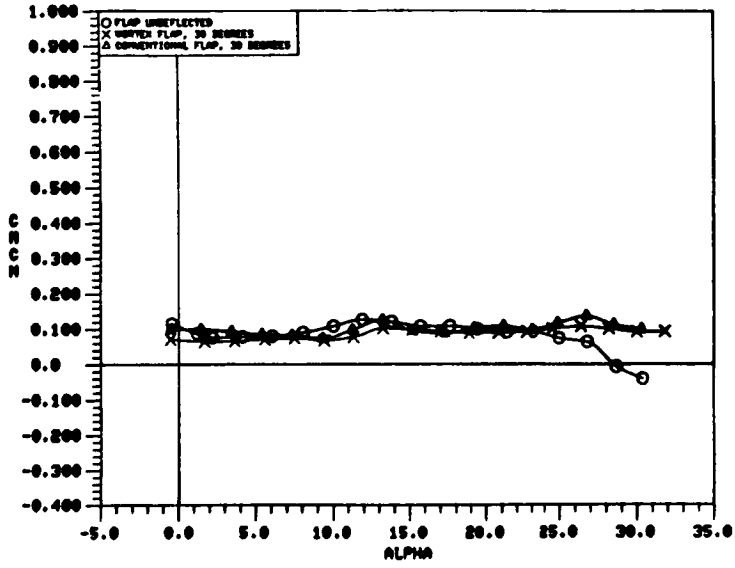

a) $C_{m_{C_N}}$ vs. α

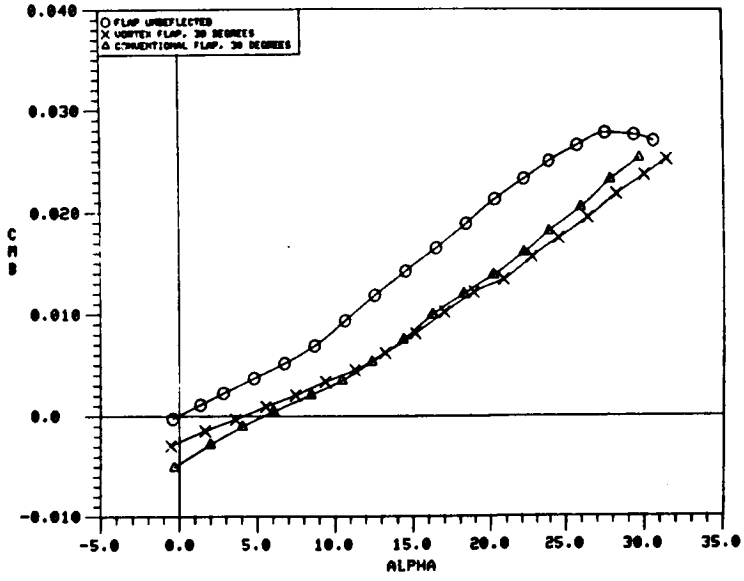

b) C_{m_β} vs. α

Figure 117. Comparison of the Static Longitudinal Stability Characteristics of the 60-Degree Cropped Delta Wing with VLM-Designed and Tapered Flaps.

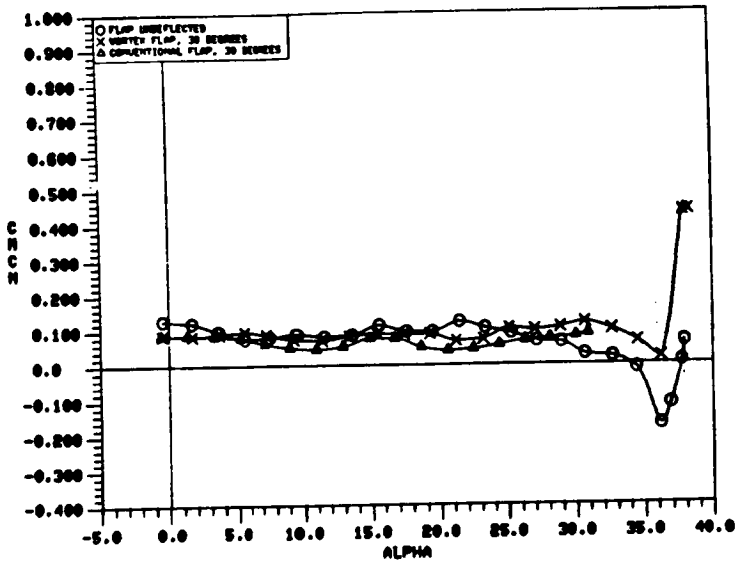

a) $C_{m_{C_N}}$ vs. α

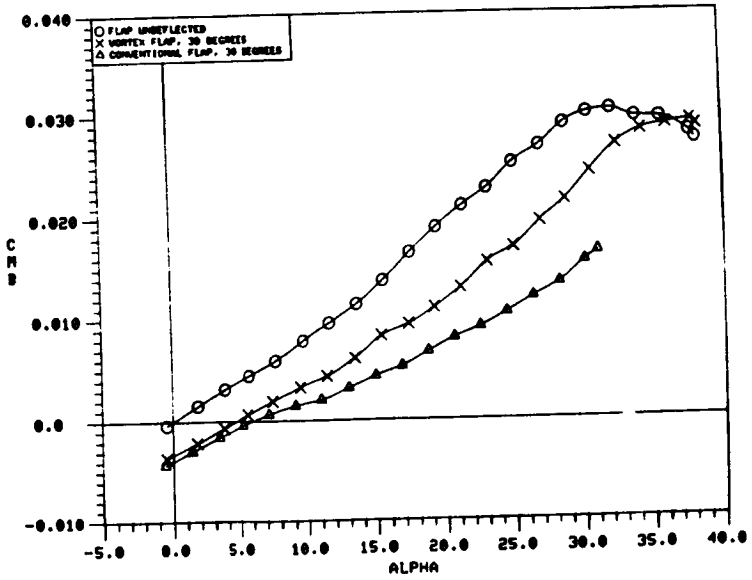

b) C_{m_β} vs. α

Figure 118. Comparison of the Static Longitudinal Stability Characteristics of the 65-Degree Cropped Delta Wing with VLM-Designed and Tapered Flaps.

O	FLAP UNDEFLECTED
X	VLM-DESIGNED FLAP, 30 DEG.
Δ	TAPERED FLAP, 30 DEG.

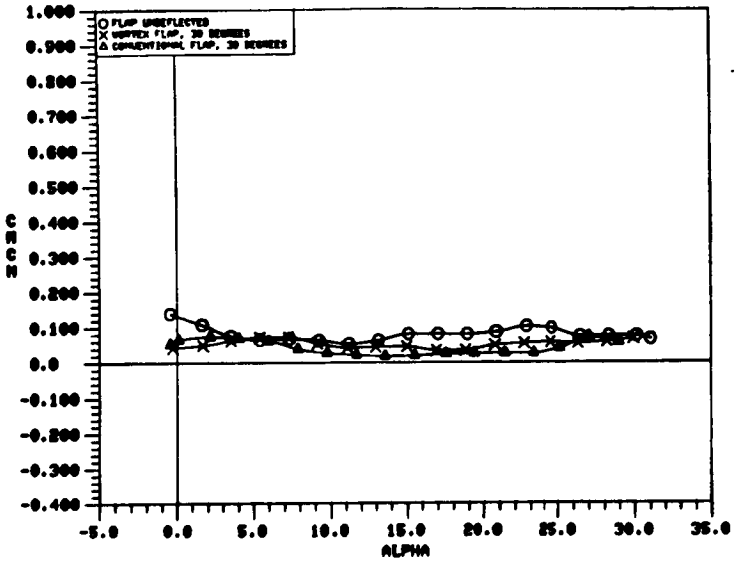

a) $C_{m_{C_N}}$ vs. α

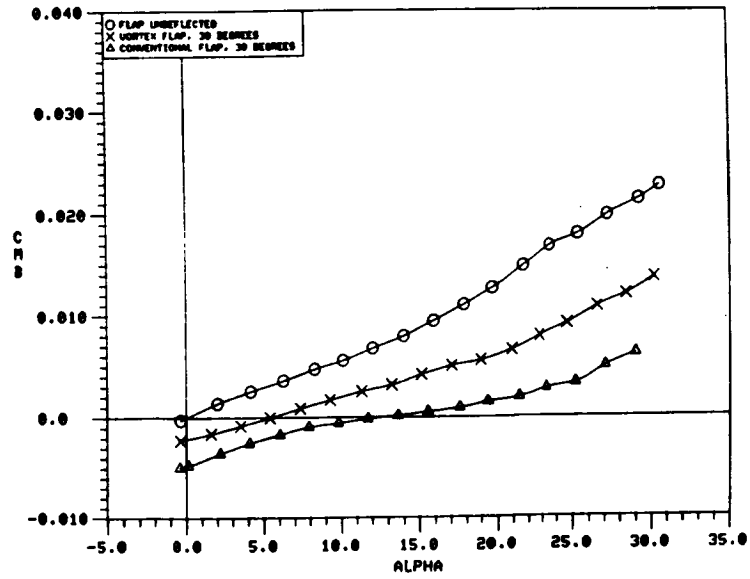

b) C_{m_β} vs. α

Figure 119. Comparison of the Static Longitudinal Stability Characteristics of the 70-Degree Cropped Delta Wing with VLM-Designed and Tapered Flaps.

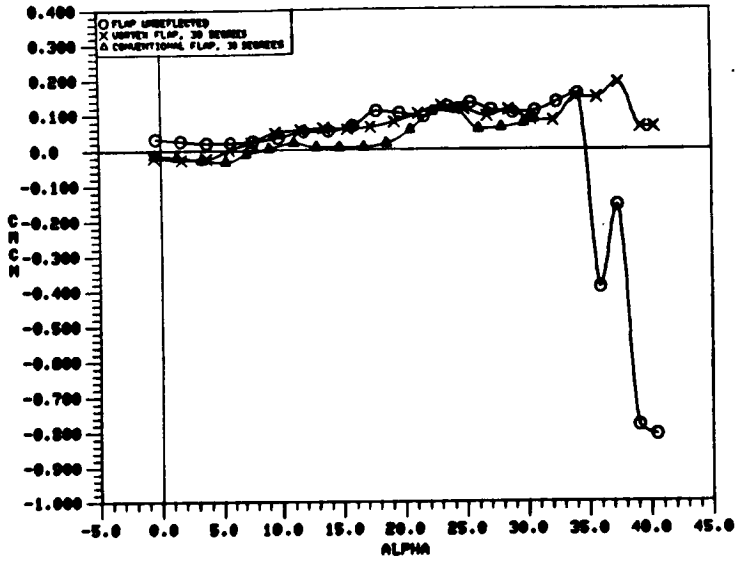

a) $C_{m_{C_N}}$ vs. α

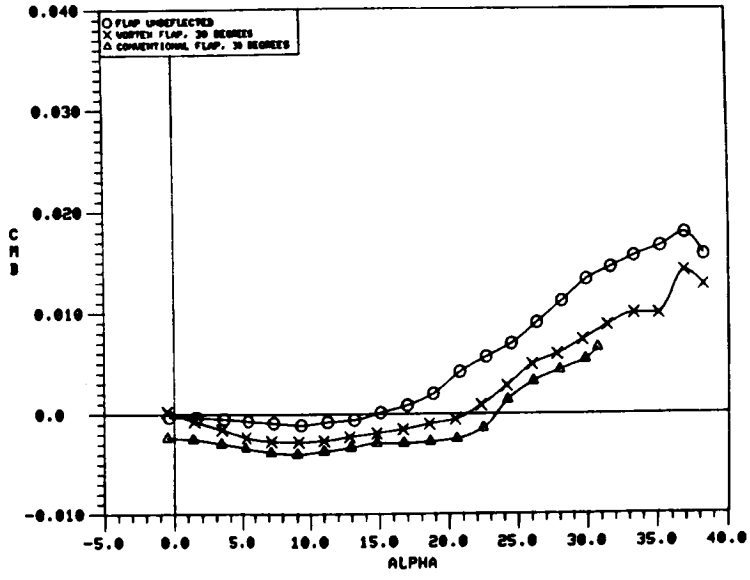

b) C_{m_β} vs. α

Figure 120. Comparison of the Static Longitudinal Stability Characteristics of the 70/50-Degree Cranked Wing with VLM-Designed and Tapered Flaps.

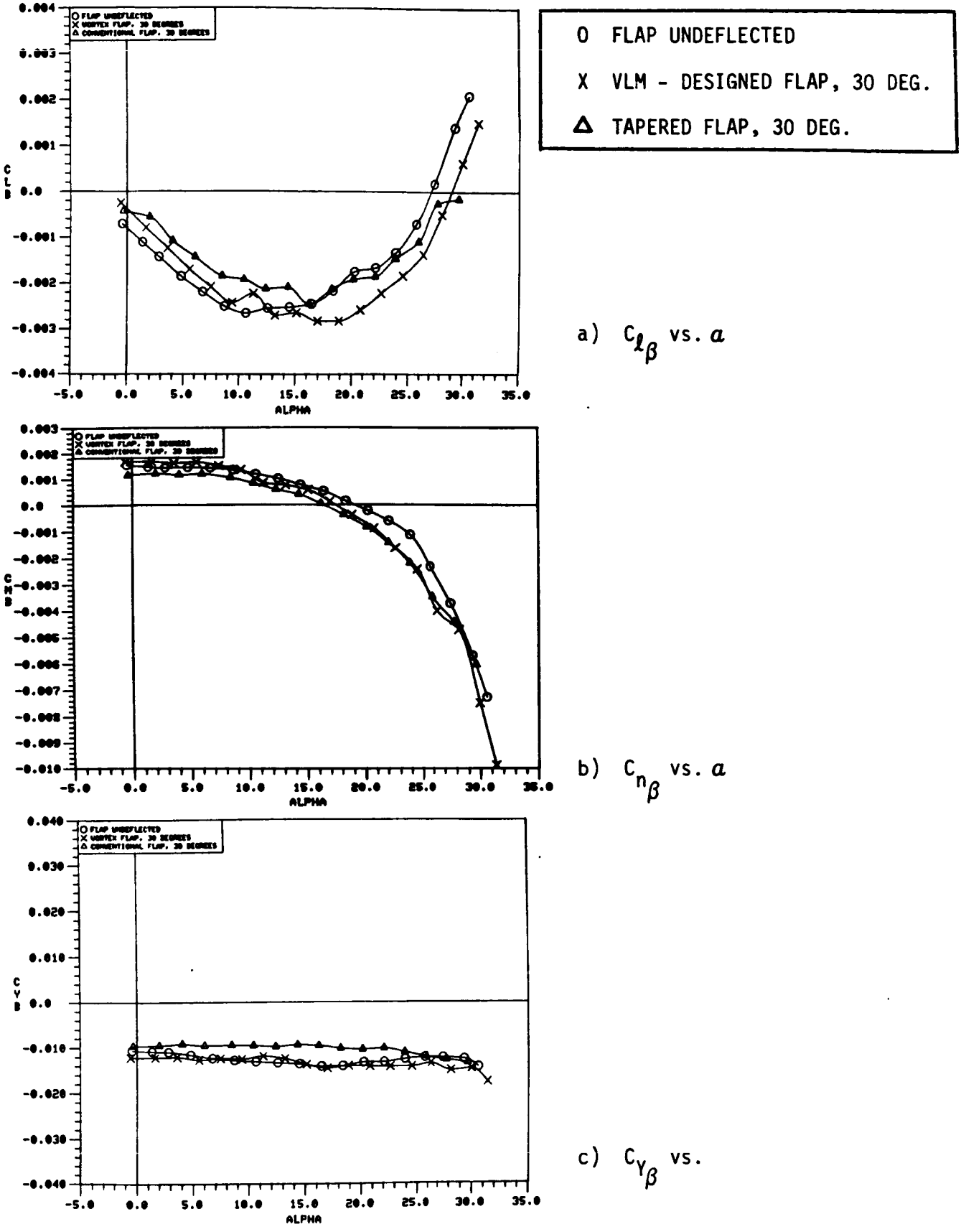

Figure 121. Comparison of the Static Lateral-Directional Stability Characteristics of the 60-Degree Cropped Delta Wing with VLM-Designed and Tapered Vortex Flaps.

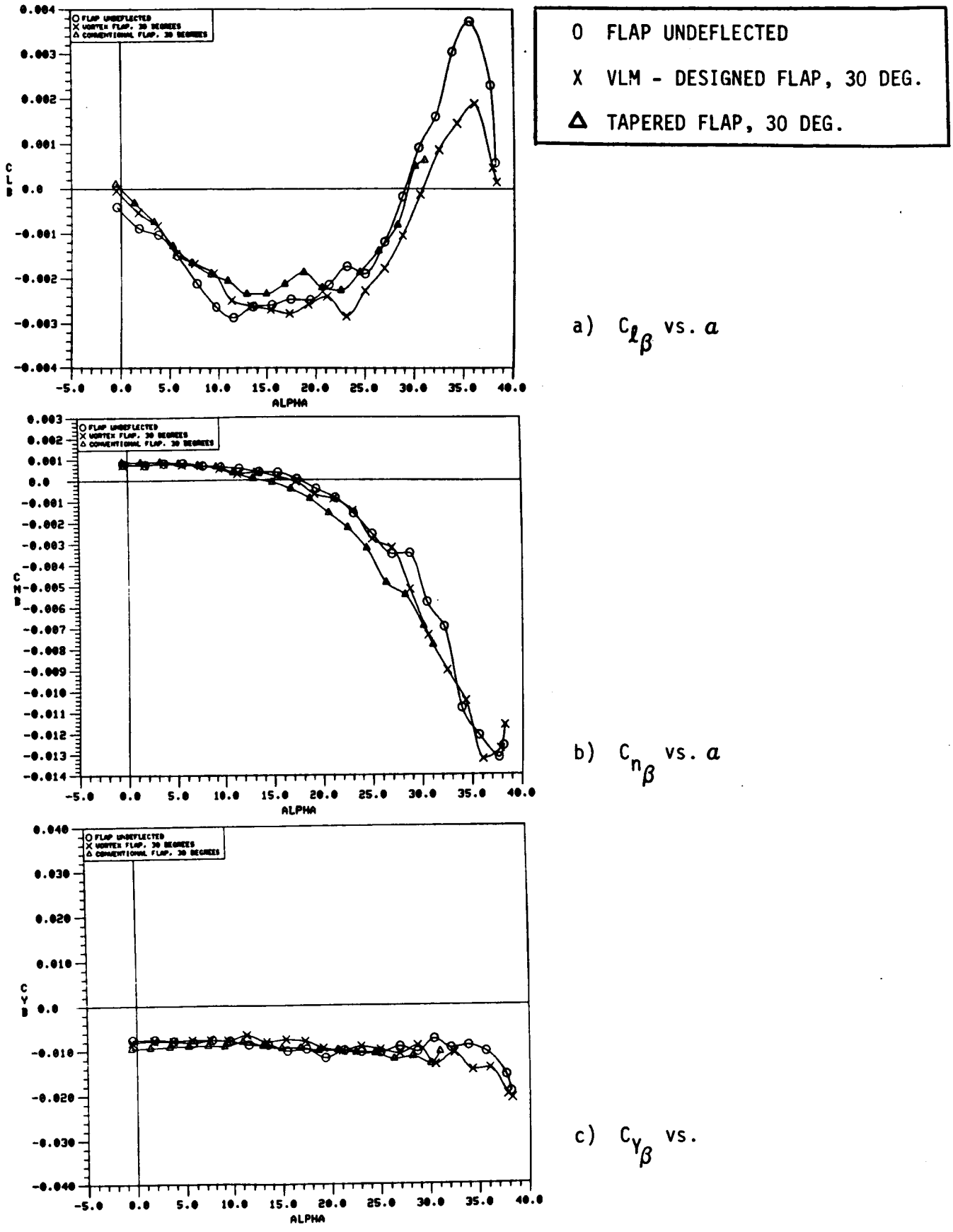

Figure 122. Comparison of the Static Lateral-Directional Stability Characteristics of the 65-Degree Cropped Delta Wing with VLM-Designed and Tapered Vortex Flaps.

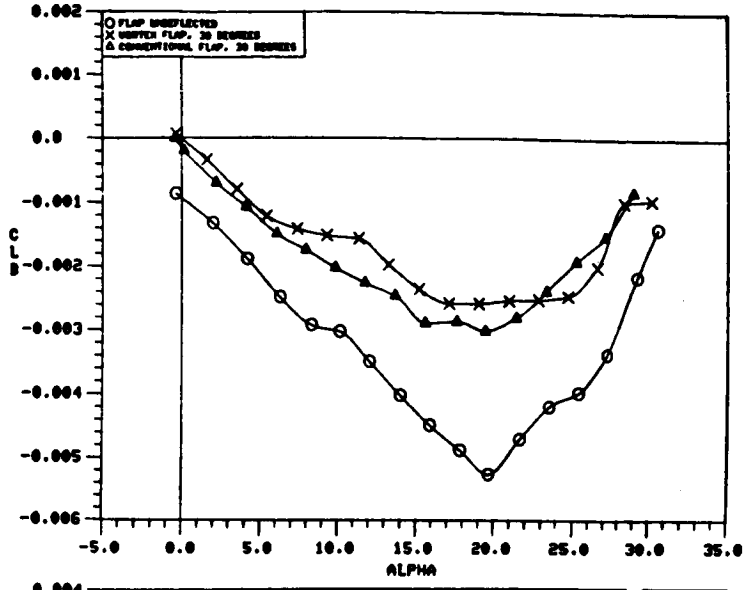

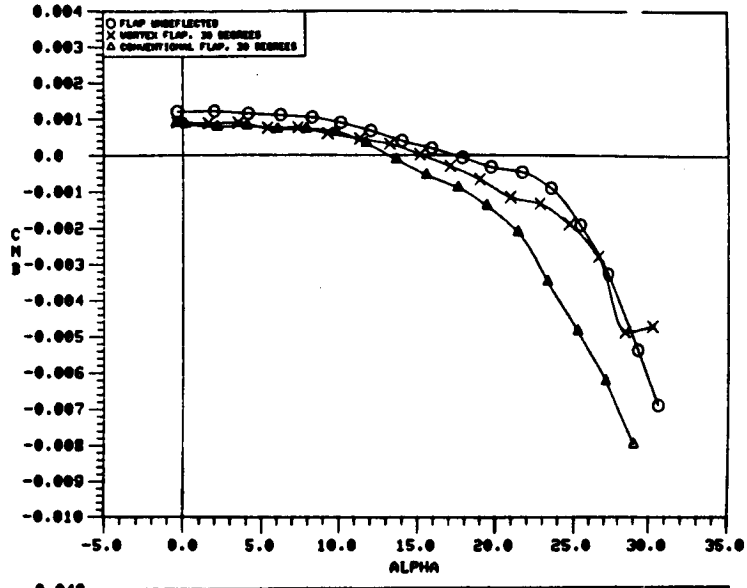

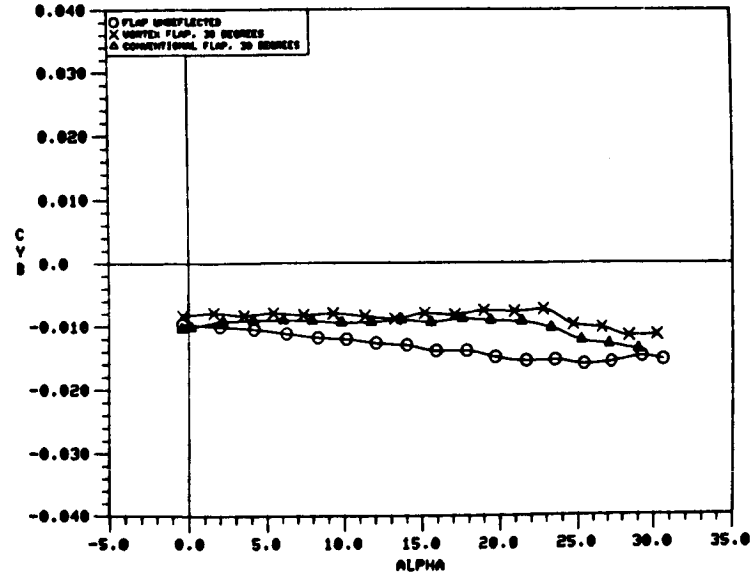

O	FLAP UNDEFLECTED
X	VLM - DESIGNED FLAP, 30 DEG.
Δ	TAPERED FLAP, 30 DEG.

a) C_{ℓ_β} vs. α

b) C_{n_β} vs. α

c) C_{Y_β} vs.

Figure 123. Comparison of the Static Lateral-Directional Stability Characteristics of the 70-Degree Cropped Delta Wing with VLM-Designed and Tapered Vortex Flaps.

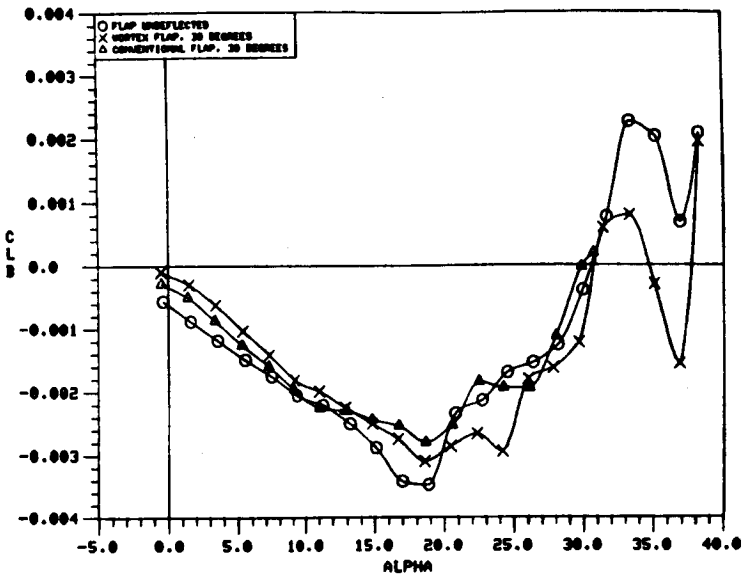

a) C_{ℓ_β} vs. α

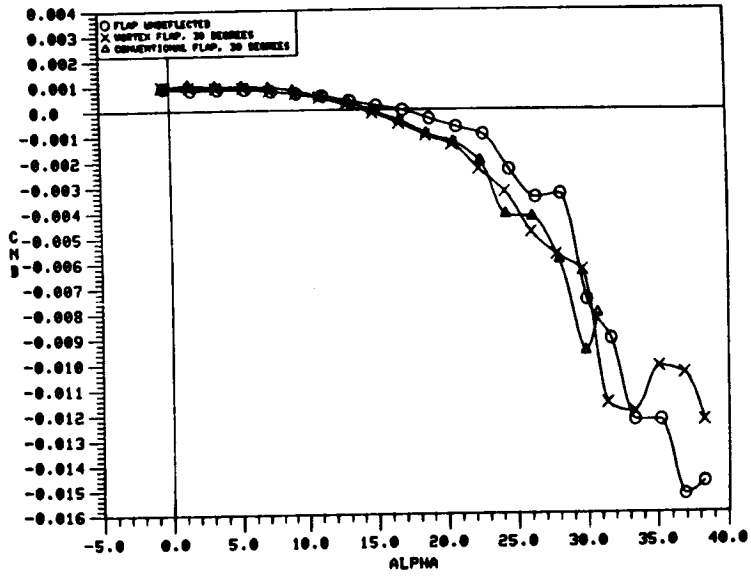

b) C_{n_β} vs. α

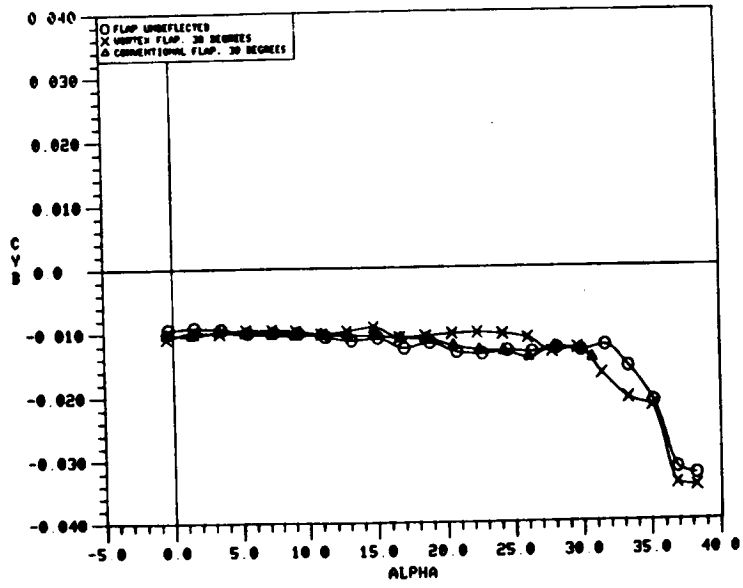

c) C_{Y_β} vs.

Figure 124. Comparison of the Static Lateral-Directional Stability Characteristics of the 70/50-Degree Cranked Wing with VLM-Designed and Tapered Vortex Flaps.

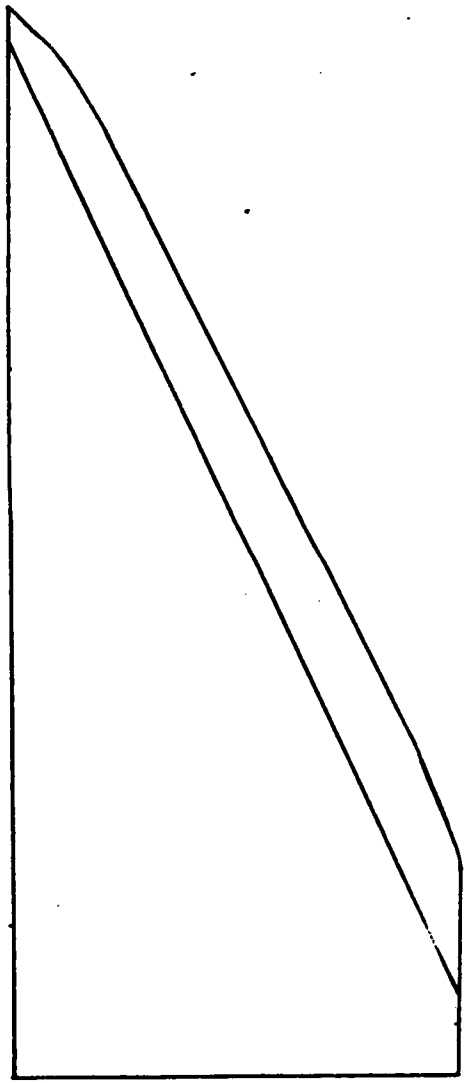

a) $\Lambda_{TE} = 0°$

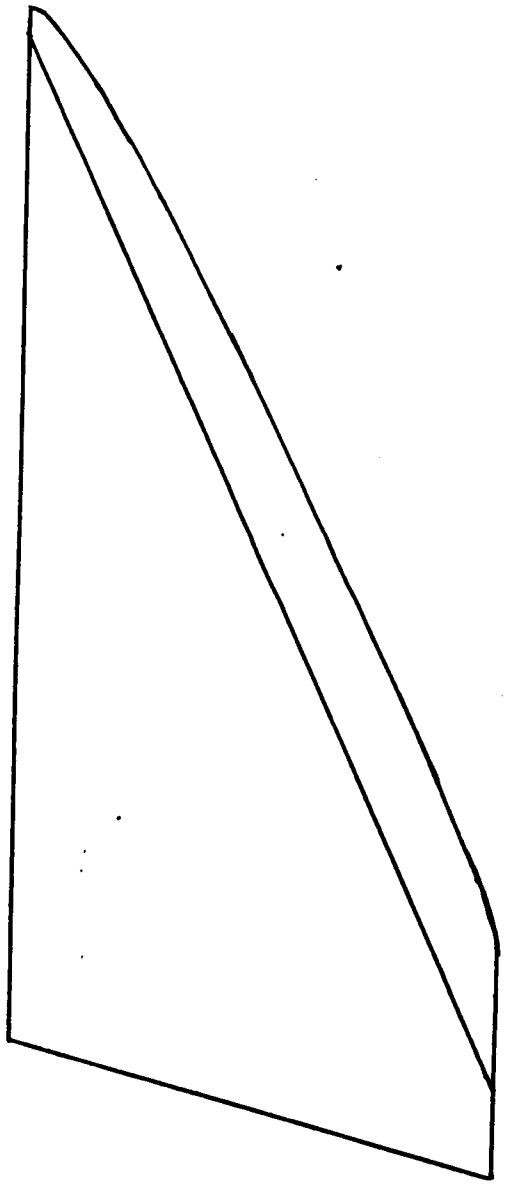

b) $\Lambda_{TE} = +15°$

Figure 125. 65-Degree Cropped Delta Wing with Trailing-Edge Sweep Variations

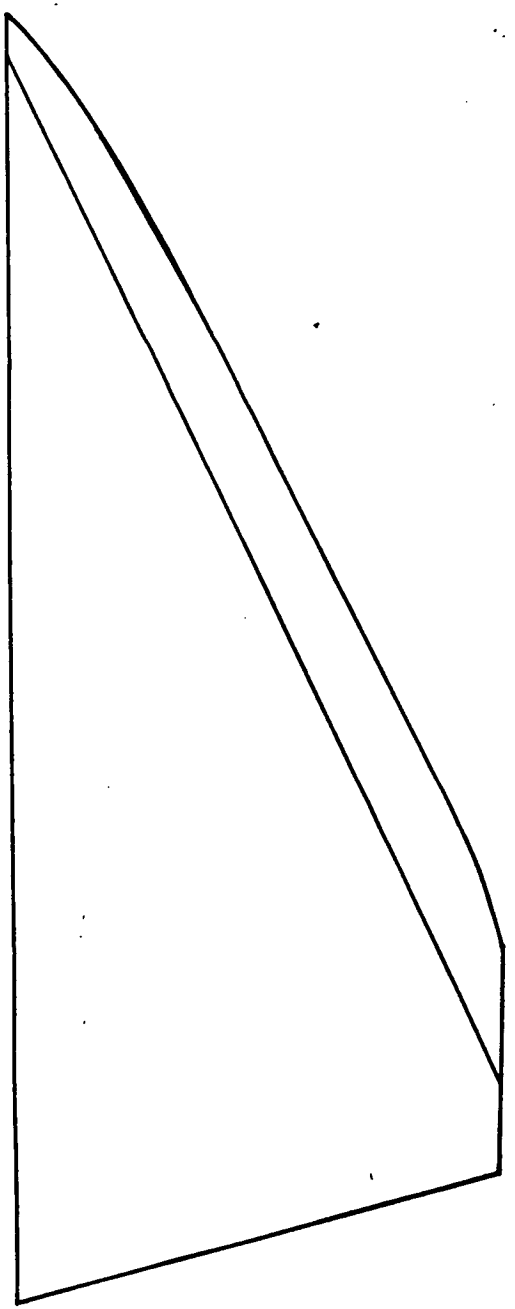

c) $\Lambda_{TE} = -15°$

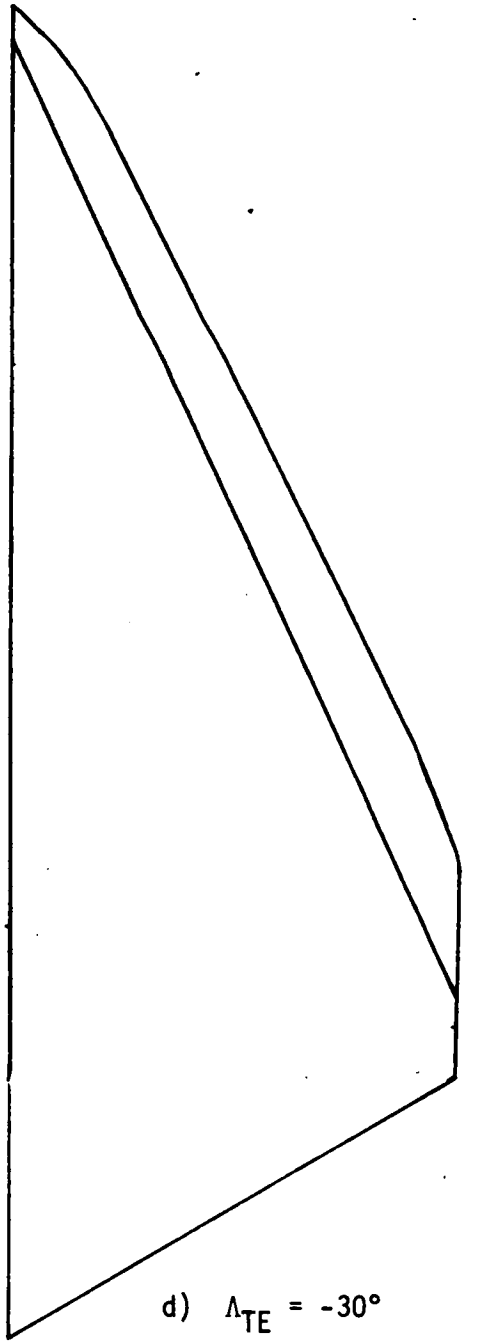

d) $\Lambda_{TE} = -30°$

Figure 125. Concluded.

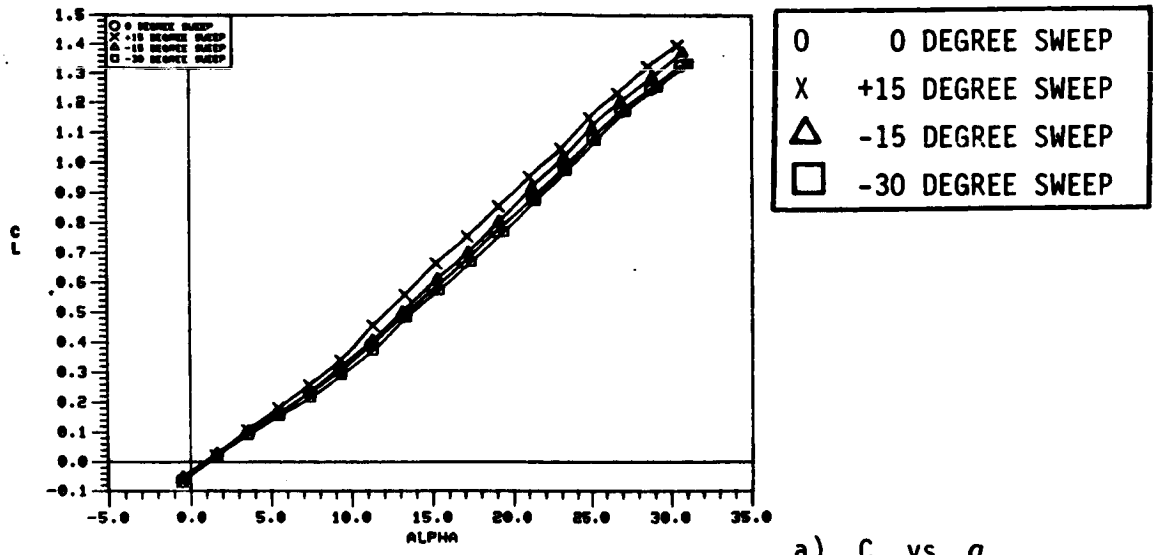

a) C_L vs. α

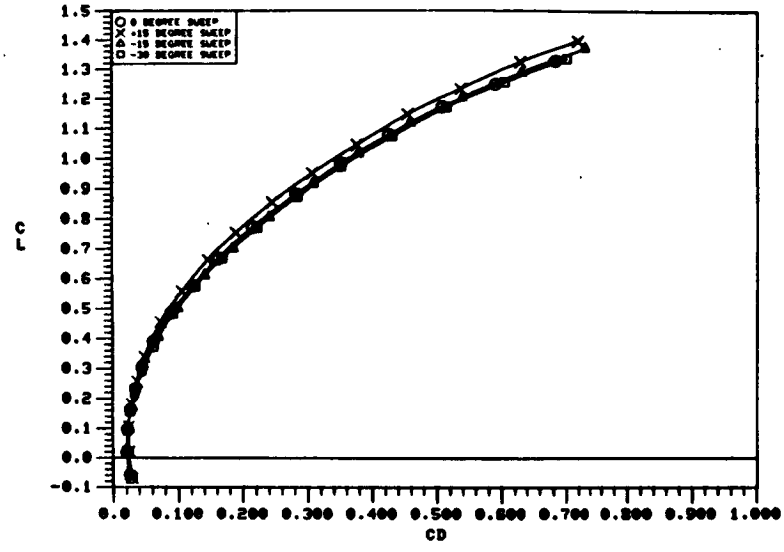

b) C_L vs. C_D

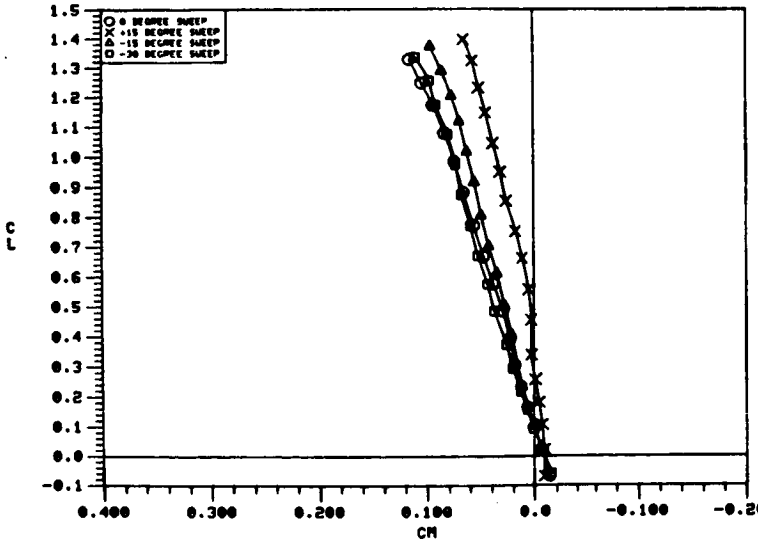

c) C_L vs. C_m

Figure 126. Effect of Trailing-Edge Sweep Variation on the 65-Degree Cropped Delta Wing Static Longitudinal Aerodynamic Characteristics.

O	0 DEGREE SWEEP
X	+15 DEGREE SWEEP
△	-15 DEGREE SWEEP
□	-30 DEGREE SWEEP

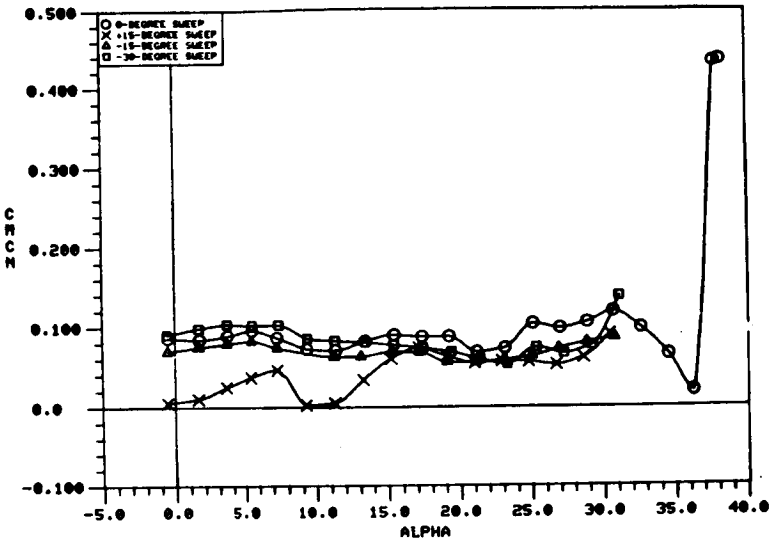

a) $C_{m_{C_N}}$ vs. α

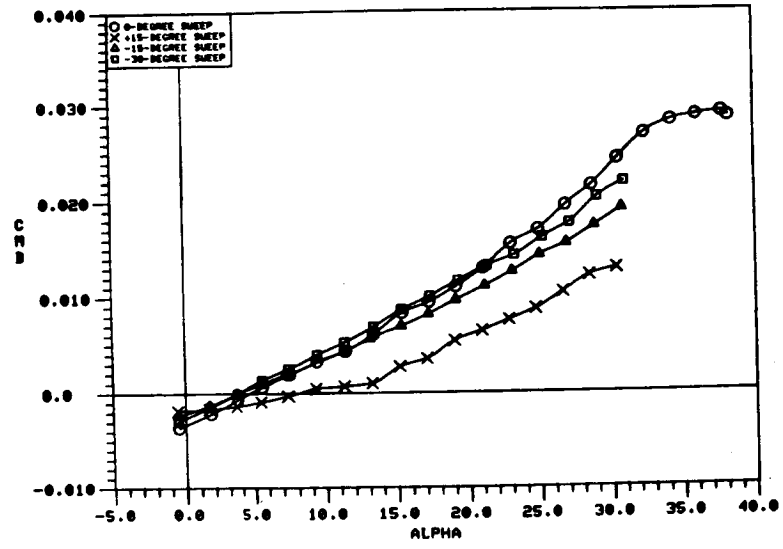

b) C_{m_β} vs. α

Figure 127. Effect of Trailing-Edge Sweep Variation on the 65-Degree Cropped Delta Wing Static Longitudinal Stability Characteristics.

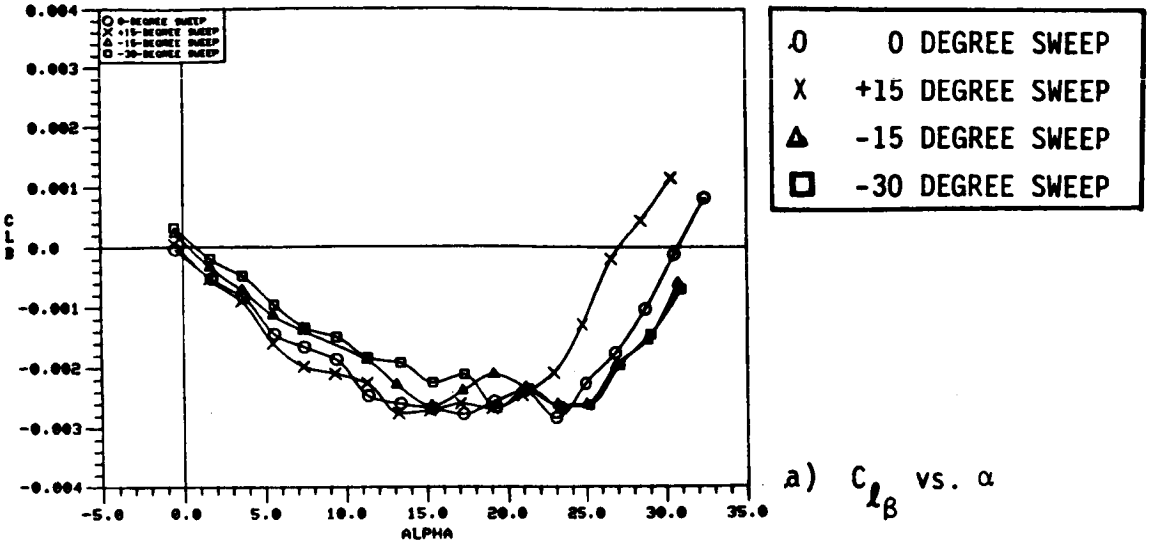

a) C_{l_β} vs. α

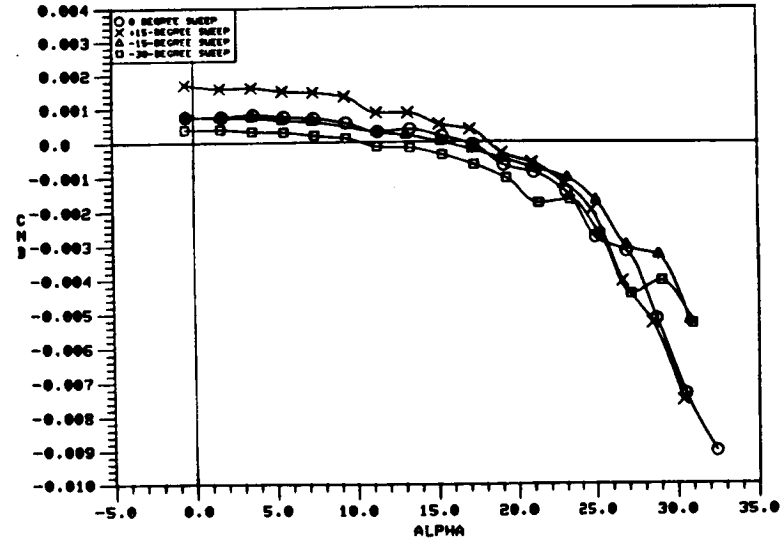

b) C_{n_β} vs. α

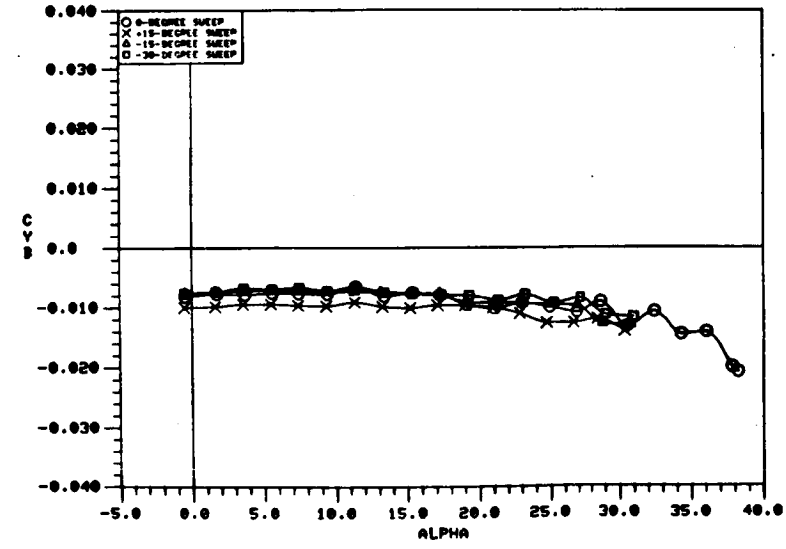

c) C_{Y_β} vs. α

Figure 128. Effect of Trailing-Edge Sweep Variation on the 65-Degree Cropped Delta Wing Static Lateral-Directional Characteristics.

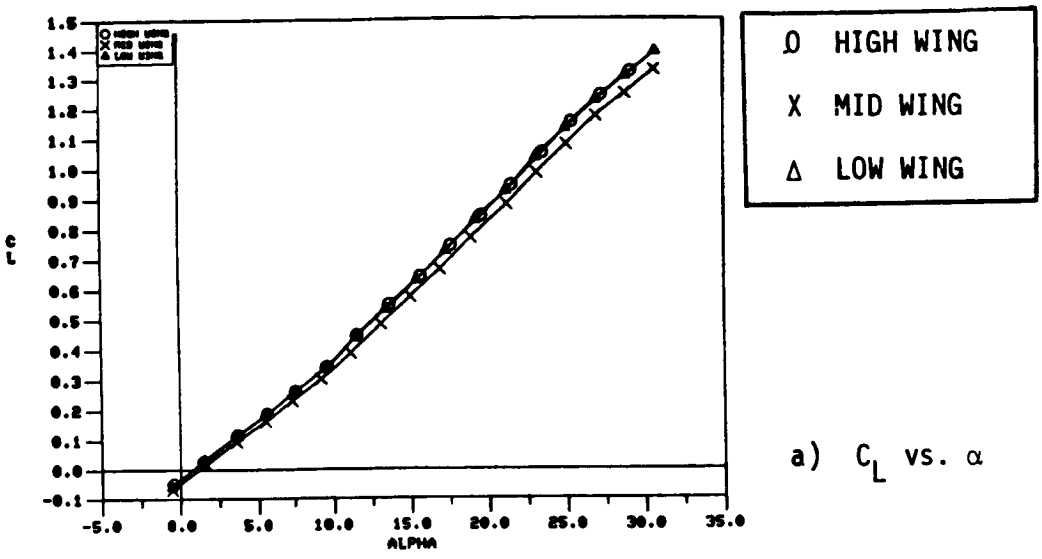

a) C_L vs. α

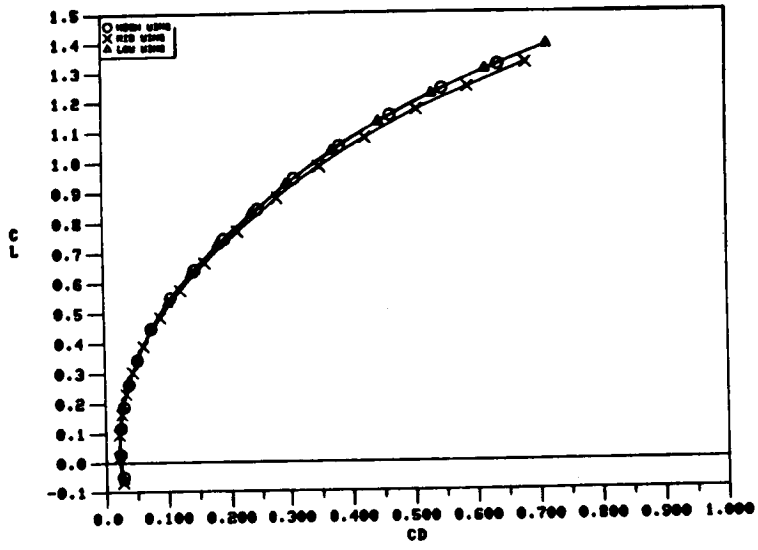

b) C_L vs. C_D

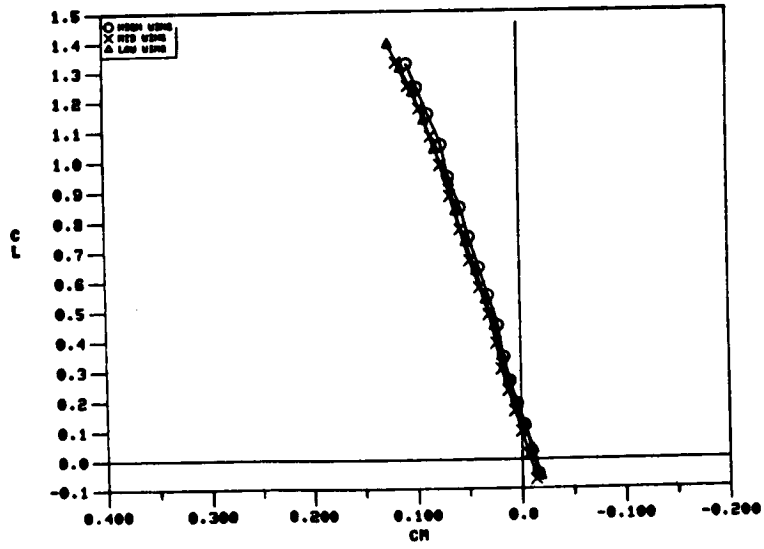

c) C_L vs. C_m

Figure 129. Effect of Wing Vertical Position on the 65-Degree Cropped Delta Wing Static Longitudinal Aerodynamic Characteristics, Vortex Flap Deflected to 30°.

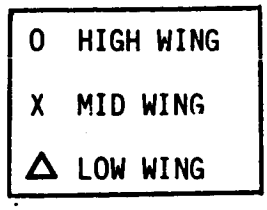

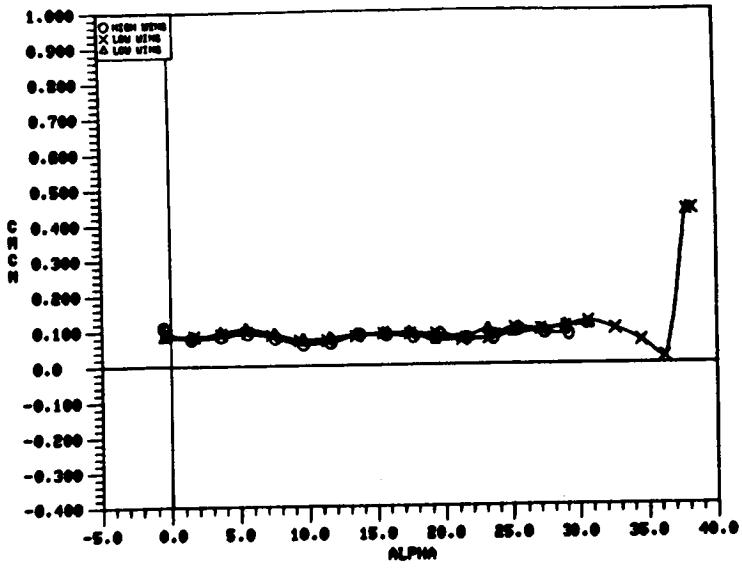

a) $C_{m_{C_N}}$ vs. α

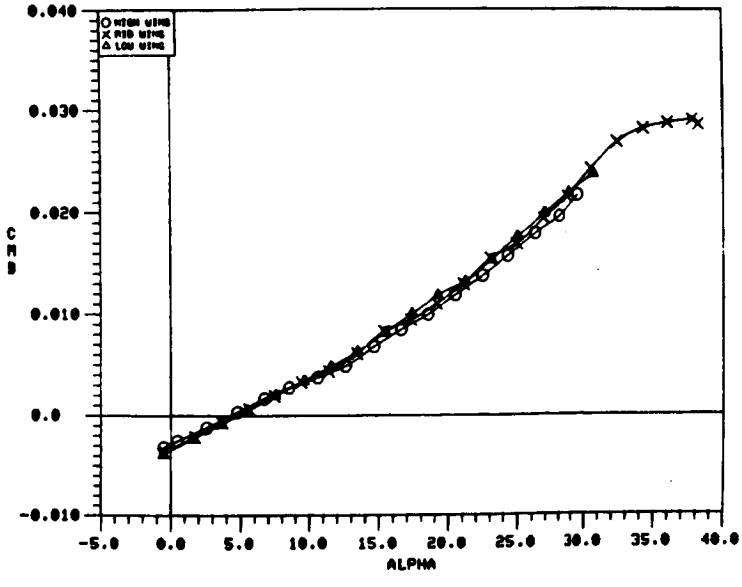

b) C_{m_β} vs. α

Figure 130. Effect of Wing Vertical Position on the 65-Degree Cropped Delta Wing Static Longitudinal Stability Characteristics, Vortex Flap Deflected to 30°.

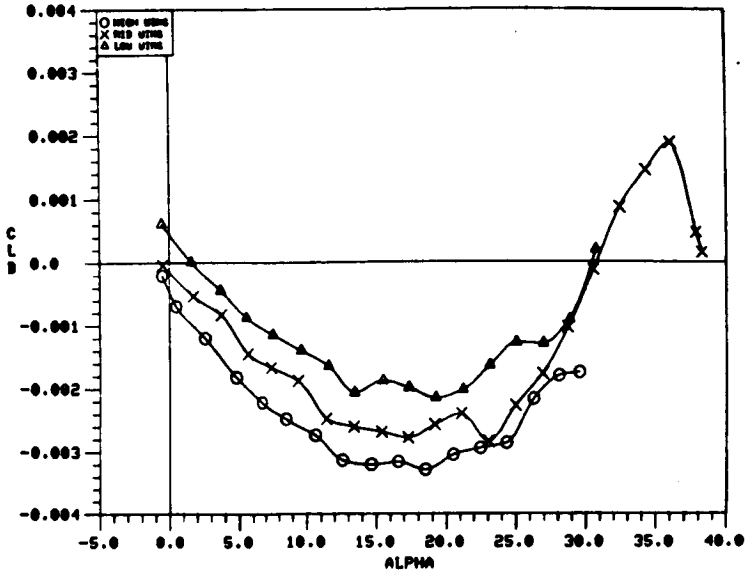

a) C_{ℓ_β} vs. α

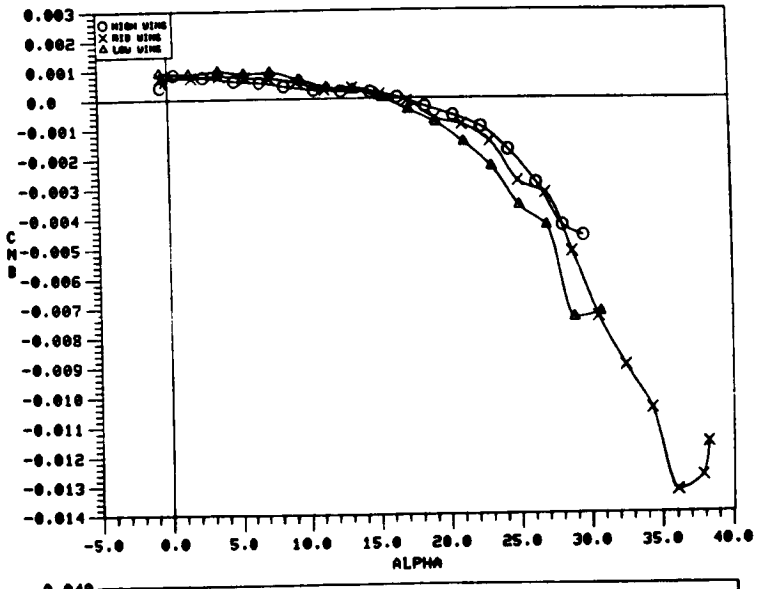

b) C_{n_β} vs. α

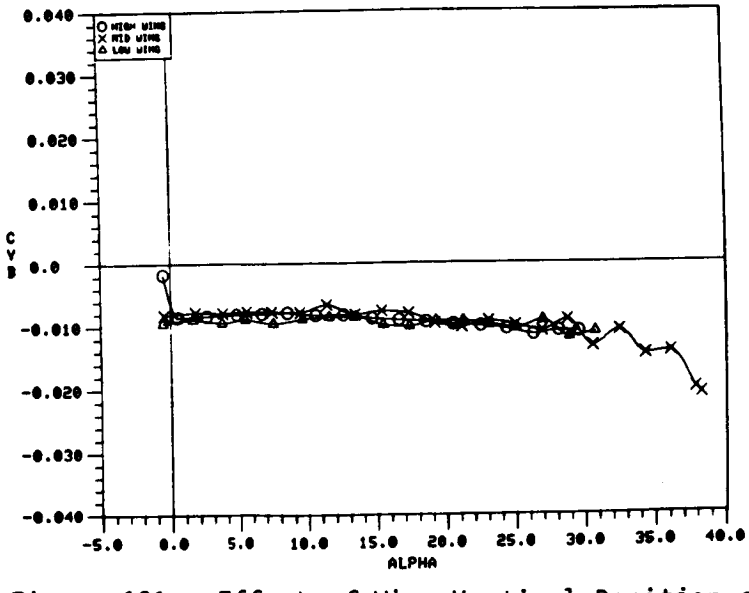

c) C_{Y_β} vs. α

Figure 131. Effect of Wing Vertical Position on the 65-Degree Cropped Delta Wing Static Lateral-Directional Stability Characteristics, Vortex Flap Deflected to 30°.

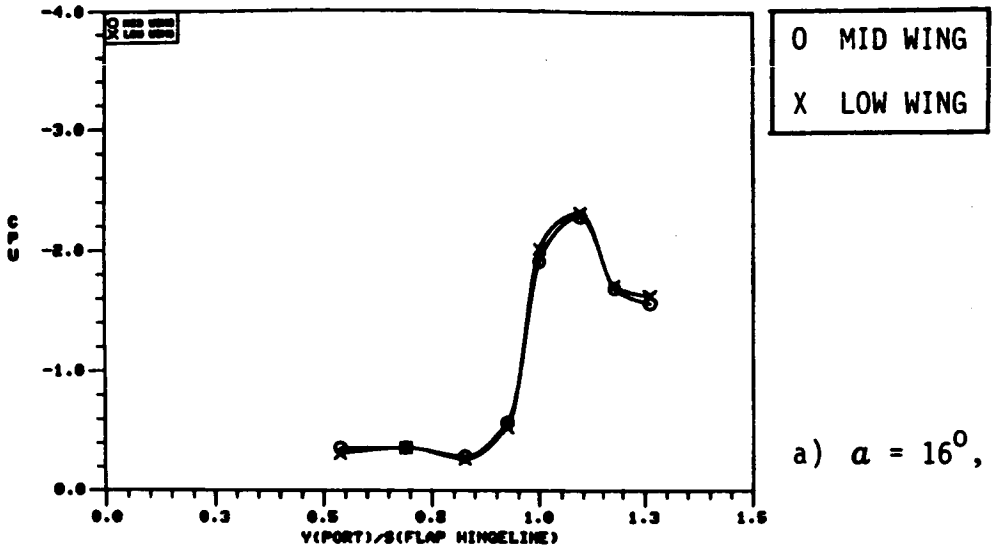

a) α = 16°, x/c = .405

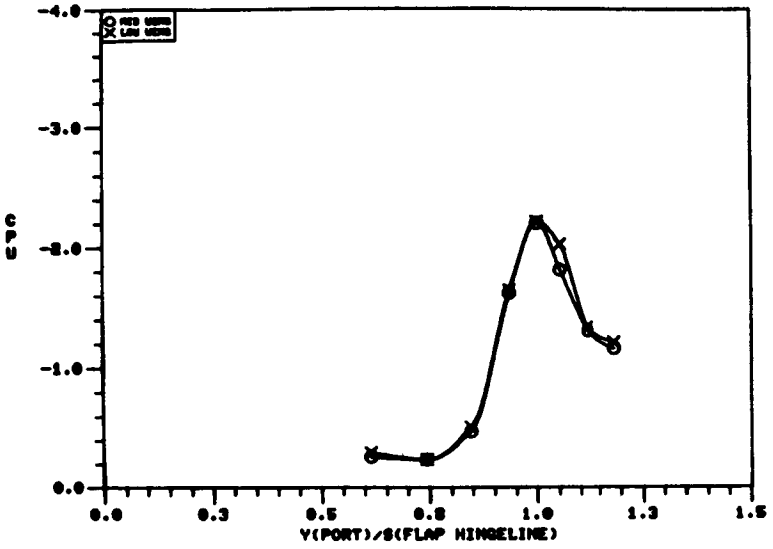

b) α = 16°, x/c = .576

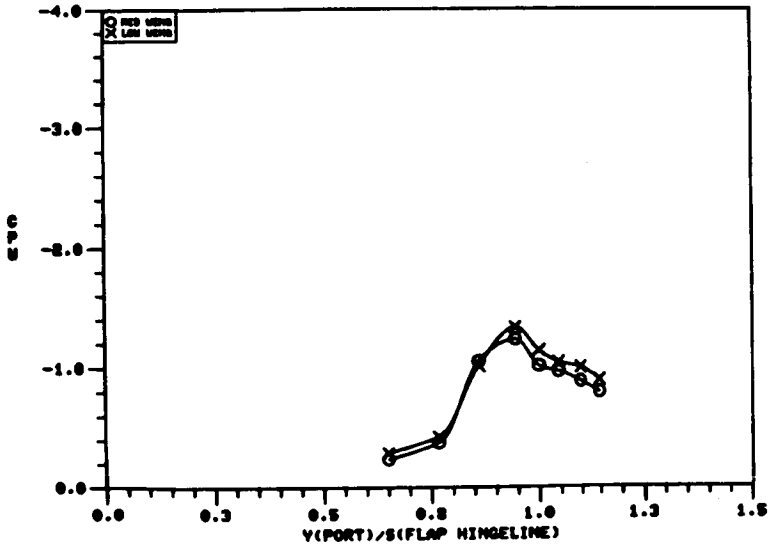

c) α = 16°, x/c = .748

Figure 132. Effect of Wing Vertical Position on the 65-Degree Cropped Delta Wing Upper Surface Static Pressure Distributions, Vortex Flap Deflected to 30°.

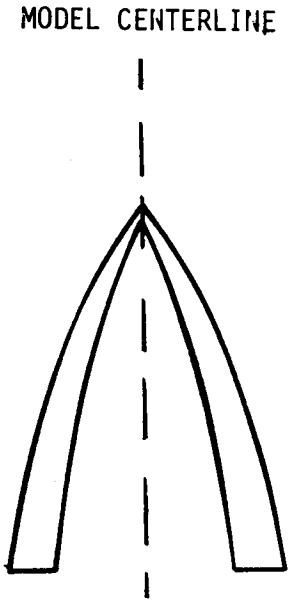

Figure 133. Empirically Designed Nose Strakes.

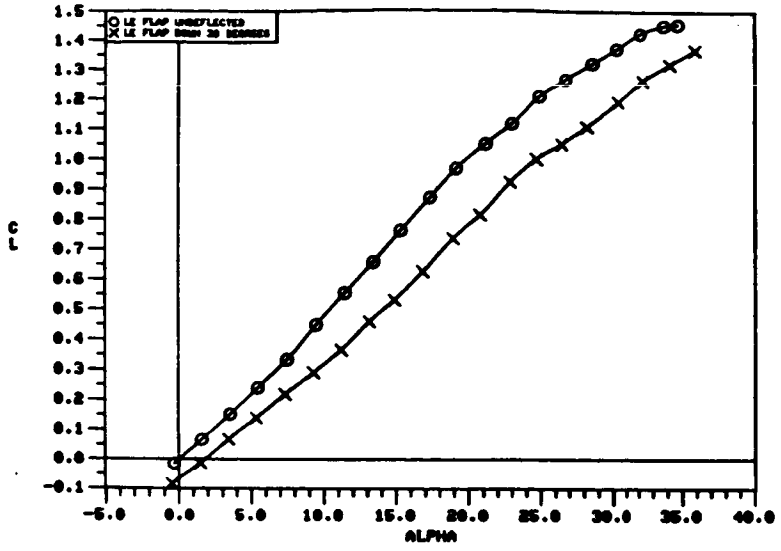

a) C_L vs. α

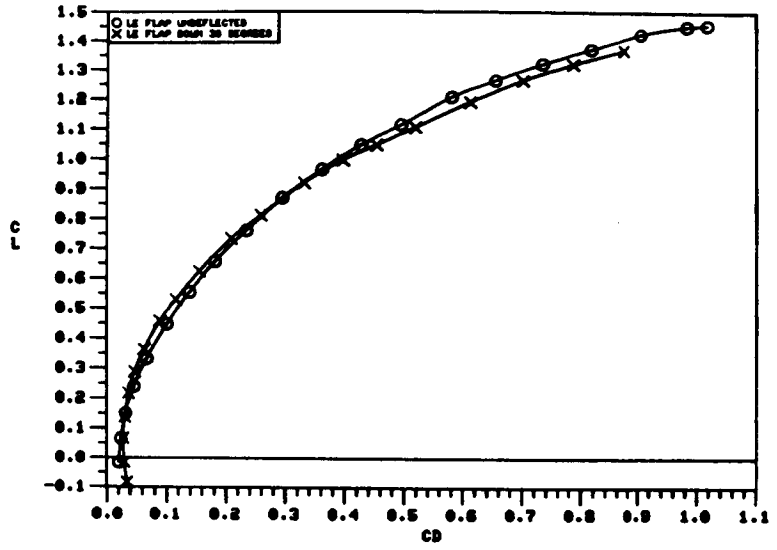

b) C_L vs. C_D

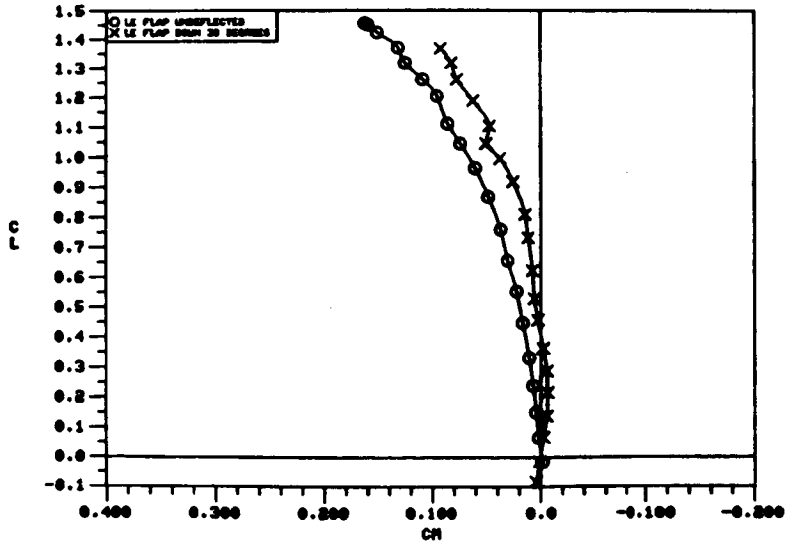

c) C_L vs. C_m

Figure 134. Effect of Deflected Vortex Flap on the Static Longitudinal Aerodynamic Characteristics of the 70/50-Degree Cranked Wing Wing with Nose Strakes.

O	LE FLAP UNDEFLECTED
X	LE FLAP DOWN 30 DEGREES

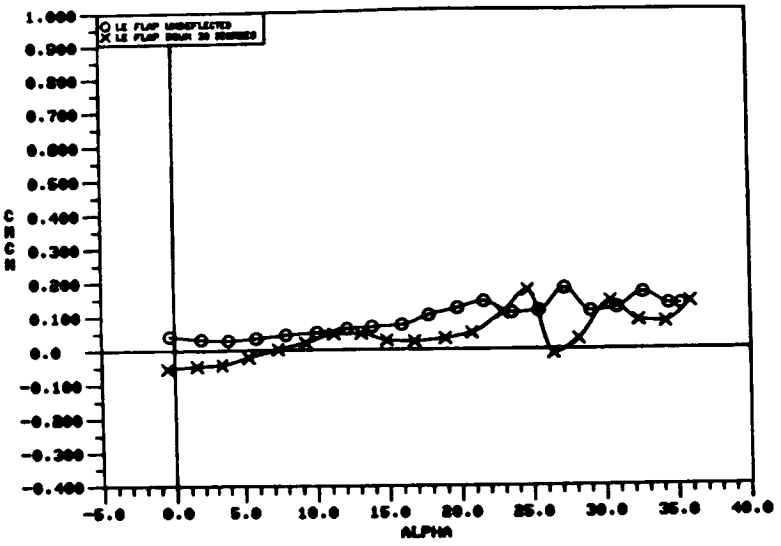

a) $C_{m_{C_N}}$ vs. α

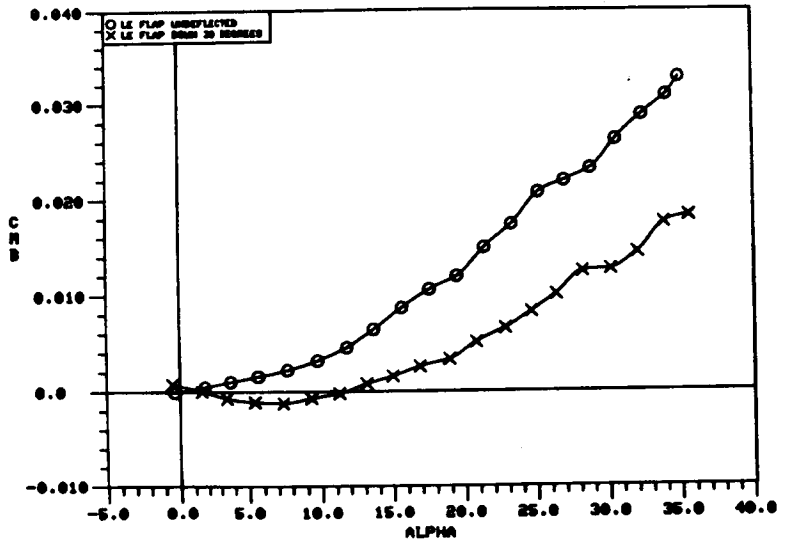

b) C_{m_β} vs. α

Figure 135. Effect of Deflected Vortex Flap on the Static Longitudinal Stability Characteristics of the 70/50-Degree Cranked Wing Wing with Nose Strakes.

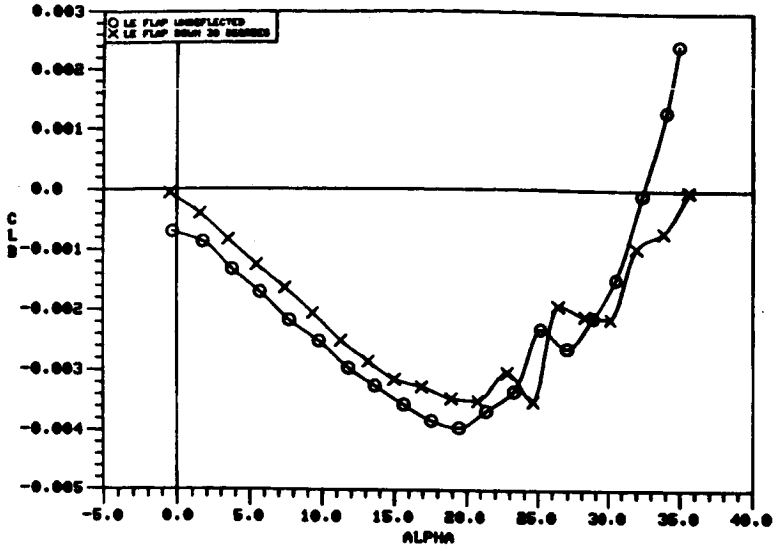

O LE FLAP UNDEFLECTED
X LE FLAP DOWN 30 DEGREES

a) C_{ℓ_β} vs. α

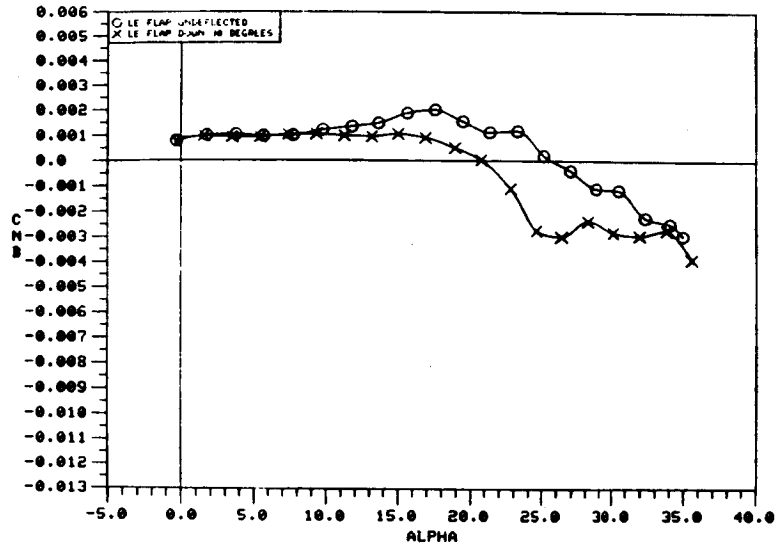

b) C_{n_β} vs. α

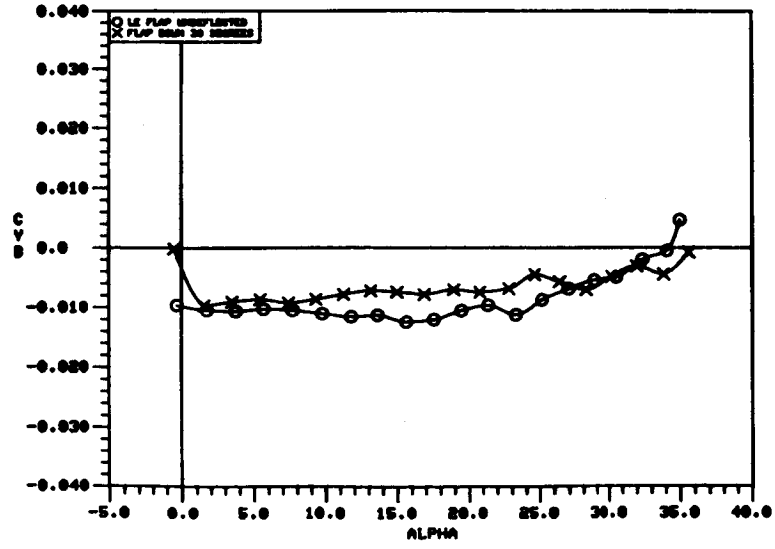

c) C_{Y_β} vs. α

Figure 136. Effect of Deflected Vortex Flap on the Static Lateral-Directional Stability Characteristics of the 70/50-Degree Cranked Wing with Nose Strakes.

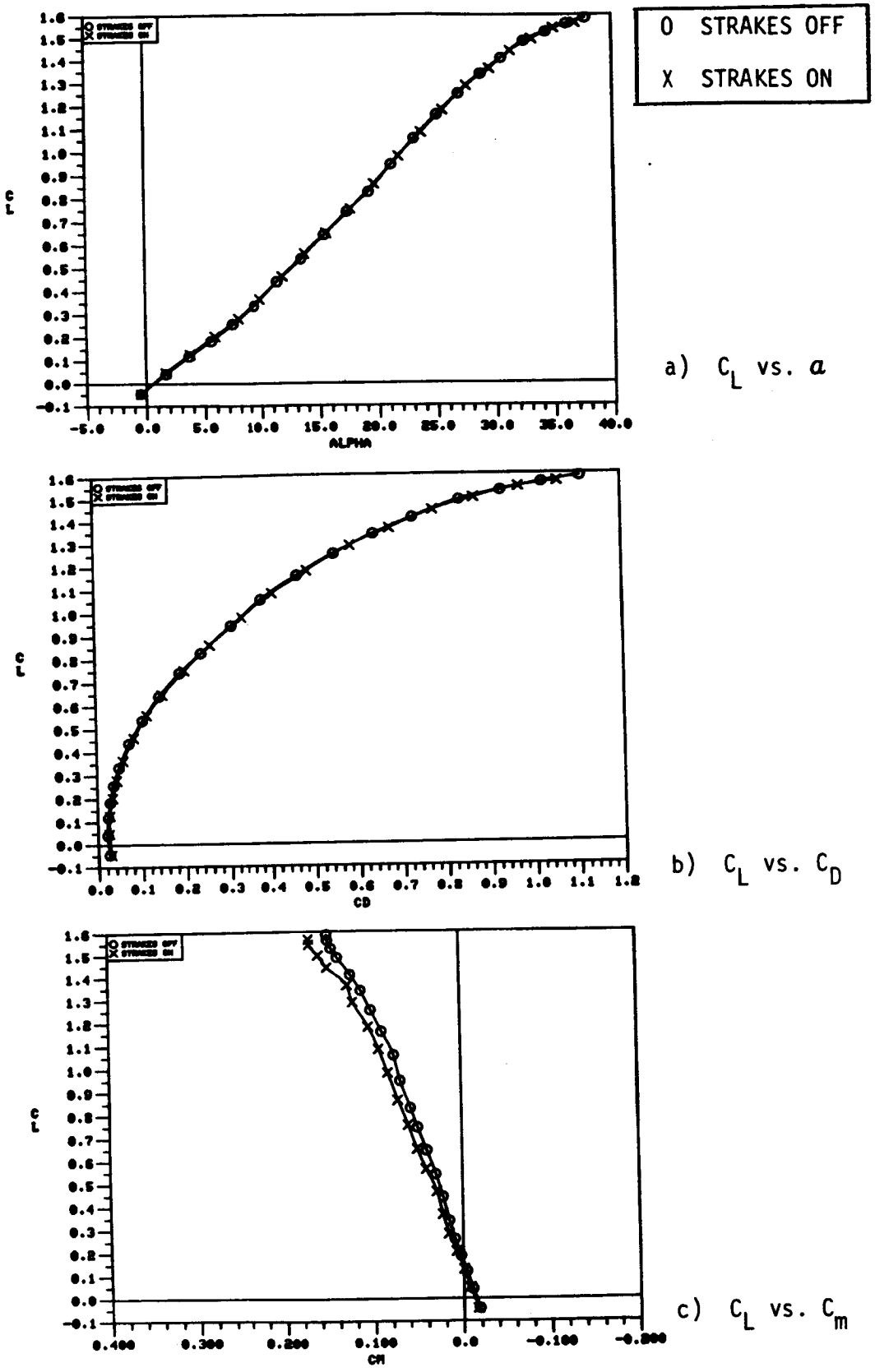

Figure 137. Effect of Nose Strakes on the 65-Degree Cropped Delta Wing Static Longitudinal Aerodynammic Characteristics.

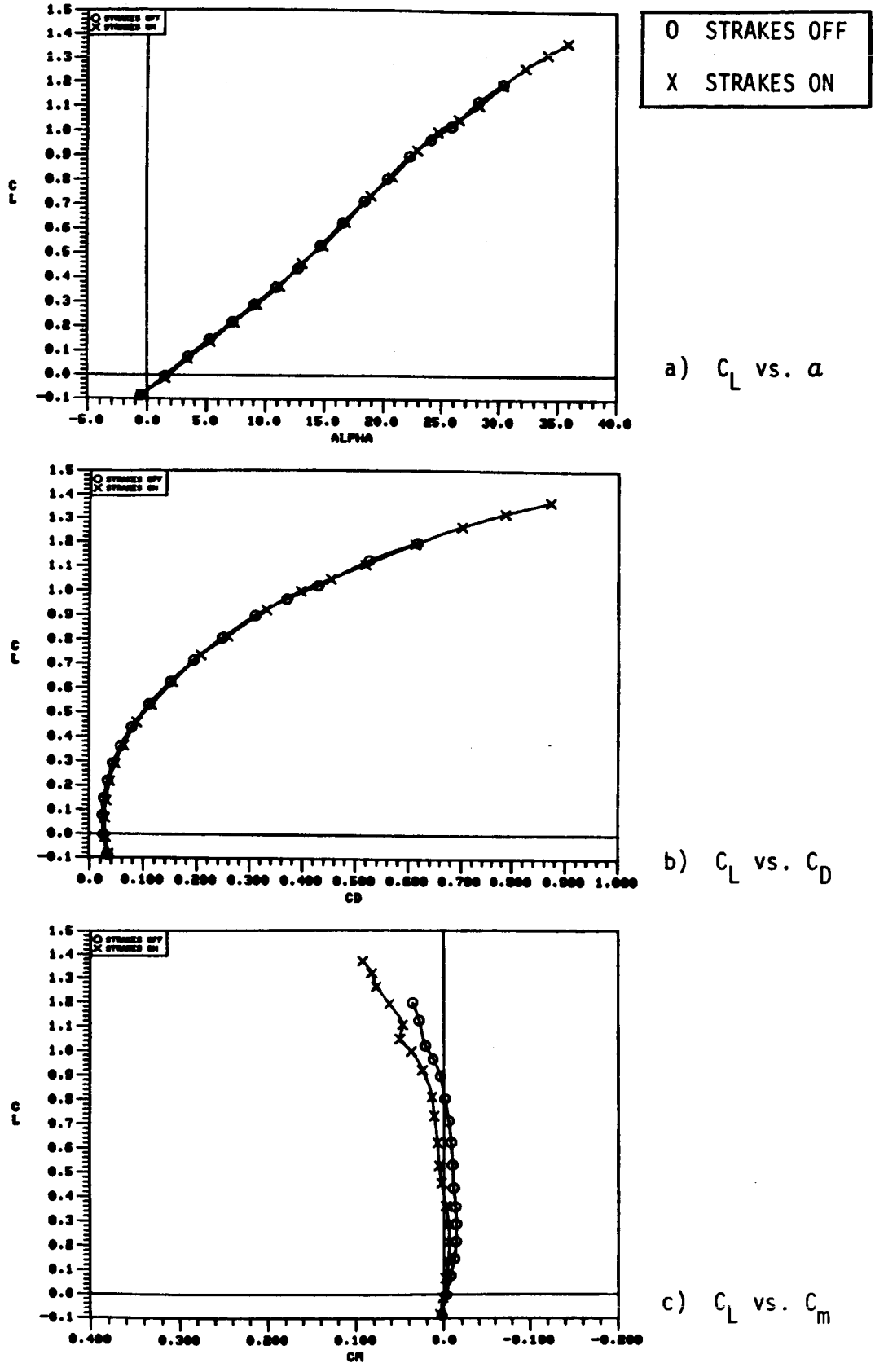

a) C_L vs. α

b) C_L vs. C_D

c) C_L vs. C_m

Figure 138. Effect of Nose Strakes on the 70/50-Degree Cranked Wing Static Longitudinal Aerodynammic Characteristics.

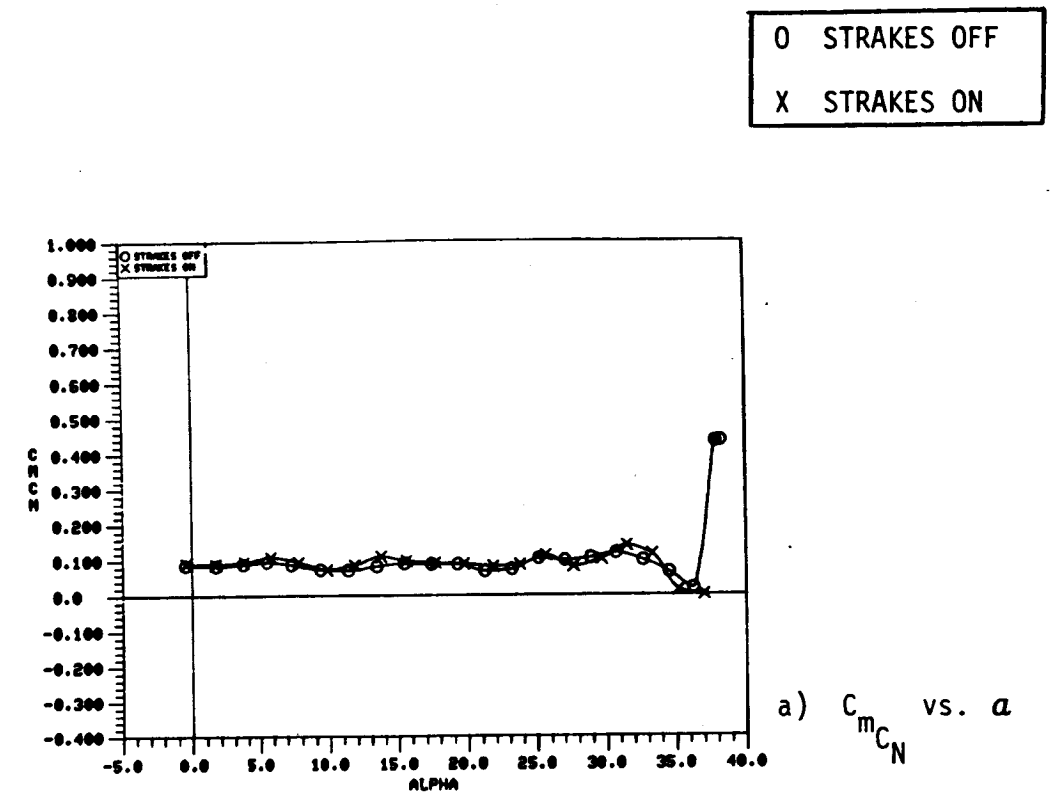

Figure 139. Effect of Nose Strakes on the 65-Degree Cropped Delta Wing Static Longitudinal Stability Characteristics.

O	STRAKES OFF
X	STRAKES ON

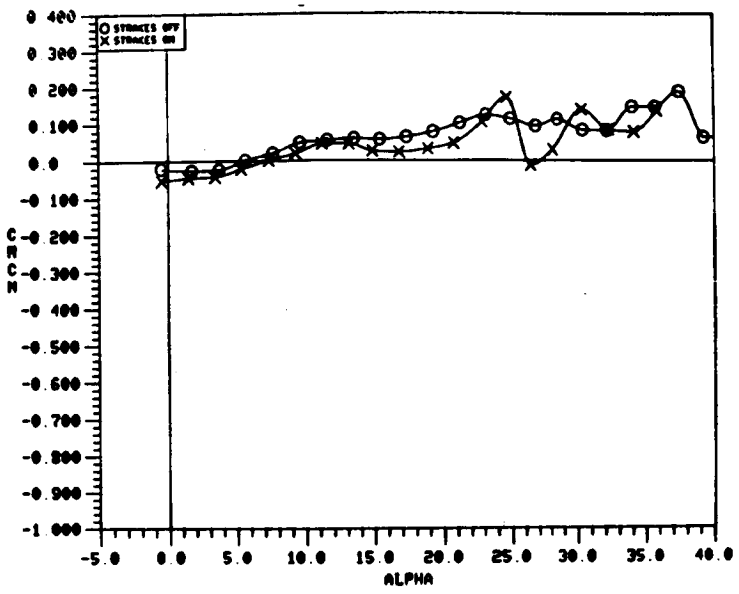

a) $C_{m_{C_N}}$ vs. α

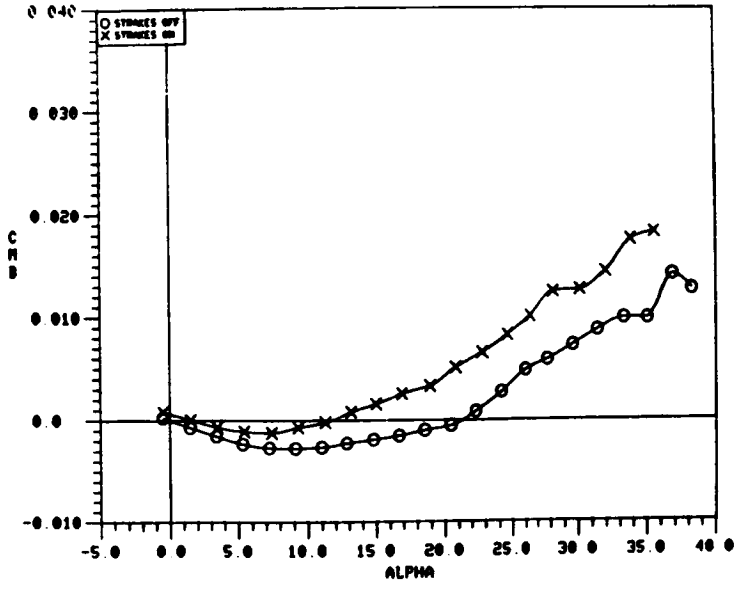

b) C_{m_β} vs. α

Figure 140. Effect of Nose Strakes on the 70/50-Degree Cranked Wing Static Longitudinal Stability Characteristics.

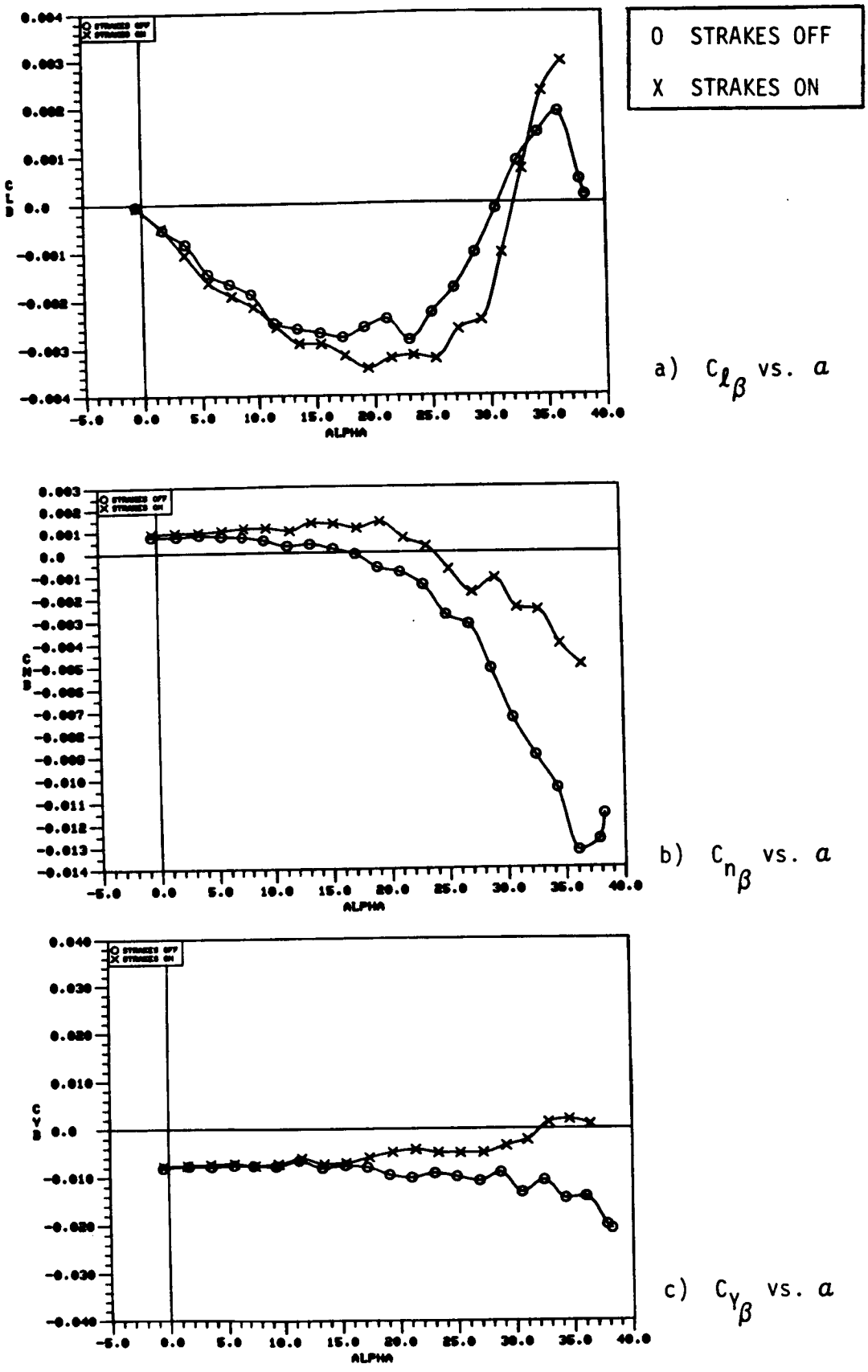

Figure 141. Effect of Nose Strakes on the 65-Degree Cropped Delta Wing Static Lateral-Directional Stability Characteristics, Vortex Flap Deflected to 30°.

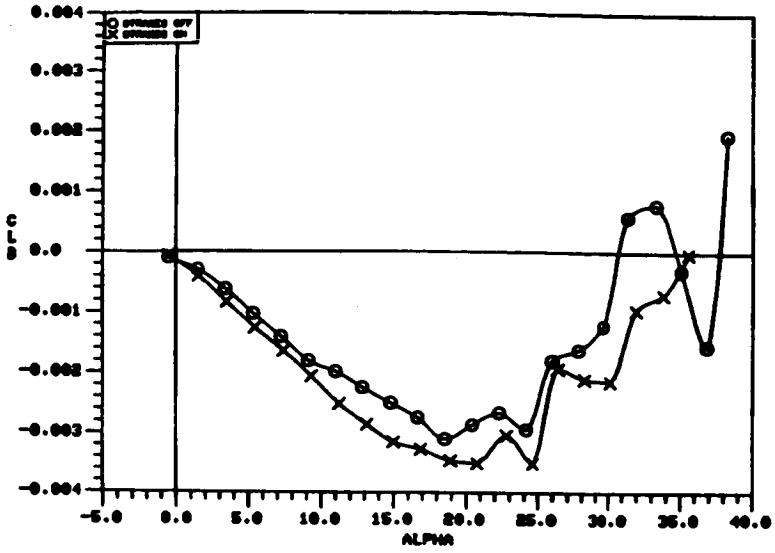

a) C_{ℓ_β} vs. α

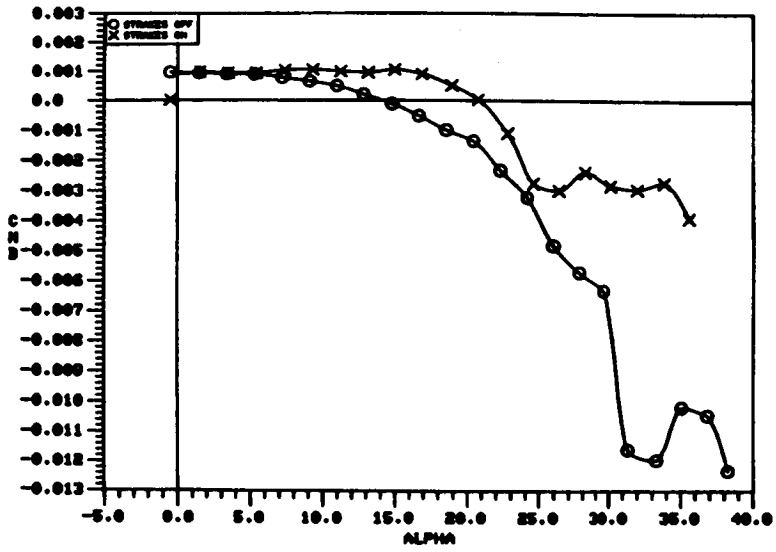

b) C_{n_β} vs. α

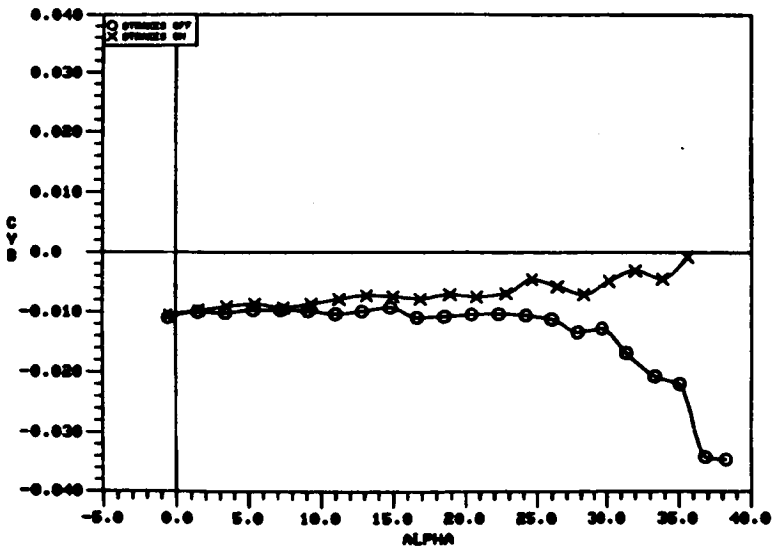

c) C_{Y_β} vs. α

Figure 142. Effect of Nose Strakes on the 70/50-Degree Cranked Wing Static Lateral-Directional Stability Characteristics, Vortex Flap Deflected to 30°.

O	STRAKES OFF
X	STRAKES ON

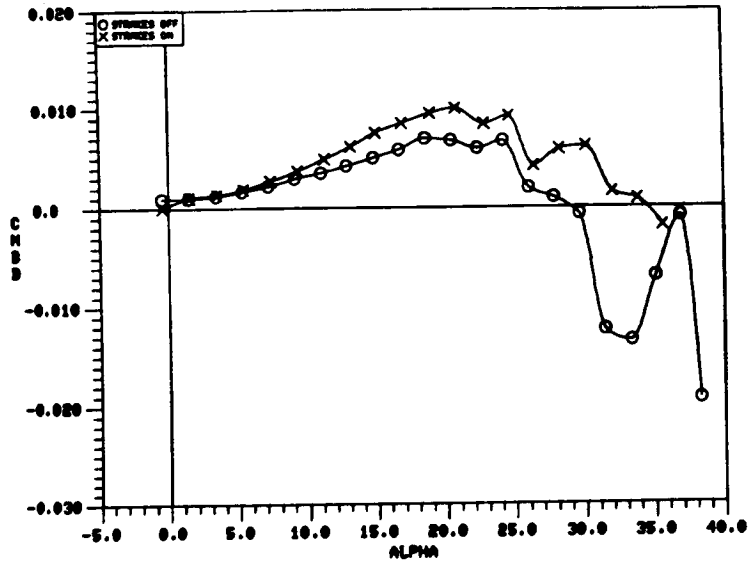

$C_{n_{\beta_{dyn}}}$ vs. α

Figure 143. Effect of Nose Strakes on the 70/50-Degree Cranked Cranked Wing Dynamic Directional Stability Parameter, Vortex Flap Deflected to 30°.

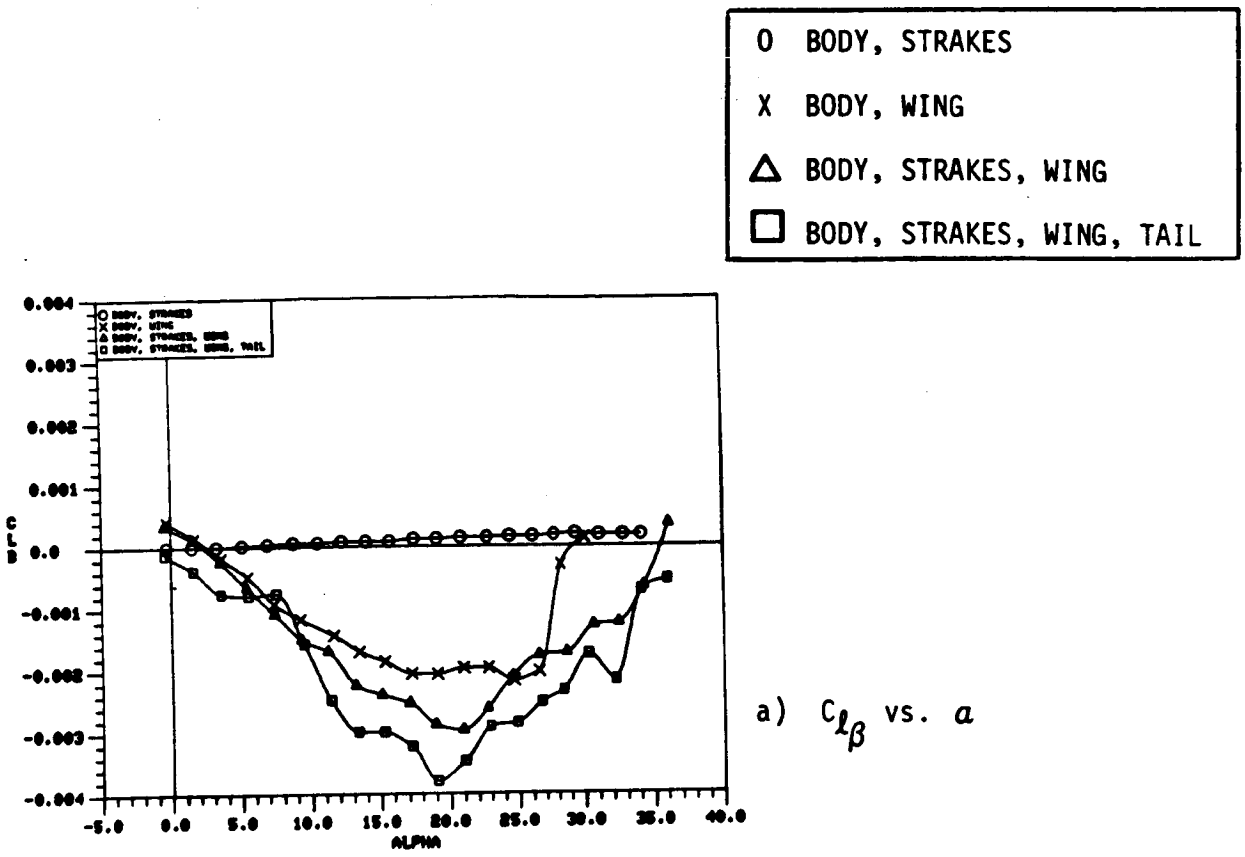

Figure 144. Contributions of Airframe Components to the Lateral-Directional Stability, of the 70/50 Degree Cranked Wing Configuration with Vortex Flap Deflected to 30°.

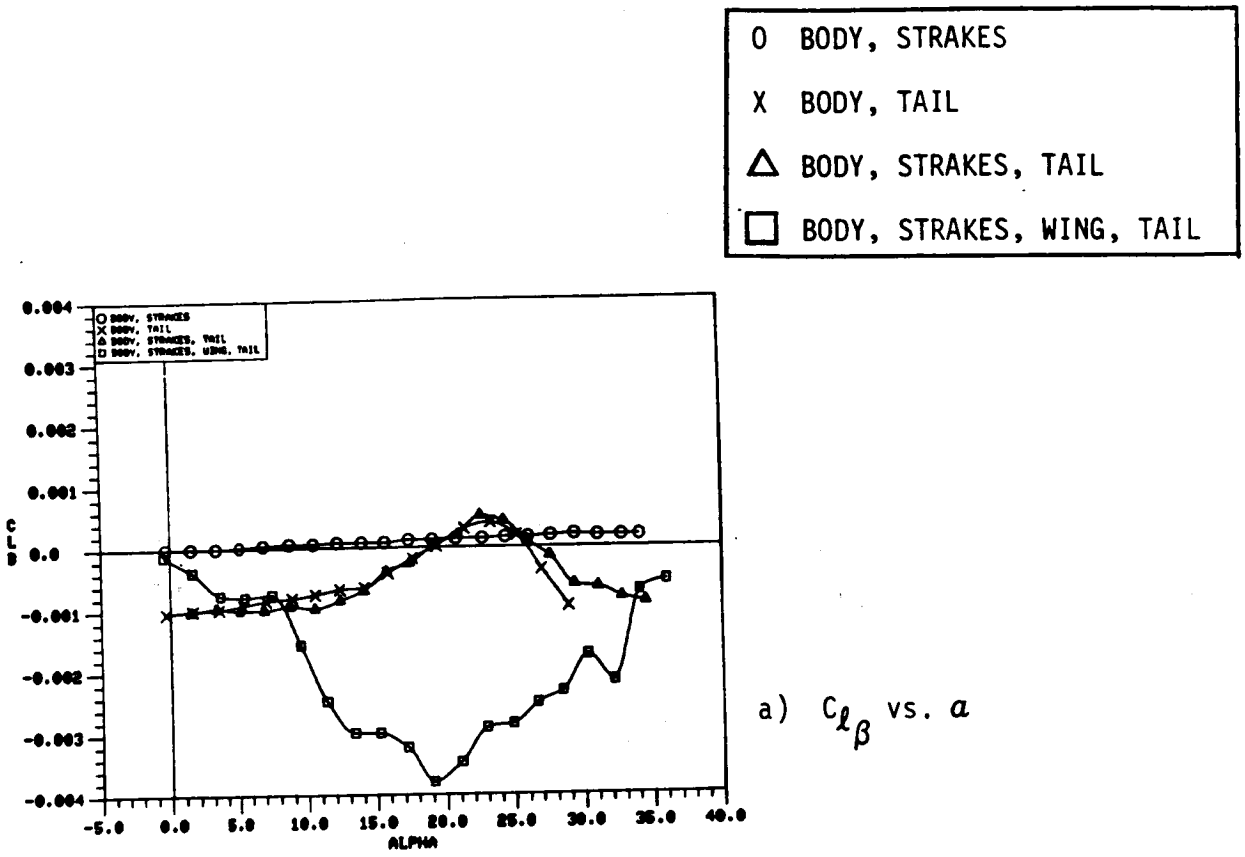

a) C_{ℓ_β} vs. α

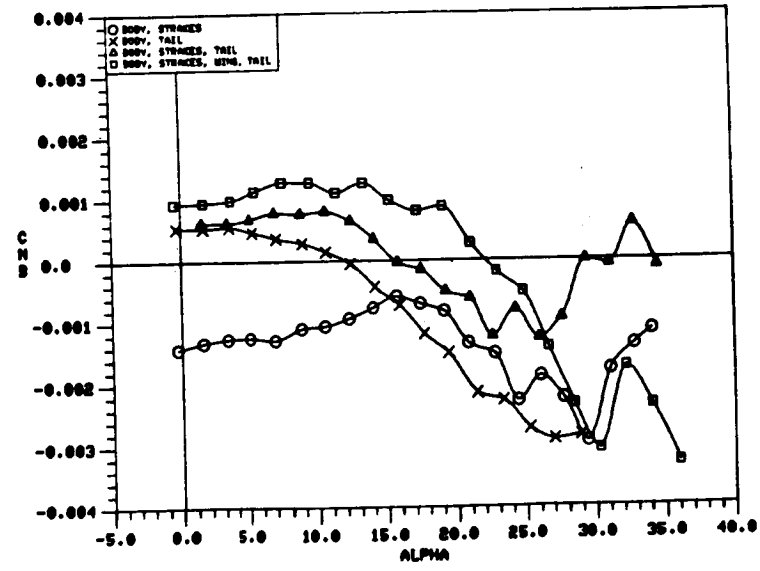

b) C_{n_β} vs. α

Figure 145. Contributions of Airframe Components to Lateral-Directional Stability of the 70/50 - Degree Cranked Wing Configuration with Vortex Flap Deflected to 30°.

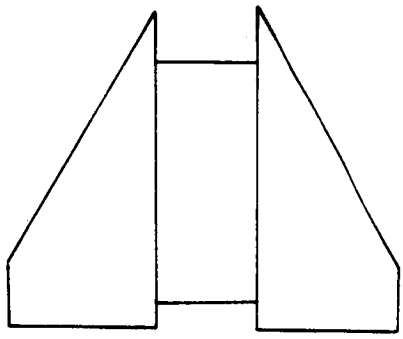

AR = 1.64

b/2 = 1.55 in.

$S = 5.5\ in^2$

$\Lambda_{LE} = 65^o$

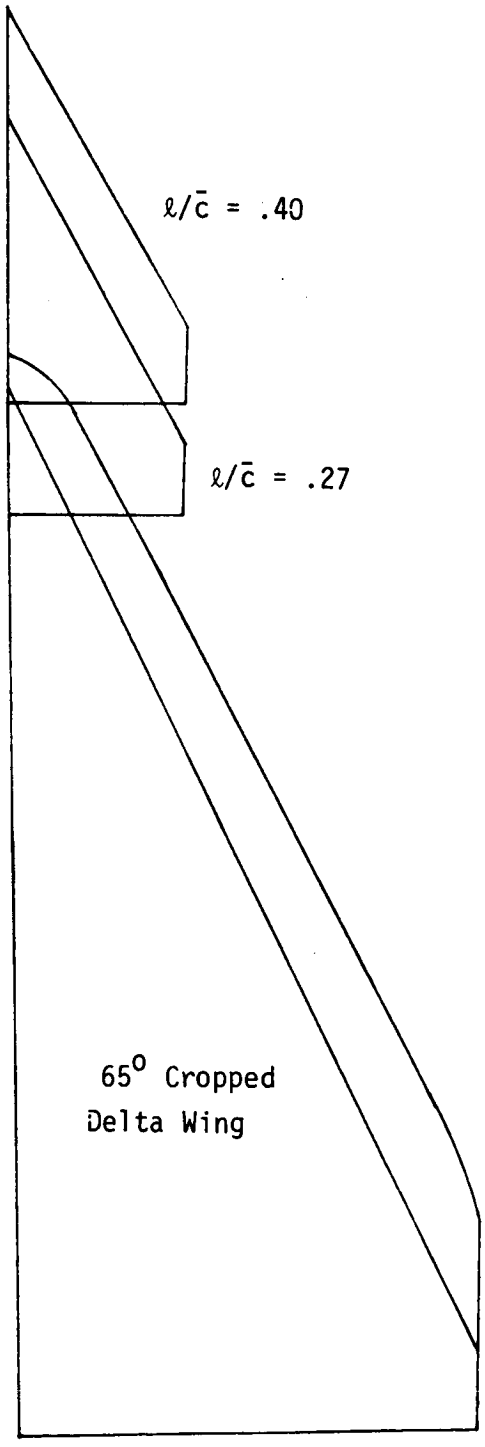

Figure 146. Empirically Designed Canards.

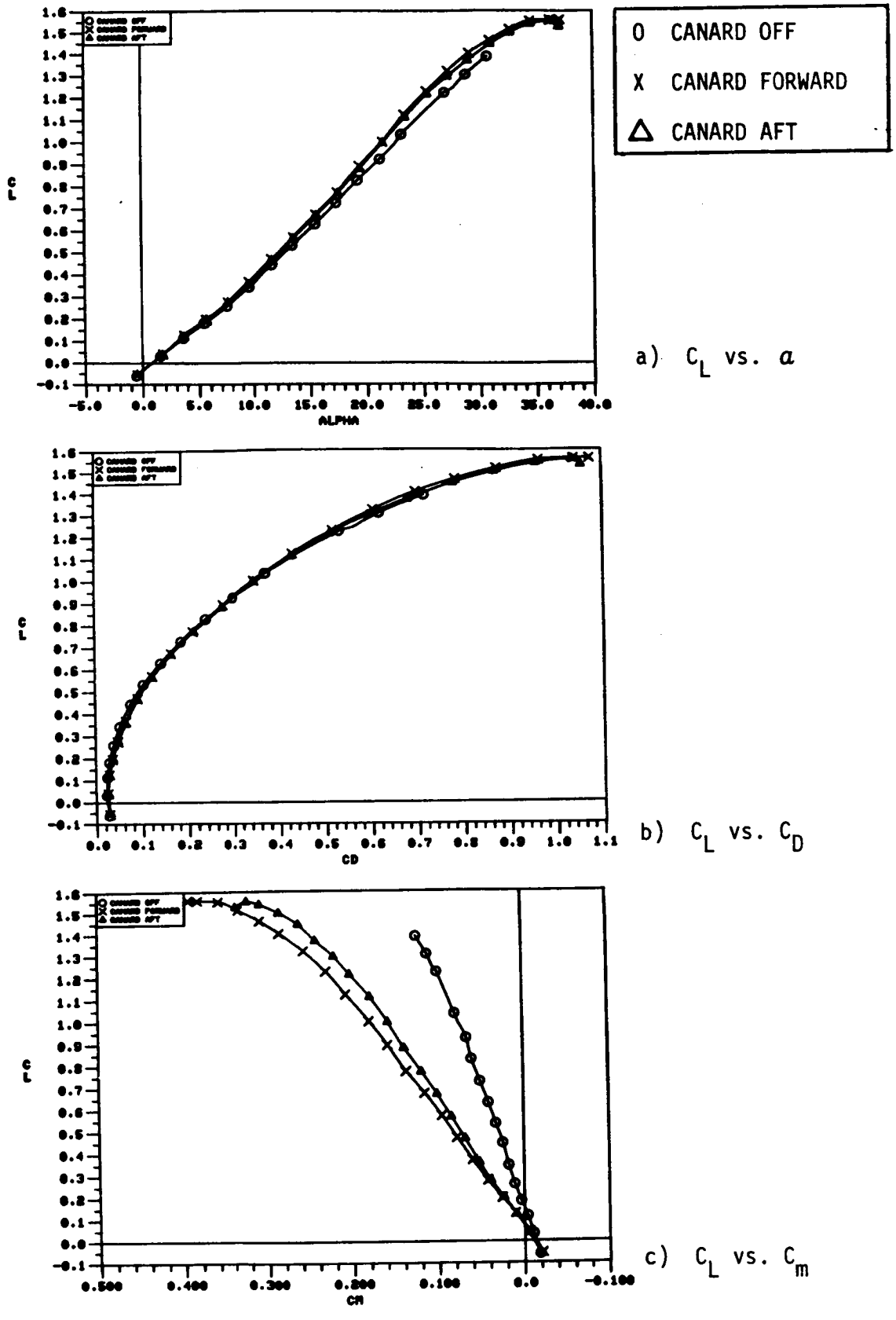

a) C_L vs. α

b) C_L vs. C_D

c) C_L vs. C_m

Figure 147. Effect of Canards on the 65-Degree Cropped Delta Wing Static Longitudinal Aerodynamic Characteristics, Vortex Flap Deflected to 30°.

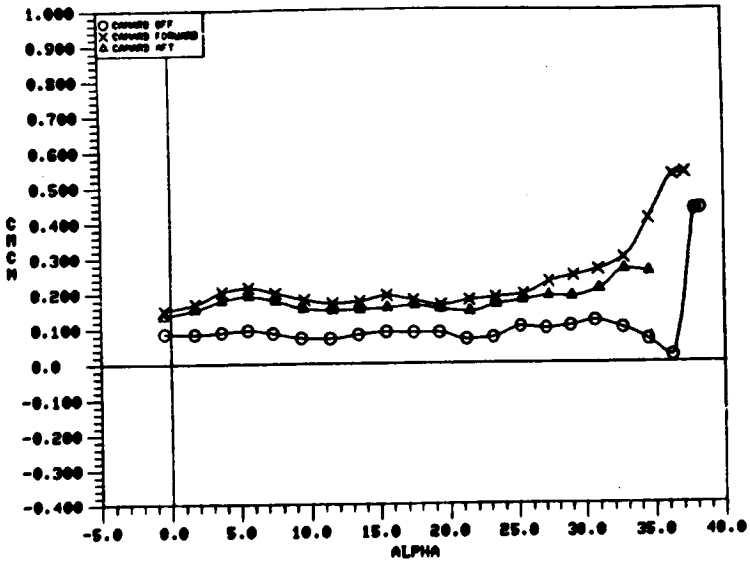

a) $C_{m_{C_N}}$ vs. α

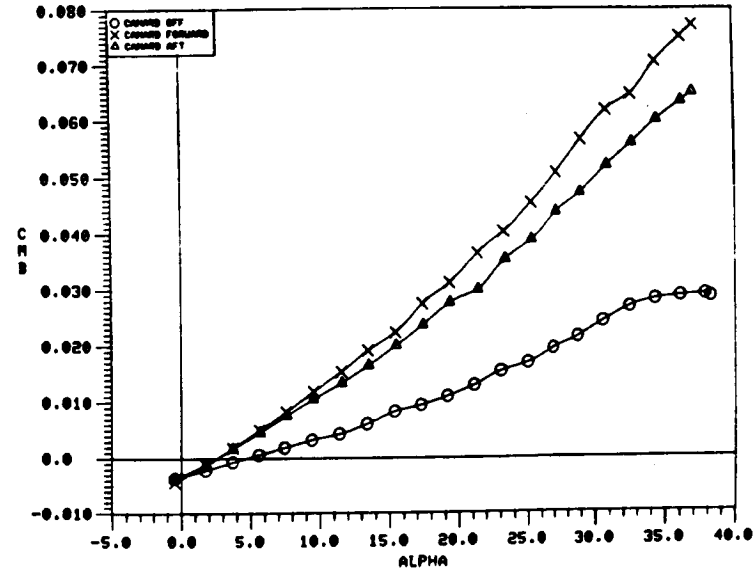

b) C_{m_β} vs.

Figure 148. Effect of Canards on the 65-Degree Cropped Delta Wing Static Longitudinal Stability Characteristics, Vortex Flap Deflected to 30°.

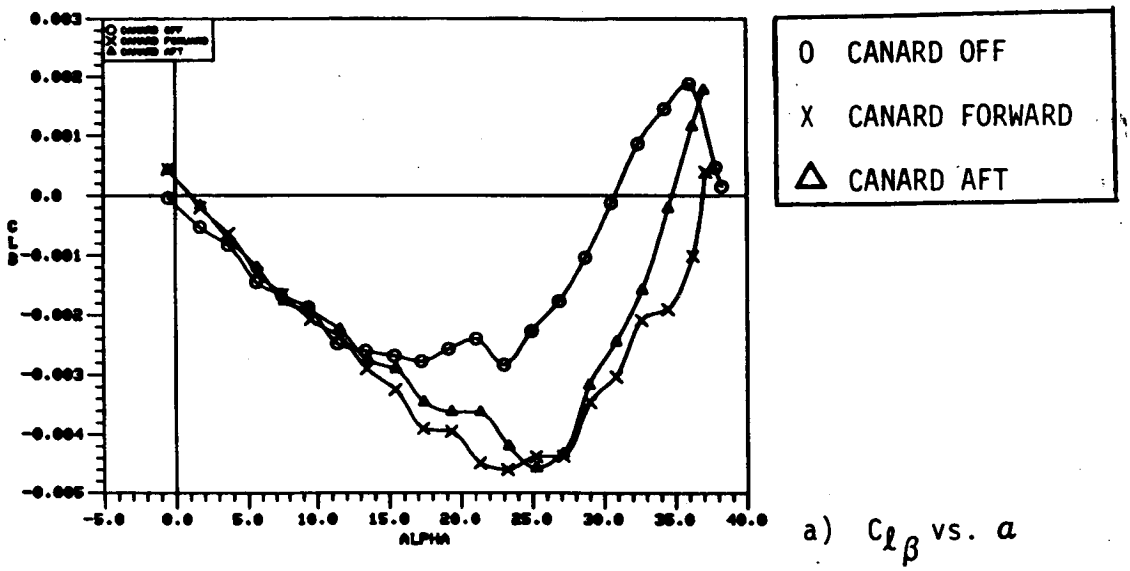

a) C_{ℓ_β} vs. α

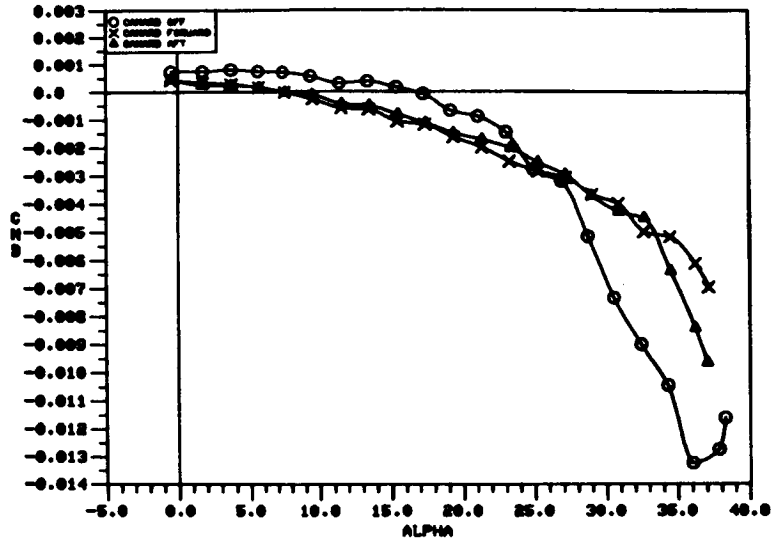

b) C_{n_β} vs. α

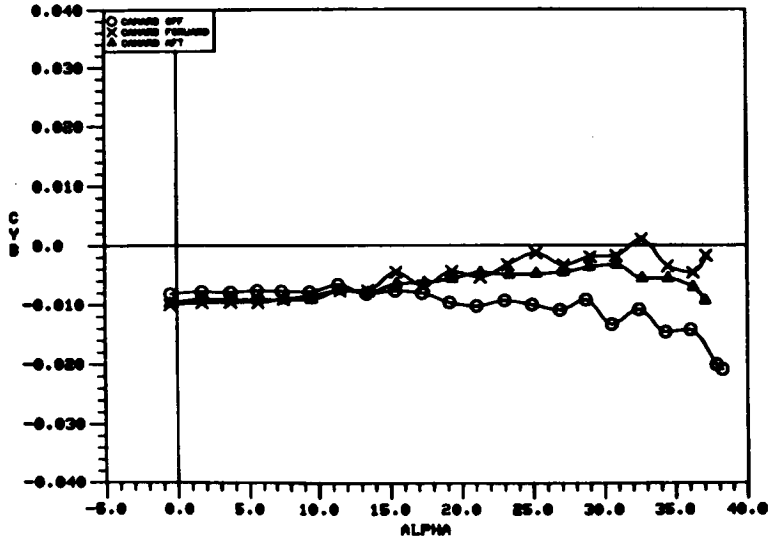

c) C_{Y_β} vs. α

Figure 149. Effect of Canards on the 65-Degree Cropped Delta Wing Static Lateral-Directional Stability Characteristics, Vortex Flap Deflected to 30°.

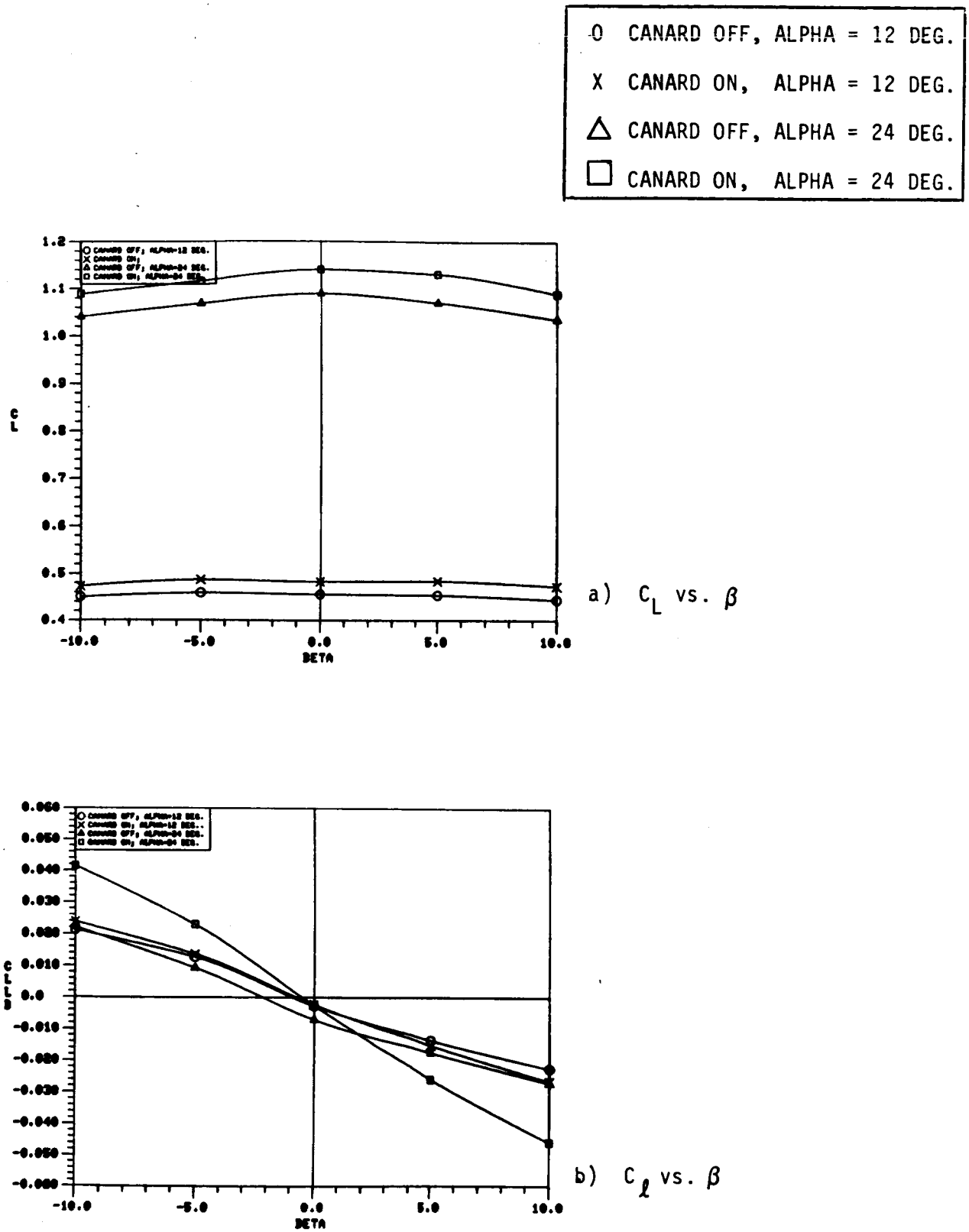

Figure 150. Effect of Canards on the 65-Degree Cropped Delta Wing Lift and Rolling Moment Variations with Sideslip, Vortex Flap Deflected to 30°.

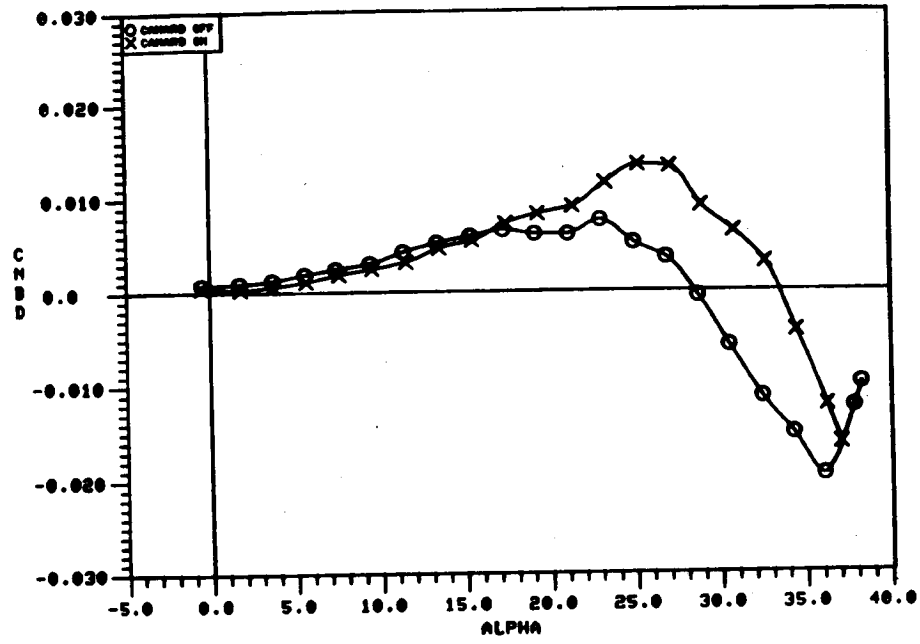

. $C_{n_{\beta_{dyn}}}$ vs. α

Figure 151. Effect of Canards on the 65-Degree Cropped Delta Wing Dynamic Directional Stability Parameter, Vortex Flap Deflected to 30°.

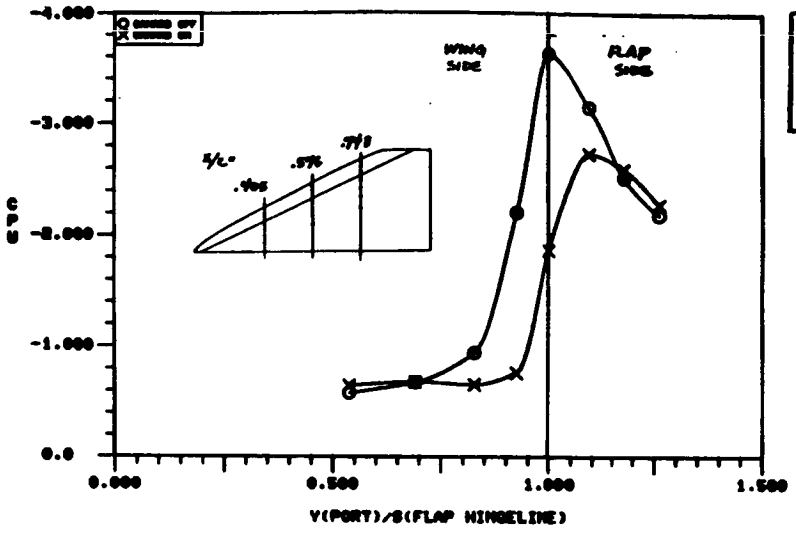

a) $\beta = 0^{o}$, x/c = .405

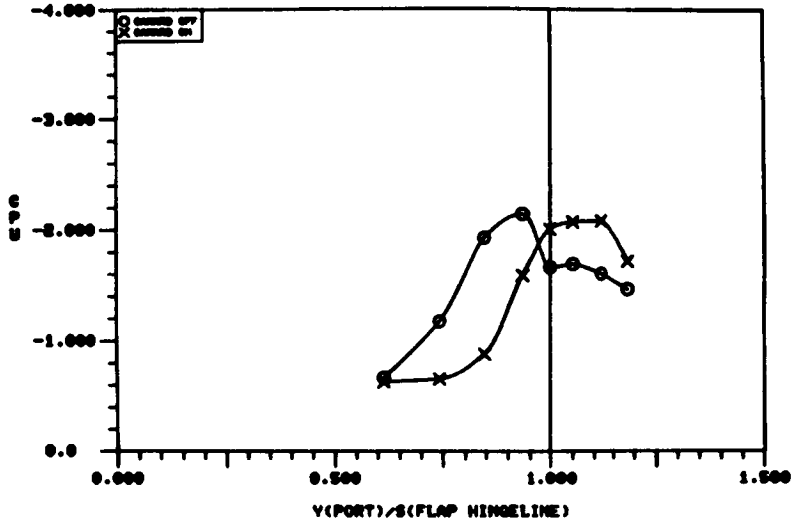

b) $\beta = 0^{o}$, x/c = .576

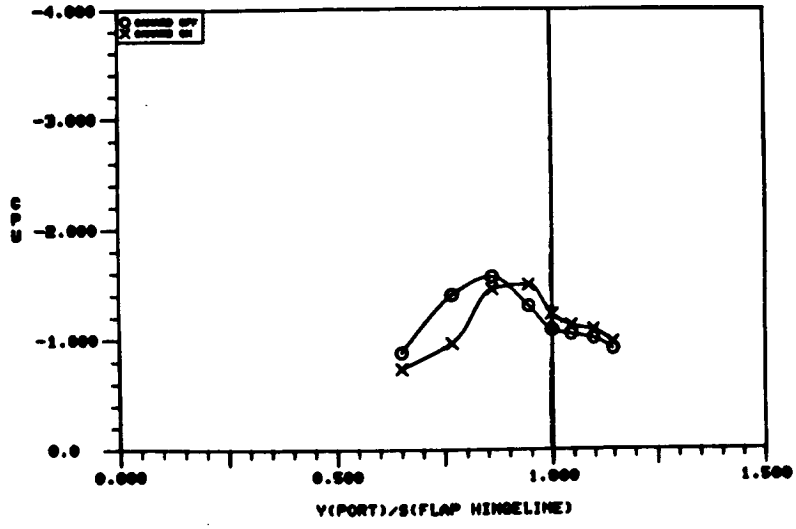

c) $\beta = 0^{o}$, x/c = .748

Figure 152. Effect of Canards on the 65-Degree Cropped Delta Wing Upper Surface Pressure Distributions at $\alpha = 24°$, $\beta = 0°$, Vortex Flap Deflected to 30°.

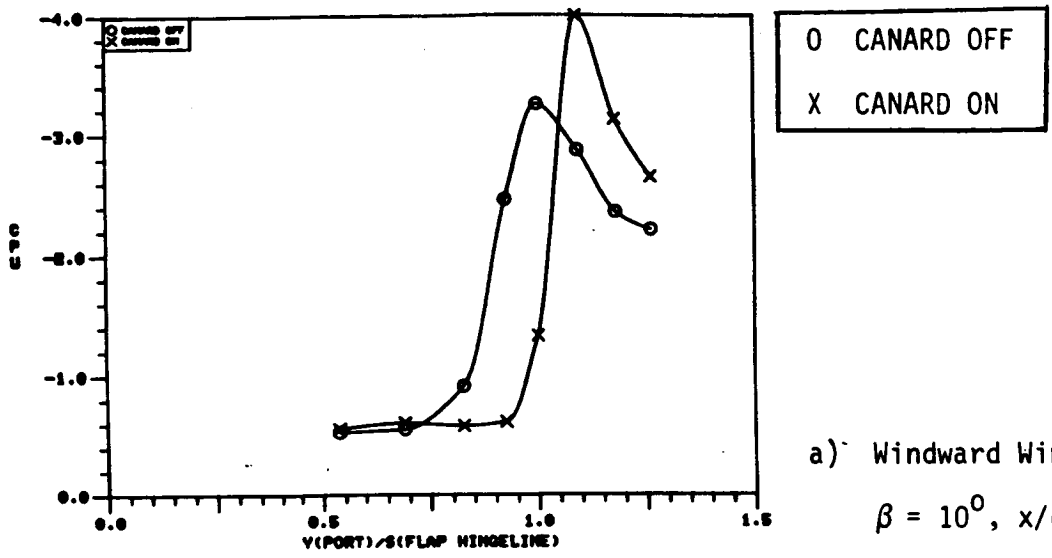

a) Windward Wing,
$\beta = 10^{o}$, x/c = .405

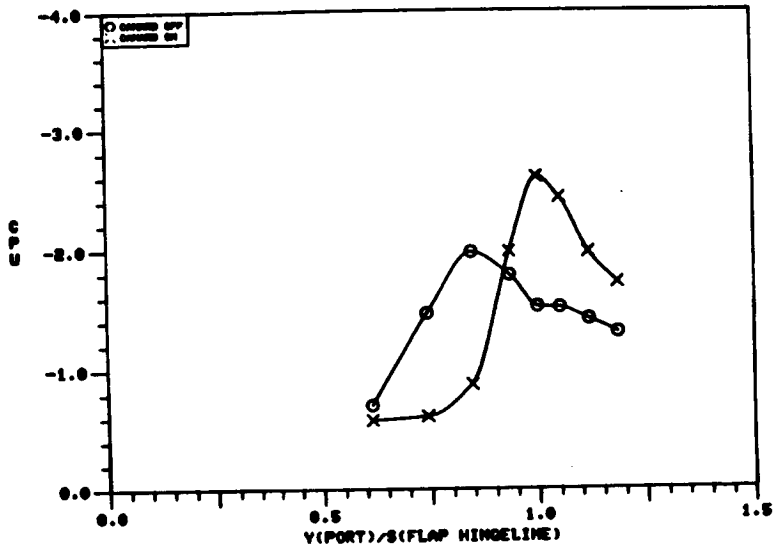

b) Windward Wing,
$\beta = 10^{o}$, x/c = .576

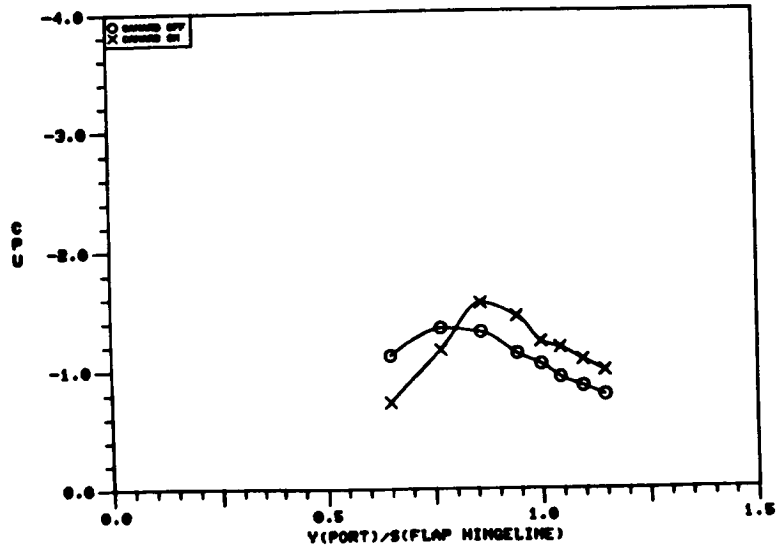

c) Windward Wing,
$\beta = 10^{o}$, x/c = .748

Figure 153. Effect of Canards on the 65-Degree Cropped Delta Wing Upper Surface Pressure Distributions in Sideslip at $\alpha = 24°$, $\beta = 10°$, Vortex Flap Deflected to 30°.

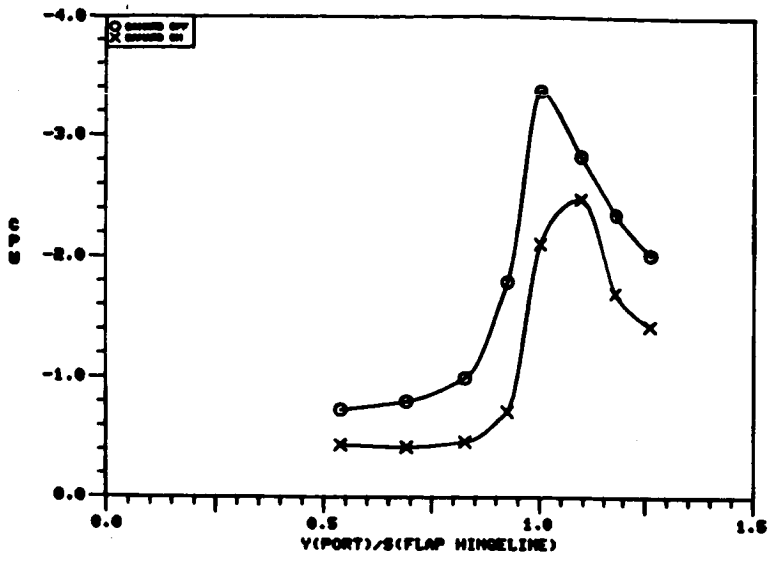

a) Leeward Wing,

$\beta = 10^{o}$, x/c = .405

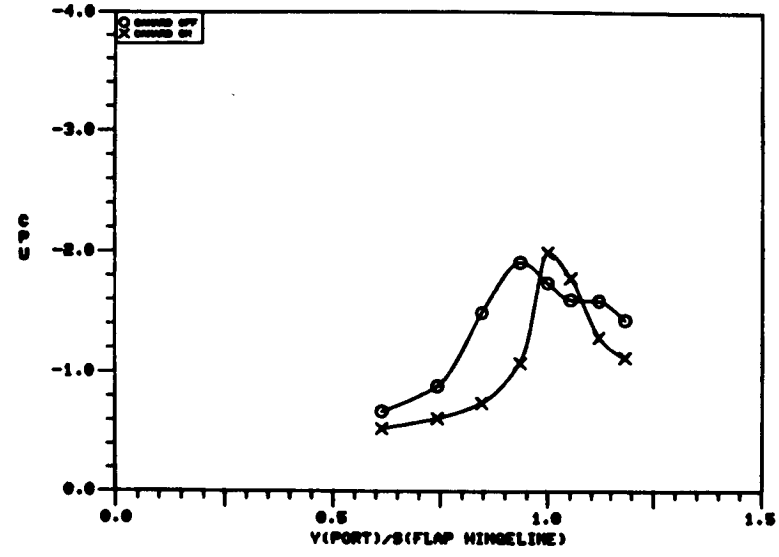

b) Leeward Wing,

$\beta = 10^{o}$, x/c = .576

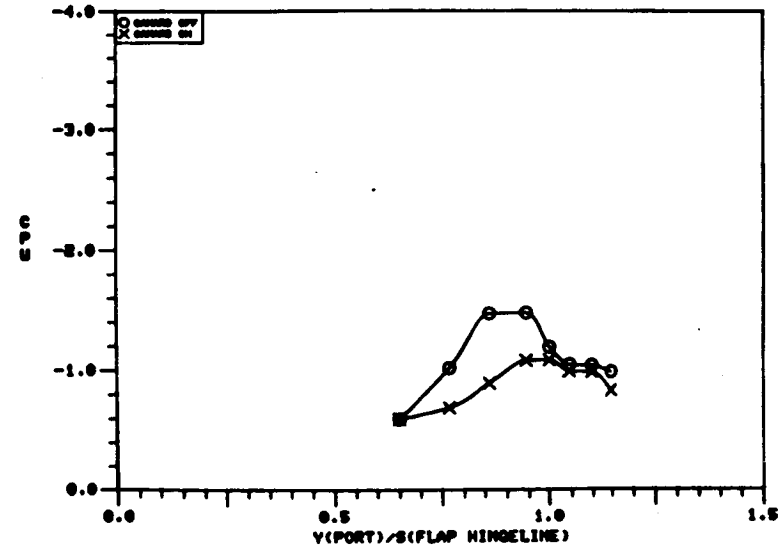

c) Leeward Wing,

$\beta = 10^{o}$, x/c = .748

Figure 153. Concluded.

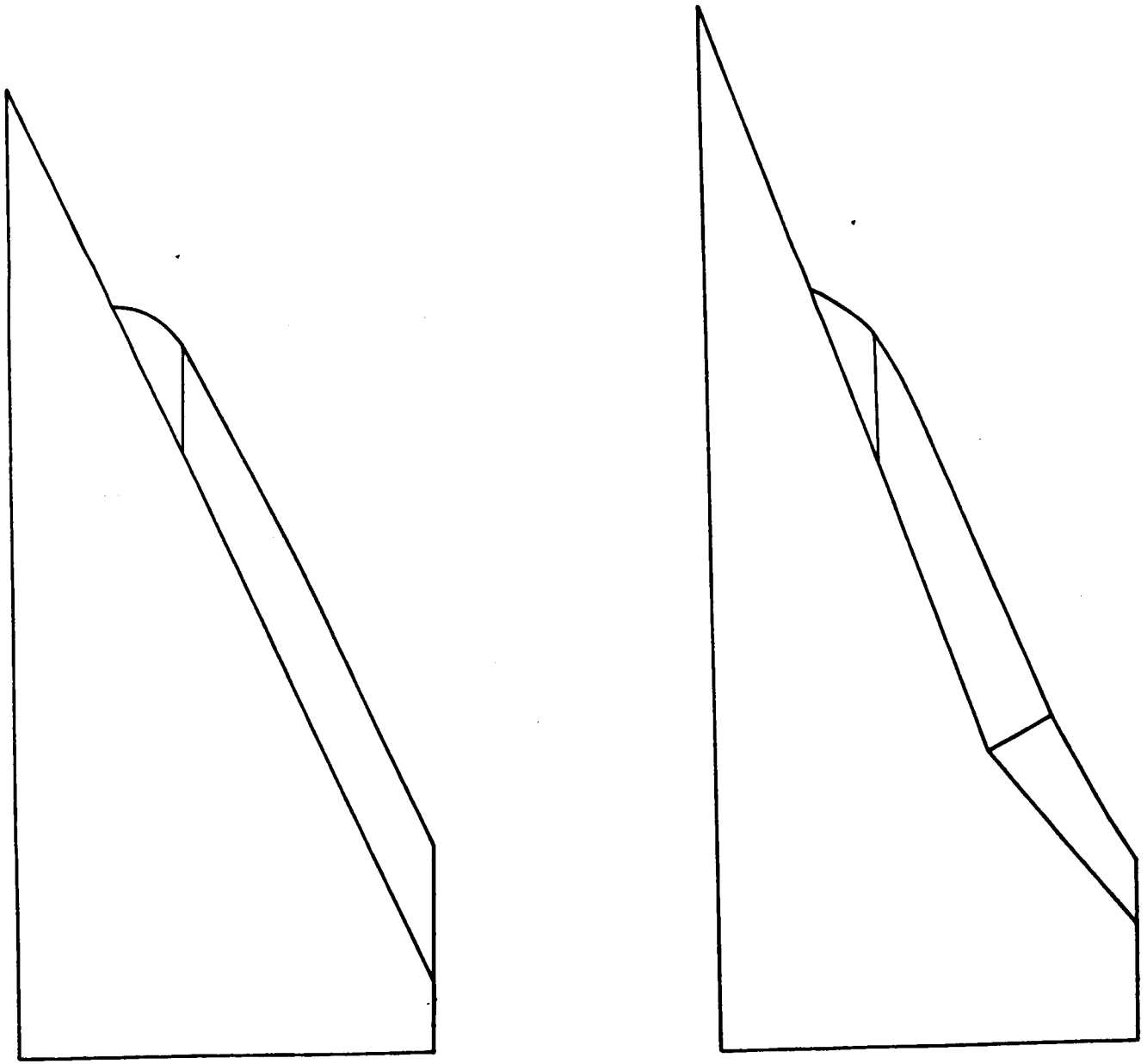

a) 65-Degree Cropped Delta Wing

b) 70/50-Degree Cranked Wing

Figure 154. Part-Span Vortex Flap Apex Modifications.

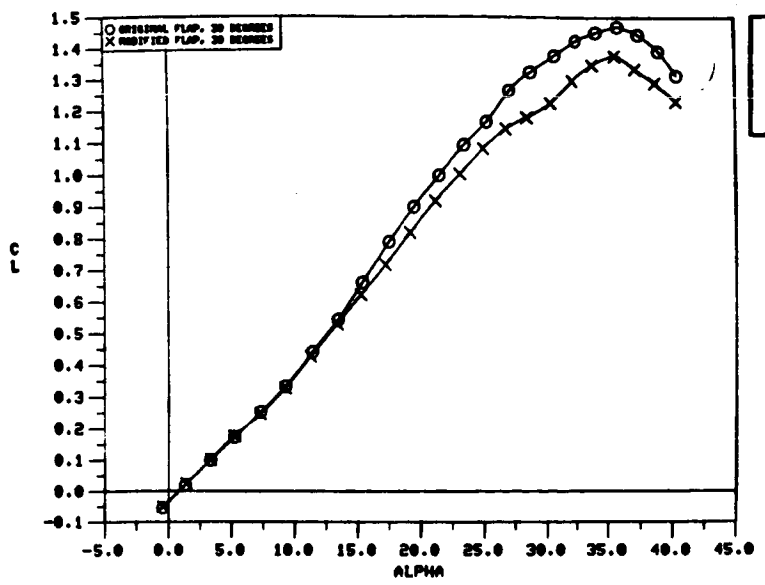

a) C_L vs. α

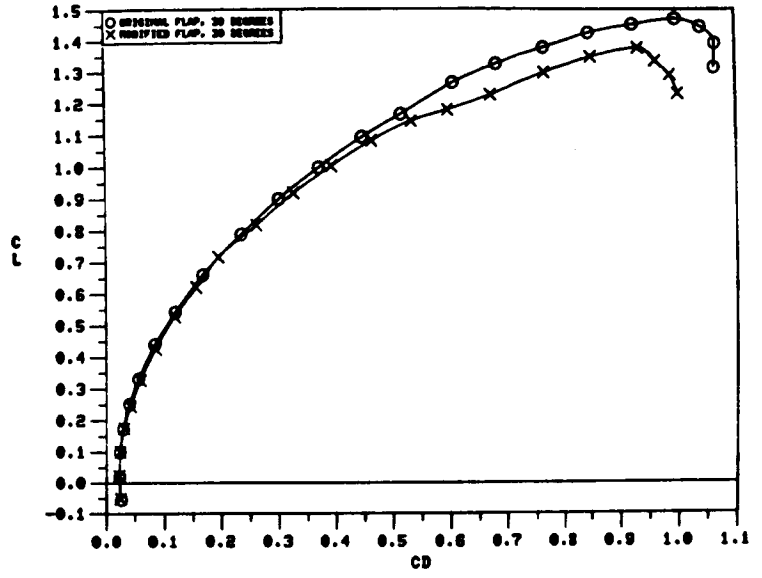

b) C_L vs. C_D

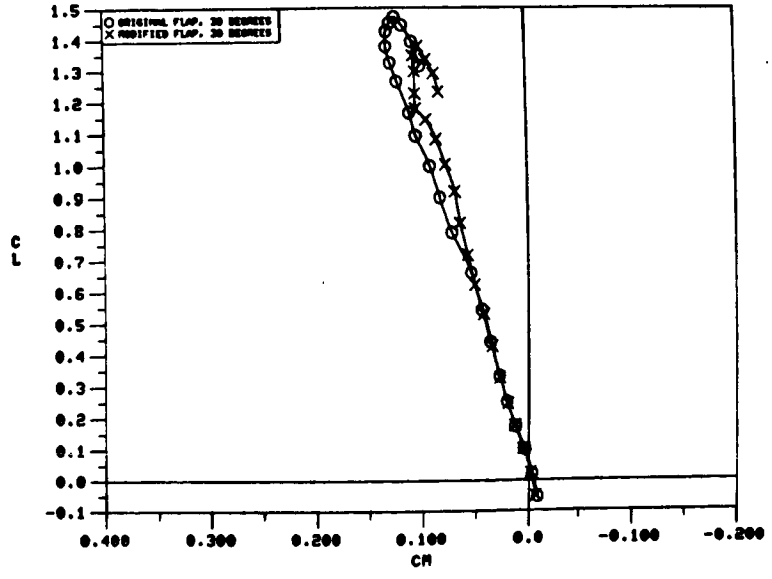

c) C_L vs. C_m

Figure 155. Effect of Flap Apex Modification on the 65-Degree Cropped Delta Wing Static Longitudinal Aerodynamic Characteristics.

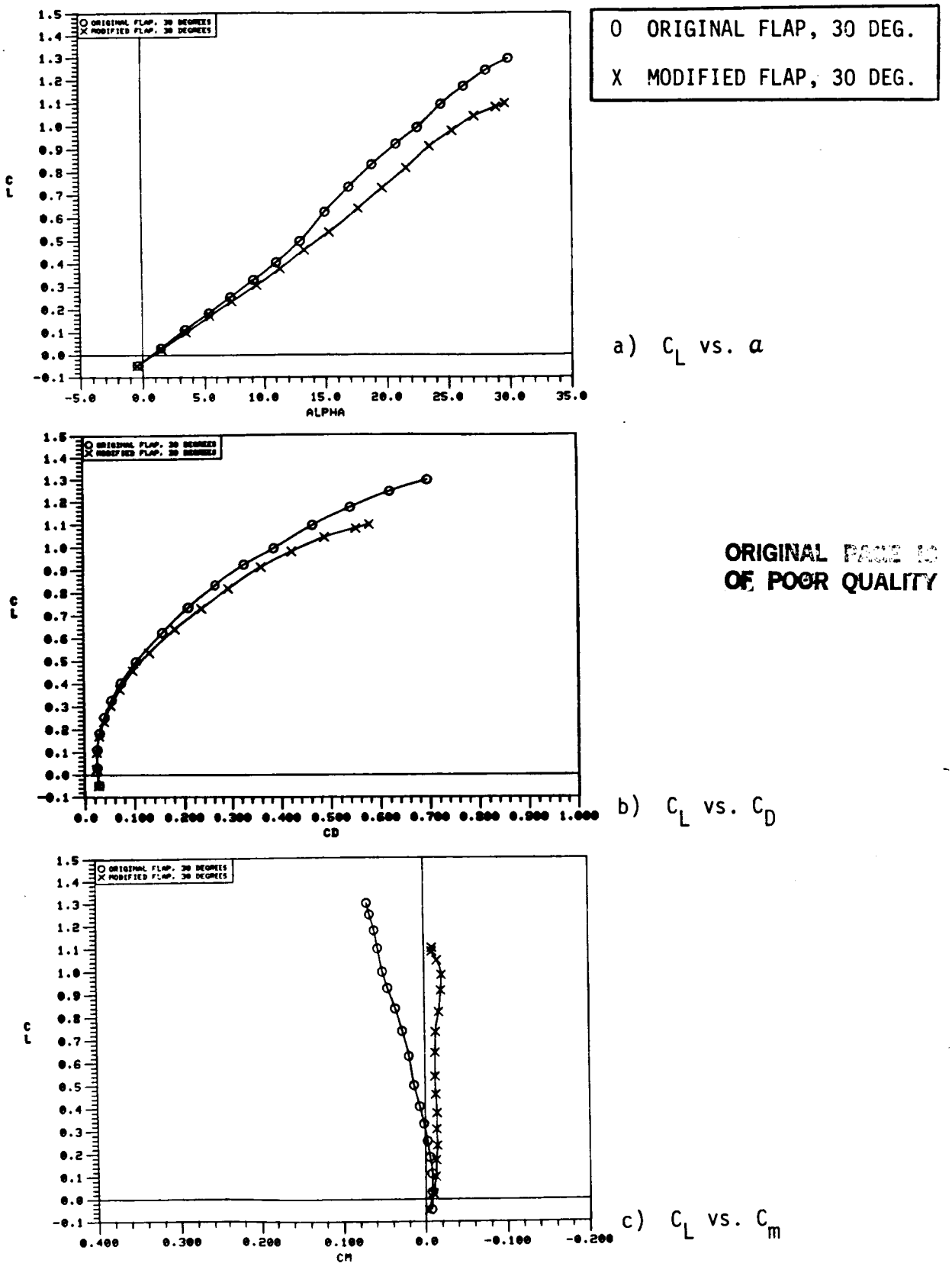

Figure 156. Effect of Flap Apex Modification on the 70/50-Degree Cranked Wing Static Longitudinal Aerodynamic Characteristics.

O ORIGINAL FLAP, 30 DEG.

X MODIFIED FLAP, 30 DEG.

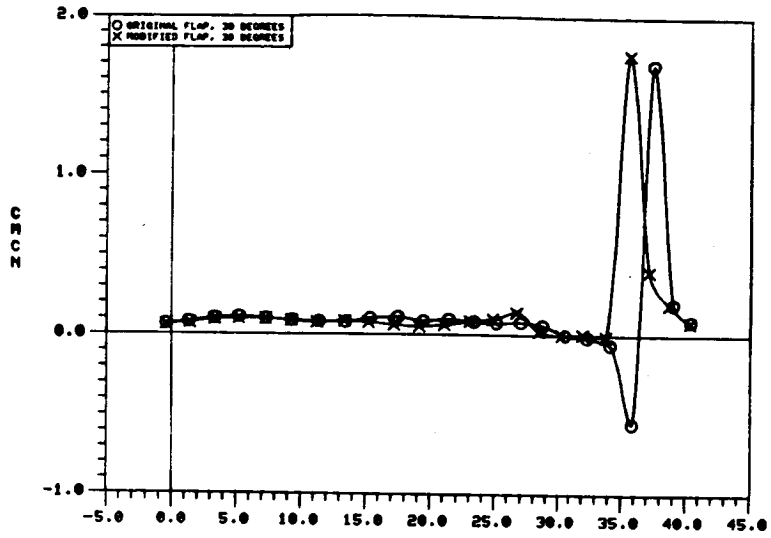

a) $C_{m_{C_N}}$ vs. α

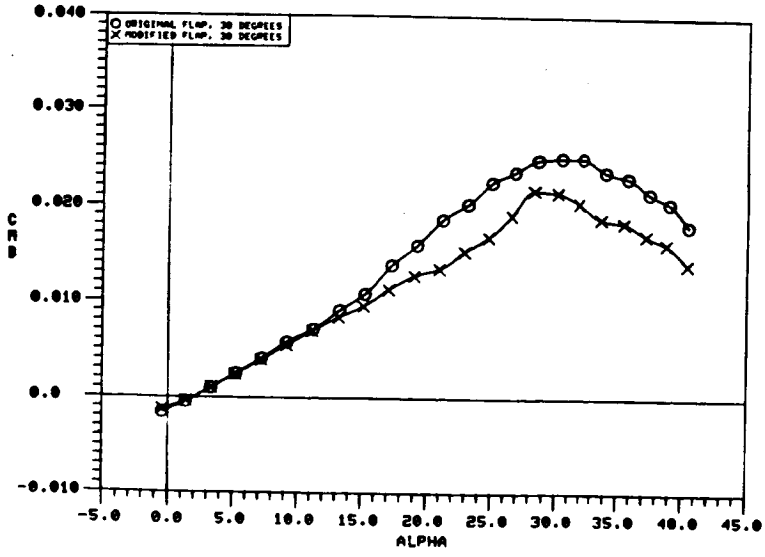

b) C_{m_β} vs. α

Figure 157. Effect of Flap Apex Modification on the 65-Degree Cropped Delta Wing Static Longitudinal Stability Characteristics.

O	ORIGINAL FLAP, 30 DEG.
X	MODIFIED FLAP, 30 DEG.

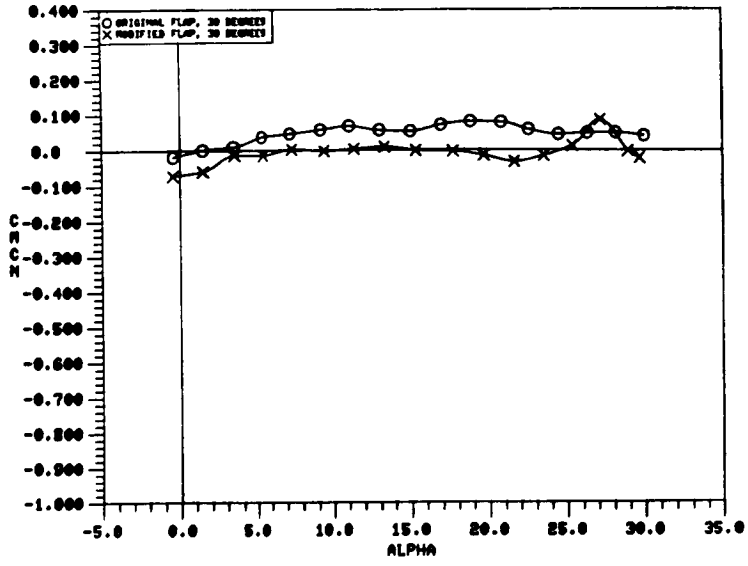

a) $C_{m_{C_N}}$ vs. α

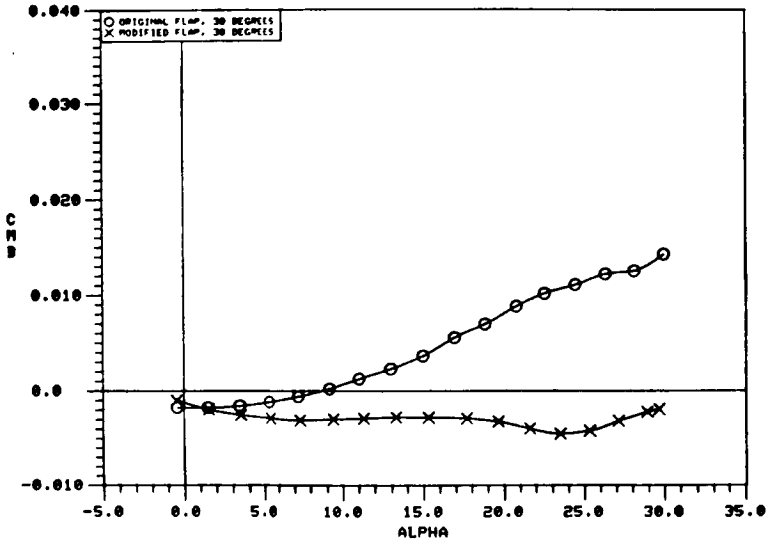

b) C_{m_β} vs. α

Figure 158. Effect of Flap Apex Modification on the 70/50-Degree Cranked Wing Static Longitudinal Stability Characteristics.

O	ORIGINAL FLAP, 30 DEG.
X	MODIFIED FLAP, 30 DEG.

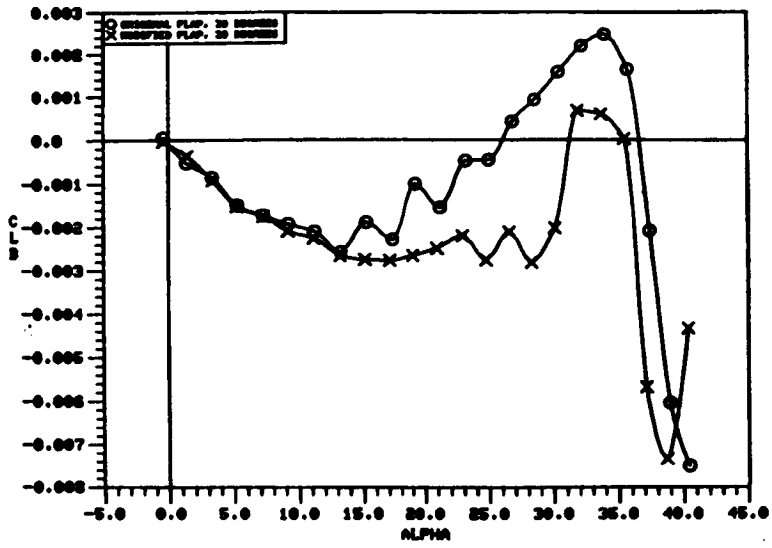

Figure 159. Effect of Flap Apex Modification on the 65-Degree Cropped Delta Wing Static Lateral Stability Characteristics.

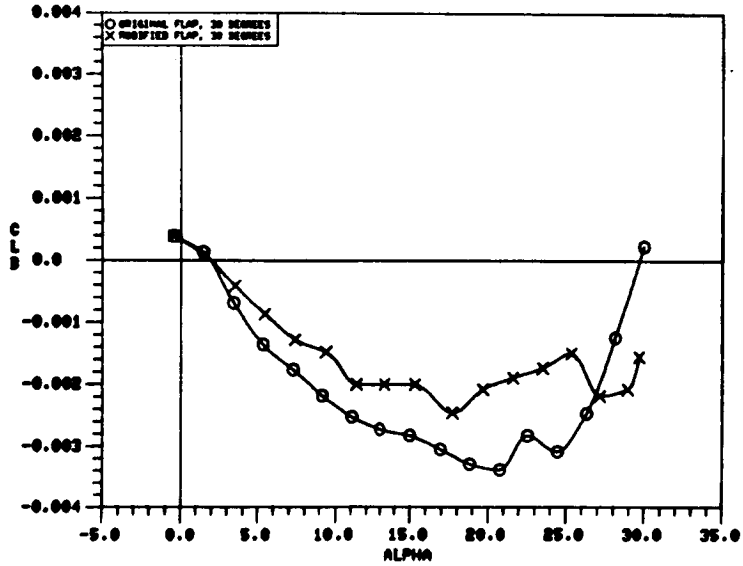

C_{l_β} vs. α

Figure 160. Effect of Flap Apex Modification on the 70/50-Degree Cranked Wing Static Lateral Stability Characteristics.

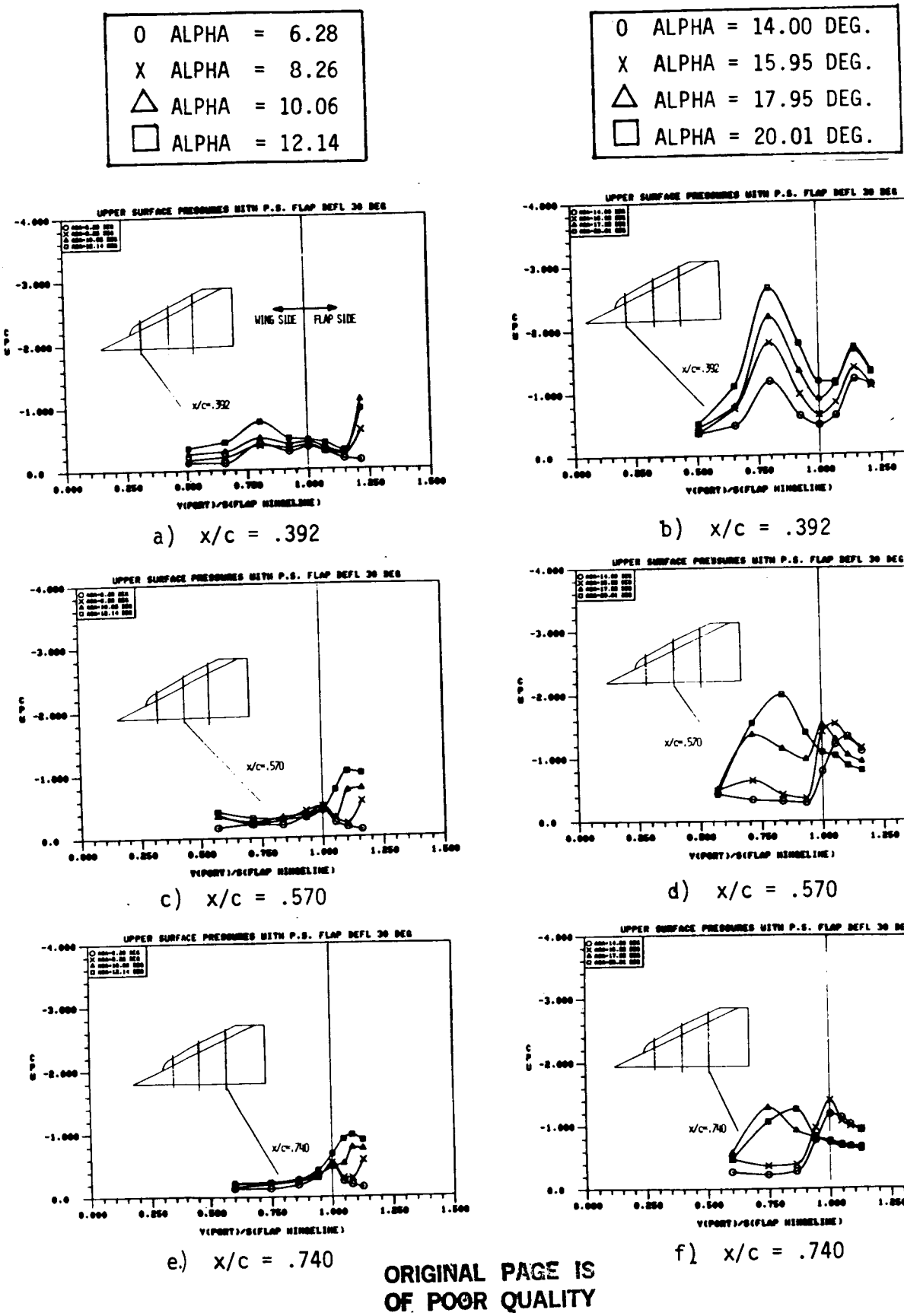

ORIGINAL PAGE IS
OF POOR QUALITY

Figure 161. Upper Surface Pressure Distributions on the 65-Degree Cropped Delta Wing with Part Span Flap. (Reference 10)

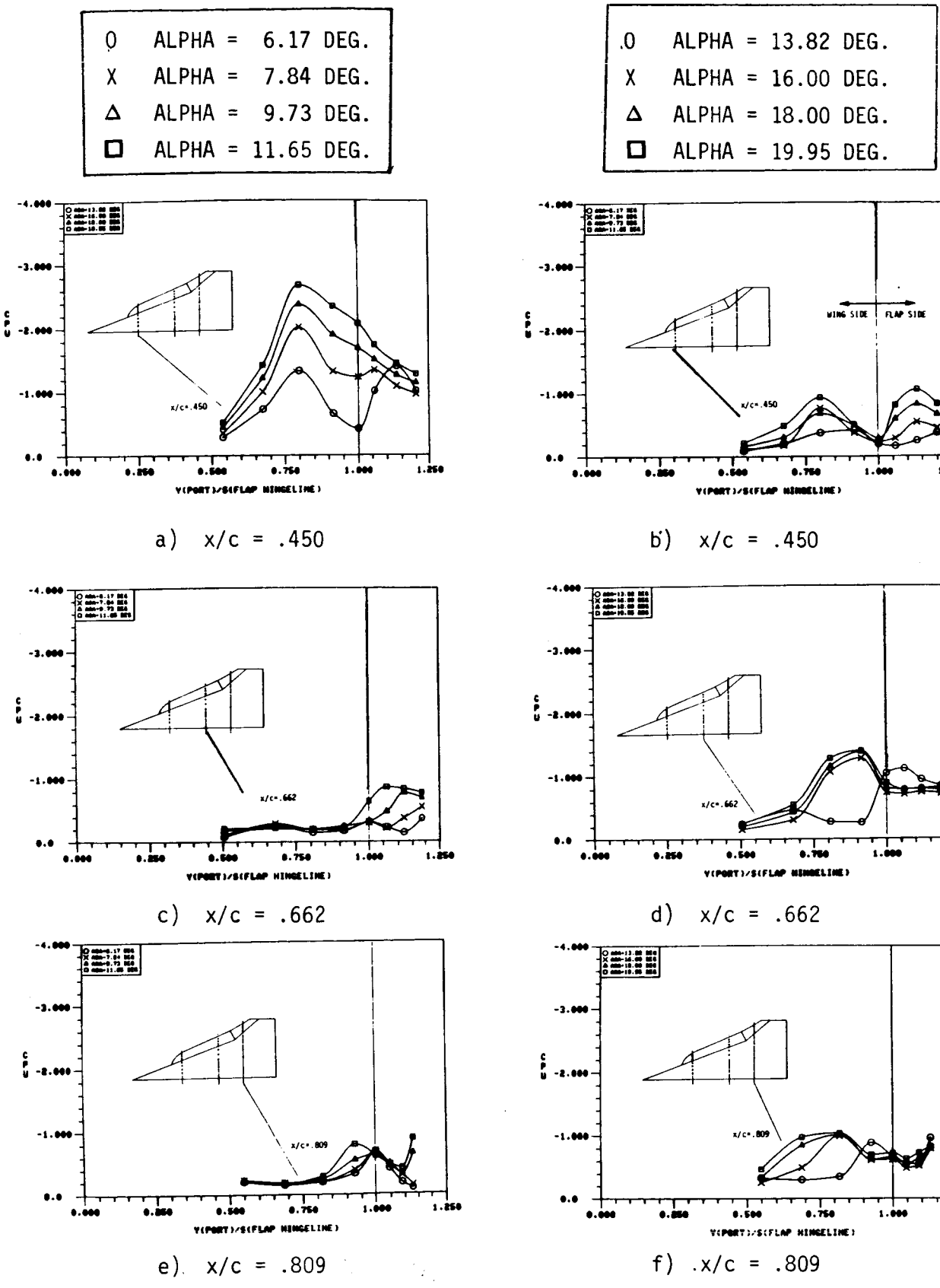

a) x/c = .450

b) x/c = .450

c) x/c = .662

d) x/c = .662

e) x/c = .809

f) .x/c = .809

Figure 162. Upper Surface Pressure Distributions on the 70/50-Degree Cranked Wing with Part Span Flap. (Reference 10)

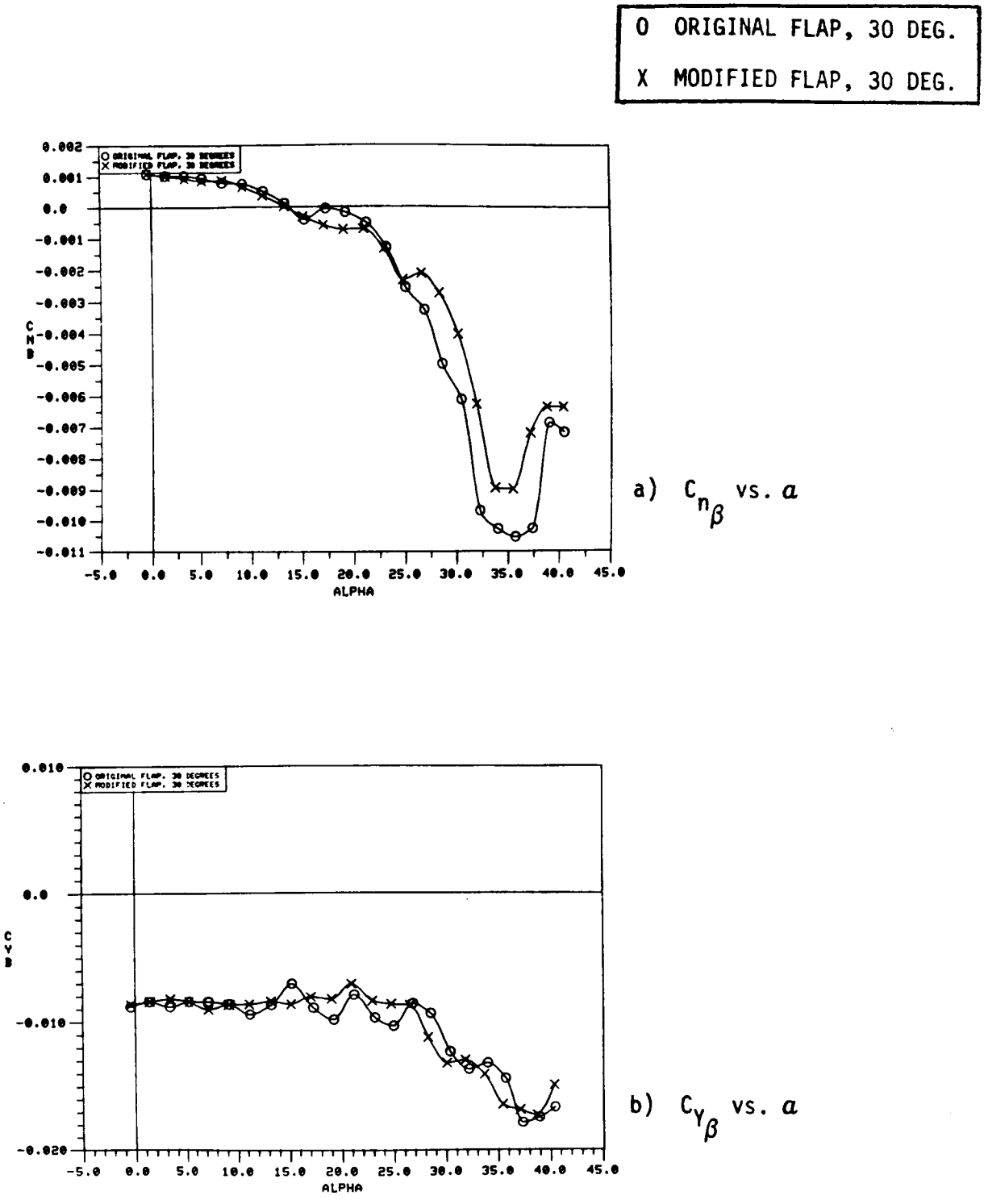

Figure 163. Effect of Flap Apex Modification on the 65-Degree Cropped Delta Wing Static Directional Stability Characteristics.

O	ORIGINAL FLAP, 30 DEG.
X	MODIFIED FLAP, 30 DEG.

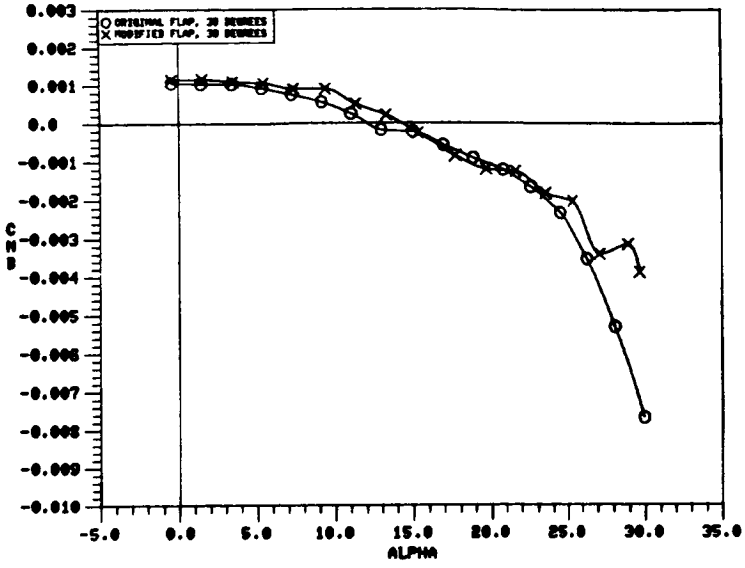

a) C_{n_β} vs. α

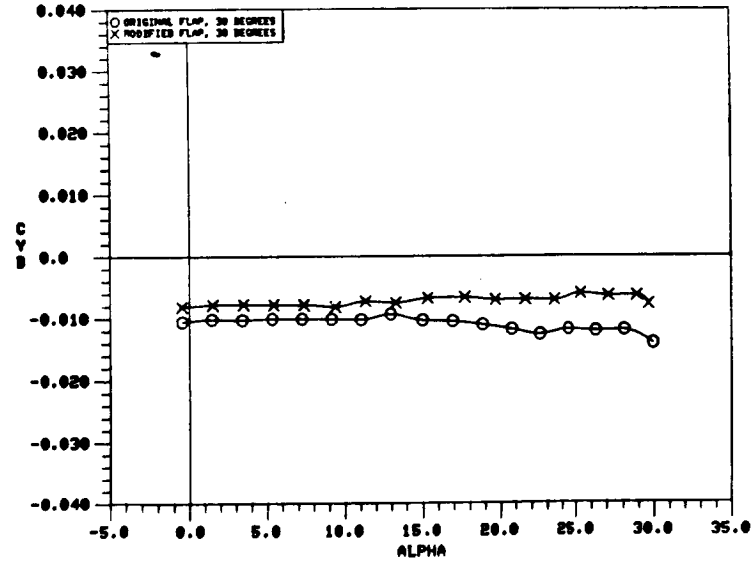

b) C_{Y_β} vs. α

Figure 164. Effect of Flap Apex Modification on the 70/50-Degree Cranked Wing Static Directional Stability Characteristics.

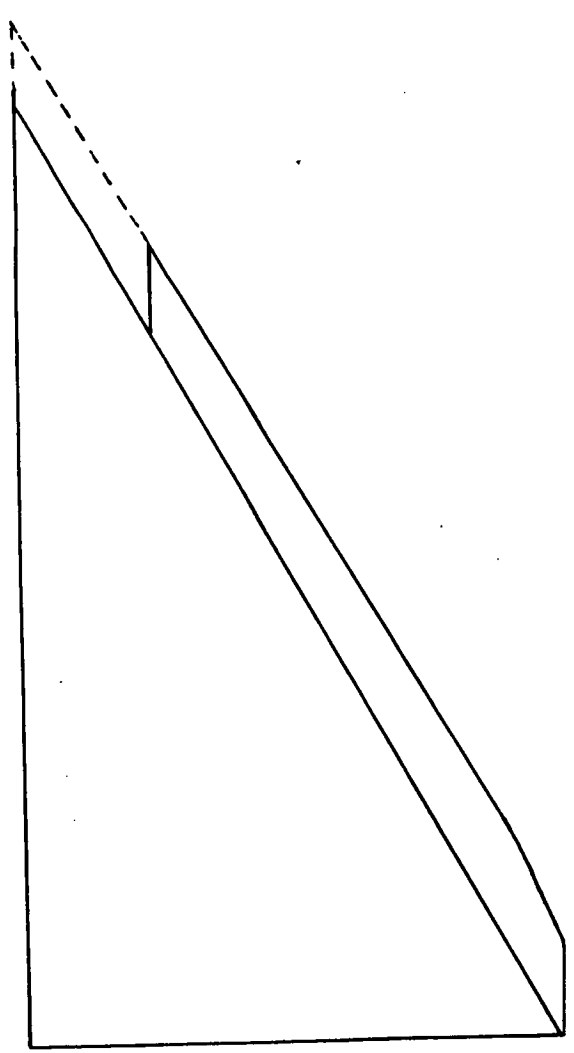

a) Removal of Inboard Flap Segment

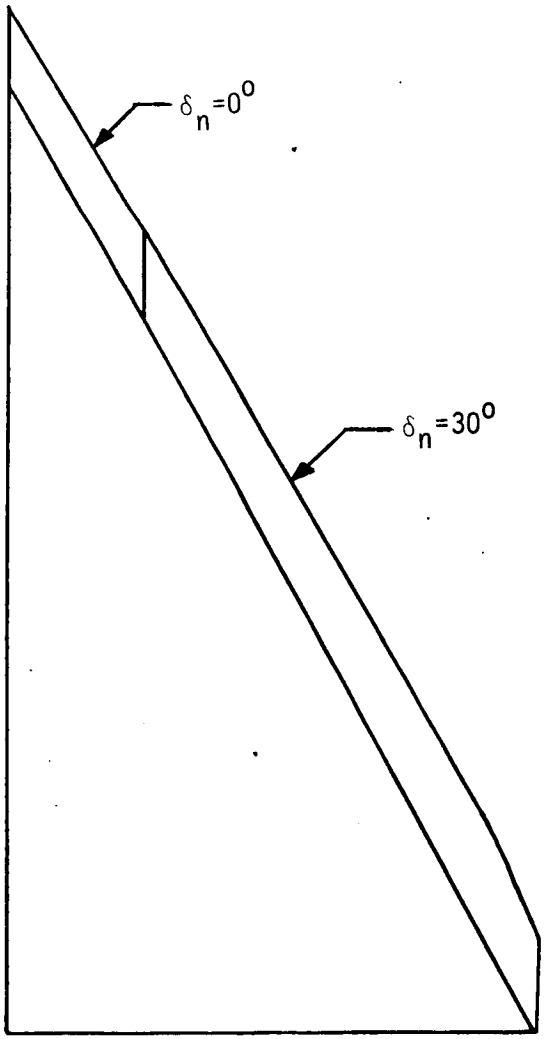

b) Differential Deflection of Flap Segments

Figure 165. Full-Span Vortex Flap Apex Modifications.

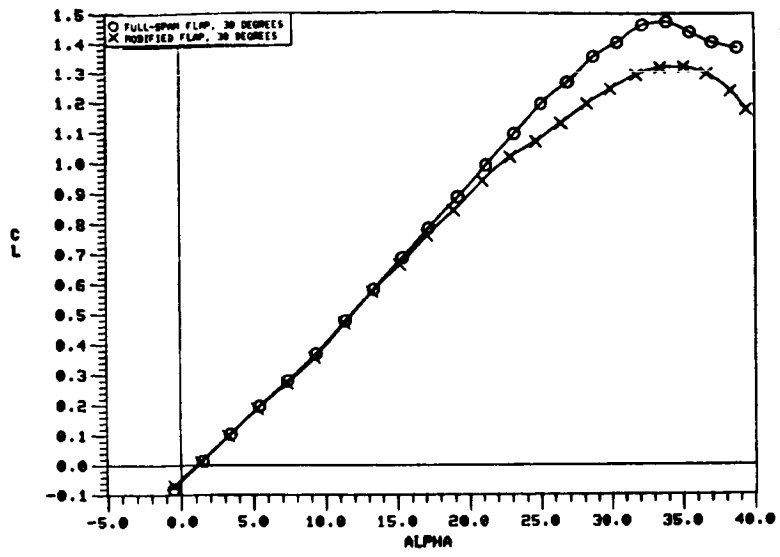

O FULL-SPAN FLAP, 30 DEGREES

X PART-SPAN FLAP, 30 DEGREES

a) C_L vs. α

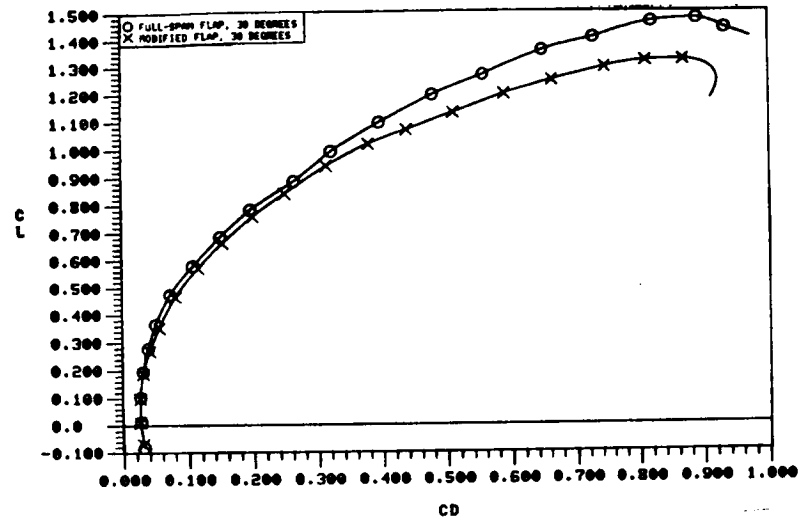

b) C_L vs. C_D

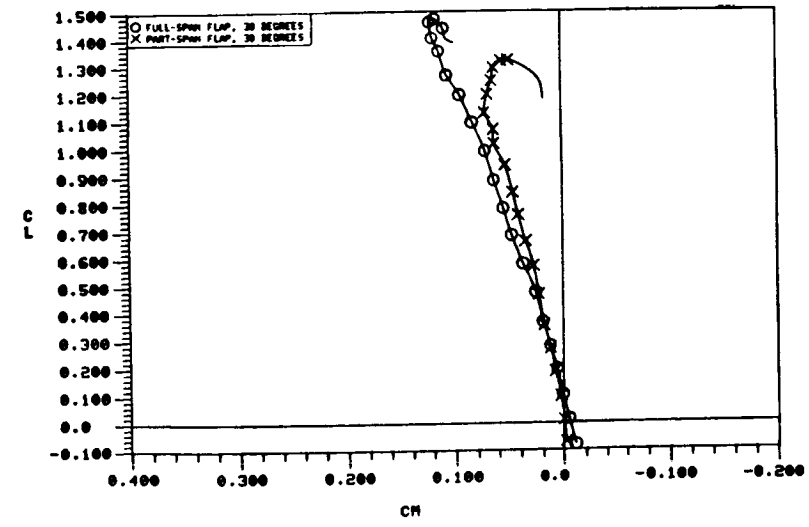

c) C_L vs. C_m

Figure 166. Effect of the Removal of the Inboard 25% of the Vortex Flap on the 60-Degree Cropped Delta Wing Static Longitudinal Aerodynamic Characteristics.

O	FULL-SPAN FLAP, 30 DEG.
X	PART-SPAN FLAP, 30 DEG.

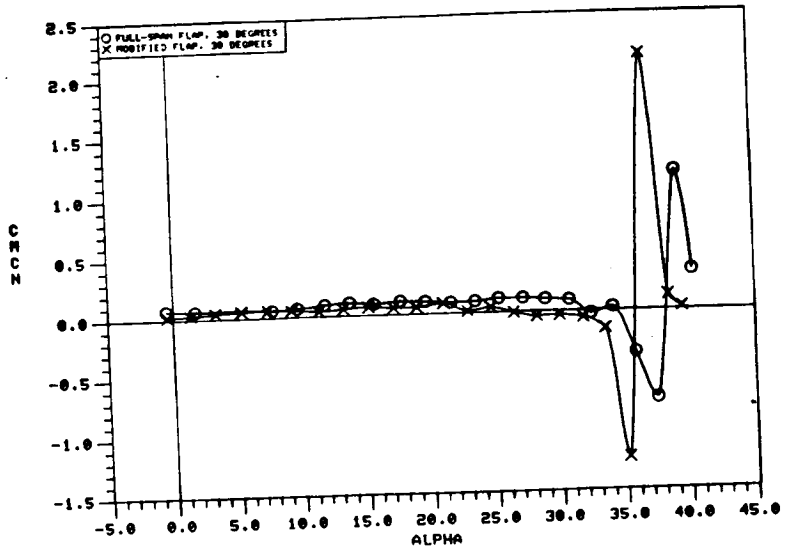

a) $C_{m_{C_N}}$ vs. α

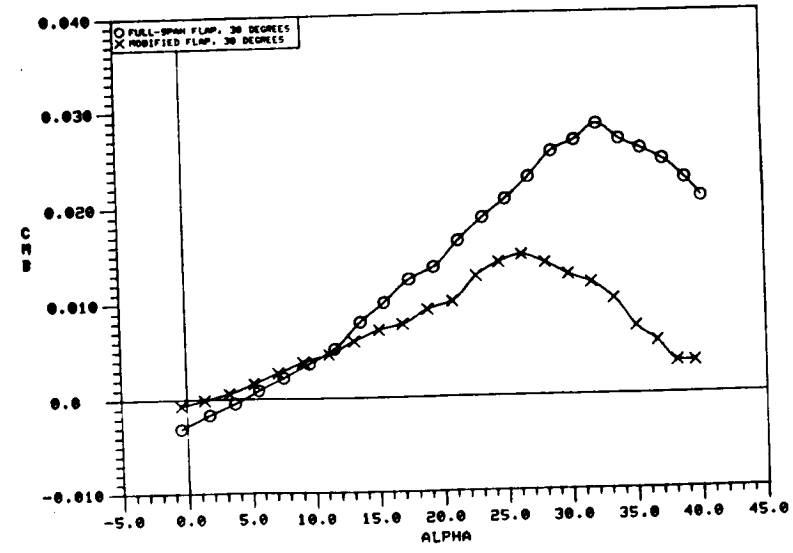

b) C_{m_β} vs. α

Figure 167. Effect of the Removal of the Inboard 25% of the Vortex Flap on the 60-Degree Cropped Delta Wing Static Longitudinal Stability Characteristics.

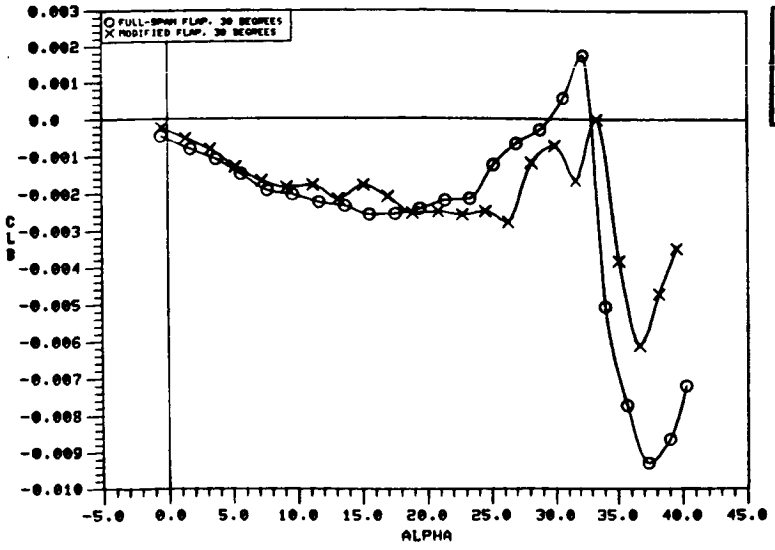

O FULL-SPAN ELAP, 30 DEG.

X PART-SPAN FLAP, 30 DEG.

a) C_{ℓ_β} vs. α

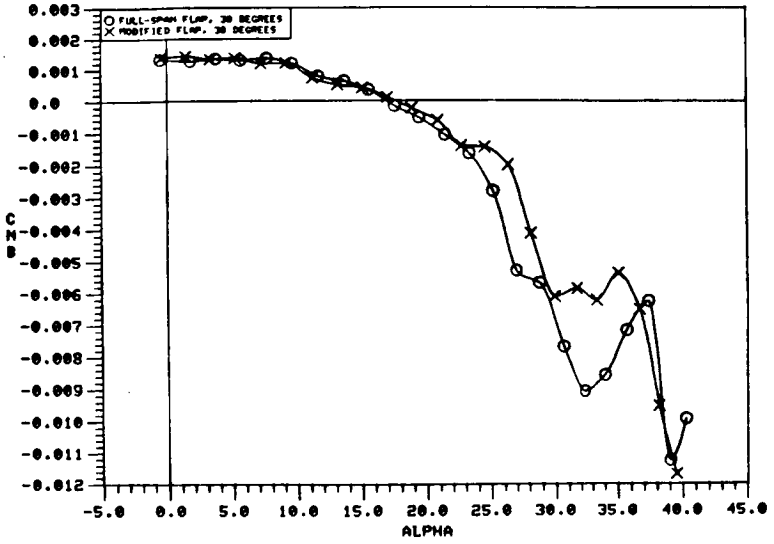

b) C_{n_β} vs. α

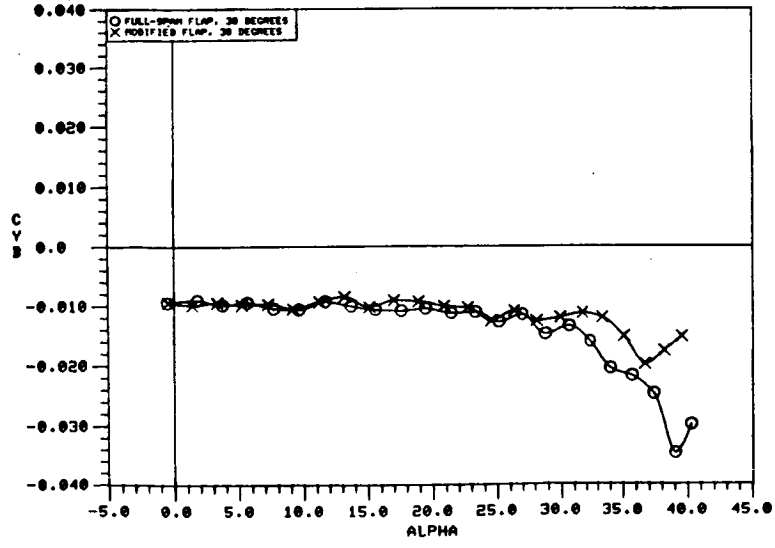

c) C_{Y_β} vs. α

Figure 168. Effect of the Removal of the Inboard 25% of the Vortex Flap on the 60-Degree Cropped Delta Wing Static Lateral-Directional Stability Characteristics.

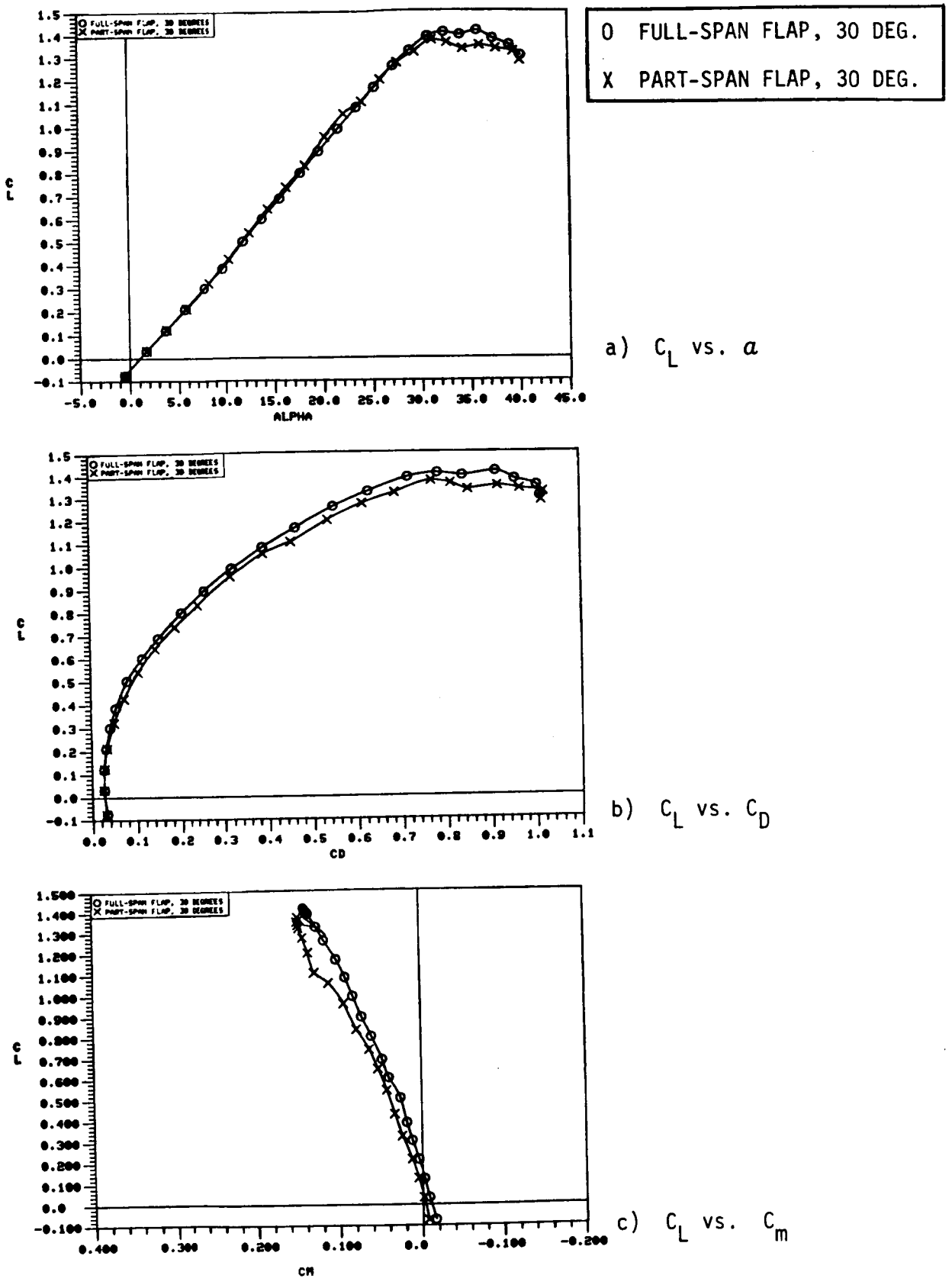

Figure 169. Effect of Flap Modification on the 60-Degree Cropped Delta Wing Static Longitudinal Aerodynamic Characteristics.

O	FULL-SPAN FLAP, 30 DEG.
X	PART-SPAN FLAP, 30 DEG.

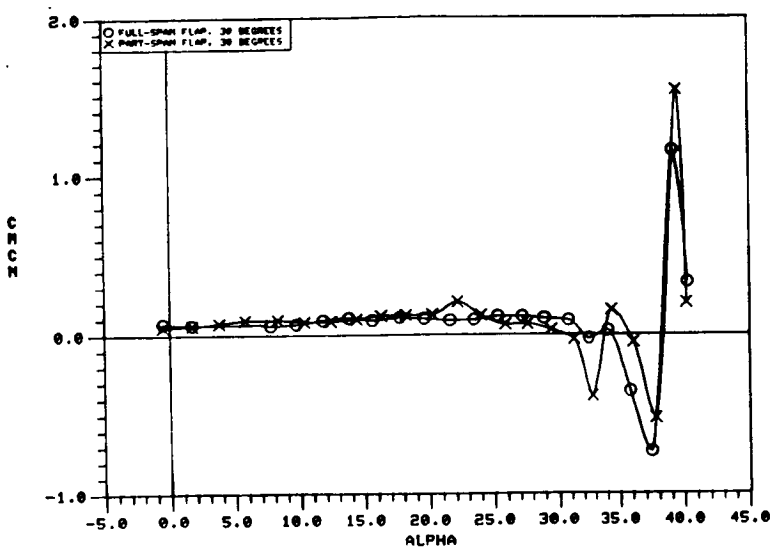

a) $C_{m_{C_N}}$ vs. α

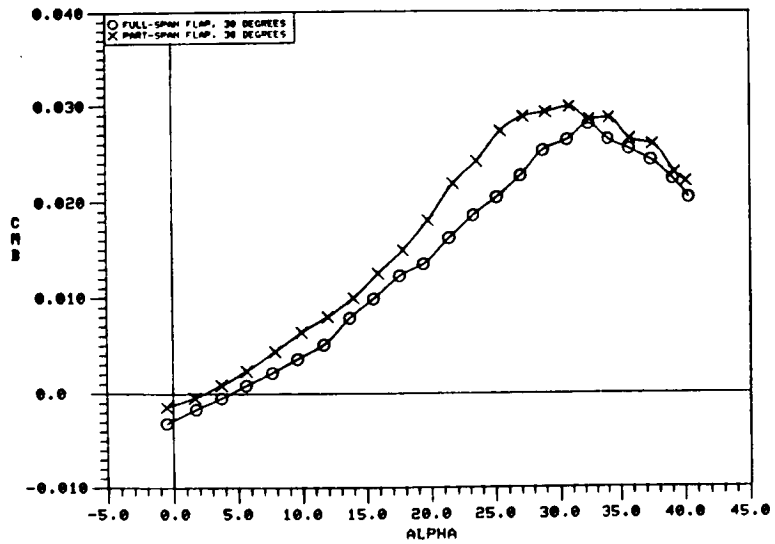

b) C_{m_β} vs. α

Figure 170. Effect of Flap Modification on the 60-Degree Cropped Delta Wing Static Longitudinal Stability Characteristics.

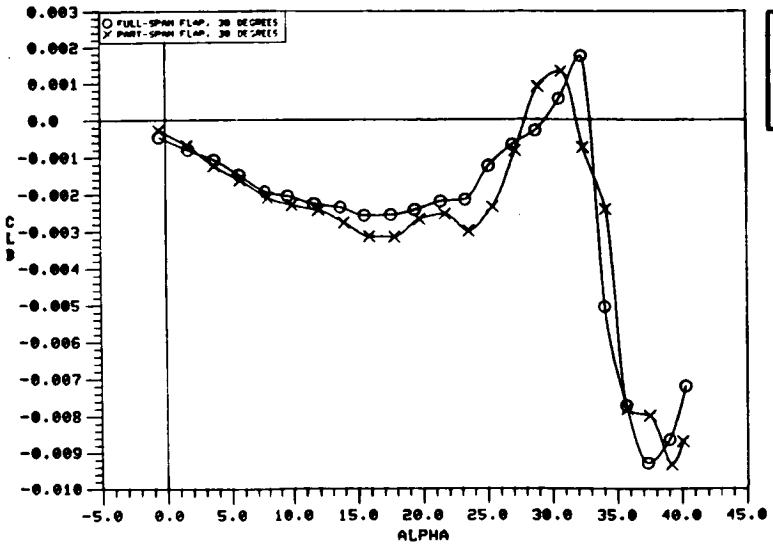

a) C_{ℓ_β} vs. α

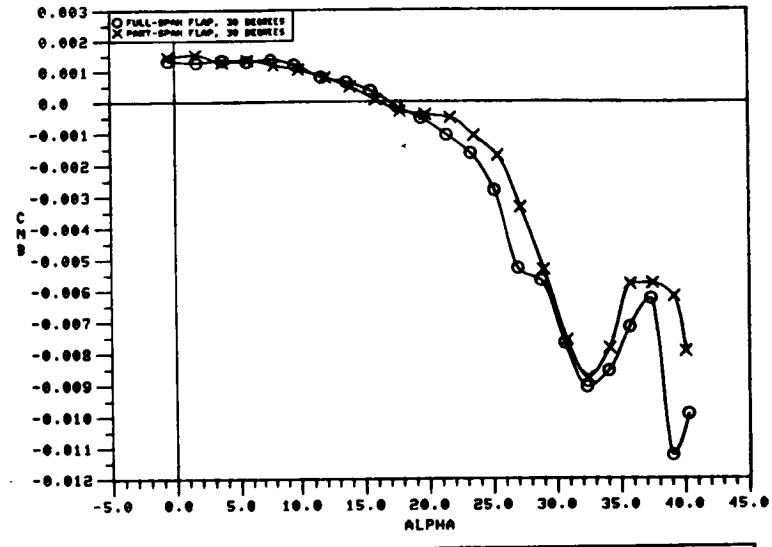

b) C_{n_β} vs. α

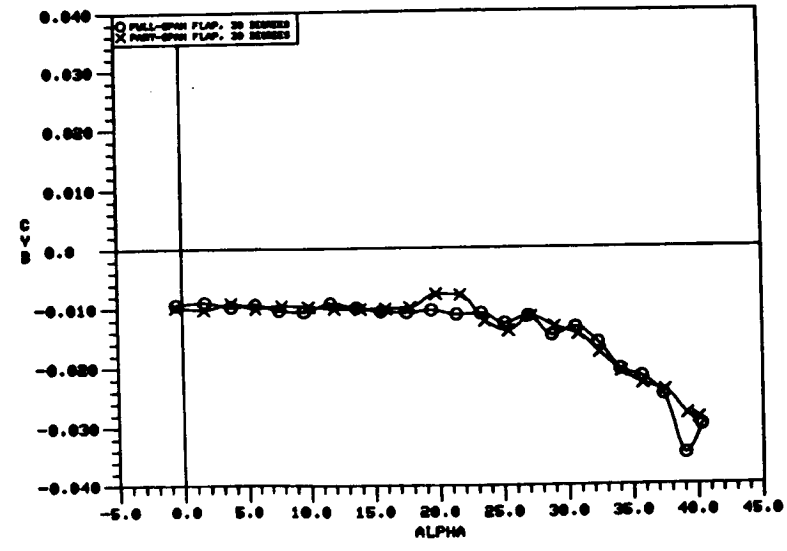

c) C_{Y_β} vs. α

Figure 171. Effect of Flap Modification on the 60-Degree Cropped Delta Wing Static Lateral-Directional Stability Characteristics.

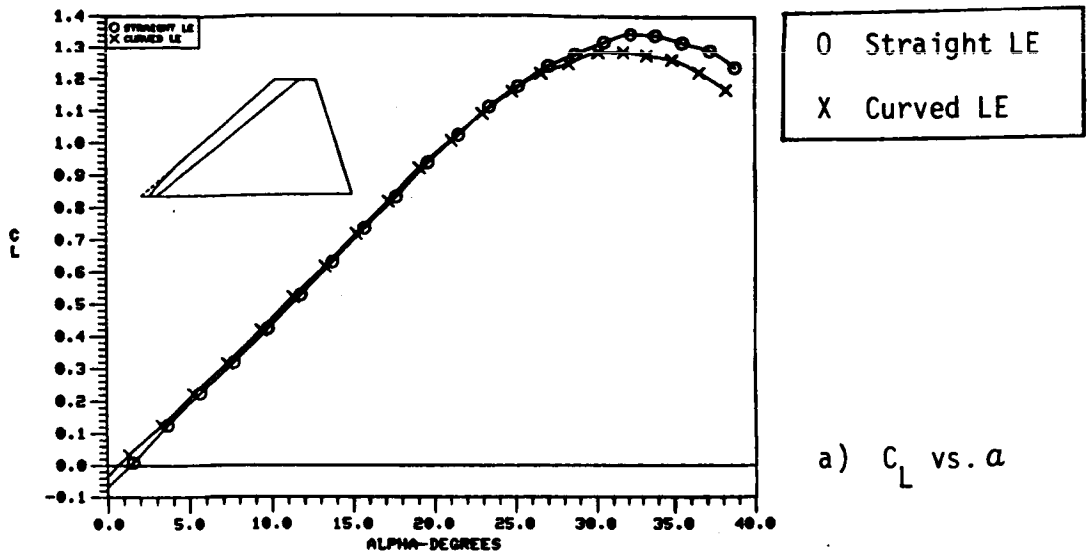

a) C_L vs. α

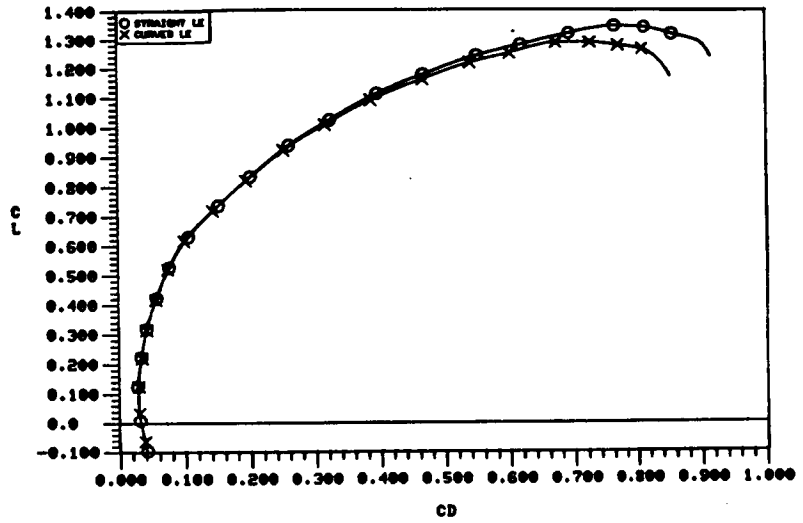

b) C_L vs. C_D

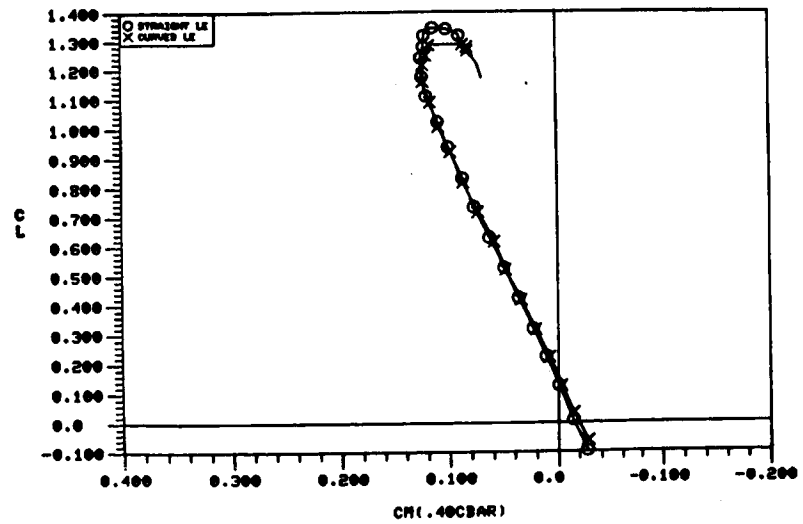

c) C_L vs. C_m

Figure 172. Effect of Flap Modification on the 50-Degree Cropped Diamond Wing Static Longitudinal Aerodynamic Characteristics.

O	Straight LE
X	Curved LE

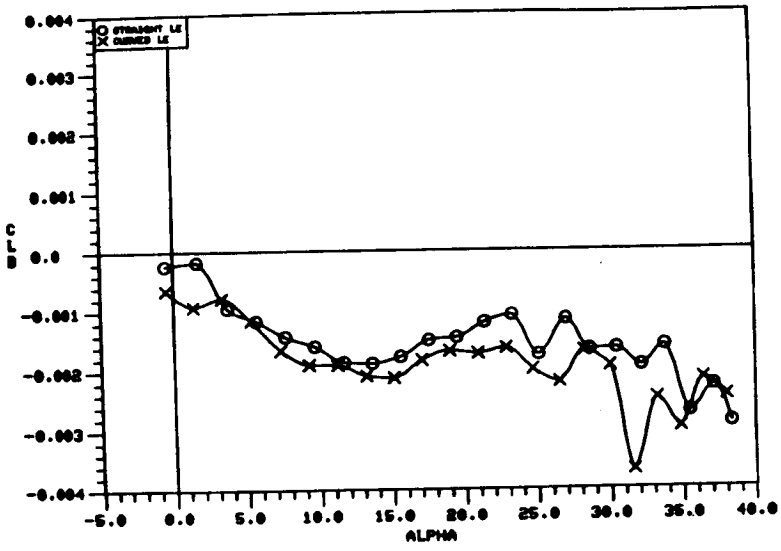

C_{ℓ_β} vs. α

Figure 173. Effect of Flap Modification on the 50-Degree Cropped Diamond Wing Static Lateral Stability Characteristics.

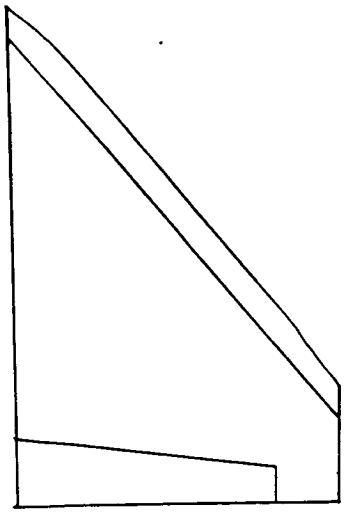

a) 50-Degree Cropped Delta Wing

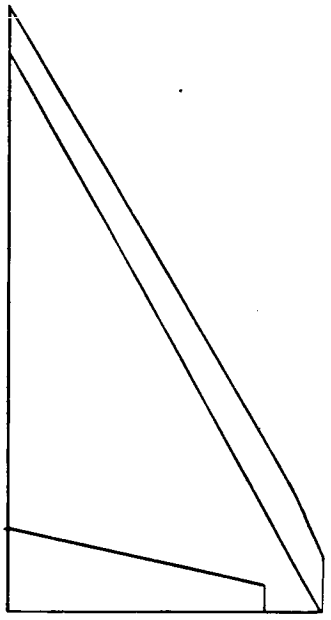

b) 60-Degree Cropped Delta Wing

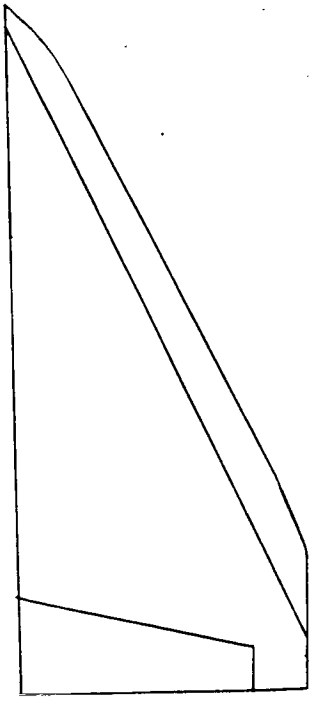

c) 65-Degree Cropped Delta Wing

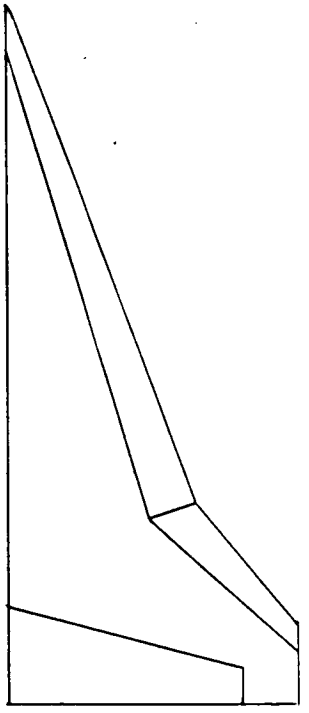

d) 70/50-Degree Cranked Wing

Figure 174. Full-Span Leading- and Part-Span Trailing-Edge Flap Geometries.

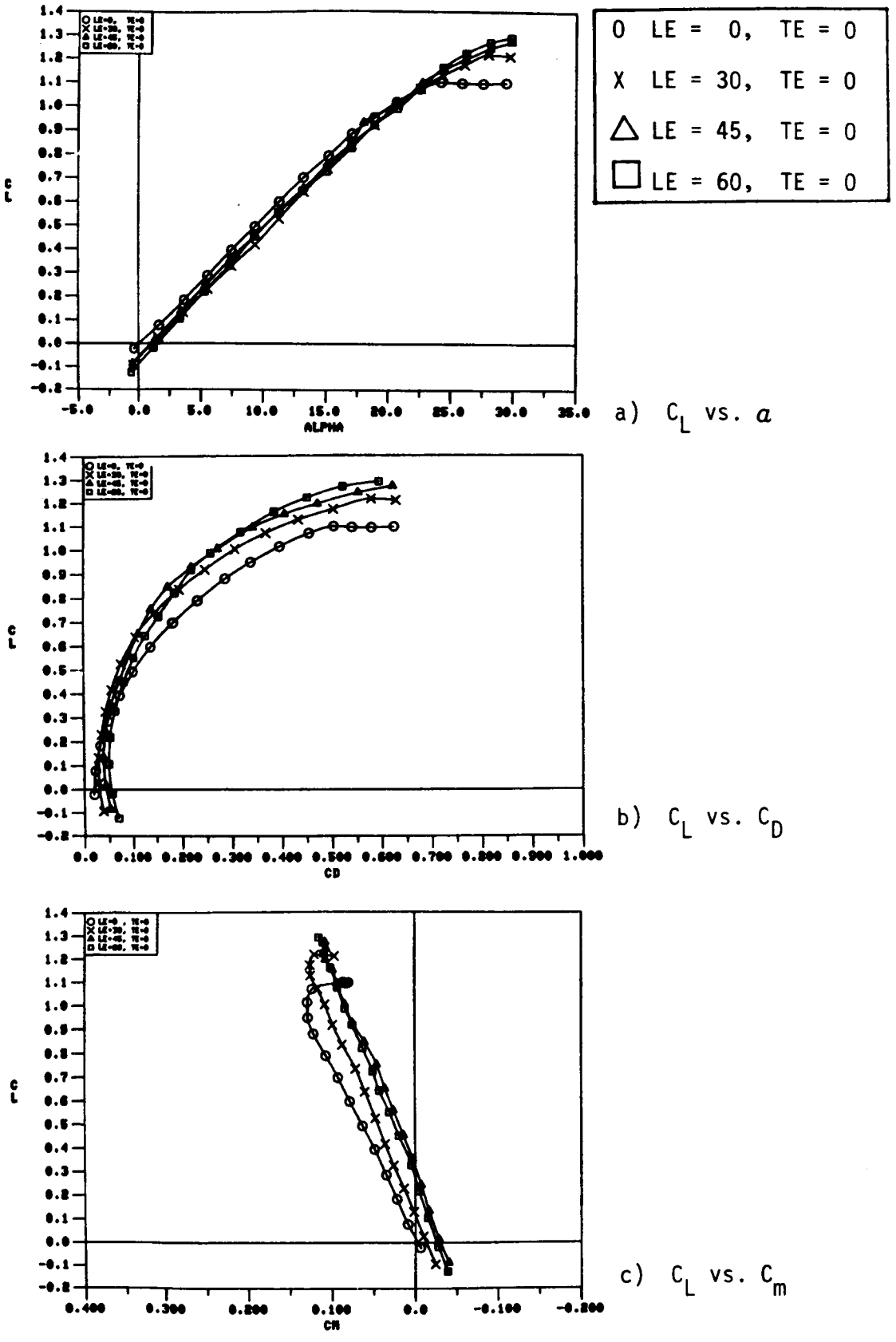

a) C_L vs. α

b) C_L vs. C_D

c) C_L vs. C_m

Figure 175. Effect of Leading-Edge Flap Deflection Angle on the 50-Degree Cropped Delta Wing Static Longitudinal Aerodynamic Characteristics.

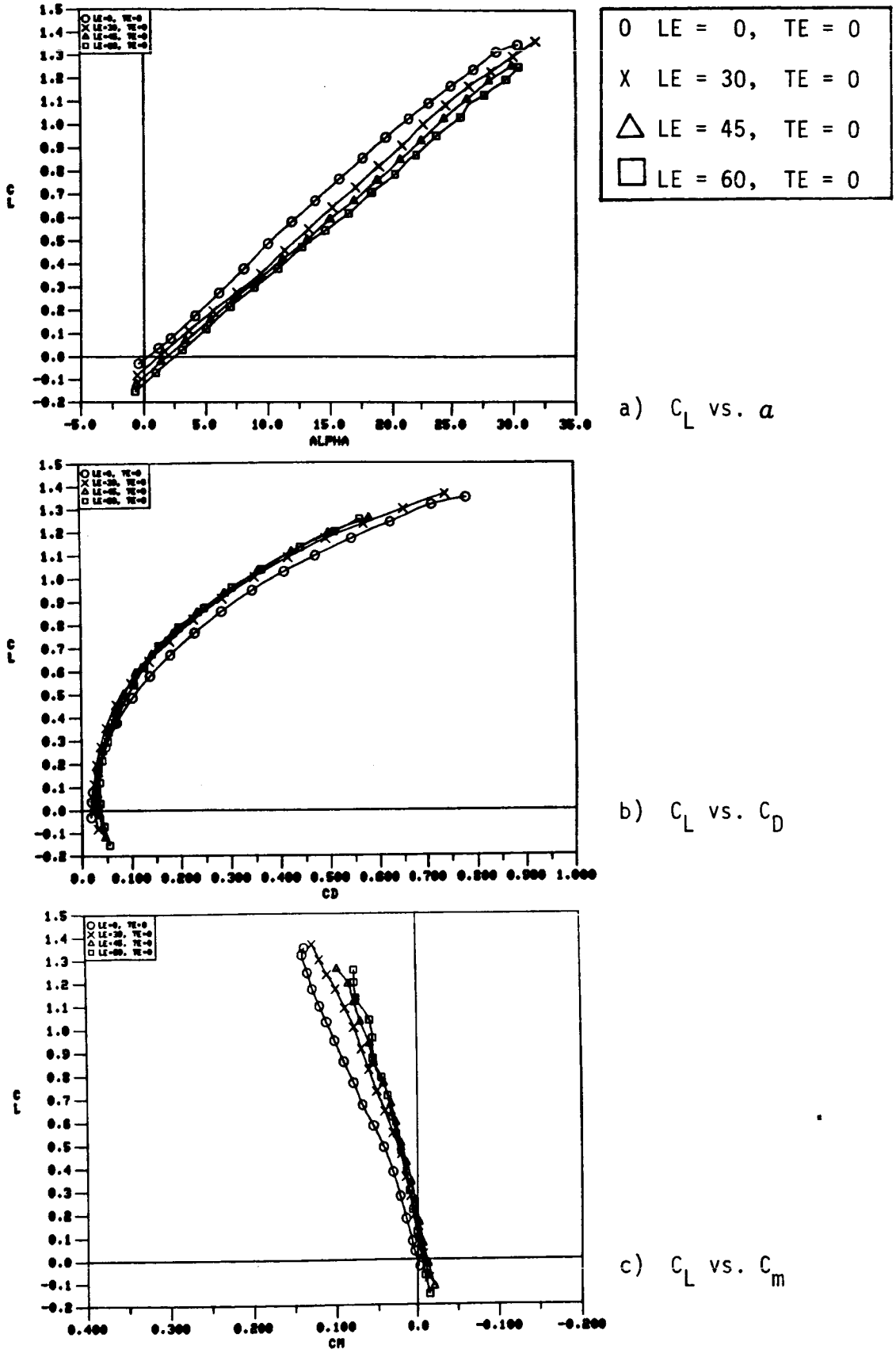

Figure 176. Effect of Leading-Edge Flap Deflection Angle on the 60-Degree Cropped Delta Wing Static Longitudinal Aerodynamic Characteristics.

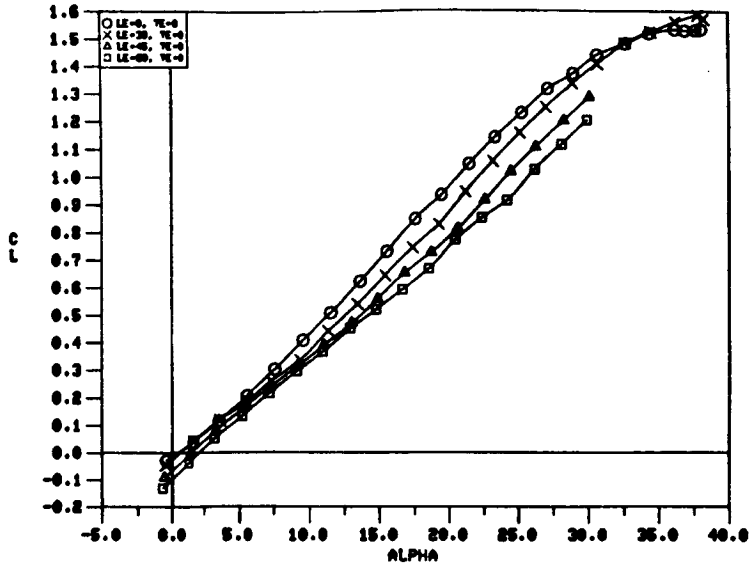

a) C_L vs. α

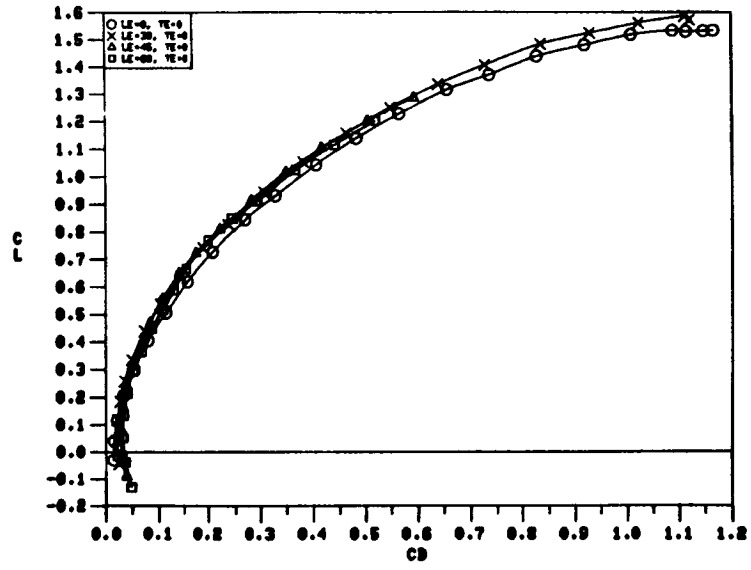

b) C_L vs. C_D

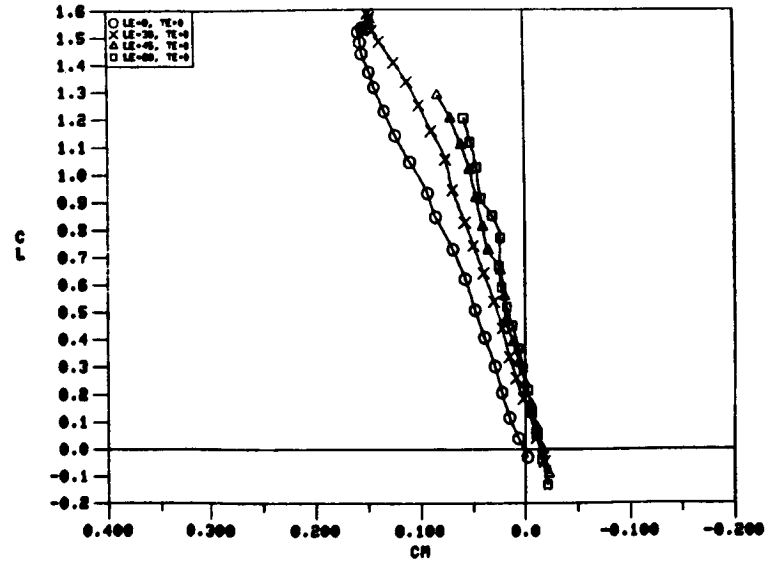

c) C_L vs. C_m

Figure 177. Effect of Leading-Edge Flap Deflection Angle on the 65-Degree Cropped Delta Wing Static Longitudinal Aerodynamic Characteristics.

0	LE = 0, TE = 0
X	LE = 30, TE = 0
△	LE = 45, TE = 0
□	LE = 60, TE = 0

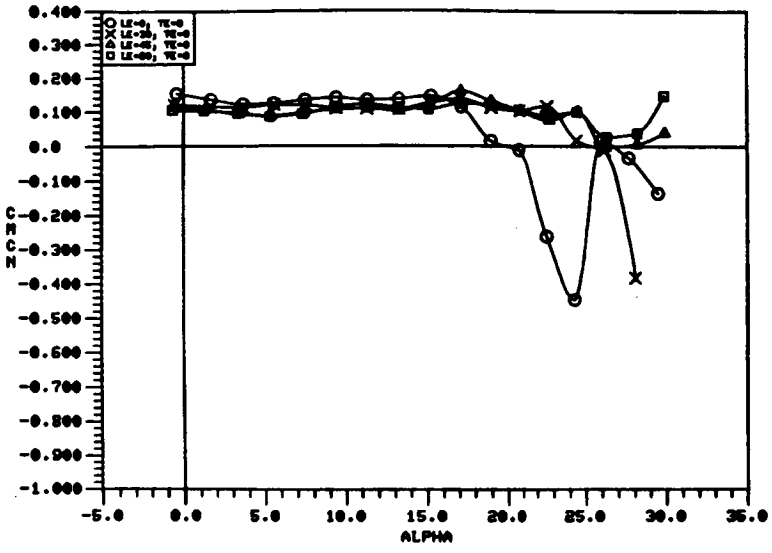

a) $C_{m_{C_N}}$ vs. α

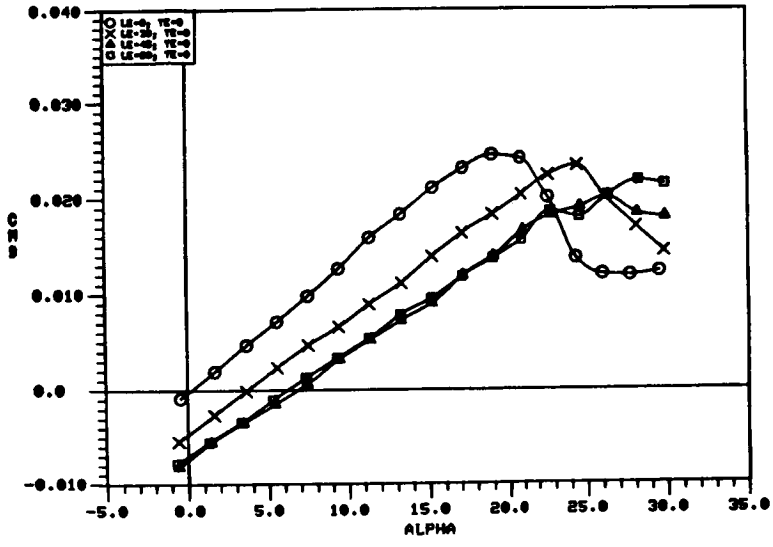

b) C_{m_β} vs. α

Figure 178. Effect of Leading-Edge Flap Deflection Angle on the 50-Degree Cropped Delta Wing Static Longitudinal Stability Characteristics.

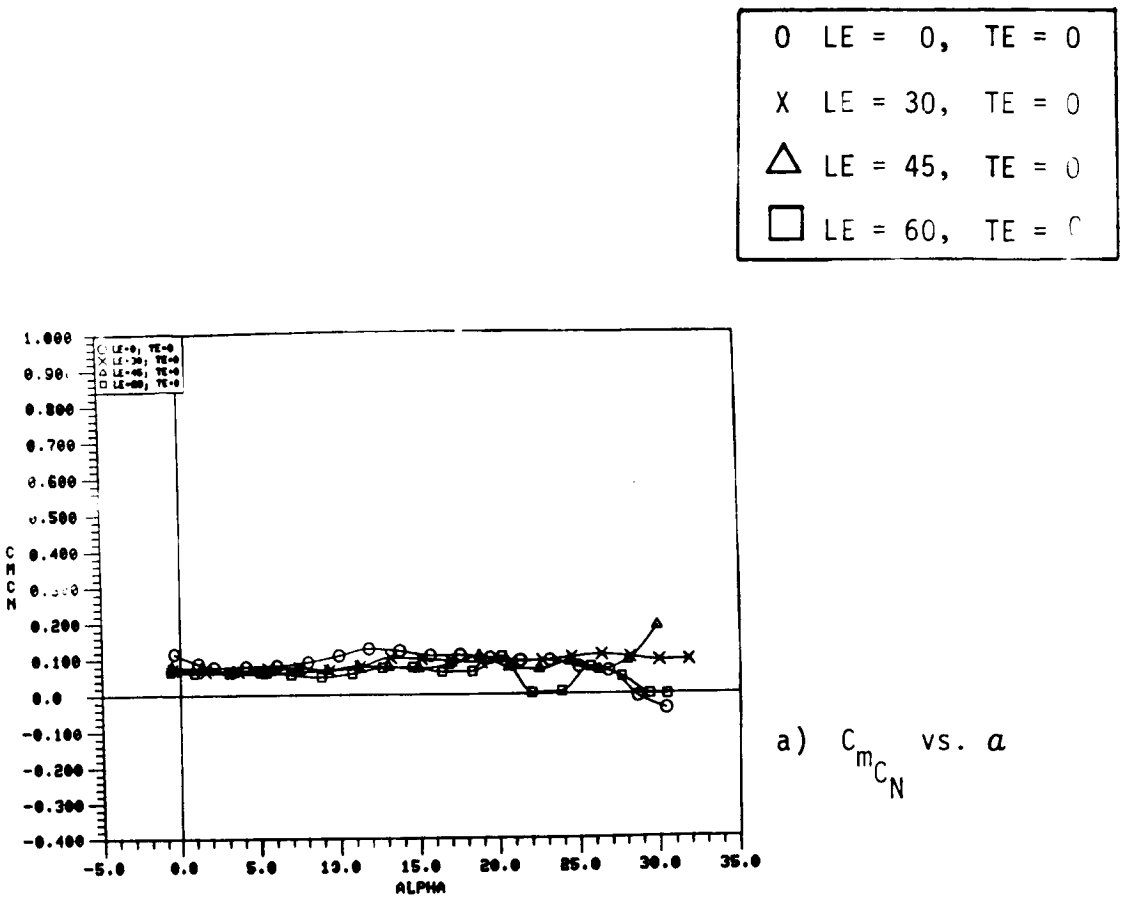

Figure 179. Effect of Leading-Edge Flap Deflection Angle on the 60-Degree Cropped Delta Wing Static Longitudinal Stability Characteristics.

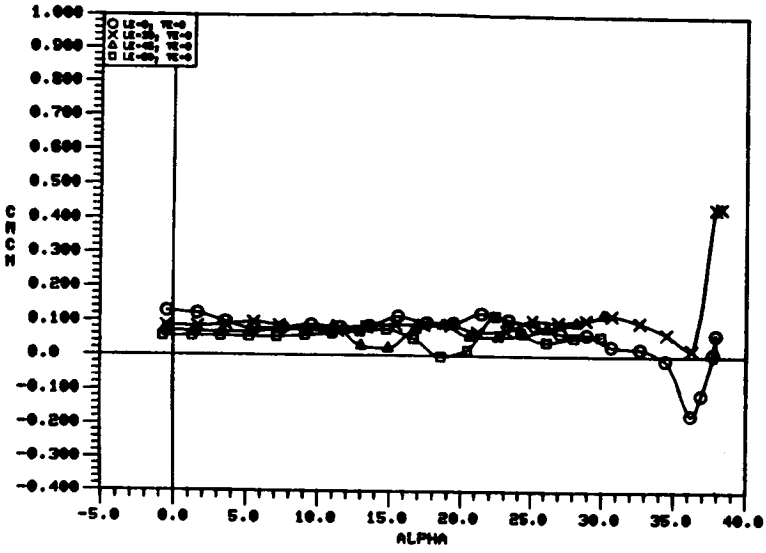

a) $C_{m_{C_N}}$ vs. α

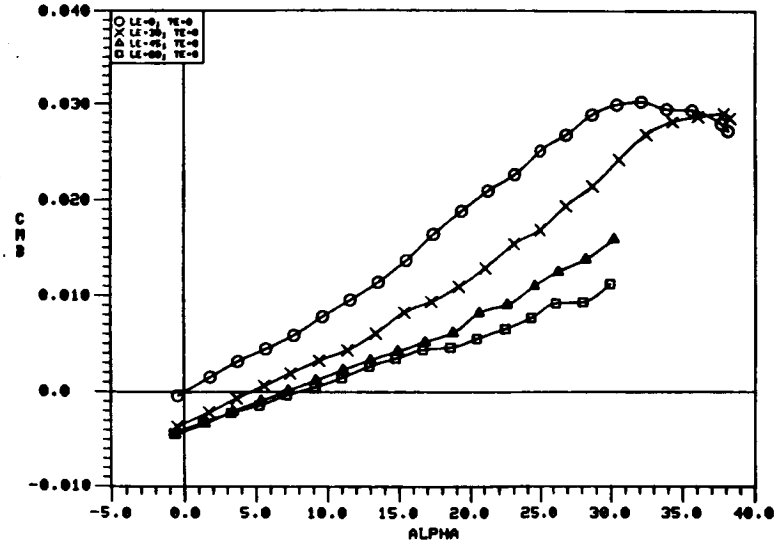

b) C_{m_β} vs. α

O	LE = 0, TE = 0
X	LE = 30, TE = 0
△	LE = 45, TE = 0
□	LE = 60, TE = 0

Figure 180. Effect of Leading-Edge Flap Deflection Angle on the 65-Degree Cropped Delta Wing Static Longitudinal Stability Characteristics.

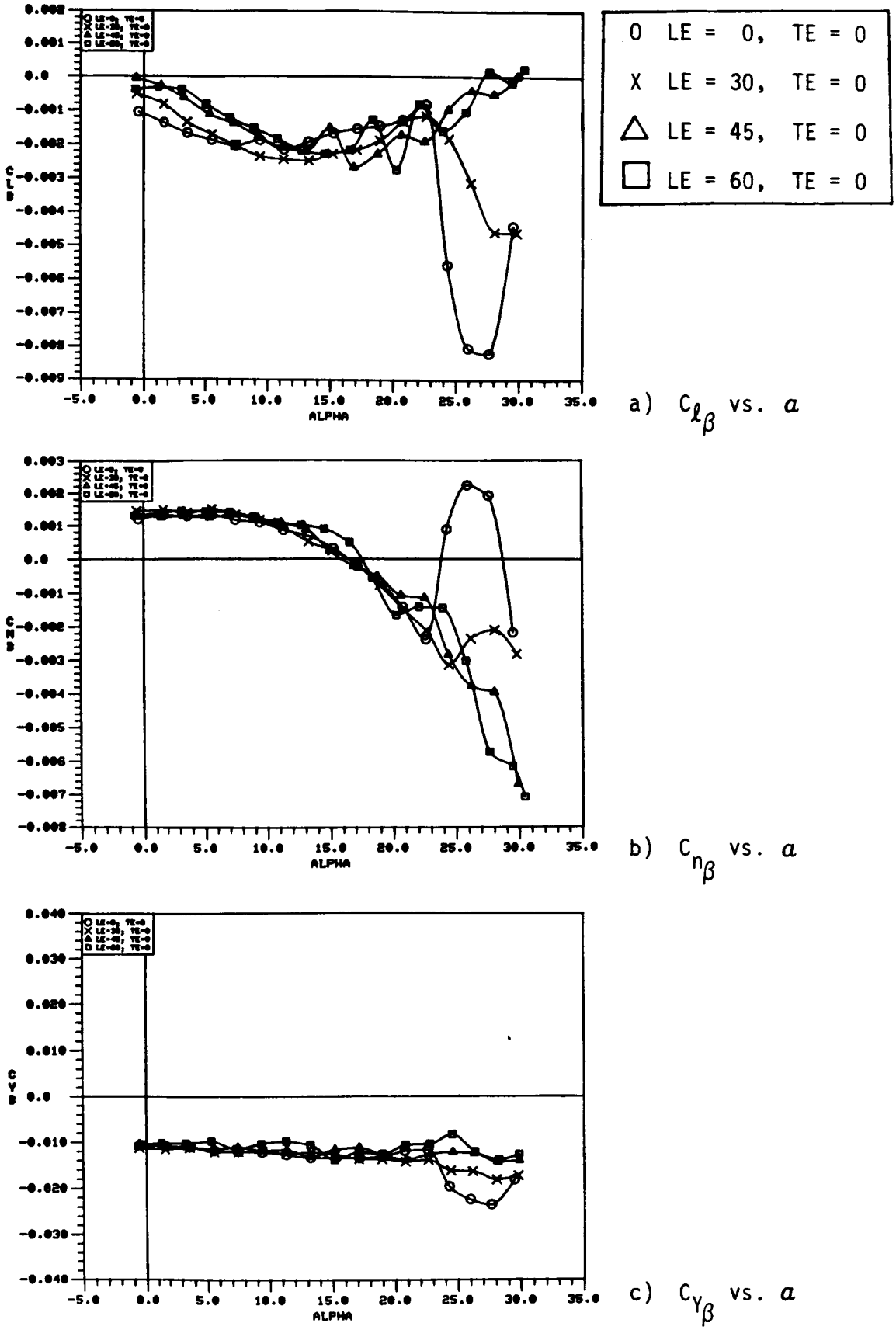

Figure 181. Effect of Leading-Edge Flap Deflection Angle on the 50-Degree Cropped Delta Wing Static Lateral-Directional Stability Characteristics.

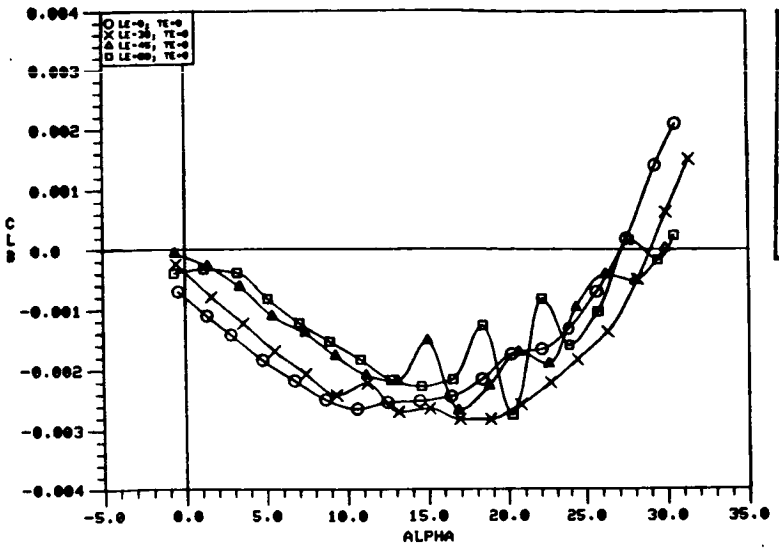

O	LE = 0,	TE = 0
X	LE = 30,	TE = 0
△	LE = 45,	TE = 0
□	LE = 60,	TE = 0

a) C_{ℓ_β} vs. α

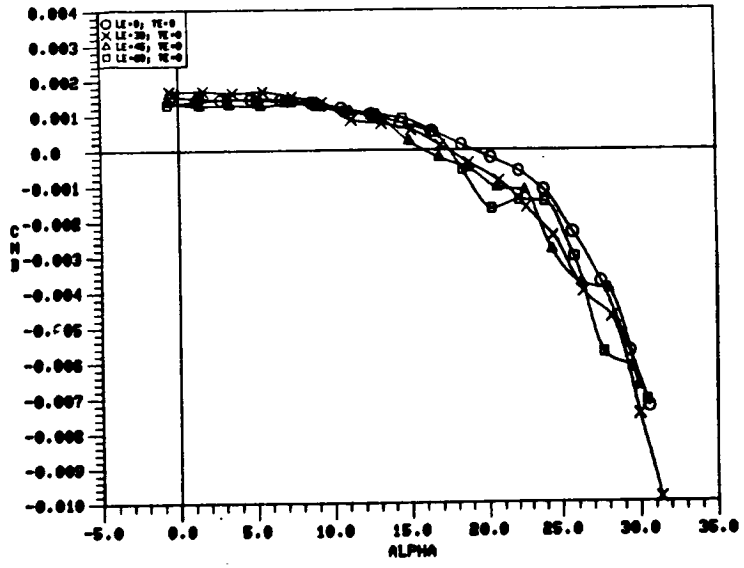

b) C_{n_β} vs. α

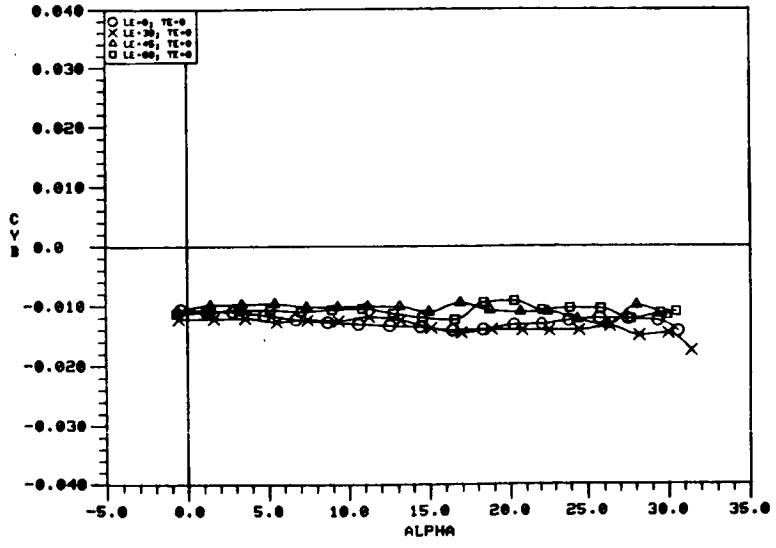

c) C_{Y_β} vs. α

Figure 182. Effect of Leading-Edge Flap Deflection Angle on the 60-Degree Cropped Delta Wing Static Lateral-Directional Stability Characteristics.

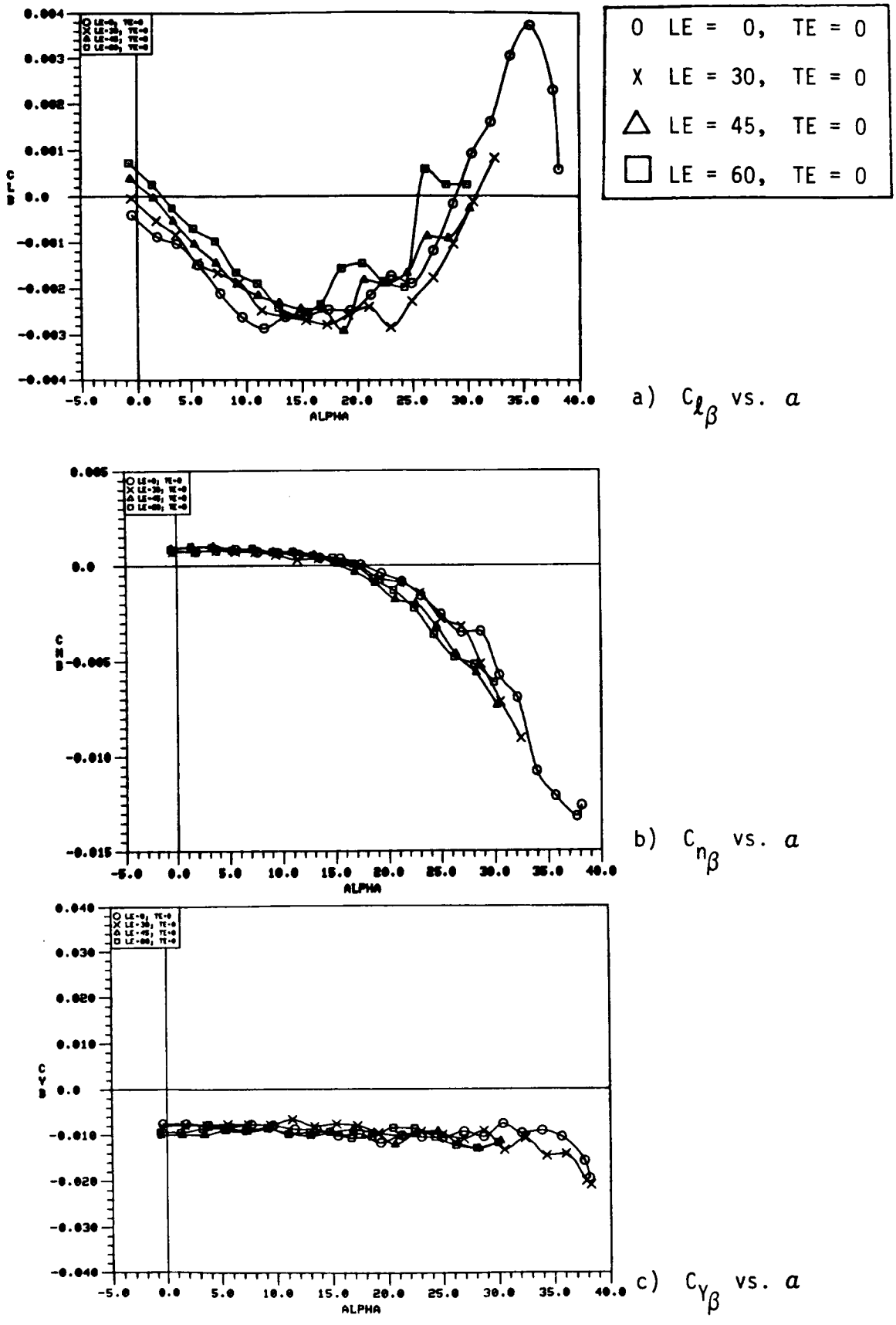

Figure 183. Effect of Leading-Edge Flap Deflection Angle on the 65-Degree Cropped Delta Wing Static Lateral-Directional Stability Characteristics.

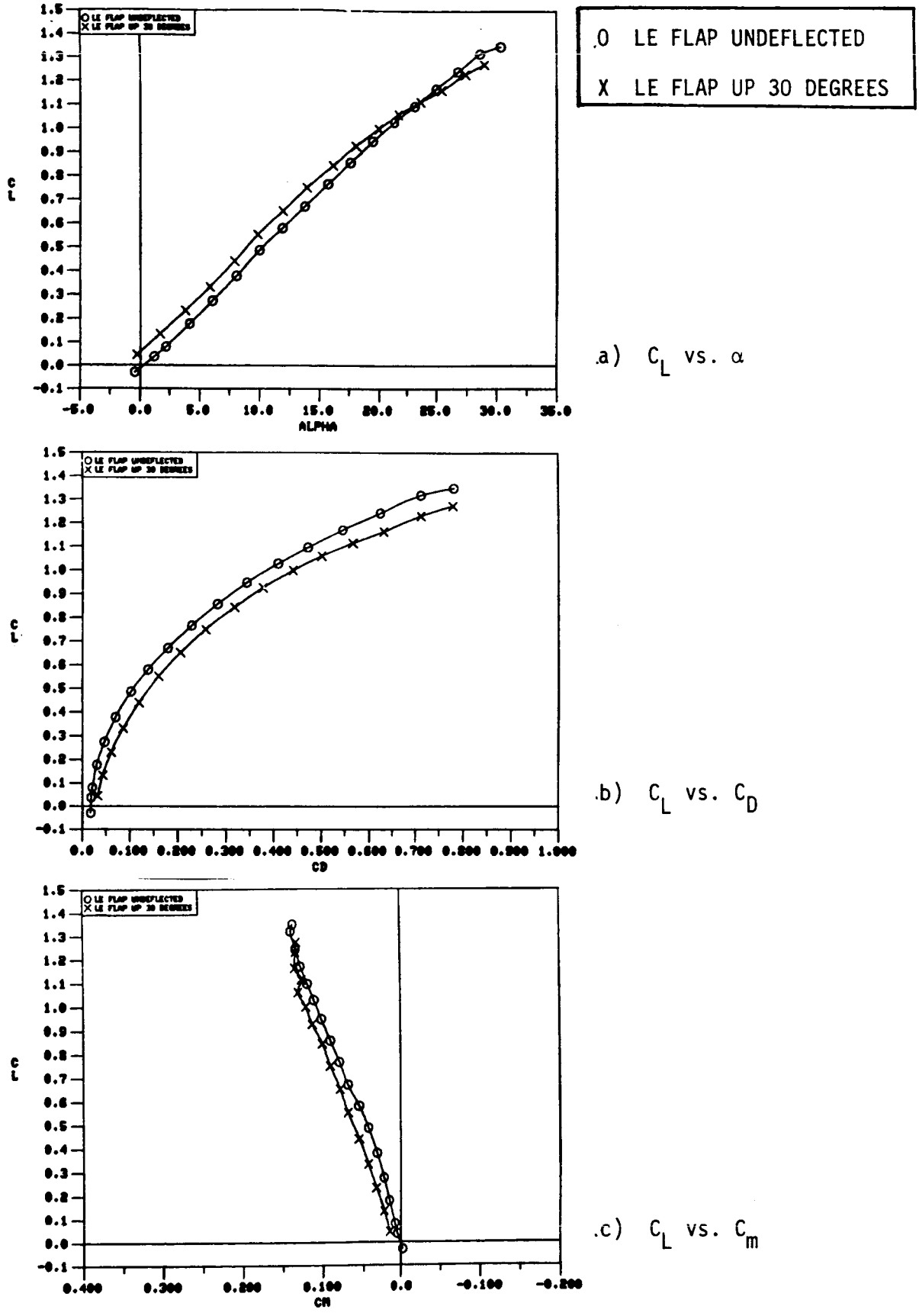

Figure 184. Effect of Inverted Leading-Edge Flap Deflection on the 60-Degree Cropped Delta Wing Static Longitudinal Aerodynamic Characteristics.

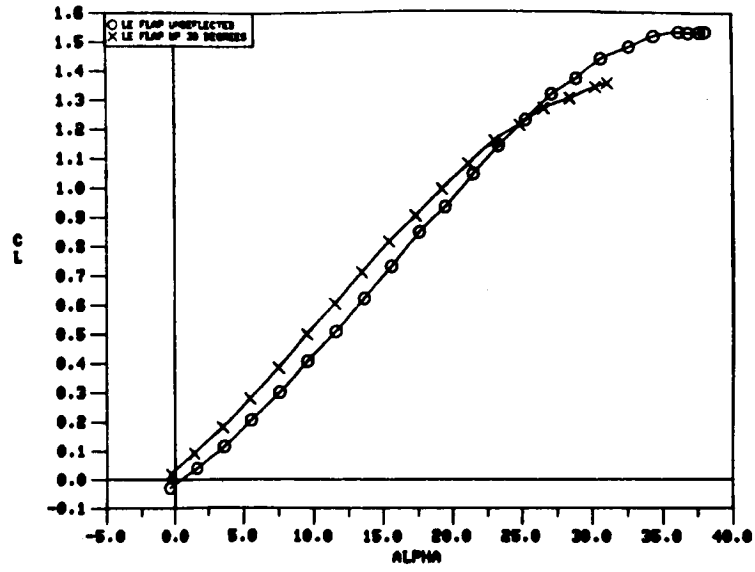

.a) C_L vs. α

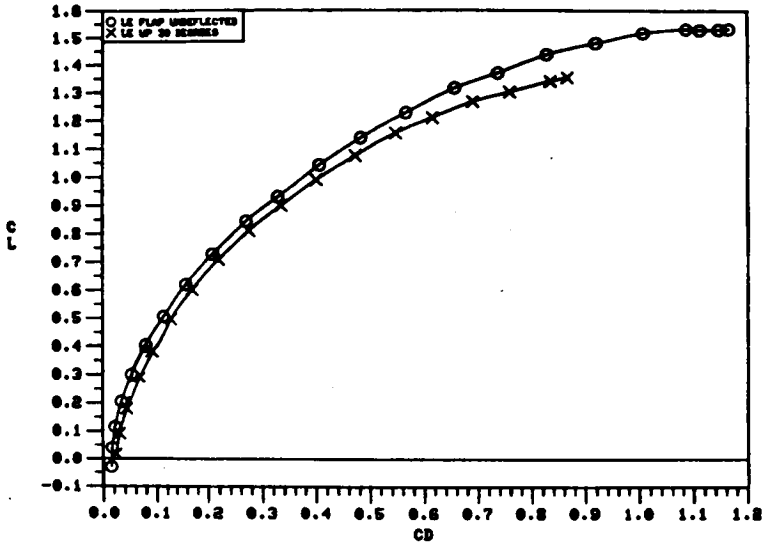

.b) C_L vs. C_D

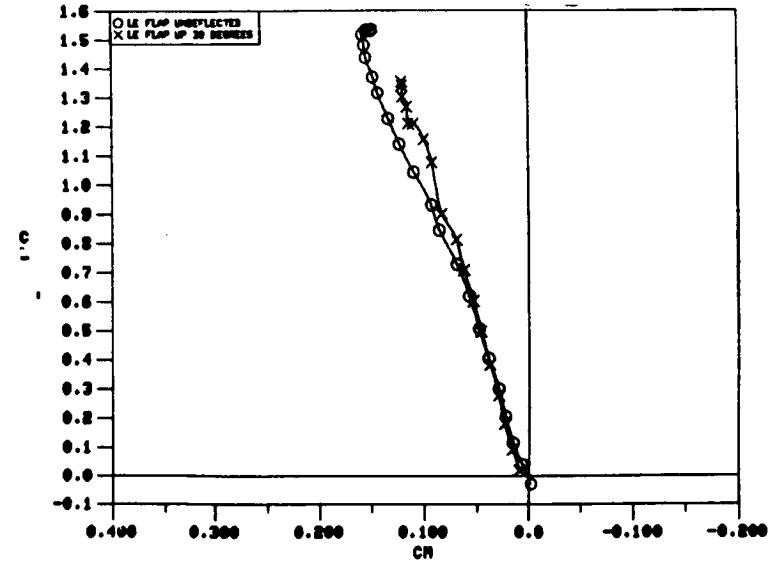

.c) C_L vs. C_m

Figure 185. Effect of Inverted Leading-Edge Flap Deflection on the 65-Degree Cropped Delta Wing Static Longitudinal Aerodynamic Characteristics.

O LE FLAP UNDEFLECTED

X LE FLAP UP 30 DEGREES

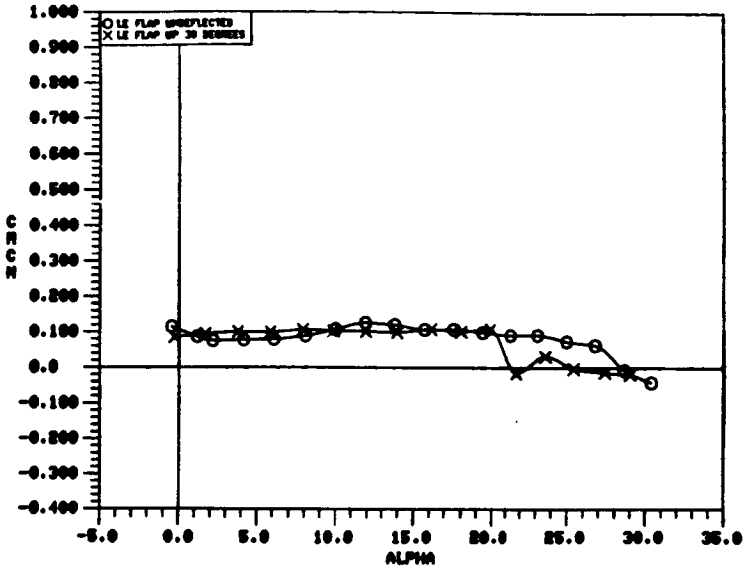

a) $C_{m_{C_N}}$ vs. α

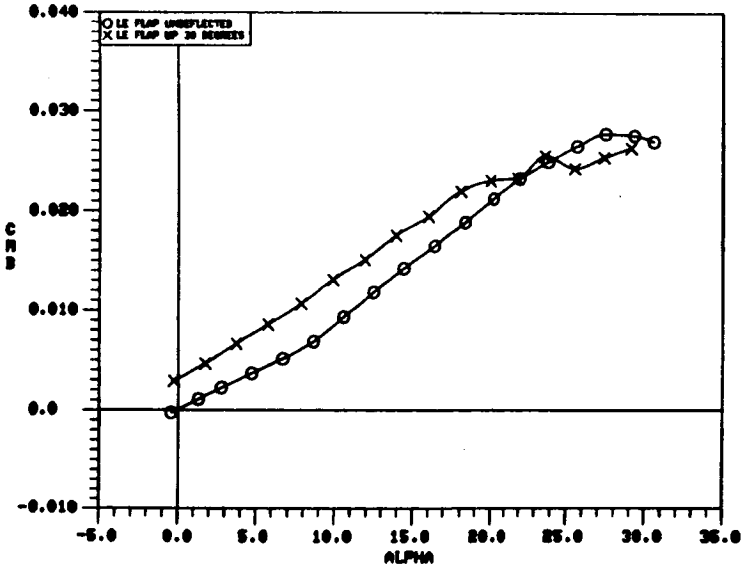

b) C_{m_β} vs. α

Figure 186. Effect of Inverted Leading-Edge Flap Deflection on the 60-Degree Cropped Delta Wing Static Longitudinal Stability Characteristics.

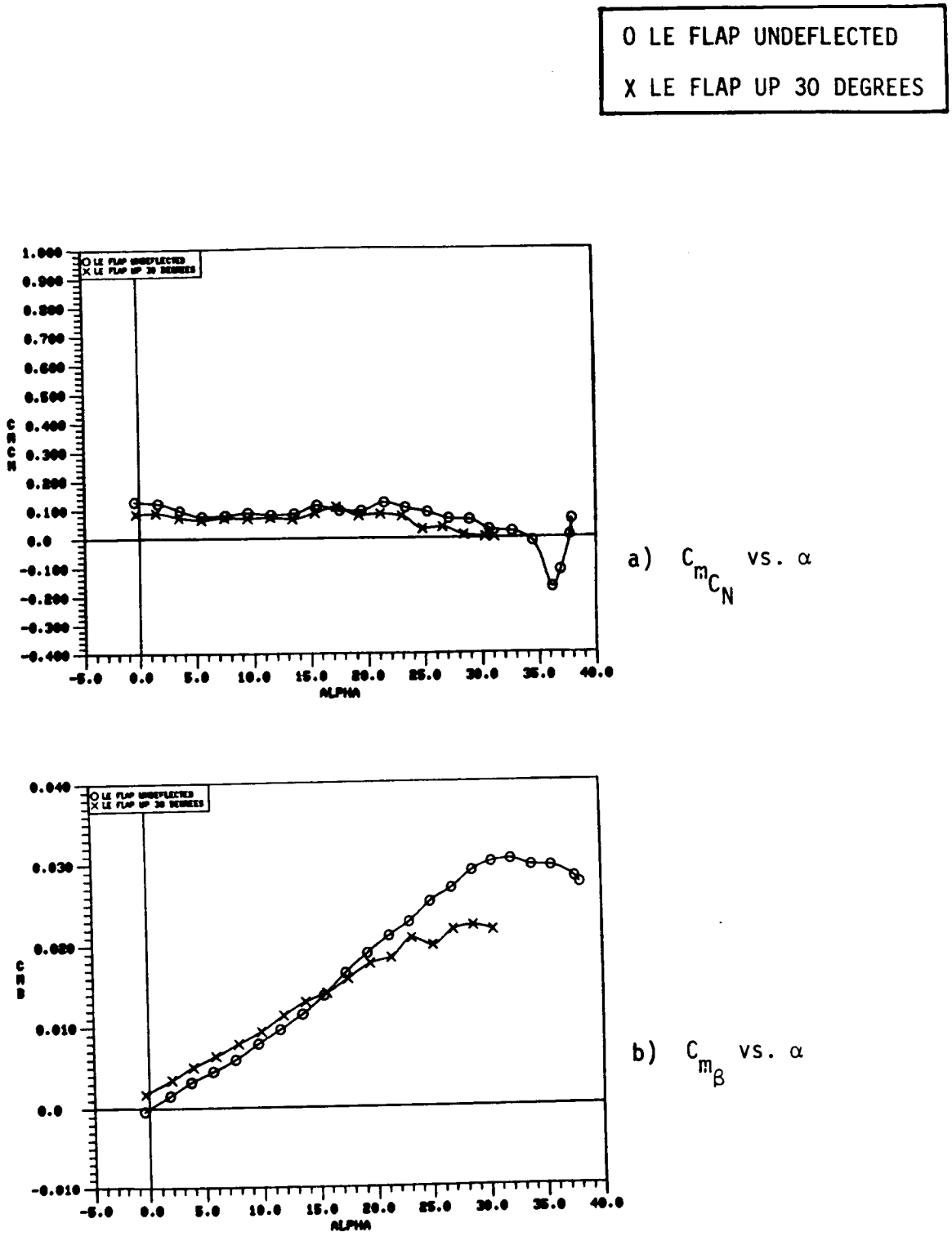

a) $C_{m_{C_N}}$ vs. α

b) C_{m_β} vs. α

Figure 187. Effect of Inverted Leading-Edge Flap Deflection on the 65-Degree Cropped Delta Wing Static Longitudinal Stability Characteristics.

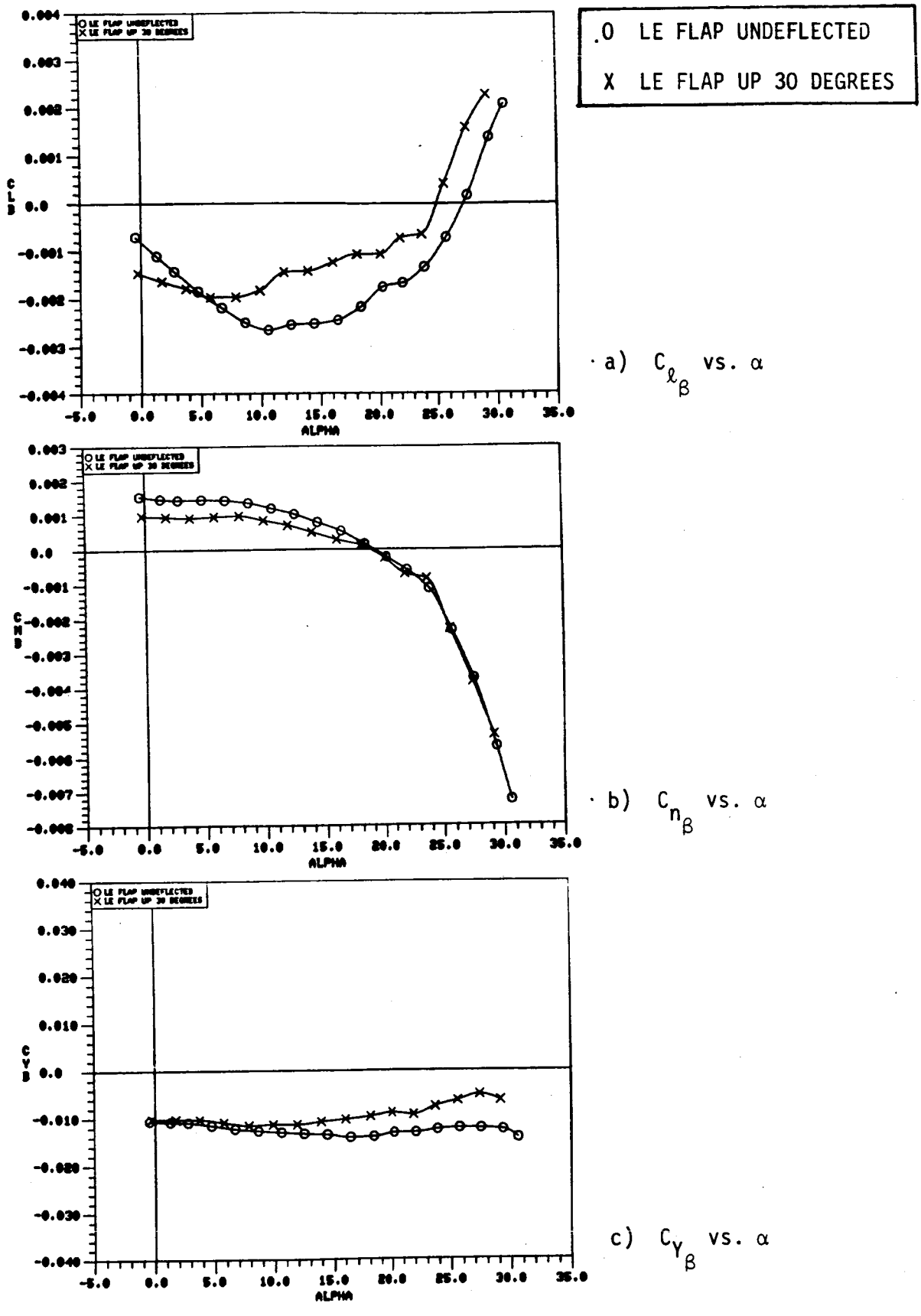

a) C_{ℓ_β} vs. α

b) C_{n_β} vs. α

c) C_{Y_β} vs. α

Figure 188. Effect of Inverted Leading-Edge Flap Deflection on the 60-Degree Cropped Delta Wing Static Lateral-Directional Stability Characteristics.

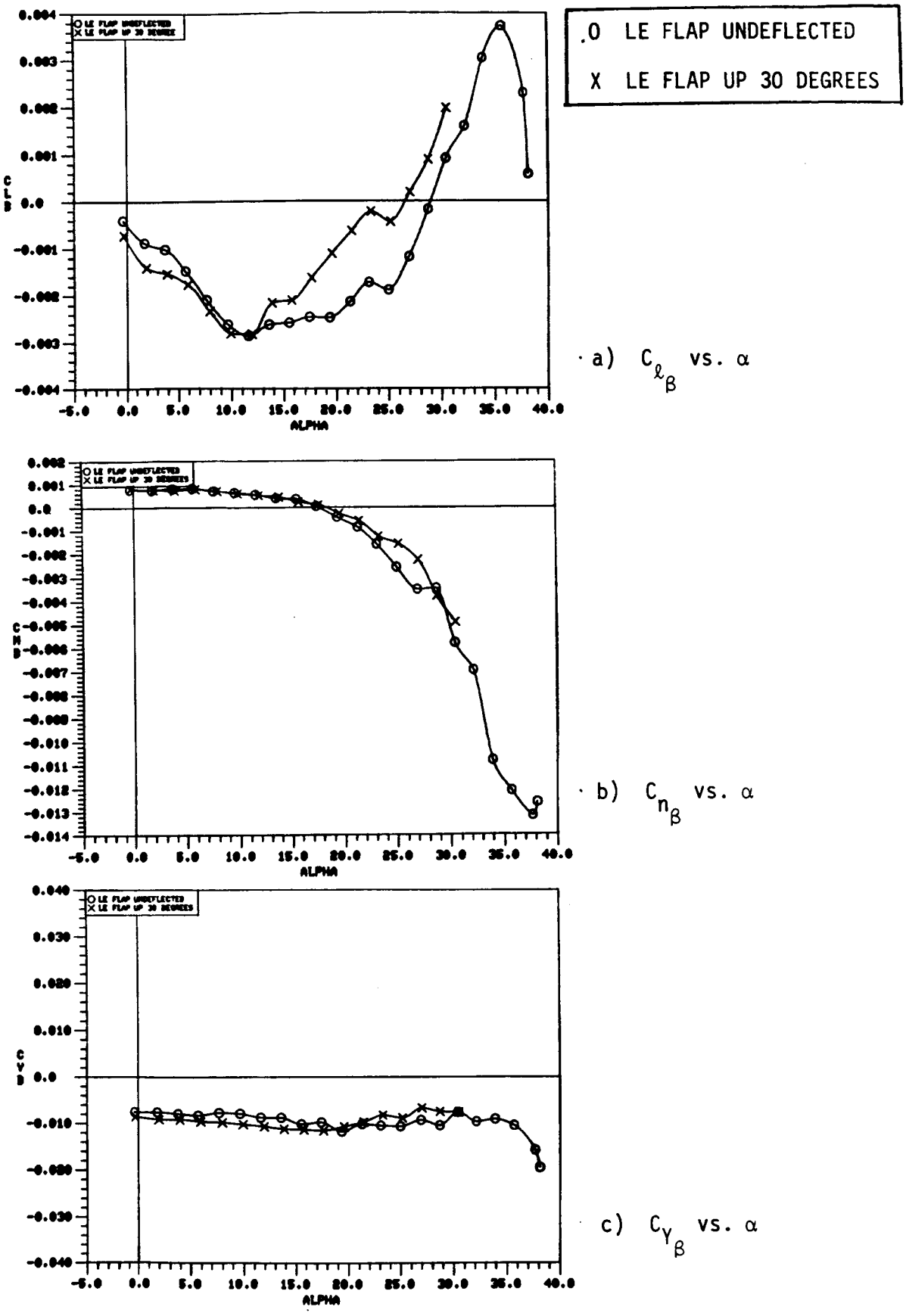

a) C_{ℓ_β} vs. α

b) C_{n_β} vs. α

c) C_{Y_β} vs. α

Figure 189. Effect of Inverted Leading-Edge Flap Deflection on the 65-Degree Cropped Delta Wing Static Lateral-Directional Stability Characteristics.

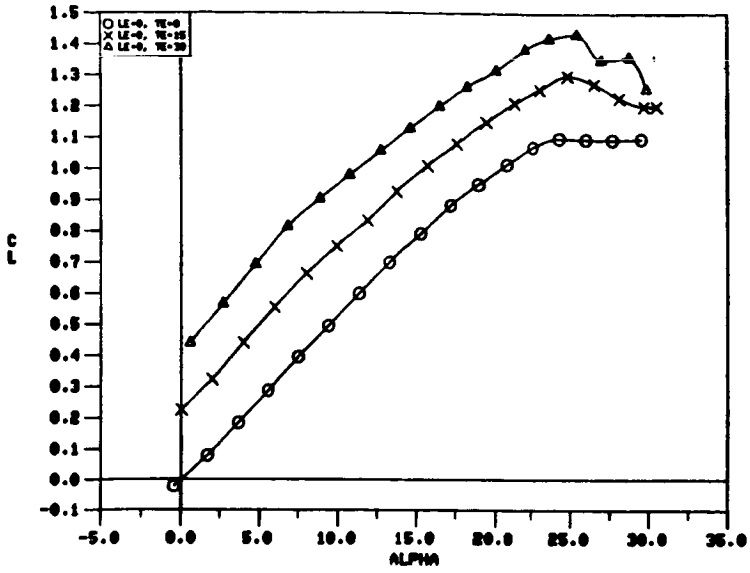

O	LE = 0,	TE =	0
X	LE = 0.	TE =	15
△	LE = 0,	TE =	30

a) C_L vs. α

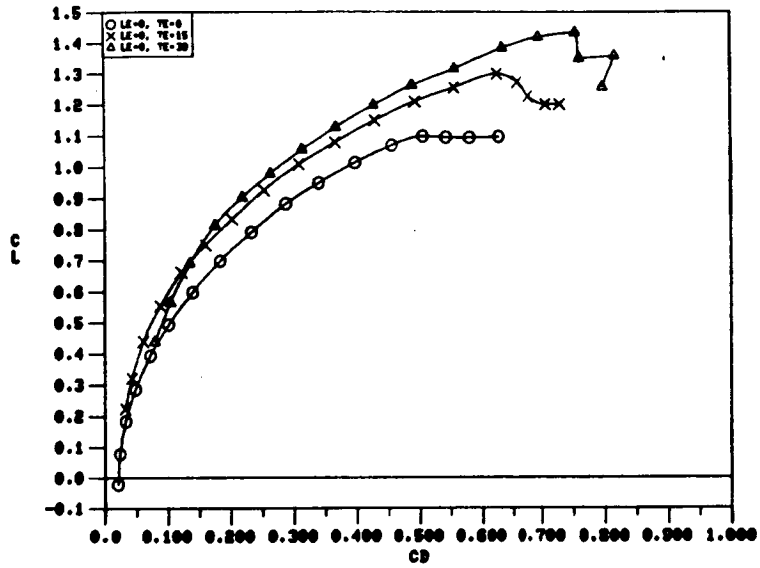

b) C_L vs. C_D

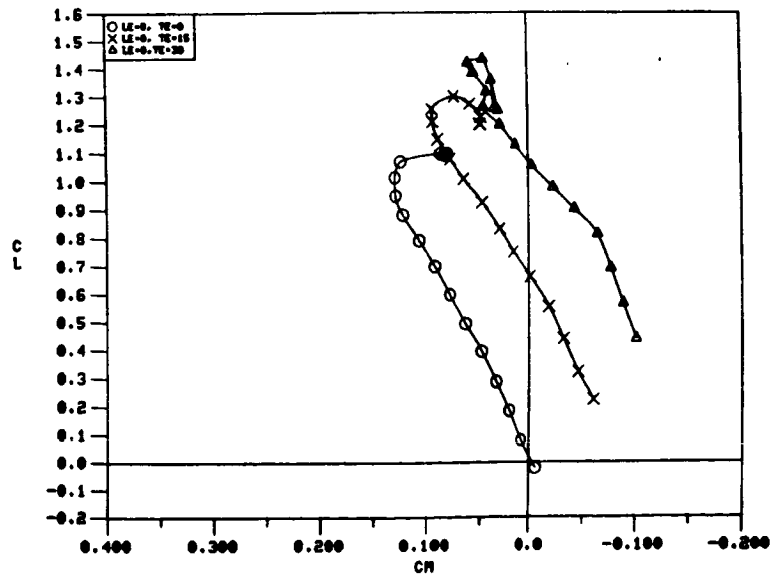

c) C_L vs. C_m

Figure 190. Effect of Trailing-Edge Flap Deflection on the 50-Degree Cropped Delta Wing Static Longitudinal Aerodynamic Characteristics with $\delta_n = 0°$.

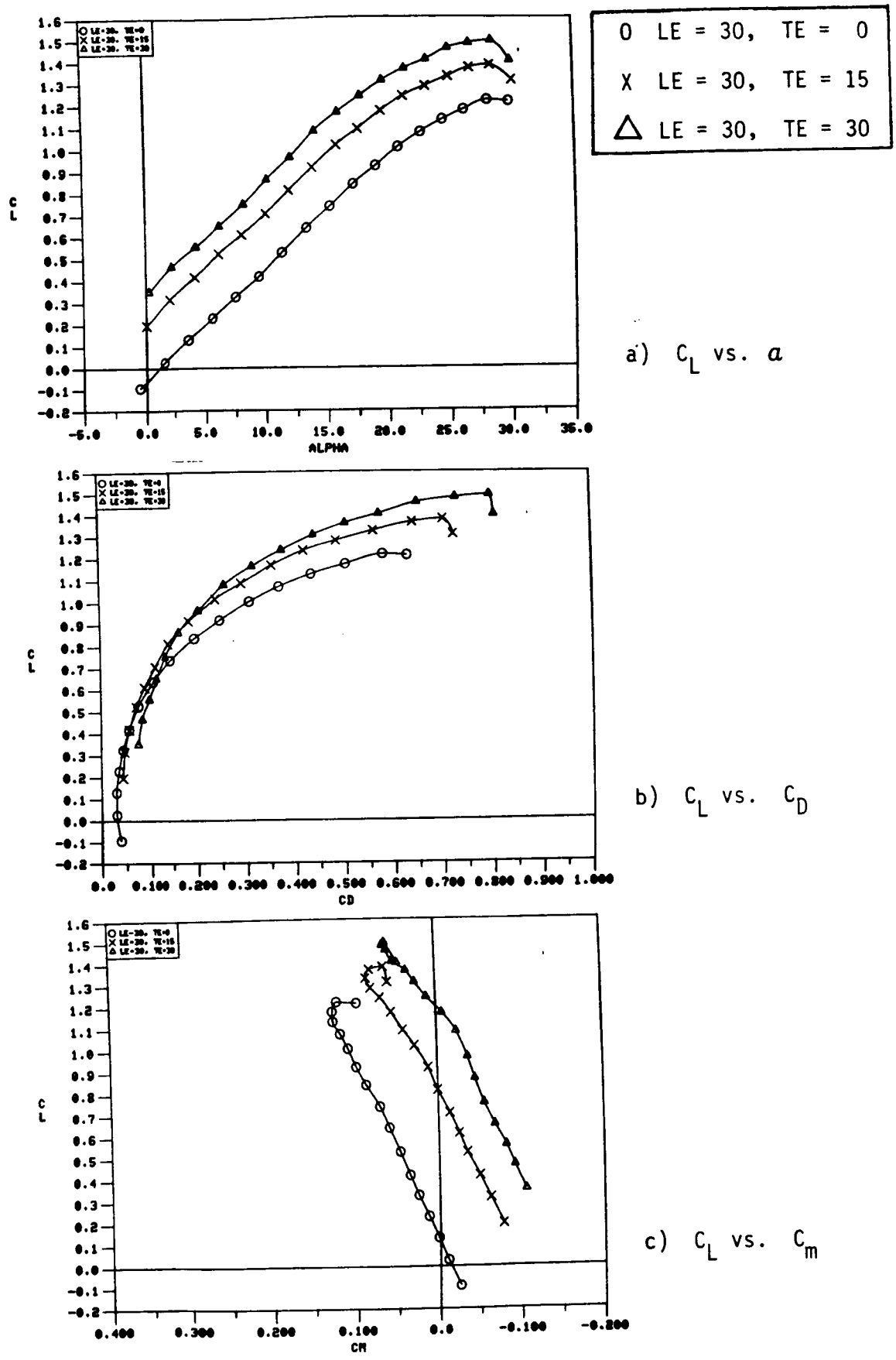

Figure 191. Effect of Trailing-Edge Flap Deflection on the 50-Degree Cropped Delta Wing Static Longitudinal Aerodynamic Characteristics with $\delta_n = 30°$.

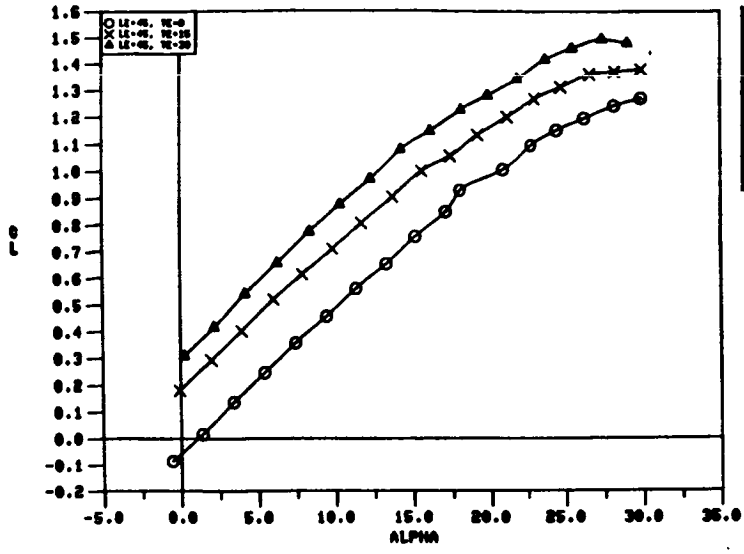

O	LE = 45, TE = 0
X	LE = 45. TE = 15
△	LE = 45, TE = 30

a) C_L vs. α

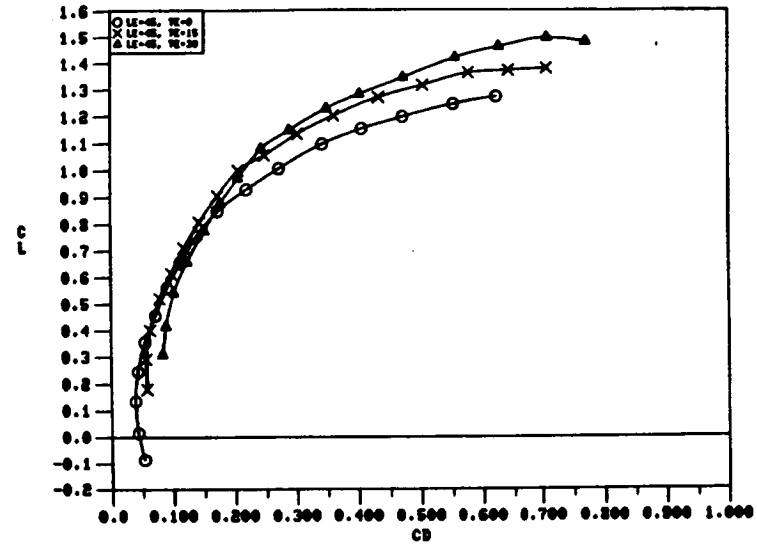

b) C_L vs. C_D

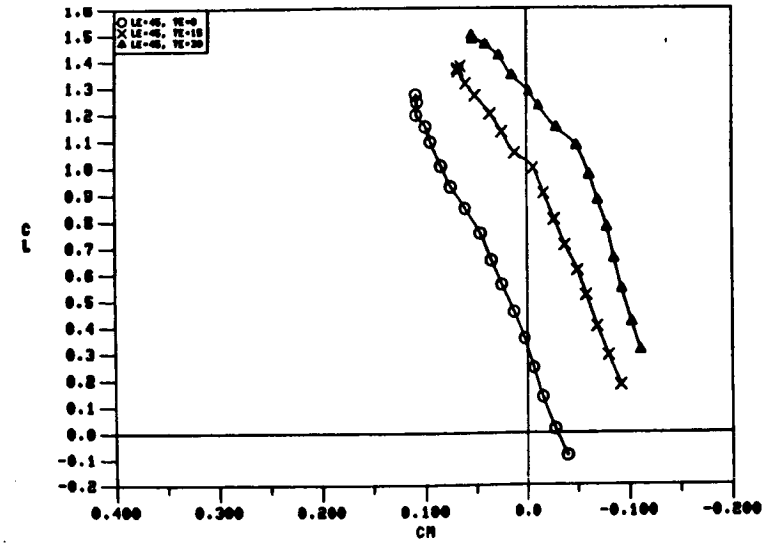

c) C_L vs. C_m

Figure 192. Effect of Trailing-Edge Flap Deflection on the 50-Degree Cropped Delta Wing Static Longitudinal Aerodynamic Characteristics with $\delta_n = 45°$.

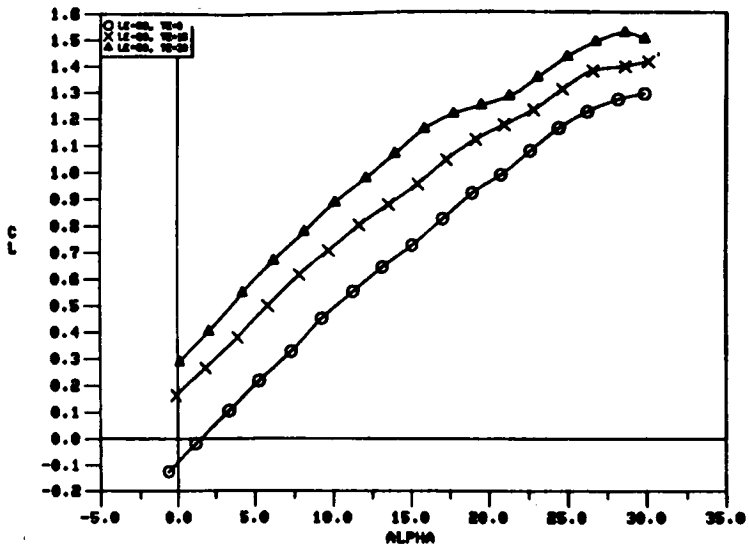

O	LE = 60,	TE =	0
X	LE = 60,	TE =	15
△	LE = 60,	TE =	30

a) C_L vs. α

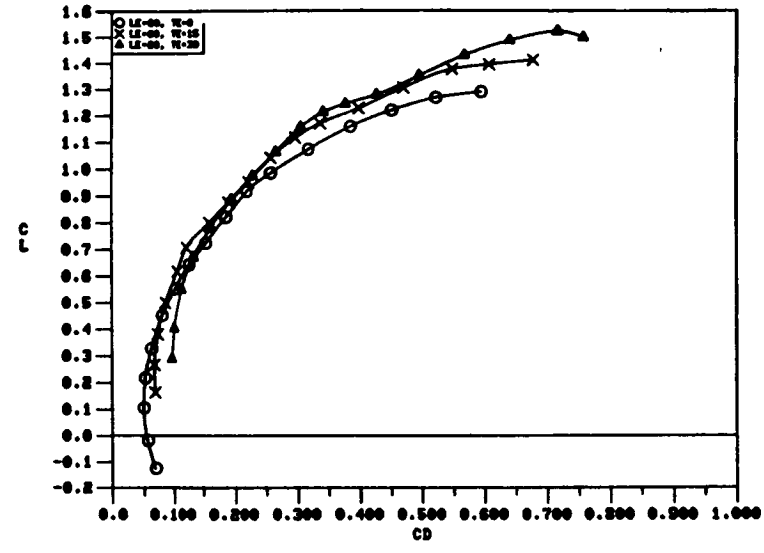

b) C_L vs. C_D

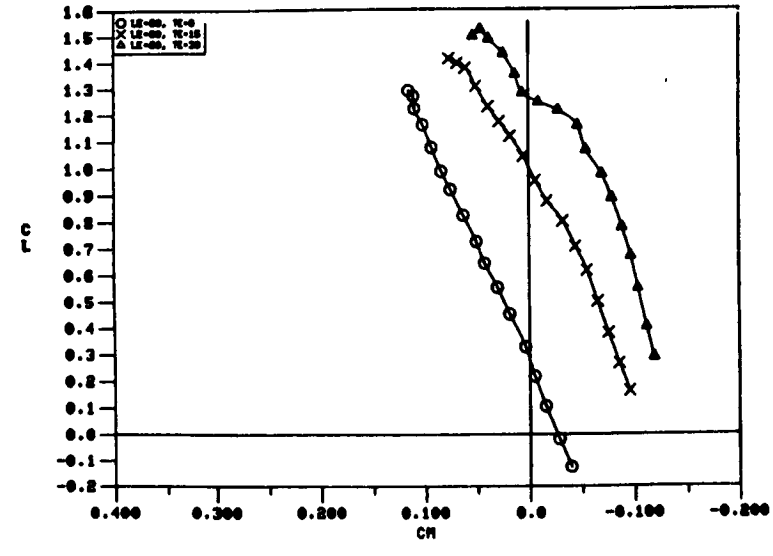

c) C_L vs. C_m

Figure 193. Effect of Trailing-Edge Flap Deflection on the 50-Degree Cropped Delta Wing Static Longitudinal Aerodynamic Characteristics with $\delta_n = 60°$.

O	LE = 0, TE = 0
X	LE = 0, TE = 15
△	LE = 0, TE = 30

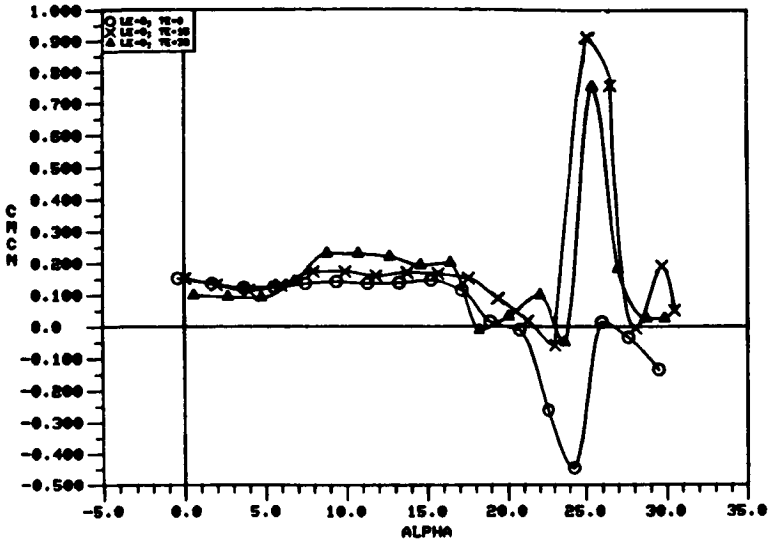

a) $C_{m_{C_n}}$ vs. α

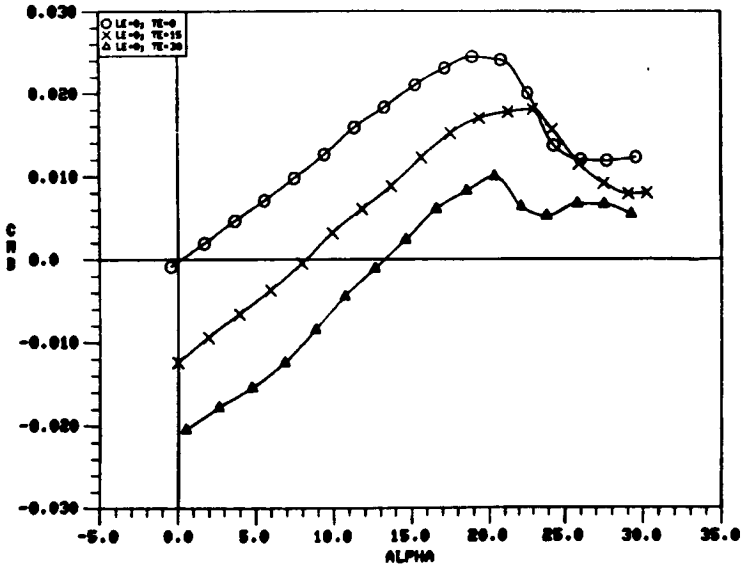

b) C_{m_β} vs. α

Figure 194. Effect of Trailing-Edge Flap Deflection on the 50-Degree Cropped Delta Wing Static Longitudinal Stability Characteristics with $\delta_n = 0°$.

O	LE = 30, TE = 0
X	LE = 30, TE = 15
△	LE = 30, TE = 30

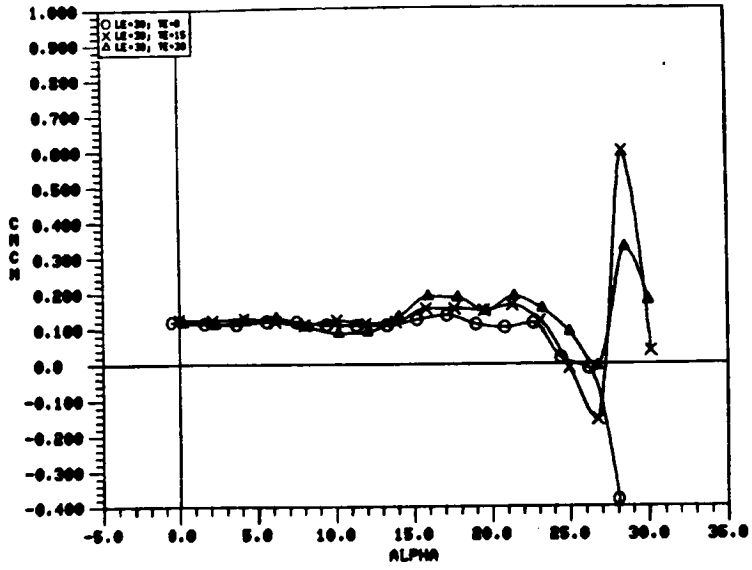

a) $C_{m_{C_n}}$ vs. α

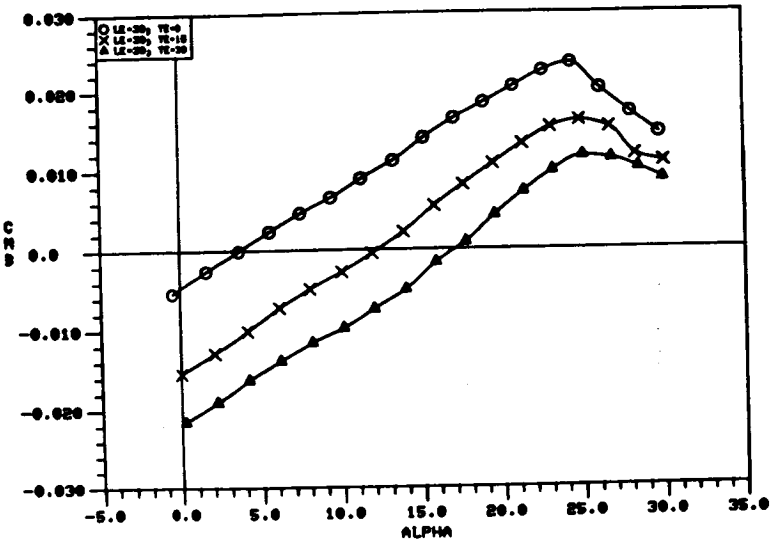

b) C_{m_β} vs. α

Figure 195. Effect of Trailing-Edge Flap Deflection on the 50-Degree Cropped Delta Wing Static Longitudinal Stability Characteristics with $\delta_n = 30°$.

O	LE = 45, TE = 0
X	LE = 45, TE = 15
△	LE = 45, TE = 30

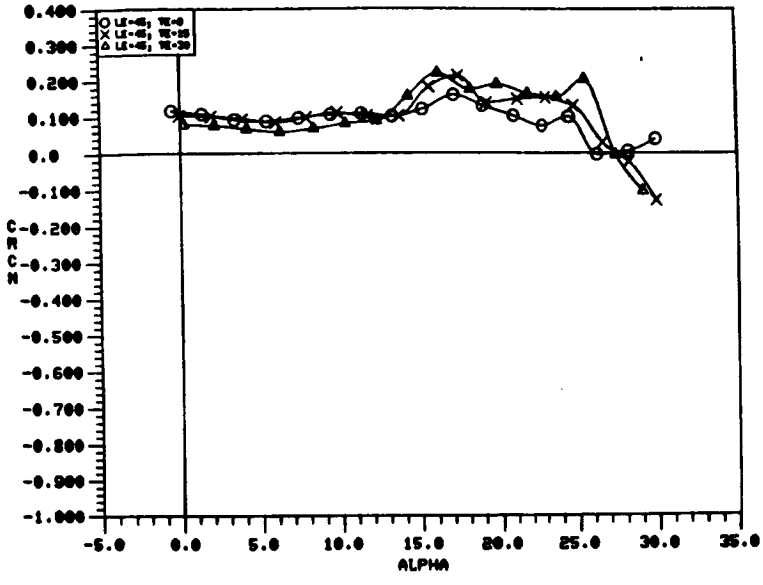

a) $C_{m_{C_n}}$ vs. α

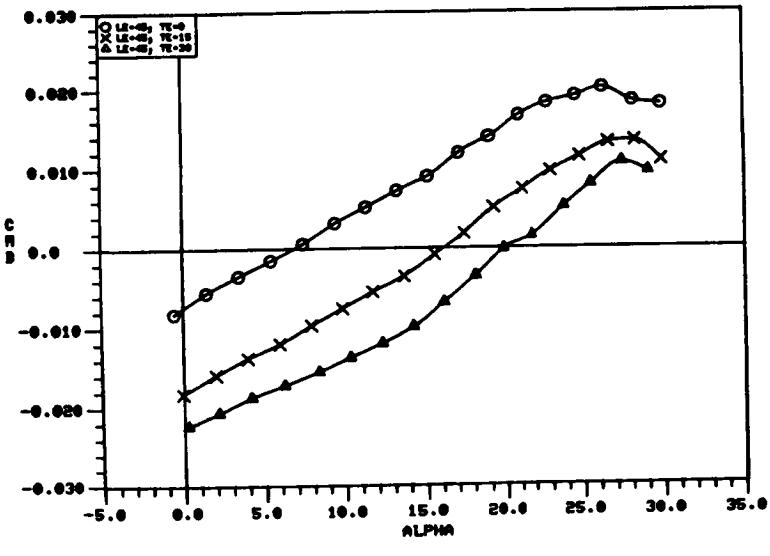

b) C_{m_β} vs. α

Figure 196. Effect of Trailing-Edge Flap Deflection on the 50-Degree Cropped Delta Wing Static Longitudinal Stability Characteristics with $\delta_n = 45°$.

O	LE = 60, TE = 0
X	LE = 60, TE = 15
△	LE = 60, TE = 30

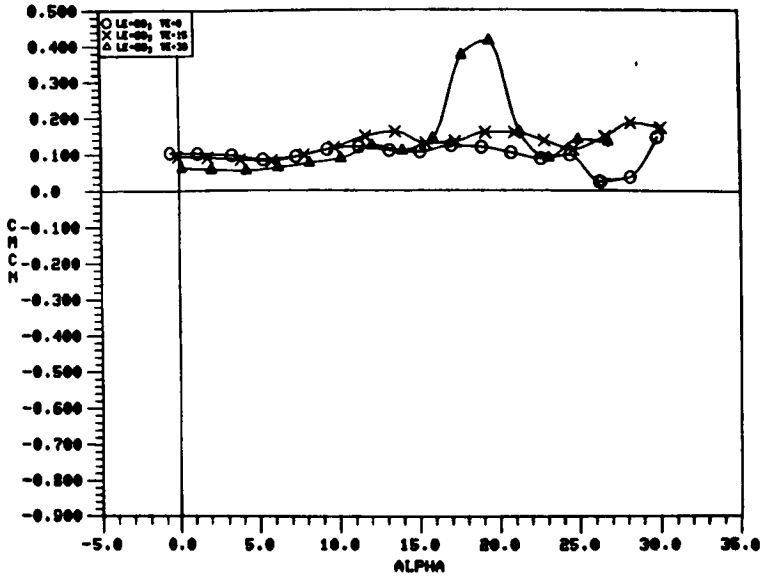

a) $C_{m_{C_n}}$ vs. α

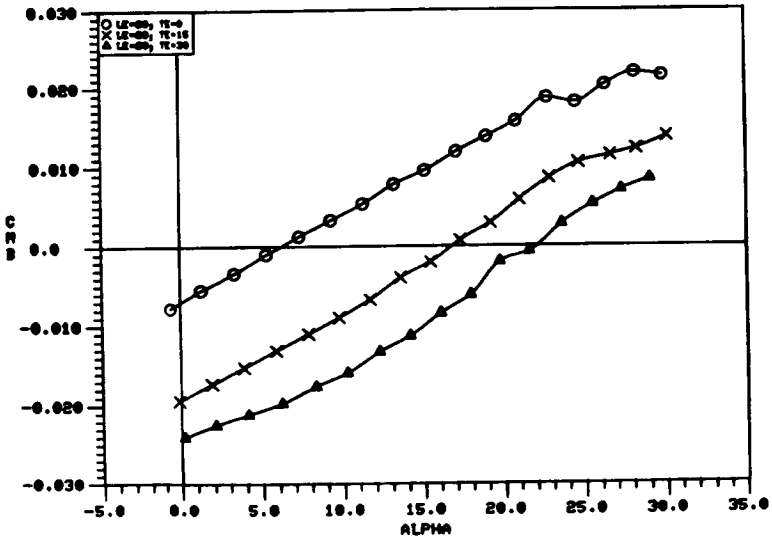

b) C_{m_β} vs. α

Figure 197. Effect of Trailing-Edge Flap Deflection on the 50-Degree Cropped Delta Wing Static Longitudinal Stability Characteristics with $\delta_n = 60°$.

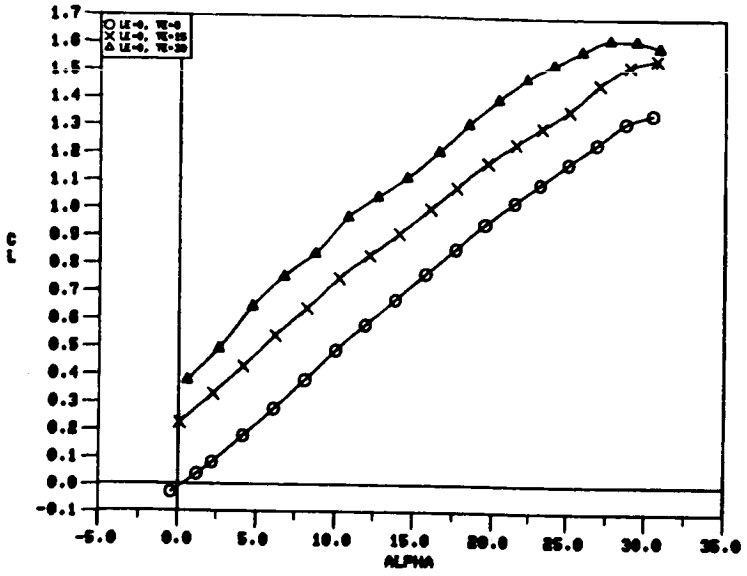

O	LE = 0,	TE =	0
X	LE = 0.	TE =	15
△	LE = 0,	TE =	30

a) C_L vs. α

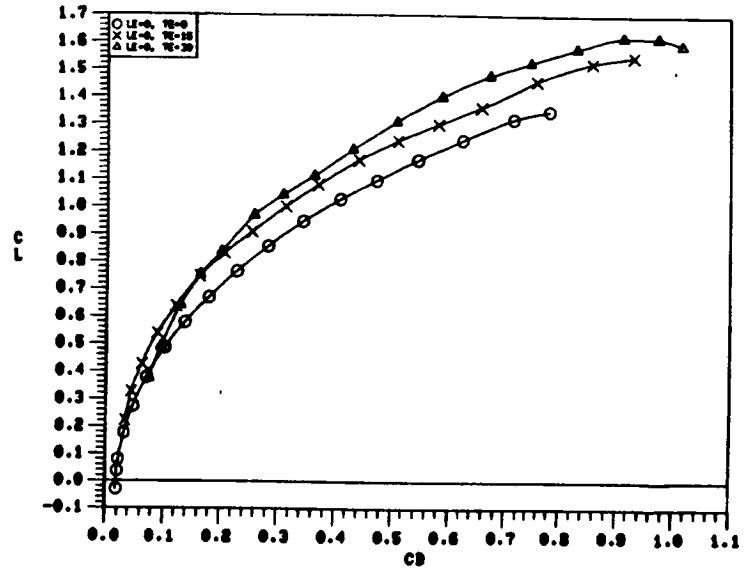

b) C_L vs. C_D

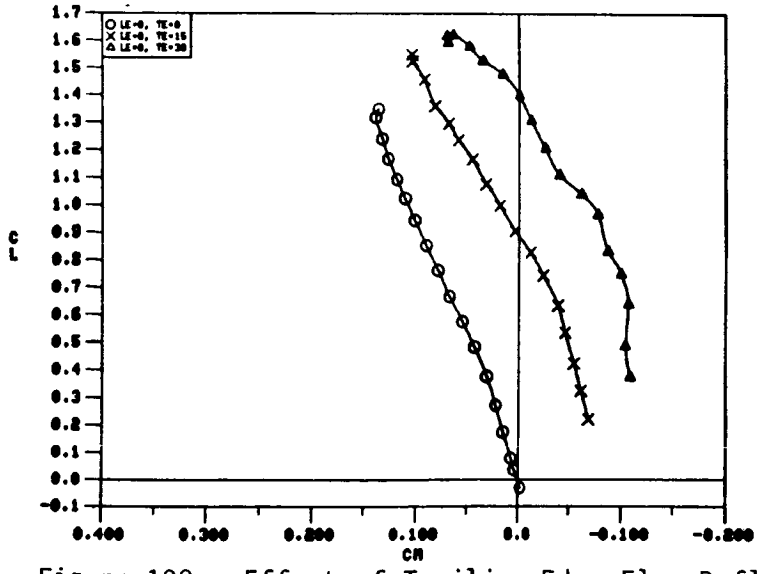

c) C_L vs. C_m

Figure 198. Effect of Trailing-Edge Flap Deflection on the 60-Degree Cropped Delta Wing Static Longitudinal Aerodynamic Characteristics with $\delta_n = 0°$.

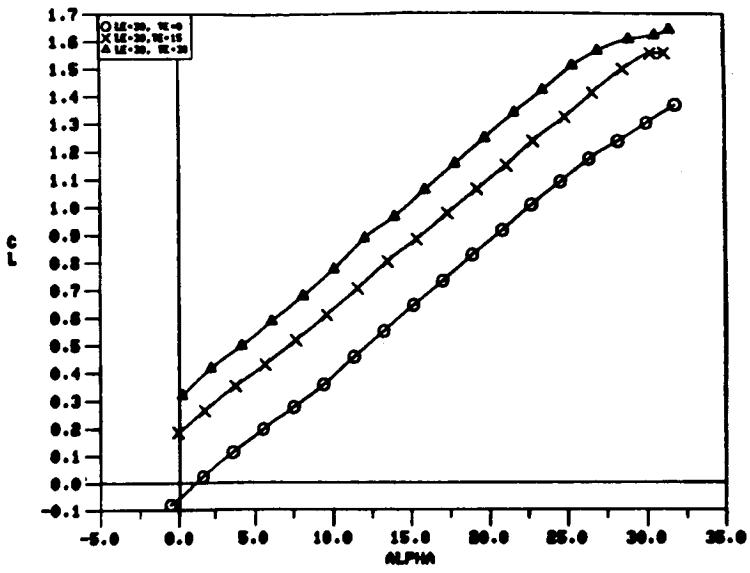

O	LE = 30,	TE =	0
X	LE = 30,	TE =	15
△	LE = 30,	TE =	30

a) C_L vs. α

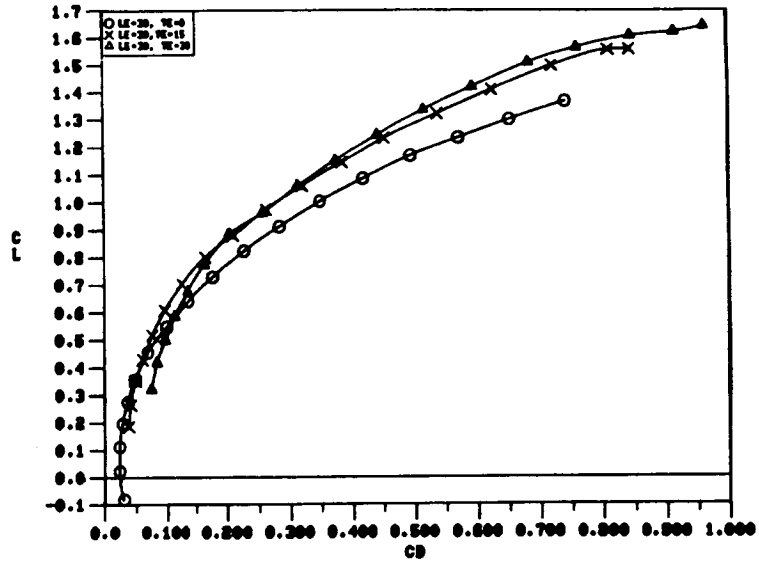

b) C_L vs. C_D

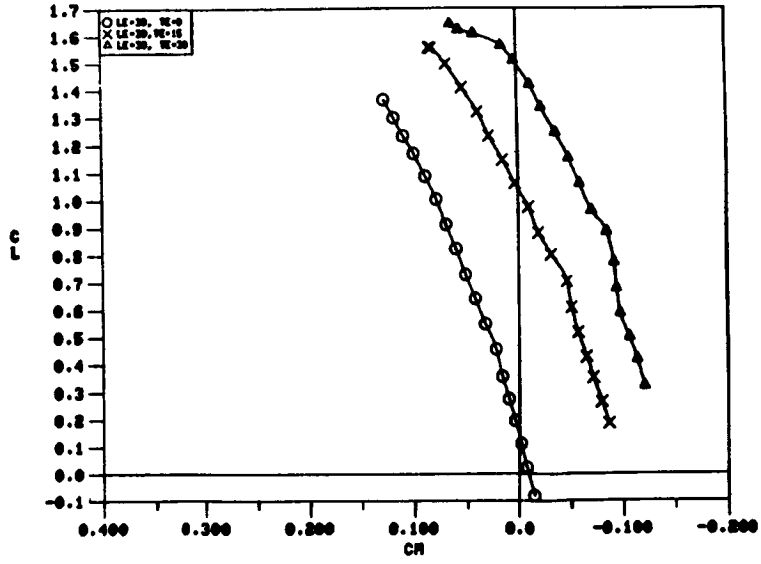

c) C_L vs. C_m

Figure 199. Effect of Trailing-Edge Flap Deflection on the 60-Degree Cropped Delta Wing Static Longitudinal Aerodynamic Characteristics with $\delta_n = 30°$.

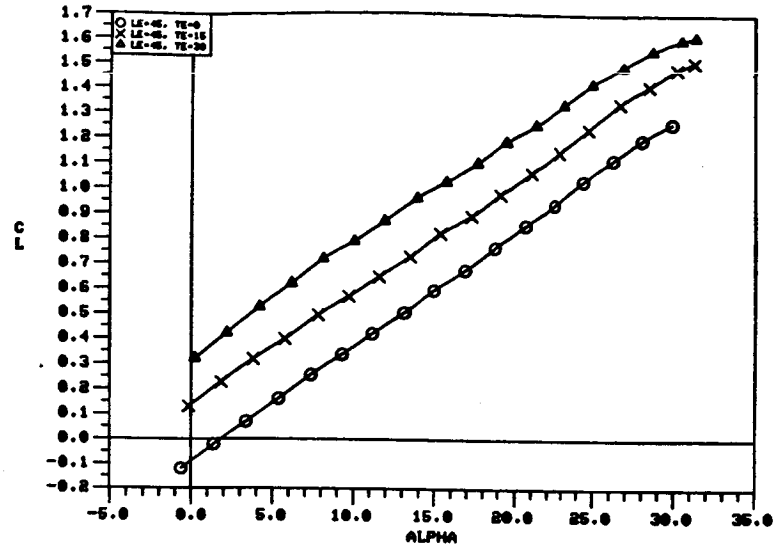

O	LE = 45,	TE =	0
X	LE = 45.	TE =	15
△	LE = 45,	TE =	30

a) C_L vs. α

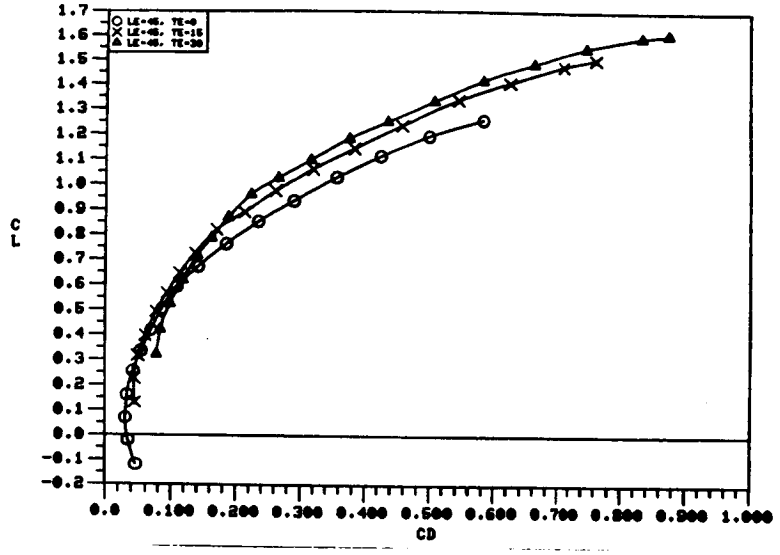

b) C_L vs. C_D

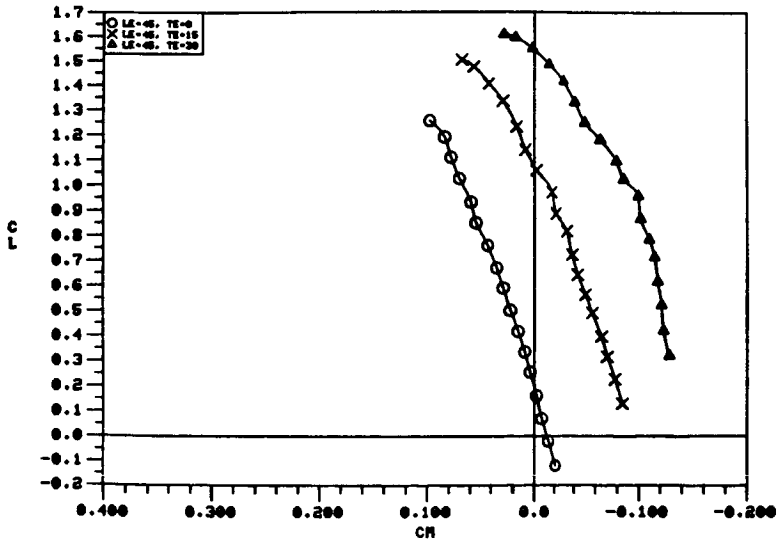

c) C_L vs. C_m

Figure 200. Effect of Trailing-Edge Flap Deflection on the 60-Degree Cropped Delta Wing Static Longitudinal Aerodynamic Characteristics with $\delta_n = 45°$.

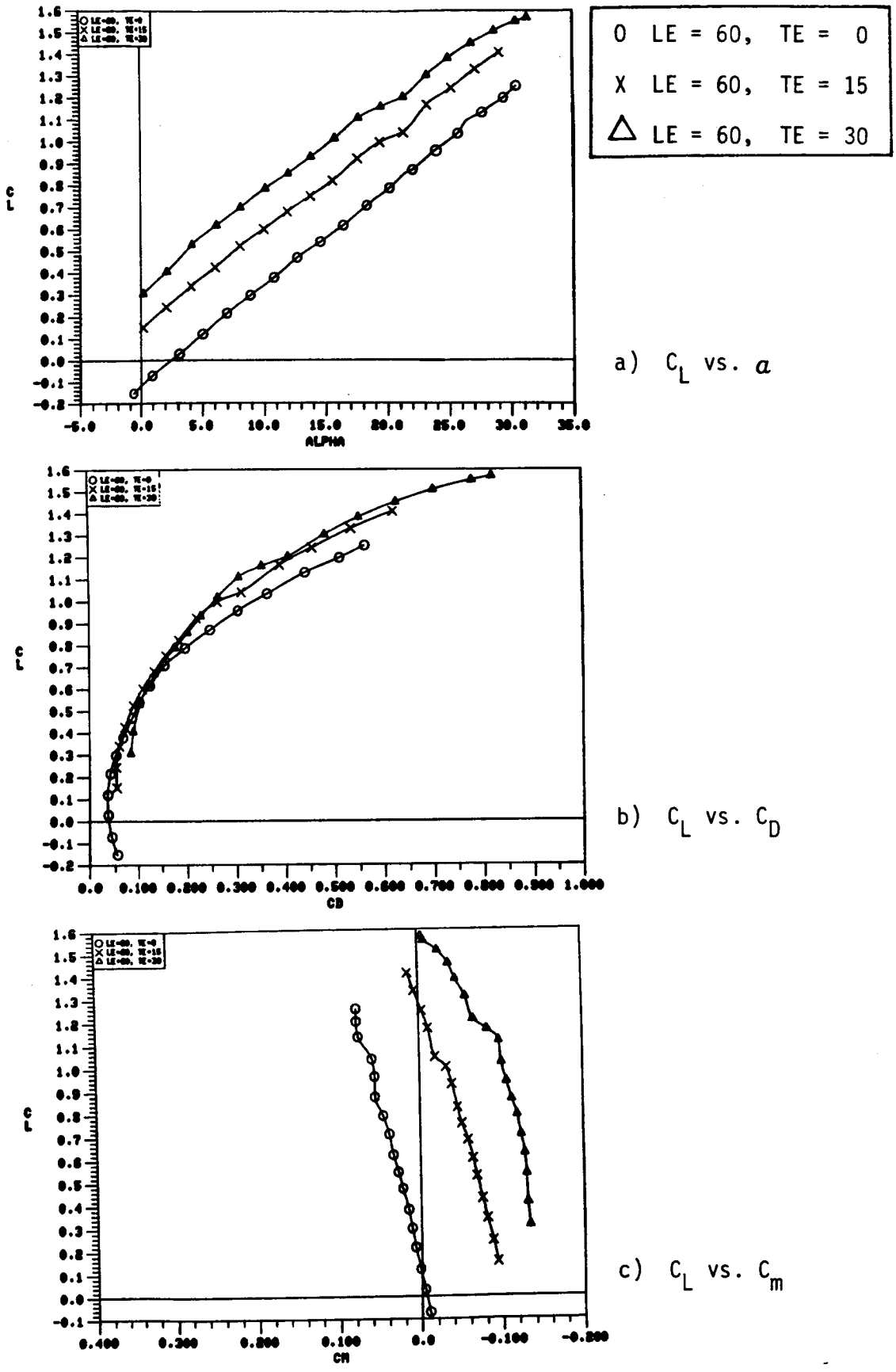

Figure 201. Effect of Trailing-Edge Flap Deflection on the 60-Degree Cropped Delta Wing Static Longitudinal Aerodynamic Characteristics with $\delta_n = 60°$.

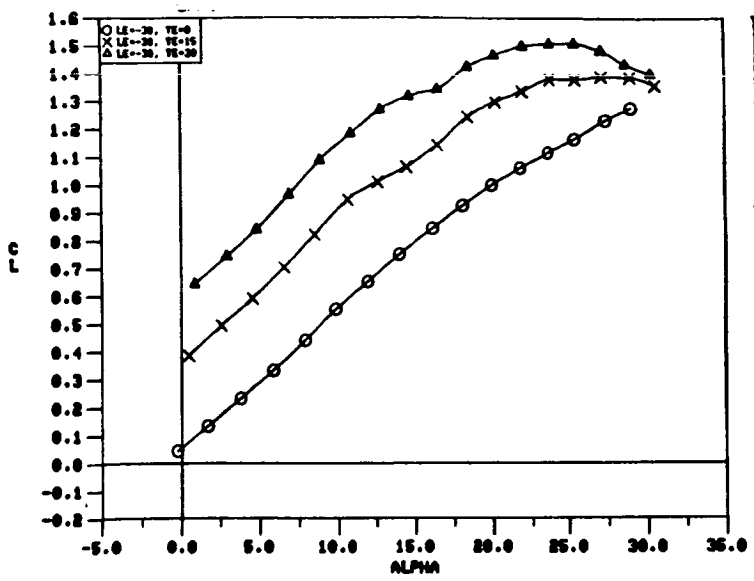

O	LE = -30,	TE =	0
X	LE = -30,	TE =	15
△	LE = -30,	TE =	30

a) C_L vs. α

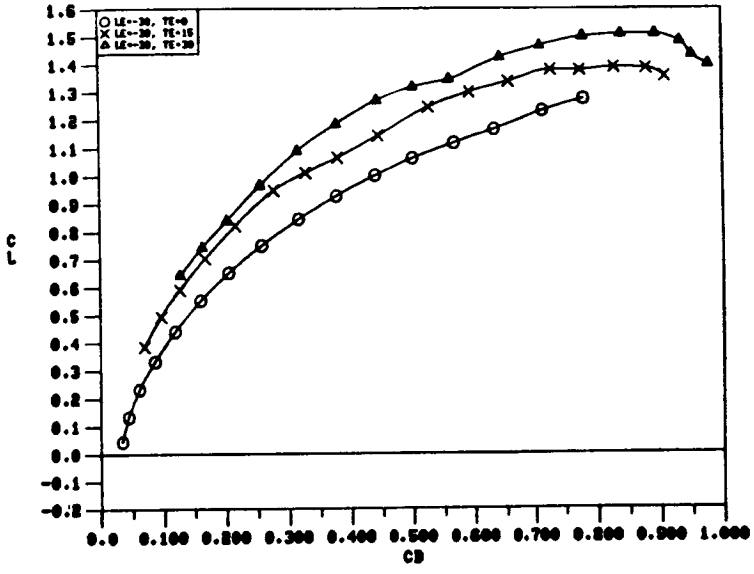

b) C_L vs. C_D

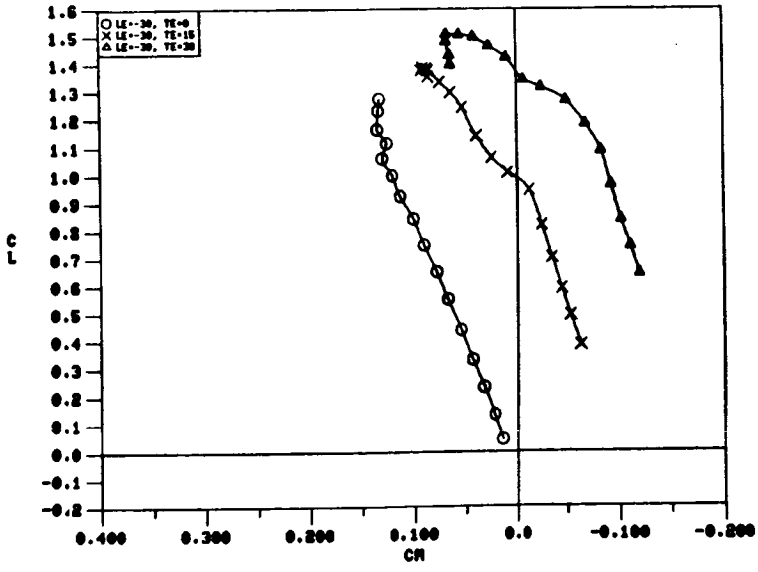

c) C_L vs. C_m

Figure 202. Effect of Trailing-Edge Flap Deflection on the 60-Degree Cropped Delta Wing Static Longitudinal Aerodynamic Characteristics with δ_n =-30°.

O	LE = 0, TE = 0
X	LE = 0, TE = 15
△	LE = 0, TE = 30

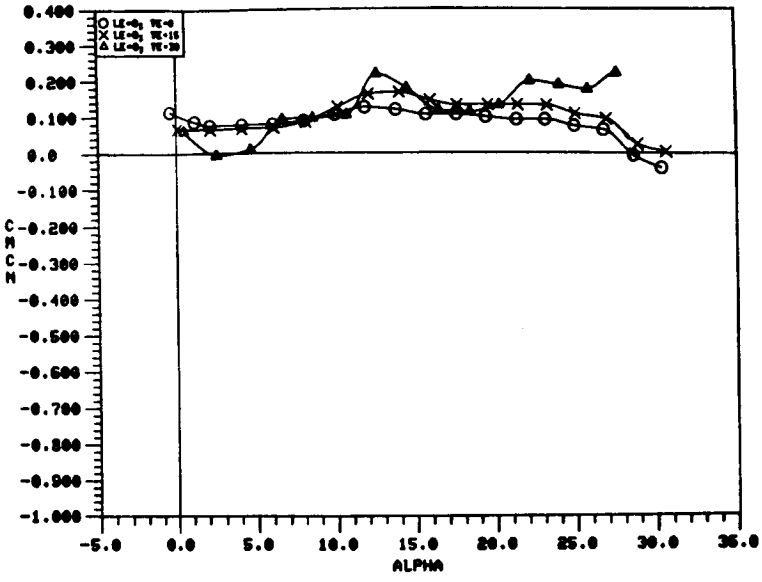

a) $C_{m_{C_n}}$ vs. α

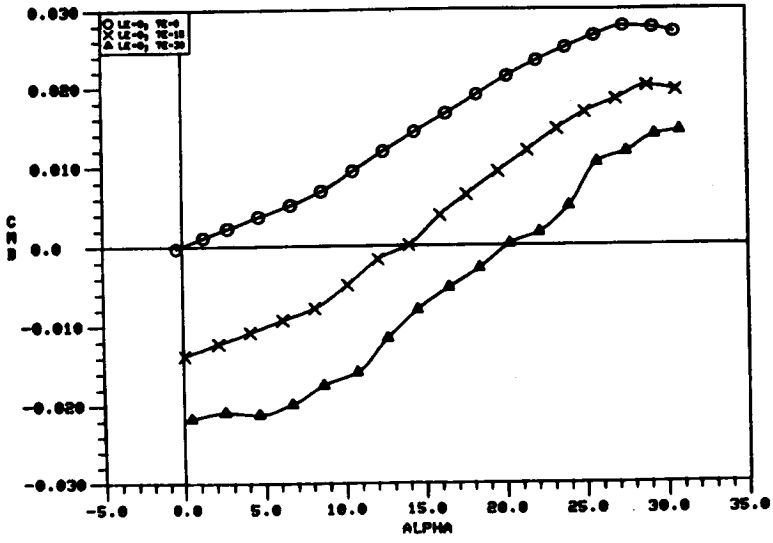

b) C_{m_β} vs. α

Figure 203. Effect of Trailing-Edge Flap Deflection on the 60-Degree Cropped Delta Wing Static Longitudinal Stability Characteristics with $\delta_n = 0°$.

O	LE = 30, TE = 0
X	LE = 30, TE = 15
△	LE = 30, TE = 30

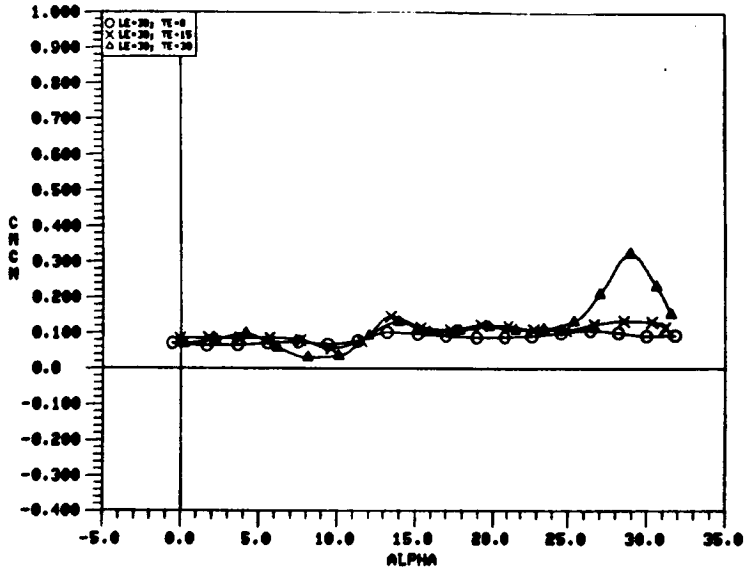

a) $C_{m_{C_{\tilde{n}}}}$ vs. α

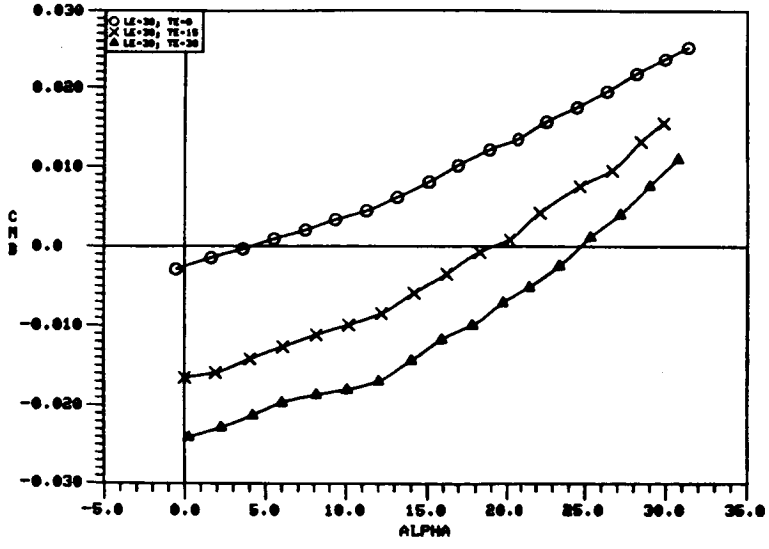

b) $C_{m_{\beta}}$ vs. α

Figure 204. Effect of Trailing-Edge Flap Deflection on the 60-Degree Cropped Delta Wing Static Longitudinal Stability Characteristics with $\delta_n = 30°$.

O	LE = 45, TE = 0
X	LE = 45, TE = 15
△	LE = 45, TE = 30

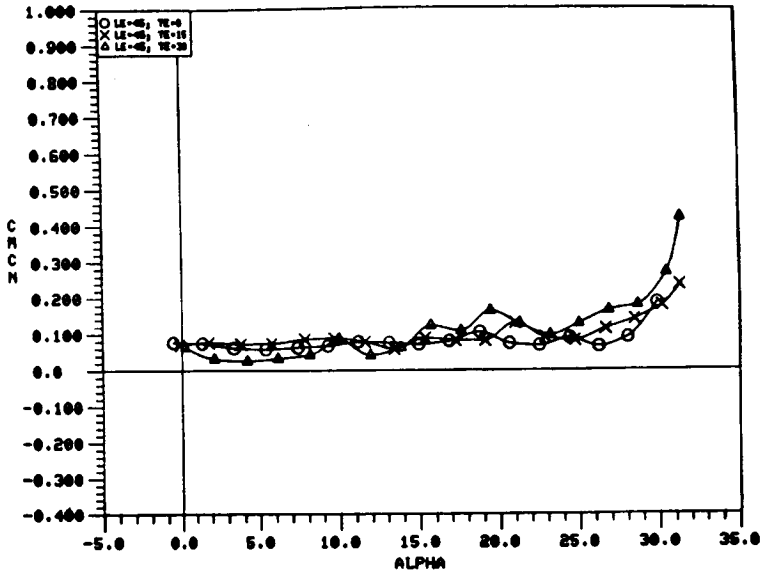

a) $C_{m_{C_n}}$ vs. α

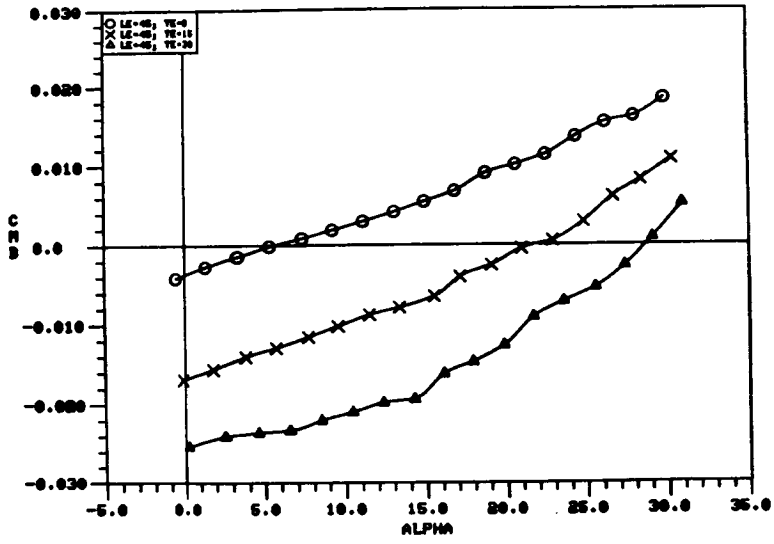

b) C_{m_β} vs. α

Figure 205. Effect of Trailing-Edge Flap Deflection on the 60-Degree Cropped Delta Wing Static Longitudinal Stability Characteristics with $\delta_n = 45°$.

O	LE = 60, TE = 0
X	LE = 60, TE = 15
△	LE = 60, TE = 30

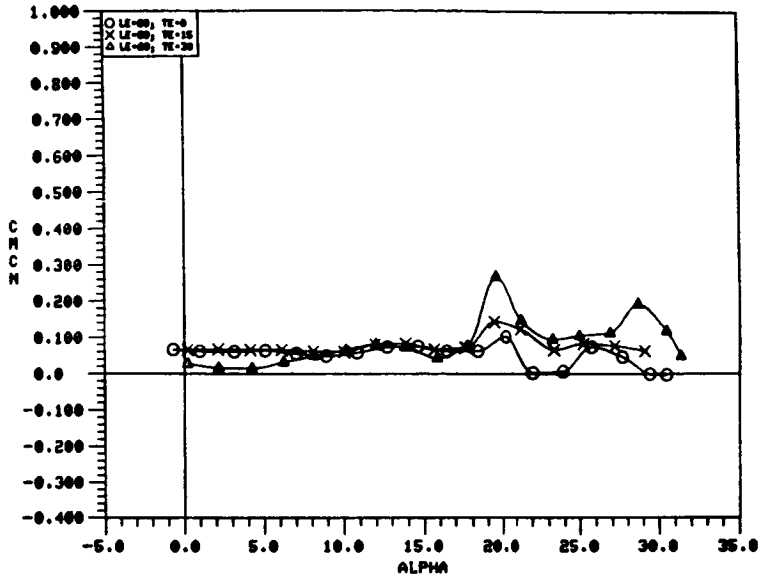

a) $C_{m_{C_n}}$ vs. α

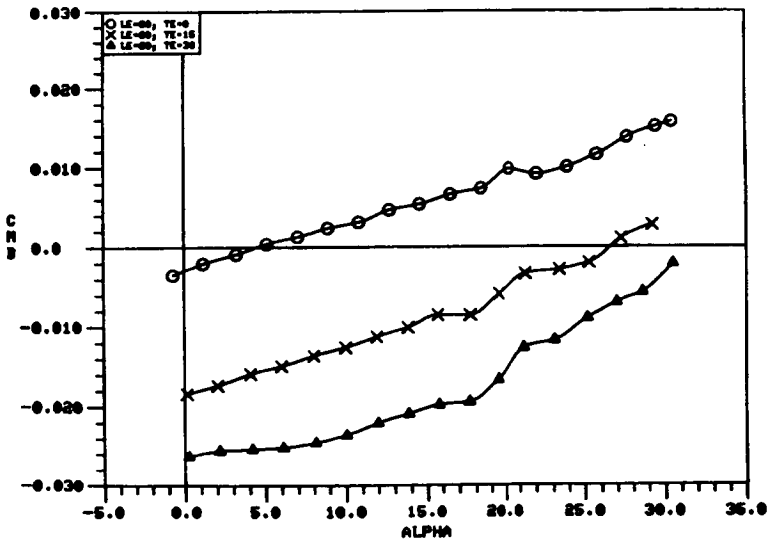

b) C_{m_β} vs. α

Figure 206. Effect of Trailing-Edge Flap Deflection on the 60-Degree Cropped Delta Wing Static Longitudinal Stability Characteristics with $\delta_n = 60°$.

O	LE = -30, TE = 0
X	LE = -30, TE = 15
△	LE = -30, TE = 30

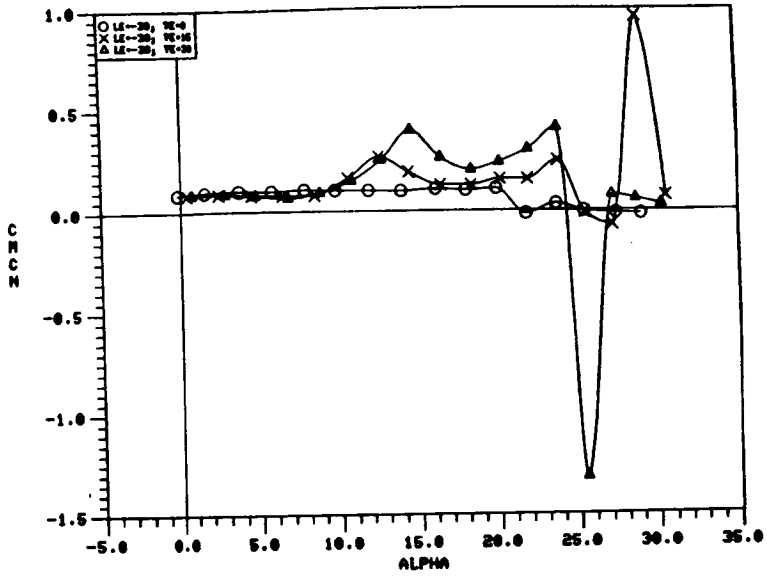

a) $C_{m_{C_N}}$ vs. α

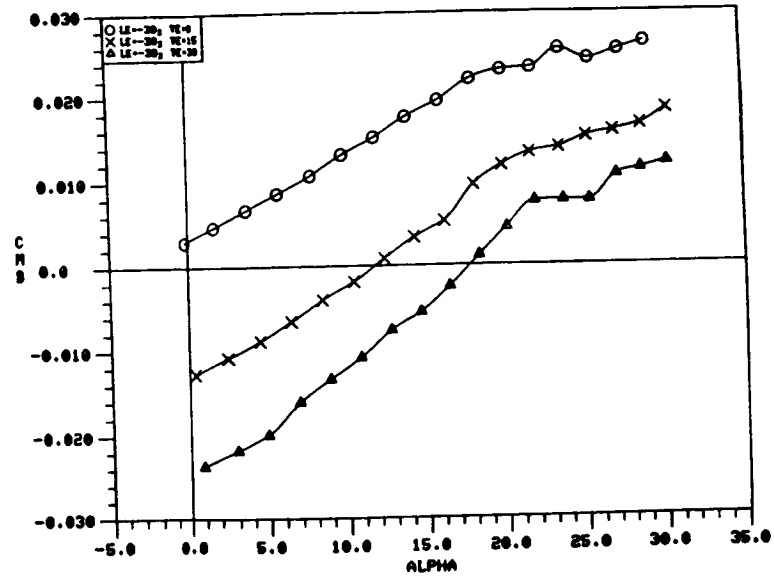

b) C_{m_β} vs. α

Figure 207. Effect of Trailing-Edge Flap Deflection on the 60-Degree Cropped Delta Wing Static Longitudinal Stability Characteristics with $\delta_n = -30°$.

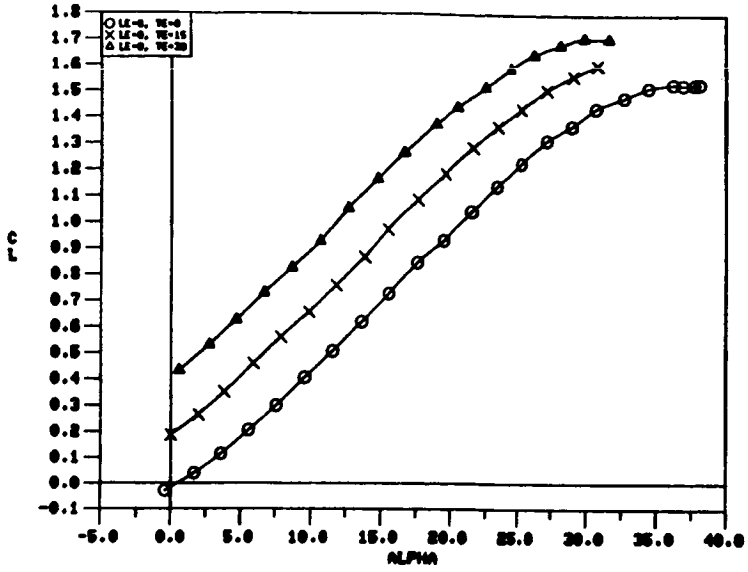

0	LE = 0, TE = 0
X	LE = 0. TE = 15
△	LE = 0, TE = 30

a) C_L vs. α

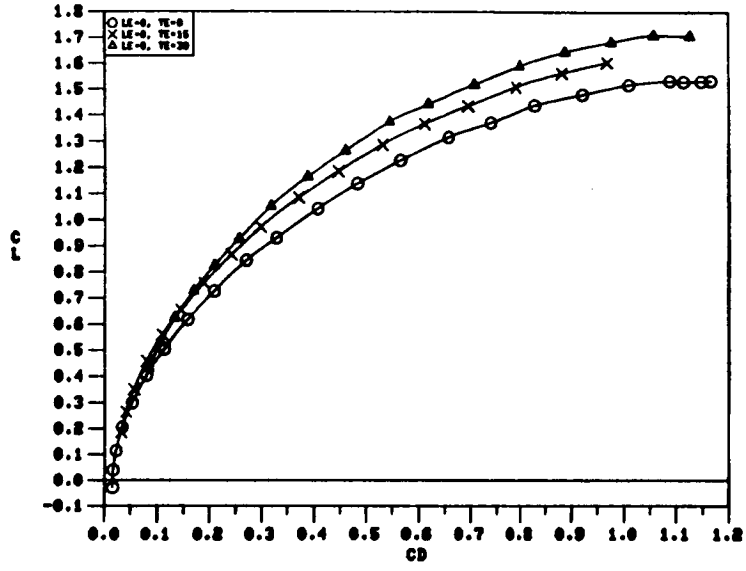

b) C_L vs. C_D

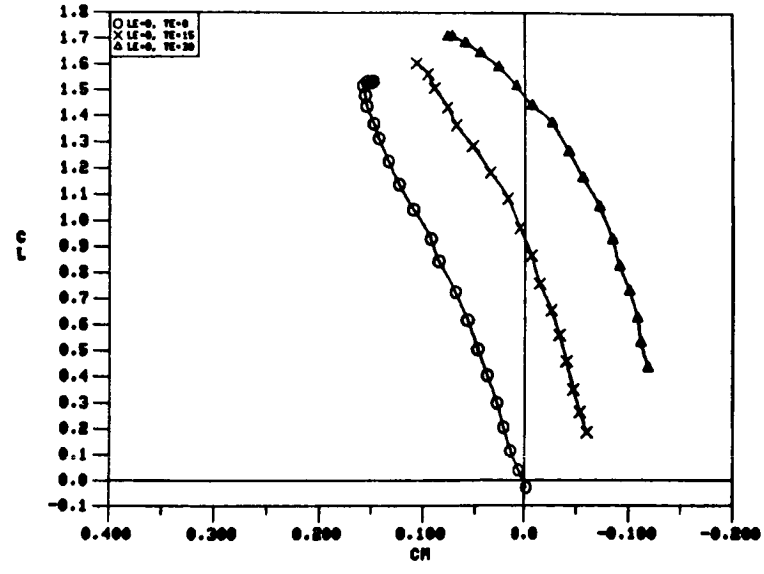

c) C_L vs. C_m

Figure 208. Effect of Trailing-Edge Flap Deflection on the 65-Degree Cropped Delta Wing Static Longitudinal Aerodynamic Characteristics with $\delta_n = 0°$.

C-4

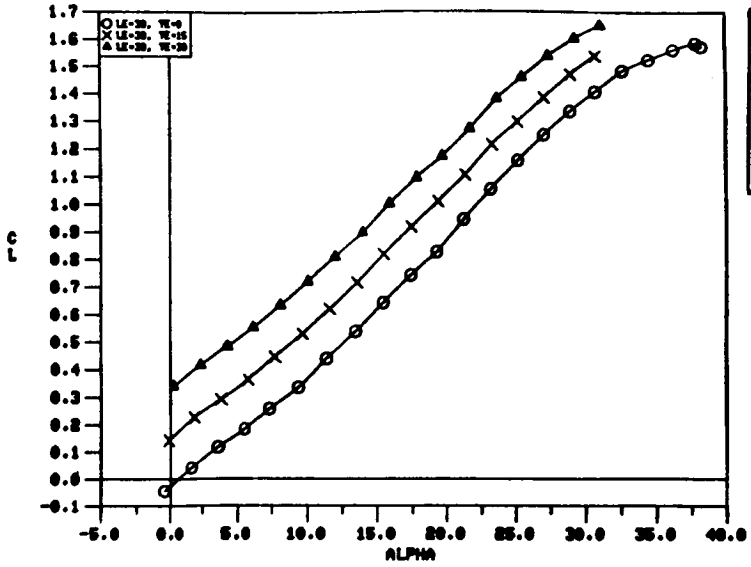

O	LE = 30,	TE =	0
X	LE = 30,	TE =	15
△	LE = 30,	TE =	30

a) C_L vs. α

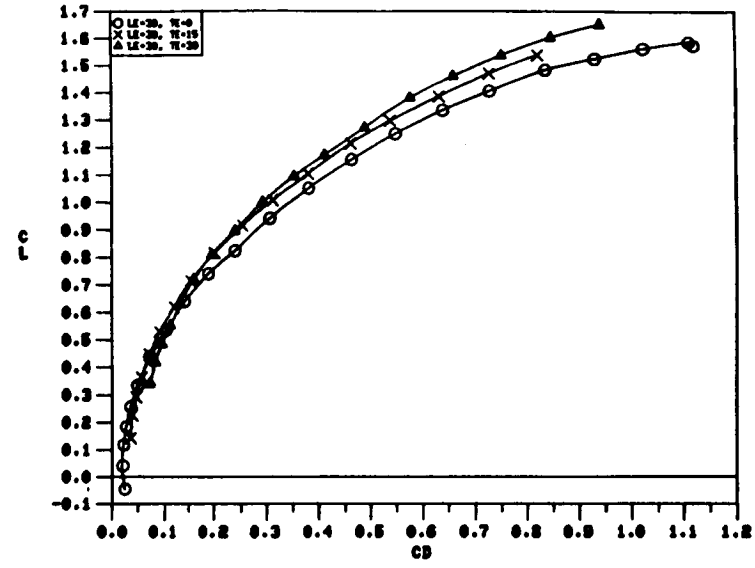

b) C_L vs. C_D

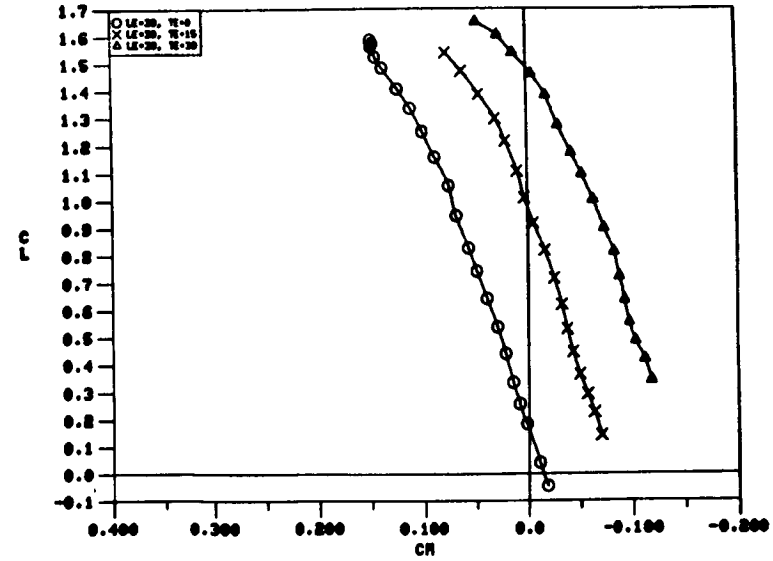

c) C_L vs. C_m

Figure 209. Effect of Trailing-Edge Flap Deflection on the 65-Degree Cropped Delta Wing Static Longitudinal Aerodynamic Characteristics with $\delta_n = 30°$.

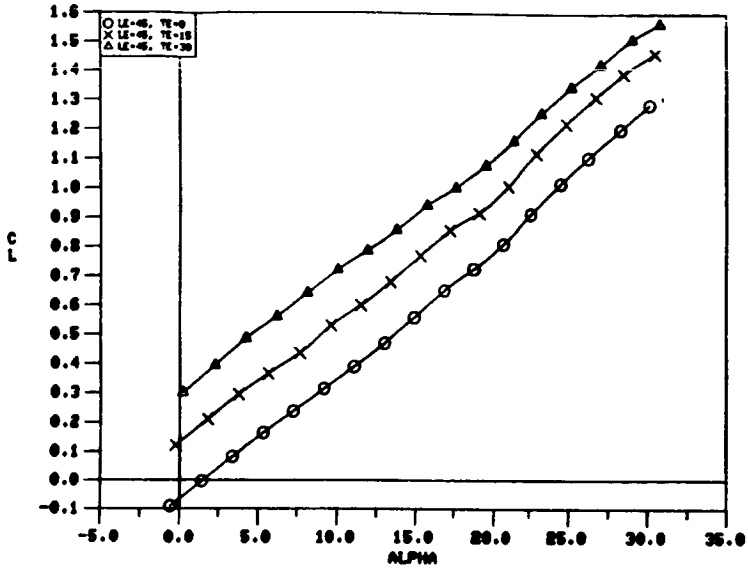

O	LE = 45,	TE =	0
X	LE = 45.	TE =	15
△	LE = 45,	TE =	30

a) C_L vs. α

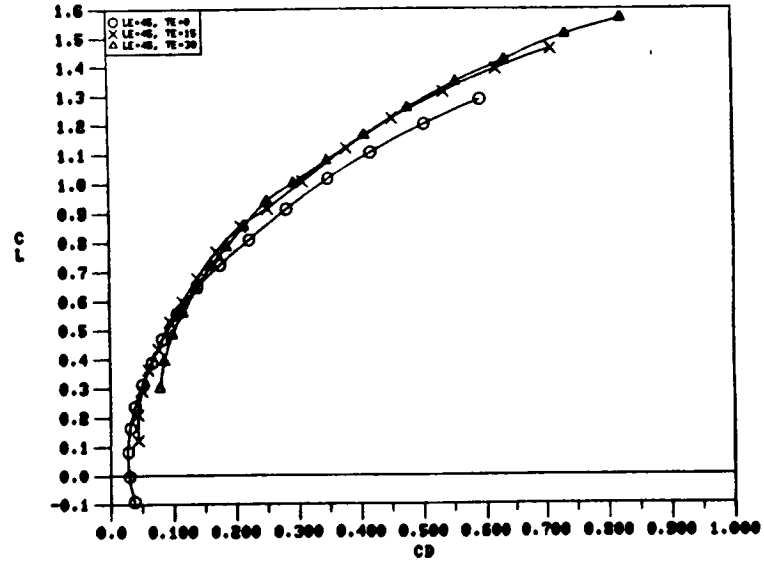

b) C_L vs. C_D

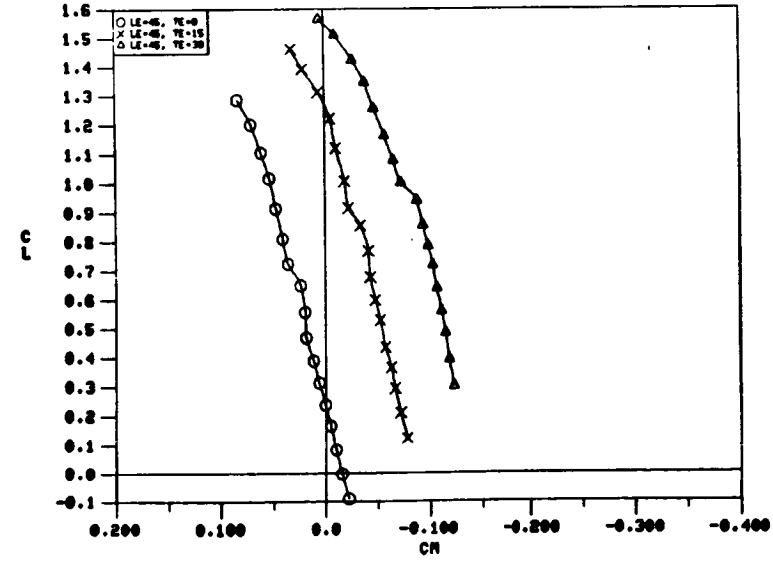

c) C_L vs. C_m

Figure 210. Effect of Trailing-Edge Flap Deflection on the 65-Degree Cropped Delta Wing Static Longitudinal Aerodynamic Characteristics with $\delta_n = 45°$.

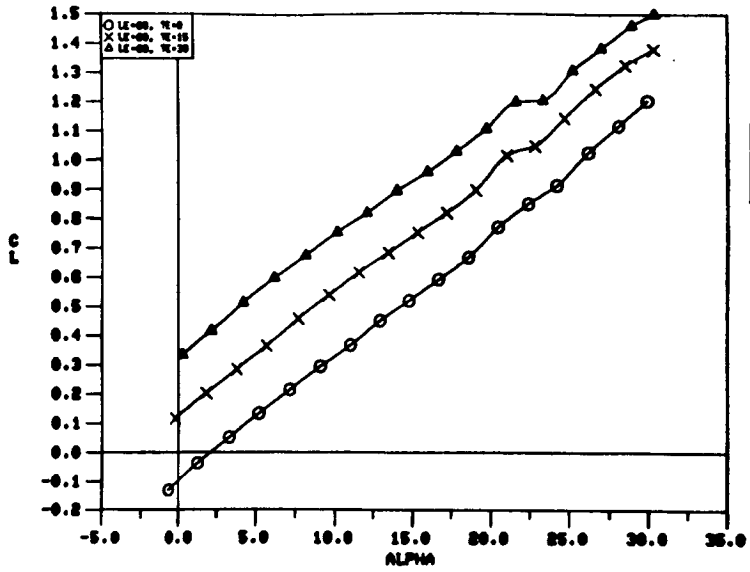

O	LE = 60,	TE =	0
X	LE = 60,	TE =	15
△	LE = 60,	TE =	30

a) C_L vs. α

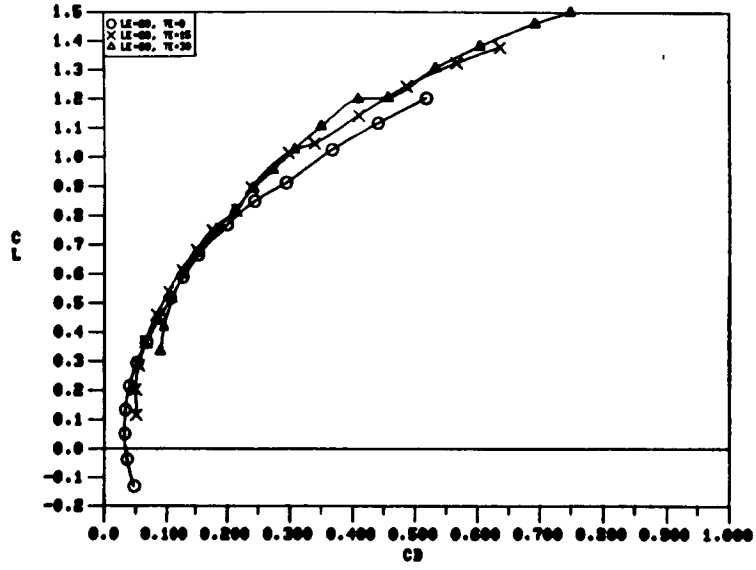

b) C_L vs. C_D

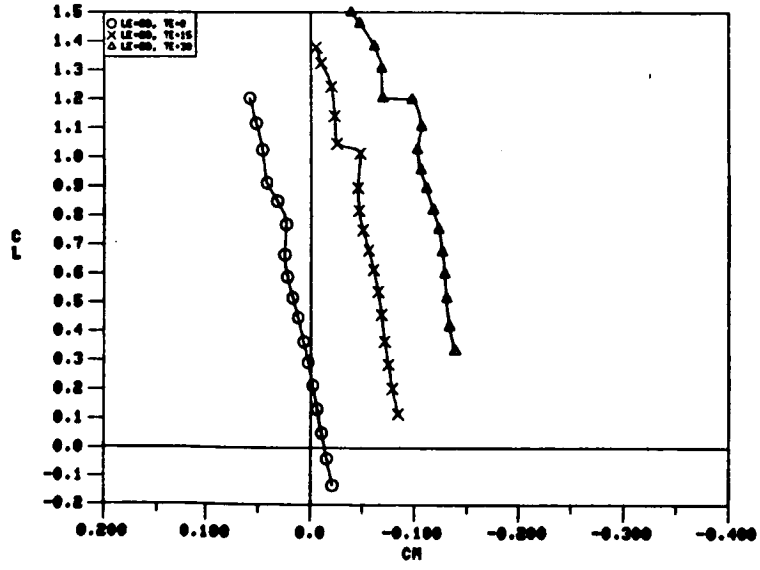

c) C_L vs. C_m

Figure 211. Effect of Trailing-Edge Flap Deflection on the 65-Degree Cropped Delta Wing Static Longitudinal Aerodynamic Characteristics with $\delta_n = 60°$.

O	LE = 0, TE = 0
X	LE = 0, TE = 15
△	LE = 0, TE = 30

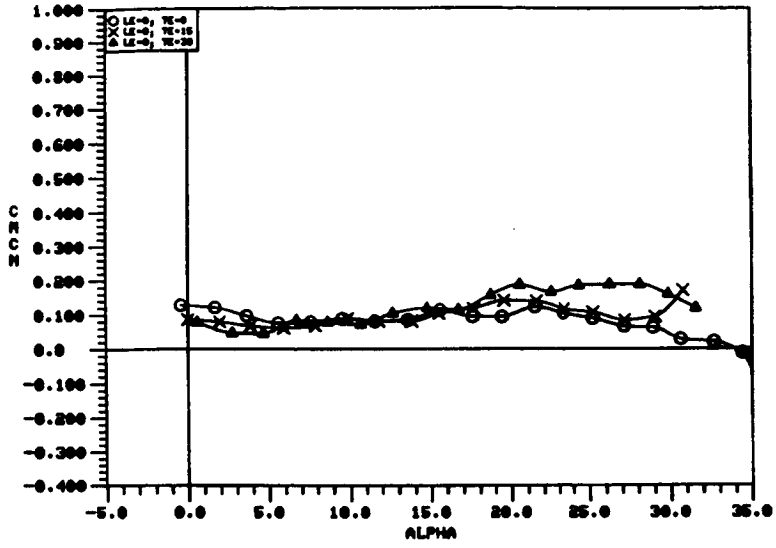

a) $C_{m_{C_n}}$ vs. α

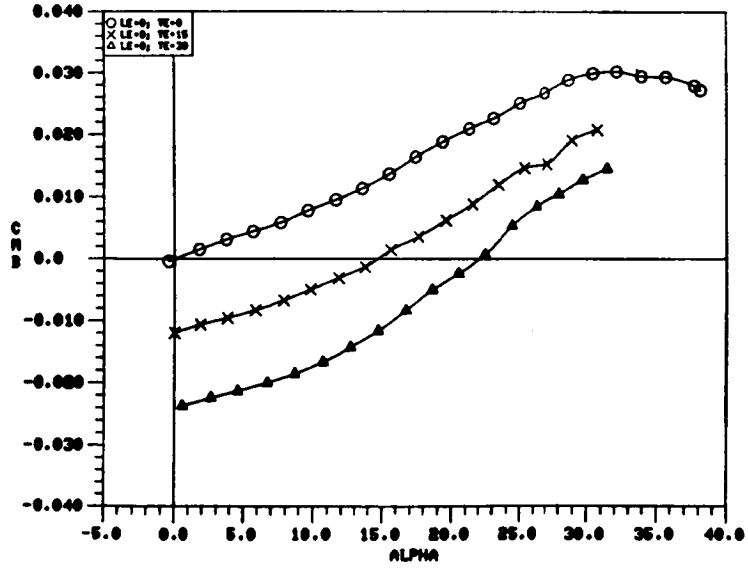

b) C_{m_β} vs. α

Figure 212. Effect of Trailing-Edge Flap Deflection on the 65-Degree Cropped Delta Wing Static Longitudinal Stability Characteristics with $\delta_n = 0°$.

O	LE = 30, TE = 0
X	LE = 30, TE = 15
△	LE = 30, TE = 30

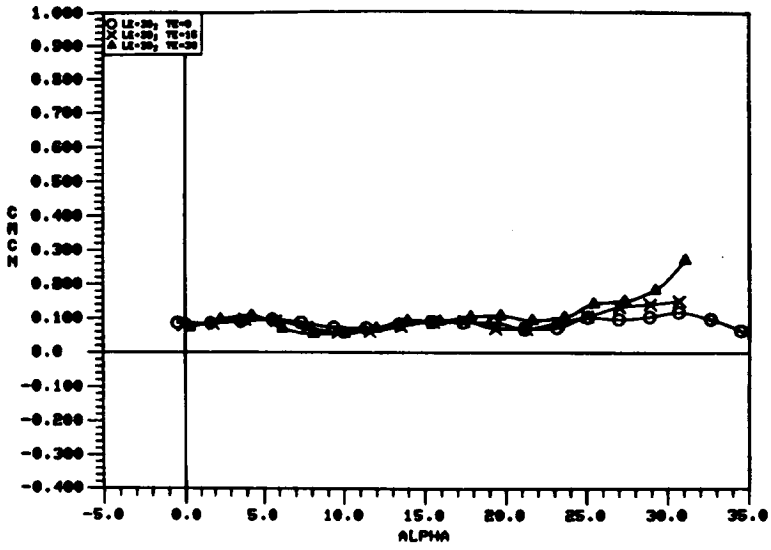

a) $C_{m_{C_n}}$ vs. α

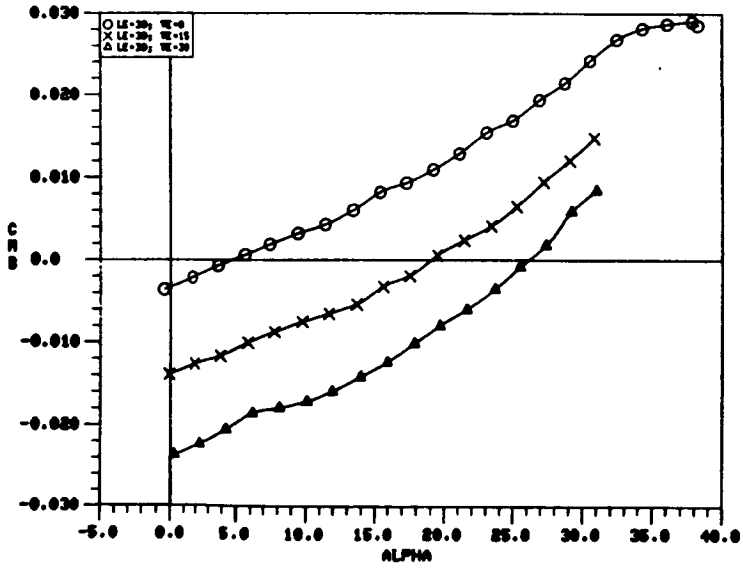

b) C_{m_β} vs. α

Figure 213. Effect of Trailing-Edge Flap Deflection on the 65-Degree Cropped Delta Wing Static Longitudinal Stability Characteristics with $\delta_n = 30°$.

O	LE = 45, TE = 0
X	LE = 45, TE = 15
△	LE = 45, TE = 30

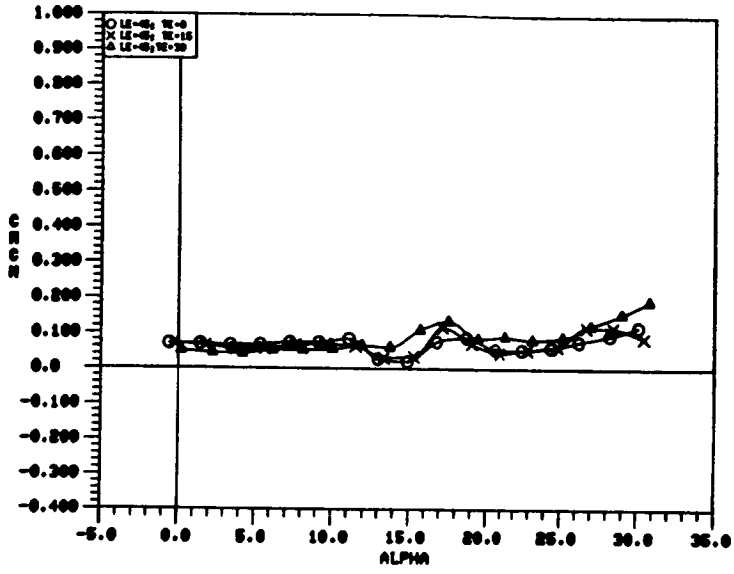

a) $C_{m_{C_n}}$ vs. α

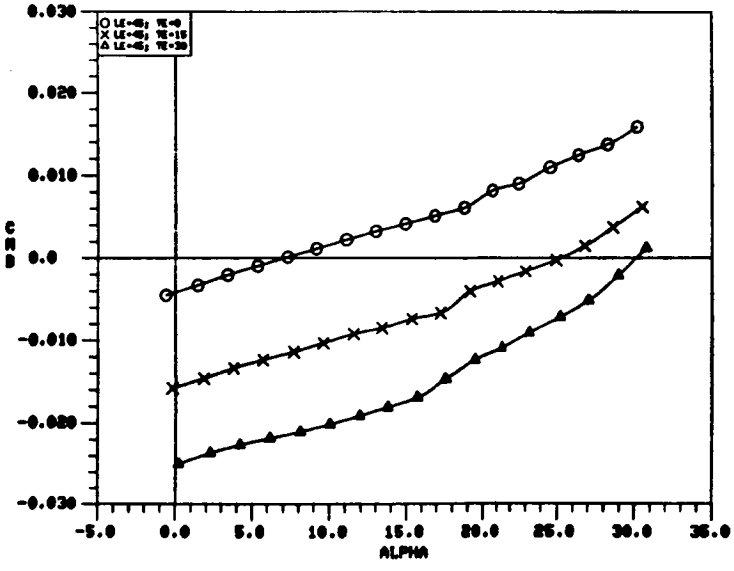

b) C_{m_β} vs. α

Figure 214. Effect of Trailing-Edge Flap Deflection on the 65-Degree Cropped Delta Wing Static Longitudinal Stability Characteristics with $\delta_n = 45°$.

O	LE = 60, TE = 0
X	LE = 60, TE = 15
△	LE = 60, TE = 30

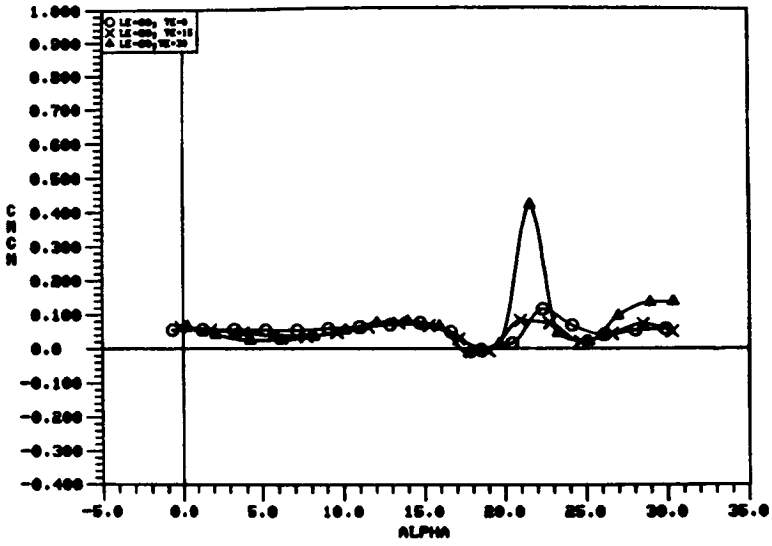

a) $C_{m_{C_n}}$ vs. α

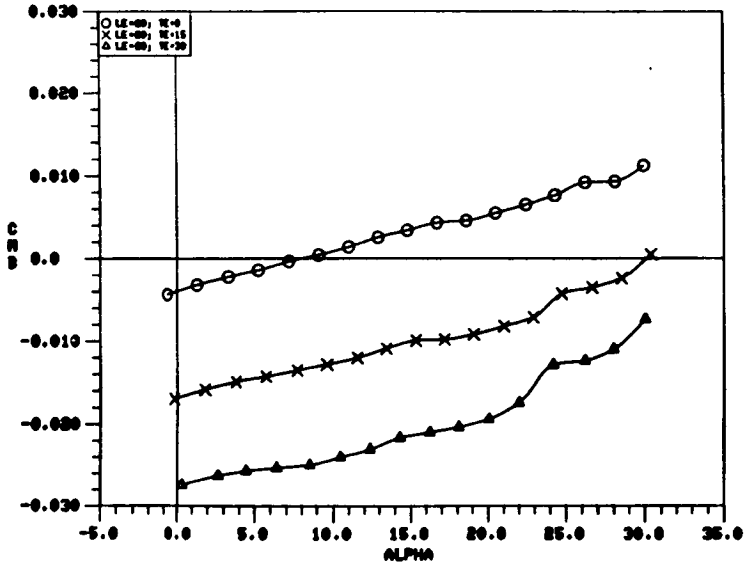

b) C_{m_β} vs. α

Figure 215. Effect of Trailing-Edge Flap Deflection on the 65-Degree Cropped Delta Wing Static Longitudinal Stability Characteristics with $\delta_n = 60°$.

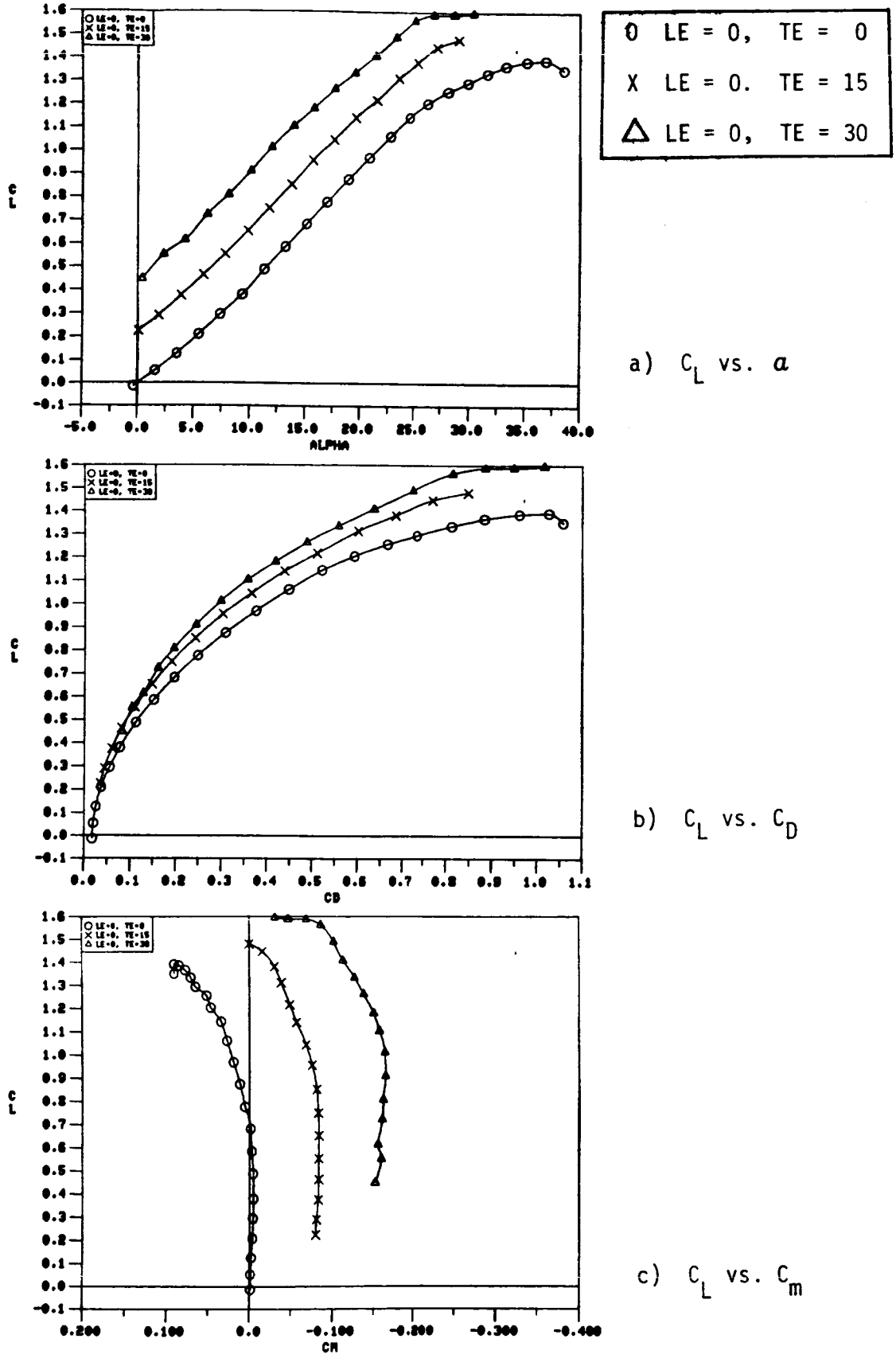

Figure 216. Effect of Trailing-Edge Flap Deflection on the 70/50-Degree Cranked Wing Static Longitudinal Aerodynamic Characteristics with $\delta_n = 0°$.

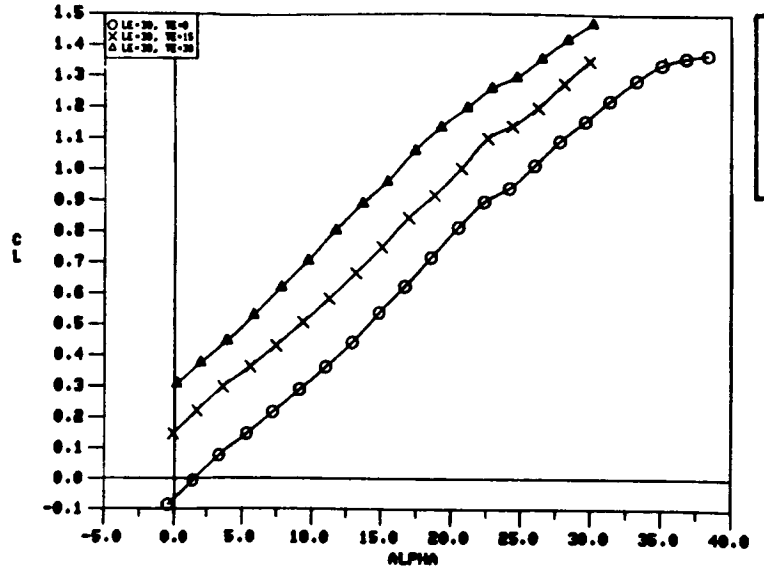

O	LE = 30,	TE =	0
X	LE = 30,	TE =	15
△	LE = 30,	TE =	30

a) C_L vs. α

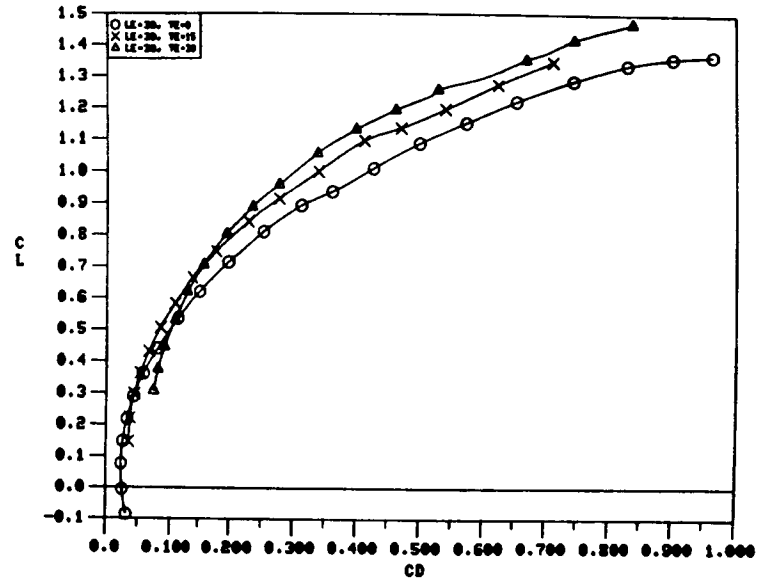

b) C_L vs. C_D

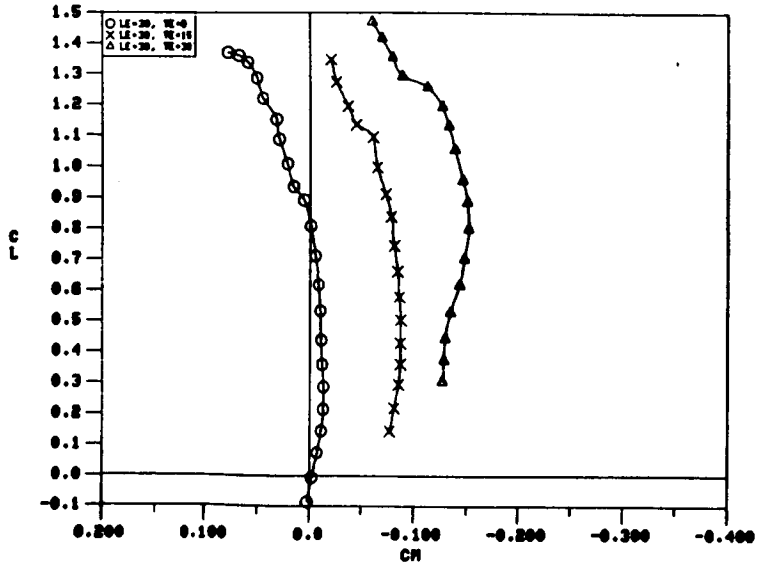

c) C_L vs. C_m

Figure 217. Effect of Trailing-Edge Flap Deflection on the 70/50-Degree Cranked Wing Static Longitudinal Aerodynamic Characteristics with $\delta_n = 30°$.

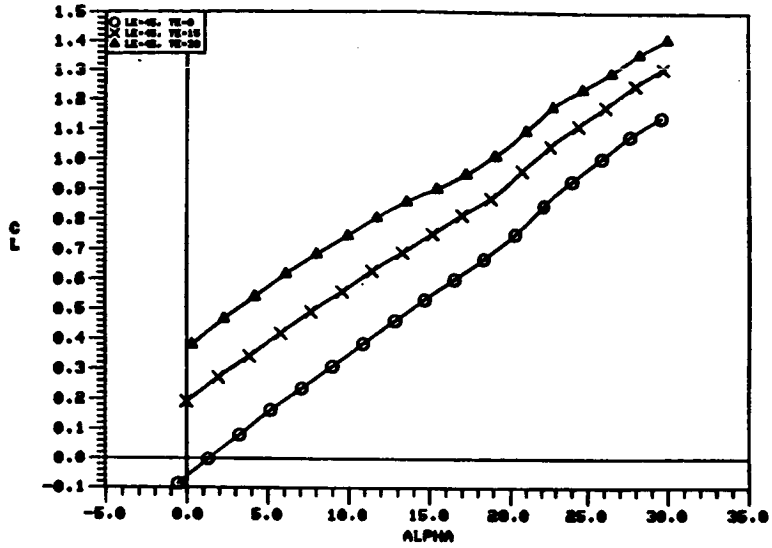

O	LE = 45,	TE =	0
X	LE = 45.	TE =	15
△	LE = 45,	TE =	30

a) C_L vs. α

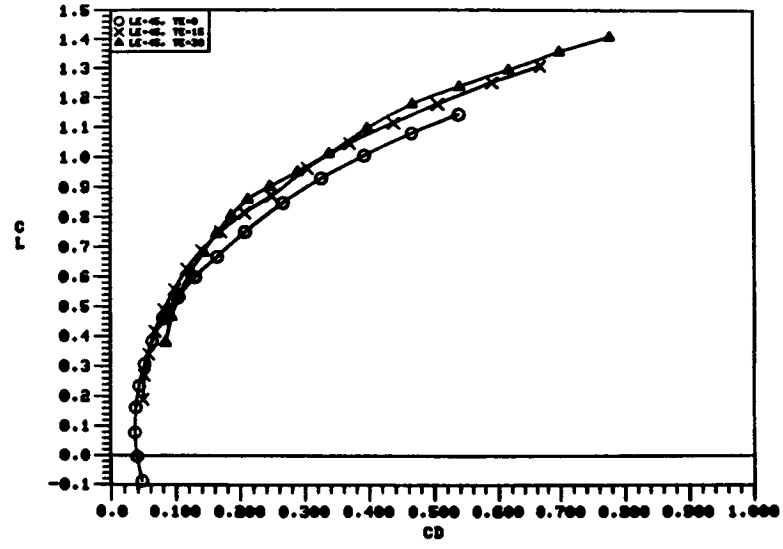

b) C_L vs. C_D

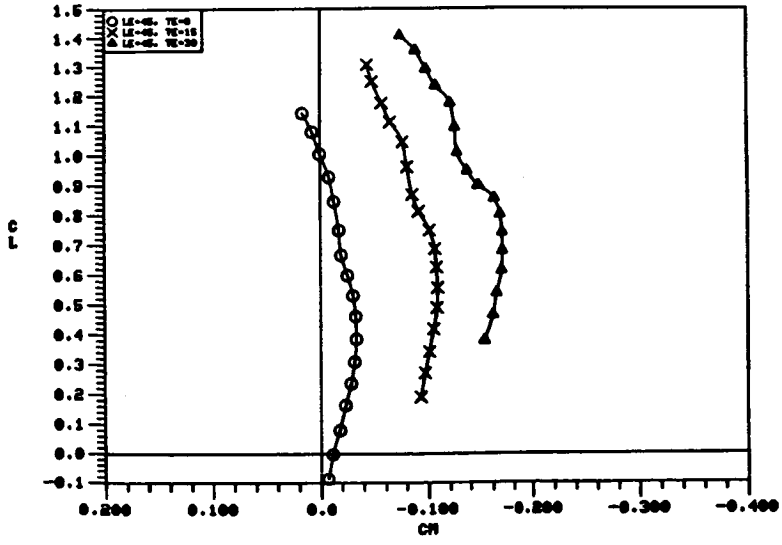

c) C_L vs. C_m

Figure 218. Effect of Trailing-Edge Flap Deflection on the 70/50-Degree Cranked Wing Static Longitudinal Aerodynamic Characteristics with $\delta_n = 45°$.

O	LE = 0, TE = 0
X	LE = 0, TE = 15
△	LE = 0, TE = 30

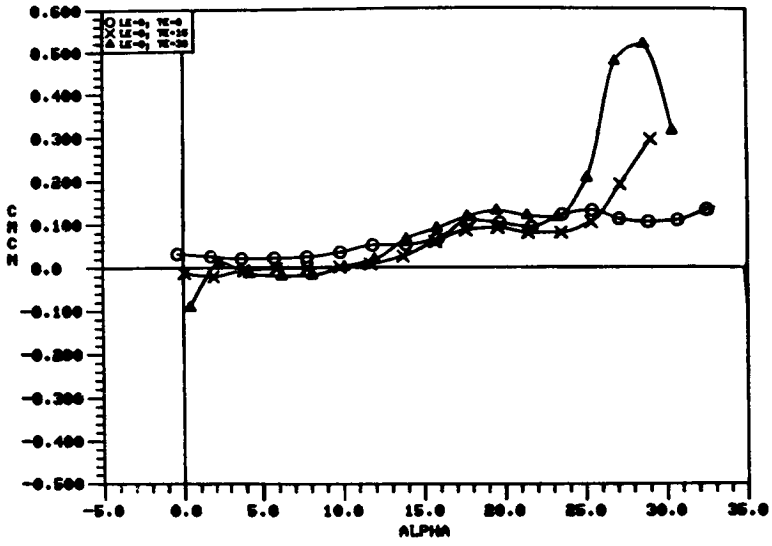

a) $C_{m_{C_n}}$ vs. α

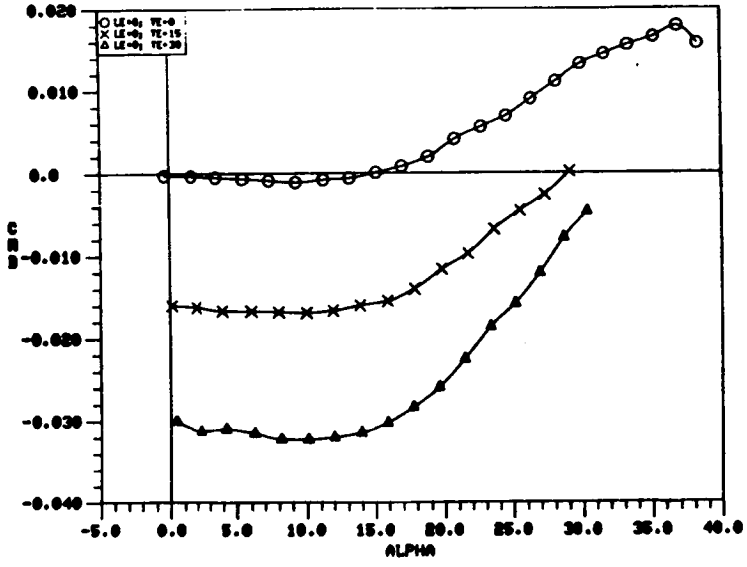

b) C_{m_β} vs. α

Figure 219. Effect of Trailing-Edge Flap Deflection on the 70/50-Degree Cranked Wing Static Longitudinal Stability Characteristics with $\delta_n = 0°$.

O	LE = 30, TE = 0
X	LE = 30, TE = 15
△	LE = 30, TE = 30

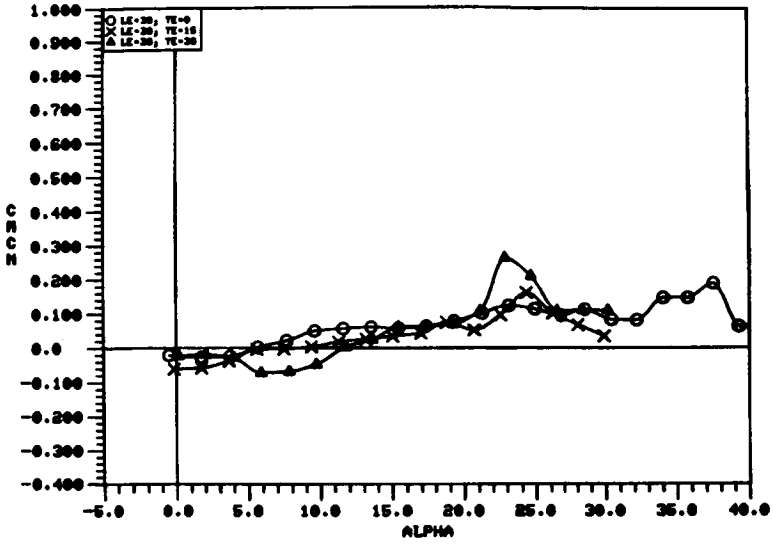

a) $C_{m_{C_{\bar{n}}}}$ vs. α

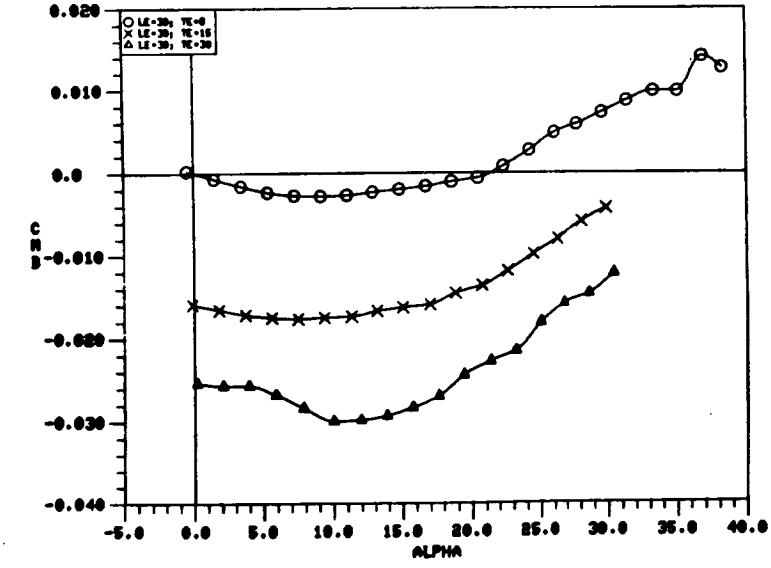

b) $C_{m_{\beta}}$ vs. α

Figure 220. Effect of Trailing-Edge Flap Deflection on the 70/50-Degree Cranked Wing Static Longitudinal Stability Characteristics with $\delta_n = 30°$.

O	LE = 45, TE = 0
X	LE = 45, TE = 15
△	LE = 45, TE = 30

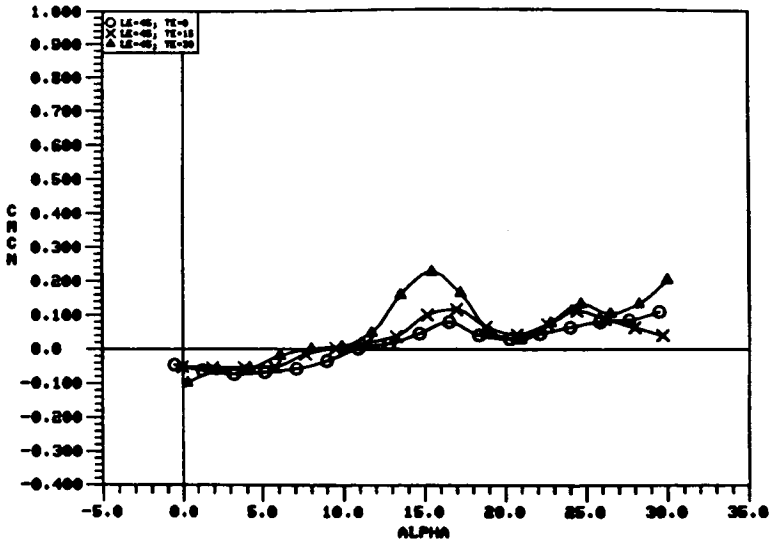

a) $C_{m_{C_n}}$ vs. α

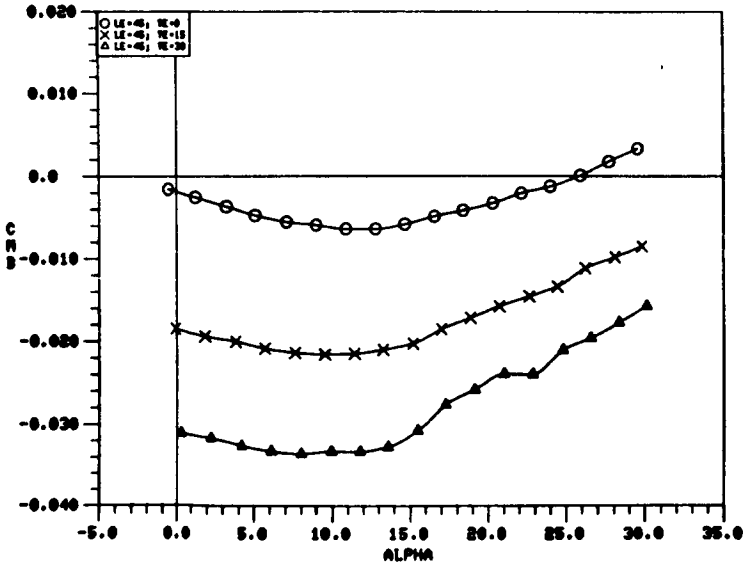

b) C_{m_β} vs. α

Figure 221. Effect of Trailing-Edge Flap Deflection on the 70/50-Degree Cranked Wing Static Longitudinal Stability Characteristics with $\delta_n = 45°$.

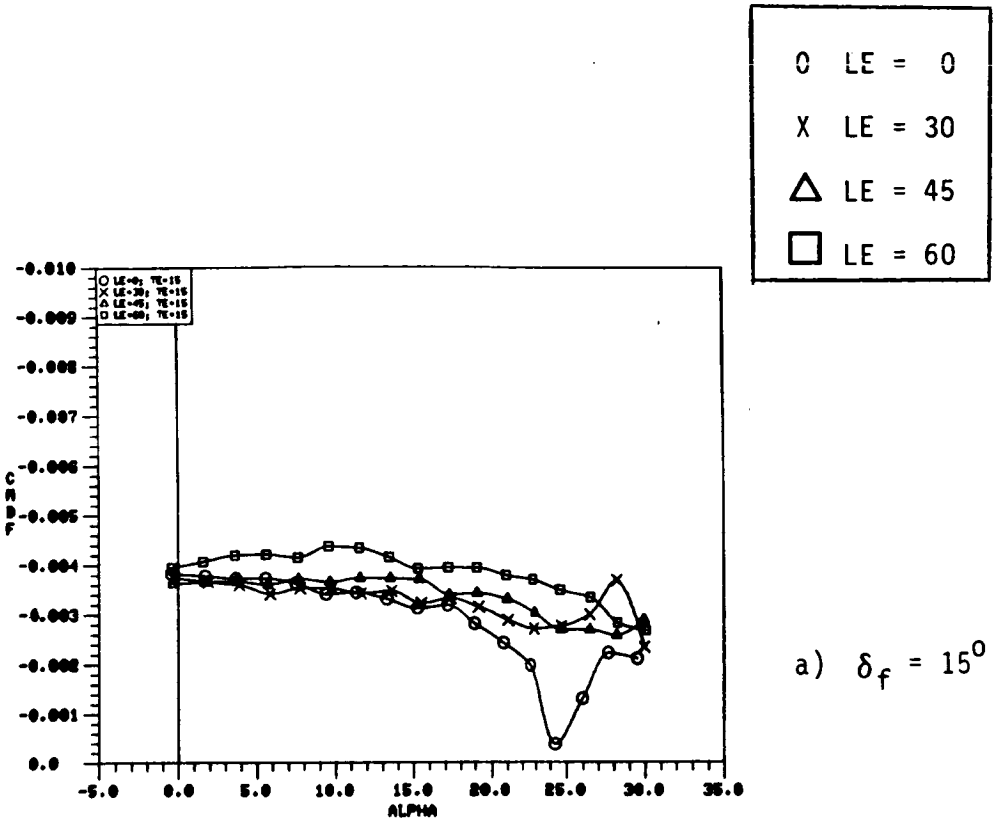

a) $\delta_f = 15^o$

$C_{m_{\delta_f}}$ vs. α

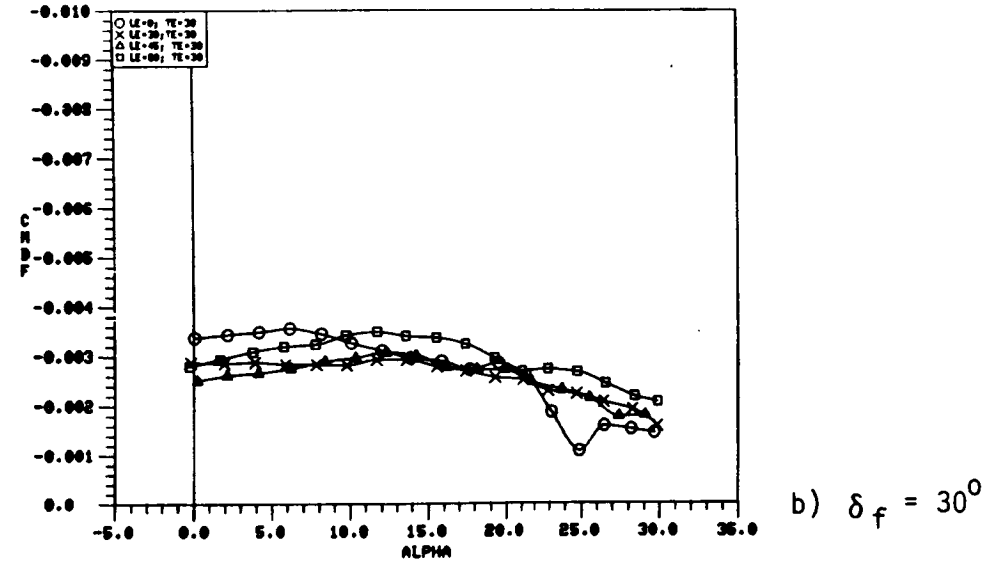

b) $\delta_f = 30^o$

$C_{m_{\delta_f}}$ vs. α

Figure 222. Effect of Vortex Flap Deflection Angle on the 50-Degree Cropped Delta Wing Longitudinal Control Derivative.

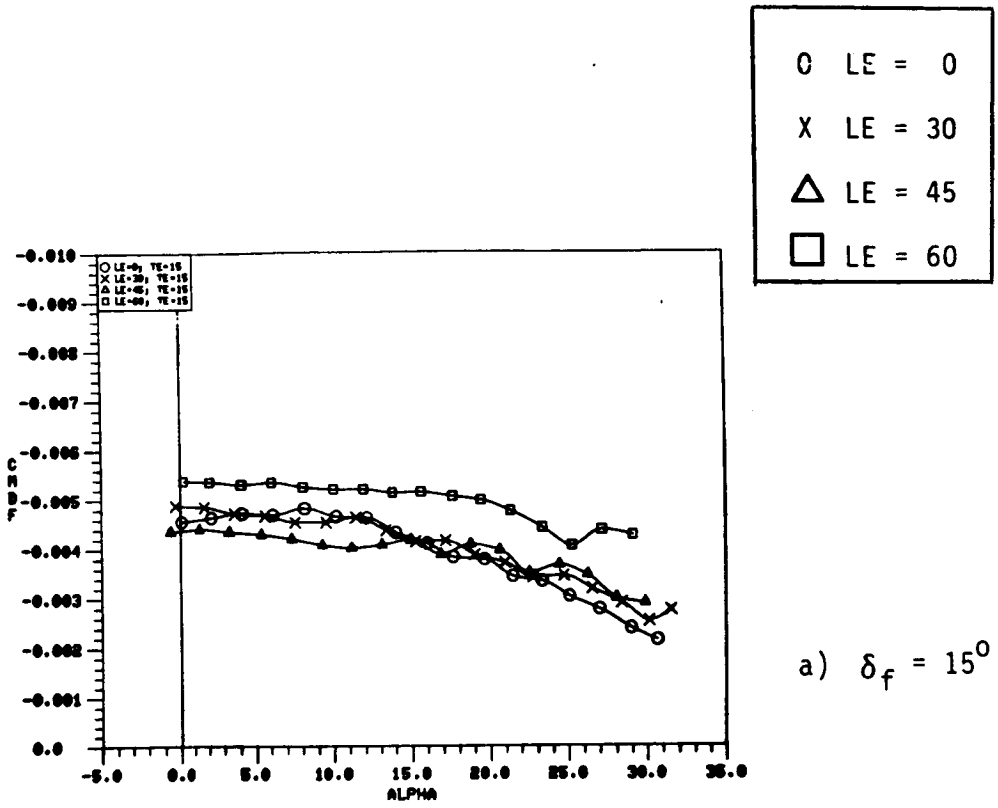

a) $\delta_f = 15^o$

$C_{m_{\delta_f}}$ vs. α

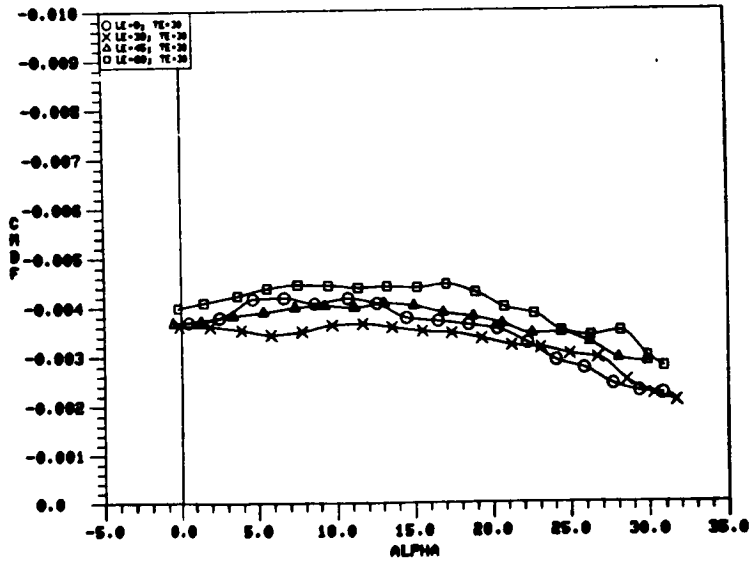

b) $\delta_f = 30^o$

$C_{m_{\delta_f}}$ vs. α

Figure 223. Effect of Vortex Flap Deflection Angle on the 60-Degree Cropped Delta Wing Longitudinal Control Derivative.

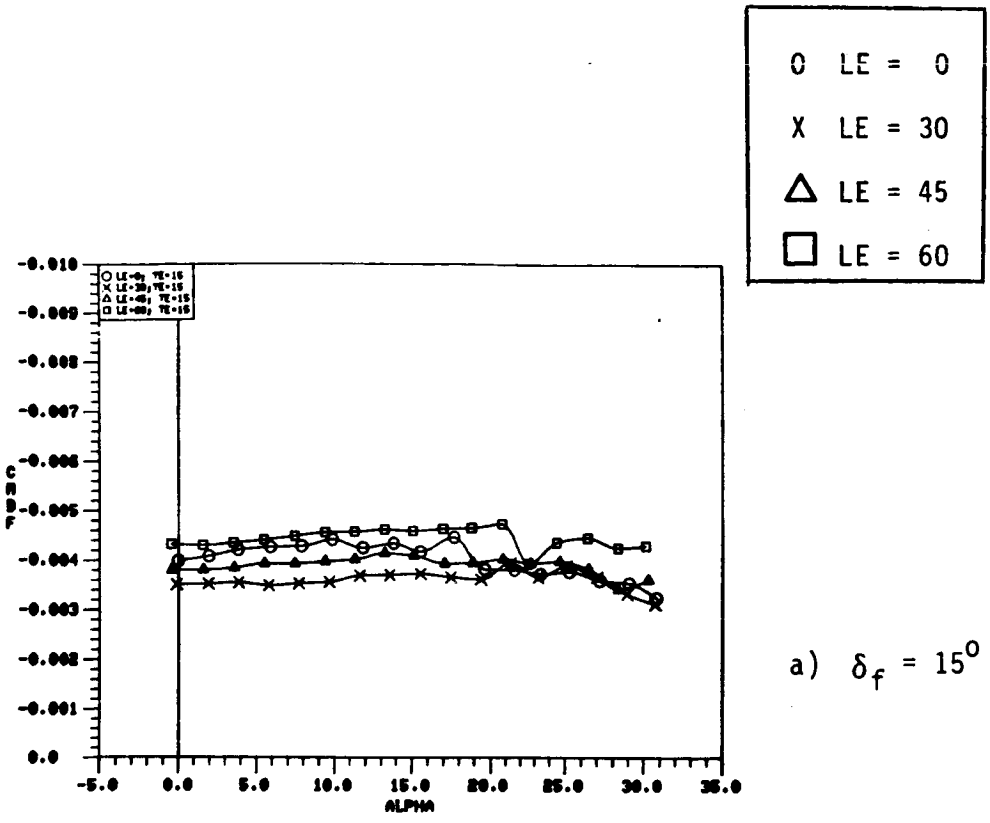

a) $\delta_f = 15^o$

$C_{m_{\delta_f}}$ vs. α

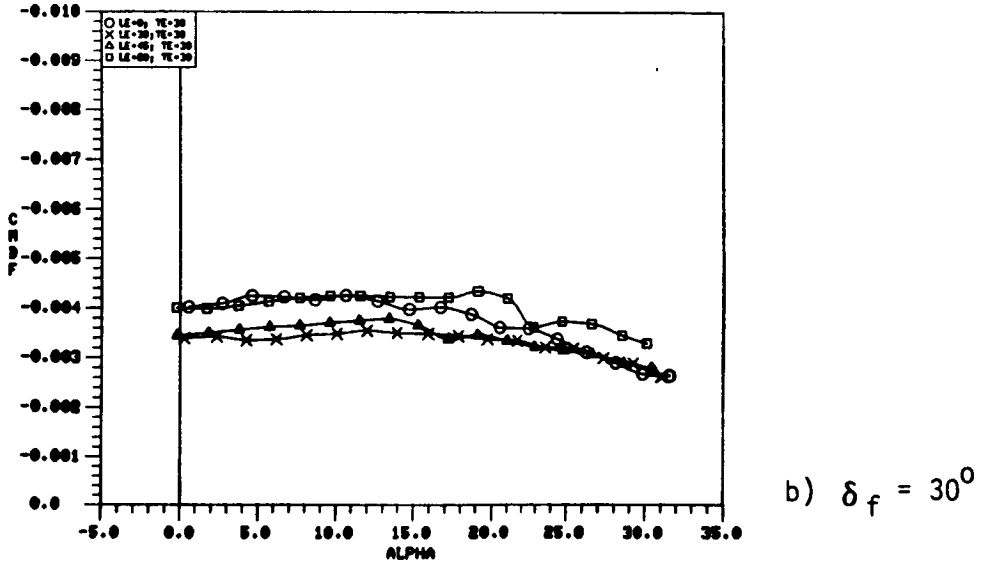

b) $\delta_f = 30^o$

$C_{m_{\delta_f}}$ vs. α

Figure 224. Effect of Vortex Flap Deflection Angle on the 65-Degree Cropped Delta Wing Longitudinal Control Derivative.

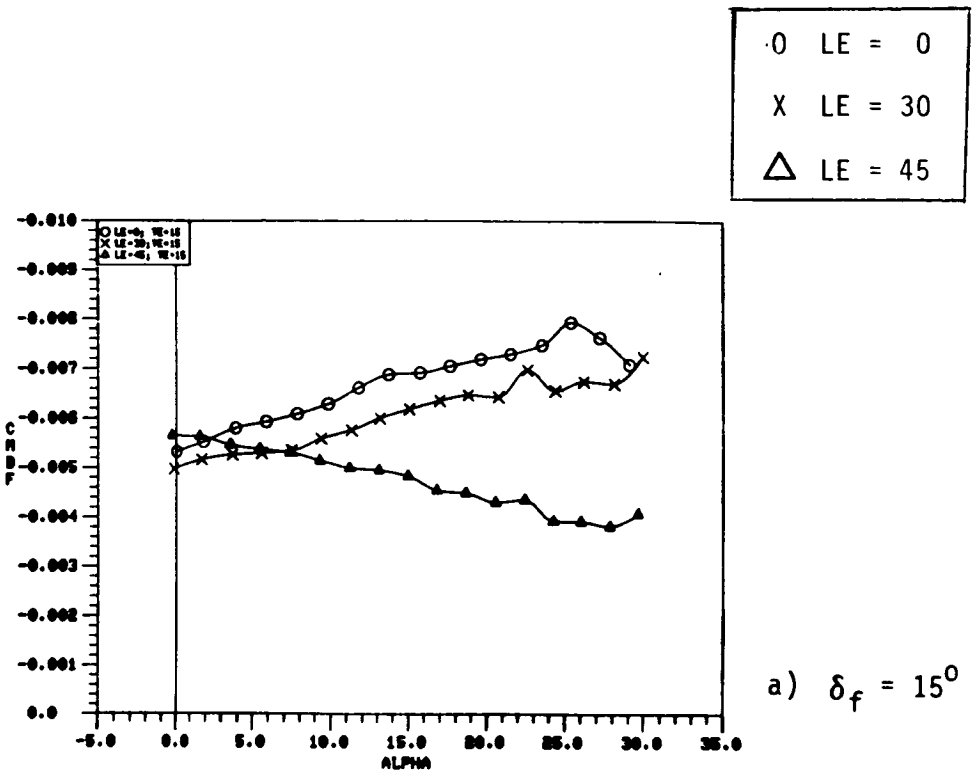

a) $\delta_f = 15^o$

$C_{m_{\delta_f}}$ vs. α

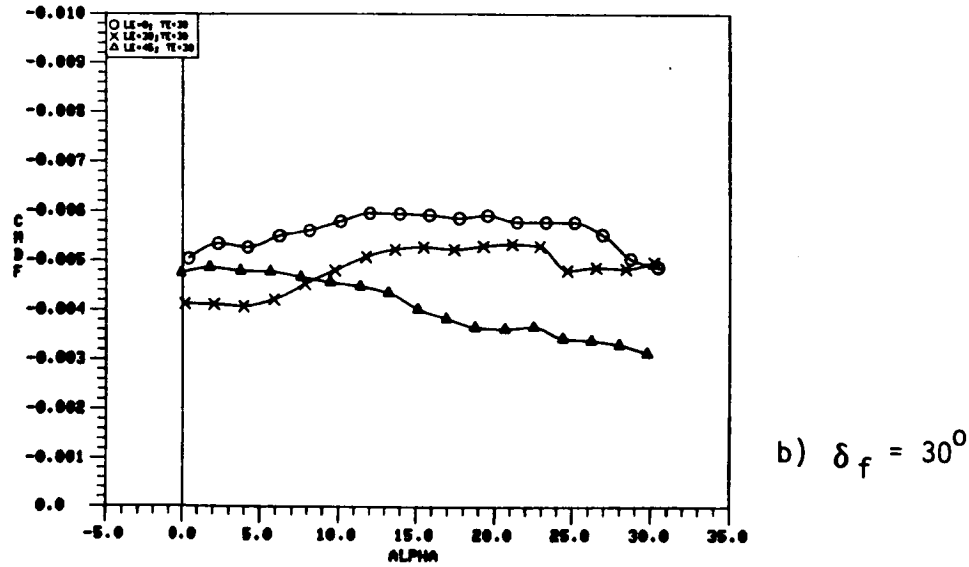

b) $\delta_f = 30^o$

$C_{m_{\delta_f}}$ vs. α

Figure 225. Effect of Vortex Flap Deflection Angle on the 70/50-Degree Cranked Wing Longitudinal Control Derivative.

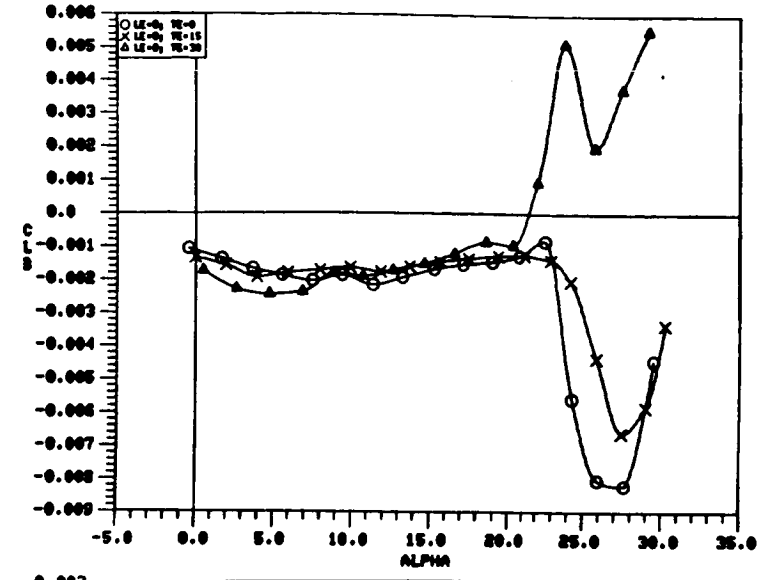

O	LE = 0,	TE =	0
X	LE = 0,	TE =	15
△	LE = 0,	TE =	30

a) C_{ℓ_β} vs. α

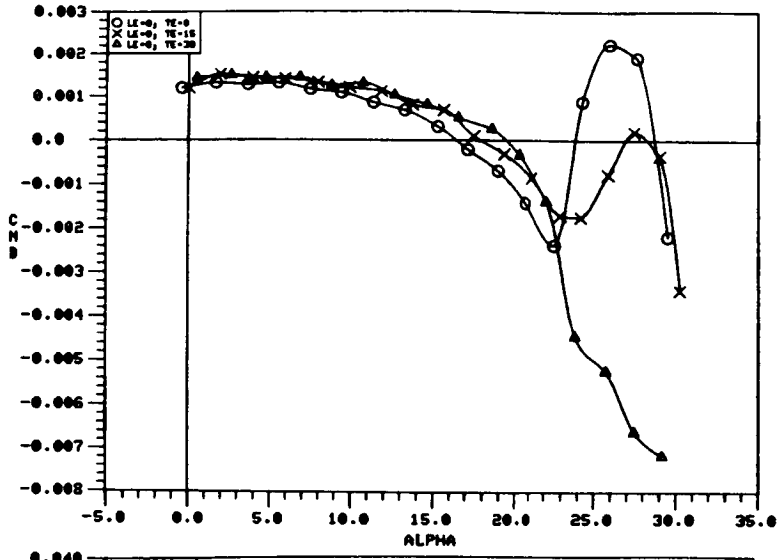

b) C_{n_β} vs. α

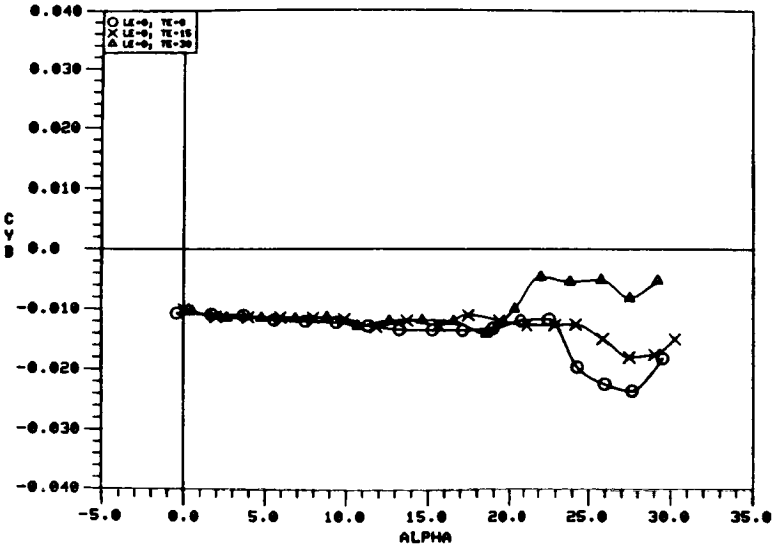

c) C_{Y_β} vs. α

Figure 226. Effect of Trailing-Edge Flap Deflection on the 50-Degree Cropped Delta Wing Static Lateral-Directional Stability Characteristics with $\delta_n = 0°$.

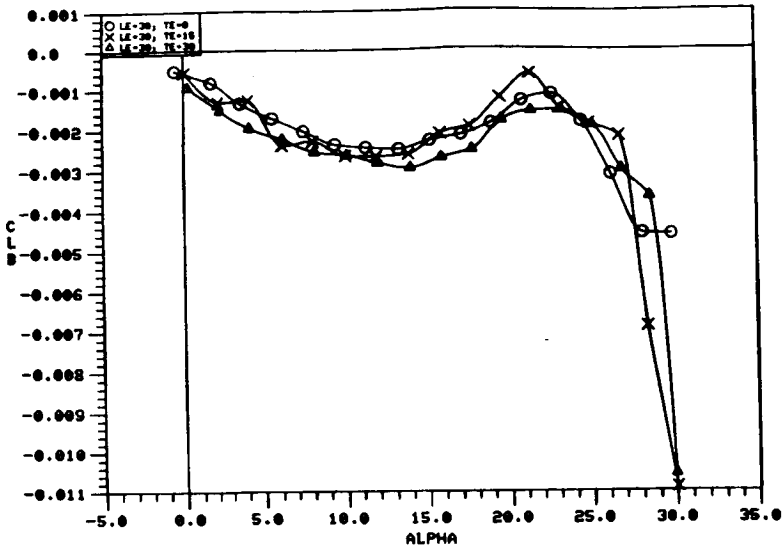

O	LE = 30,	TE =	0
X	LE = 30,	TE =	15
△	LE = 30,	TE =	30

a) C_{ℓ_β} vs. α

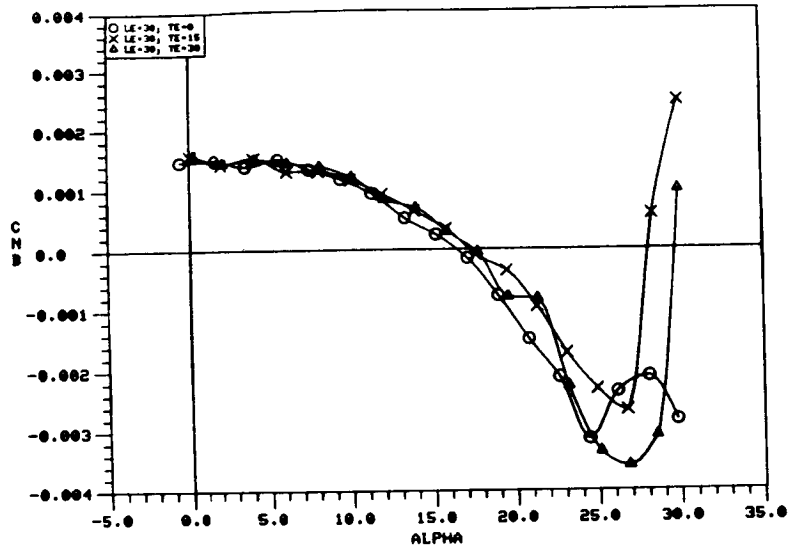

b) C_{n_β} vs. α

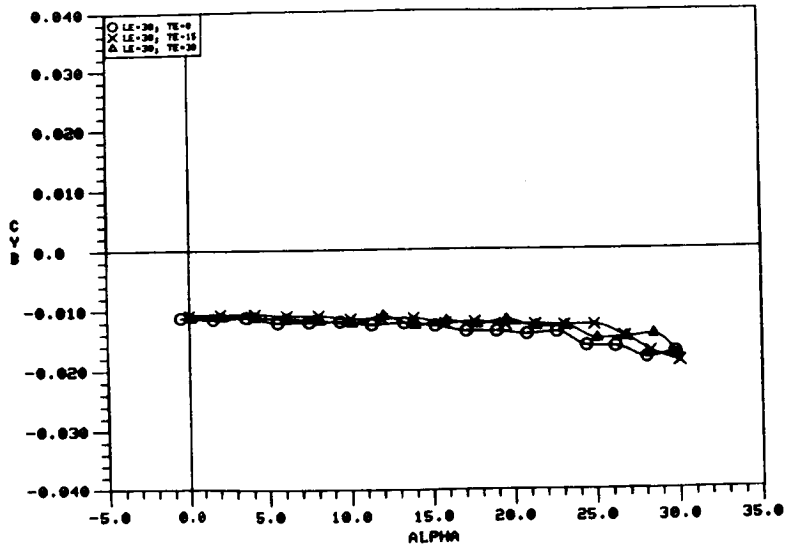

c) C_{Y_β} vs. α

Figure 227. Effect of Trailing-Edge Flap Deflection on the 50-Degree Cropped Delta Wing Static Lateral-Directional Stability Characteristics with $\delta_n = 30°$.

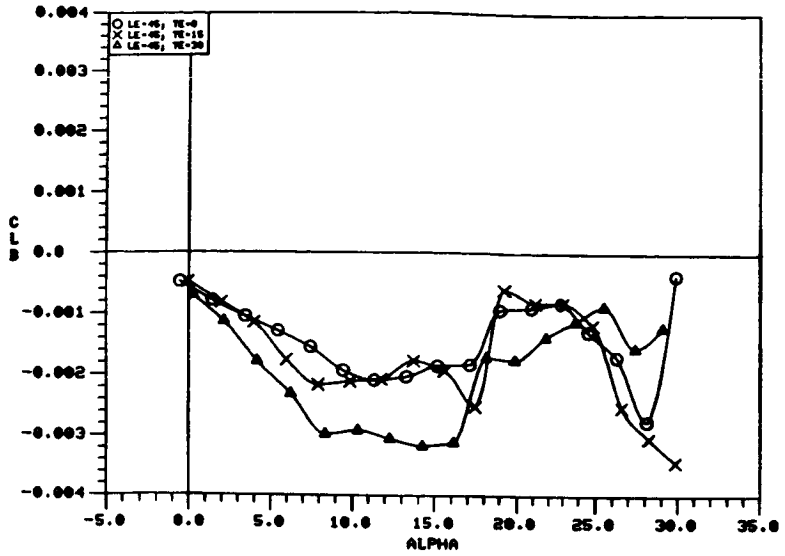

O	LE = 45,	TE =	0
X	LE = 45,	TE =	15
△	LE = 45,	TE =	30

a) C_{ℓ_β} vs. α

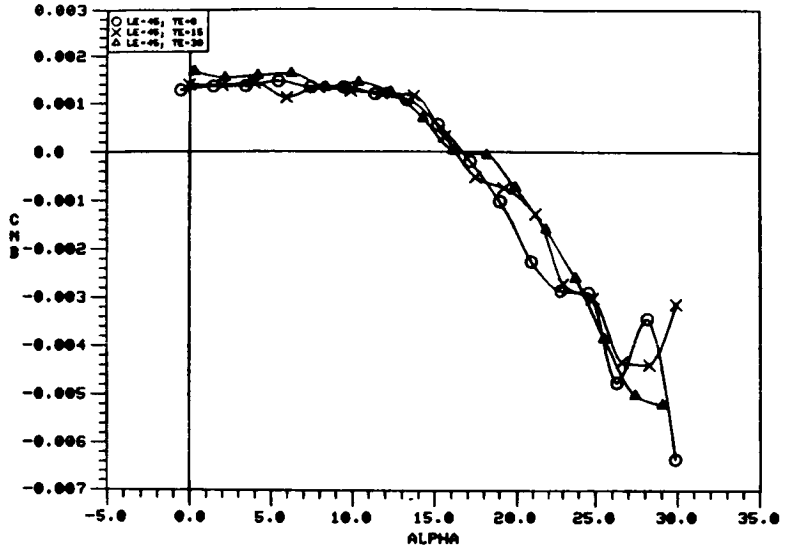

b) C_{n_β} vs. α

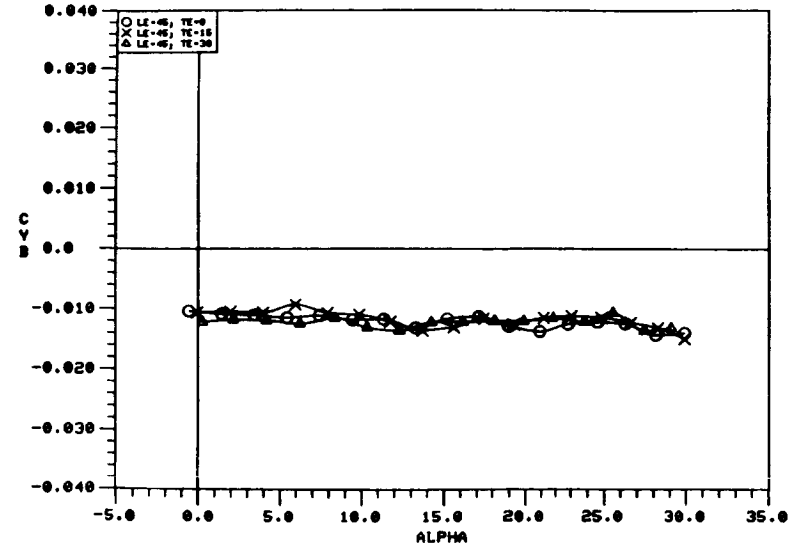

c) C_{Y_β} vs. α

Figure 228. Effect of Trailing-Edge Flap Deflection on the 50-Degree Cropped Delta Wing Static Lateral-Directional Stability Characteristics with $\delta_n = 45°$.

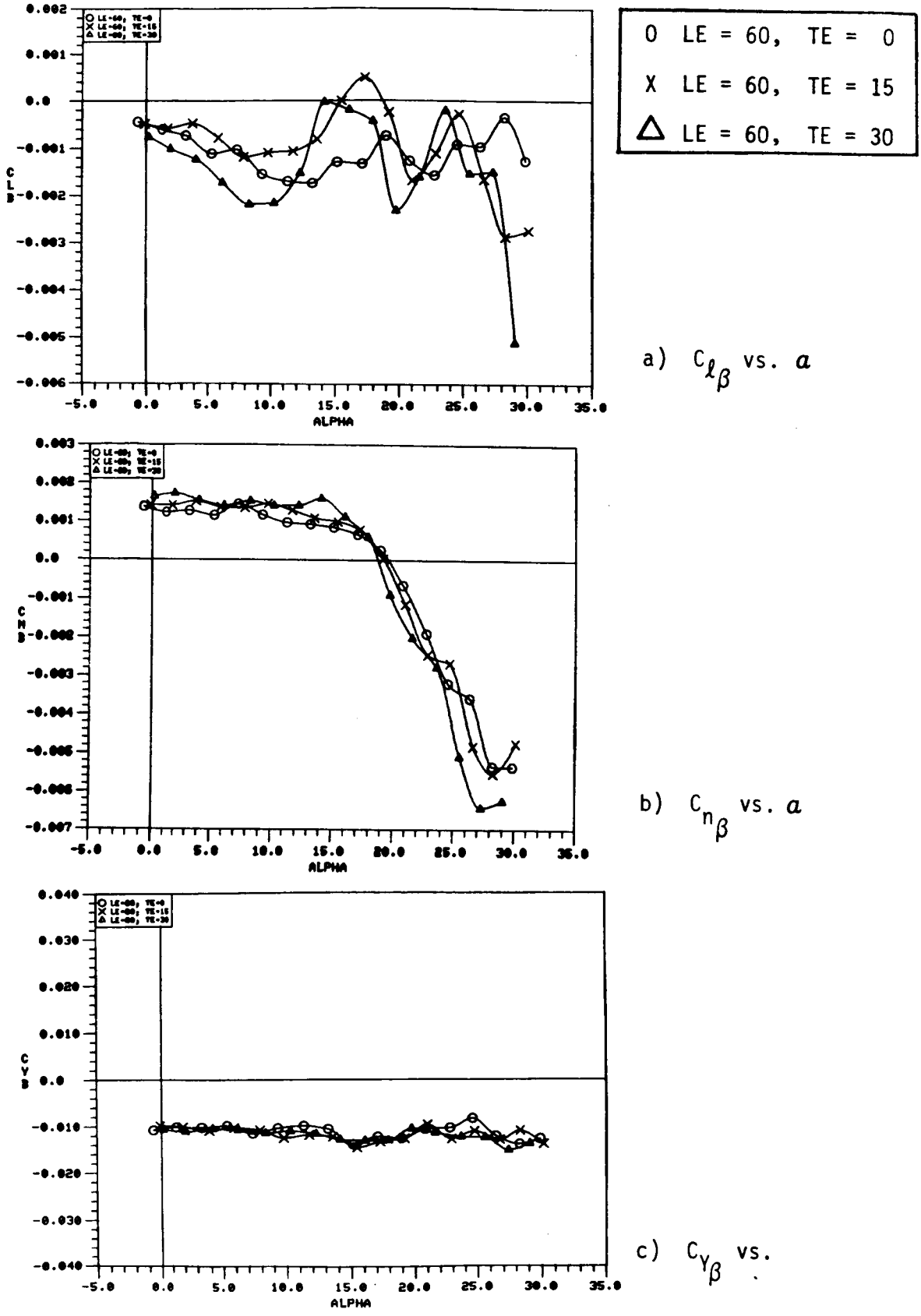

Figure 229. Effect of Trailing-Edge Flap Deflection on the 50-Degree Cropped Delta Wing Static Lateral-Directional Stability Characteristics with $\delta_n = 60°$.

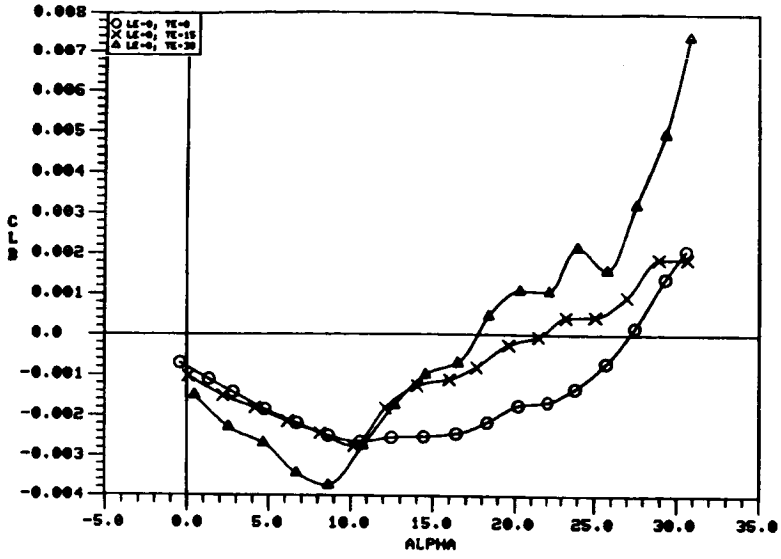

O	LE = 0,	TE =	0
X	LE = 0,	TE =	15
△	LE = 0,	TE =	30

a) C_{ℓ_β} vs. α

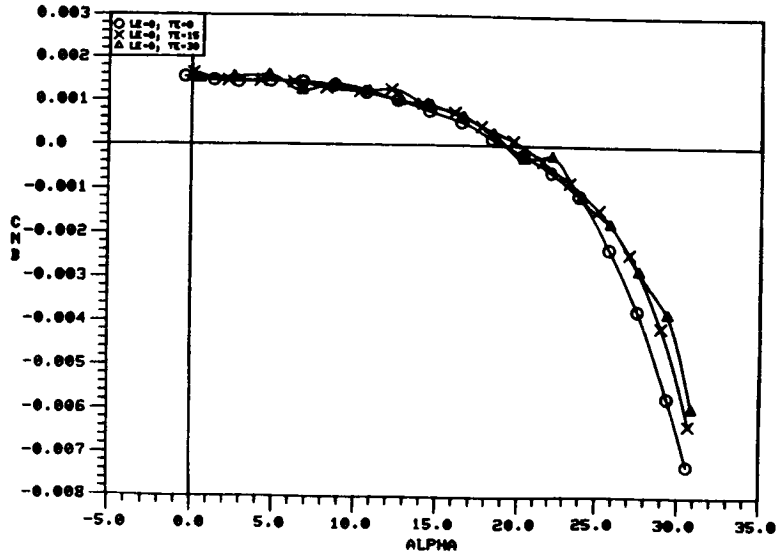

b) C_{n_β} vs. α

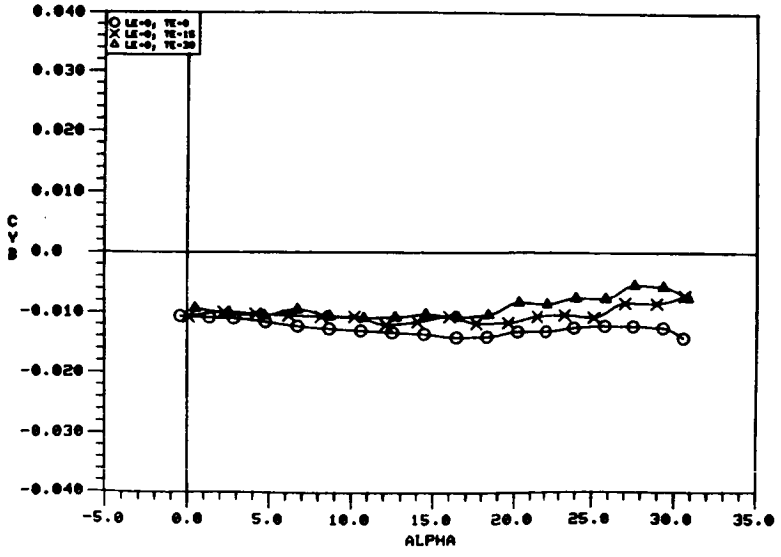

c) C_{Y_β} vs. α

Figure 230. Effect of Trailing-Edge Flap Deflection on the 60-Degree Cropped Delta Wing Static Lateral-Directional Stability Characteristics with $\delta_n = 0°$.

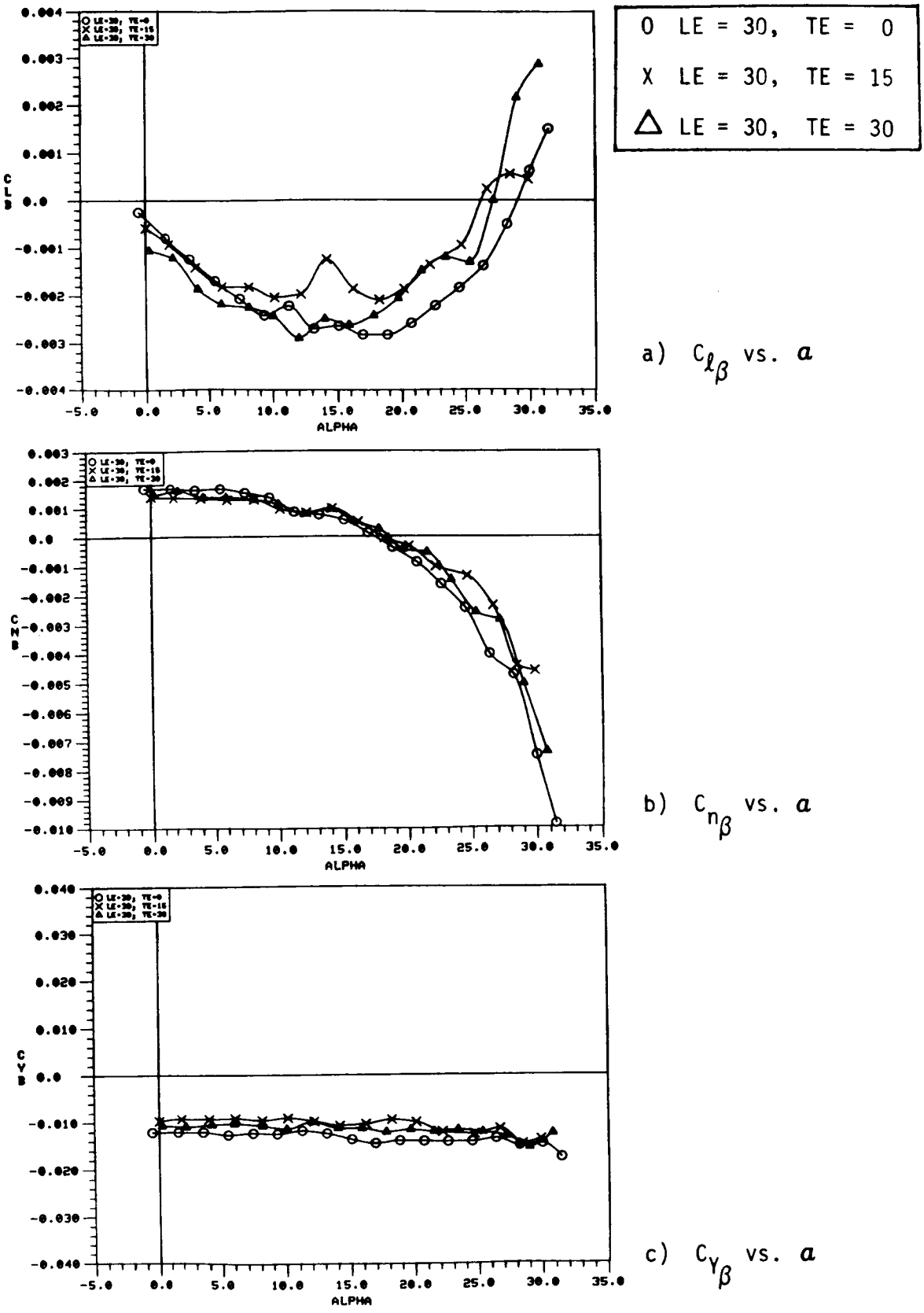

Figure 231. Effect of Trailing-Edge Flap Deflection on the 60-Degree Cropped Delta Wing Static Lateral-Directional Stability Characteristics with $\delta_n = 30°$.

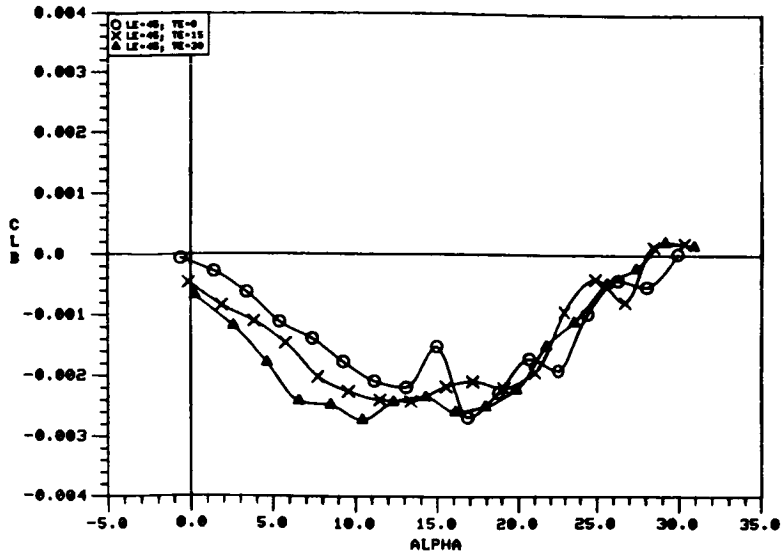

O	LE = 45,	TE =	0
X	LE = 45,	TE =	15
△	LE = 45,	TE =	30

a) C_{ℓ_β} vs. α

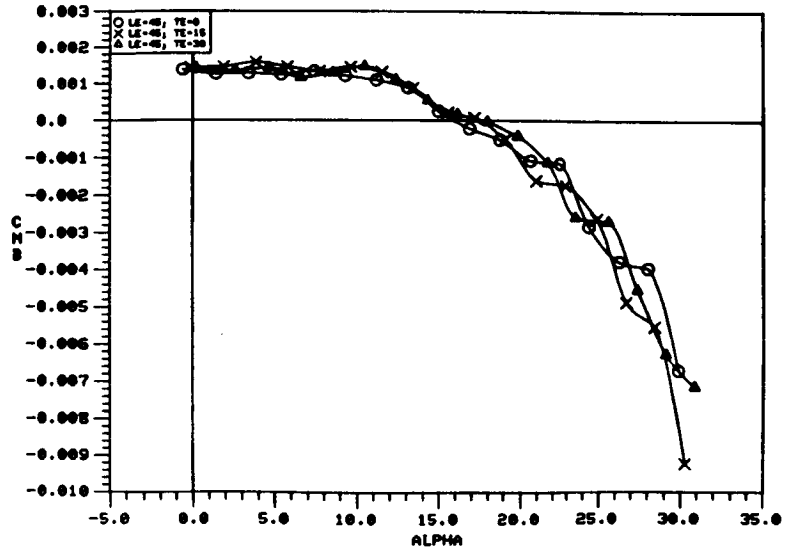

b) C_{n_β} vs. α

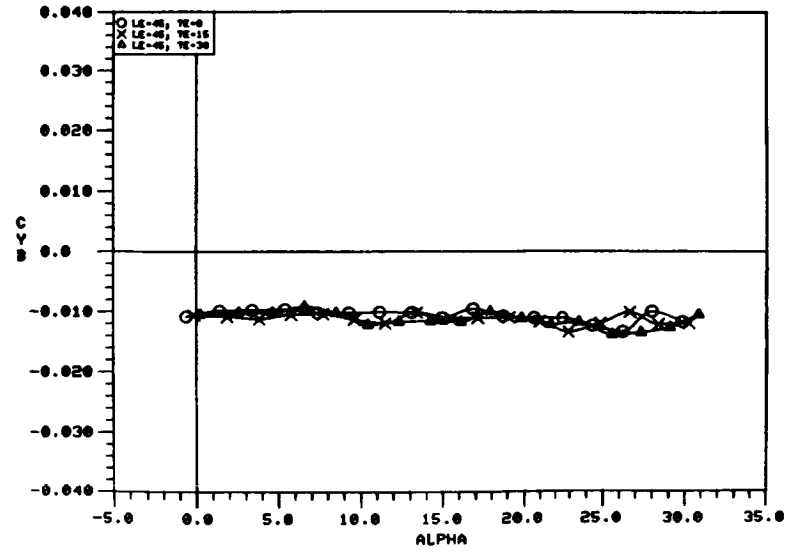

c) C_{Y_β} vs. α

Figure 232. Effect of Trailing-Edge Flap Deflection on the 60-Degree Cropped Delta Wing Static Lateral-Directional Stability Characteristics with δ_n = 45°.

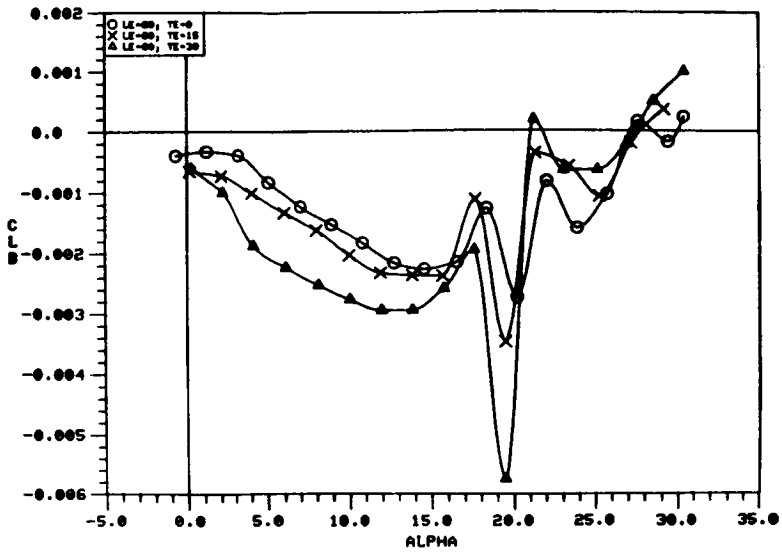

O	LE = 60,	TE =	0
X	LE = 60,	TE =	15
△	LE = 60,	TE =	30

a) C_{ℓ_β} vs. α

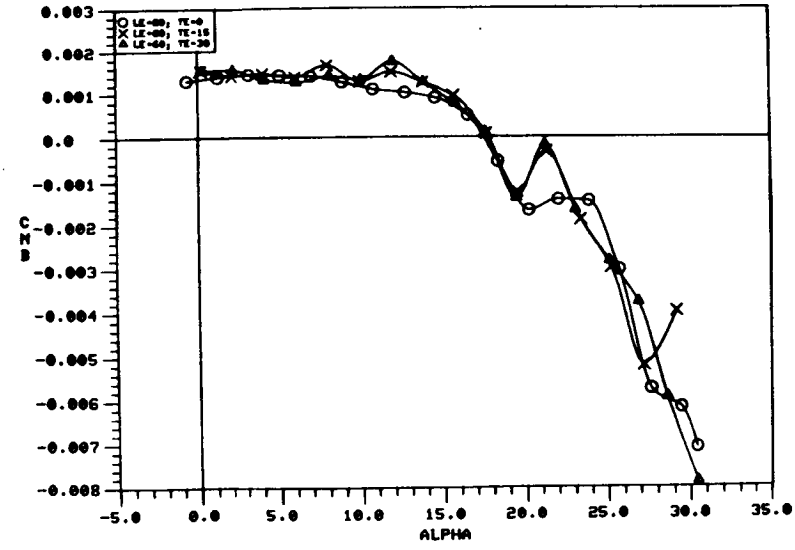

b) C_{n_β} vs. α

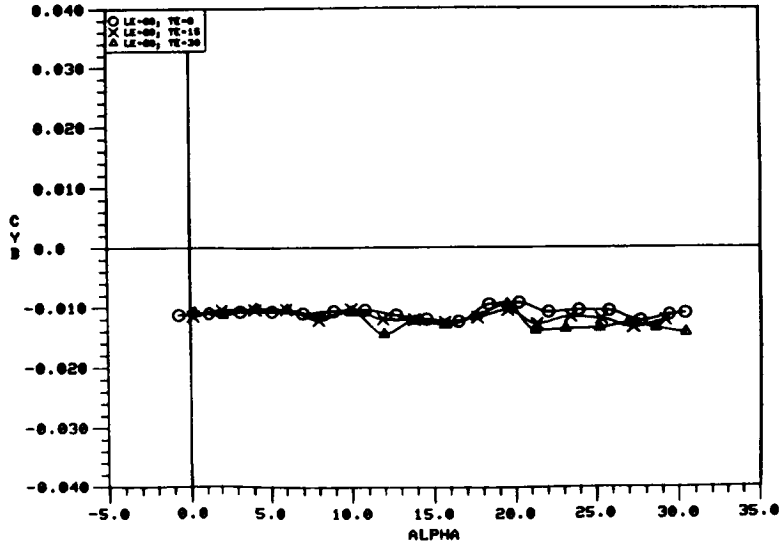

c) C_{Y_β} vs.

Figure 233. Effect of Trailing-Edge Flap Deflection on the 60-Degree Cropped Delta Wing Static Lateral-Directional Stability Characteristics with $\delta_n = 60°$.

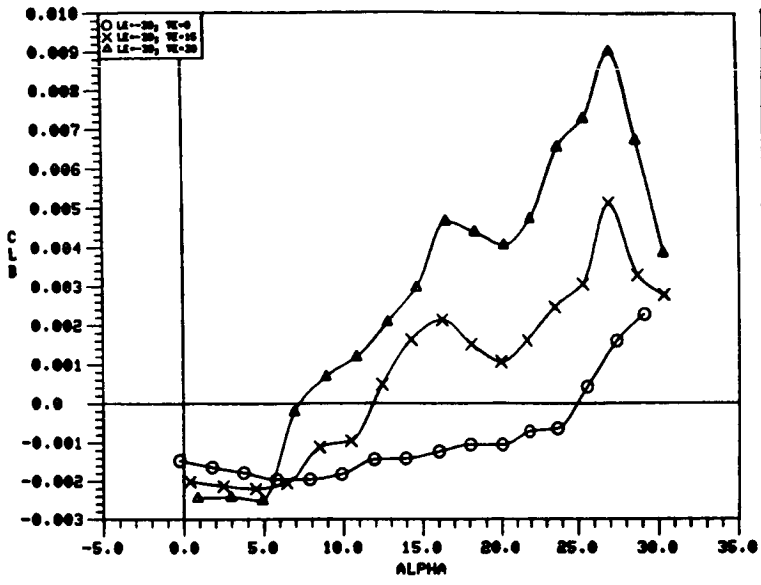

0 LE = -30, TE = 0

X LE = -30, TE = 15

△ LE = -30, TE = 30

a) C_{ℓ_β} vs. α

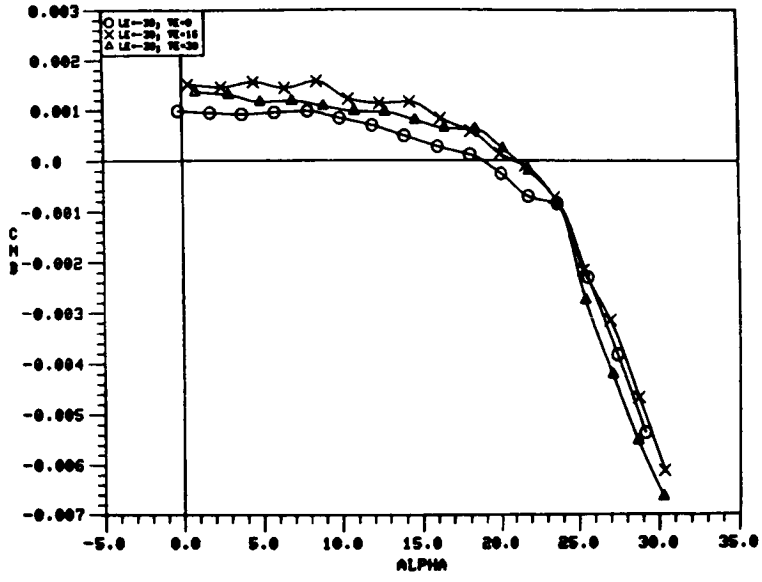

b) C_{n_β} vs. α

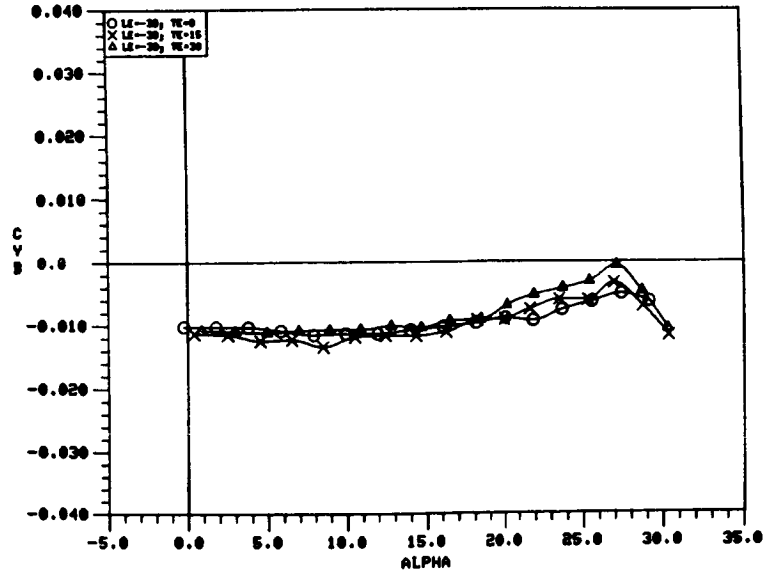

c) C_{Y_β} vs. α

Figure 234. Effect of Trailing-Edge Flap Deflection on the 60-Degree Cropped Delta Wing Static Lateral-Directional Stability Characteristics with δ_n =-30°.

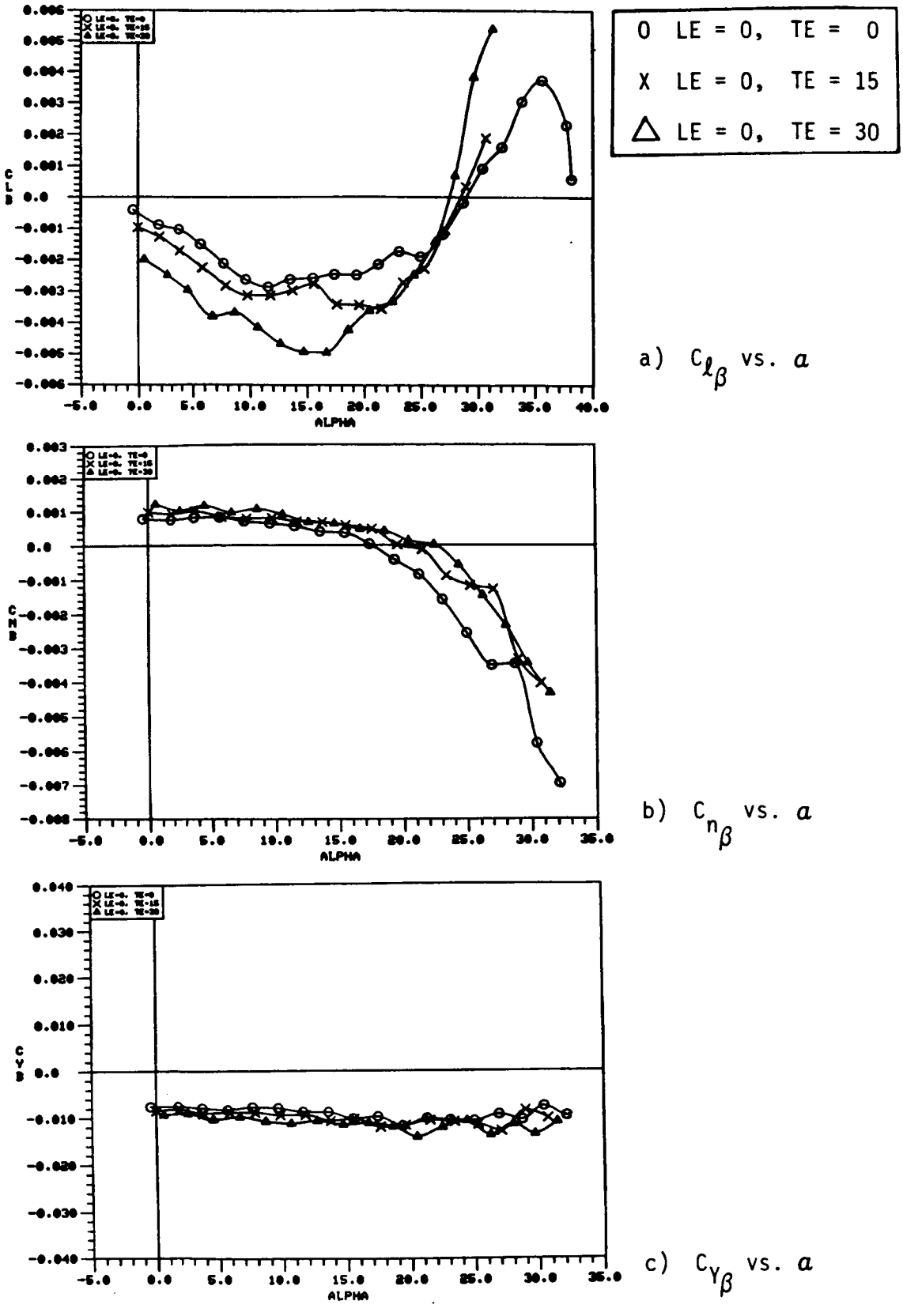

Figure 235. Effect of Trailing-Edge Flap Deflection on the 65-Degree Cropped Delta Wing Static Lateral-Directional Stability Characteristics with $\delta_n = 0°$.

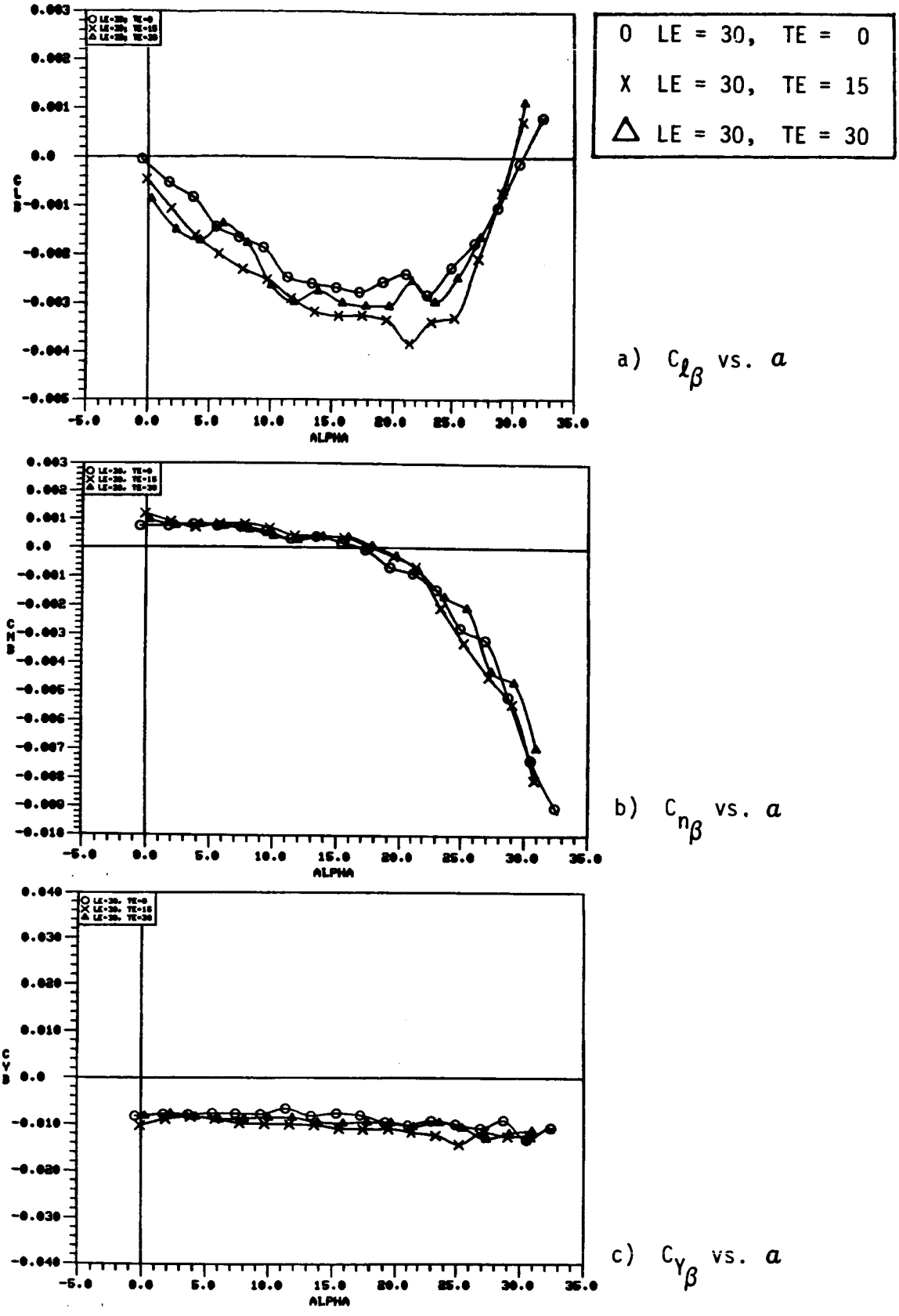

Figure 236. Effect of Trailing-Edge Flap Deflection on the 65-Degree Cropped Delta Wing Static Lateral-Directional Stability Characteristics with $\delta_n = 30°$.

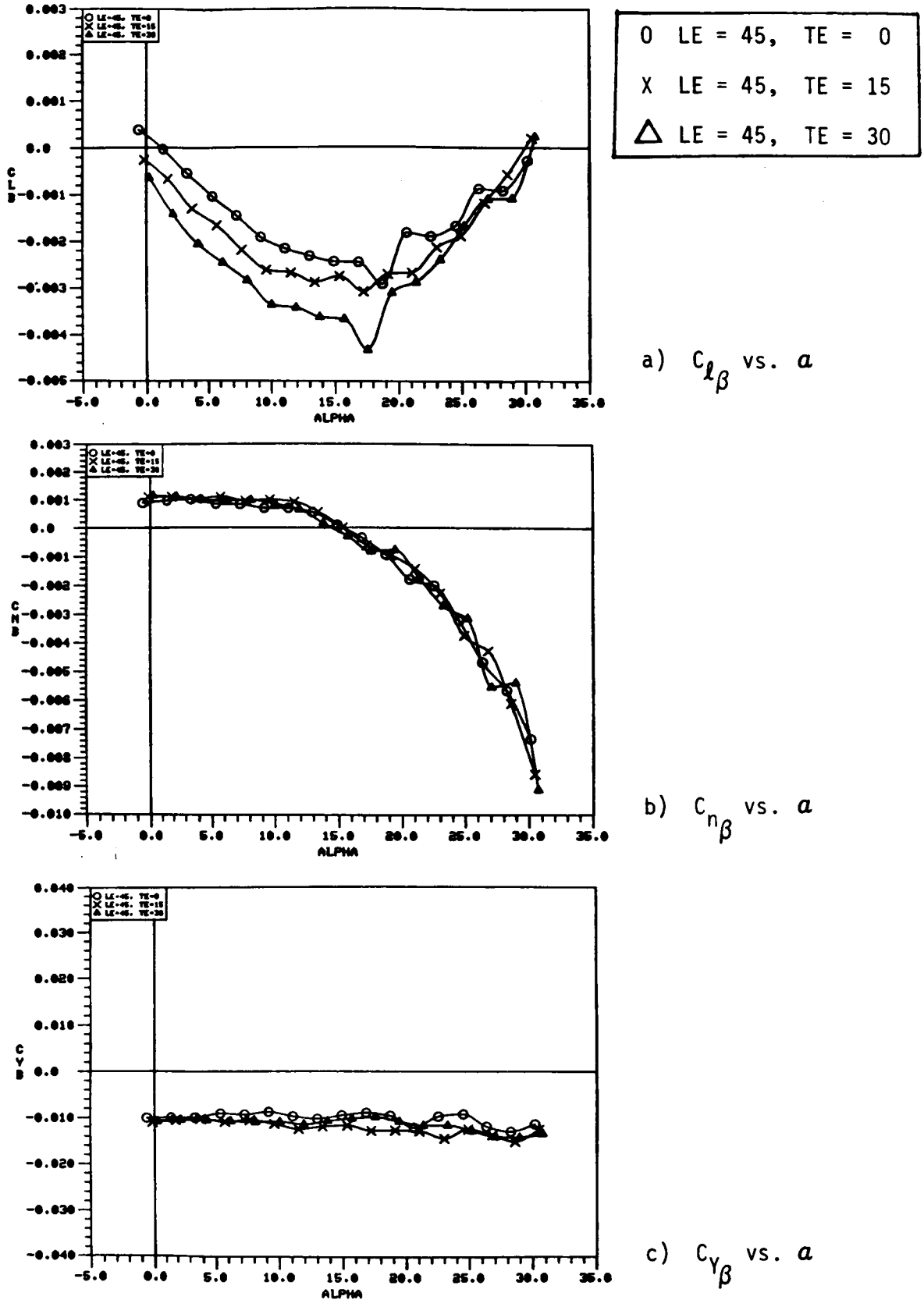

Figure 237. Effect of Trailing-Edge Flap Deflection on the 65-Degree Cropped Delta Wing Static Lateral-Directional Stability Characteristics with $\delta_n = 45°$.

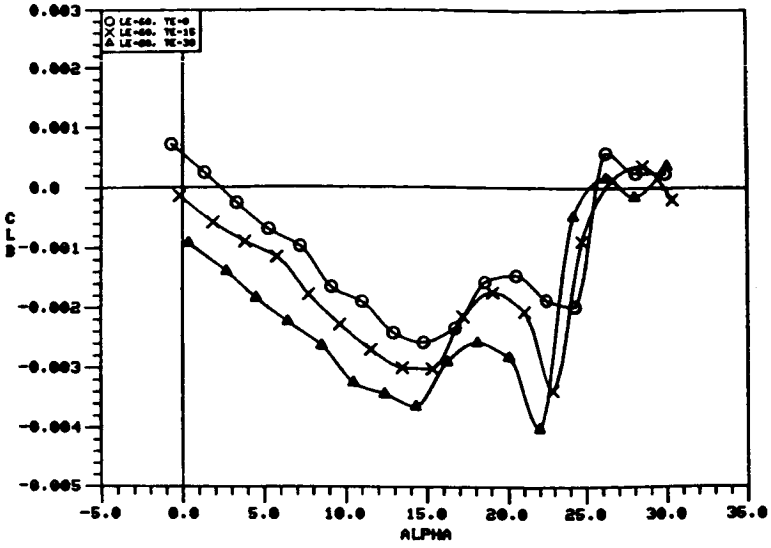

0	LE = 60,	TE =	0
X	LE = 60,	TE =	15
△	LE = 60,	TE =	30

a) C_{ℓ_β} vs. α

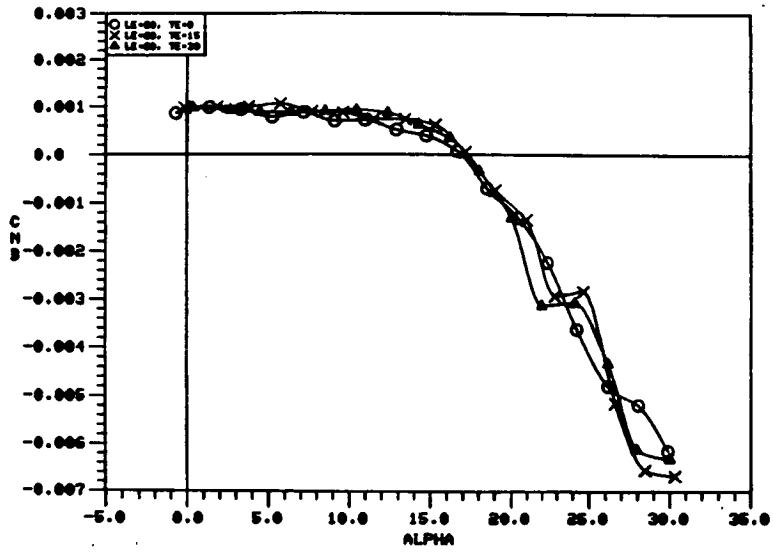

b) C_{n_β} vs. α

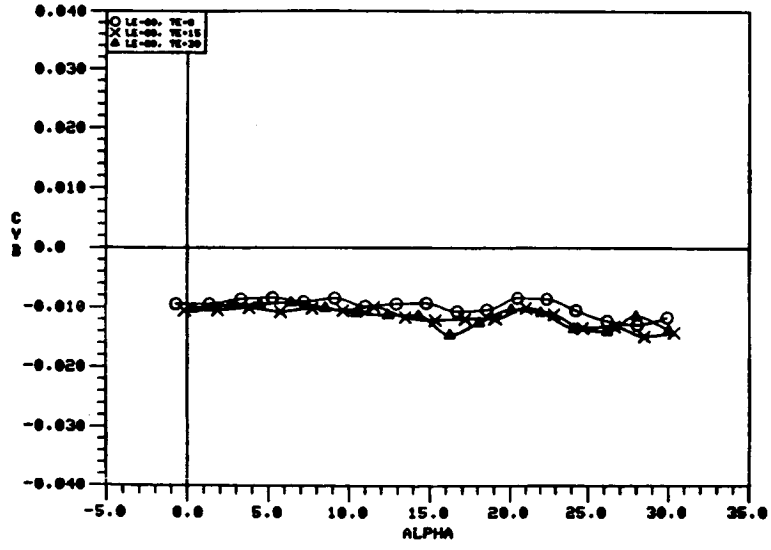

c) C_{Y_β} vs.

Figure 238. Effect of Trailing-Edge Flap Deflection on the 65-Degree Cropped Delta Wing Static Lateral-Directional Stability Characteristics with $\delta_n = 60°$.

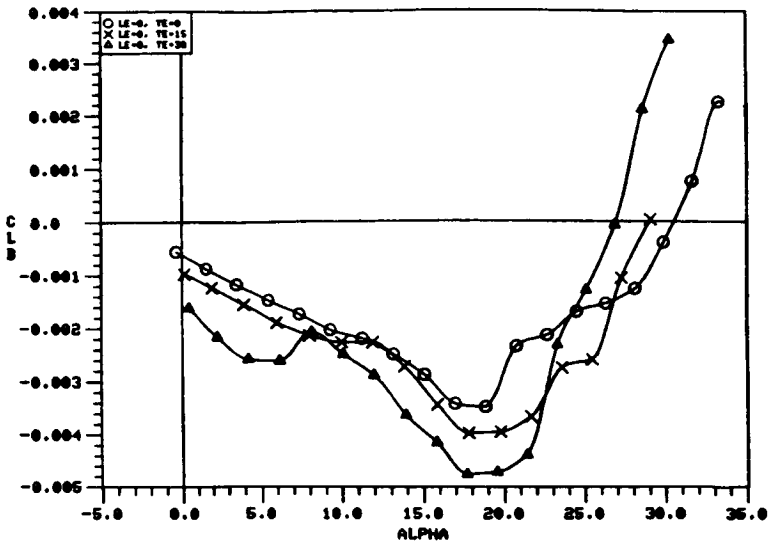

O	LE = 0,	TE =	0
X	LE = 0,	TE =	15
△	LE = 0,	TE =	30

a) C_{ℓ_β} vs. α

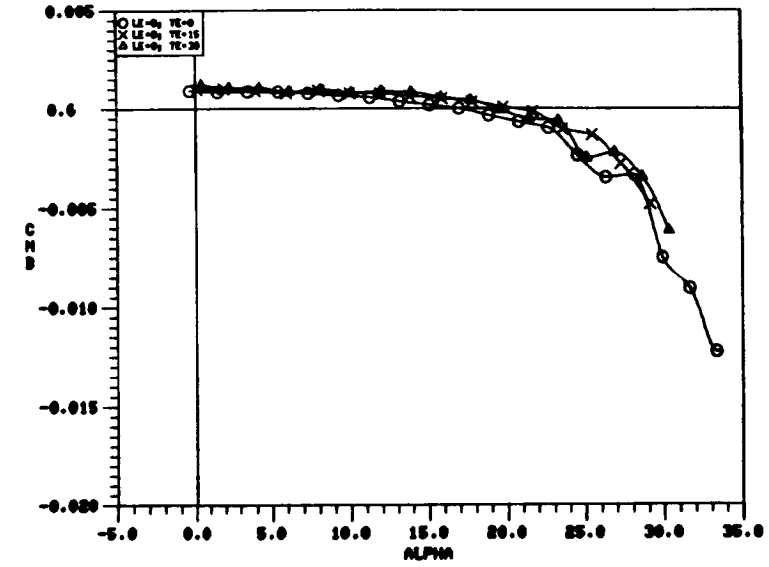

b) C_{n_β} vs. α

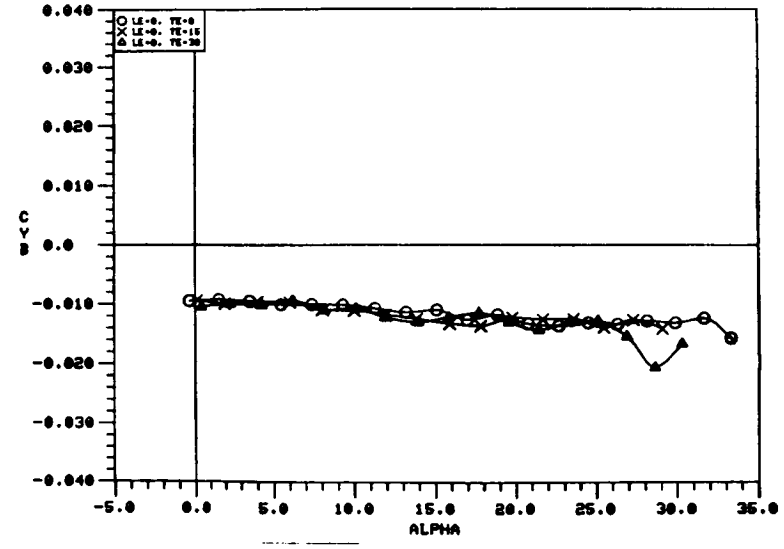

c) C_{Y_β} vs. α

Figure 239. Effect of Trailing-Edge Flap Deflection on the 70/50-Degree Cranked Wing Static Lateral-Directional Stability Characteristics with $\delta_n = 0°$.

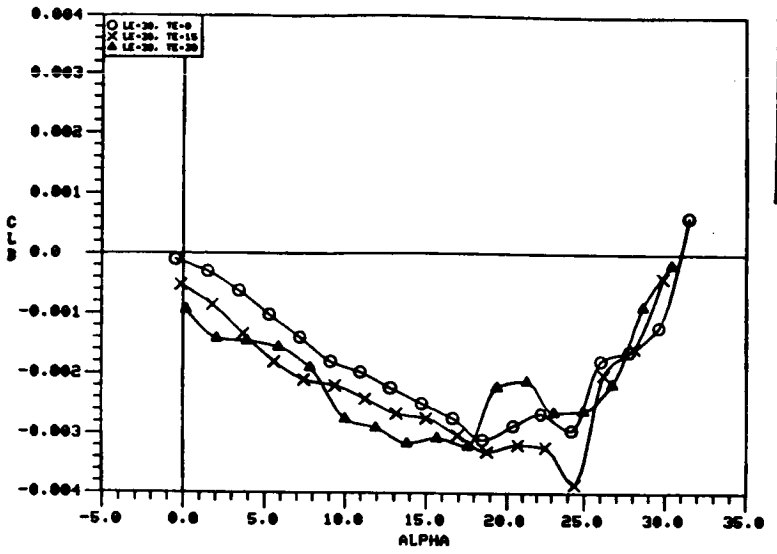

O	LE = 30,	TE =	0
X	LE = 30,	TE =	15
△	LE = 30,	TE =	30

a) C_{ℓ_β} vs. α

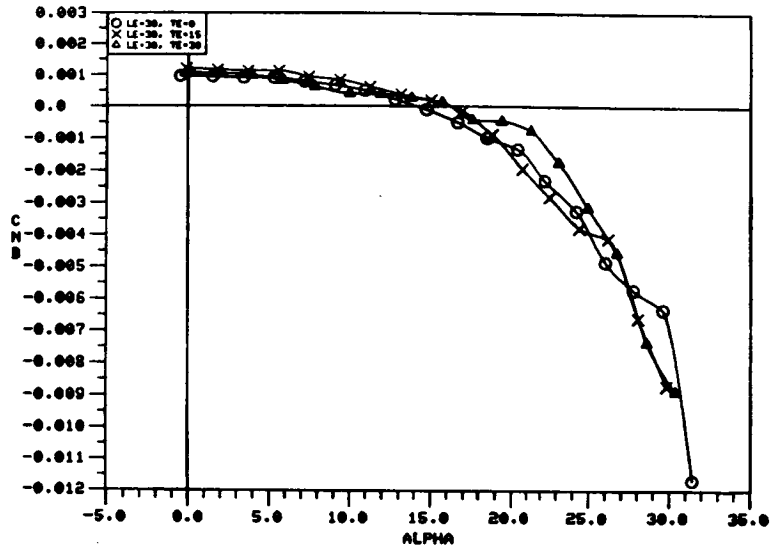

b) C_{n_β} vs. α

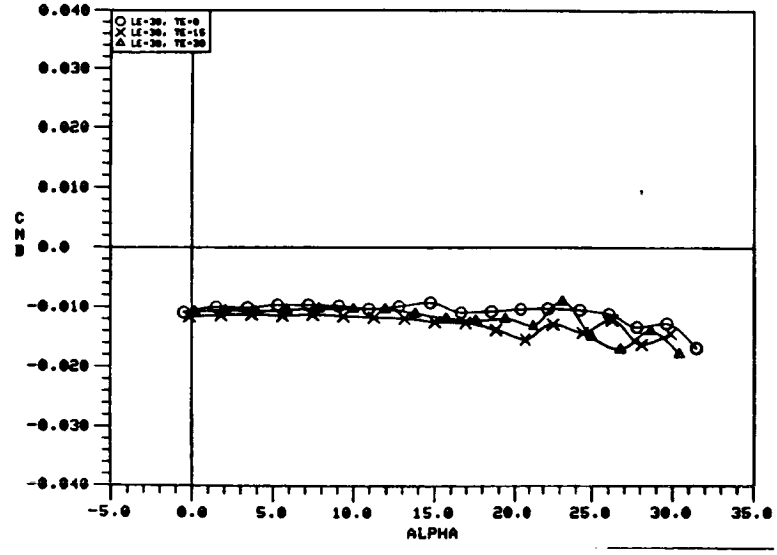

c) C_{Y_β} vs. α

Figure 240. Effect of Trailing-Edge Flap Deflection on the 70/50-Degree Cranked Wing Static Lateral-Directional Stability Characteristics with $\delta_n = 30°$.

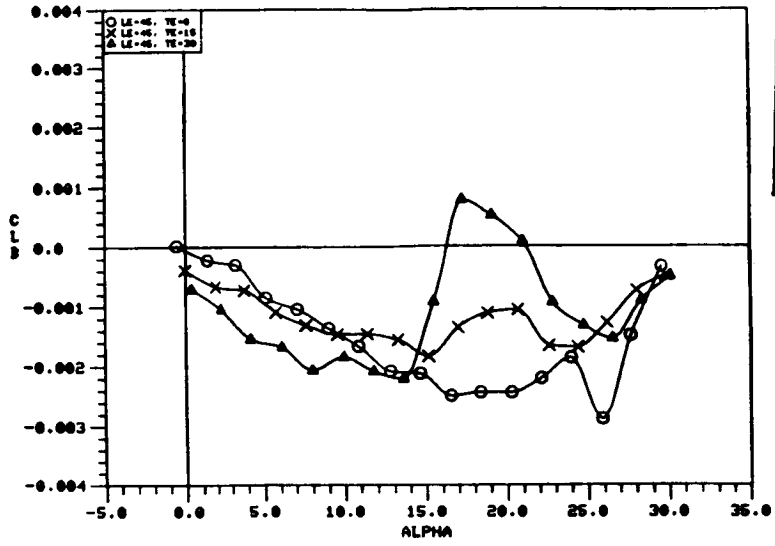

a) C_{ℓ_β} vs. α

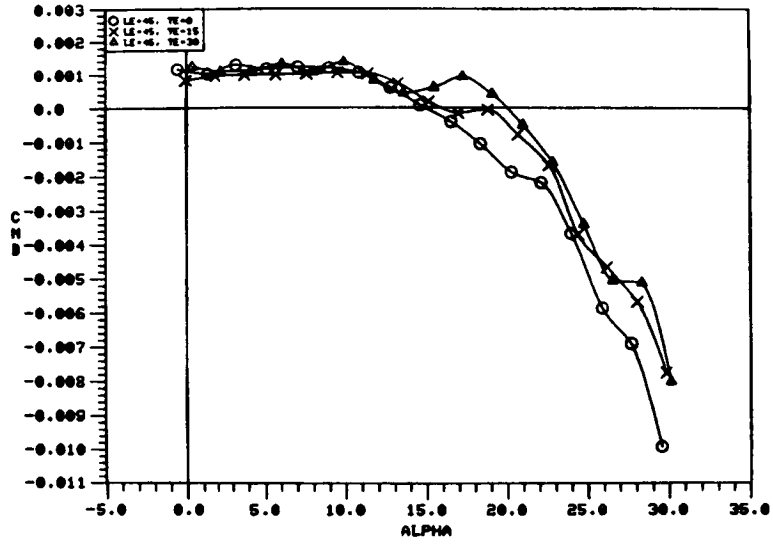

b) C_{n_β} vs. α

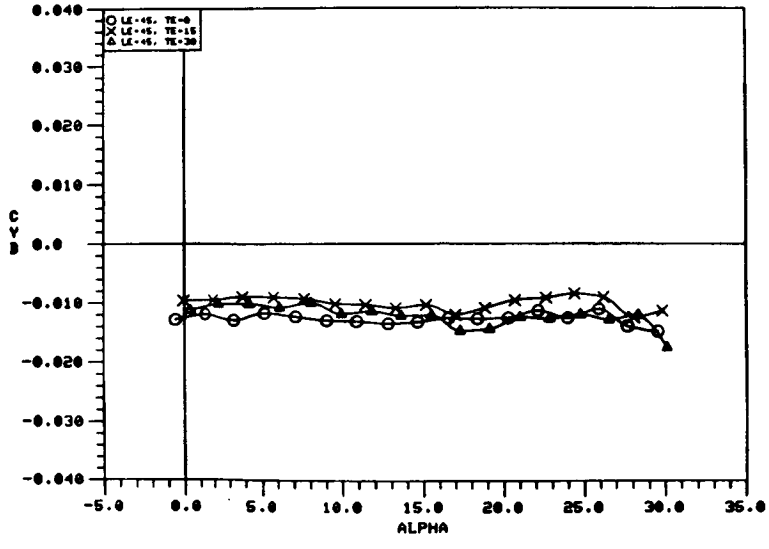

c) C_{Y_β} vs. α

Figure 241. Effect of Trailing-Edge Flap Deflection on the 70/50-Degree Cranked Wing Static Lateral-Directional Stability Characteristics with $\delta_n = 45°$.

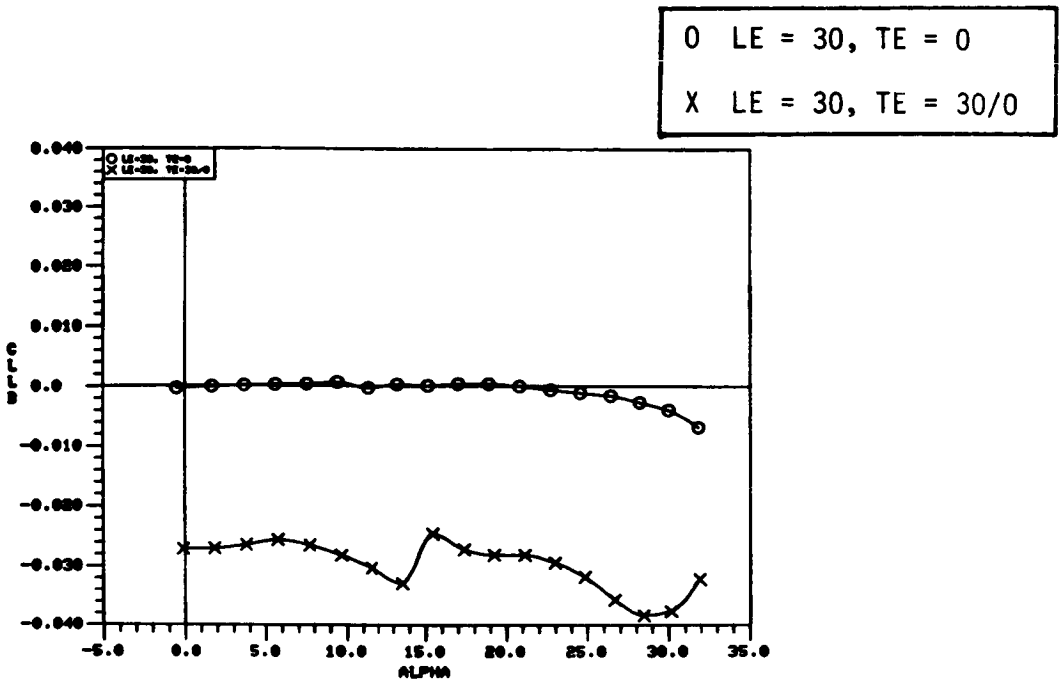

C_ℓ vs. α

Figure 242. Incremental Rolling Moment of the 60-Degree Cropped Delta Wing due to Differential Trailing-Edge Flap Deflection.

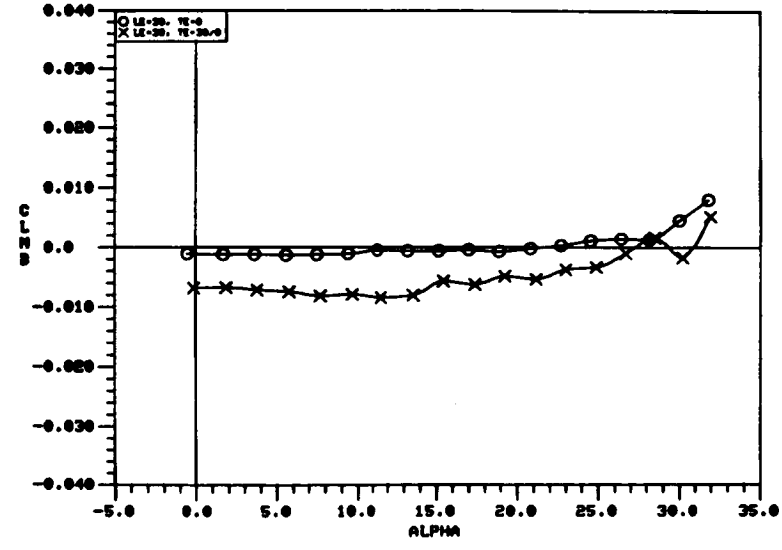

C_n vs. α

Figure 243. Incremental Yawing Moment of the 60-Degree Cropped Delta Wing due to Differential Trailing-Edge Flap Deflection.

O	LE = 30,	TE = 0,	β = 0
X	LE = 30,	TE = 0,	β = 5
Δ	LE = 30,	TE = 30/0,	β = 0
$\square$	LE = 30,	TE = 30/0,	β = 5

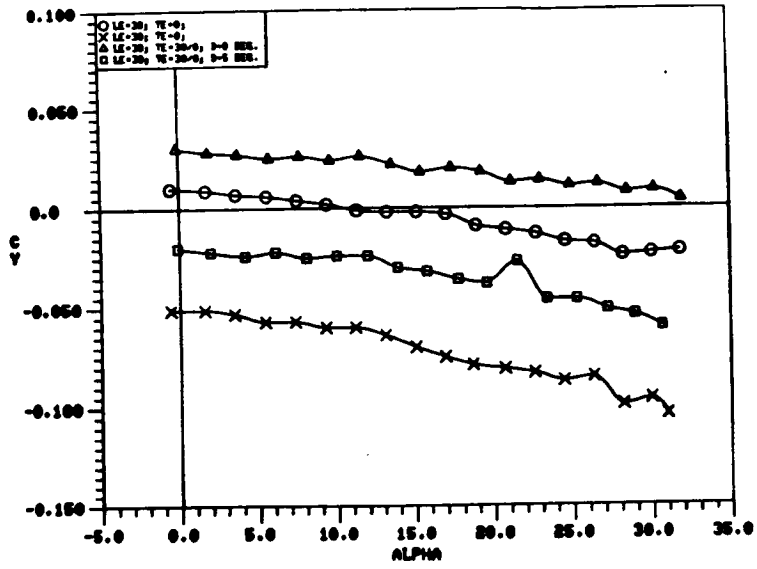

C_Y vs. α

Figure 244. Effect of Differential Trailing-Edge Flap Deflection on the 60-Degree Cropped Delta Wing Sideforce Characteristics.

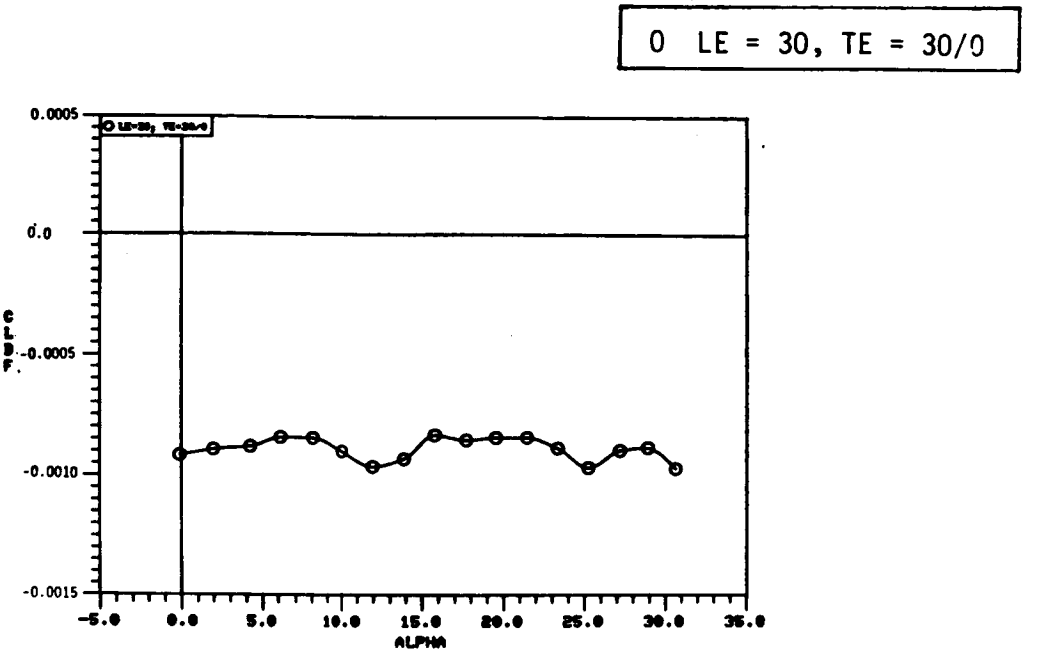

$C_{\ell_{\delta_f}}$ vs. α

Figure 245. Lateral Control of the 60-Degree Cropped Delta Wing due to Differential Trailing-Edge Flap Deflection.

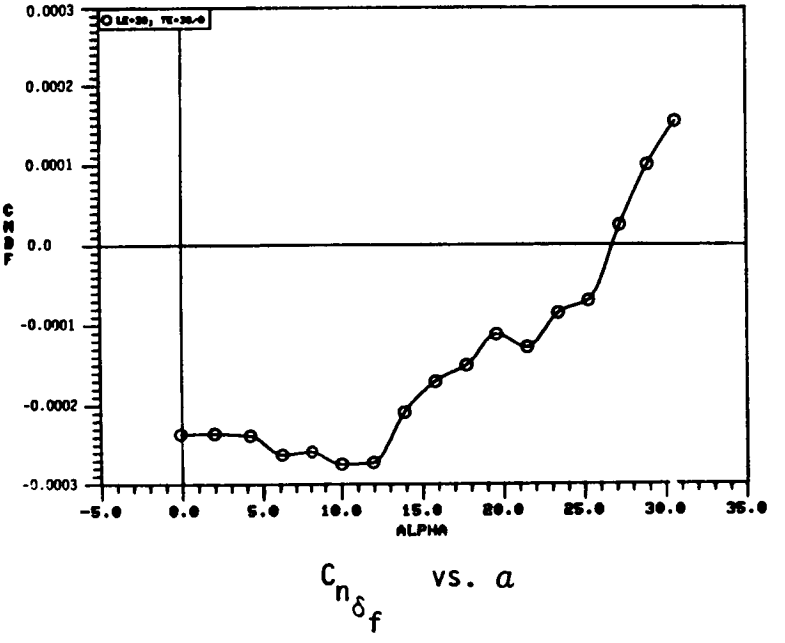

$C_{n_{\delta_f}}$ vs. α

Figure 246. Directional Control of the 60-Degree Cropped Delta Wing due to Differential Trailing-Edge Flap Deflection.

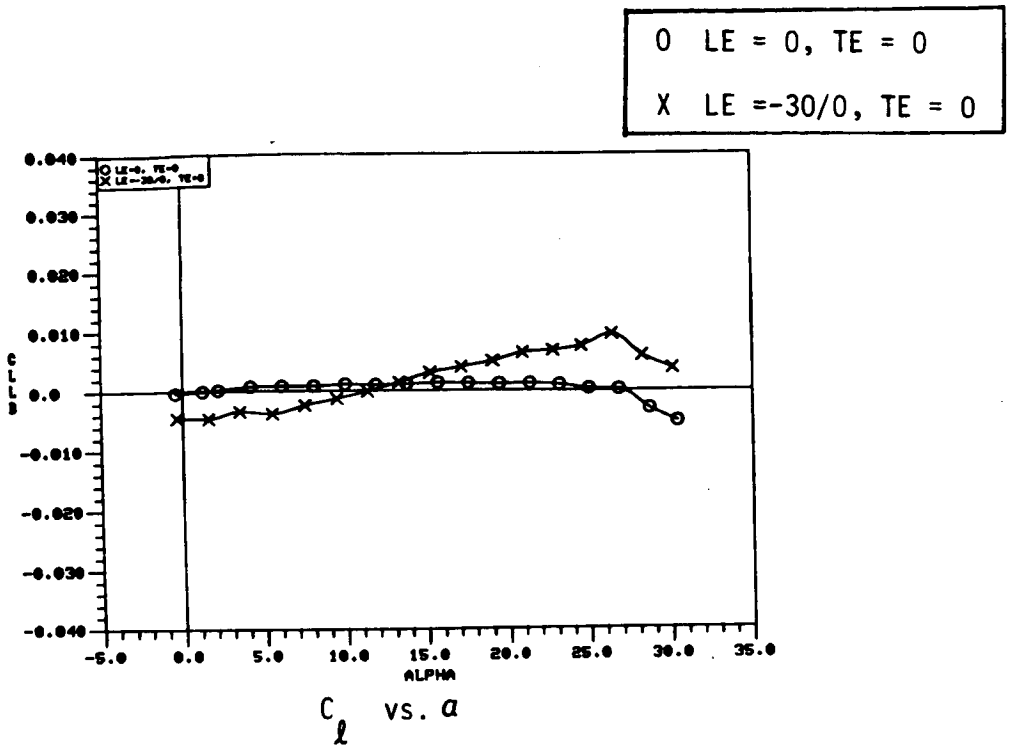

C_{ℓ} vs. α

Figure 247. Incremental Rolling Moment of the 60-Degree Cropped Delta Wing due to Differentially Inverted Leading-Edge Flaps.

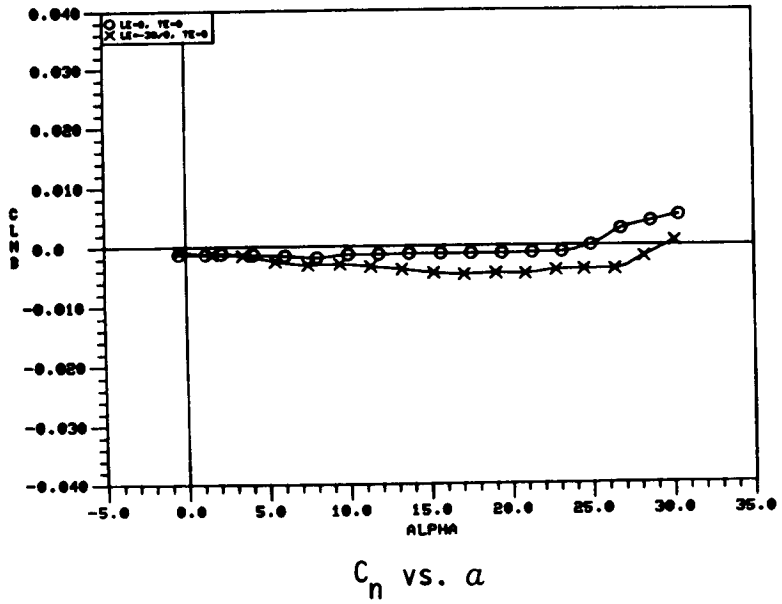

C_n vs. α

Figure 248. Incremental Yawing Moment of the 60-Degree Cropped Wing due to Differentially Inverted Leading-Edge Flaps.

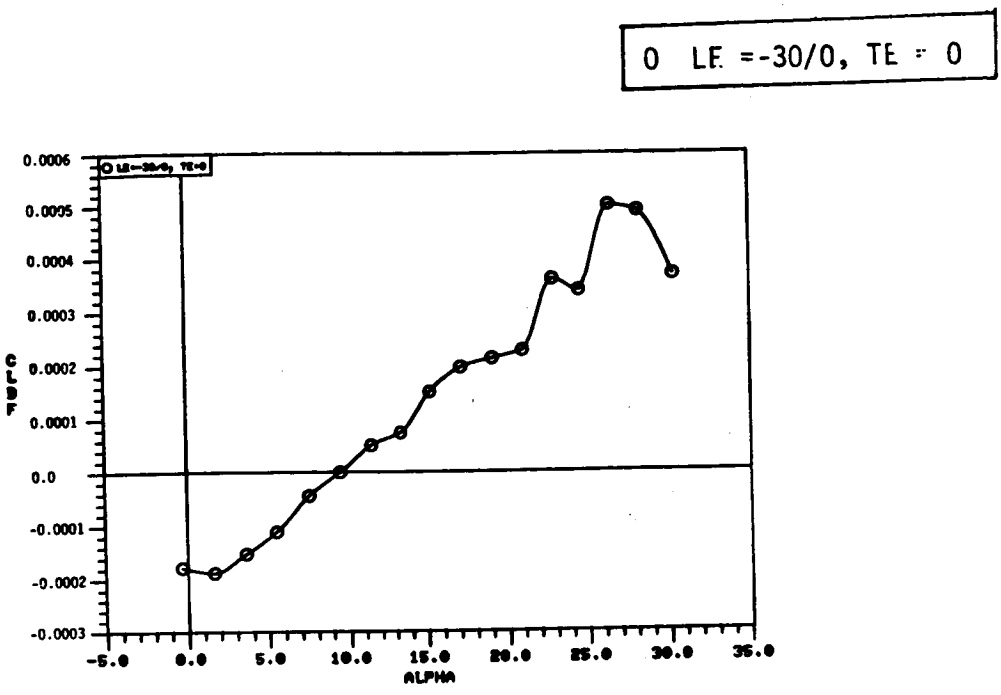

$C_{\ell_{\delta_n}}$ vs. α

Figure 249. Lateral Control of the 60-Degree Cropped Delta Wing due to Differentially Inverted Leading-Edge Flaps.

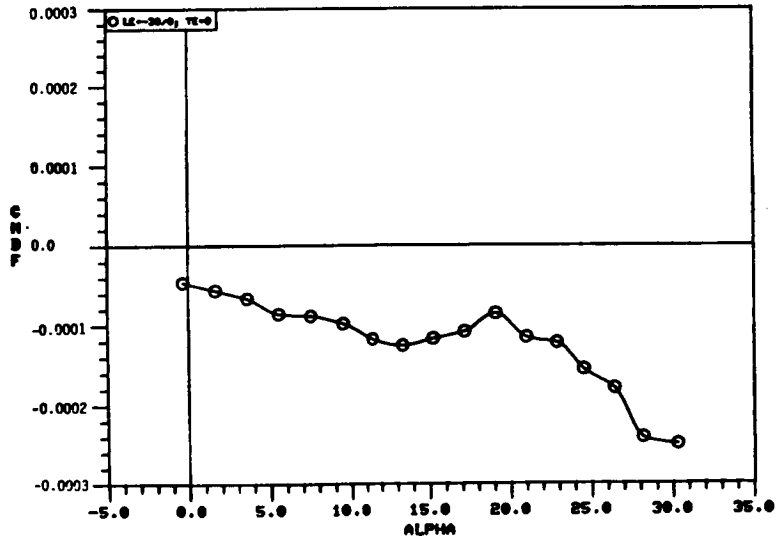

$C_{n_{\delta_f}}$ vs. α

Figure 250. Directional Control of the 60-Degree Cropped Delta Wing due to Differentially Inverted Leading-Edge Flaps.

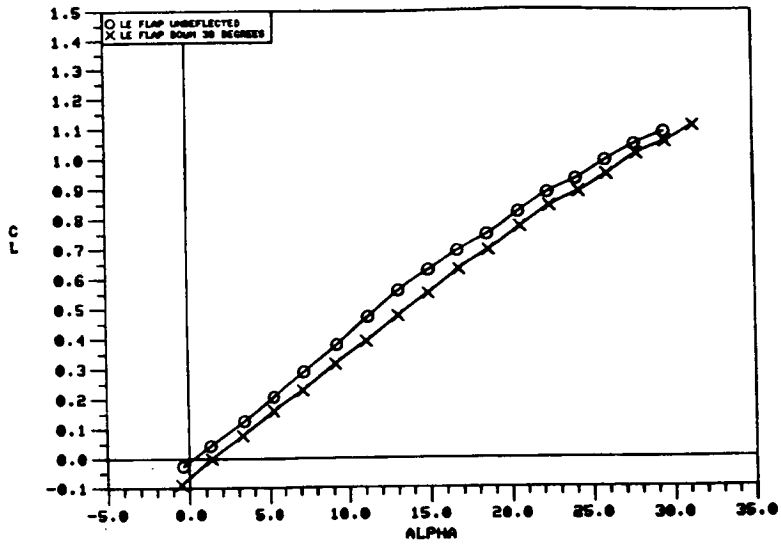

O LE FLAP UNDEFLECTED
X LE FLAP DOWN 30 DEGREES

a) C_L vs. α

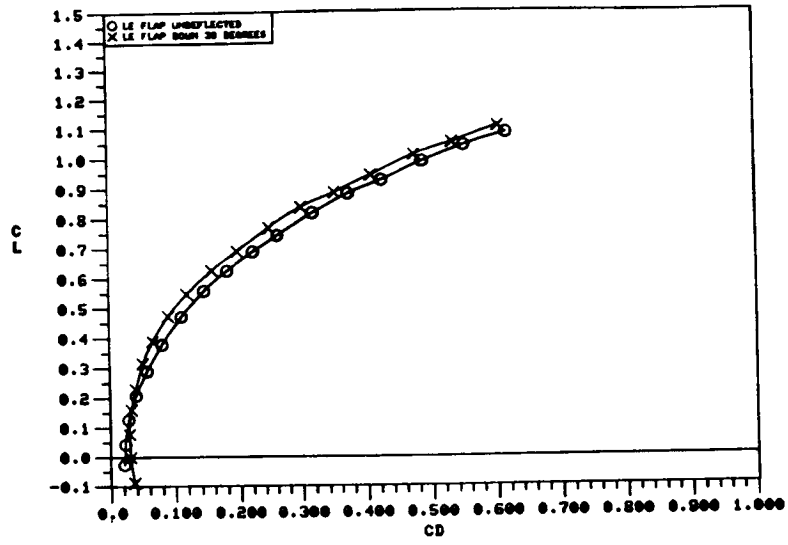

b) C_L vs. C_D

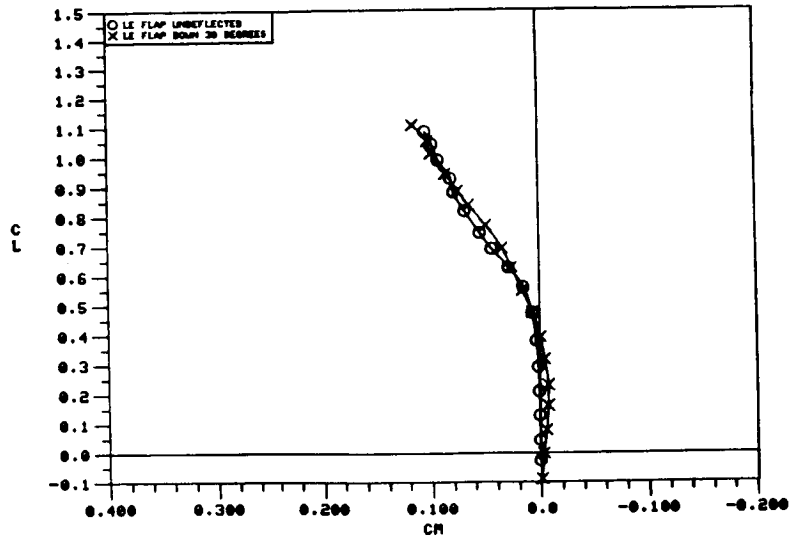

c) C_L vs. C_m

Figure 251. Effect of Deflected Vortex Flap on the Static Longitudinal Aerodynamic Characteristics of the 70/50-Degree Cranked Wing with Outboard Fins.

O	LE FLAP UNDEFLECTED
X	LE FLAP DOWN 30 DEGREES

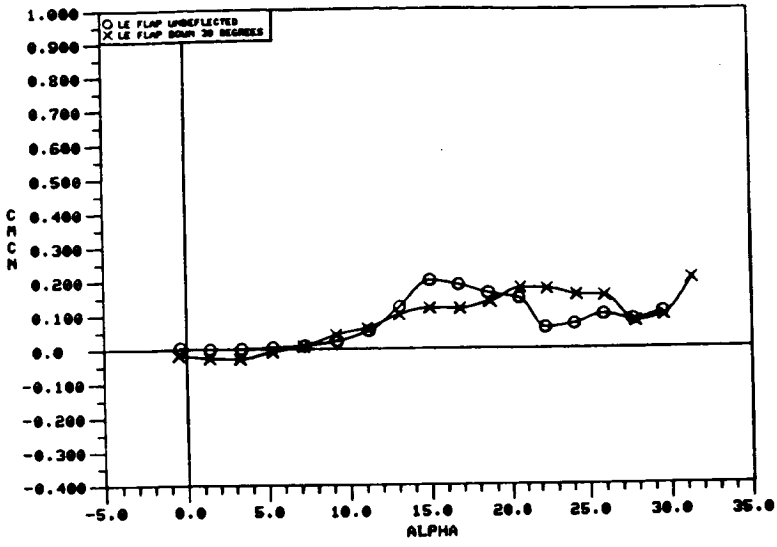

a) $C_{m_{C_N}}$ vs. α

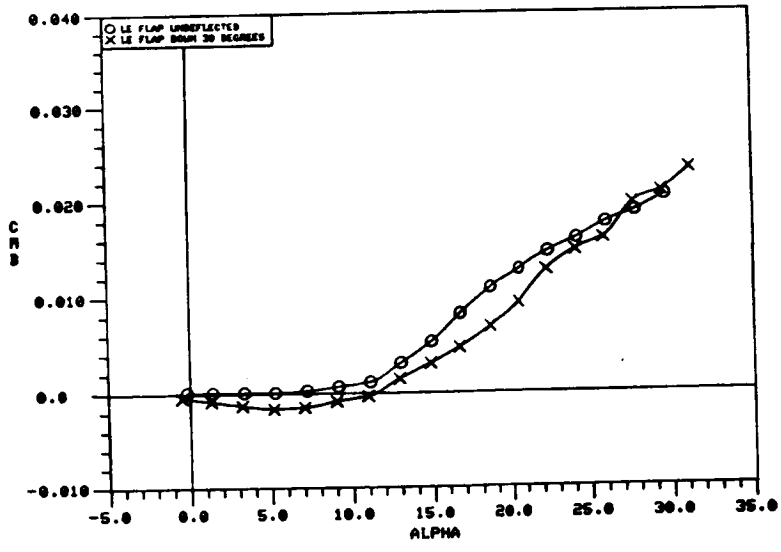

b) C_{m_β} vs. α

Figure 252. Effect of Deflected Vortex Flap on the Static Longitudinal Stability Characteristics of the 70/50-Degree Cranked Wing with Outboard Fins.

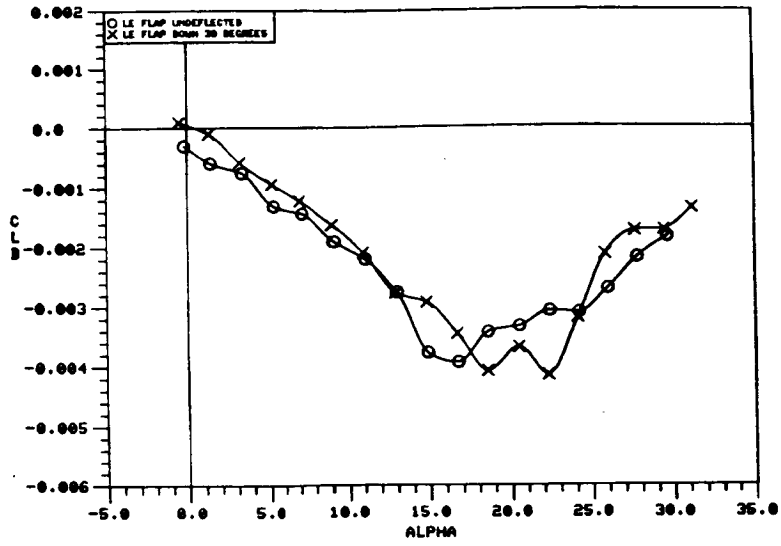

a) C_{ℓ_β} vs. α

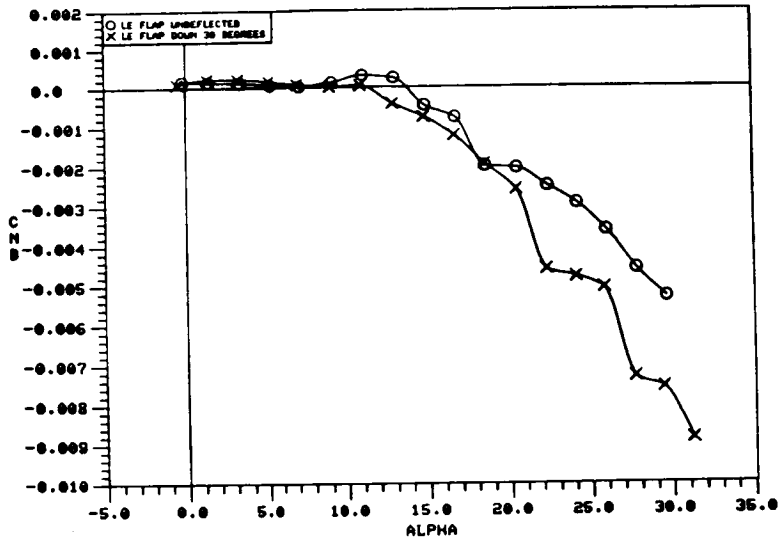

b) C_{n_β} vs. α

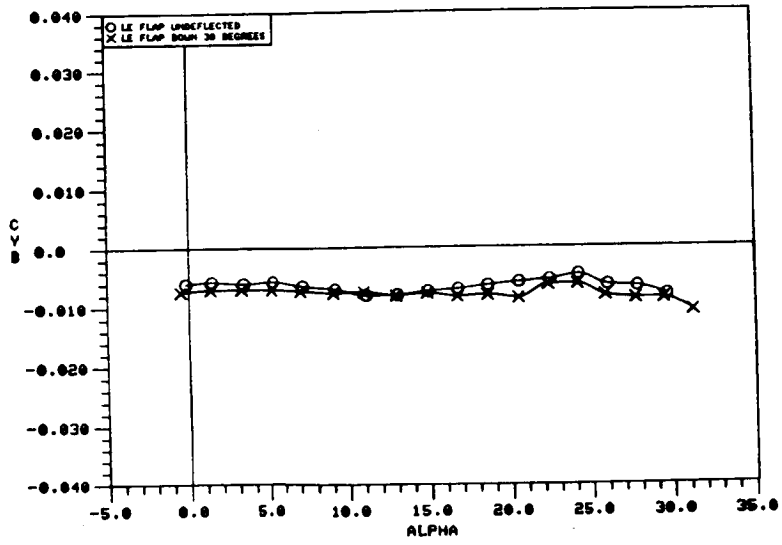

c) C_{Y_β} vs. α

Figure 253. Effect of Deflected Vortex Flap on the Static Lateral-Directional Stability Characteristics of the 70/50-Degree Cranked Wing with Outboard Fins.

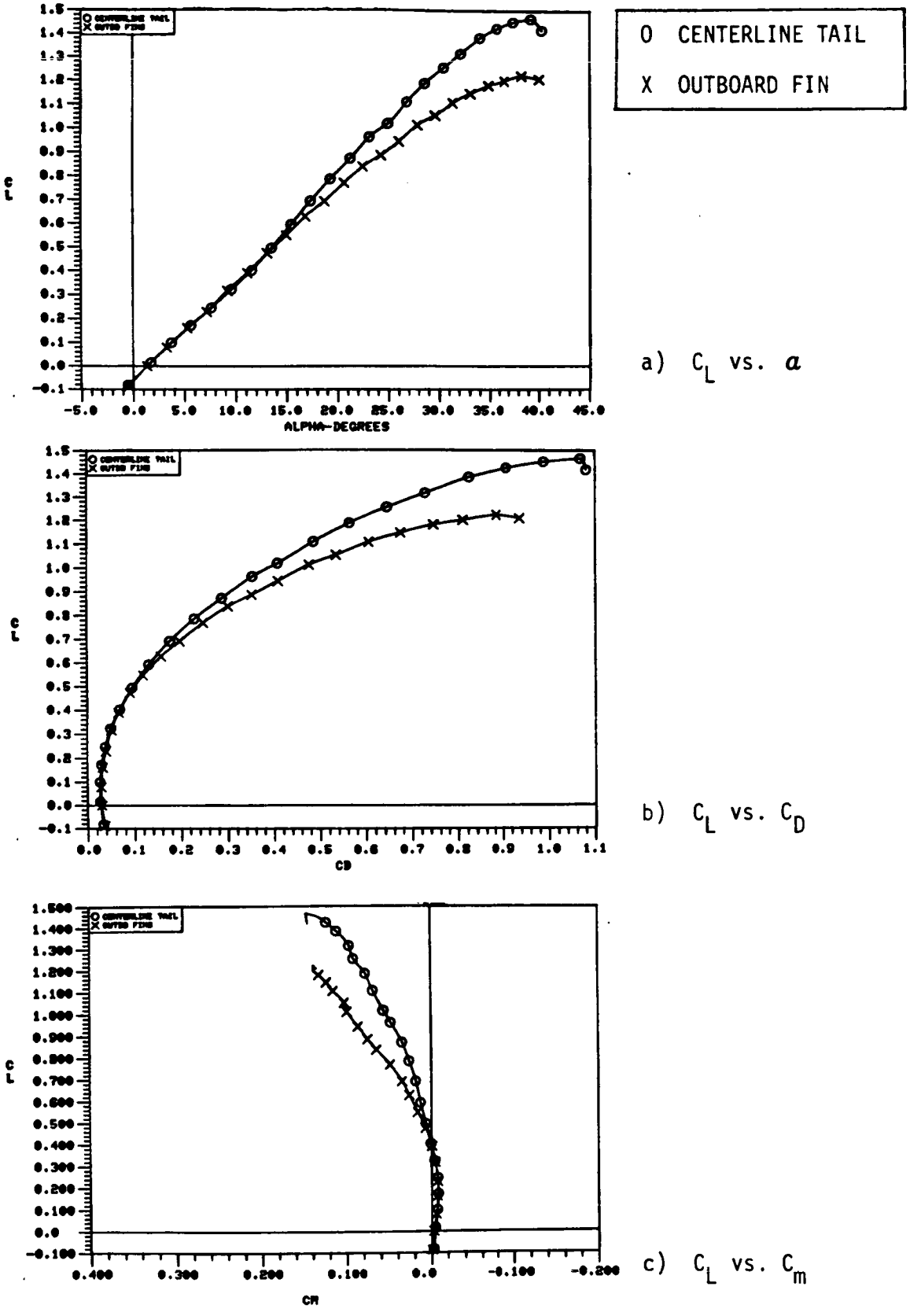

a) C_L vs. α

b) C_L vs. C_D

c) C_L vs. C_m

Figure 254. Effect of Outboard Fins on the 70/50-Degree Cranked Wing Static Longitudinal Aerodynamic Characteristics, Vortex Flap Deflected to 30°.

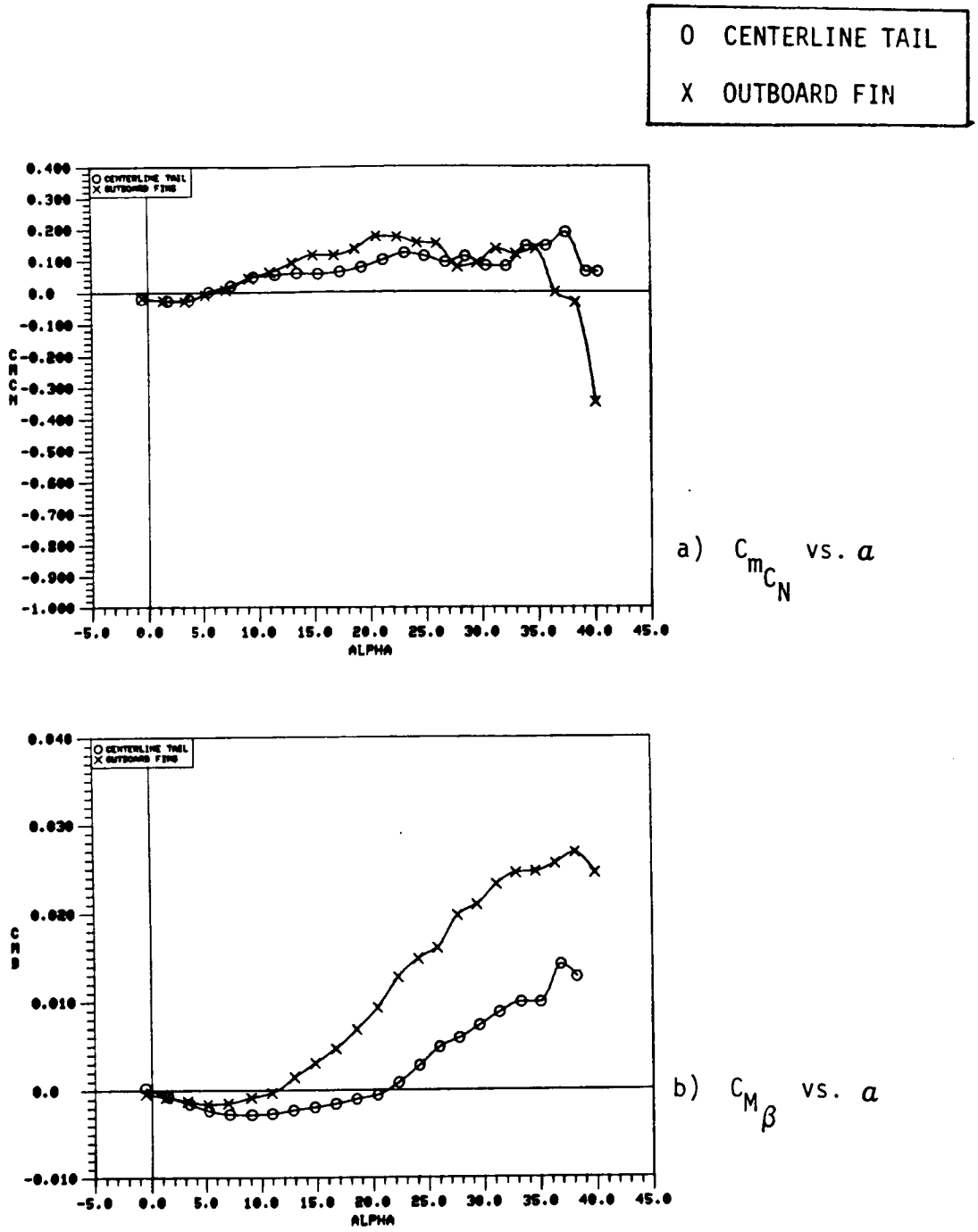

Figure 255. Effect of Outboard Fins on the 70/50-Degree Cranked Wing Static Longitudinal Stability Characteristics, Vortex Flap Deflected to 30°.

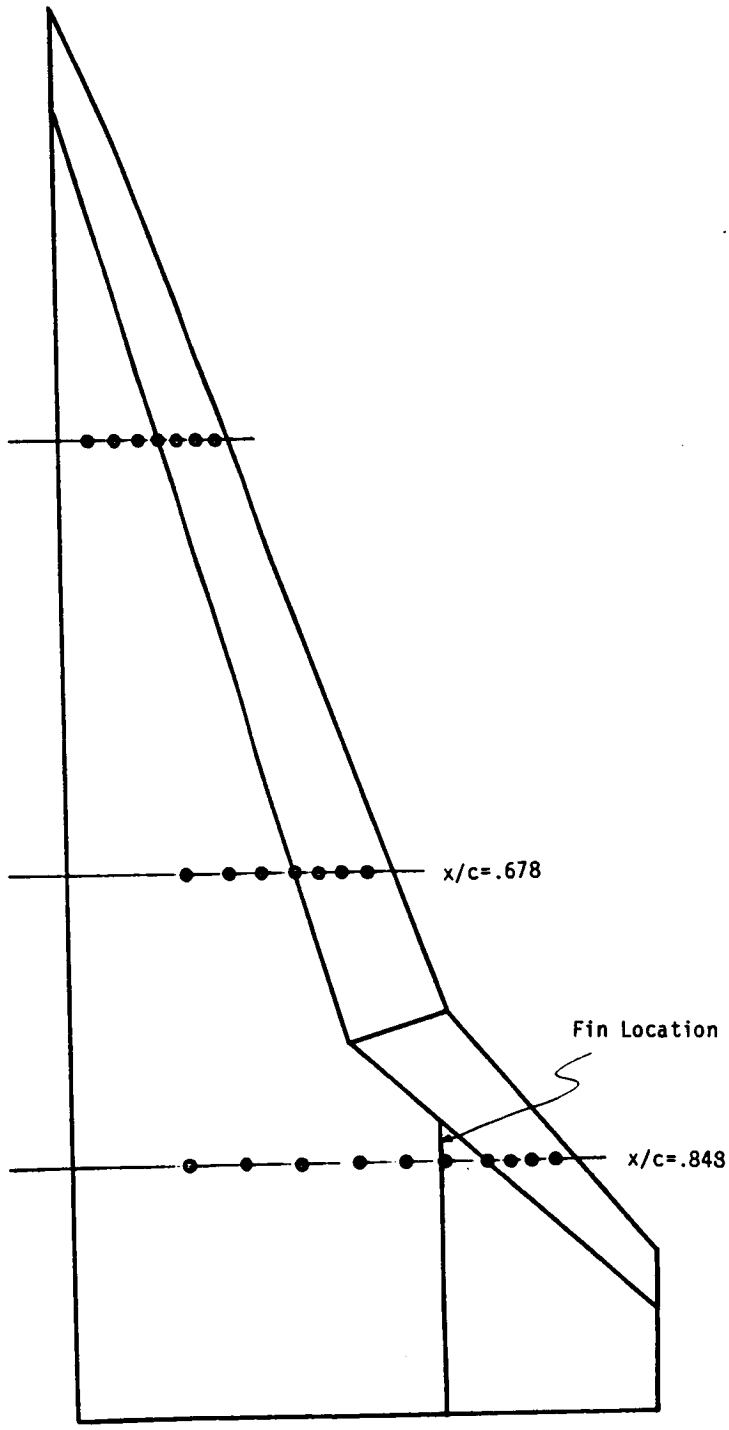

Figure 256. Location of Upper Surface Pressure Ports on the 70/50-Degree Cranked Wing.

O	CENTERLINE TAIL
X	OUTBOARD FIN

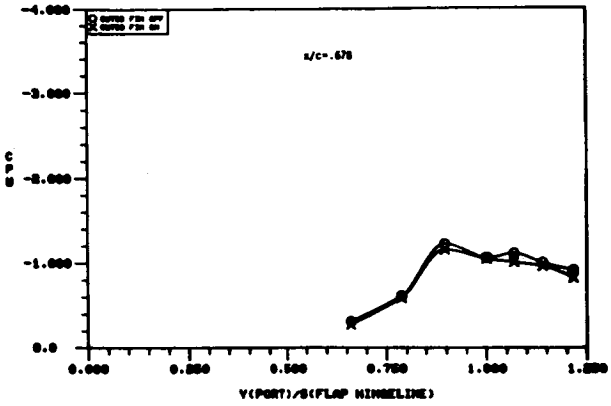

a) α = 16°, x/c = .678

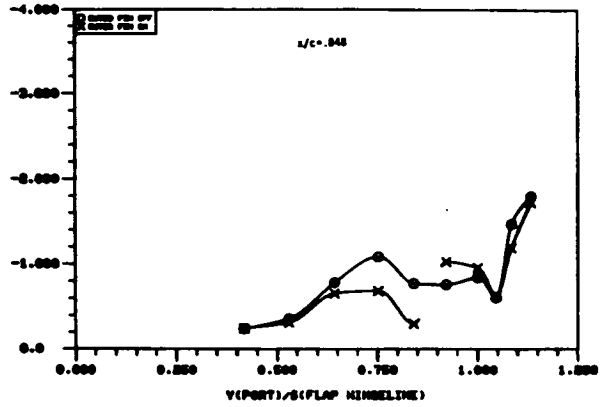

b) α = 16°, x/c = .848

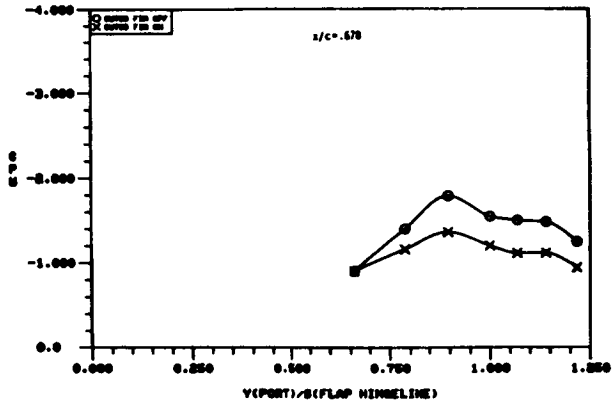

c) α = 24°, x/c = .678

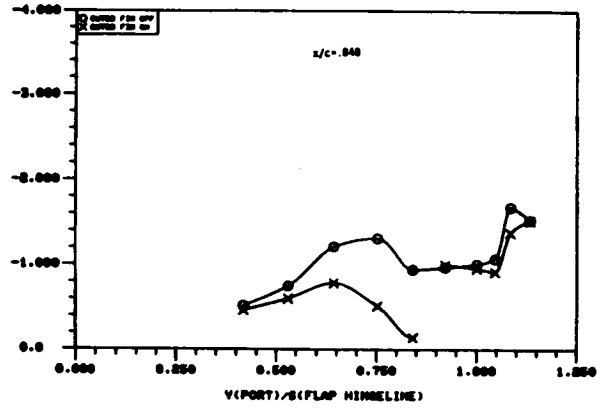

d) α =24°, x/c = .848

Figure 257. Effect of Outboard Fins on the 70/50-Degree Cranked Wing Upper Surface Static Pressure Distribution at Zero Sideslip, Vortex Flap Deflected to 30°.

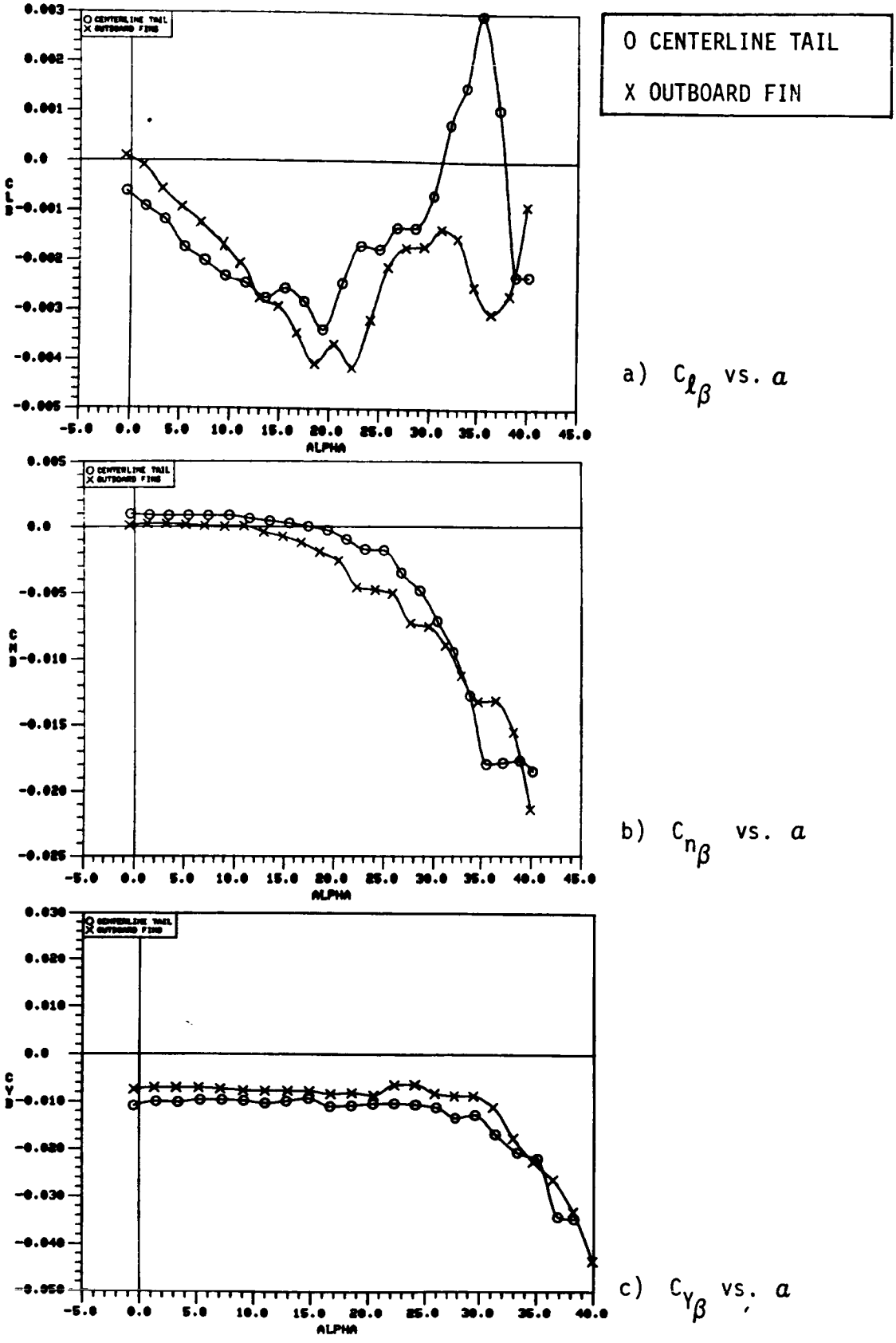

Figure 258. Effect of Outboard Fins on the 70/50-Degree Cranked Wing Static Lateral-Directional Stability Characteristics. Vortex Flap Deflected to 30°.

O	CENTERLINE TAIL
X	OUTBOARD FIN

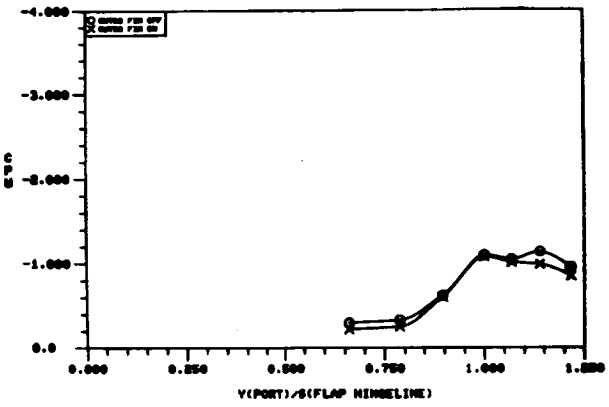

a) Leeward Wing,
$\beta = 5^{o}$, $\alpha = 16^{o}$, x/c = .678

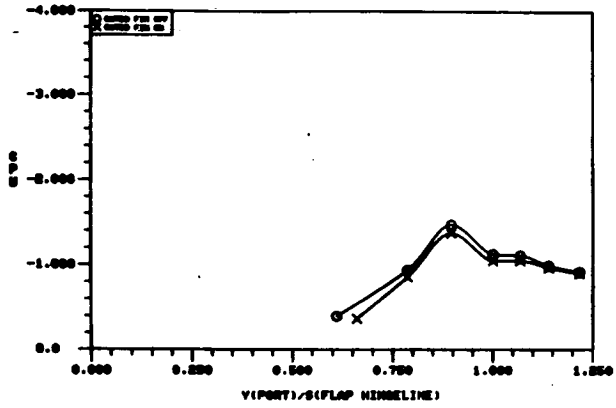

b) Windward Wing,
$\beta = 5^{o}$, $\alpha = 16^{o}$, x/c = .678

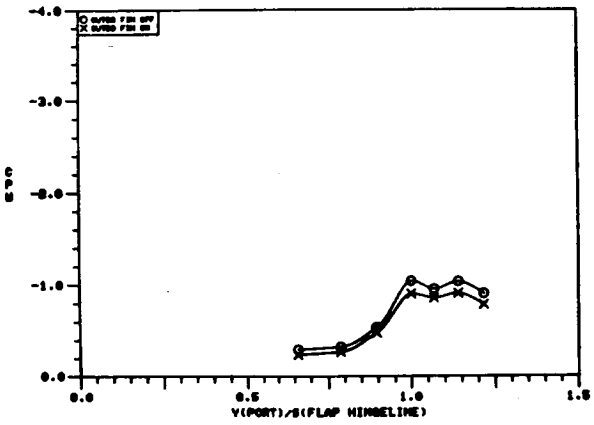

c) Leeward Wing,
$\beta = 10^{o}$, $\alpha = 16^{o}$, x/c = .678

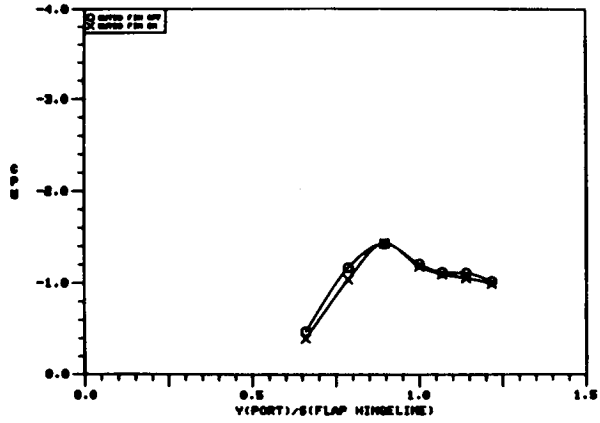

d) Leeward Wing,
$\beta = 10^{o}$, $\alpha = 16^{o}$, x/c = .678

Figure 259. Effect of Outboard Fins on the 70/50-Degree Cranked Wing Upper Surface Static Pressure Distributions in Sideslip, Vortex Flap Deflected to 30°.

O	CENTERLINE TAIL
X	OUTBOARD FIN

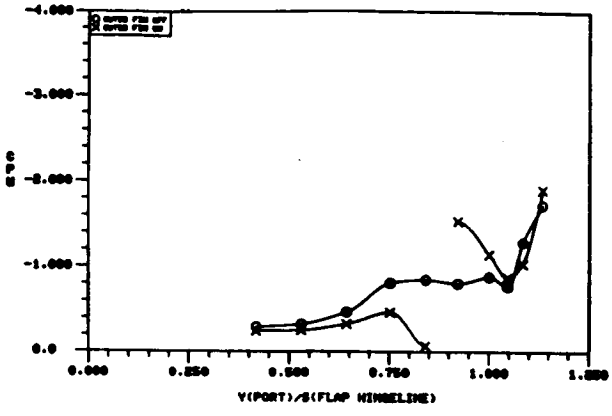

a) Leeward Wing,
$\beta = 5^0$, $\alpha = 16^0$, x/c = .848

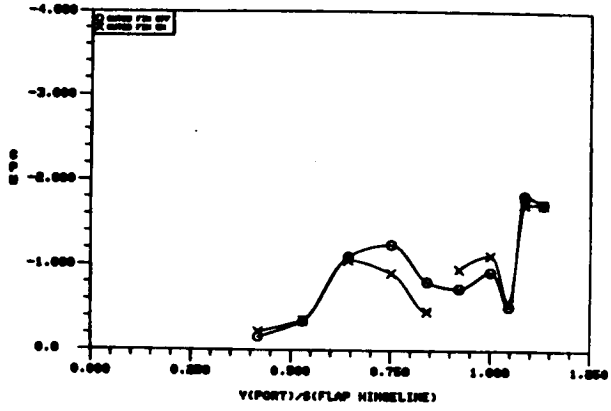

b) Windward Wing,
$\beta = 5^0$, $\alpha = 16^0$, x/c = .848

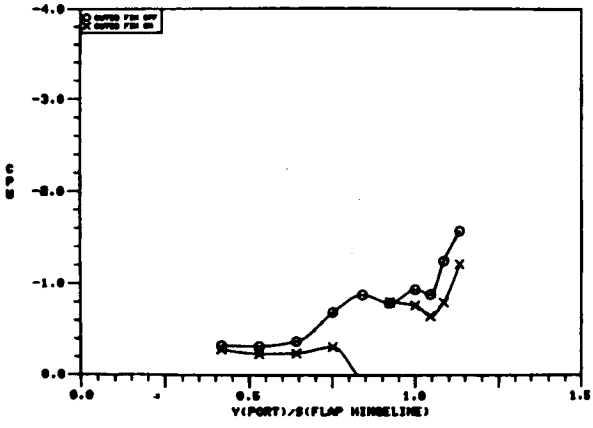

c) Leeward Wing,
$\beta = 10^0$, $\alpha = 16^0$, x/c = .848

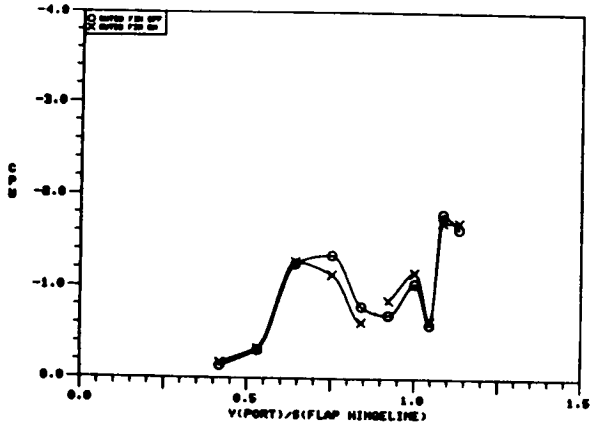

d) Windward Wing,
$\beta = 10^0$, $\alpha = 16^0$, x/c = .848

Figure 259. Continued.

O CENTERLINE TAIL

X OUTBOARD FIN

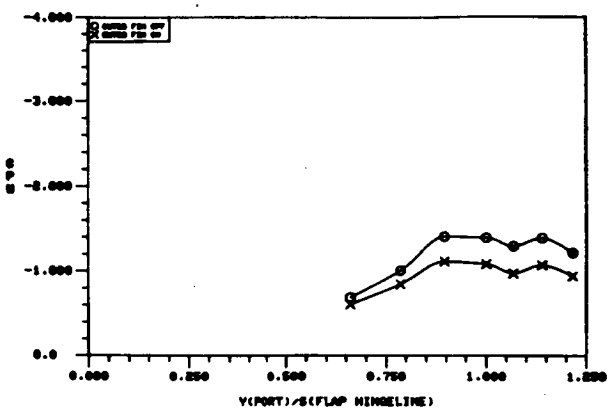

a) Leeward Wing,
$\beta = 5^{o}$, $\alpha = 24^{o}$, x/c = .678

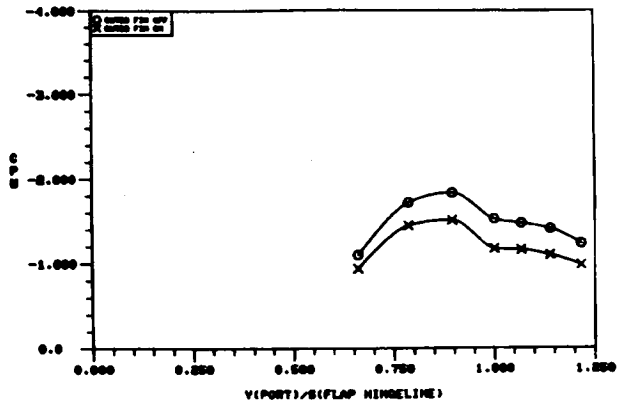

b) Windward Wing,
$\beta = 5^{o}$, $\alpha = 24^{o}$, x/c = .678

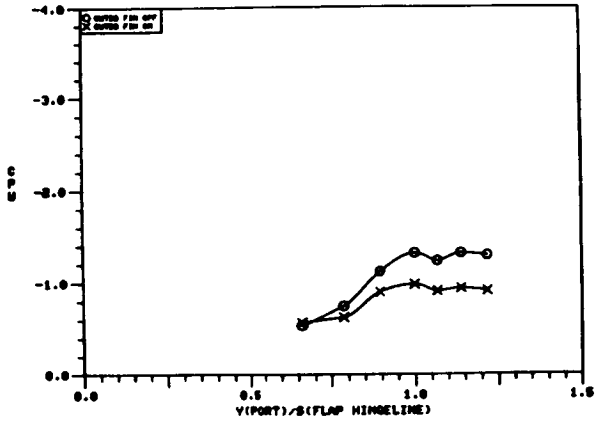

c) Leeward Wing,
$\beta = 10^{o}$, $\alpha = 24^{o}$, x/c = .678

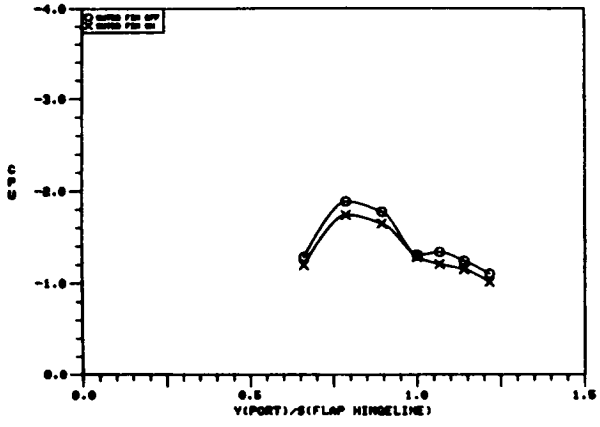

d) Windward Wing,
$\beta = 10^{o}$, $\alpha = 24^{o}$, x/c = .678

Figure 259. Continued.

O	CENTERLINE TAIL
X	OUTBOARD FIN

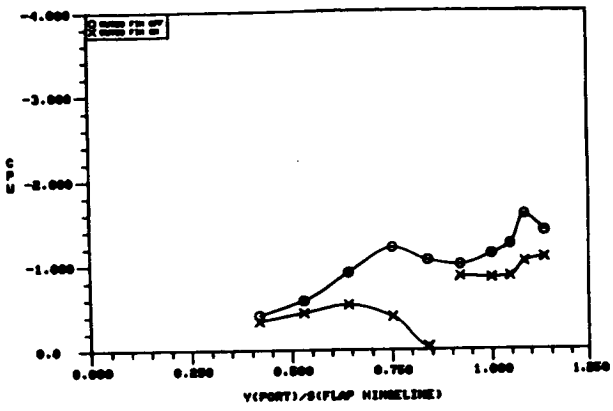

a) Leeward Wing,
$\beta = 5^{o}$, $\alpha = 24^{o}$, x/c = .848

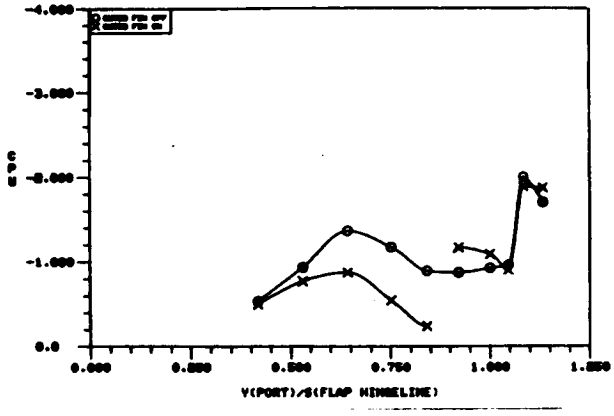

b) Windward Wing,
$\beta = 5^{o}$, $\alpha = 24^{o}$, x/c = .848

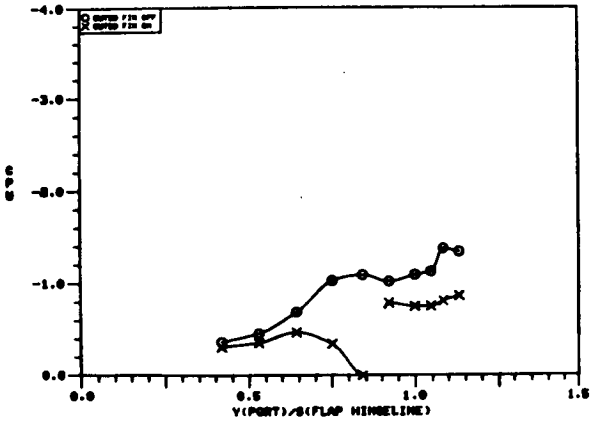

c) Leeward Wing,
$\beta = 10^{o}$ $\alpha = 24^{o}$, x/c = .848

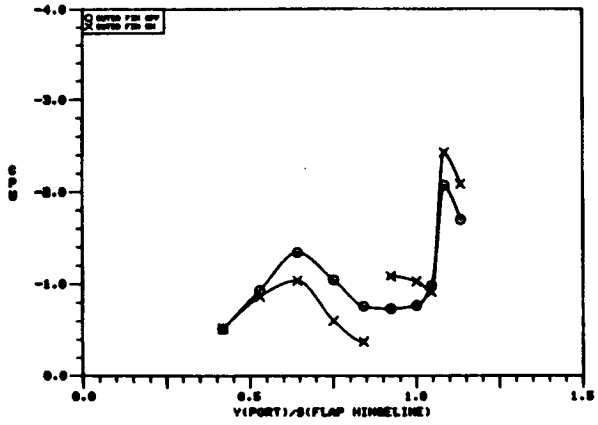

d) Windward Wing,
$\beta = 10^{o}$, $\alpha = 24^{o}$, x/c = .848

Figure 259. Concluded.

O	OUTBOARD FIN, ALPHA = 16 DEG.
X	CENTERLINE TAIL, ALPHA = 16 DEG.
△	OUTBOARD FIN, ALPHA = 24 DEG.
□	CENTERLINE TAIL, ALPHA = 24 DEG.

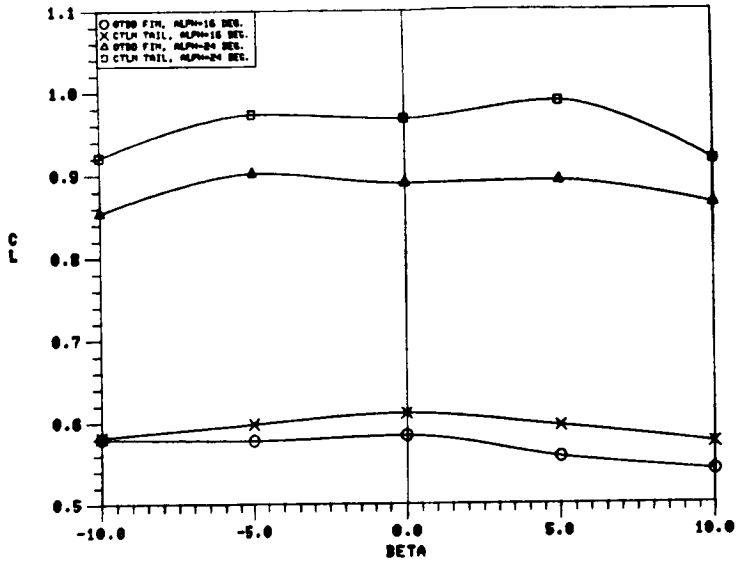

a) C_L vs. β

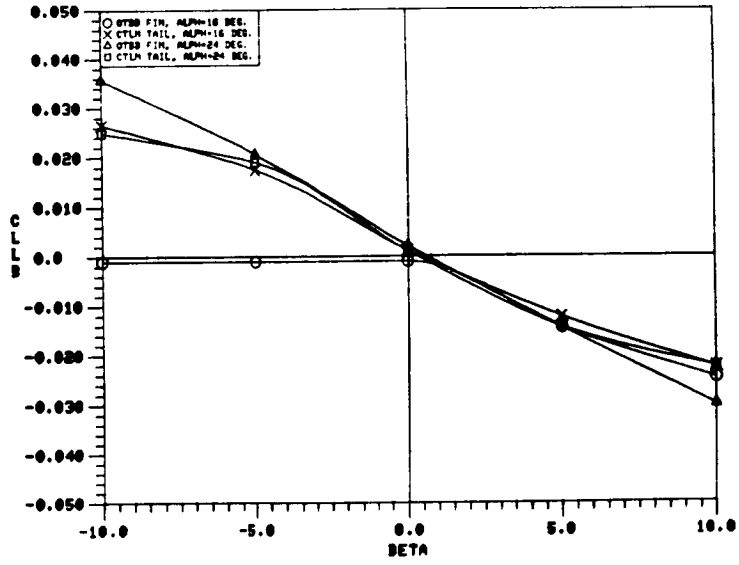

b) C_ℓ vs. β

Figure 260. Effect of Outboard Fins on the 70/50-Degree Cranked Wing Lift and Rolling Moment Variations with Sideslip, Vortex Flap Deflected to 30°.

O	CENTERLINE TAIL
X	OUTBOARD FIN

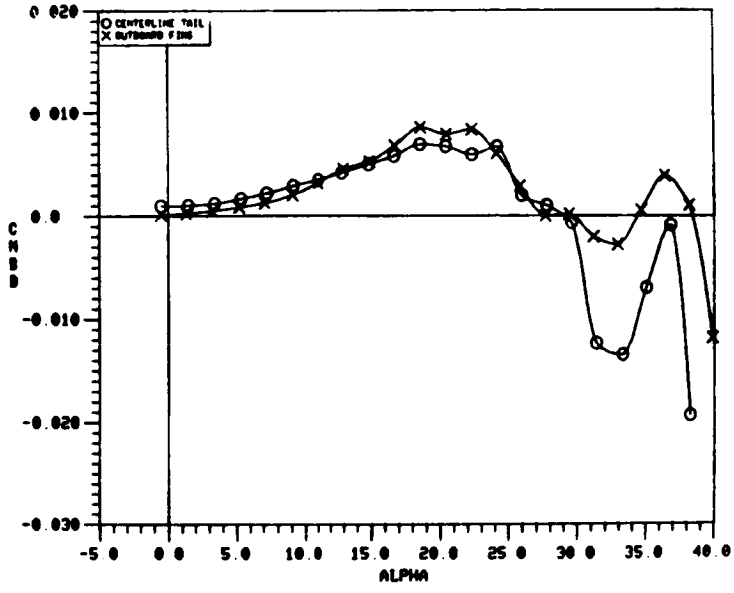

$C_{n_{\beta_{dyn}}}$ vs. α

Figure 261. Effect of Outboard Fins on the 70/50-Degree Cranked Wing Dynamic Directional Stability Parameter, Vortex Flap Deflected to 30°.

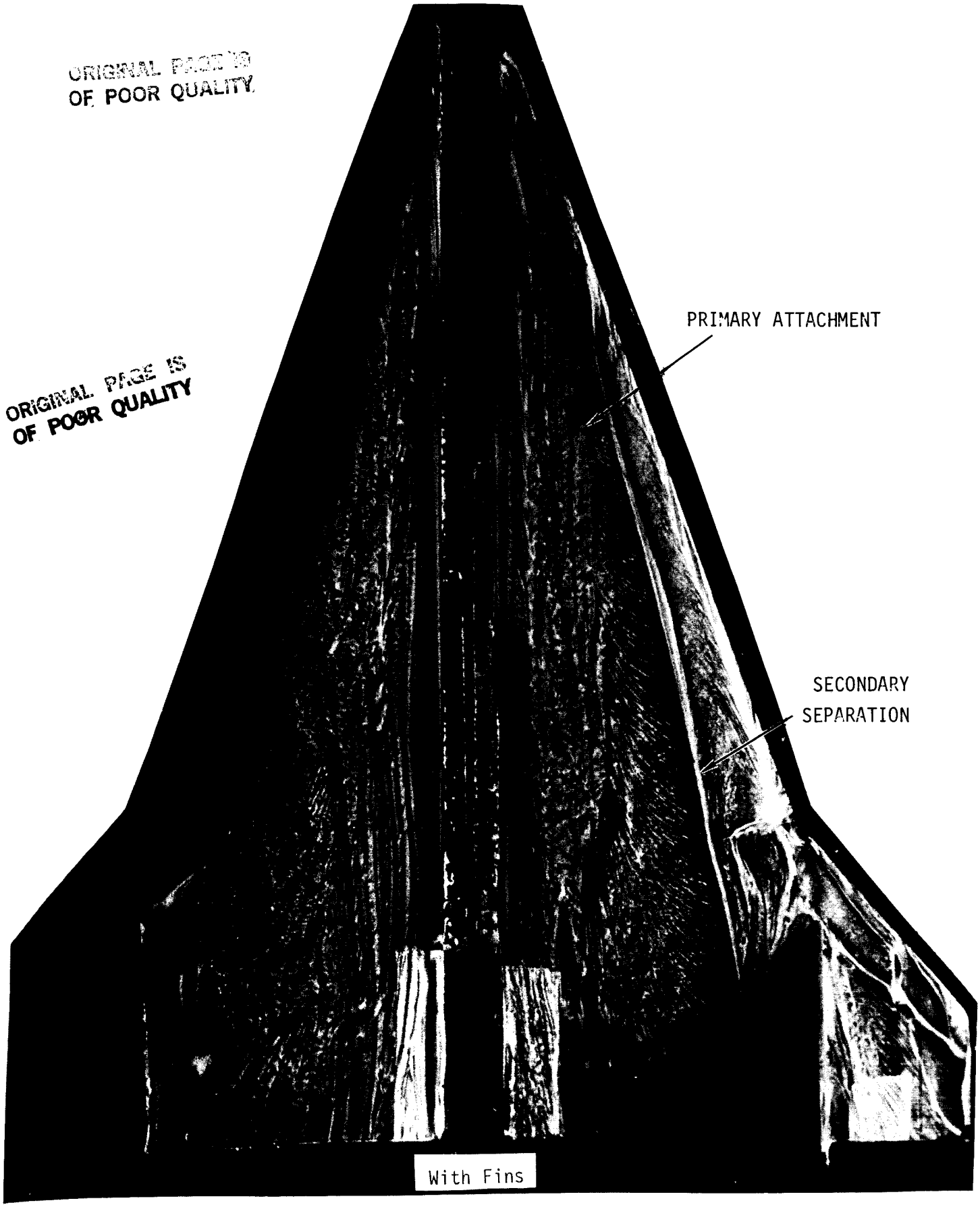

Figure 262. Upper Surface Flow Patterns on the 70/50-Degree Cranked Wing With and Without Outboard Fins, at $\alpha = 16°$, $\beta = 5°$.

ORIGINAL PAGE IS
OF POOR QUALITY

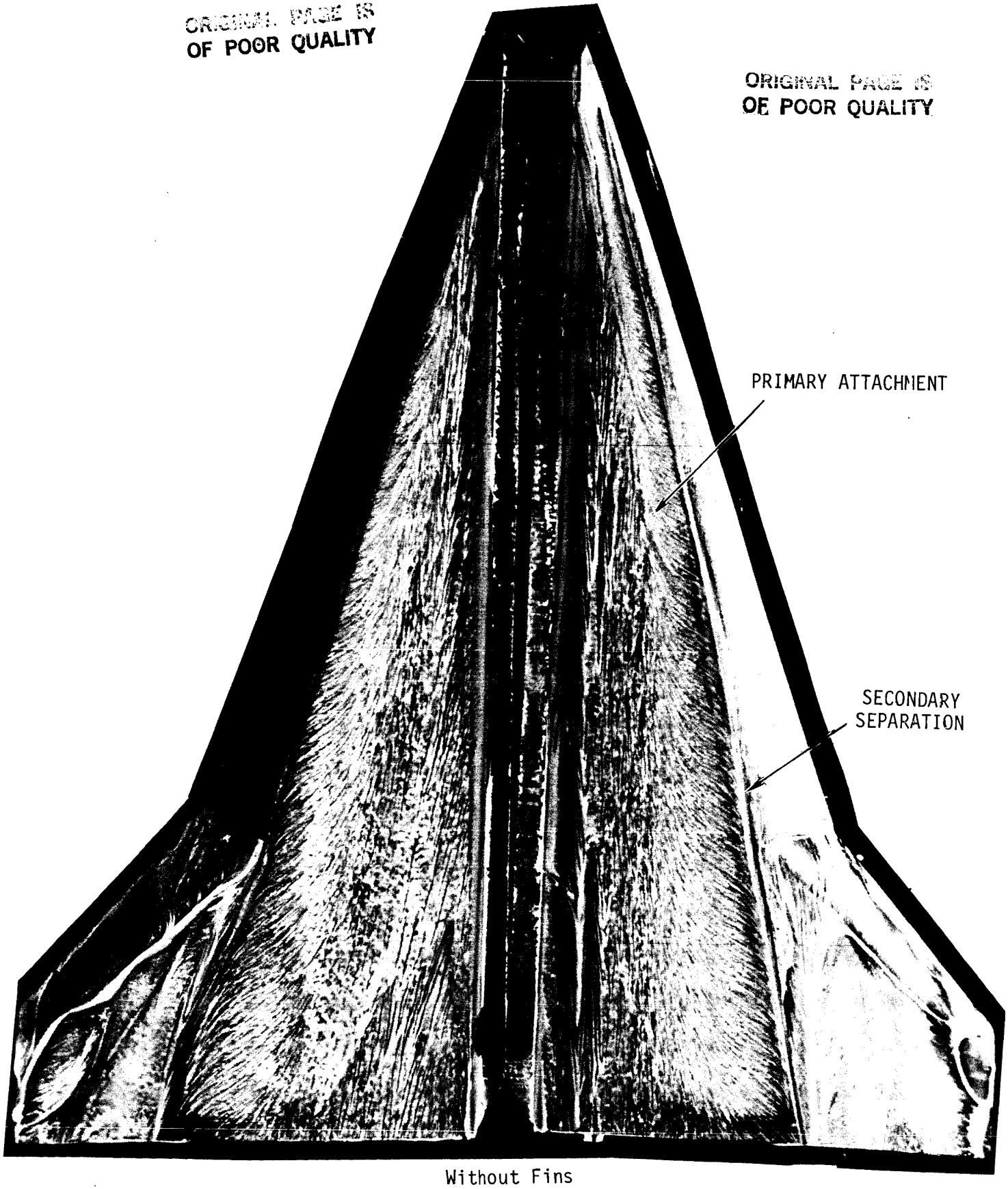

Without Fins

Figure 262. Continued.

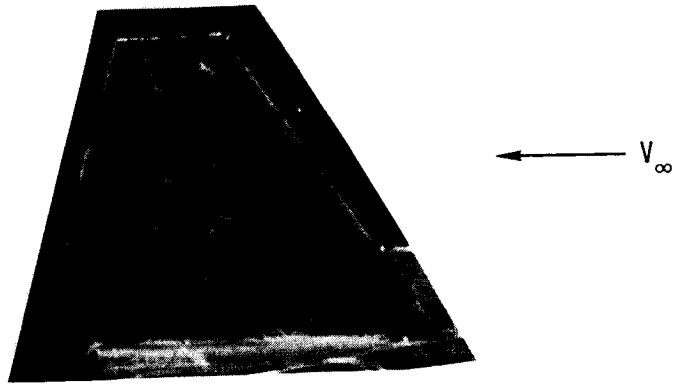

a) Pressure Side of Windward Fin

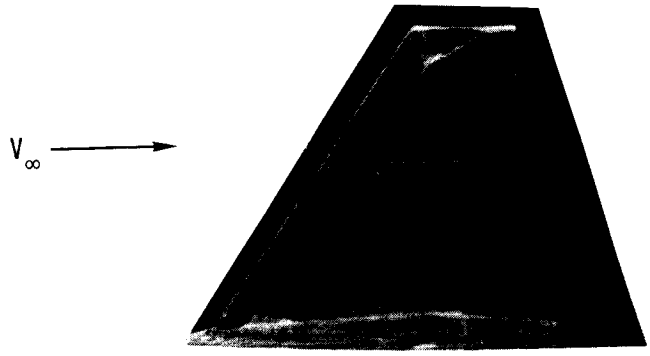

b) Suction Side of Windward Fin

Figure 262. Continued.

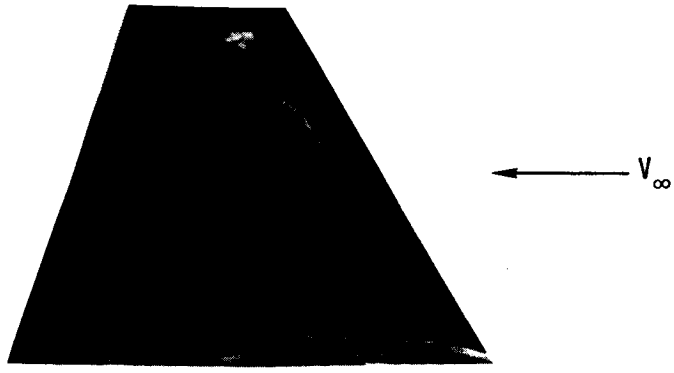

c) Pressure Side of Leeward Fin

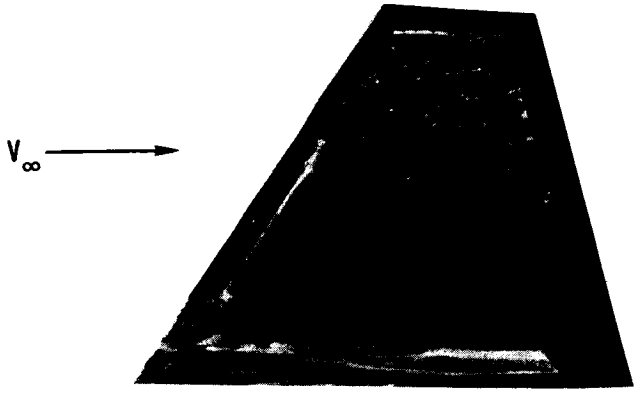

d) Suction Side of Leeward Fin

Figure 262. Concluded.

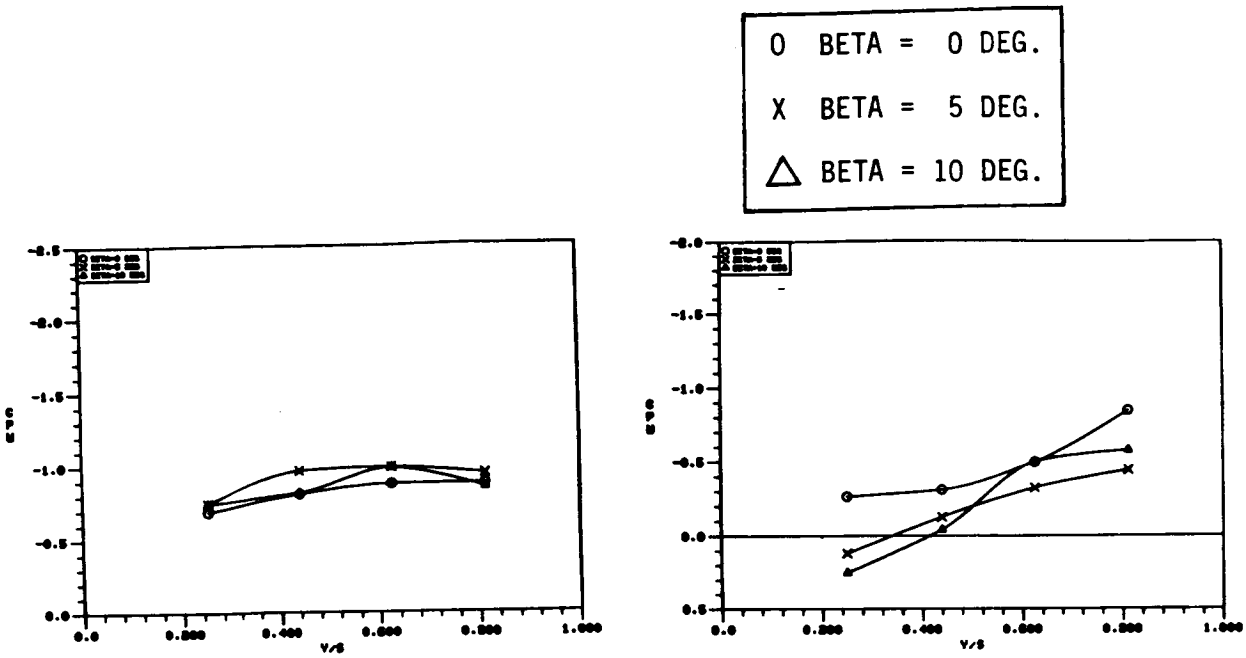

a) Suction Side of Leeward Fin, $\alpha = 16^{o}$, x/c = .24

b) Pressure Side of Leeward Fin, $\alpha = 16^{o}$, x/c = .24

c) Suction Side of Leeward Fin, $\alpha = 16^{o}$, x/c = .57

d) Pressure Side of Leeward Fin, $\alpha = 16^{o}$, x/c = .57

Figure 263. Effect of Sideslip Angle on the Outboard Fin Surface Static Pressure Distributions.

O	BETA = 0 DEG.
X	BETA = 5 DEG.
△	BETA = 10 DEG.

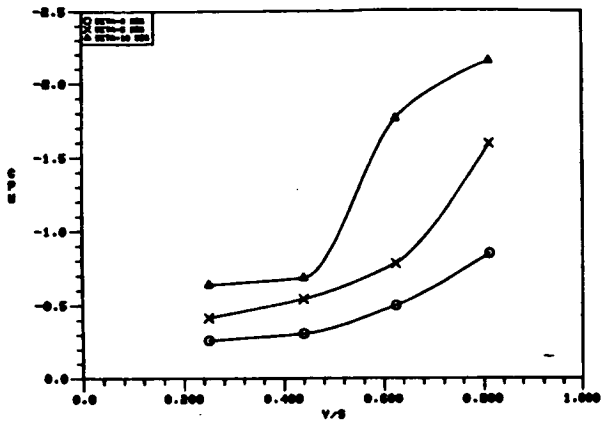

a) Suction Side of Windward Fin, $\alpha = 16^{o}$ x/c = .24

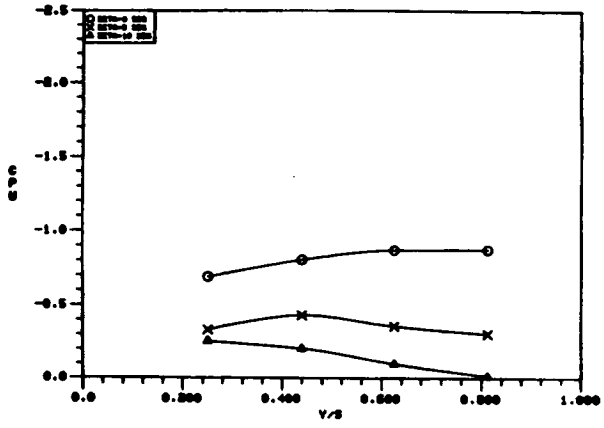

b) Pressure Side of Windward Fin, $\alpha = 16^{o}$, x/c = .24

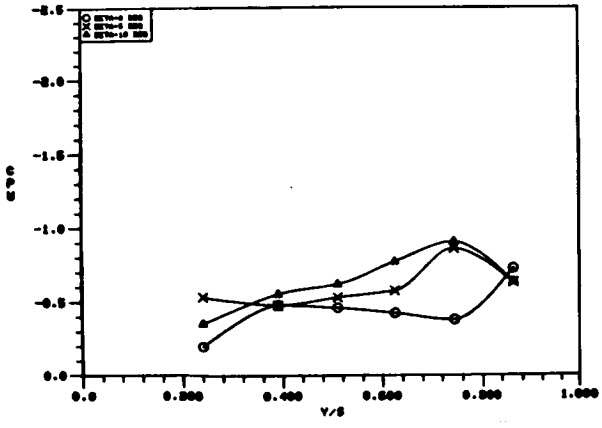

c) Suction Side of Windward Fin, $\alpha = 16^{o}$, x/c = .57

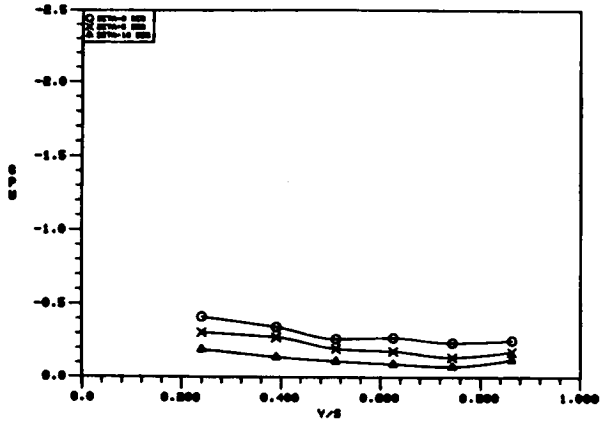

d) Pressure Side of Windward Fin, $\alpha = 16^{o}$, x/c = .57

Figure 263. Continued.

O	BETA = 0 DEG.
X	BETA = 5 DEG.
△	BETA = 10 DEG.

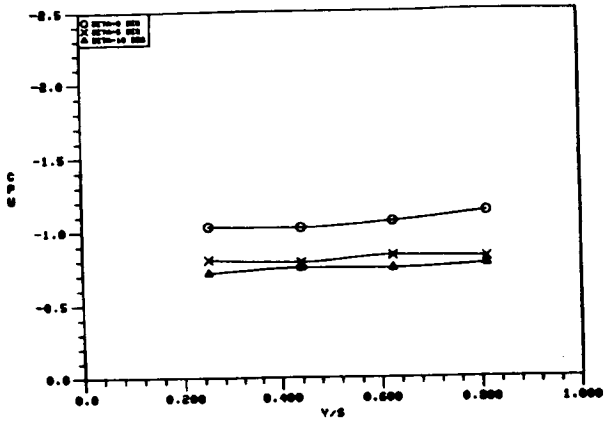

a) Suction Side of Leeward Fin, $\alpha = 24^{o}$, x/c = .24

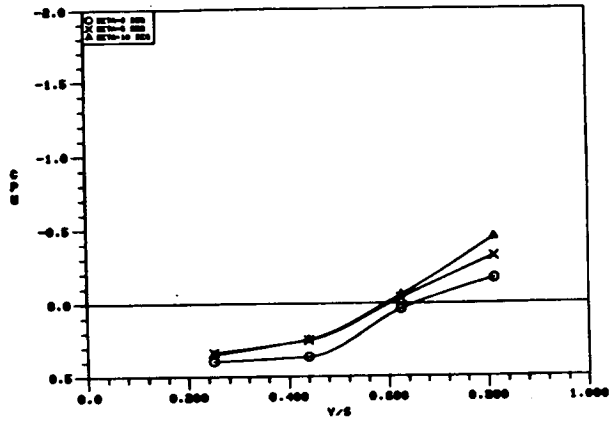

b) Pressure Side of Leeward Fin, $\alpha = 24^{o}$, x/c = .24

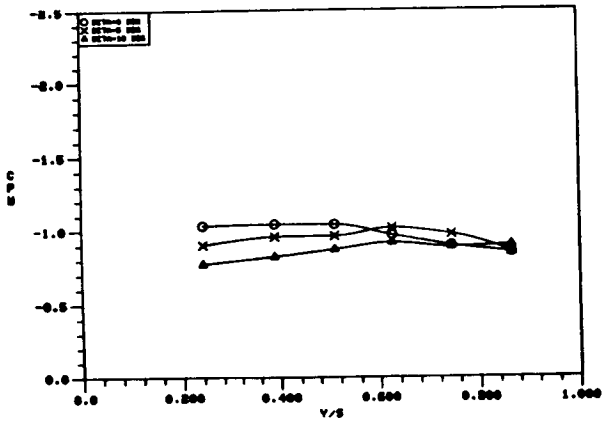

c) Suction Side of Leeward Fin, $\alpha = 24^{o}$, x/c = .57

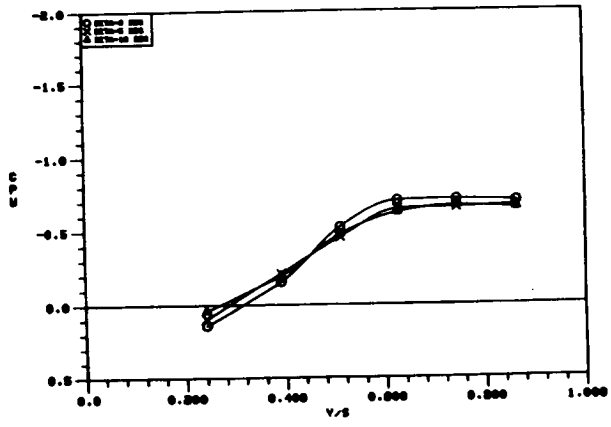

d) Pressure Side of Leeward Fin, $\alpha = 24^{o}$, x/c = .57

Figure 263. Continued.

O	BETA = 0 DEG.
X	BETA = 5 DEG.
△	BETA = 10 DEG.

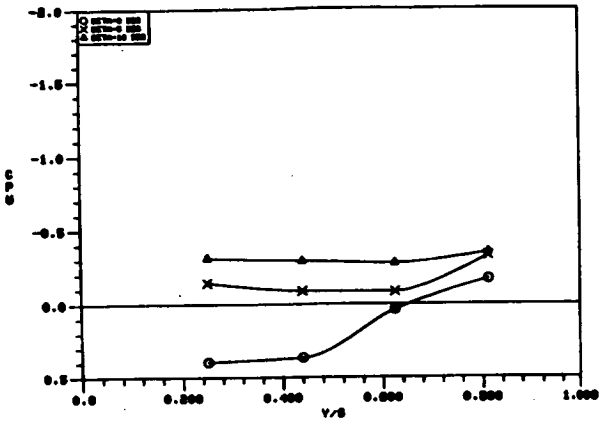

a) Suction Side of Windward Fin, $\alpha = 24^{o}$, x/c = .24

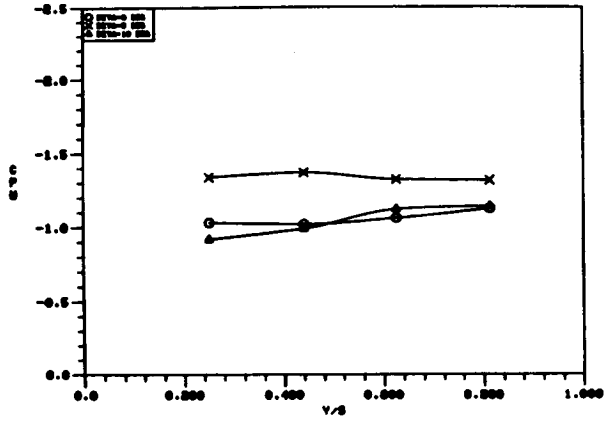

b) Pressure Side of Windward Fin, $\alpha = 24^{o}$, x/c = .24

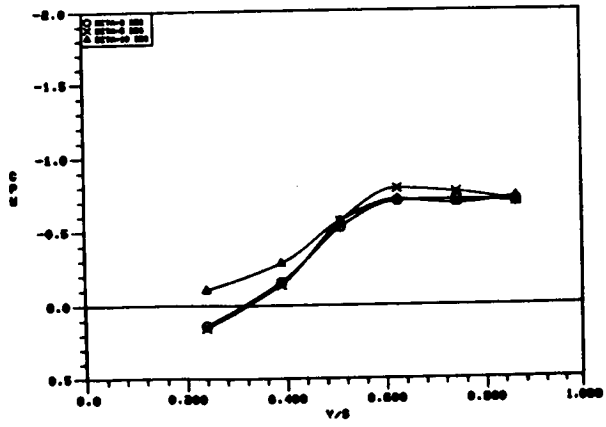

c) Suction Side of Windward Fin, $\alpha = 24^{o}$, x/c = .57

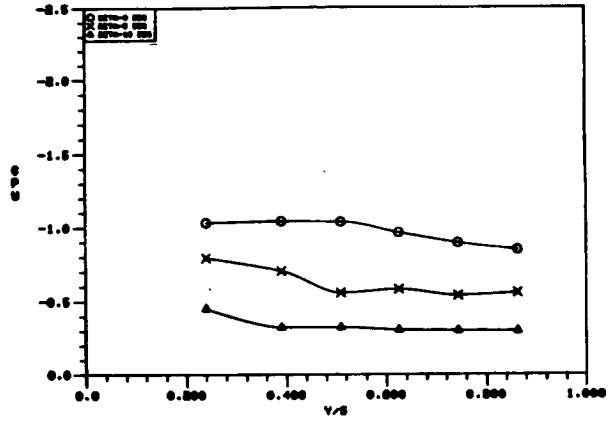

d) Pressure Side of Windward Fin, $\alpha = 24^{o}$, x/c = .57

Figure 263. Concluded.

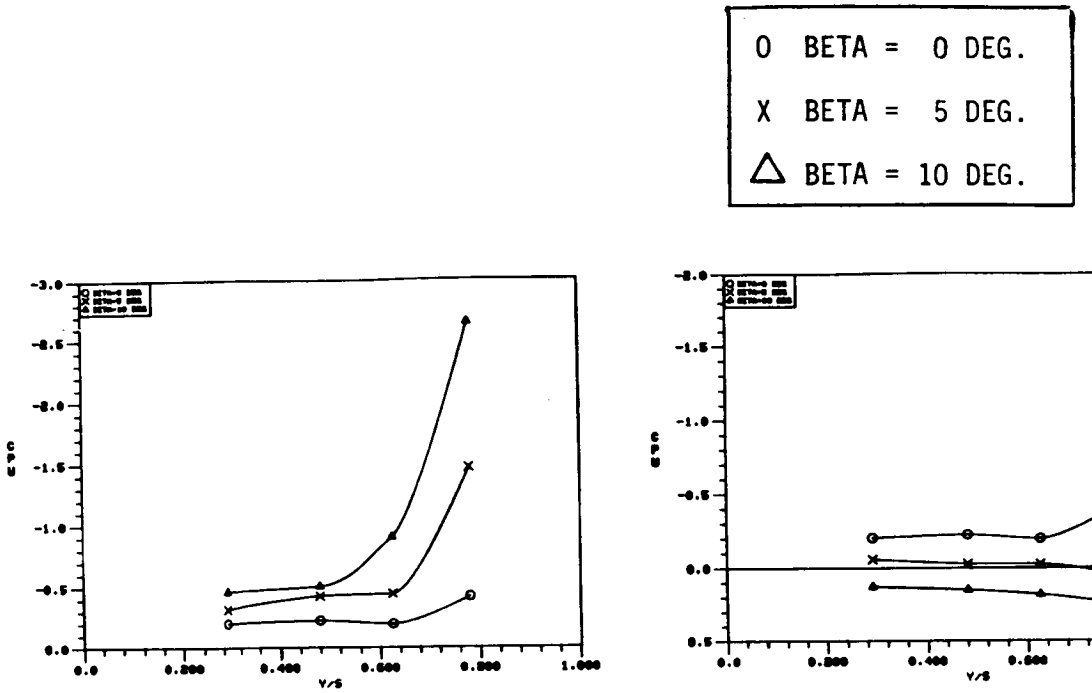

a) Suction Side, $\alpha = 16^{o}$, x/c = .24

b) Pressure Side, $\alpha = 16^{o}$, x/c = .24

c) Suction Side, $\alpha = 16^{o}$, x/c = .47

d) Pressure Side, $\alpha = 16^{o}$, x/c = .47

Figure 264. Effect of Sideslip Angle on the Centerline Tail Surface Static Pressure Distributions.

O	BETA = 0 DEG.
X	BETA = 5 DEG.
△	BETA = 10 DEG.

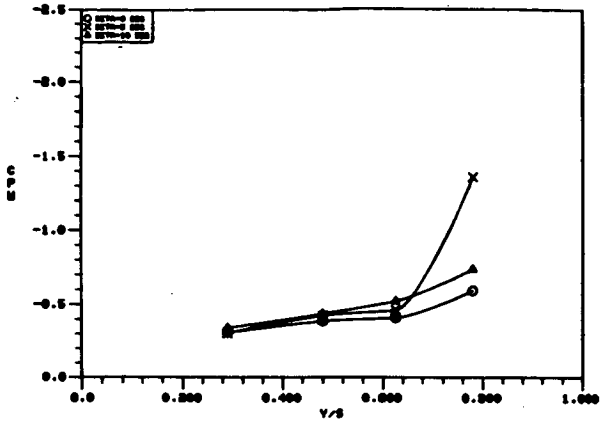

a) Suction Side, $\alpha = 24^{o}$, x/c = .24

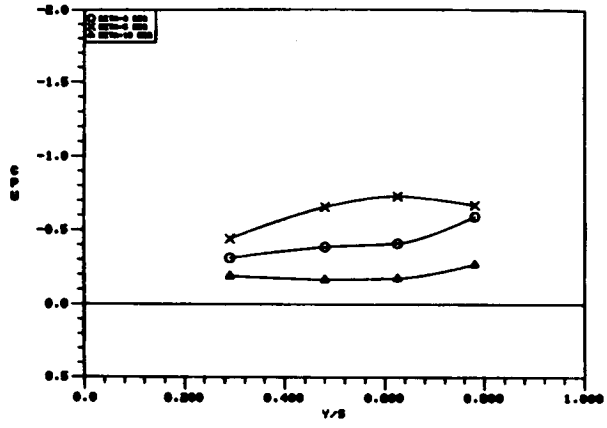

b) Pressure Side, $\alpha = 24^{o}$, x/c = .24

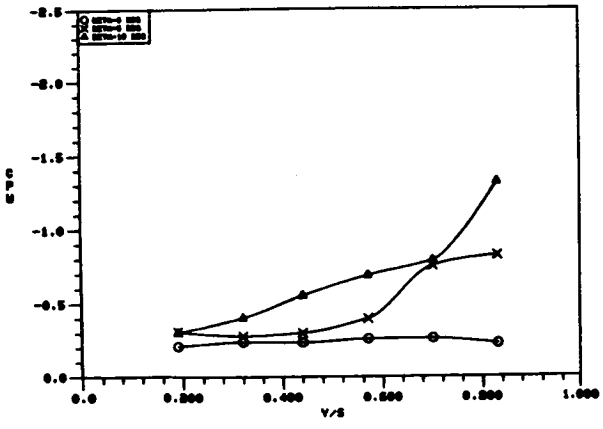

c) Suction Side, $\alpha = 24^{o}$, x/c = .47

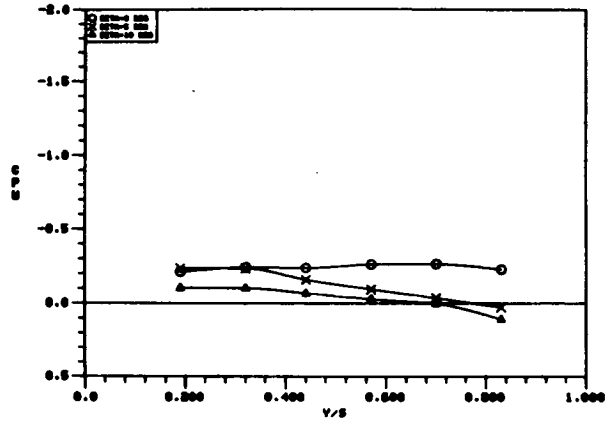

d) Pressure Side, $\alpha = 24^{o}$, x/c = .47

Figure 264. Concluded.

O TAIL UNDEFLECTED

X TAIL DEFLECTED, +10 DEG.

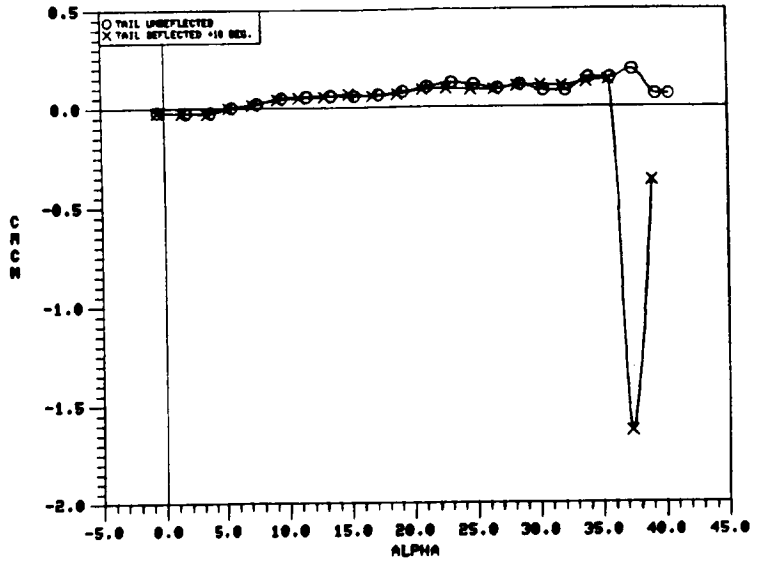

a) $C_{m_{C_N}}$ vs. α

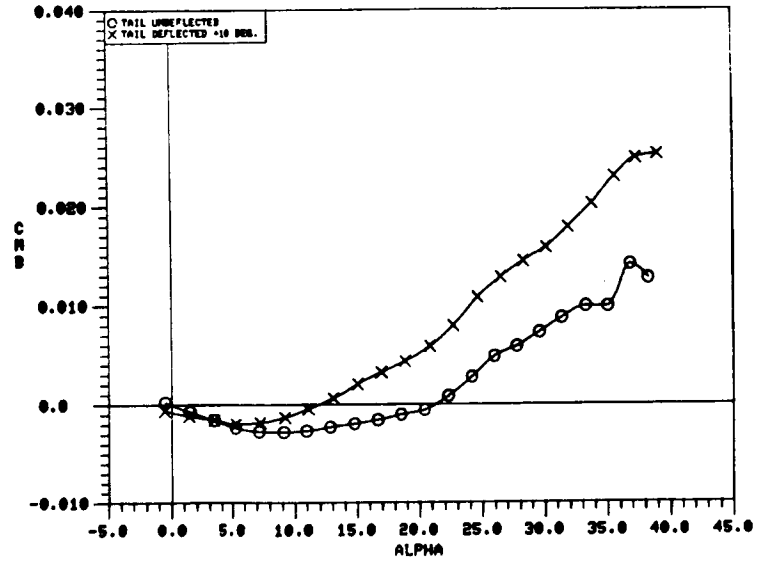

b) C_{m_β} vs. α

Figure 265. Effect of Centerline Tail Deflection on the 70/50-Degree Cranked Wing Static Longitudinal Stability Characteristics, δ_v = +10°, Vortex Flap Deflected to 30°.

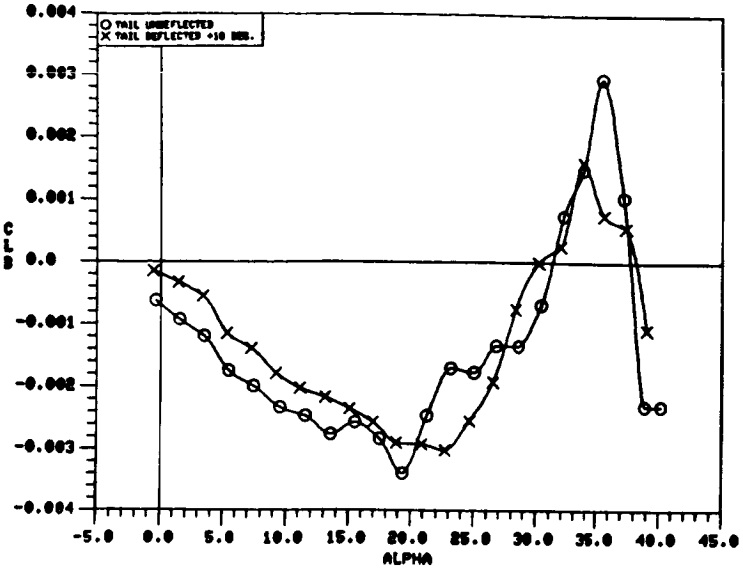

O TAIL UNDEFLECTED

X TAIL DEFLECTED, +10 DEG.

a) C_{ℓ_β} vs. α

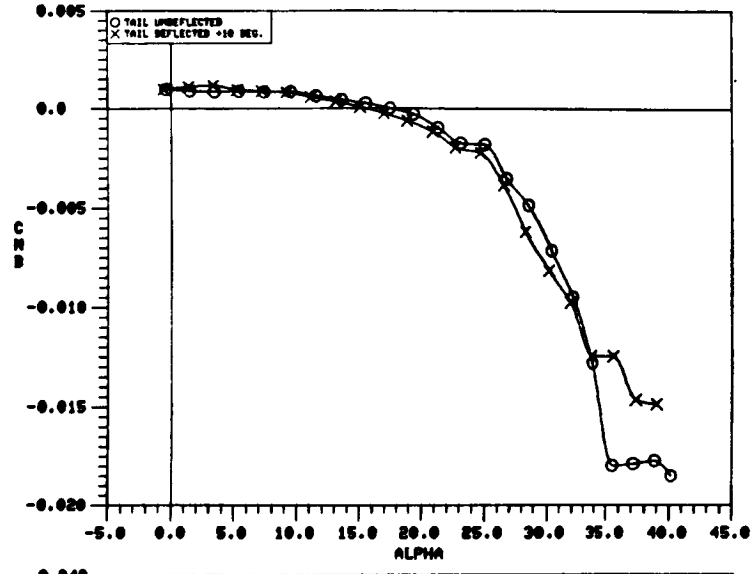

b) C_{n_β} vs. α

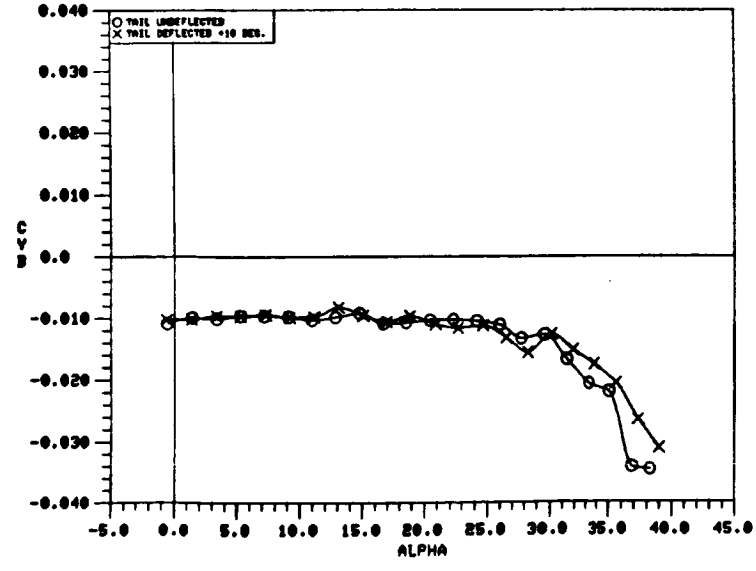

c) C_{Y_β} vs. α

Figure 266. Effect of Centerline Tail Deflection on the 70/50-Degree Cranked Wing Static Lateral-Directional Stability Characteristics, δ_v = +10°, Vortex Flap Deflected to 30°.

O FINS UNDEFLECTED

X FINS DEFLECTED, - 10 DEG.

△ FINS DEFLECTED, +10 DEG.

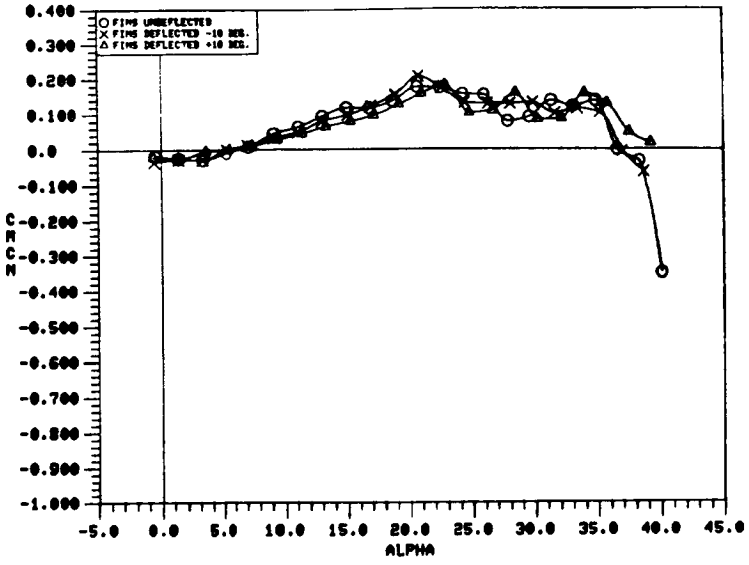

a) $C_{m_{C_N}}$ vs. α

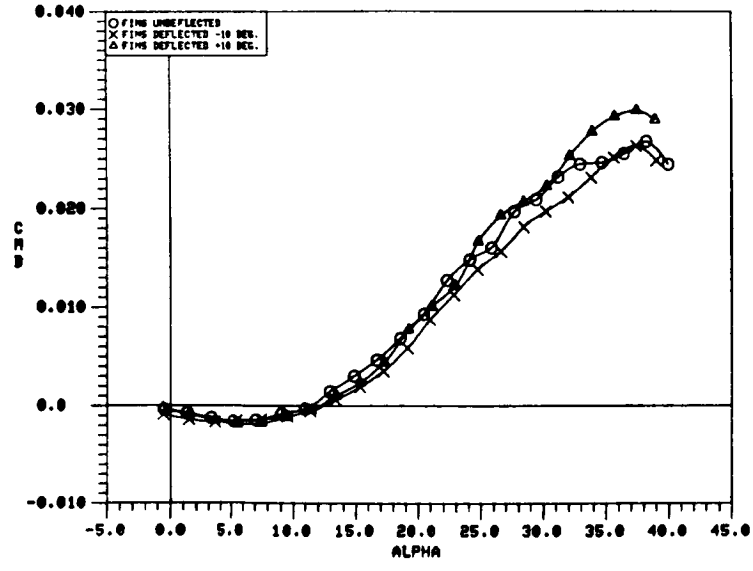

b) C_{m_β} vs. α

Figure 267. Effect of Symmetric Outboard Fin Deflection on the 70/50-Degree Cranked Wing Static Longitudinal Stability Characteristics, δ_v = +10°, Vortex Flap Deflected to 30°.

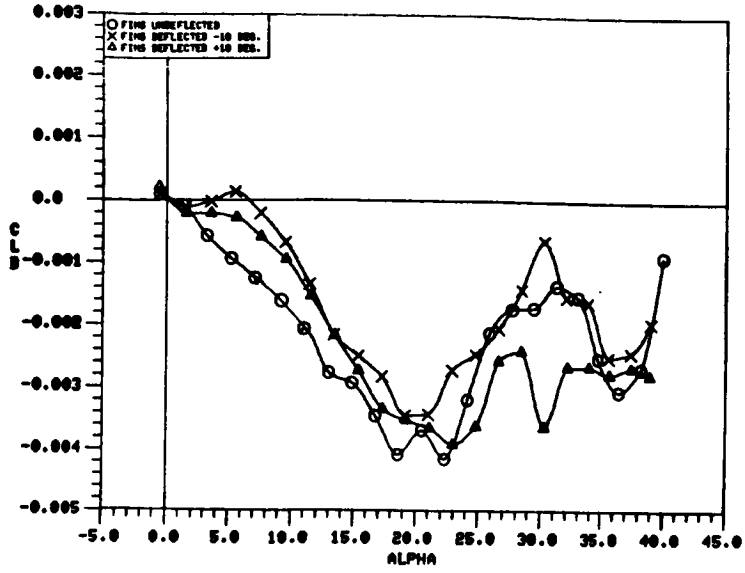

O FINS UNDEFLECTED

X FINS DEFLECTED, -10 DEG.

△ FINS DEFLECTED, +10 DEG.

a) C_{ℓ_β} vs. α

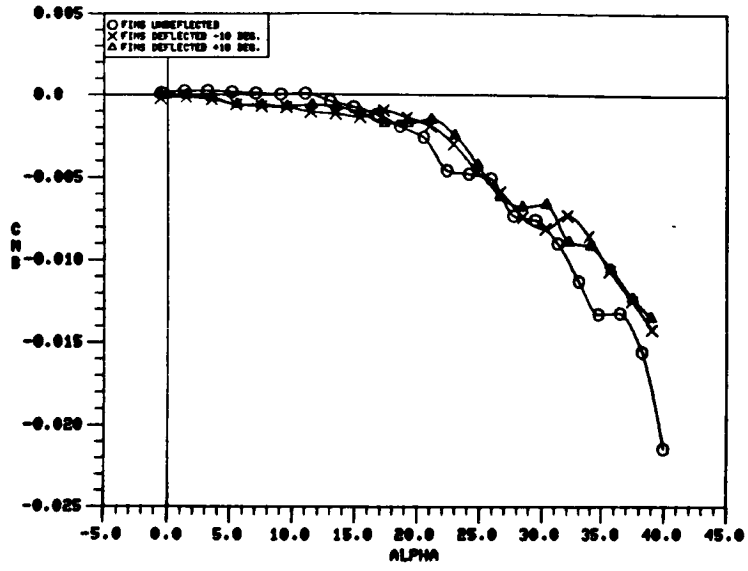

b) C_{n_β} vs. α

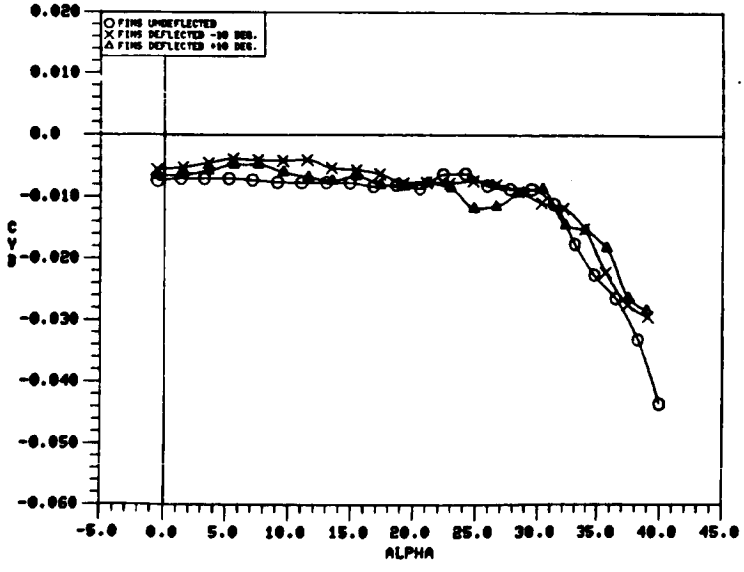

c) C_{Y_β} vs. α

Figure 268. Effect of Symmetric Outboard Fin Deflection on the 70/50-Degree Cranked Wing Static Lateral-Directional Stability Characteristics, δ_V = +10°, Vortex Flap Deflected to 30°.

O	FINS DEFLECTED +10 DEG.
X	FINS DEFLECTED -10 DEG.

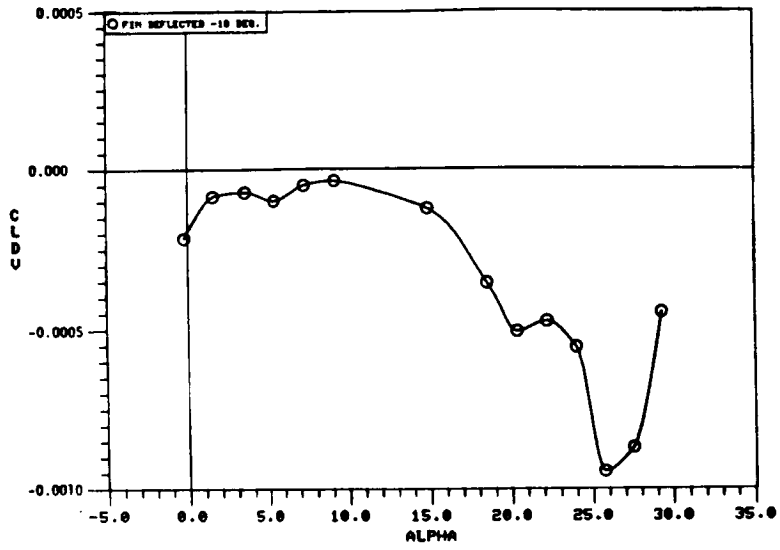

a) $C_{\ell_{\delta_V}}$ vs. α

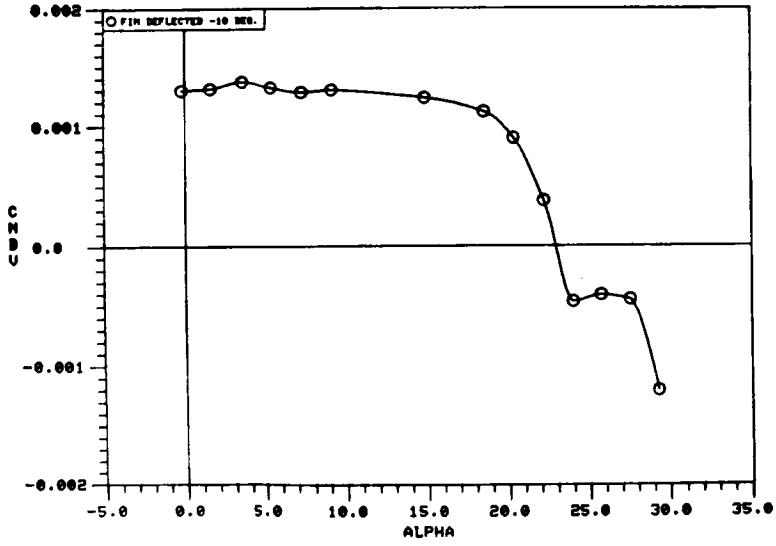

b) $C_{n_{\delta_V}}$ vs. α

Figure 269. Effect of Symmetric Outboard Fin Deflection on the 70/50-Degree Cranked Wing Lateral-Directional Control Derivatives, Vortex Flap Deflected to 30°.

O	CENTERLINE TAIL, 10 DEG.
X	OUTBOARD FINS, 10 DEG.

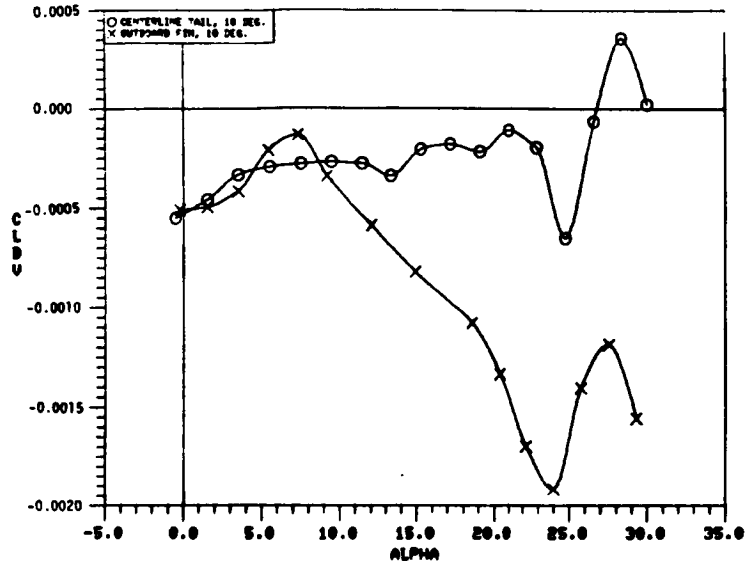

a) $C_{\ell_{\delta_V}}$ vs. α

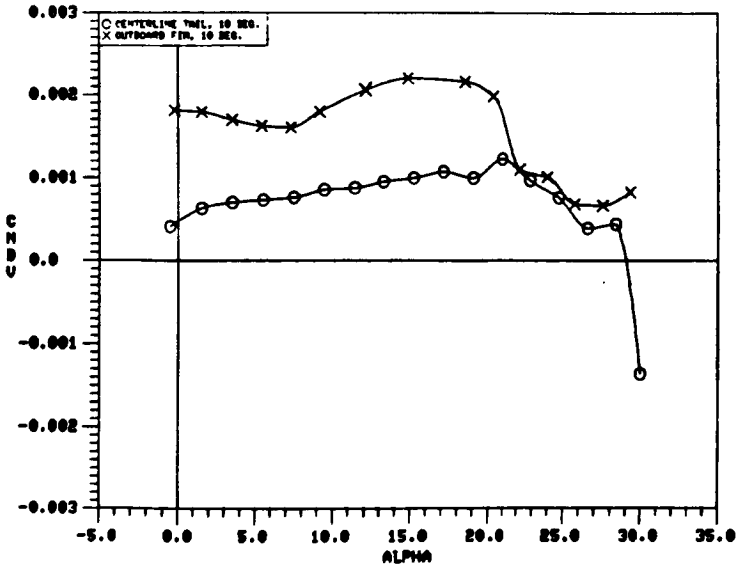

b) $C_{n_{\delta_V}}$ vs. α

Figure 270. Comparison of the Centerline Tail and Outboard Fin Deflection Effects on the 70/50-Degree Cranked Wing Lateral-Directional Control Derivatives, Vortex Flap Deflected to 30°.

1. Report No.	2. Government Accession No.	3. Recipient's Catalog No.
NASA CR-172439		

4. Title and Subtitle	5. Report Date
VORTEX FLAP TECHNOLOGY: A STABILITY AND CONTROL ASSESSMENT	November 1984
	6. Performing Organization Code
7. Author(s)	8. Performing Organization Report No.
K. M. Carey and G. E. Erickson	NOR-84-158
	10. Work Unit No.
9. Performing Organization Name and Address Northrop Corporation, Aircraft Division One Northrop Avenue Hawthorne, CA 90250	11. Contract or Grant No. NAS1-17533
	13. Type of Report and Period Covered Contractor Report
12. Sponsoring Agency Name and Address National Aeronautics and Space Administration Washington, D.C. 20546	14. Sponsoring Agency Code

15. Supplementary Notes

Langley Technical Monitor: Long P. Yip
Final Report

16. Abstract

A comprehensive low-speed wind tunnel investigation was performed of leading-edge vortex flaps applied to representative aircraft configurations. A determination was made of the effects of analytically- and empirically-designed vortex flaps on the static longitudinal and lateral-directional aerodynamics, stability, and control characteristics of fighter wings having leading-edge sweep angles of 45 to 76.5 degrees. The sensitivity to several configuration modifications was assessed, which included the effects of flap planform, leading- and trailing-edge flap deflection angles, wing location on the fuselage, forebody strakes, canards, and centerline and outboard vertical tails. Six-component forces and moments, wing surface static pressure distributions, and surface flow patterns were obtained using the Northrop 21- by 30-inch low-speed wind tunnel.

17. Key Words (Suggested by Author(s))	18. Distribution Statement
Vortex Flows, Vortex Breakdown, High Angle-of-Attack Aerodynamics, Stability and Control, Subsonic Wind Tunnel Tests, Vortex Flaps, Fighter Aircraft	[redacted]

19. Security Classif. (of this report)	20. Security Classif. (of this page)	21. No. of Pages	22. Price
Unclassified	Unclassified	361	